NASA Conference Publication 3347

The 1996 NASA Aerospace Battery Workshop

Compiled by
J.C. Brewer

Proceedings of a workshop sponsored by the
NASA Aerospace Flight Battery Systems Program
and held in Huntsville, Alabama
December 3–5, 1996

February 1997

NASA Conference Publication 3347

The 1996 NASA Aerospace Battery Workshop

Compiled by
J.C. Brewer
Marshall Space Flight Center • MSFC, Alabama

Proceedings of a workshop sponsored by the
NASA Aerospace Flight Battery Systems Program
and held in Huntsville, Alabama
December 3–5, 1996

National Aeronautics and Space Administration
Marshall Space Flight Center • MSFC, Alabama 35812

February 1997

Preface

This document contains the proceedings of the 29th annual NASA Aerospace Battery Workshop, hosted by the Marshall Space Flight Center on December 3-5, 1996. The workshop was attended by scientists and engineers from various agencies of the U.S. Government, aerospace contractors, and battery manufacturers, as well as international participation in like kind from a number of countries around the world.

The subjects covered included nickel-cadmium, nickel-hydrogen, silver-zinc, nickel-metal hydride, and lithium- based technologies.

Introduction

The NASA Aerospace Battery Workshop is an annual event hosted by the Marshall Space Flight Center. The workshop is sponsored by the NASA Aerospace Flight Battery Systems Program which is managed out of NASA Lewis Research Center and receives support in the form of overall objectives, guidelines, and funding from Code AE / Code S, NASA Headquarters.

The 1996 Workshop was held on three consecutive days and was divided into five sessions. The first day consisted of a General / Primary Battery Session and a Nickel-Hydrogen Battery On-Orbit Reconditioning Experience Focused Session. The second day consisted of a Nickel-Hydrogen Session and a Nickel-Cadmium Session. The third and final day was devoted to an Other Secondary Technologies Session which covered sodium-sulfur, nickel-zinc, nickel-metal hydride, and lithium ion technologies.

On a personal note, I would like to take this opportunity to thank all of the many people that contributed to the organization and production of this workshop:

The NASA Aerospace Flight Battery Systems Program, for their financial support as well as their input during the initial planning stages of the workshop.

Bob Bechtel and **Eric Lowery**, NASA Marshall Space Flight Center; **Gopal Rao**, NASA Goddard Space Flight Center; **Harry Brown**, Naval Surface Warfare Center, Crane Division; and **Doug Hafen**, Lockheed Martin, for serving as Session Organizers, which involved soliciting presentations, organizing the session agenda, and orchestrating the session during the workshop;

Huntsville Hilton, for doing an outstanding job in providing an ideal setting for this workshop and for the hospitality that was shown to all who attended;

Marshall Space Flight Center employees, for their help in stuffing envelopes, registering attendees, handling the audience microphones, and flipping transparancies during the workshop.

Finally, I want to thank all of you that attended and/or prepared and delivered presentations for this workshop. You were the key to the success of this workshop.

Jeff Brewer
NASA Marshall Space Flight Center

Table of Contents

Preface iii

Introduction v

General / Primary Battery Session 1

NASA Aerospace Flight Battery Systems Program Update
Michelle Manzo and Patricia O'Donnell, NASA Lewis Research Center 3

Modeling the Behavior of Zn-AgO Batteries During High Rates of Discharge
Woo-kum Lee and J.W. Van Zee, University of South Carolina 47

Electrolyte Loss Tendencies of Primary Silver-Zinc Cells
Lawrence H. Thaller and Gordon L. Juvinall, The Aerospace Corporation 77

JPL Experience with the Mars Pathfinder, Mission Simulation Battery
Dave Perrone and Richard Ewell, Jet Propulsion Laboratory 93

Investigation of an Aberrant Cell Voltage During the Filling of a Large Lithium Thionyl Chloride Cell
Lawrence H. Thaller and Michael V. Quinzio, The Aerospace Corporation; presented by Margot L. Wasz, The Aerospace Corporation 115

Galileo Probe Battery System
B.P. Dagarin, R.K. Taenaka, and E.J. Stofel, Hughes Space and Communications Company 133

Nickel-Hydrogen Battery On-Orbit Reconditioning Experience Focused Session 145

Nickel-Hydrogen Battery Reconditioning
Erik L. Levine, Space Systems / Loral 147

The In-Orbit Battery Reconditioning Experience on Board the Orion 1 Spacecraft
S.A. Hoover and S. Daughtridge, Orion Satellite Corporation; P.J. Johnson and S.T. King, Matra Marconi Space UK Ltd. 187

The INTELSAT Experience with Reconditioning of NiH_2 Batteries
Frank Scalici, Andrew Dunnet, and Daphne Xu, International Telecommunications Satellite Organization 207

Telstar 401 Reconditioning Experience
Dr. Dean W. Maurer, McKnight Associates Inc. 219

On-Orbit Health Check of Hubble Space Telescope Nickel-Hydrogen Batteries
Gopalakrishna M. Rao and Harry Wajsgras, NASA Goddard Space Flight Center; Stanley J. Krol, Jr., Lockheed Martin Technical Operations Inc.; and Betty Colhoun, Computer Sciences Corp. 231

NiH_2 Battery Reconditioning for LEO Applications
J.D. Armantrout and D.P. Hafen, Lockheed Martin Missiles and Space 263

Nickel-Hydrogen Session 281

Development of Sintered Fiber Nickel Electrodes for Aerospace Batteries
Jennifer Francisco, Dennis Chiappetti, and Jack Brill, Eagle-Picher Industries, Inc. 283

Studies of the Codeposition of Cobalt Hydroxide and Nickel Hydroxide
C.H. Ho, M. Murthy, and J.W. Van Zee, University of South Carolina 289

Nickel-Hydrogen Battery Fault Clearing at Low State of Charge
C. Lurie, TRW Space and Electronics Group 333

EOS-AM1 Nickel Hydrogen Cell Interim Life Test Report
C.W. Bennett, Lockheed Martin Missiles and Space; D.J. Keys and G.M. Rao, NASA Goddard Space Flight Center; H.E. Wannemacher, Jackson and Tull; and H. Vaidyanathan, COMSAT Laboratories 351

SSTI-Lewis Spacecraft Nickel-Hydrogen Battery
R.F. Tobias, TRW Space and Electronics Group 381

New Developments in Nickel-Hydrogen Dependent Pressure Vessel (DPV) Cell and Battery Design
Dwight B. Caldwell, Chris L. Fox, and Lee E. Miller, Eagle-Picher Industries, Inc. 405

SAFT Nickel Hydrogen Cell and Battery Update
Dr. Yannick Borthomieu and Annie Sennet, SAFT Advanced and Industrial Battery Group 413

Nickel-Cadmium Session 437

Battery Performance of ADEOS (Advanced Earth Observing Satellite) and Ground Simulation Test Results
K. Koga, Y. Suzuki, S. Kuwajima, and H. Kusawake, National Space Development Agency of Japan 439

The In-Orbit Performance of Batteries on the SKYNET 4 Spacecraft Fleet: A Nickel-Cadmium Success Story
P.J. Johnson and P.E. Miles, Matra Marconi Space UK Ltd. 451

FAST Spacecraft Battery Design and Performance
David S. Jung, Gopalakrishna Rao, and Anisa Ahmad, NASA Goddard Space Flight Center 469

Results of V/T Verification
Steve Hall, Naval Surface Warfare Center, Crane Division; and Michelle Manzo, NASA Lewis Research Center 493

Design and Performance Data for 81 Ah FNC Cells
F. Cohen, Rocketdyne; and M. Anderman, Acme Aerospace 499

Application of First Principles Ni-Cd and Ni-H_2 Battery Models to Spacecraft Operations
Paul Timmerman, Ratnakumar Bugga, and Salvador DiStefano, Jet Propulsion Laboratory . . 517

Other Secondary Technologies Session 545

Sodium Sulfur Battery Cell Experiment (NaSBE)
J. Christopher Garner, U.S. Naval Research Laboratory 547

Low-Earth-Orbit (LEO) Life Cycle Evaluation of Nickel-Zinc Batteries
D. Coates, E. Ferreira, M. Nyce, and A. Charkey, Energy Research Corporation 565

Burp Charging Nickel Metal Hydride Cells
Eric Darcy, NASA Johnson Space Center; and Richard Pollard, University of Houston; presented by Bob Bragg, NASA Johnson Space Center 577

Low Temperature Synthesis, Chemical and Electrochemical Characterization of $LiNi_xCo_{1-x}O_2$ ($0 < x < 1$) Cathode Materials for Rechargeable Lithium Ion Batteries
K.S. Nanjundaswamy, D. Standlee, and C.O. Kelly, Eagle-Picher Industries Inc.; and R.V. Whiteley, Jr., Pacific University 599

1996 NASA Aerospace Battery Workshop Attendance List 605

General / Primary Battery Session

NASA AEROSPACE FLIGHT BATTERY SYSTEMS PROGRAM UPDATE

MICHELLE MANZO
PATRICIA O'DONNELL
NASA LEWIS RESEARCH CENTER
CLEVELAND, OHIO 44135

1996 NASA AEROSPACE BATTERY WORKSHOP
HUNTSVILLE HILTON
HUNTSVILLE, ALABAMA

DECEMBER 3-5, 1996

BACKGROUND

NASA AEROSPACE FLIGHT BATTERY SYSTEMS PROGRAM - INITIATED IN 1985 TO ADDRESS CONCERNS WITH AEROSPACE BATTERIES

INITIAL CONCERNS - QUALITY, RELIABILITY - PROVIDE BRIDGE BETWEEN DEVELOPMENT AND FLIGHT USE

PROGRAM EVOLVED TO PROVIDE SUPPORT TO NASA ENTERPRISES IDENTIFIED IN RECENT REORGANIZATION

PROGRAM PLAN REVISED TO REFLECT AGENCY'S STRATEGIC PLAN AND SUPPORT FOR NASA ENTERPRISES

The NASA Aerospace Flight Battery Systems Program represents a unified NASA wide effort with the overall objective of providing NASA with the policy and posture which will increase the safety, performance, and reliability of space power systems. The program was initiated in 1985 to address problems experienced with aerospace batteries.

Since the initiation of the program the agency has undergone a reorganization. A strategic plan has been developed to guide the agency over the next 25 years. In the past year, the NASA Aerospace Flight Battery Systems Program has been realigned to be consistent with the NASA strategic plan. The major objectives of the program have been revised to directly support the enterprises that have been identified in the new strategic plan.

BATTERY PROGRAM SUPPORT OF NASA ENTERPRISES

	PRIMARY CUSTOMERS	GOALS	RELEVANCE OF BATTERY PROGRAM
MISSION TO PLANET EARTH ENTERPRISE	Policy Makers Science and Education Communities	Demonstrate new instruments, technologies and procedures - small smart spacecraft and instruments Evolve EOS science and technology and demonstrate new instruments, technologies, and procedures	Evolve new battery technologies that enable MTPE missions Demonstrate battery technologies and advancements
AERONAUTICS ENTERPRISE	Aero Industry US Gov't Agencies	Provide advanced technologies for unpiloted airborne Earth/space observing platforms	Evolve and demonstrate battery technologies to support unpiloted platforms
HUMAN EXPLORATION AND DEVELOPMENT OF SPACE ENTERPRISE	Science and Education Communities Commercial Sectors	Achieve routine space travel Provide safe, reliable, low-cost transportation Operate international Space Station cost effectively	Evolve and validate lightweight battery technologies with improved life & performance, Lower cost batteries
SPACE SCIENCE ENTERPRISE	Science and Education Communities Technology Innovators	Lower cost missions Robotic missions Develop demonstrate and infuse new technology to enable and enhance all missions	Lower cost batteries Lightweight, low volume batteries New technologies to enable missions Cooperative government development, technology transfer to industry

NASA has been reorganized into four major enterprise areas: Mission to Planet Earth, Aeronautics, Human Exploration and Development of Space, and Space Science. Customers and goals have been identified for each enterprise. The chart above also relates the Battery Program to the work in each of the Enterprises. Batteries are critical to the path defined for each of the NASA enterprises.

PROGRAM OBJECTIVES

DEVELOP, MAINTAIN AND PROVIDE TOOLS FOR THE VALIDATION AND ASSESSMENT OF AEROSPACE BATTERY TECHNOLOGIES

ACCELERATE THE READINESS OF TECHNOLOGY ADVANCES AND PROVIDE INFUSION PATHS FOR EMERGING TECHNOLOGIES

PROVIDE NASA PROJECTS WITH THE REQUIRED DATABASE AND VALIDATION GUIDELINES FOR TECHNOLOGY SELECTION OF HARDWARE AND PROCESSES RELATING TO AEROSPACE BATTERIES

DISSEMINATE VALIDATION AND ASSESSMENT TOOLS, QUALITY ASSURANCE, RELIABILITY, AND AVAILABILITY INFORMATION TO THE NASA AND AEROSPACE BATTERY COMMUNITIES

ENSURE THAT SAFE, RELIABLE BATTERIES ARE AVAILABLE FOR NASA's FUTURE MISSIONS

The objectives of the NASA Aerospace Flight Battery Systems Program are listed above.

APPROACH

MAINTAIN CURRENT BATTERY TECHNOLOGY

INCREASE FUNDAMENTAL UNDERSTANDING OF PRIMARY AND SECONDARY CELLS

ESTABLISH SPECIFICATIONS, DESIGN AND OPERATIONAL GUIDELINES FOR PRIMARY AND SECONDARY CELLS AND BATTERIES

PROVIDE IMPROVED PROCESS CONTROL

OPEN AND MAINTAIN COMMUNICATION LINES WITHIN NASA AND THE AEROSPACE COMMUNITY

The approach to achieving the program objectives involves:

1) maintaining current battery technology;
2) increasing the fundamental understanding of primary and secondary cells;
3) establishing specifications and design and operational guidelines for primary and secondary cells and batteries;
4) providing for improved process control;
5) opening and maintaining communication lines within NASA and the aerospace community

PROGRAM TASK RESPONSIBILITIES

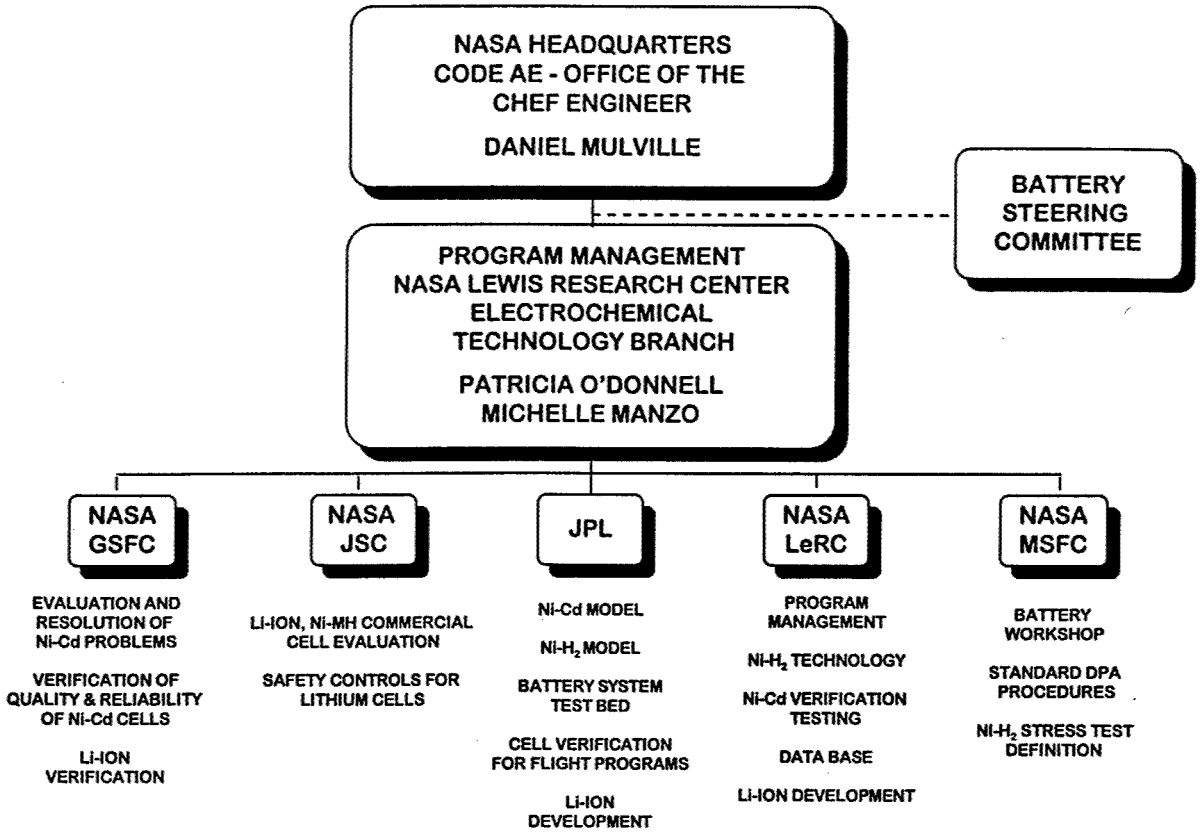

The majority of the NASA centers are involved in the execution of specific tasks within the program. The Lewis Research Center Program Manager has full responsibility for technical management, cost and scheduling of the program. The NASA Lewis Research Center Program Manager also provides continuing coordination with all the NASA centers, Jet Propulsion Laboratory (JPL), NASA Headquarters and the NASA Aerospace Flight Battery Systems Steering Committee.

The NASA Aerospace Flight Battery Systems Steering Committee provides advice on battery issues. The Committee is chaired by the Battery Program manager, membership is comprised of one representative from each of the NASA centers, the Aerospace Corporation, the Air Force, the Navy and the CIA .

PROGRAM ORGANIZATION

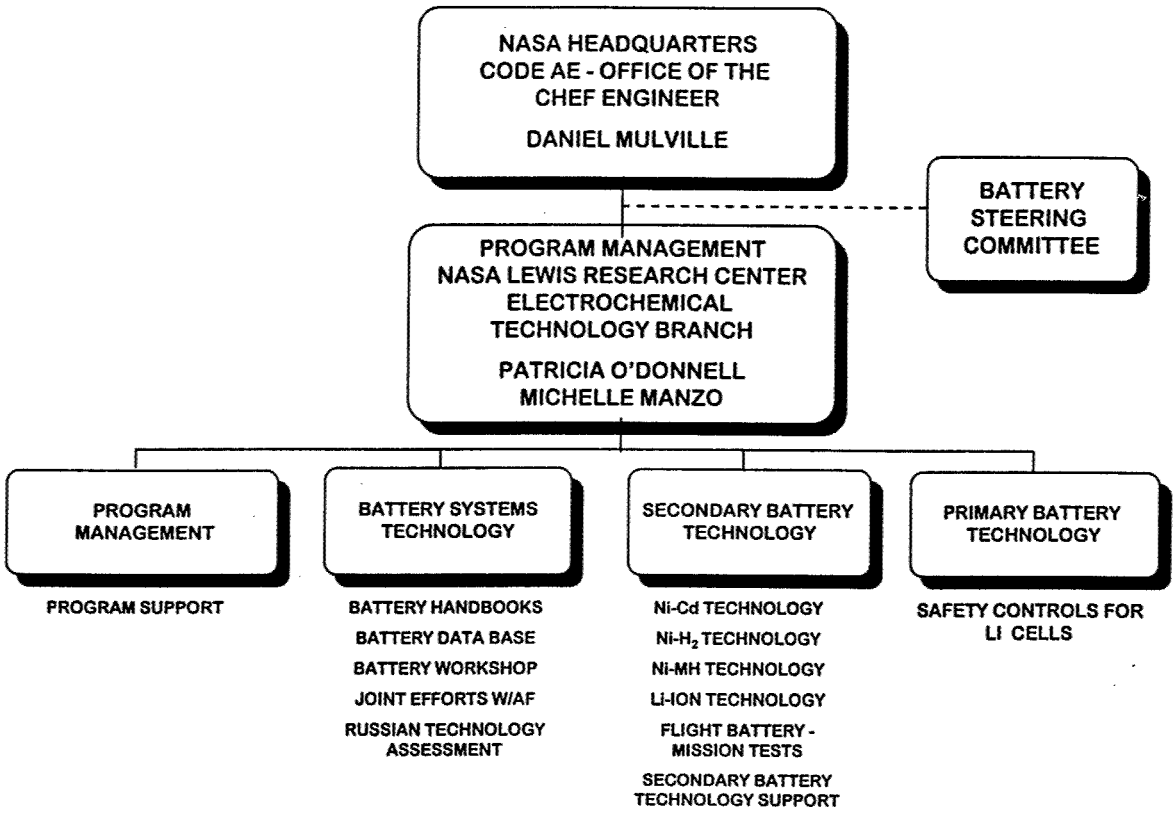

This program is designed to enhance the safety, reliability, and performance of NASA's aerospace primary and secondary batteries as well as battery power systems. The NASA Aerospace Flight Battery Systems Program is organized under four major task areas: Program Management, Battery Systems Technology, Secondary Battery Technology, and Primary Battery Technology. The program is sponsored by the Office of the Chief Engineer, Code AE and the NASA Lewis Research Center (LeRC) , as the lead center, has the overall responsibility for management of the program. Dr. Patricia O'Donnell of the Lewis Research Center is the program manager.

BATTERY SYSTEMS TECHNOLOGY TASK

OBJECTIVES:

TO IMPROVE RELIABILITY OF ENERGY STORAGE SPACE POWER SYSTEM DESIGN, INTEGRATION, AND CHECKOUT

ADDRESS SYSTEMS ASPECTS - INTEGRATION OF CELLS INTO BATTERIES AND BATTERIES INTO POWER SYSTEMS

TASKS:

NASA BATTERY HANDBOOKS

BATTERY DATA BASE

NASA BATTERY WORKSHOP

RUSSIAN BATTERY TECHNOLOGY ASSESSMENT

JOINT EFFORTS WITH THE AIR FORCE

The Battery Systems Technology Task addresses the overall systems aspects associated with the integration of cells into batteries and batteries into power systems. The objective is to improve the reliability of energy storage, space power system design, integration, and checkout.

Sub-tasks under the Battery Systems Technology Task are listed above.

NASA BATTERY HANDBOOKS

OBJECTIVE: DEFINE GOOD CONSISTENT PRACTICES FOR THE DESIGN, INTEGRATION AND CHECKOUT, AND TESTING OF PRIMARY AND SECONDARY BATTERY SYSTEMS. PROVIDE GUIDELINES AND REQUIREMENTS TO ENSURE MISSION SUCCESS

NASA HANDBOOK FOR NICKEL-HYDROGEN BATTERIES *

HANDBOOK FOR HANDLING AND STORAGE OF NICKEL-CADMIUM BATTERIES *

PRIMARY BATTERY DESIGN AND SAFETY GUIDELINES HANDBOOK *

GUIDELINES DOCUMENT FOR NICKEL-CADMIUM CELLS

GUIDELINES DOCUMENT FOR NICKEL-HYDROGEN CELLS

GUIDELINES DOCUMENT FOR SILVER-ZINC CELLS

* COMPLETED - PUBLISHED

A number of handbooks has been published since the program was initiated in 1985. Some of the more recent publications are listed above. Present efforts in this area focus on the development of "Guidelines/Checklist" type documents for nickel-cadmium, nickel-hydrogen and silver-zinc technologies.

NASA BATTERY HANDBOOKS

NICKEL-CADMIUM GUIDELINES DOCUMENT - JPL
NICKEL-HYDROGEN GUIDELINES DOCUMENT - LeRC
SILVER-ZINC GUIDELINES DOCUMENT - MSFC

DOCUMENTS TO SERVE AS GUIDELINE AND CHECKLIST FOR THE PROCUREMENT OF CELLS FOR FLIGHT PROJECTS

AID IN DEVELOPMENT OF SPECIFICATIONS FOR PROCUREMENT

RATIONALE FOR SELECTION OF DESIGN FEATURES FOR SPECIFIC APPLICATIONS

REPRESENTATIVE VALUES AND RANGES FOR TECHNICAL SPECIFICATIONS FOR CRITICAL DESIGN PARAMETERS

CONTRACTS WITH AEROSPACE CORPORATION TO PRODUCE DOCUMENTS

The purpose of the guidelines documents is to provide guidance in the areas of overall design considerations, selection of design features /components for specific applications and to provide background for the proper selection of cells for a specific mission.

BATTERY DATA BASE - LeRC

OBJECTIVE: DEVELOP DATA BASE FOR THE DISSEMINATION OF TECHNICAL NOTES, POLICY DOCUMENTATION AND TEST DATA THROUGHOUT THE AGENCY

DATA BASE IS FUNCTIONAL - OPERATION HAS BEEN DEMONSTRATED

OPERATIONAL CYCLE TEST DATA - POST 1990 DATA FROM CRANE TESTING HAS BEEN ENTERED INTO THE DATA BASE AND IS AVAILABLE ON-LINE

LOCKHEED MARTIN TEST DATA IS BEING INCORPORATED INTO DATA BASE

The Battery Data Base subtask addresses a NASA Battery System Data Base Environment to serve the NASA battery community for the dissemination of technical cell cycle data for the testing at Crane. The majority of the NASA cell test data base resides at the Naval Weapons Support Center, Crane, IN. The Crane data has been organized and structured into a battery test data base. Cycle test data for tests run since 1990 is available on-line.

NASA BATTERY WORKSHOP - MSFC

OBJECTIVE: PROVIDE FORUM FOR OPEN COMMUNICATION OF BATTERY RELATED ACTIVITIES

WORKSHOP ADDRESSES TECHNOLOGY STATUS OF ESTABLISHED AND EMERGING TECHNOLOGIES

SUBJECTS COVERED GENERALLY INCLUDE:

- RESEARCH AND DEVELOPMENT WORK ON STATE-OF-THE-ART AEROSPACE BATTERY TECHNOLOGIES,
- FLIGHT AND GROUND TEST DATA
- ON-ORBIT OPERATION AND PROBLEM RESOLUTION EFFORTS
- FOCUSED TOPIC TO ADDRESS CURRENT ISSUES RELATING TO AEROSPACE BATTERIES

The NASA Battery Workshop comes under the sponsorship of the NASA Aerospace Flight Battery Systems Program. Previously held at NASA Goddard, the Marshall Space Flight Center has hosted yearly Workshops since December 1990. The workshop serves as a forum for open communication of battery related activities between industry and government.

RUSSIAN BATTERY TECHNOLOGY EVALUATION

OBJECTIVE: DEVELOP SEPARATOR SPECIFICATIONS FOR Ag/Zn CELL DESIGNS BASED ON EVALUATION OF RUSSIAN TECHNOLOGY

NAVY PROGRAM WITH NASA INVOLVMENT

INCORPORATE IMPROVED SEPARATORS IN DOMESTIC CELLS

SEPARATOR ASSESSMENT UNDERWAY
- CYCLE TESTING
- STORAGE TESTING - WET STAND
- DPA

This task was initiated to assess claims of the superiority of Russian Ag-Zn cell technology over domestic silver-zinc technology. In side-by-side tests, Russian cells out-performed cells manufactured in the USA. The tests indicated that the separator may be the component responsible for the improved performance. The present effort is a follow-on to the original evaluation that incorporates candidate separator materials into cells for evaluation. This is a primarily a Navy effort with NASA involvement.

COOPERATIVE EFFORTS WITH THE AIR FORCE

OBJECTIVE: LEVERAGE FUNDS BY COMBINING RESOURCES WITH THE AIR FORCE FOR THE DEVELOPMENT OF EFFORTS TO SUPPORT THE VERIFICATION OF SECONDARY CELLS/BATTERIES FOR AEROSPACE APPLICATIONS.

AREAS OF COMMON INTEREST

COMMON PRESSURE VESSEL (CPV) NICKEL-HYDROGEN BATTERIES

SINGLE PRESSURE VESSEL (SPV) NICKEL-HYDROGEN BATTERIES

INDIVIDUAL PRESSURE VESSEL (IPV) NICKEL HYDROGEN CELLS

SUPER NICKEL-CADMIUM CELLS

DEPENDANT PRESSURE VESSEL (DPV) NICKEL-HYDROGEN BATTERIES

NASA and the Air Force share common interests in aerospace batteries. In order to leverage efforts in these times of shrinking budgets, a Memorandum of Understanding between NASA and the Air Force was signed that permits cooperation in the area of "Joint Spacecraft Battery Verification." Areas of common interest have been identified as shown on the chart above.

COOPERATIVE EFFORTS WITH THE AIR FORCE

JOINT TASKS

CPV EVALUATION

45AH, 2-CELL CPV'S

AF TEST PLAN WITH NASA INPUT - 3 PACKS - 2 LEO, 1 GEO

Ni-H_2 STORAGE TEST

5 YEAR STORAGE - CYCLE TO COMPARE WITH UNSTORED

SUPER Ni-Cd STORAGE TEST

COMPARISON OF STORAGE TEMPERATURES - 0°C & 20°C AND CELL LOTS

The joint tasks that have been initiated to date are as follows:

CPV Evaluation - The Air Force has 21, 45 Ah, 2-cell CPV's for technology evaluation that are part of the program. The Air Force and NASA have jointly agreed upon the test conditions for the three packs so that the data will be useful to both agencies.

Ni-H_2 Storage Test - NASA is funding the life cycle tests for Ni-H_2 cells that had been stored for five years as part of an Air Force test on the effects of storage on the cycle life of Ni-H_2 cells. The cells are being cycled at the same conditions used for the sister packs that were cycled without storage.

Super Ni-Cd Storage Test - The effects of storage on super-Ni-Cd cells has long been a concern. This task evaluates the effects of storage temperature and cell lot on the capacity and cycle life of super Ni-Cd cells.

SECONDARY BATTERY TECHNOLOGY TASK

OBJECTIVES:

IMPROVE PERFORMANCE, QUALITY, SAFETY AND RELIABILITY OF SECONDARY BATTERY SYSTEMS.

MAINTAIN AND IMPROVE ESTABLISHED TECHNOLOGIES AND AID IN DEVELOPMENT OF EMERGING TECHNOLOGIES

TASKS:

NICKEL-CADMIUM BATTERY TECHNOLOGY
NICKEL-HYDROGEN BATTERY TECHNOLOGY
NICKEL-METAL HYDRIDE BATTERY TECHNOLOGY
LITHIUM-ION BATTERY TECHNOLOGY
FLIGHT BATTERY MISSION TESTS
SECONDARY BATTERY TECHNOLOGY SUPPORT

The Secondary Battery Technology Task was established to improve the performance, quality, safety, and reliability of secondary battery systems. This task is presently structured to maintain and improve established technologies such as nickel-cadmium and nickel-hydrogen, and to aid in the development and assimilation of emerging technologies such as lithium ion and nickel-metal hydride.

The Secondary Battery Technology Task areas are listed on the chart above.

NICKEL-CADMIUM BATTERY TECHNOLOGY
VERIFICATION OF SECONDARY CELLS

OBJECTIVE: PROVIDE INDEPENDENT VERIFICATION OF MANUFACTURING FLIGHT CELLS BY PROCURING AND TESTING REPRESENTATIVE CELLS FROM VARIOUS MANUFACTURERS

FOREIGN CELL EVALUATION - LeRC

SANYO CELLS	25, 35 AH CELLS
SAFT CELLS	21, 50 AH CELLS

ADVANCED Ni-Cd EVALUATION - LeRC, GSFC

SUPER Ni-Cd CELLS	25, 21 AH CELLS
	10, 50 AH CELLS
MAGNUM Ni-Cd CELLS	25, 21 AH CELLS

ALTERNATE SOURCE CELL EVALUATION - LeRC

ACME CELLS	12 EA 18 & 55AH CELLS
	NYLON & PP SEPARATORS

In order to support flight programs and address NASA's future needs with respect to nickel-cadmium cells, the NASA Aerospace Flight Battery Systems Program has a subtask that involves the evaluation of current technology Ni-Cd cells from the following sources: Hughes, SAFT, Sanyo, and Acme.

NICKEL-CADMIUM CELL VERIFICATION

VERIFICATION TEST PLAN

REPEAT PORTIONS OF MANUFACTURERS INSPECTION ACCEPTANCE TESTS

RUN NASA STANDARD ACCEPTANCE TEST PROCEDURE FOR INFORMATION ONLY

PERFORM LIFE CYCLE TESTING

1 PACK	PERFORM V/T CHARACTERIZATION
1 PACK	ACCELERATED GEO
3 PACKS	LEO REGIME @ VARIOUS TEMPERATURES

Cells have been procured in groups of 20-25 and being evaluated according to the plan outlined above. The testing involves a repeat of a portion of the manufacturer's acceptance tests to verify performance, running the NASA Standard Acceptance Test procedure, for information only, to establish a common standard data base among the cells from the various manufacturers, and finally, cycle life testing under a variety of conditions.

NICKEL-CADMIUM CELL VERIFICATION

LIFE CYCLE TEST REGIMES FOR Ni-Cd CELL EVALUATION

TEST/ PACK	DESCRIPTION	DOD (%)	TEMP (°C)	DETAILS OF REGIME
1	V/T CHARACTERIZATION - SHOCK/VIBRATION			V/T CHARACTERIZATION - PROCEDURE
2	STANDARD STRESS TEST	40	20	CHARGE - 1 HR, 0.8C TO V/T LIMIT, TAPER DISCHARGE - 0.8C FOR 30 MINUTES - TO 40% DOD
3	HIGH TEMPERATURE STRESS TEST	40	30	CHARGE - 0.8C TO V/T LIMIT, TAPER DISCHARGE - 0.8C FOR 30 MINUTES - TO 40% DOD
4	LOW TEMPERATURE STRESS TEST	40	0	CHARGE - 0.8C TO V/T LIMIT, TAPER DISCHARGE - 0.8C FOR 30 MINUTES - TO 40% DOD
5	ACCELERATED GEO	80	10	2 WEEK SUN PERIODS/RECONDITIONING TBD

PLAN REQUIRES MINIMUM OF 25 CELLS - IF ONLY 20 CELLS ARE AVAILABLE - THE SAME PACK WILL BE USED FOR TESTS 1 AND 5.

The chart above summarizes the test conditions for the test packs of nickel-cadmium cells.

NICKEL- CADMIUM LEO TEST SUMMARY

11/21/96

PACK ID	VENDOR	DESCRIPTION	CAP (AH)	# OF CELLS ORIG	CONDITIONS DOD (%)	CONDITIONS TEMP (oC)	STATUS CYCLES	COMMENTS
6000A	HUGHES	ADVANCED Ni-Cd - Z/PS	20	5	40	20	28723	Stopped Testing
6001A	HUGHES	ADVANCED Ni-Cd - Z/PS	20	5	40	20	28308	Stopped Testing
6002A	HUGHES	ADVANCED Ni-Cd - PP/PBI	20	5	40	20	25359	Stopped Testing
6003A	HUGHES	ADVANCED Ni-Cd - Z/PBI	20	8	40	20	25219	Stopped Testing
6004A	HUGHES	ADVANCED Ni-Cd - Z/PS	20	8	25	30	25892	Stopped Testing
6005A	HUGHES	ADVANCED Ni-Cd - Z/PS	20	8	40	30	18909	Stopped Testing
6006A	HUGHES	SUPER Ni-Cd - Z/PBI +ADD	20	8	40	20	21601	Stopped Testing
6024S	SAFT		24	5	40	0	39238	
6120S	SAFT	VOS A	20	5	40	20	20900	Stopped Testing
6124S	SAFT	VOS B	24	5	40	20	26091	Stopped Testing
6140S	SAFT		40	5	40	20	19298	
6601S	SAFT	Ni-Cd	50	5	40	0	9611	
6621S	SAFT	Ni-Cd	50	5	40	20	10077	
6631S	SAFT	Ni-Cd	50	5	40	30	10006	Failed at 30, temp reduced to 10
6601R	SANYO	Ni-Cd - advanced cell	35	5	40	0	12752	
6620R	SANYO	Ni-Cd - advanced cell	35	5	40	20	13107	
6621R	SANYO	Ni-Cd - standard cell	35	5	40	20	12705	
6631R	SANYO	Ni-Cd - advanced cell	35	5	40	30	12972	

NICKEL- CADMIUM LEO TEST SUMMARY - CONTINUED

11/21/96

PACK ID	VENDOR	DESCRIPTION	CAP (AH)	# OF CELLS ORIG	CONDITIONS DOD (%)	CONDITIONS TEMP (oC)	STATUS CYCLES	COMMENTS
0020E	EP-CS	Magnum Ni-Cd	21	5	40	20	3988	
0031E	EP-CS	Magnum Ni-Cd	21	5	40	30	3917	
6601E	EP-CS	Magnum Ni-Cd	21	5	40	0	3666	
0020H	EP-CS	Super Ni-Cd	21	5	40	20	4859	
0031H	EP-CS	Super Ni-Cd	21	5	40	30	3938	
0601H	EP-CS	Super Ni-Cd	21	5	40	0	4488	
0018N	ACME	Nylon	18	5	40	20	5338	
0018P	ACME	Polypropylene	18	5	40	20	5337	
0055N	ACME	Nylon	55	5	40	20	5385	
0055P	ACME	Polypropylene	55	5	40	20	5340	
0121M	EP-CS	Magnum Ni-Cd	21	5	40	20	10667	
6122M	EP-CS	Magnum Ni-Cd	10		40	20	13687	
6522M	EP-CS	Magnum Ni-Cd	50		40	20	12982	
0106M	EP-CS	Magnum Ni-Cd	21	5	VAR	0	8004	
6106M	EP-CS	Magnum Ni-Cd	10	5	VAR	0	11645	
6506M	EP-CS	Magnum Ni-Cd	50		VAR	0	12126	

NICKEL-CADMIUM BATTERY TECHNOLOGY

APPLIED NICKEL-CADMIUM TECHNOLOGY - JPL

OBJECTIVE: DEVELOPMENT OF Ni-Cd PERFORMANCE MODEL FOR PREDICTION OF BATTERY PERFORMANCE UNDER SPECIFIED SPACECRAFT OPERATIONAL CONDITIONS

BASED ON FIRST PRINCIPLES

DESKTOP - MACINTOSH VERSION OF MODEL IS UNDERGOING FIELD TESTING

CAPABILITIES SUMARIZED IN *J.ELECTROCHEM SOC* ***143,*** *803* (1996)

CURRENT PLANS INVOLVE THE FOLLOWING REFINEMENTS
- INCLUDE DEGRADATION CAPABILITIES,
- BETTER DEFINED CHEMICAL EQUATIONS,
- MORE SOPHISTICATED ALGORITHMS
- IMPLEMENTATION ON DESKTOP COMPUTERS

The Jet Propulsion Laboratory is responsible for the Applied Nickel-Cadmium Technology subtask. This subtask involves the development of an electrochemical model of the nickel-cadmium system that involves physical, chemical, and electrochemical studies at the component and cell levels. The model will be used to develop an accelerated test which can be used to determine the quality and reliability of flight lot cells without extensive life testing and to predict the performance of a battery from a set of spacecraft operating conditions. The model is scheduled for completion this fiscal year.

NICKEL-HYDROGEN BATTERY TECHNOLOGY

CELL COMPONENT AND IPV DESIGN EVALUATION - LeRC

OBJECTIVE: PROVIDE INDEPENDENT VERIFICATION OF DESIGN AND COMPONENT VARIATIONS TO MANUFACTURING FLIGHT CELLS BY PROCURING AND TESTING REPRESENTATIVE CELLS FROM VARIOUS MANUFACTURES

VERIFICATION OF 26% KOH

CELLS FROM HUGHES, EAGLE PICHER, GATES, YARDNEY

EVALUATION OF DESIGN FEATURES

CATALYZED WALL WICK
CELL STACKING
ADVANCED DESIGN FEATURES IN ISS DESIGN CELLS
350Ah, 5 ½" HUGHES CELL - EVALUATION

EVALUATION OF CELL COMPONENTS

NICKEL ELECTRODE IMPREGNATION PROCESS
SEPARATOR
PASSIVATION OF ELECTRODE PLAQUE

The major goal of the Nickel-Hydrogen Technology subtask is to evaluate design features for incorporation into nickel-hydrogen cells for NASA missions. The Lewis Research Center has responsibility for the Nickel-Hydrogen Technology subtask. Currently, the effects of the NASA advanced design features and the effects of 26% vs 31% KOH, cell design variations including stacking arrangements and impregnation processes are being evaluated in flight cells being tested at Crane.

NICKEL-HYDROGEN CELL TEST STATUS

PACK ID	VENDOR	DESCRIPTION	CAP (AH)	# OF CELLS ORIG	# OF CELLS LEFT	CONDITIONS DOD (%)	CONDITIONS TEMP (oC)	STATUS CYCLES	DATE	FAILURES
5000L	HUGHES	26% KOH - AF STANDARD	50	3	0	80	10	-	-	15314,19500,23700
5000L	HUGHES	31% KOH - AF STANDARD	50	3	0	80	10	-	-	3729,4165,11355
5001L	EPI	NASA ADV DESIGN w/ CAT WW	125	3	3	60	10	42792	11/18/96	
5001L	EPI	NASA ADV DESIGN w/o CAT WW	125	3	0	60	10	-		9588,13900,20575
5007L	GATES	26% KOH	65	5	5	60	10	25879	11/18/96	
5007L	GATES	31% KOH	65	5	0	60	10	-	-	10824,10975,11455,12244,12471
5004L	EPI	26% KOH - AQUEOUS	65	3	3	60	10	25787	11/18/96	
5004L	EPI	31% KOH - AQUEOUS	65	3	3	60	10	25787	11/18/96	
5004L	EPI	26% KOH - ALCOHOLIC	65	3	3	60	10	25787	11/18/96	
5004L	EPI	31% KOH - ALCOHOLIC	65	3	3	60	10	25787	11/18/96	
3008L	EPI	BTB DESIGN w/CAT WW	65	3	0	60	10	-	-	10931, 12236, 12236
3008L	EPI	RECIRCULATION	65	3	2	60	10	23700	11/18/96	20100
5006L	YTP	26% KOH	56	3	2	60	10	22862	11/18/96	21907
5006L	YTP	31% KOH	56	3	0	60	10	-	-	12503, 12949, 12949
5002L	EPI	PE FILM/PE PAPER	50	3	0	60	10	0	-	LOW CAPACITY - NO LEO
5002L	EPI	PE FILM/PP FELT	50	3	0	60	10	0	-	LOW CAPACITY - NO LEO
5002L	EPI	ASBESTOS	50	3	0	60	10	-	-	2309,2309,2756
5002L	EPI	PE FILM/ZIRCAR	50	3	0	60	10	-	-	All @ ~6700
5008	HUGHES	PASSIVATED		3		60	10	13195	11/18/96	
5008	HUGHES	NON PASSIVATED		3		60	10	13195	11/18/96	
3002L	EPI	CPV	10	10	9	40	10	12776	11/18/96	CELL REMOVED FOR DPA
3003L	JCI	CPV	50	1	1	35	10	9915	11/18/96	

There are many design variations for nickel-hydrogen cells. The systematic testing being performed in this task is intended to differentiate between the design features and components. Cells from various manufactures with varied design features are being tested. The status of the current tests on cells is summarized above.

NICKEL-HYDROGEN BATTERY TECHNOLOGY

LOCKHEED-MARTIN IPV CELL TESTING

SUPPORT FOR LOCKHEED-MARTIN IPV Ni-H_2TESTS

- CELL DESIGN VARIABLES AND TEST HISTORIES MADE AVAILABLE
- CELL DATA TRANSFERRED TO CRANE FOR INCORPORATION INTO THE DATA BASE

The life cycle testing at Lockheed-Martin in Denver is the longest running nickel-hydrogen test program. NASA began supporting this program in 1992. In return for this support, all of the information relating these cells has been made available to NASA. This includes the pack histories, cell design information, DPA results and all cycle test data. The cycle test data is being incorporated into the NASA data base at Crane.

LOCKHEED-MARTIN NI-H2 LIFE TEST - CELL CHARACTERISTICS

ONGOING TESTS HIGHLIGHTED

VENDOR	CAP AH	DIA IN	DOD %	TEMP °C	# OF CELLS	STACK CONFIG	KOH %	SEP	SINTER	IMPREG	COMMENTS
EP-J	50	3.5	40	10	16	RECIRC	31	ZIRCAR	DRY	AQUEOUS	
EP-J	50	3.5	40	20	8	RECIRC	31	ZIRCAR	DRY	AQUEOUS	
EP-J	50	3.5	60	10	8	RECIRC	31	ZIRCAR	DRY	AQUEOUS	
EP-J	50	3.5	60	20	4	RECIRC	31	ZIRCAR	DRY	AQUEOUS	
EP-J	50	3.5	60	10	8	RECIRC	26	ZIRCAR	DRY	AQUEOUS	
GATES	50	3.5	40	10	16	RECIRC	31	ZIRCAR	DRY	AQUEOUS	
GATES	50	3.5	40	20	8	RECIRC	31	ZIRCAR	DRY	AQUEOUS	
GATES	50	3.5	60	10	8	RECIRC	31	ZIRCAR	DRY	AQUEOUS	
GATES	50	3.5	60	20	4	RECIRC	31	ZIRCAR	DRY	AQUEOUS	
YARDNEY	50	3.5	40	10	6	RECIRC	31	ASB/ZIR	SLURRY	AQUEOUS	
YARDNEY	50	3.5	60	10	6	RECIRC	26	ASB/ZIR	SLURRY	AQUEOUS	CONST CHG
YARDNEY	50	3.5	60	10	6	RECIRC	31	ASB/ZIR	SLURRY	AQUEOUS	CONST CHG
YARDNEY	50	3.5	60	10	3	RECIRC	26	ASB/ZIR	SLURRY	AQUEOUS	MOD CHG
YARDNEY	50	3.5	60	10	3	RECIRC	31	ASB/ZIR	SLURRY	AQUEOUS	MOD CHG
EP-J	50	3.5	40	10	4	BTB	31	ZIRCAR	DRY	AQUEOUS	COMSAT
[illegible]	[illegible]	[illegible]	[illegible]	[illegible]	[illegible]	[illegible]	[illegible]	ZIRCAR	[illegible]	AQUEOUS	
[illegible]	[illegible]	[illegible]	[illegible]	[illegible]	[illegible]	RECIRC	[illegible]	ZIRCAR	[illegible]	AQUEOUS	
[illegible]	[illegible]	[illegible]	[illegible]	[illegible]	[illegible]	RECIRC	[illegible]	ZIRCAR	[illegible]	AQUEOUS	
YARDNEY	100	4.5	40	10	4	RECIRC	31	ZIRCAR	SLURRY	AQUEOUS	DUAL STK
[illegible]	[illegible]	[illegible]	[illegible]	[illegible]	[illegible]	RECIRC	[illegible]	ZIRCAR	SLURRY	AQUEOUS	[illegible]

The chart above lists the design features for the cells in the Lockheed-Martin program. Ongoing tests are highlighted.

LOCKHEED-MARTIN NICKEL-HYDROGEN LIFE TEST STATUS

ONGOING TESTS HIGHLIGHTED

MANUFACT-URER	CAP AH	DIA IN	DOD %	TEMP °C	# OF CELLS	CELLS REMAIN	CYCLES	AVG EODV	AVG EOCV	C:D
EP-J	50	3.5	40	10	16	0	42259			
EP-J	50	3.5	40	20	8	0	24309			
EP-J	50	3.5	60	10	8	0	9499			
EP-J	50	3.5	60	20	4	0	5304			
[illegible]	50	[illegible]	[illegible]	[illegible]	[illegible]	[illegible]	35662	[illegible]	[illegible]	[illegible]
GATES	50	[illegible]	[illegible]	[illegible]	[illegible]	[illegible]	30268	[illegible]	[illegible]	[illegible]
GATES	50	3.5	40	20	8	0	36612			
GATES	50	3.5	60	10	8	0	10232			
GATES	50	3.5	60	20	4	0	9013			
YARDNEY	50	3.5	40	10	6	0	22318			
YARDNEY	50	3.5	60	10	6	0	10746			
YARDNEY	50	3.5	60	10	6	0	7717			
YARDNEY	50	3.5	60	10	3	0	11018			
YARDNEY	50	3.5	60	10	3	0	8210			
EP-J-COMSAT	50	3.5	40	10	4	0	14691			
[illegible]	[illegible]	[illegible]	[illegible]	[illegible]	[illegible]	[illegible]	[illegible]	[illegible]	[illegible]	[illegible]
[illegible]	[illegible]	[illegible]	[illegible]	[illegible]	[illegible]	[illegible]	[illegible]	[illegible]	[illegible]	[illegible]
[illegible]	[illegible]	[illegible]	[illegible]	[illegible]	[illegible]	[illegible]	[illegible]	[illegible]	[illegible]	[illegible]
YARDNEY	100	4.5	40	10	4	0	25545			
[illegible]	[illegible]	[illegible]	[illegible]	[illegible]	[illegible]	[illegible]	[illegible]	[illegible]	[illegible]	[illegible]

The chart above summarizes the status of the ongoing tests in the Lockheed-Martin program. Ongoing tests are highlighted.

NICKEL-HYDROGEN BATTERY TECHNOLOGY

CPV BATTERY EVALUATION

OBJECTIVE: EVALUATE POTENTIAL OF EMERGING CPV TECHNOLOGY TO MEET NASA's FUTURE NEEDS. DEVELOP DATA BASE TO INSURE OPTIMUM BATTERY MANAGEMENT AND SUPPORT FOR MISSIONS

EVALUATION OF 2.5" CPV BATTERIES - LeRC

10, 2 CELL, 10AH CPV BATTERIES EAGLE PICHER
LEO LIFE TEST, 40% DOD, 10°C
12,700 CYCLES - ONE CELL REMOVED FOR DPA

CHARACTERIZATION OF 2.5" CPV BATTERIES - JPL

CHARACTERIZATION/MISSION SIMULATION TESTS ON 2.5"CPV TESTS

JOINT TASK WITH AIR FORCE - 3.5" CPV BATTERIES

21, 2-CELL, 45AH CPV BATTERIES - EAGLE PICHER
3 PACKS - 2 LEO 40% DOD -5 °C, 10 °C, 1 GEO

As NASA missions change to smaller, less expensive satellites with volume and weight concerns, there is a need to incorporate new technologies to meet these needs. CPV batteries are being baselined for a number of NASA missions. This task provides a data base that will aid in insuring optimum battery management for systems using this technology.

NICKEL-HYDROGEN BATTERY TECHNOLOGY

SPV BATTERY EVALUATION - LeRC

OBJECTIVE: EVALUATE POTENTIAL OF EMERGING SPV TECHNOLOGY TO MEET NASA'S FUTURE NEEDS

JOHNSON CONTROLS - SPV BATTERY

28 VOLT, 50 AH BATTERY
35% DOD, 10°C ~10,000 CYCLES
JOINT EVALUATION WITH ISS

As NASA missions change to smaller, less expensive satellites with volume and weight concerns, there is a need to incorporate new technologies to meet these needs. SPV batteries are being considered for future NASA missions. This task provides a data base that will aid in insuring optimum battery management for systems using this technology.

NICKEL-HYDROGEN BATTERY TECHNOLOGY

NICKEL-HYDROGEN MODEL - JPL

OBJECTIVE - DEVELOP A COMPUTER MODEL CAPABLE OF PREDICTING ORBITAL PERFORMANCE OF A NICKEL-HYDROGEN BATTERY USING A CELL LEVEL ELECTROCHEMICAL MODEL BASED ON FUNDAMENTAL PHENOMENA

DEVELOPMENT PARALLELS Ni-Cd MODEL

PRELIMINARY VERSION OF THE MODEL THAT OPERATES ON A PC IS AVAILABLE AND UNDER EVALUATION

PLANS INCLUDE
- CONTINUED VALIDATION AND CALIBRATION
- INCORPORATION OF THERMAL MODEL

JPL is responsible for developing a computer model for nickel-hydrogen batteries that parallels the work done on the nickel-cadmium model.

NICKEL-HYDROGEN BATTERY TECHNOLOGY

DEVELOPMENT OF Ni-H_2 STRESS TEST - MSFC

OBJECTIVE: DEFINE AND VERIFY A STRESS TEST FOR NICKEL-HYDROGEN, COMPARABLE TO THE 40% DOD, 20°C TEST FOR NICKEL-CADMIUM CELLS

60% DOD, 10°C - PRELIMINARY PROFILE FOR THE STRESS TEST

MATRIX DEVELOPED FOR IDENTIFICATION OF TEST CONDITIONS

TEMPERATURE	DEPTH OF DISCHARGE		
20°C	35%	50%	65%
10°C	45%	60%	75%

EAGLE PICHER 48 AH CELLS FOR AXAF
AVERAGE CAPACITY AT 10°C -63.5AH AT C/2, WHERE C=48,

The Marshall Space Flight Center is responsible for the task defining the conditions for a nickel-hydrogen stress test similar to the 40%DOD, 20 °C test currently used for Ni-Cd cells. An analysis of the nickel-hydrogen data base resulted in a preliminary recommendation of 60% DOD, 10°C as the comparable Ni-H_2 test conditions. A matrix has been developed to identify the appropriate test conditions. Eagle Picher 48 Ah cells, similar to those ordered for AXAF are being used in this evaluation.

NICKEL-HYDROGEN BATTERY TECHNOLOGY

DEVELOPMENT OF Ni-H_2 STRESS TEST - MSFC

STRESS TEST STATUS

EARLY FAILURES

65% DOD - 20°C 961-1177 CYCLES
75% DOD - 10°C 1085-1188 CYCLES
60% DOD - 10°C 2037-2400 CYCLES
50% DOD - 20°C 2375-3200 CYCLES

CONTINUING TESTS

35% DOD - 20°C
45% DOD - 10°C

CAUSE OF FAILURES IS UNDER INVESTIGATION

Testing of the cells per the matrix discussed on the previous chart has begun. To date four, of the packs have experienced early failures after less than 3200 cycles. The cause of the failures is under investigation.

NICKEL-METAL HYDRIDE TECHNOLOGY

NICKEL-METAL HYDRIDE TECHNOLOGY EVALUATION

OBJECTIVE EVALUATE POTENTIAL OF Ni-MH TECHNOLOGY TO MEET NASA's FUTURE NEEDS

EVALUATION OF AEROSPACE DESIGN CELLS - LeRC

EAGLE PICHER - 6-10Ah CELLS - 40%DOD, 10°C
- 3 FAILURES - 10000, 14047, 16129 CYCLES
- ONGOING TESTS - 17556 CYCLES

SANYO - 25 - 35Ah CELLS -
- CHARACTERIZATION TESTS COMPLETED
- TO BE RUN IN Ni-Cd VERIFICATION PROFILE

Nickel-metal hydride batteries have the potential to replace nickel-cadmium and in some cases nickel-hydrogen batteries. This task is evaluating this potential. Aerospace design cells from Eagle Picher are on LEO life test at 40% DOD, 10°C. Aerospace design cells from Sanyo are being evaluated in tests that parallel the nickel-cadmium verification tests previously discussed.

NICKEL-METAL HYDRIDE TECHNOLOGY

CHARACTERIZATION OF CELLS FROM OVONICS - GSFC

6.7 Ah CELLS

CALORIMETRIC ANALYSIS, CAPACITY, CHARGE RETENTION

6 CELLS - ACCELERATED GEO CYCLES - 240 CYCLES

LEO CYCLES - 20°C, 40% DOD - 830 CYCLES TO FAILURE

GSFC is responsible for basic calorimetric measurements on nickel-metal hydride cells. Cells from Ovonic Battery Company are being evaluated in LEO and GEO cycle regimes.

NICKEL-METAL HYDRIDE TECHNOLOGY

NI-MH COMMERCIAL CELL EVALUATION - JSC

EVALUATE Ni-MH POTENTIAL FOR EVA's, IVA's FOR SPACE STATION

DETERMINE BEST AVAILABLE COMMERCIAL Ni-MH

EVALUATE CHARGE METHODOLOGY
- BURP CHARGING DEMONSTRATED ADVANTAGES -
  - CHARGE EFFICIENCY, MINIMIZE CHARGE DURATION, INCREASED CAPACITY & CYCLE LIFE
- 900 - 100% DOD CYCLES WITH SANYO 4/3 A CELLS

Ni-MH DEMONSTRATED GOOD ABUSE TOLERANCE

DEVELOP AND CERTIFY NI-MH BATTERY FOR EMU BACKPACK, ADVANCED HELMET LIGHTS, CUFF CHECK LIST

JSC is evaluating nickel-metal hydride batteries, chargers and charge methods for use in IVA's and EVA's. Replacement of primary batteries with secondary batteries for in-cabin applications on the space shuttle and for the space station has the potential of significant cost savings.

LITHIUM -ION BATTERY TECHNOLOGY

OBJECTIVE EVALUATE POTENTIAL OF Li-ION TECHNOLOGY TO MEET NASA's FUTURE NEEDS. ENABLE TECHNOLOGY DEVELOPMENT FOR AEROSPACE APPLICATIONS

Li-ION TECHNOLOGY ASSESSMENT - JPL

TECHNOLOGY REVIEW - STATUS ASSESSED FOR AEROSPACE APPLICATIONS

EVALUATE COMERCIAL PRODUCTS FROM SONY, SAFT, SANYO, & YARDNEY

DOCUMENTATION OF MANUFACTURING PROCESSES

DEVELOPMENT OF GUIDELINES DOCUMENTS

NASA is evaluating the potential of Lithium Ion technology to meet our future needs. Li-Ion is an enabling technology for many NASA missions. This technology offers the potential for reduced weight and volume.

The preliminary assessment consists of a review of the status of the technology available from the various manufacturers and characterization and life-cycle testing of today's technology.

LITHIUM -ION BATTERY TECHNOLOGY

LITHIUM ION CELL CHARACTERIZATION - GSFC

CHARACTERIZATION, CYCLE TESTING, DPA OF CELLS FROM CURRENT MANUFACTURERS

SAFT - 3.5" CELLS EVALUATED FOR TEMPERATURE EFFECTS ON CAPACITY, VOLTAGE AND SELF DISCHARGE

Li-ION DESIGN DEVELOPMENT - LeRC

IMPROVE ANODE - MODIFY CARBON SUBSTRATES TO FACILITATE Li ION INSERTION AND INCREASE Li CAPACITY

LITHIUM -ION BATTERY TECHNOLOGY

LI-ION COMMERCIALCELL EVALUATION - JSC

INCORPORATION OF NEW TECHNOLOGY BATTERIES INTO GFE EQUIPMENT - LAPTOP COMPUTERS, CAMCORDERS - REQUIRES UNDERSTANDING OF SAFETY ISSUES RELATING TO SPACE USE AND QUALIFICATION OF NEW TECHNOLOGY

OBTAIN COMMERCIAL CELLS - PERFORM EVALUATION
- CHARACTERIZATION,
- CHARGE CONTROL PARAMETERS,
- PERFORMANCE
- THERMAL CHARACTERIZATION
- ABUSE TOLERANCE

FLIGHT BATTERY MISSION TESTS

TOPEX - JPL
MISSION SIMULATION TESTS

MARS GLOBAL SURVEYOR - JPL
20 AH 2-CELL CPV's
STRESS TEST, MISSION SIMULATION, PERFORMANCE VERIFICATION

CLARK SATELLITE SPV DESIGN EVALUATION - LeRC
15AH, 28 VOLT , FLIGHT SPARE, I&T BATTERIES

BATTERY TEST BED - JPL
MISSION SUPPORT - GRO, UARS, EUVE, TOPEX.
MANAGE DIVERGENT CELLS/BATTERIES - FACILITY SIMULATE MPS POWER SYSTEM

NASA projects are beginning to baseline non-traditional battery systems for future missions. In order to increase the data base on these systems and to provide timely support, these technologies are being investigated as part of the battery program. In many cases these efforts are entered into jointly with the programs or other NASA codes. The test data and experience provide benefits throughout the agency.

SECONDARY BATTERY TECHNOLOGY SUPPORT

DEVELOPMENT OF DPA TEST PROCEDURES - MSFC

OBJECTIVE: DEFINE GENERAL GUIDELINES TO BE FOLLOWED BY FACILITIES PERFORMING DPA PROCEDURES ON NICKEL-CADMIUM AND NICKEL-HYDROGEN CELLS

AVAILABLE PROCEDURES HAVE BEEN EVALUATED

DRAFT GUIDELINES DOCUMENTS HAVE BEEN PREPARED

AEROSPACE WILL WRITE MANUAL

The Marshall Space Flight Center has the responsibility for developing and establishing guidelines for NASA for the performance of destructive physical analyses for Ni-Cd and Ni-H_2 chemistries. Current DPA procedures used in the industry are being evaluated in an effort to identify a standard procedure for the agency. Drafts of the guidelines documents have been prepared.

SECONDARY BATTERY TECHNOLOGY SUPPORT

DEVELOPMENT OF SEPARATOR TEST PROCEDURES - LeRC

OBJECTIVE: DESIGN AND DEVELOPMENT OF UNIFORM RELIABLE TEST PROCEDURES FOR EVALUATING CANDIDATE SEPARATOR MATERIALS FOR Ni-Cd, Ni-H_2 & Ni-MH CELLS

DETAILED PROCEDURES FOR STANDARD TESTS TO EVALUATE SEPARATORS HAVE BEEN DEVELOPED

PUBLICATION BY END OF FISCAL YEAR

The Lewis Research Center has produced a manual that recommends standard separator test procedures. The manual defines improved tests that will more closely evaluate separator characteristics as related to the actual cell environment. Publication of a document containing the recommended test procedures is expected before the end of the fiscal year.

PRIMARY BATTERY TECHNOLOGY TASK

OBJECTIVE:

IMPROVE PERFORMANCE, QUALITY, SAFETY AND RELIABILITY OF PRIMARY BATTERY SYSTEMS

TASK

SAFETY CONTROLS FOR LITHIUM CELLS

The objective of the Primary Battery Technology Task is to improve the performance, reliability and safety of primary battery systems. The Johnson Space Center has primary responsibility for work performed in the primary battery area.

The major task in the primary battery technology area is the development of safety controls for primary Li-BCX Cells.

SAFETY CONTROLS FOR LITHIUM CELLS

OBJECTIVE INCREASE SHORT CIRCUIT HAZARD TOLERANCE BY REDUCING MOLARITY OF ELECTROLYTE AND THUS REDUCE CAPABILITY TO SUSTAIN HIGH SHORT CIRCUIT CURRENT FOR EXTENDED TIME

Li-BCX CELLS FROM WGL - C, D, DD

DETERMINE MINIMUM CONCENTRATION TO MAINTAIN CAPACITY REQUIREMENTS WHILE REDUCING SHORT CIRCUIT CURRENT TO PREVENT VENTING OR RUPTURE

PERFORMANCE, ABUSE, SHELF LIFE DETERMINATIONS AND QUALIFICATION OF CELLS WITH REDUCED ELECTROLYTE LEVELS

LEVELS ESTABLISHED FOR C AND D CELLS, DD EFFORT IS UNDERWAY

Successful implementation of safety controls for Li-BCX cells will result in the elimination of the need to fly the cells with a waiver . The approach used in this task is to reduce the electrolyte concentration to a level that will no longer support a short circuit current and thus prevent cell venting and ruptures.

SUMMARY REMARKS

BATTERY PROGRAM HAS BEEN REALIGNED TO BE CONSISTENT WITH NASA's STRATEGIC PLAN

EMPHASIS HAS SHIFTED FROM RELIABILITY, QUALITY ASSURANCE ROLE TO BROAD SUPPORT FOR NASA ENTERPRISES

BATTERY PROGRAM HAS RESULTED IN INCREASED COMMUNICATION AND COOPERATION AMONG NASA CENTERS AND WITHIN THE AEROSPACE BATTERY COMMUNITY

THE PROGRAM ADDRESSES FLIGHT BATTERY ISSUES RELATING TO NASA's FLIGHT PROGRAMS

The NASA Aerospace Flight Battery Systems Program has been realigned to be consistent with NASA's strategic plan. Emphasis in the program has been shifted to provide broad support for each of the NASA enterprises.

The program has provided for increased communication within the agency and with the battery industry as well. The program addresses flight battery and related flight power system activities which are essential for ensuring safe and reliable performance.

Modeling the Behavior of Zn-AgO Batteries During High Rates of Discharge

Woo-kum Lee and J.W. Van Zee

Center for Electrochemical Engineering
Department of Chemical Engineering
University of South Carolina

Center of Electrochemical Engineering
Department of Chemical Engineering
University of South Carolina
Columbia, SC 29208

Outline

- Objectives
- Electrode Reactions
- Prototype Battery
- Model Development
- Model Predictions
  - Concentration Distributions
  - Heat Generation Rates

J.W. Van Zee, Dec. 3, 1996
NASA Aerospace Battery Workshop

Center of Electrochemical Engineering
Department of Chemical Engineering
University of South Carolina
Columbia, SC 29208

Long-Term Model-Objectives

- Determine Local Heat Generation Rates
  - function of x,y,z in a cell
  - function of plate position
  - function of time & discharge rate
  - function of cycle
  - function of charge rate
- For Heat Removal:
  - Consider Alternate Grid Designs
  - External Cooling

Center of Electrochemical Engineering
Department of Chemical Engineering
University of South Carolina
Columbia, SC 29208

Electrode Reactions

- Positive Electrode

$$Ag_2O + H_2O + 2e- \xrightarrow{\text{discharge}} 2Ag + OH^- \quad U^{\Theta} = 0.342\ V$$

$$2AgO + H_2O + 2e- \xrightarrow{\text{discharge}} Ag_2O + OH^- \quad U^{\Theta} = 0.642\ V$$

- Negative Electrode

$$Zn(OH)_4^{-2} \longleftrightarrow ZnO + 2(OH)^- \quad K_{eq} = 0.003$$

$$ZnO + H_2O + 2e- \xleftarrow{\text{discharge}} Zn + 2\ OH^- \quad U^{\Theta} = -1.35\ V$$

J.W. Van Zee, Dec. 3, 1996
NASA Aerospace Battery Workshop

Center of Electrochemical Engineering
Department of Chemical Engineering
University of South Carolina
Columbia, SC 29208

Prototype Battery

- 135 A-h Capacity
- 12-25 knots
- 50 -250 Amps 10 -100 mA/cm^2
- 250 V
- 168 cells ÷ 24 cells/case = 7 cases
- 15 in^2
- Nylon, Cellophane, FRSC = 0.130 in.
- AgO, Zn thick. = 0.039, 0.060 in.

Center of Electrochemical Engineering
Department of Chemical Engineering
University of South Carolina
Columbia, SC 29208

Schematic of a 135 A-hr Zn/AgO Battery

(Only 15 of the 24 positive (Ag) and 25 negative (Zn) plates are shown
separators not shown

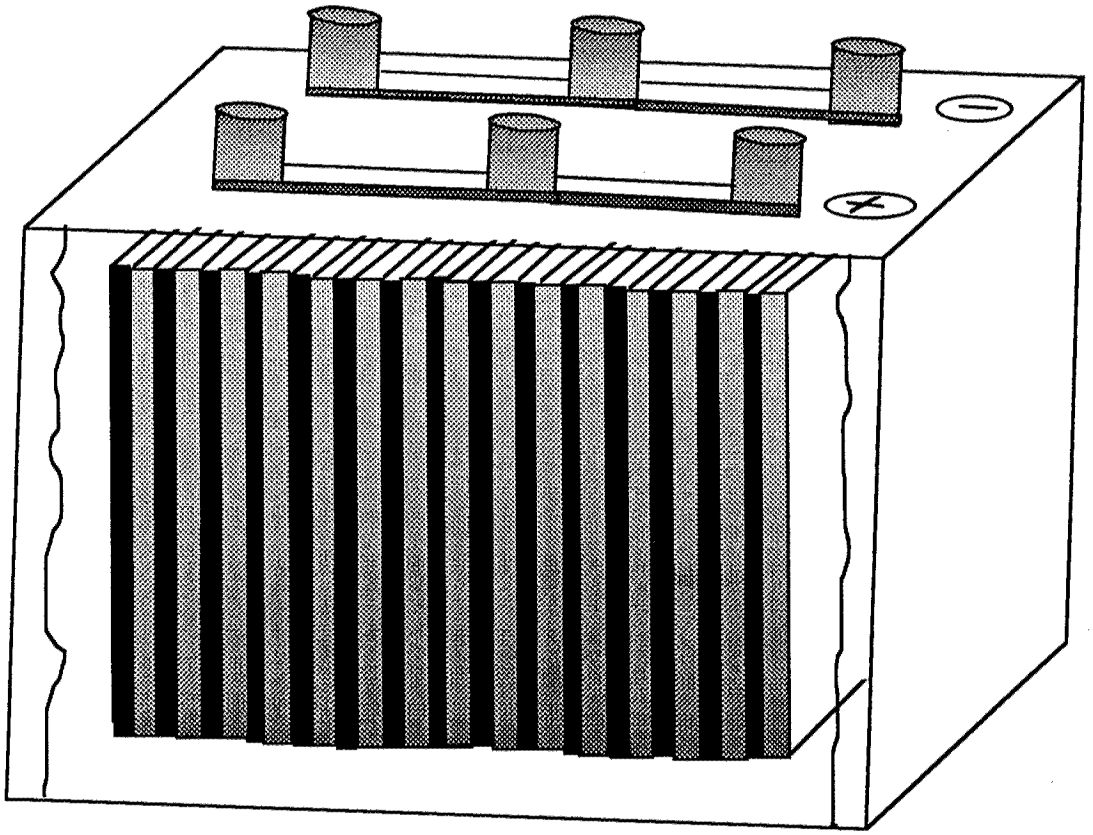

Alternate Electrode Designs

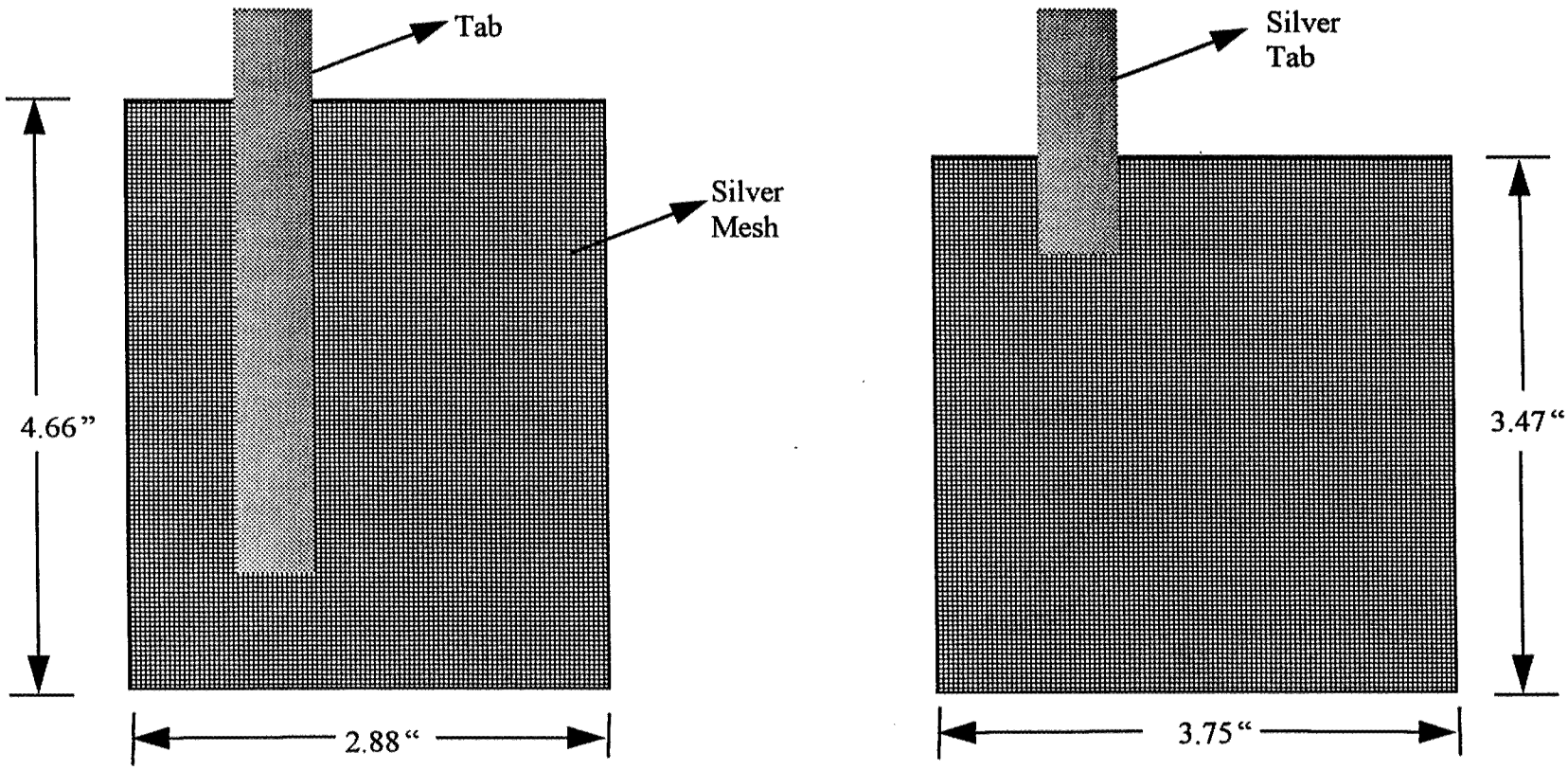

Present Assumptions

- - One-Dimensional Transport.
- - No Convection in the Porous Electrode.
- - Dilute Solution Theory.
- - Constant Porosity.
- - Large Matrix Conductivity

Center of Electrochemical Engineering
Department of Chemical Engineering
University of South Carolina
Columbia, SC 29208

One-dimensional flux expression

$$\frac{N_i}{\varepsilon} = -\frac{D_i}{\tau}\frac{\partial C_i}{\partial x} - \frac{F z_i D_i C_i}{\tau R T}\frac{\partial \phi_2}{\partial x}$$

J.W. Van Zee, Dec. 3, 1996
NASA Aerospace Battery Workshop

Center of Electrochemical Engineering
Department of Chemical Engineering
University of South Carolina
Columbia, SC 29208

Governing Equations- in Zn electrode

$$\varepsilon_{Zn} \frac{\partial C_{K^+}}{\partial t} = -\nabla \cdot N_{K^+}$$

$$\varepsilon_{Zn} \frac{\partial C_{OH^-}}{\partial t} = -\frac{as_{OH^-} i_n}{nF} - \nabla \cdot N_{OH^-} + 2R$$

$$\varepsilon_{Zn} \frac{\partial C_{Zn(OH)_4^{-2}}}{\partial t} = -\frac{as_{Zn(OH)_4^{-2}} \cdot i_n}{nF} - \nabla \cdot N_{Zn(OH)_4^{-2}} - R$$

Center of Electrochemical Engineering
Department of Chemical Engineering
University of South Carolina
Columbia, SC 29208

Governing Equations- in Zn electrode (cont.)

$$\frac{\partial M_{ZnO}}{\partial t} = -\frac{A_s i_n s_{ZnO}}{nF}$$

$$\sum z_i C_i = 0$$

$$\frac{\partial i_2}{\partial x} = a i_n$$

Center of Electrochemical Engineering
Department of Chemical Engineering
University of South Carolina
Columbia, SC 29208

Butler-Volmer Equation

$$i_n = i_o \left\{ y \left(\frac{C_{OH^-}}{C_{OH^-,ref}} \right)^2 \exp\left(\frac{F\alpha_a}{RT}\eta_a\right) - \left(1 - y\right) \exp\left(-\frac{F\alpha_c}{RT}\eta_c\right) \right\}$$

where $y = M_{Zn}/M^o_{ZnO}$ and $1-y = M_{ZnO}/M^o_{ZnO}$

Center of Electrochemical Engineering
Department of Chemical Engineering
University of South Carolina
Columbia, SC 29208

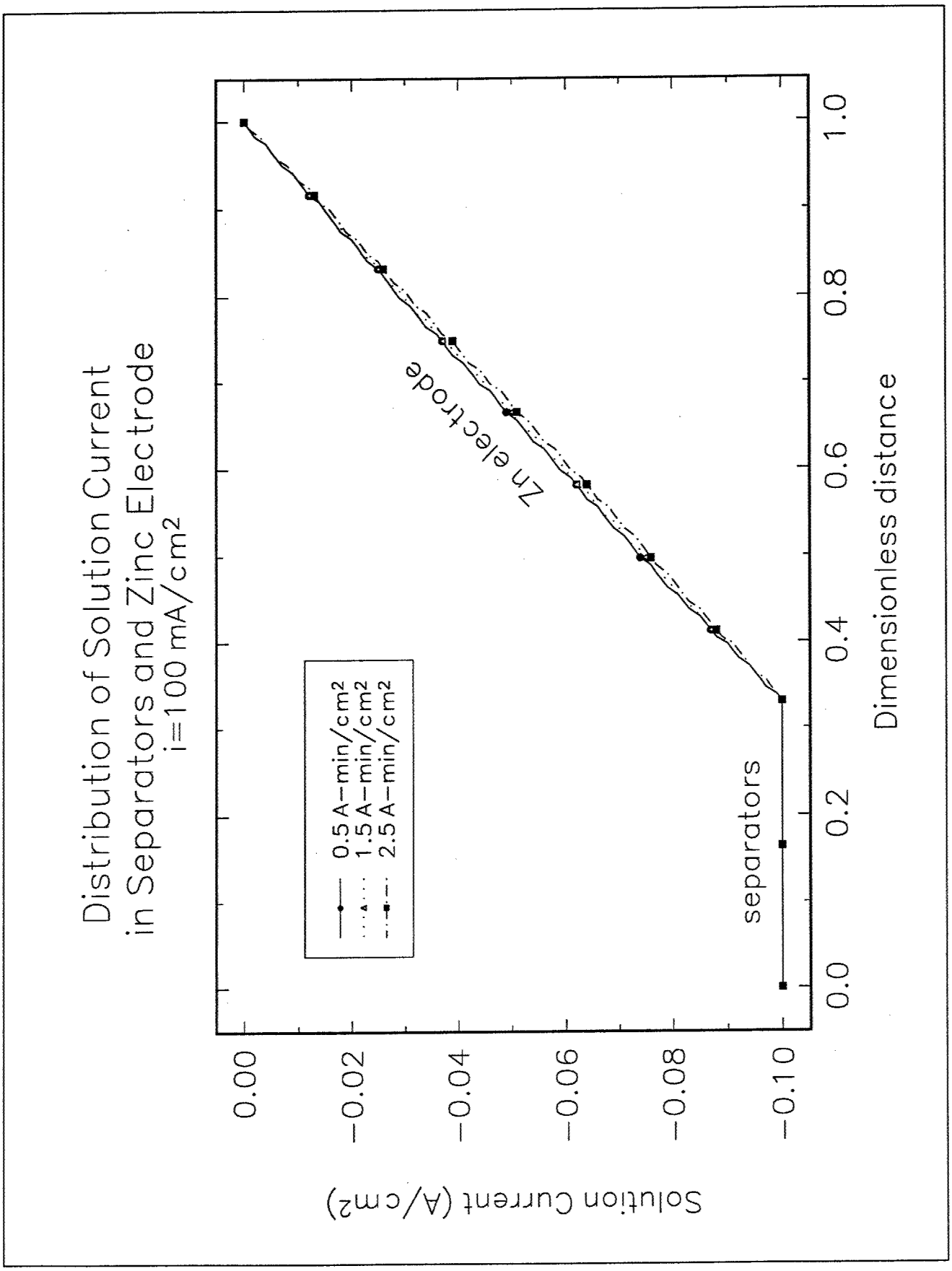
Distribution of Solution Current
in Separators and Zinc Electrode
i=100 mA/cm2
0.5A-min/cm2
1.5A-min/cm2
2.5A-min/cm2
Zn electrode
separators
Solution Current (A/cm2)
0.00
-0.02
-0.04
-0.06
-0.08
-0.10
0.0
0.2
0.4
0.6
0.8
1.0
Dimensionless distance

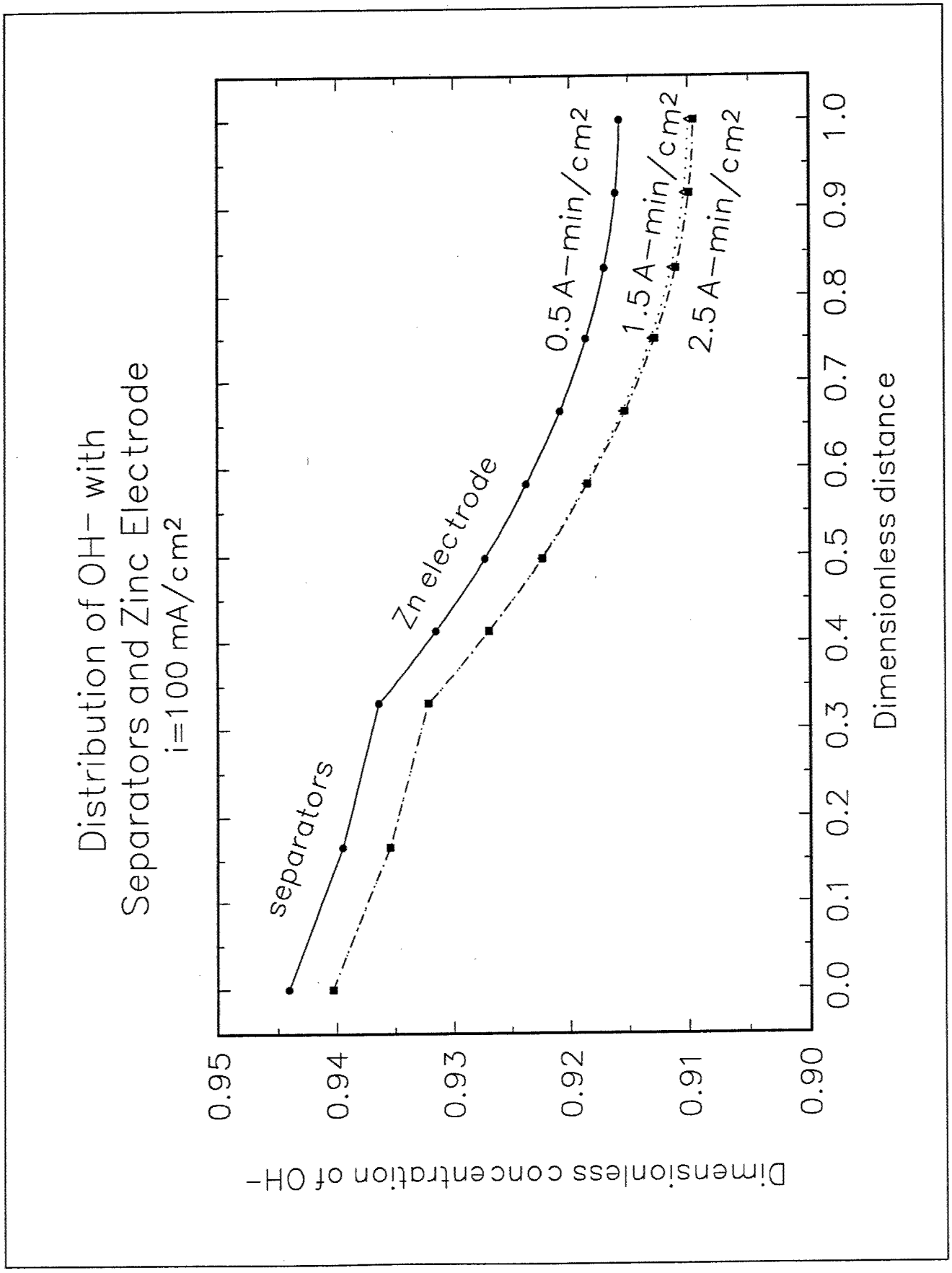
Distribution of OH- with
Separators and Zinc Electrode
i=100 mA/cm2
separators
Zn electrode
0.5A-min/cm2
1.5A-min/cm2
2.5A-min/cm2
0.95
0.94
0.93
0.92
0.91
0.90
Dimensionless concentration of OH-
0.0
0.1
0.2
0.3
0.4
0.5
0.6
0.7
0.8
0.9
1.0
Dimensionless distance

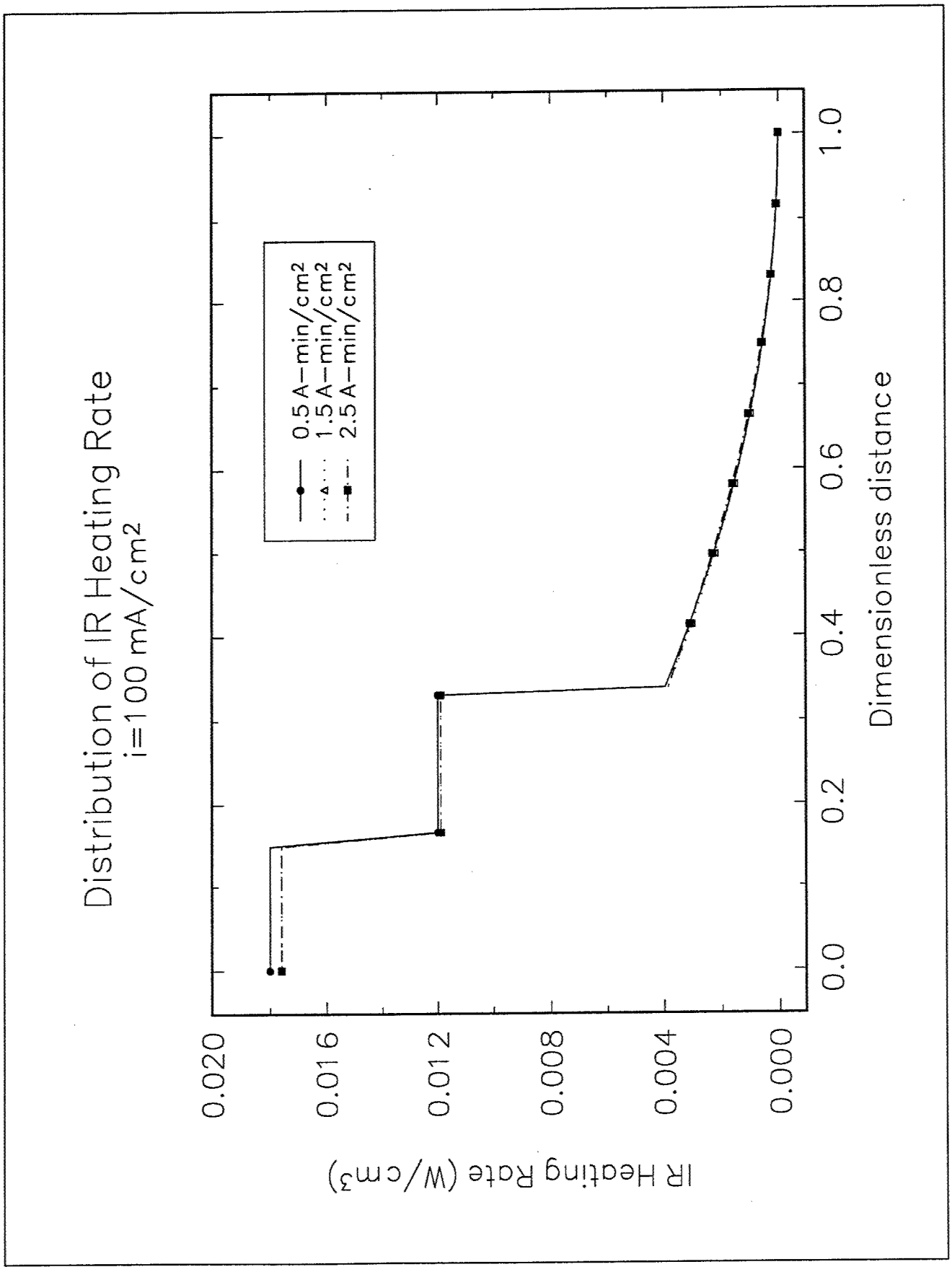
Distribution of IR Heating Rate
i=100 mA/cm2
0.5A–min/cm2
1.5A–min/cm2
2.5A–min/cm2
IR Heating Rate (W/cm3)
0.020
0.016
0.012
0.008
0.004
0.000
0.0
0.2
0.4
0.6
0.8
1.0
Dimensionless distance

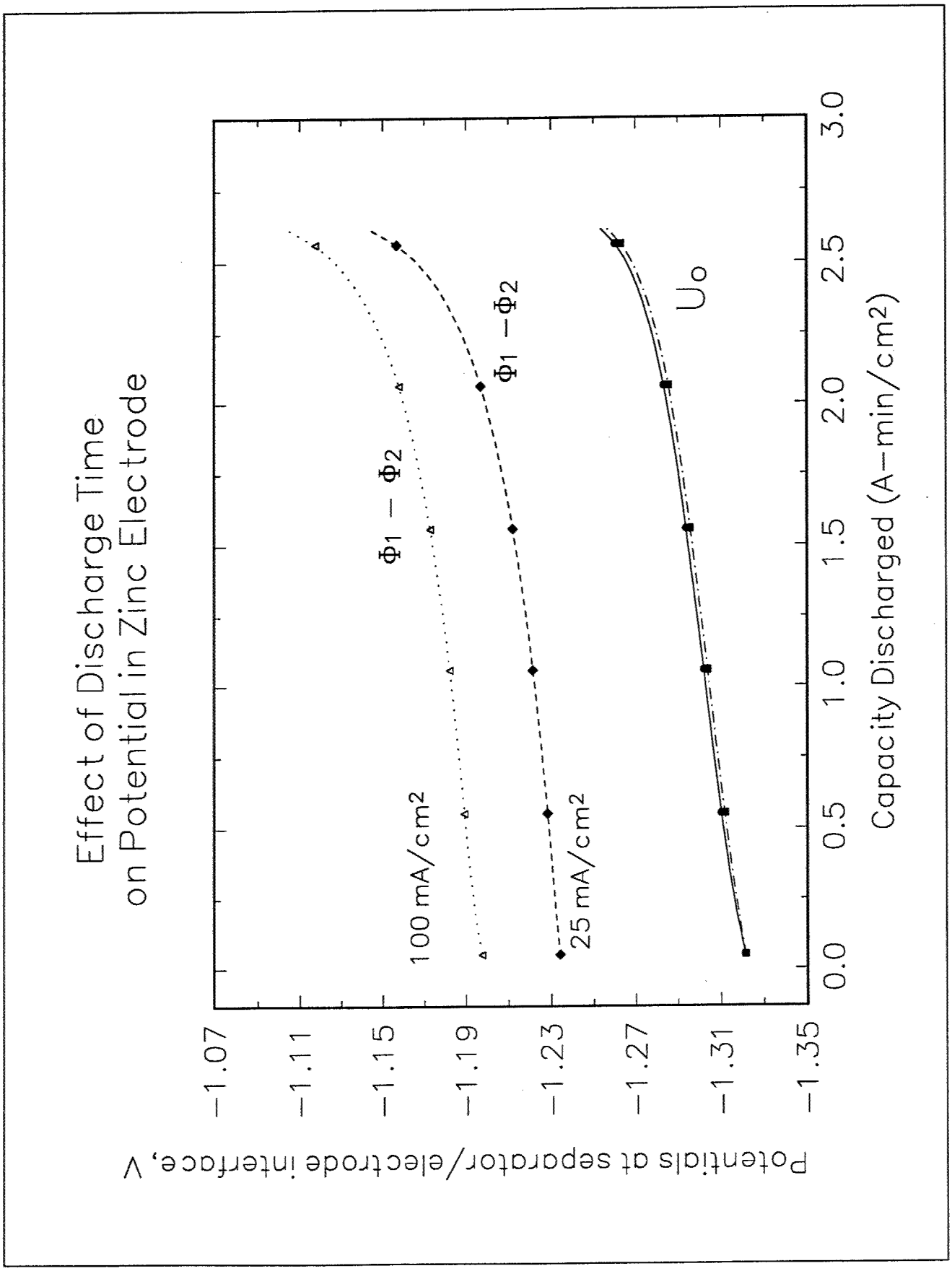
Effect of Discharge Time
on Potential in Zinc Electrode
Potentials at separator/electrode interface, V
−1.07
−1.11
−1.15
−1.19
−1.23
−1.27
−1.31
−1.35
0.0
0.5
1.0
1.5
2.0
2.5
3.0
Capacity Discharged (A−min/cm2)
100 mA/cm2
Φ1 − Φ2
25 mA/cm2
Φ1 −Φ2
Uo

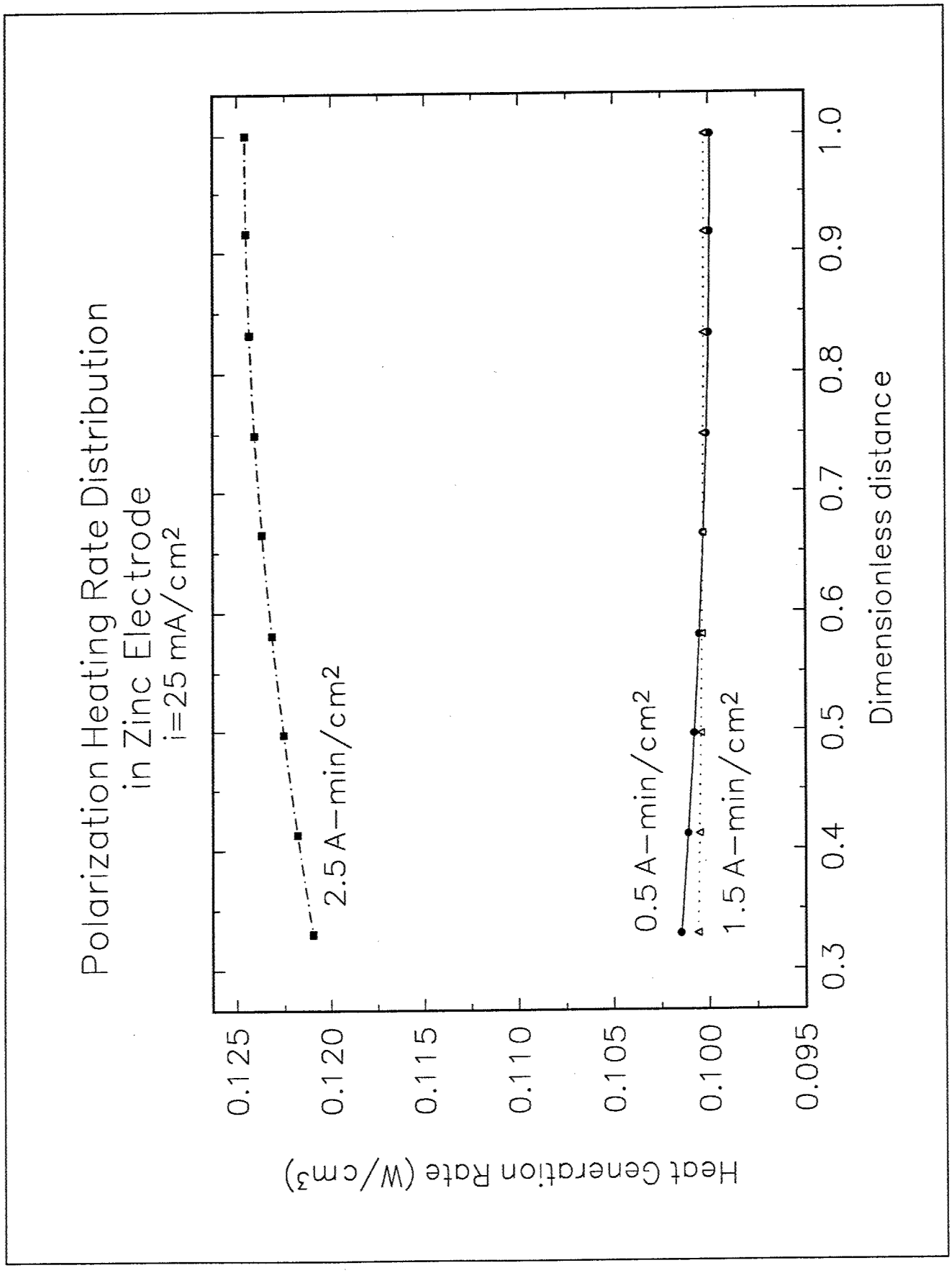
Polarization Heating Rate Distribution
in Zinc Electrode
i=25 mA/cm2
2.5 A-min/cm2
0.5 A-min/cm2
1.5 A-min/cm2
Heat Generation Rate (W/cm3)
0.125
0.120
0.115
0.110
0.105
0.100
0.095
0.3
0.4
0.5
0.6
0.7
0.8
0.9
1.0
Dimensionless distance

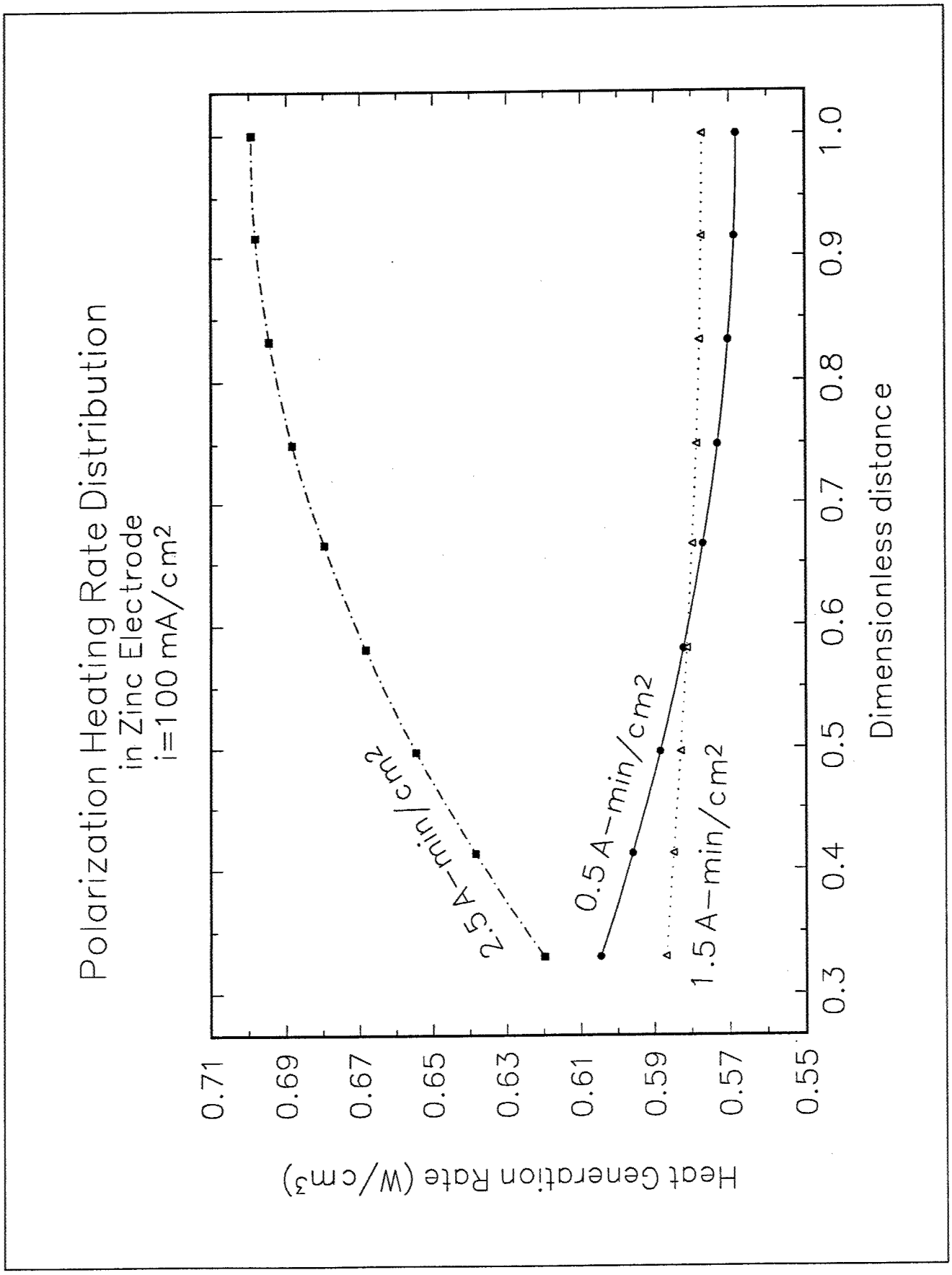
Polarization Heating Rate Distribution
in Zinc Electrode
i=100 mA/cm2
Heat Generation Rate (W/cm3)
0.71
0.69
0.67
0.65
0.63
0.61
0.59
0.57
0.55
0.3
0.4
0.5
0.6
0.7
0.8
0.9
1.0
Dimensionless distance
2.5 A-min/cm2
0.5 A-min/cm2
1.5 A-min/cm2

Distribution of OH^- Concentration

Silver electrode (i=25 mA/cm^2)

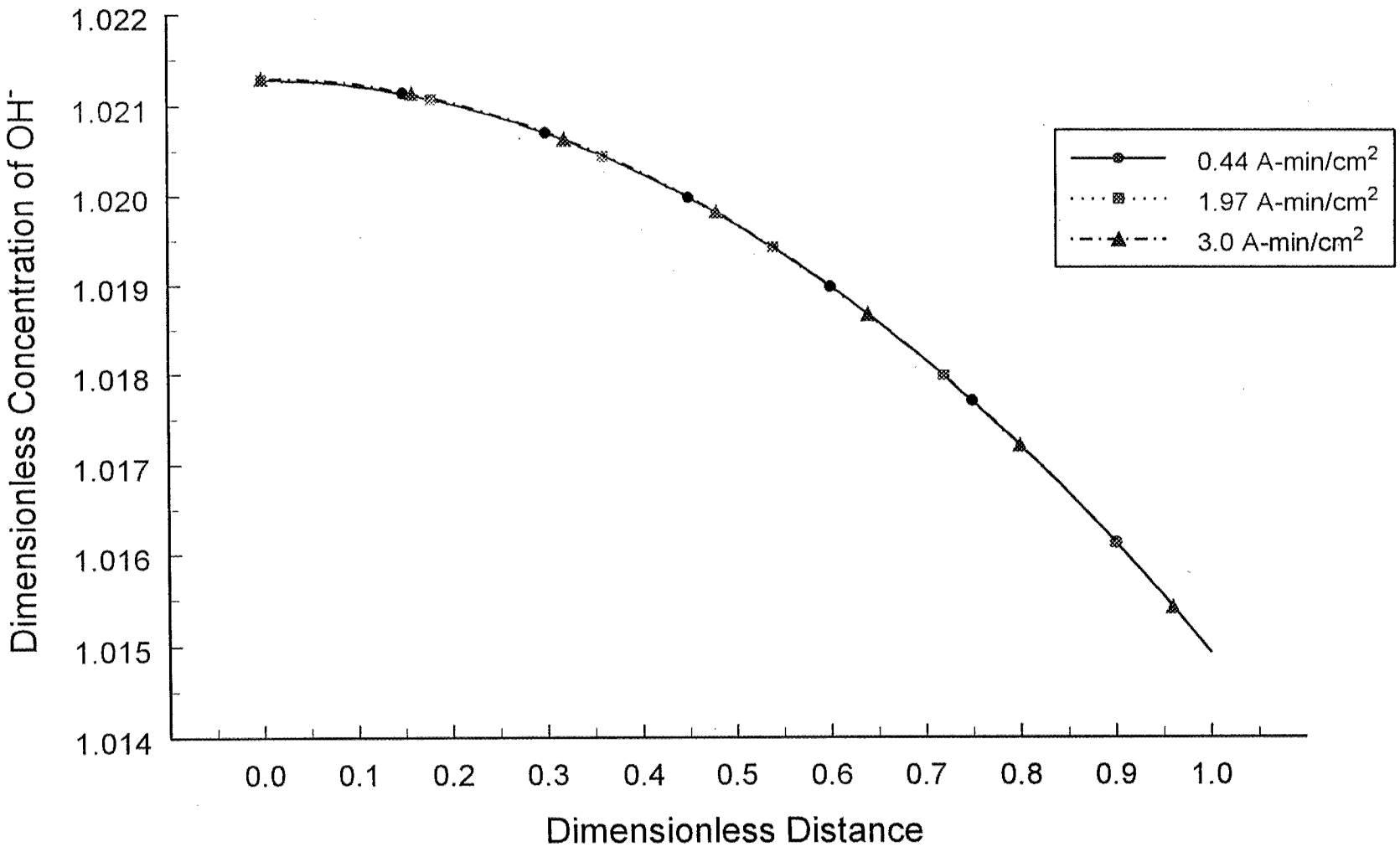

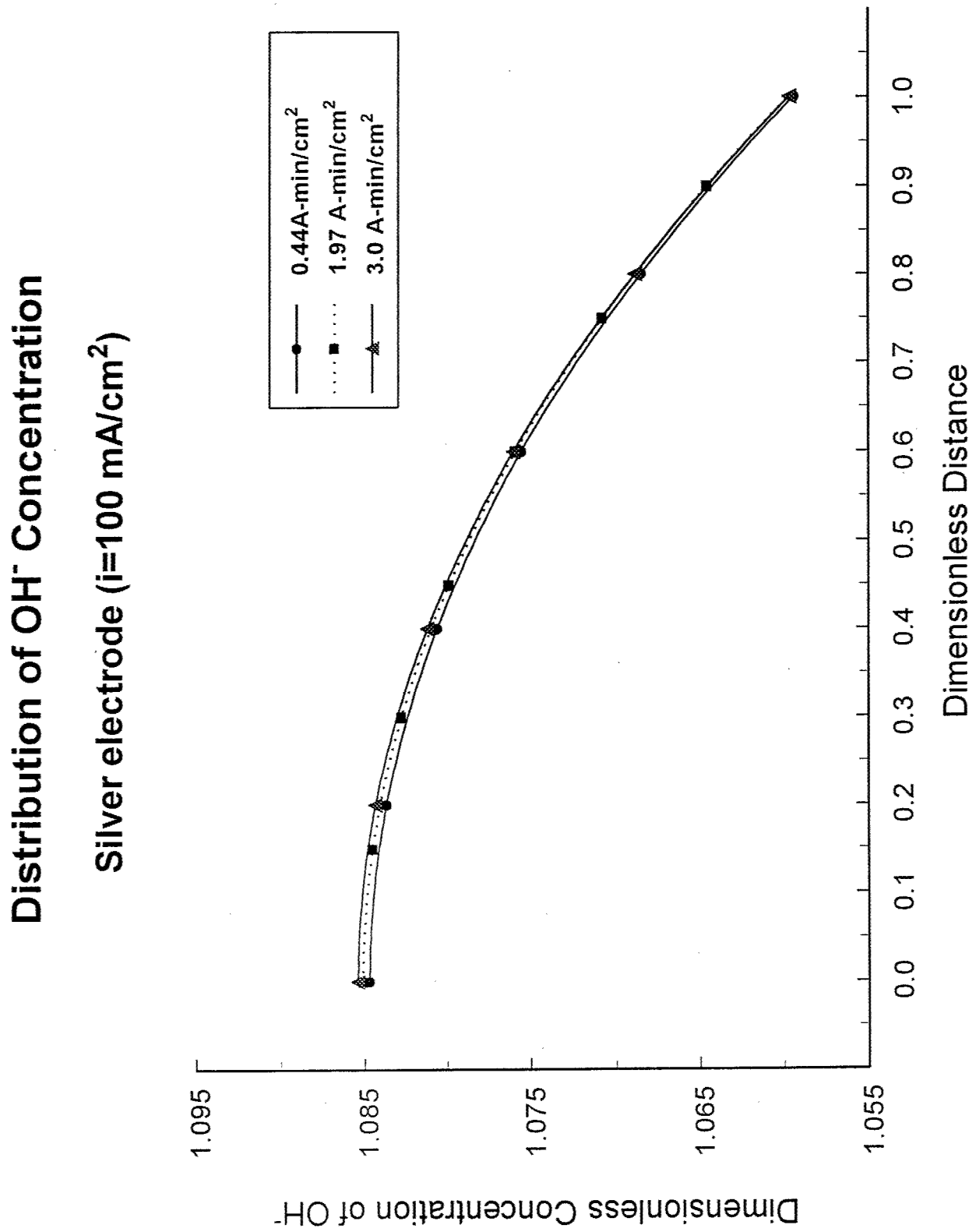
Distribution of OH⁻ Concentration
Silver electrode (i=100 mA/cm²)
0.44A-min/cm²
1.97 A-min/cm²
3.0 A-min/cm²
1.095
1.085
1.075
1.065
1.055
Dimensionless Concentration of OH⁻
0.0
0.1
0.2
0.3
0.4
0.5
0.6
0.7
0.8
0.9
1.0
Dimensionless Distance

The Effect of Capacity on Potential

Silver electrode (at x=1.0)

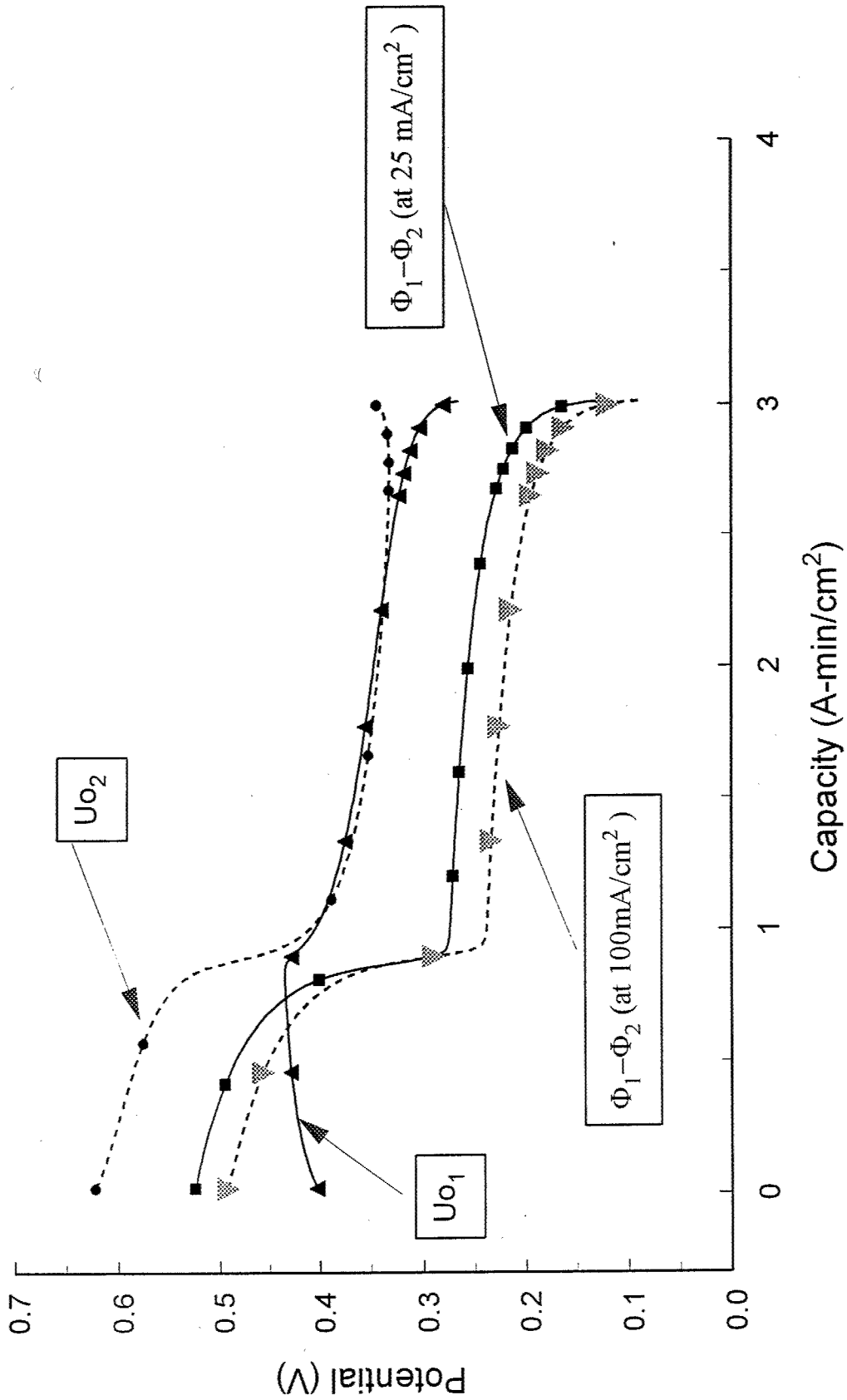

Effect of Current Density on Silver Mole Fractions at 0.44 A-min/cm^2 of Discharge

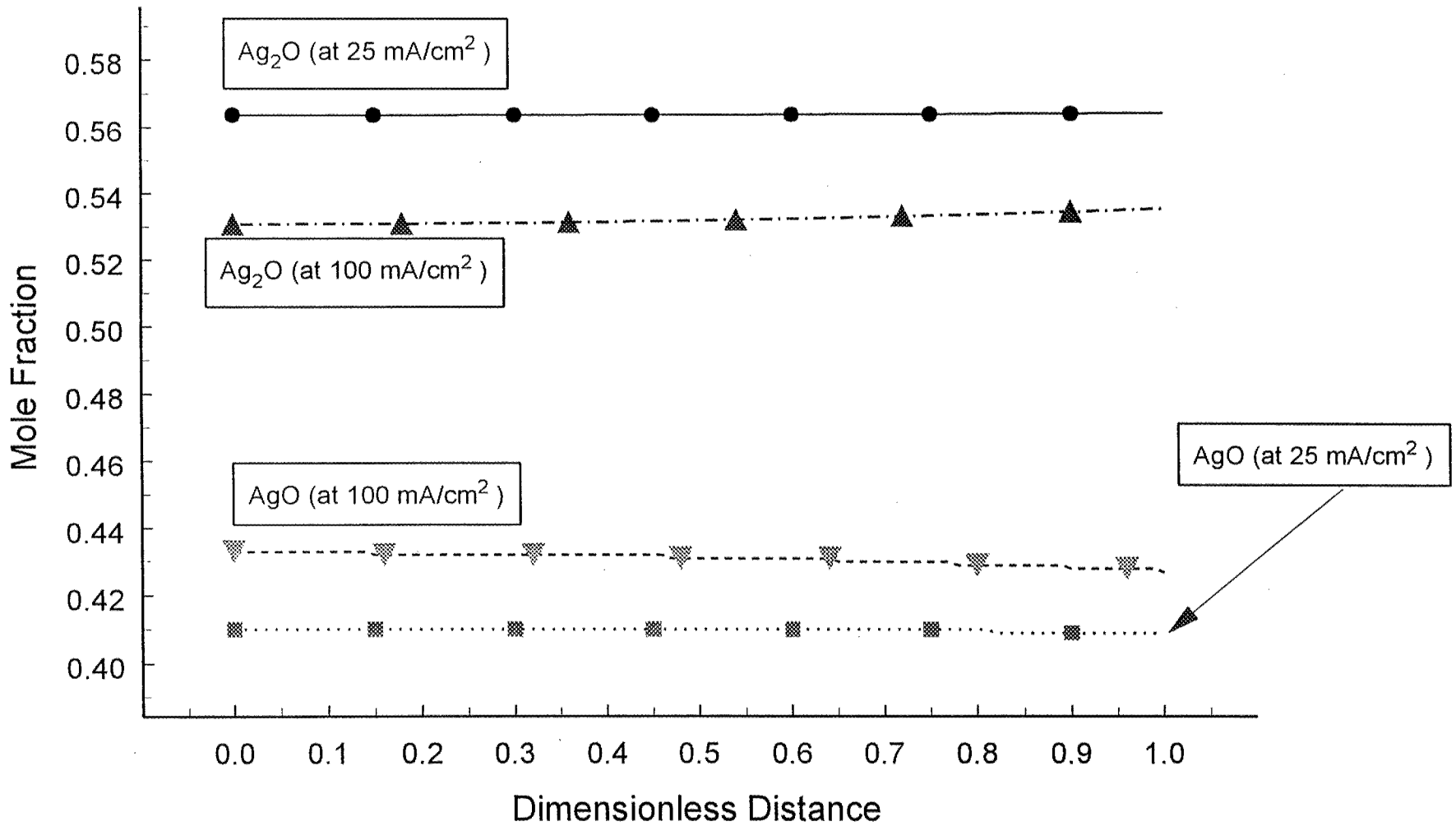

Effect of Current Density on Silver Mole Fractions at 0.88 A-min/cm^2 of Discharge

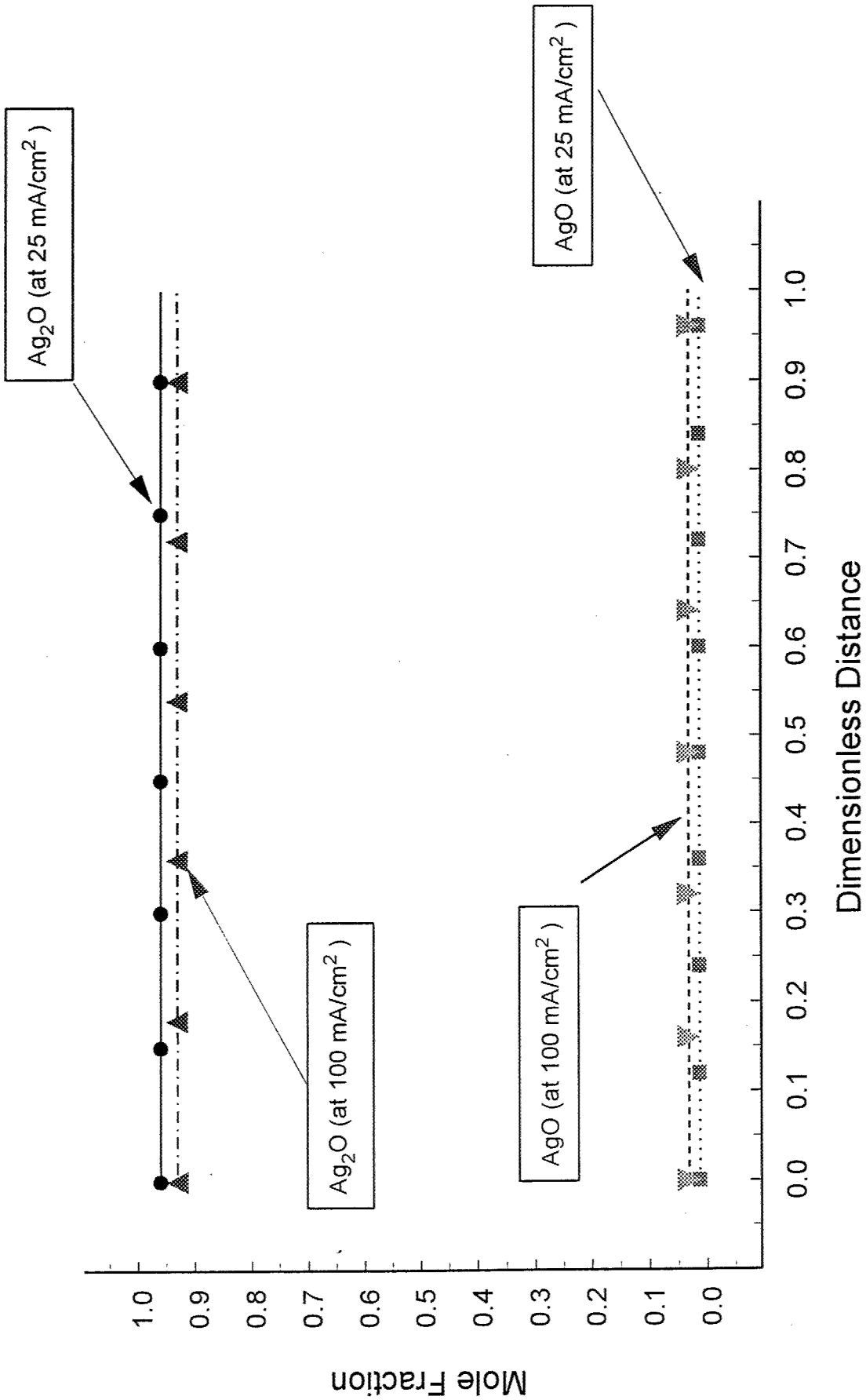

Effect of Current Density on Silver Mole Fractions at 1.97 A-min/cm^2 of Discharge

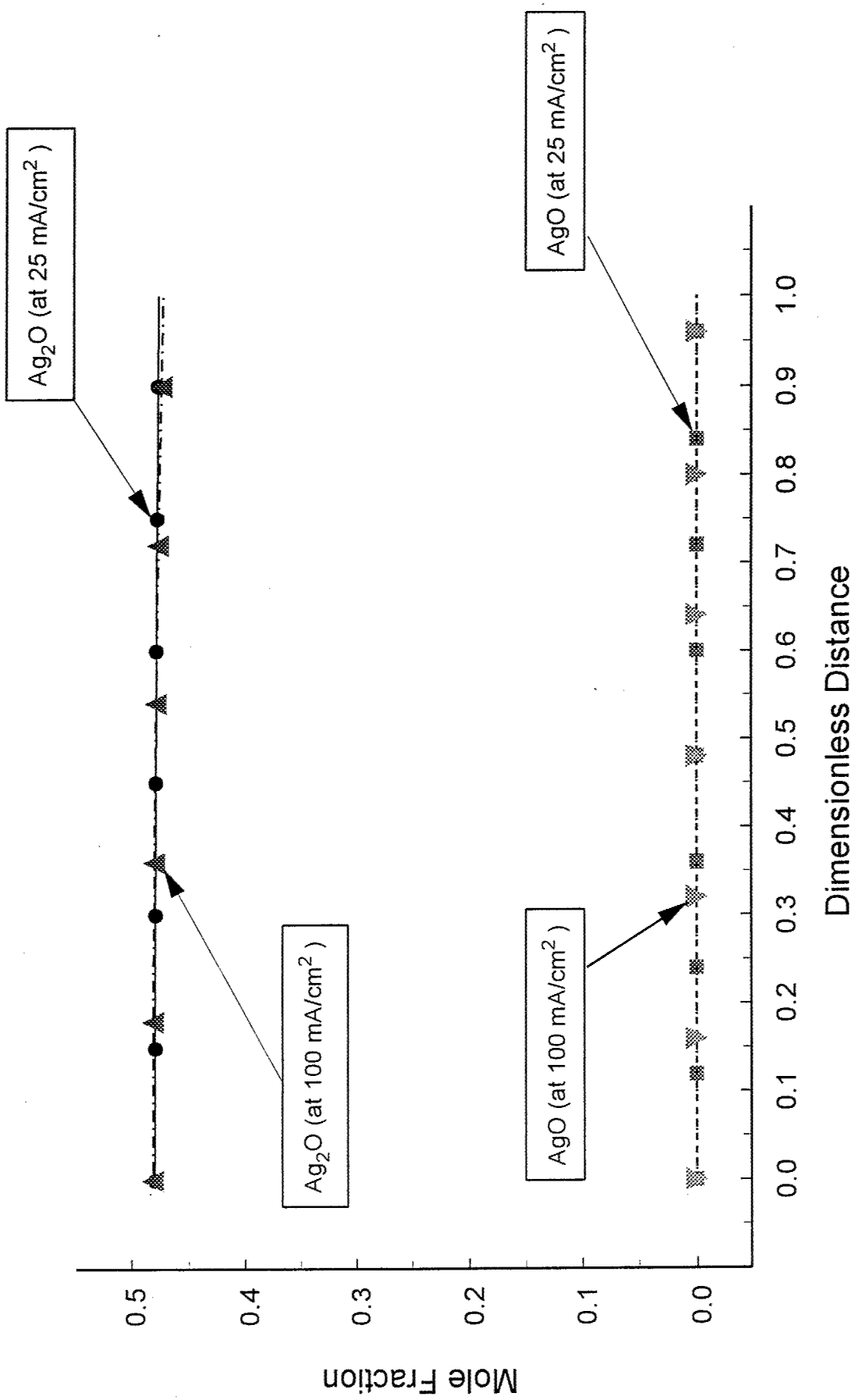

Heating Rate from Reaction 2 Polarization

Silver electrode (i=25mA/cm^2)

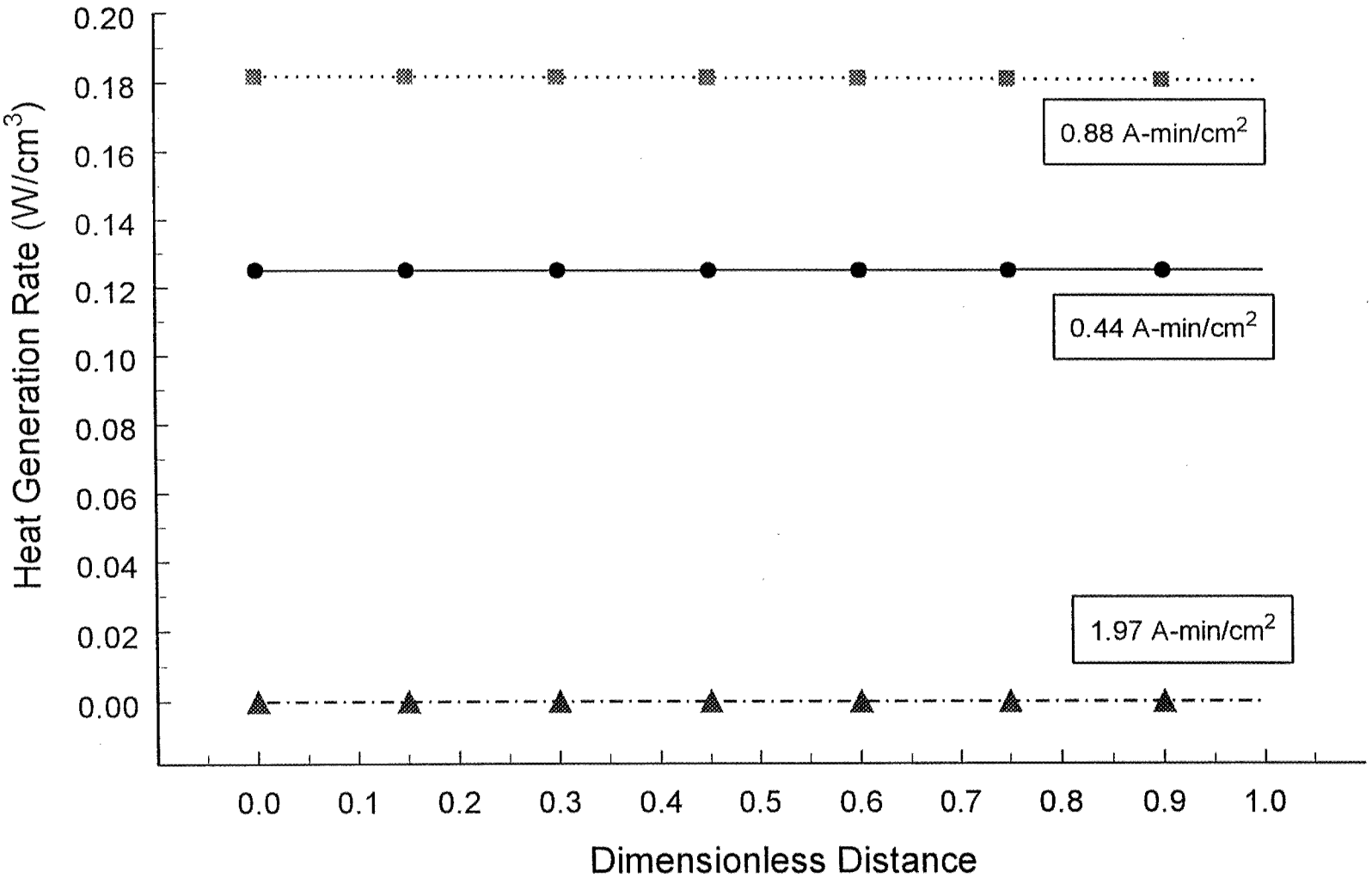

Heating Rate from Reaction 1 Polarization

Silver electrode (i=25 mA/cm^2)

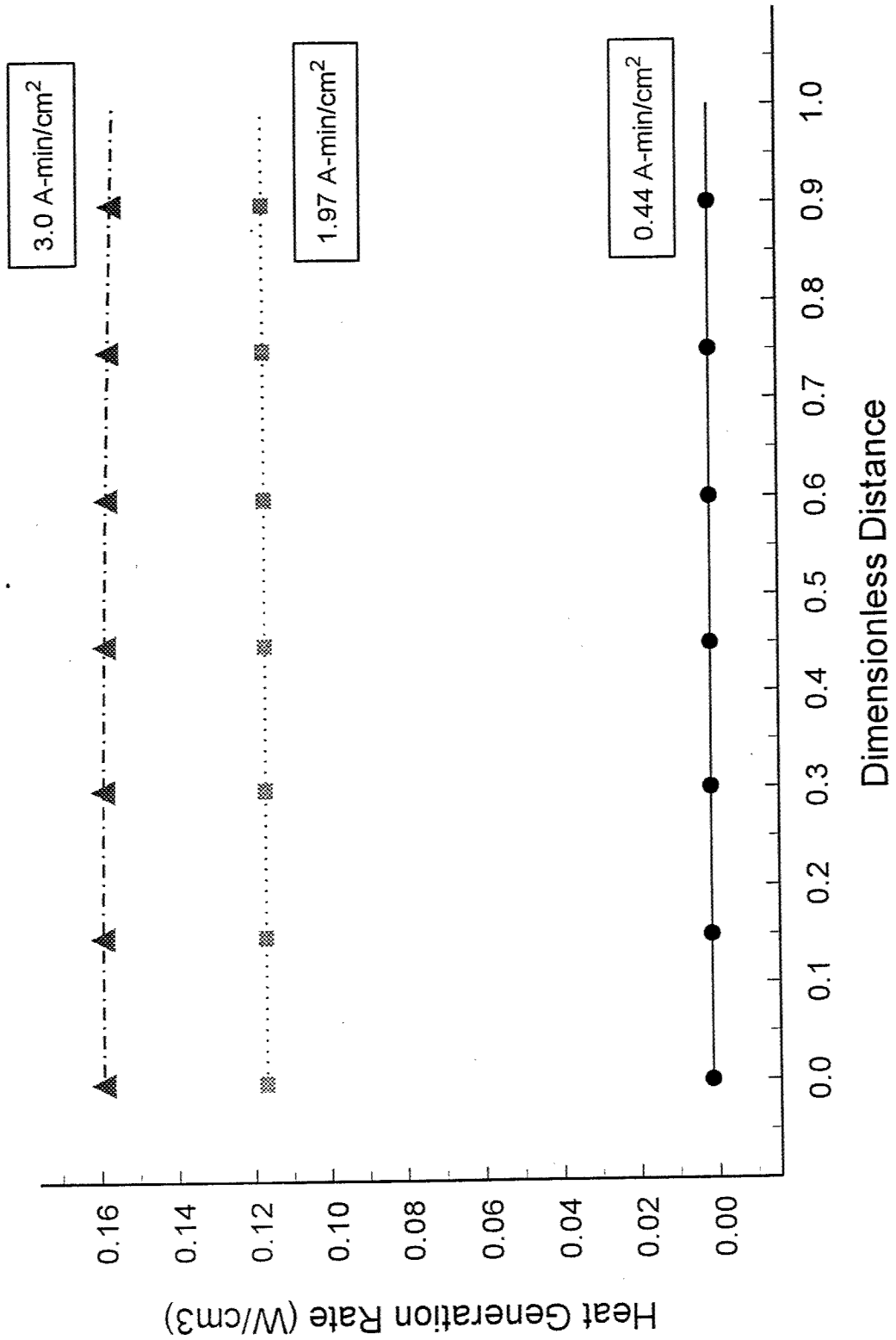

Total Heating Rate from Polarization

Silver electrode (i=25 mA/cm^2)

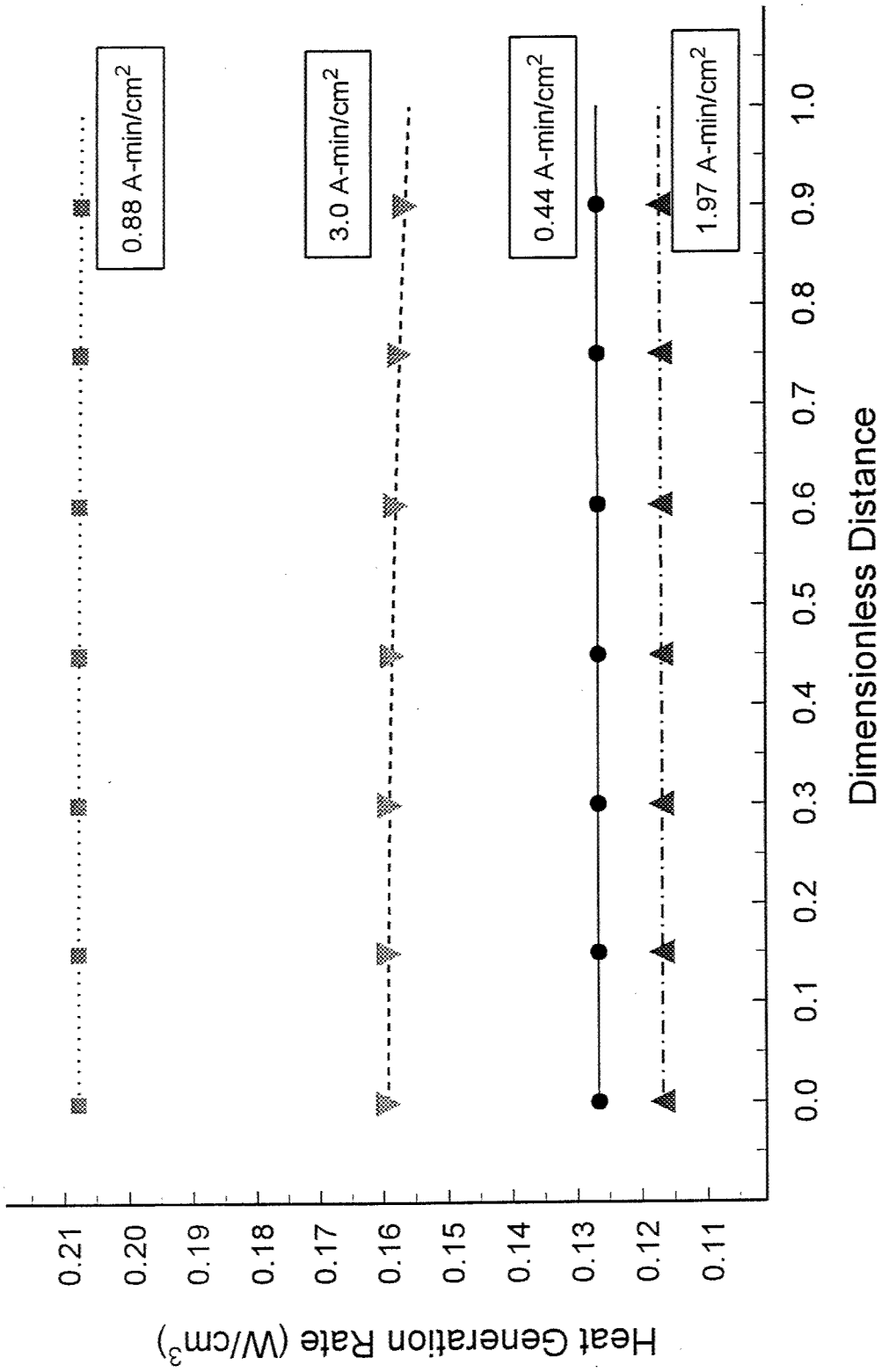

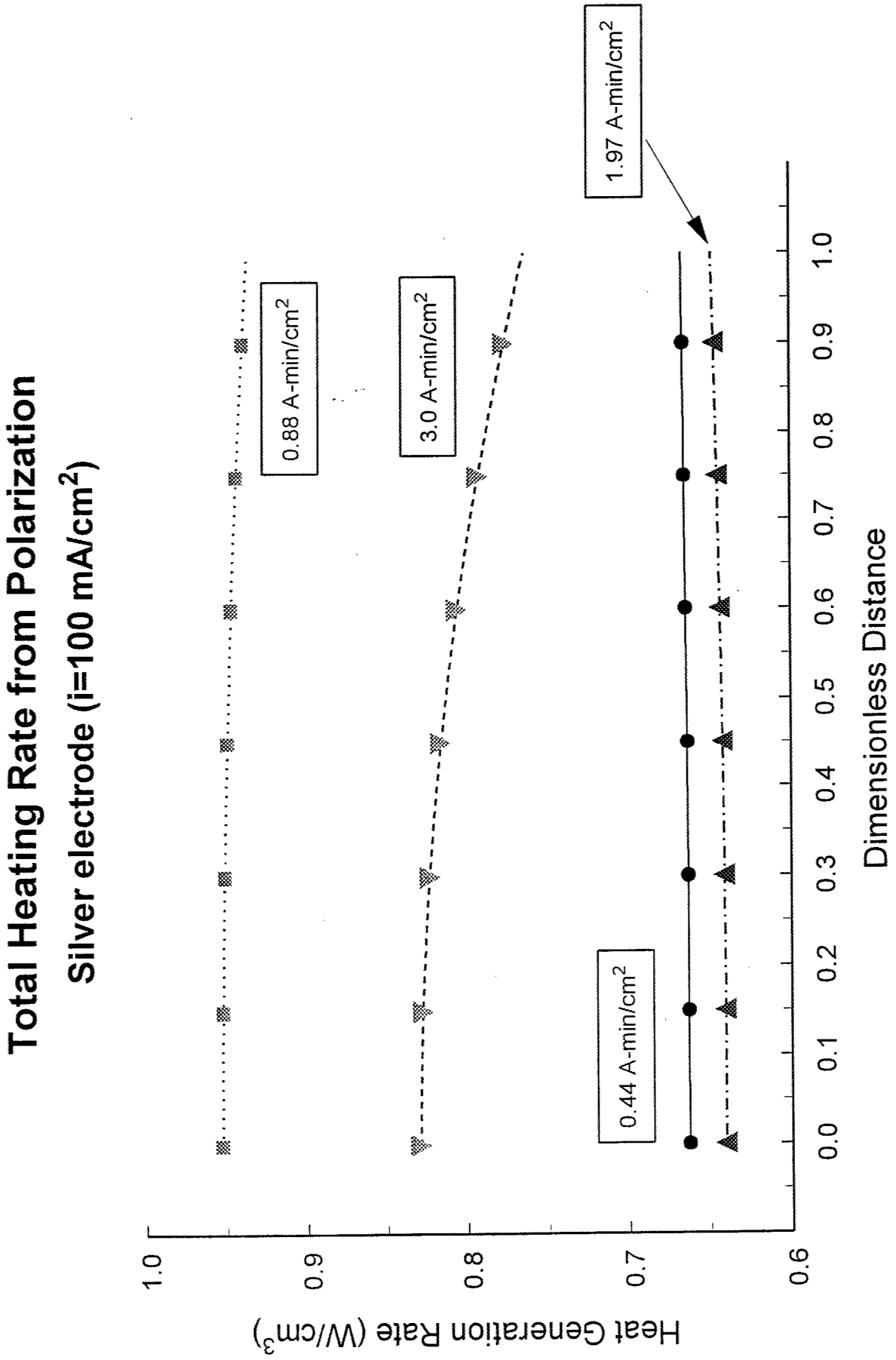
Total Heating Rate from Polarization
Silver electrode (i=100 mA/cm2)
0.88 A-min/cm2
3.0 A-min/cm2
1.97 A-min/cm2
0.44 A-min/cm2
Heat Generation Rate (W/cm3)
1.0
0.9
0.8
0.7
0.6
0.0
0.1
0.2
0.3
0.4
0.5
0.6
0.7
0.8
0.9
1.0
Dimensionless Distance

Summary & Future Work

- First Principles Model Developed
- Local Isothermal Heat Generation Predicted
- Include Temperature Feedback
  - Kinetics, conductivity, thermodynamics
- Extend to 3-D Current Distribution
- Solve 3-D Temperature Distribution

Center of Electrochemical Engineering
Department of Chemical Engineering
University of South Carolina
Columbia, SC 29208

Acknowledgments

- ONR Grant No. N00014-96-1-0795
- Naval Underwater Warfare Center, Newport
  - Mr. Steve Tucker
  - Mr. Chris Egan
- J.R. Moden, JRM Inc., Bristol, RI

Center of Electrochemical Engineering
Department of Chemical Engineering
University of South Carolina
Columbia, SC 29208

THE AEROSPACE CORPORATION

Electrolyte Loss Tendencies of Primary Silver-Zinc Cells

Lawrence H. Thaller and Gordon L. Juvinall
Energy Technology Department
The Aerospace Corporation

M2-275
POBox 92957
Los Angeles, CA 90009

(310) 336-5180
thaller@courier8.aero.org

THE AEROSPACE CORPORATION

OUTLINE

- BACKGROUND
- CHEMISTRY ISSUES
- TRENDS IN CELL DESIGN
- FLIGHT USAGE
- STATIC VOLUME-BASED MODEL
- APPLICATION TO EXISTING DESIGNS
- CONCLUSIONS

THE AEROSPACE CORPORATION

BACKGROUND

- SILVER ZINC CELLS WIDELY USED
- RECENT TRENDS EMPHASIZE LONGER WET STAND TIMES
- DESIGN MODS TREND TOWARD WETTER CELLS
- WETTER CELLS INCREASE THE PROBABILITY OF EXPELLED ELECTROLYTE
- THERE HAVE BEEN SEVERAL INSTANCES OF ELECTROLYTE LOSS PROBLEMS WITH FLIGHT ARTICLES
- ELECTROLYTE LOSS CAN RESULT FROM SEVERAL DIFFERENT PROBLEMS
- A TASK WAS CARRIED OUT TO INVESTIGATE A CELL'S TENDENCY TO LOSE ELECTROLYTE

Silver-zinc batteries are used in applications where high energy density and high discharge rates are required. These batteries are mostly used in the primary mode where they are not required to be recharged. All launch vehicles use silver-zinc batteries in sizes ranging from about one ampere hour (Ah) to 250 Ah. For the launch vehicle applications addressed here, batteries are assembled except for the introduction of electrolyte and carefully stored until they are called up for use. At that time, electrolyte is added as part of the overall activation process prior to installation on the vehicle. Once the cells are filled, reactions take place that can result in small amounts of electrolyte being expelled from them. There have been several recorded instances where electrolyte expulsion has resulted in the rejection of either that particular battery or the entire production lot of batteries that were felt to have a generic problem. An in-flight failure of a battery suggested that the problem resulted from the effects of small amounts of electrolyte forming an ionic conduction path inside the battery box. This presentation will review the causes for the different kinds of problems within a cell that can result in the expulsion of small amounts of electrolyte. It will also present a static volume based model that was found to be useful in estimating the tendencies for different silver-zinc cell designs to expel electrolyte after they are activated and what precautions and remedies are available to minimize or preclude this problem. In applying this model to four different cell designs, it accurately predicted a problem with a cell design that was felt to be responsible for an inflight battery failure due to the expulsion of electrolyte from the cells.

THE AEROSPACE CORPORATION

CHEMISTRY ISSUES

- CELL PERFORMANCE DEPENDS ON ELECTROLYTE CONCENTRATION AND AMOUNT
- GASSING RATE DEPENDS ON AMALGAMATION
- OXALATE PROBLEM DEPENDS ON AMOUNT OF ELECTROLYTE

The amount of electrolyte and the concentration of potassium hydroxide required for the cell's intended application is determined by the mass transport and the super saturation limits of the zincate ion under the conditions the cell is being discharged and the duration over which the discharge is required. Foundation studies carried out at Naval Research Laboratory in the late 1940s were instrumental in helping manufacturers establish their own design codes in terms of surface area, porosity, and electrolyte quantities.

Zinc is an amphoteric metal, and thus is thermodynamically unstable in aqueous potassium hydroxide. The reaction of the zinc with aqueous potassium hydroxide solution results in hydrogen evolution. In practice, the rate of hydrogen evolution is reduced by amalgamation of the zinc electrodes and by stringent quality control measures. The addition of mercury to the zinc electrodes (amalgamation) raises the hydrogen overvoltage and effectively inhibits the evolution of hydrogen by "local action", which is essentially corrosion of the zinc. Normally, the mercury constitutes about 1% to 2% by weight of the finished anode. Increasing the mercury content from 1% to 2% decreases the rate of evolution of hydrogen by a factor of ten.

Besides the electrolyte requirements being dictated by current density (milliamperes per square centimeter) and capacity (milliampere-hours per square centimeter) there are other factors to be considered as well. The amount of electrolyte affects the rate of growth of potassium oxalate crystals that form within the layers of cellulosic separator material. These crystals, which result from the interaction of potassium hydroxide with cellophane, can lead to tears in the separator during the rigors of launch. Very often this results in potentially dangerous short circuits within the cell. The concentration of electrolyte affects the rate of formation of potassium oxalate as well as the gassing rate at the zinc electrodes.

THE AEROSPACE CORPORATION

TRENDS IN CELL DESIGN

- LONGER WET STAND TIMES
  - From 15 days towards 90 days
  - More electrolyte
  - More separator
- WETTER CELLS MORE PRONE TO EXPEL ELECTROLYTE
- ABSORBENT PADS CAN BE USED

Cells are of course designed so that excessive amounts of electrolyte will not be expelled. However, many of the current cell types were originally designed twenty or thirty years ago. Since that time, there has been an effort to extend the wet stand time from 15 days (for the very short wet stand limits associated with batteries using cells with only a few layers of separator) to up to 90 days for some requalified cell types. It is well known that extra layers of cellophane separator material can increase the wet stand time, but at the expense of an increased internal resistance. The addition of more electrolyte is another method used to increase the wet stand time since it retards the growth of oxalate crystals mentioned above. For these reasons, the net free volumes within some of these designs have gotten smaller.

THE AEROSPACE CORPORATION

CAUSES OF ELECTROLYTE LOSS

- POOR AMALGAMATION STEP
- NORMAL VENTING OF CELLS
- IMPROPER PRESSURE ON "O" RING SEAL
- EXCESS ELECTROLYTE DURING FILLING
- DISPLACEMENT OF ELECTROLYTE BY HYDROGEN IN ZINC ELECTRODES
- INADEQUATE HEAD SPACE

This chart lists the major factors that have caused electrolyte to be expelled from silver zinc cells. Different manufacturers use different methods of amalgamating their zinc plates. From time to time the amalgamation levels or quality are ineffective or the surface of the zinc plates are unusually high. Either of these situations can result in excessive gassing when the cells are first filled. Following the addition of electrolyte, gassing will take place, but the vent valve will allow the hydrogen gas to be vented as the pressure builds up. As the gas escapes, small droplets of electrolyte can also be expelled as well. If the vent valve has been improperly seated against the "O" ring, hydrogen gas along with small amounts of liquid can be lost from the interior of the cell via this path. Another problem that is seen occasionally is caused by excess amounts of electrolyte being added to the cell as a consequence of incorrect amounts contained in the filling bottles that are assigned to each cell. However, cell designs that have an inadequate amount of free volume will be the main issue to be addressed in this presentation. Much of the electrolyte is designed to be held within the pore structure of the electrodes and separators. Zinc electrodes are typically 65% porous. The hydrogen gas forming at the zinc surfaces within the pore structure of these electrodes can push electrolyte out into the free volume of the cell. If there is an inadequate amount of head space within the cell, the electrolyte can be pushed out through the vent valve and onto the top of the cell.

THE AEROSPACE CORPORATION

CELL FILLING PRIOR TO FLIGHT

- REMOVE VENT VALVE
- ATTACH FILL TUBE
- VACUUM BACK FILL CELL
- LET STAND "N" DAYS
- APPLY VACUUM "Y" TIMES
- INSTALL VENT VALVE
- MONITOR CELL/BATTERY VOLTAGE
- INSTALL ON SPACECRAFT

A general list of steps that are followed during the normal processing of a silver zinc battery at the launch site. These procedures are specific to the contractor, but the major elements are the same. Batteries are stored refrigerated and without electrolyte. The cells are filled with a prescribed amount of electrolyte that is contained with a fill bottle (one for each cell) by a vacuum back filling process and then allowed to stand for a period of time during which the open circuit voltages are monitored and the battery voltage under a test load is measured for compliance to specifications. Depending on the contractor, one or more reapplications of vacuum are applied to redistribute the electrolyte within the porous elements within the cell and at the same time disengage and remove the hydrogen gas trapped within the zinc electrodes. The cell vents are then installed and tightened to the proper torque and finally the battery installed on the spacecraft.

CELL BACKFILLING SETUP

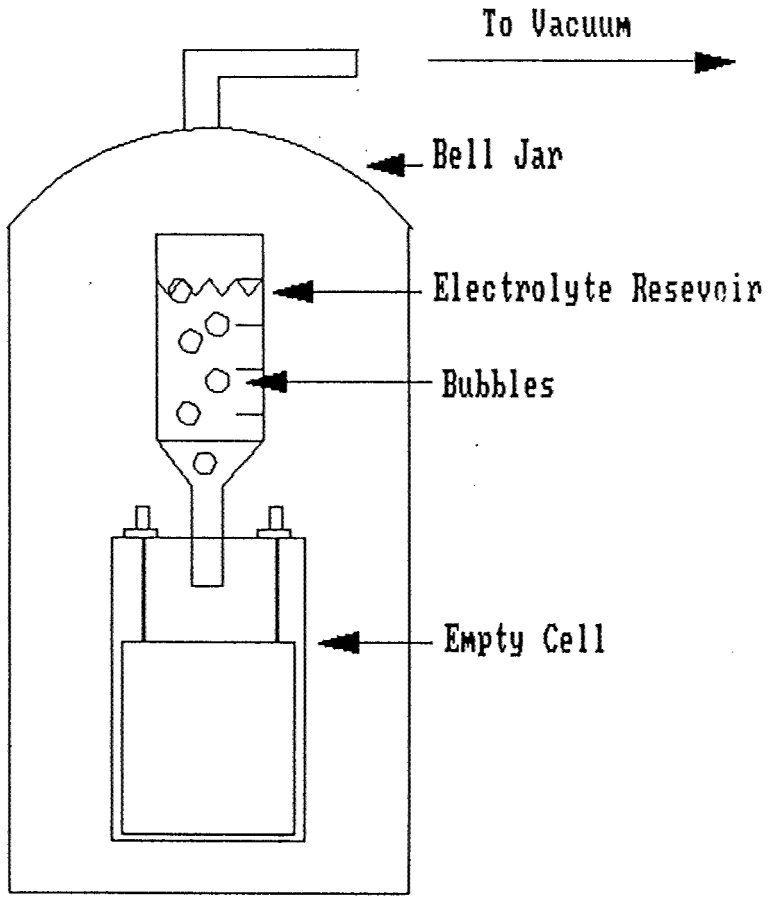

A schematic of a vacuum filling fixture. In actual practice, all the cells of the battery are filled at one time. In one arrangement, plastic tubes which are connected at one end to the individual reservoirs are threaded into the opening at the cell top at the other end. This threaded opening is later used for the insertion of the vent valve.

THE AEROSPACE CORPORATION

FLIGHT USAGE

- CELL VENT VALVE OPENS IN THE RANGE OF 3-5 PSI DIFFERENTIAL
- BATTERY HOUSING VENTS AT ABOUT 11 PSI DIFFERENTIAL
- WHEN VEHICLE REACHES ALTITUDE, BATTERY VENTS TO SPACE
- VEHICLES GOING TO GEO CAN VENT SEVERAL TIMES
- LOSS OF 1.5 VOLTS DUE TO SHORTED CELL DOES NOT CREATE A PROBLEM
- LOSS OF A FULL BATTERY DOES

This chart lists a short description of the pressure environment the battery will see during its short useful life in space. To be noted is the fact that a battery will be expected to vent at an altitude when the outside pressure drops below about 1 psia. At this point the individual cells will also vent as they adjust to the lower pressures inside the battery box. This coupled with the slow or not so slow reaction of the zinc with the electrolyte will produce a small amount of hydrogen gas that will vent first to the battery box and then to space given the proper levels of differential pressure.

CELL TOP AND VENT VALVE

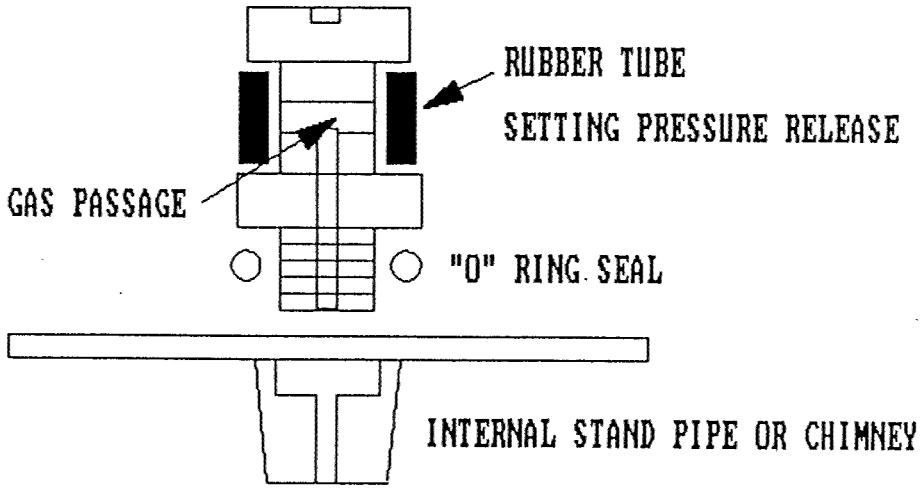

A close up view of the vent valve that is placed on each cell. The short piece of rubber tubing stretched around the gas passage within the valve allows pressure to be relieved as the rubber band is stretched away from the opening and then will reseal as the pressure is released.

THE AEROSPACE CORPORATION

STATIC CELL MODEL

- DISASSEMBLE AN UNACTIVATED CELL
- MEASURE THICKNESS, WEIGHT, POROSITY, ETC.
- DETERMINE VOLUME OF ALL INTERNAL COMPONENTS AND THAT OF THE CELL
- CALCULATE NET INTERIOR FREE VOLUME
- DETERMINE VOLUME OF ELECTROLYTE IN ZINC ELECTRODES
- DETERMINE WHETHER CELL CAN EXPEL ELECTROLYTE

This chart outlines the steps in developing a static volume-based model of a silver zinc cell. It starts with an unactivated cell that will be completely disassembled. Each component is weighed and measured. For the electrodes, the active material must be removed so the substrates can be weighed as well. Knowing the density of the materials used, the volumes of each part can be determined. As a double check on all these volume calculations, a cell's internal volume is also determined prior to disassembley by using standard gas expansion techniques. This requires a cell to be connected to a standard volume and allowing the gas to expand into the cell that has been taken to a known pressure. The two values for net internal volume as defined in the next charts agreed to within 2%.

THE AEROSPACE CORPORATION

CELL VOLUME DEFINITIONS

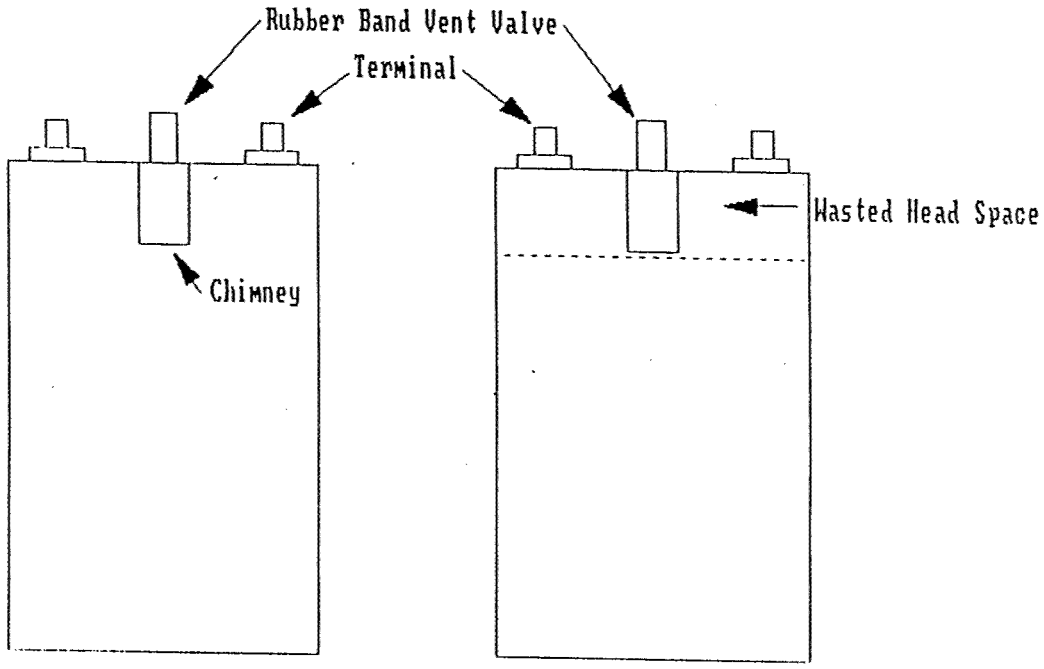

Gross Interior Cell Volume *Net Interior Cell Volume*

These three charts describe how the different cell volumes that are within a cell are defined. The chimney that sticks down into the cell in effect wastes some of the head space but is needed to prevent electrolyte loss in case a cell is inverted. From the Net Interior Cell Volume, the pieces and parts of the plates and separators are accounted for and then subtracted. Finally after the electrolyte is added, the Net Interior Free Volume can be determined. However, depending on the amount of hydrogen gas trapped within the pores of the zinc plate material, different amounts of free electrolyte will be inside the cell.

THE AEROSPACE CORPORATION

CELL VOLUME DEFINITIONS

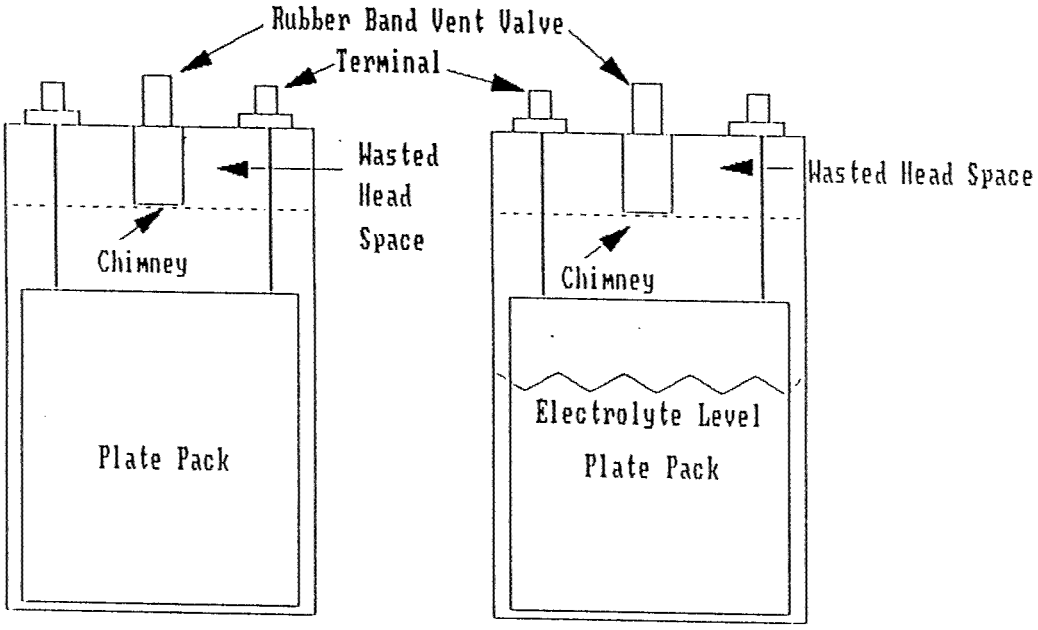

Gross Interior Free Volume *Net Interior Free Volume*

THE AEROSPACE CORPORATION

CELL VOLUME DEFINITION

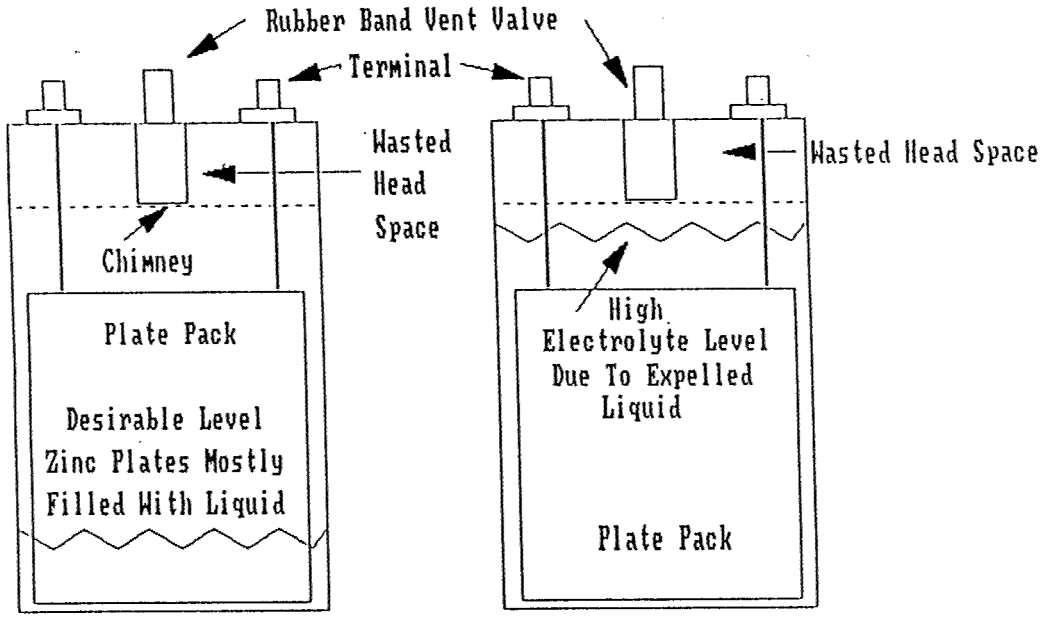

Desirable electrolyte distribution *Undesirable electrolyte distribution*

RESULTS FROM FOUR TYPICAL CELLS

Cell Parameter	145 Ah	13.5 Ah	10 Ah	4.5 Ah
Zinc Porosity	68.7 %	66.5 %	62.7%	57.5 %
Net Cell Interior Volume	359 cc	77 cc	57 cc	19 cc
Gross Free Vol	218 cc	47 cc	39 cc	11 cc
Net Free Vol	44 cc	12 cc	16 cc	2.8 cc
Minimum Free Electrolyte Vol	1.1 cc	-0.7 cc*	-4.1 cc	2.0 cc
Permissible Loss from Zn	41 %	80 %	163 %**	114 %

* Pore volume greater than electrolyte fill ** No gross expulsion possible

By applying the model to four different cell designs, the different cell volumes were determined. Cell designs where the porous volume within the zinc electrodes is large compared to the Net Free Volume are subject to electrolyte being forced from them during the course of cell standing or during discharge. When the permissible loss is greater than 100%, it means that all of the electrolyte contained with the zinc plates could be displaced by hydrogen gas and there would be no danger for electrolyte loss from the problem being addressed here. If electrolyte loss is asssociated with this type of cell design the problems may be related to surfactants in the electrolyte or or separator, or to vent valves that were improperly tightened during final battery processing.

CONCLUSIONS

- SILVER ZINC CELLS ARE NOT HERMETICALLY SEALED
- VARIOUS FLIGHT PROGRAMS HAVE EXPERIENCED ELECTROLYTE LOSS PROBLEMS
- SEVERAL DIFFERENT CAUSES FOR EXCESSIVE ELECTROLYTE LOSS HAVE BEEN SEEN
  - Some related to quality issues
  - Some related to inappropriate cell designs
- STATIC MODELING CAN BE HELPFUL FOR ESTIMATING ELECTROLYTE LOSS TENDENCIES

Since silver zinc cells are not hermetically sealed, care must be taken to prevent the loss of electrolyte which can result in shorting paths within the battery box. Prelaunch battery processing is important in being able to minimize any problems with expelled electrolyte. Just as important are the quality issues related to amalgamation, soponifiable impurities, and the electrolyte quantities contained in the individual filling bottles. Static modeling of the cell design can be useed to determine the electrolyte loss tendencies of that individual cell design.

JPL Experience With The Mars Pathfinder, Mission Simulation Battery

NASA Battery Workshop
December 3, 4, and 5 1996
Huntsville, Alabama

Dave Perrone and Richard Ewell
Jet Propulsion Laboratory

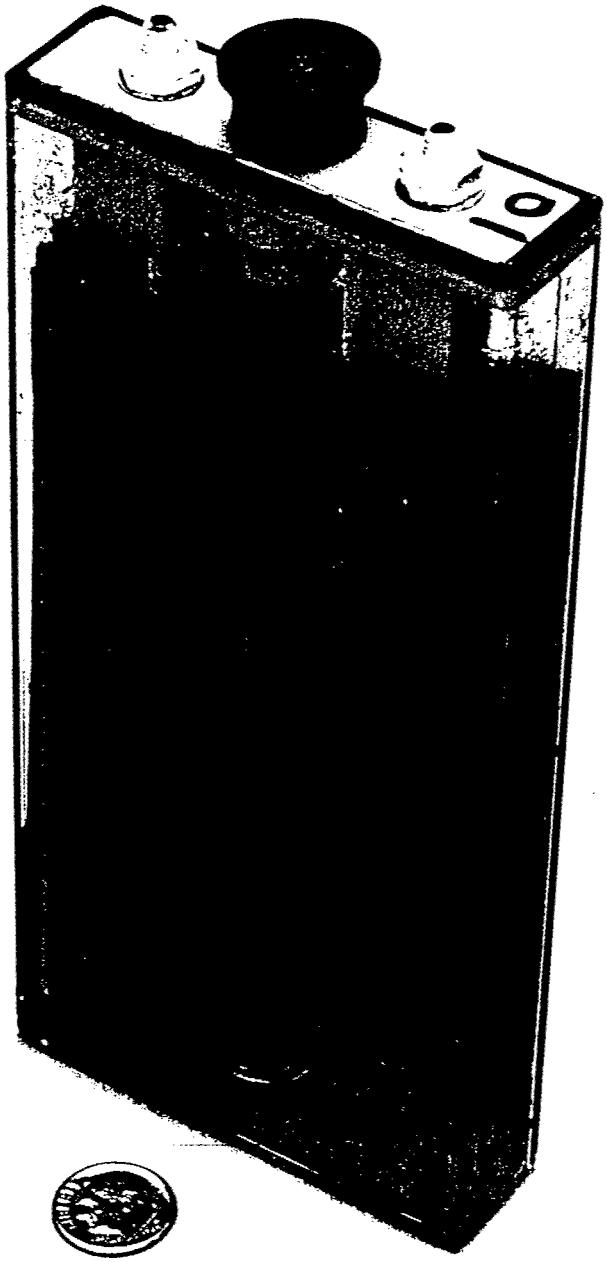

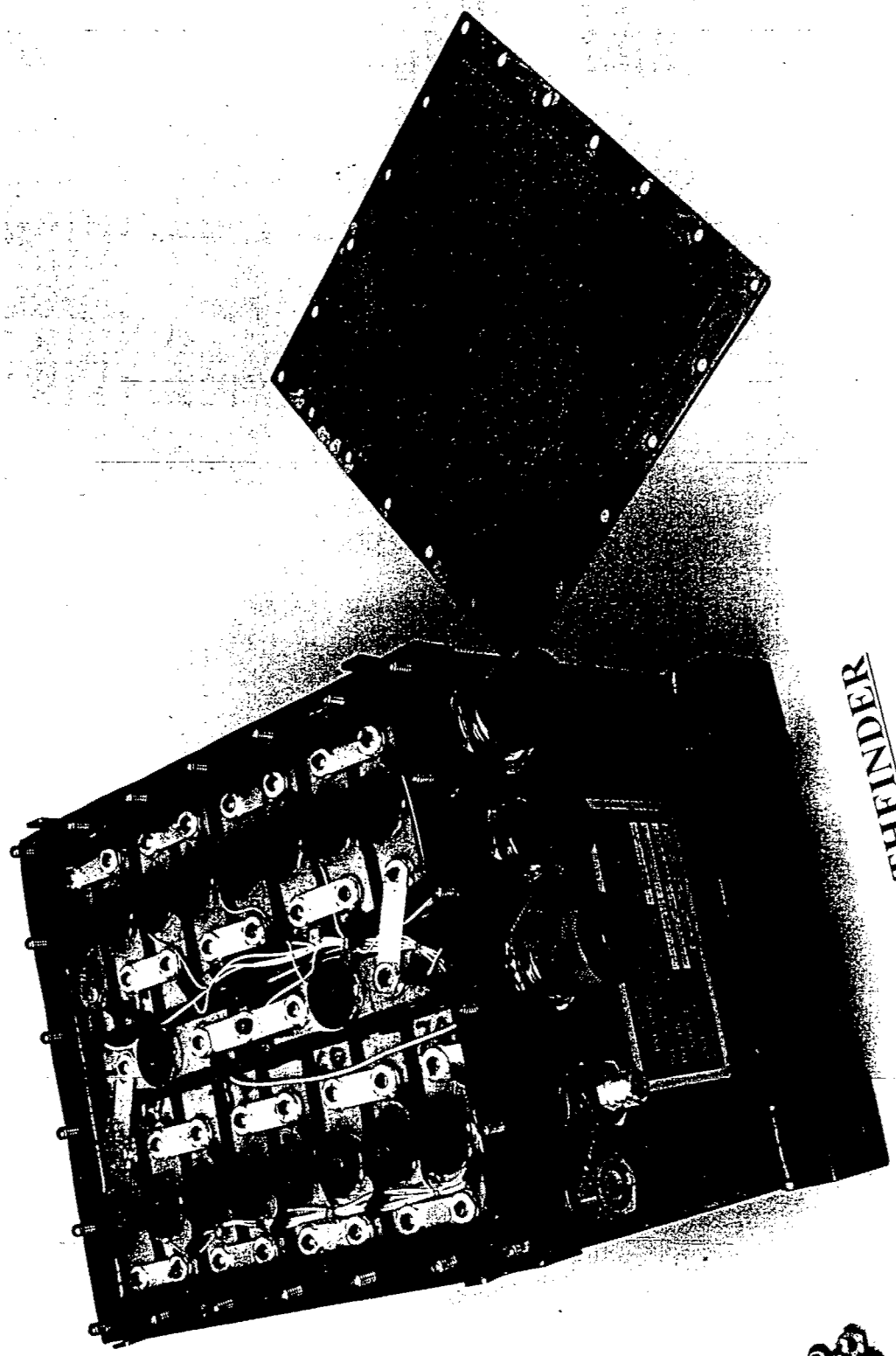

MARS PATHFINDER

18 cell, 40 Ampere-hour, Ag-Zn Battery

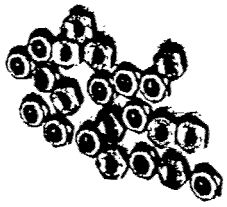

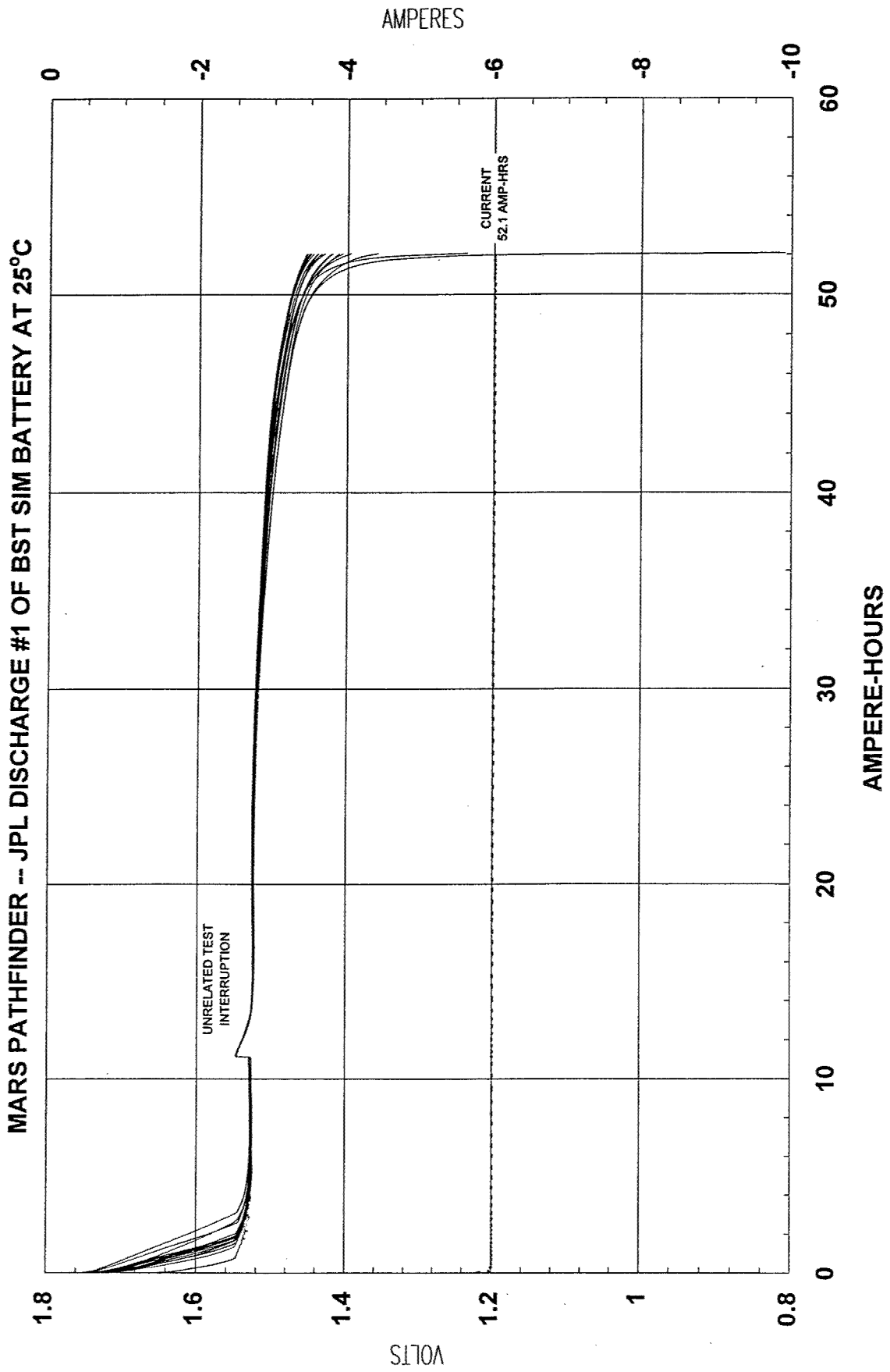

D. PERRONE 12/5/96 3:46 PM

Mars Pathfinder Battery - Expected Mission Profile

- **4 months discharge at 1 to 2 mA**
  - battery is inverted for duration
  - ambient temperature at 15°C
- **Launch**
  - battery remains inverted
  - 4.2A for 81 minutes
  - 6.0A for 50 minutes
- **Cruise**
  - ambient temperature from 10° to -5°C
  - stand in a partial state of charge (~ 40 ampere-hours)
- **Entry, Descent, and Landing**
  - 40 Ampere-hours
- **Mars Surface Operation**
  - 30 cycles at 50% depth of discharge

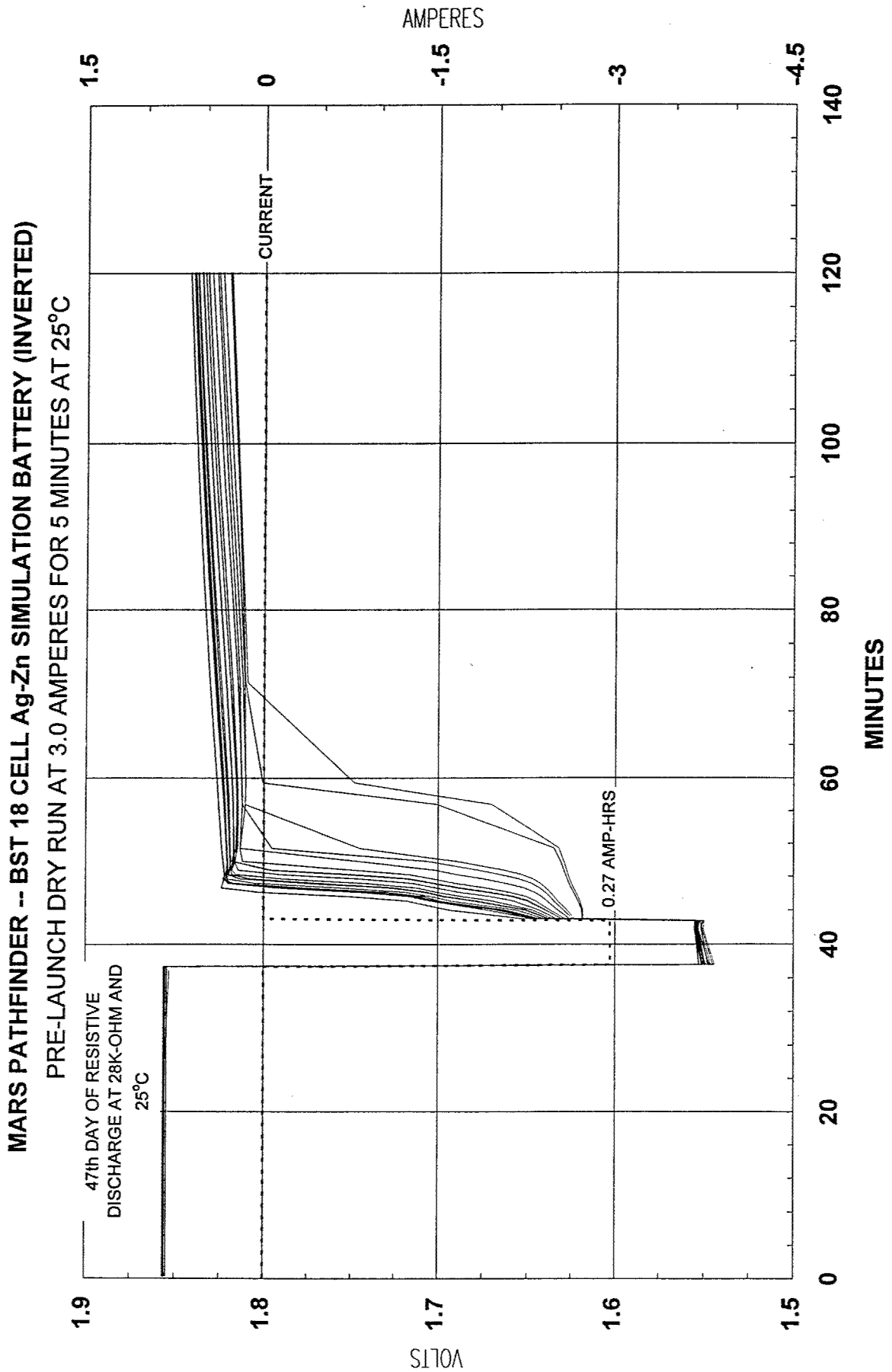

D. PERRONE 12/5/96 3:46 PM

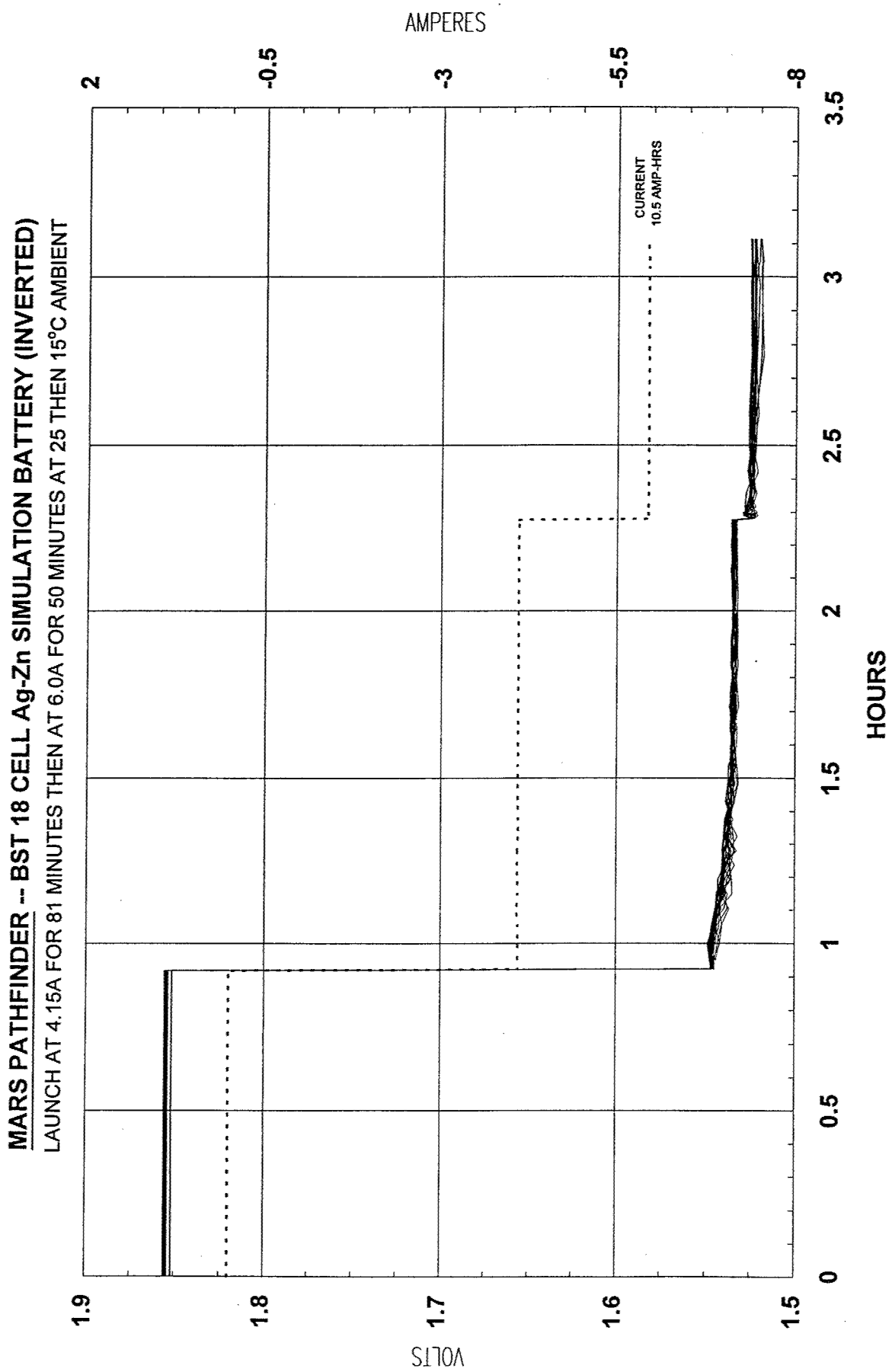

D. PERRONE 12/5/96 3:46 PM

MARS PATHFINDER -- BST 18 CELL, 40 AMPERE-HOUR, Ag-Zn SIMULATION BATTERY

CHARGE #4 FOR 12 HOURS AT 1.960 VPC THEN 12 HOURS AT 1.860 VPC AT 25°C
FOLLOWS 7 MONTHS WITH 28KOHM RESISTIVE LOAD

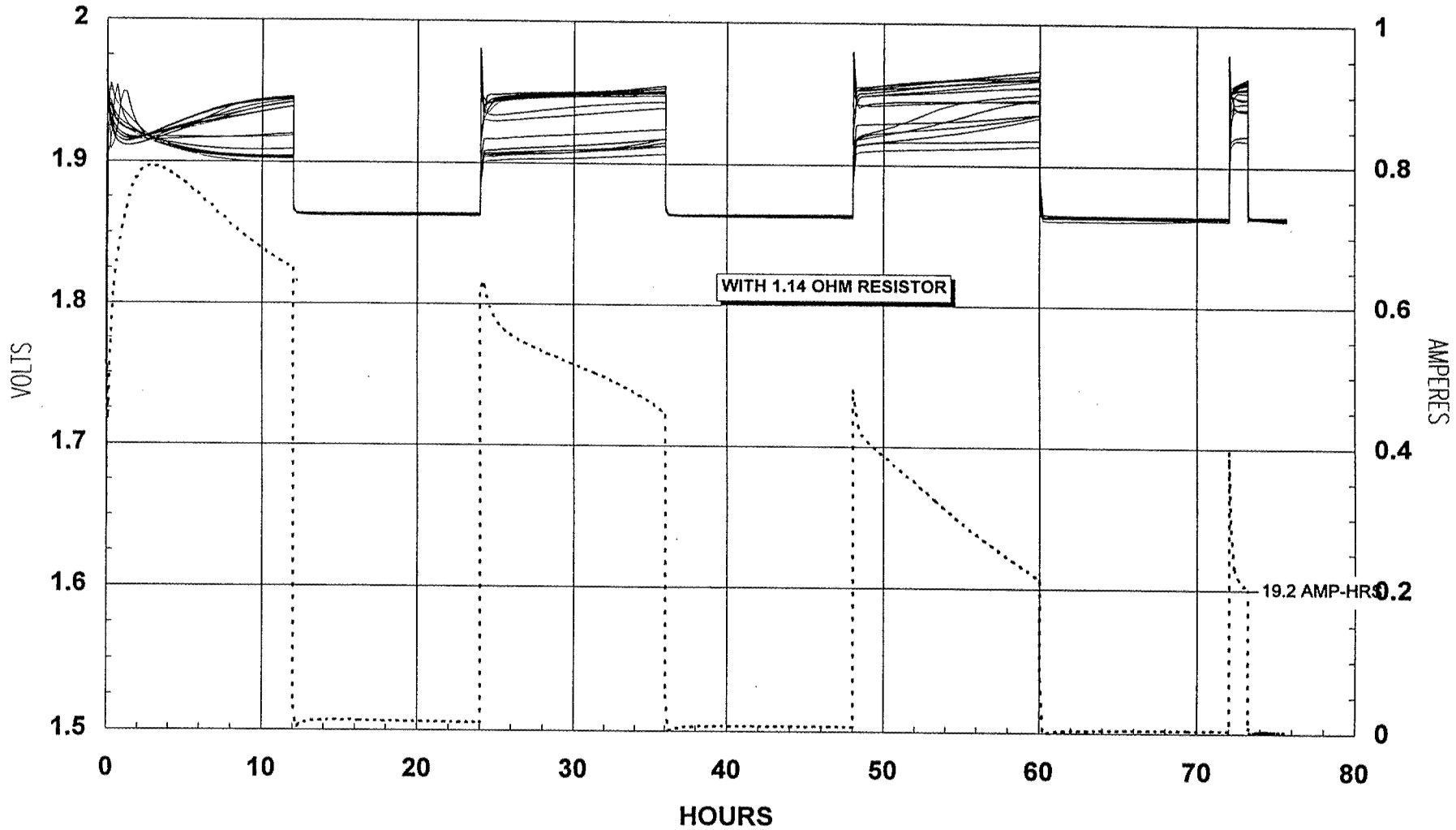

D. PERRONE 12/5/96 3:47 PM

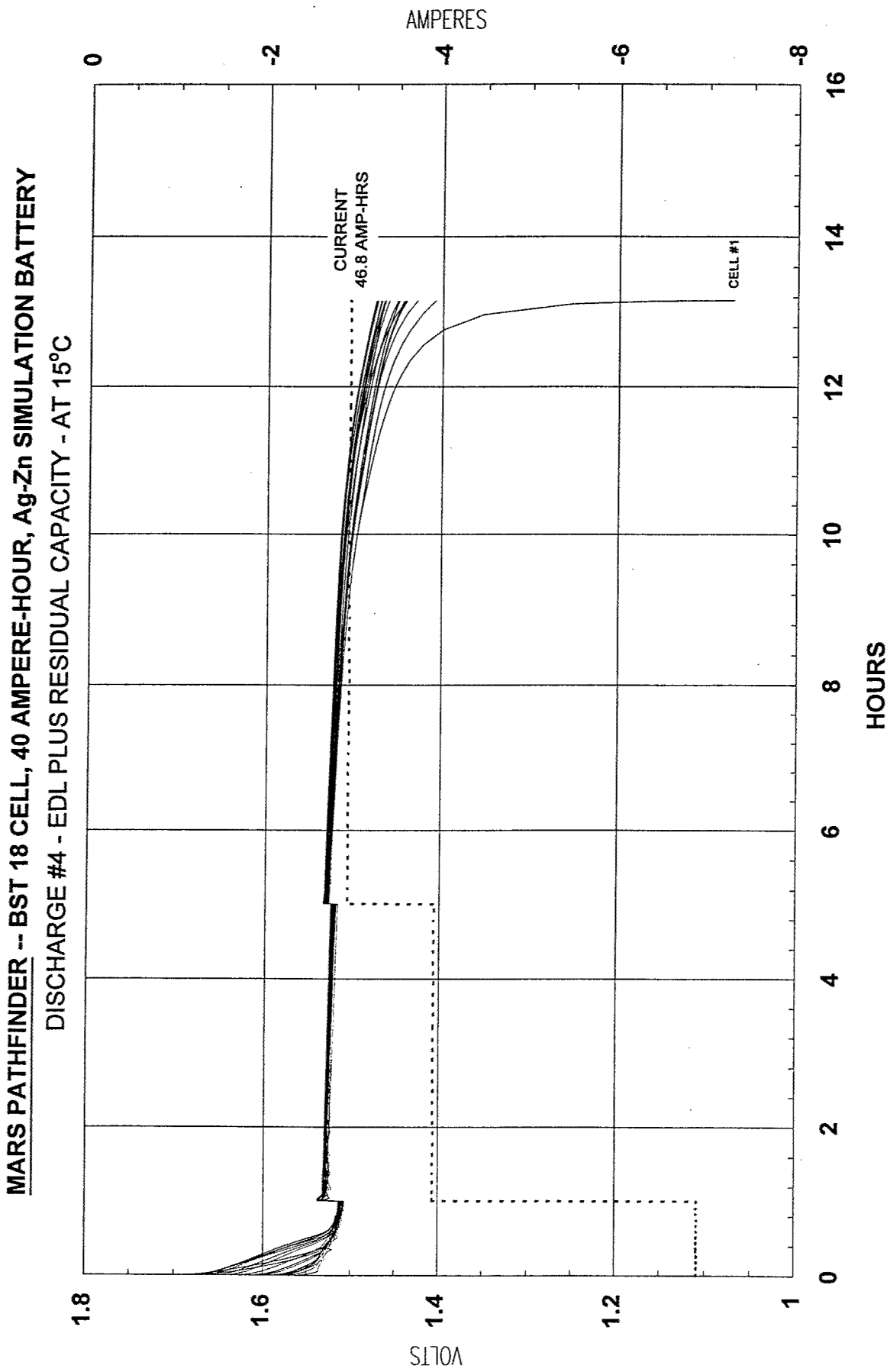

D. PERRONE 12/5/96 3:47 PM

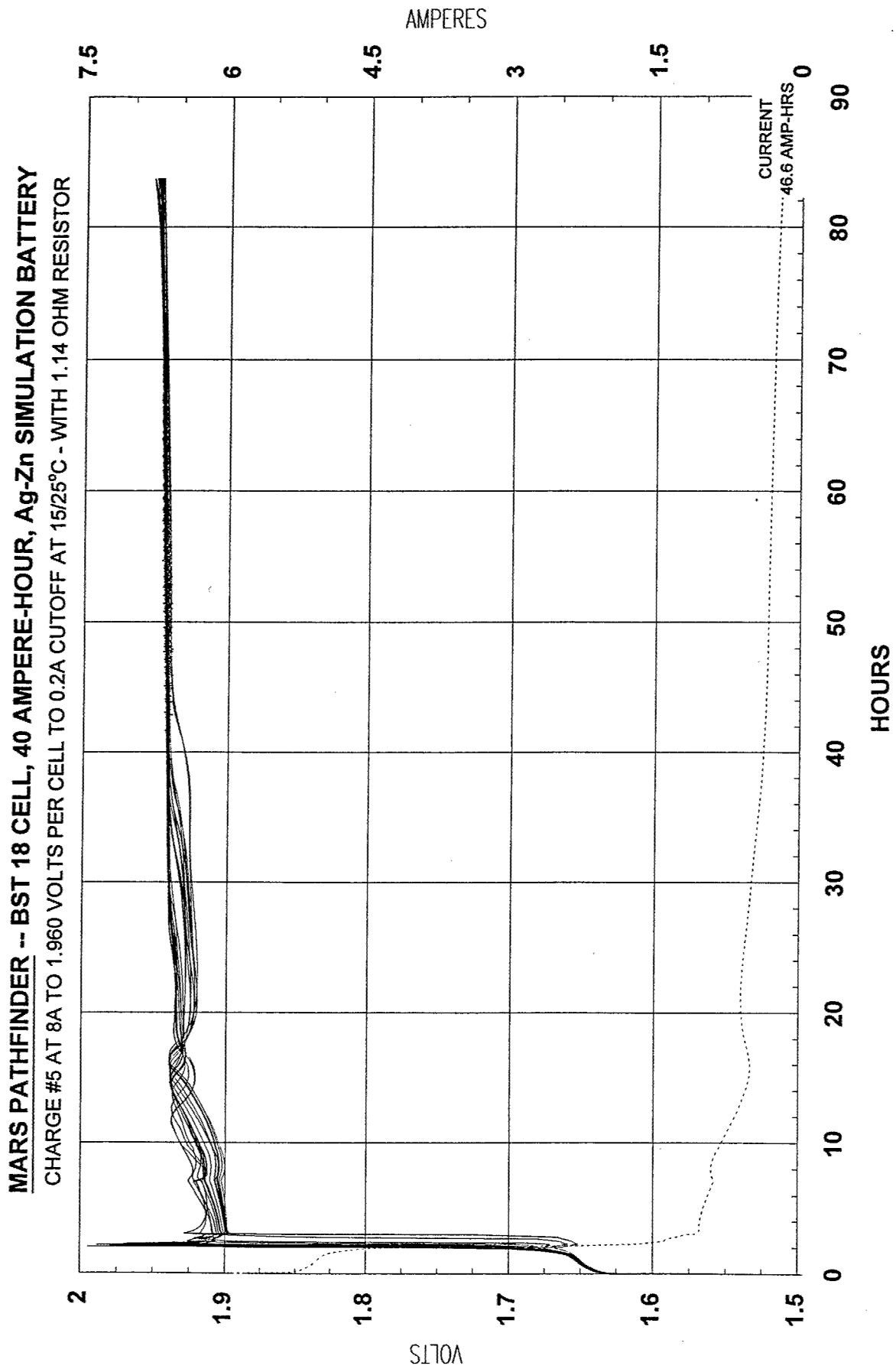

D. PERRONE 12/5/96 3:47 PM

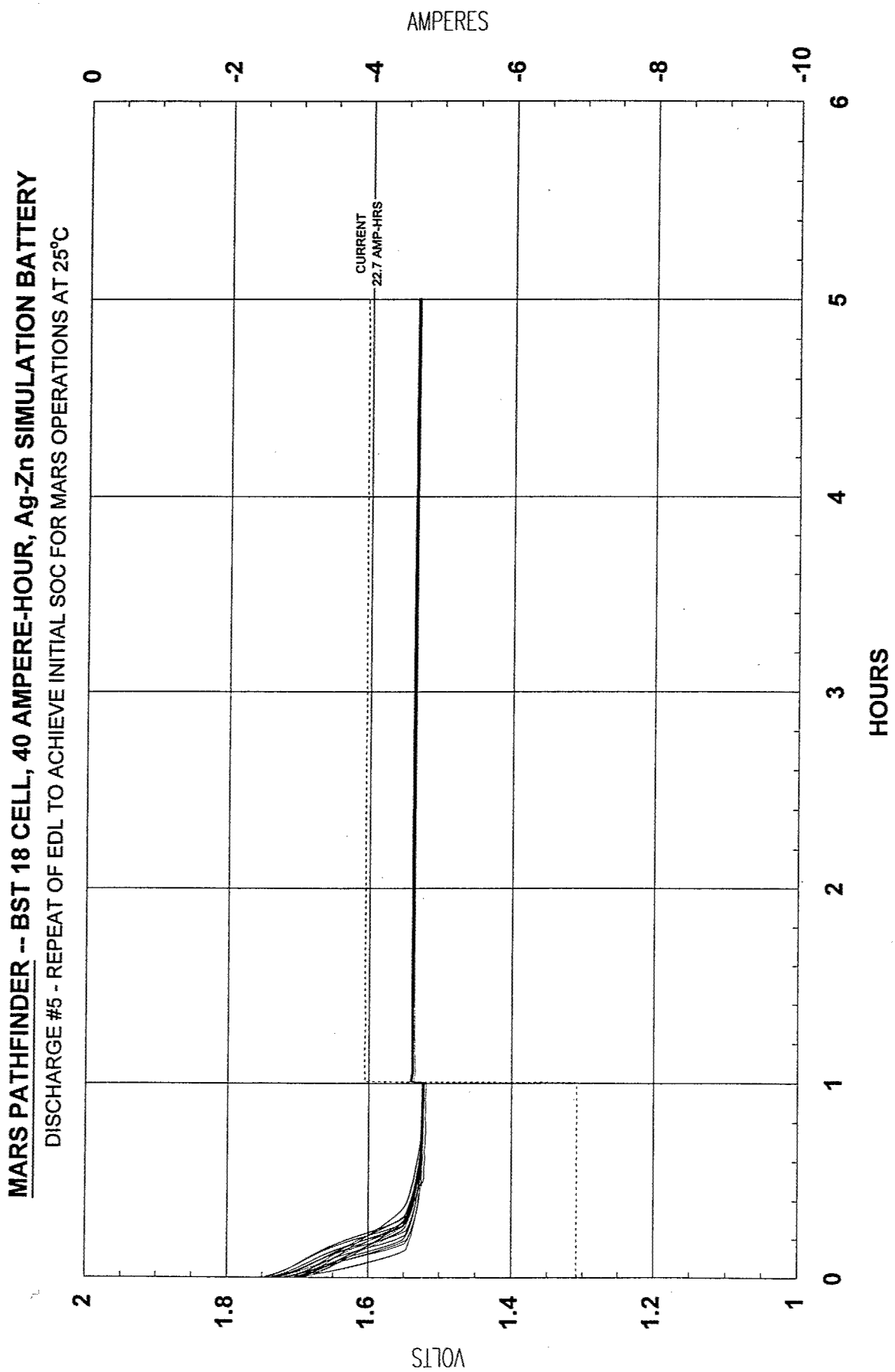

D. PERRONE 12/5/96 3:47 PM

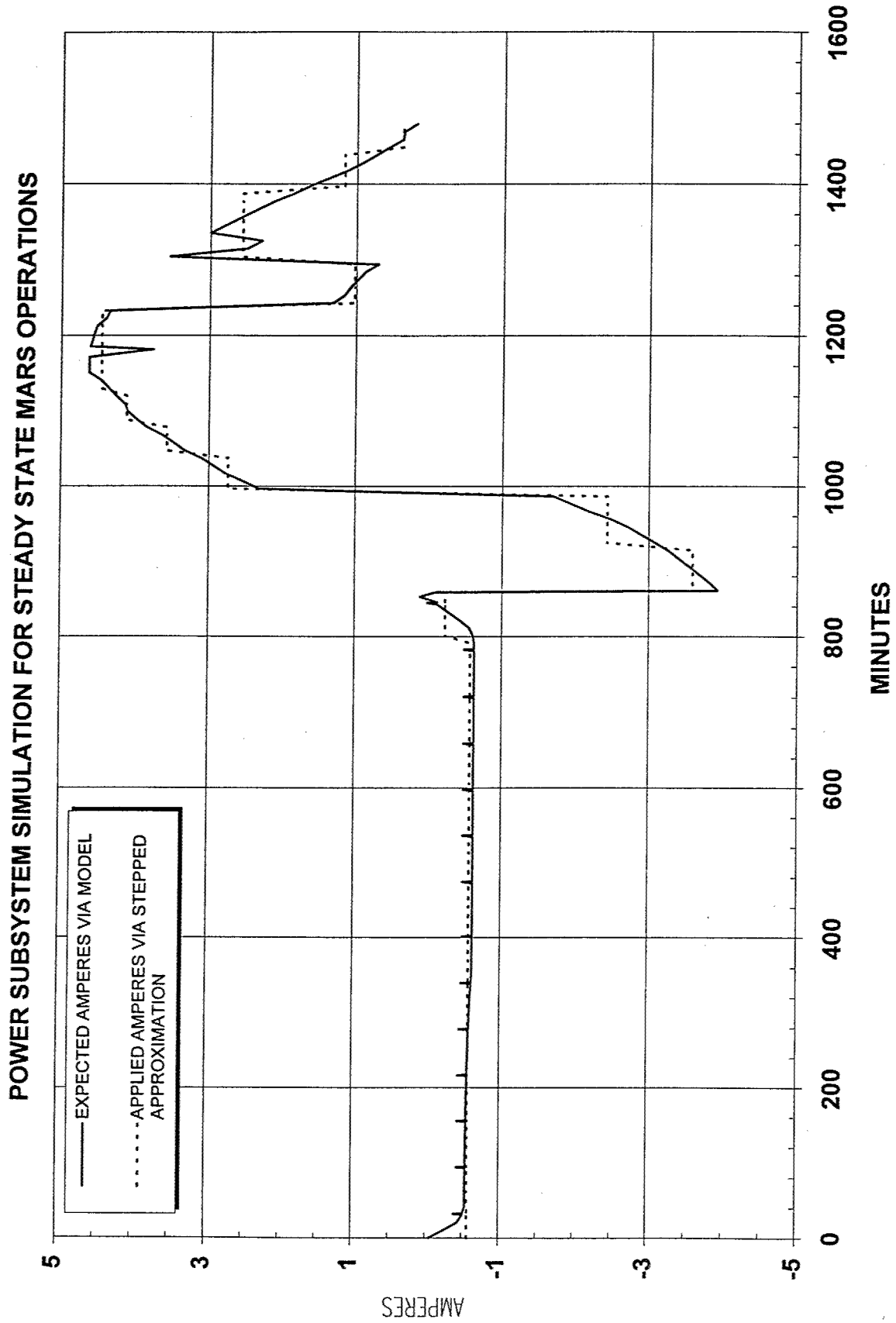

DEP 12/5/96 3:53 PM

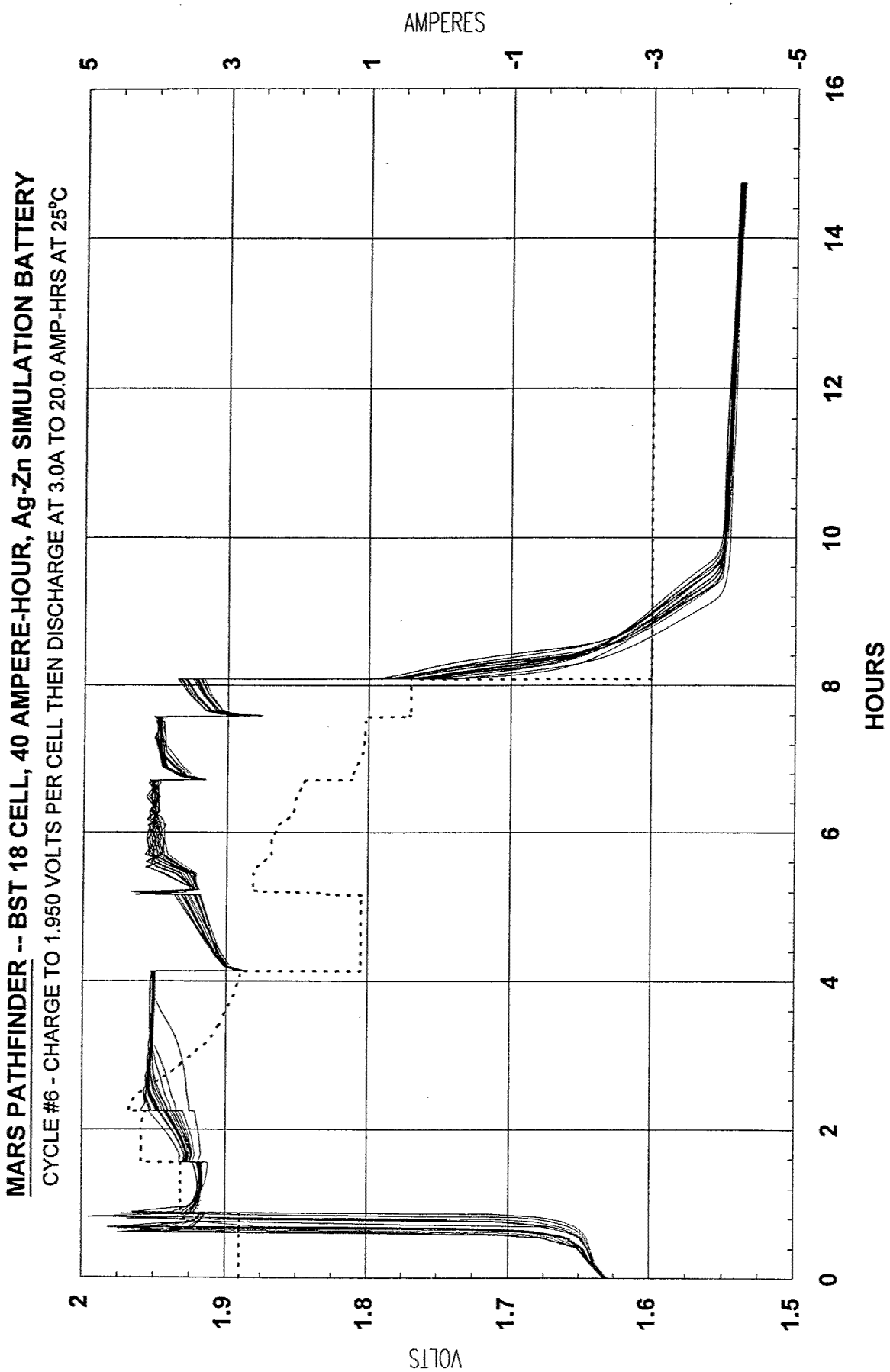

D. PERRONE 12/5/96 3:49 PM

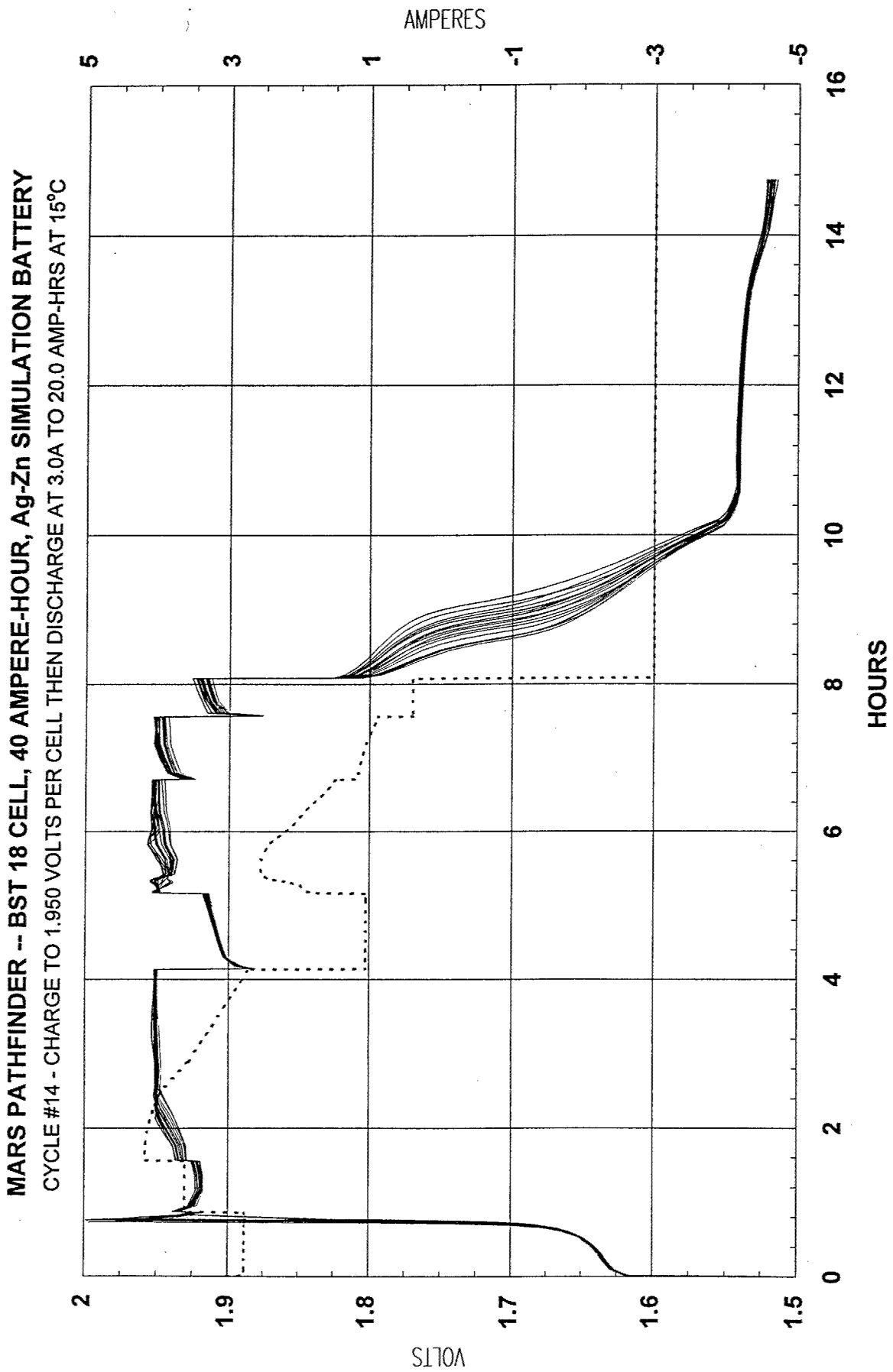
MARS PATHFINDER -- BST 18 CELL, 40 AMPERE-HOUR, Ag-Zn SIMULATION BATTERY
CYCLE #14 - CHARGE TO 1.950 VOLTS PER CELL THEN DISCHARGE AT 3.0A TO 20.0 AMP-HRS AT 15°C
AMPERES
5
3
1
-1
-3
-5
VOLTS
2
1.9
1.8
1.7
1.6
1.5
HOURS
0
2
4
6
8
10
12
14
16
D. PERRONE 12/5/96 3:50 PM

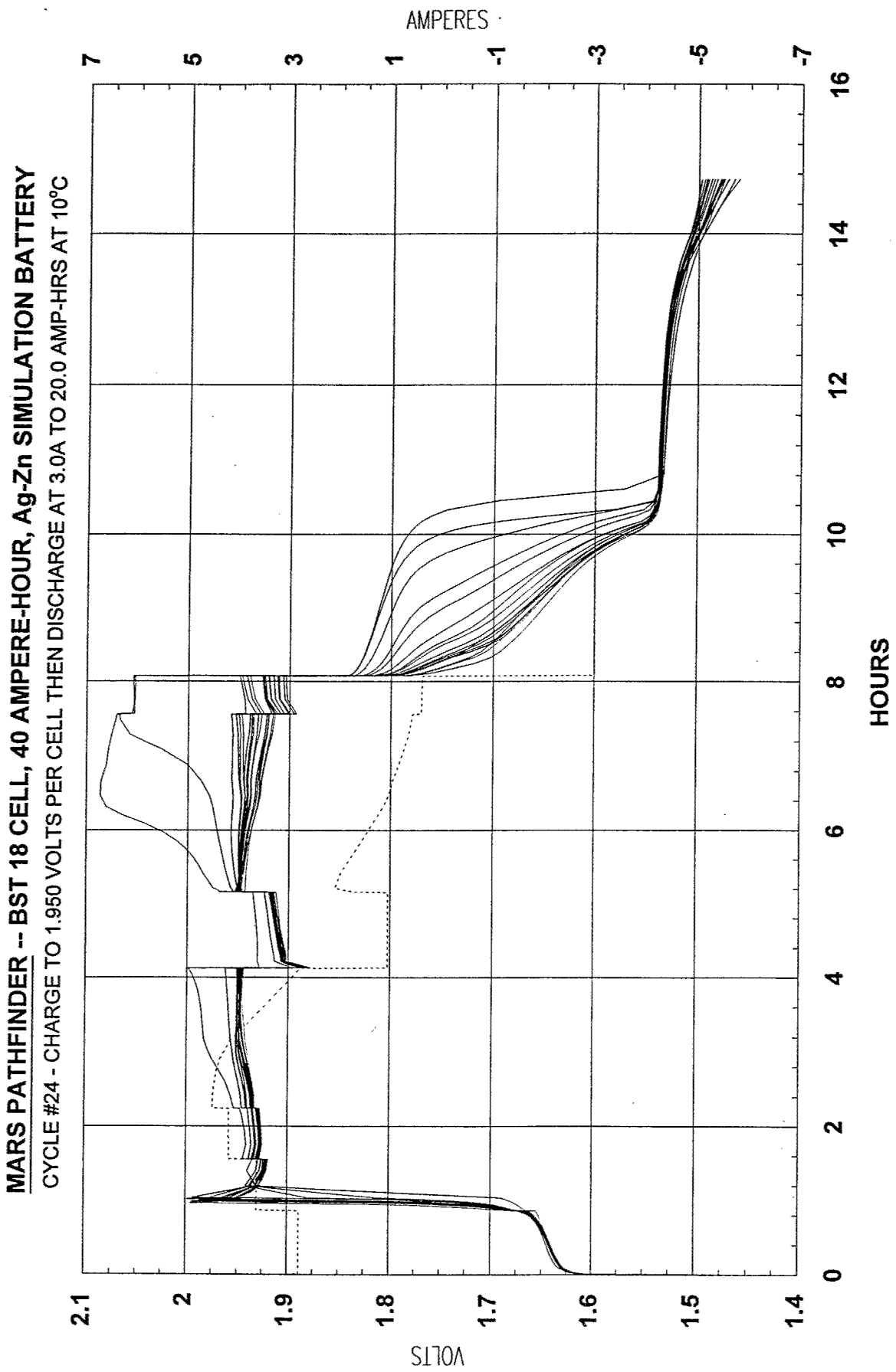

D. PERRONE 12/5/96 3:50 PM

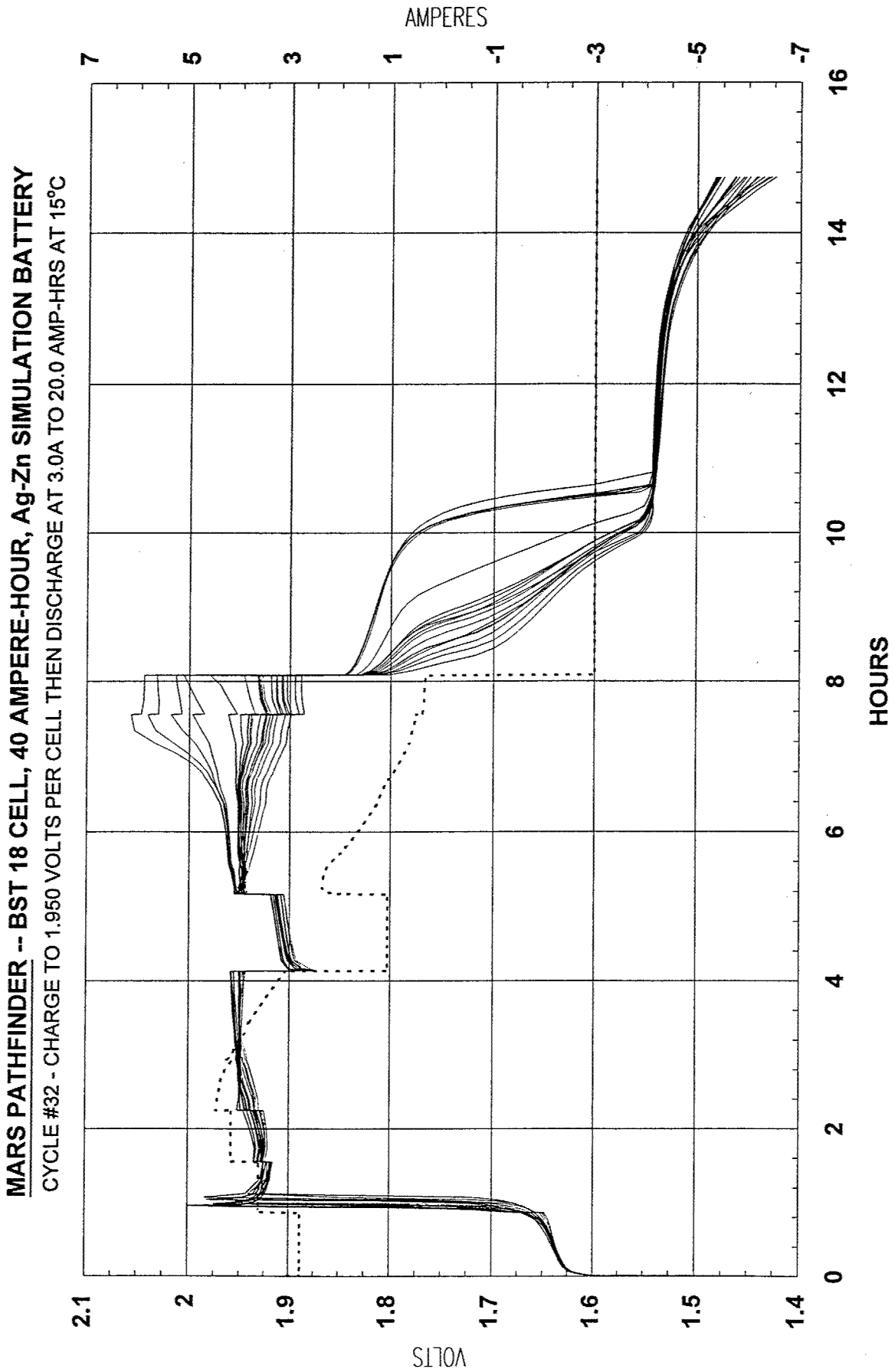

D. PERRONE 12/5/96 3:50 PM

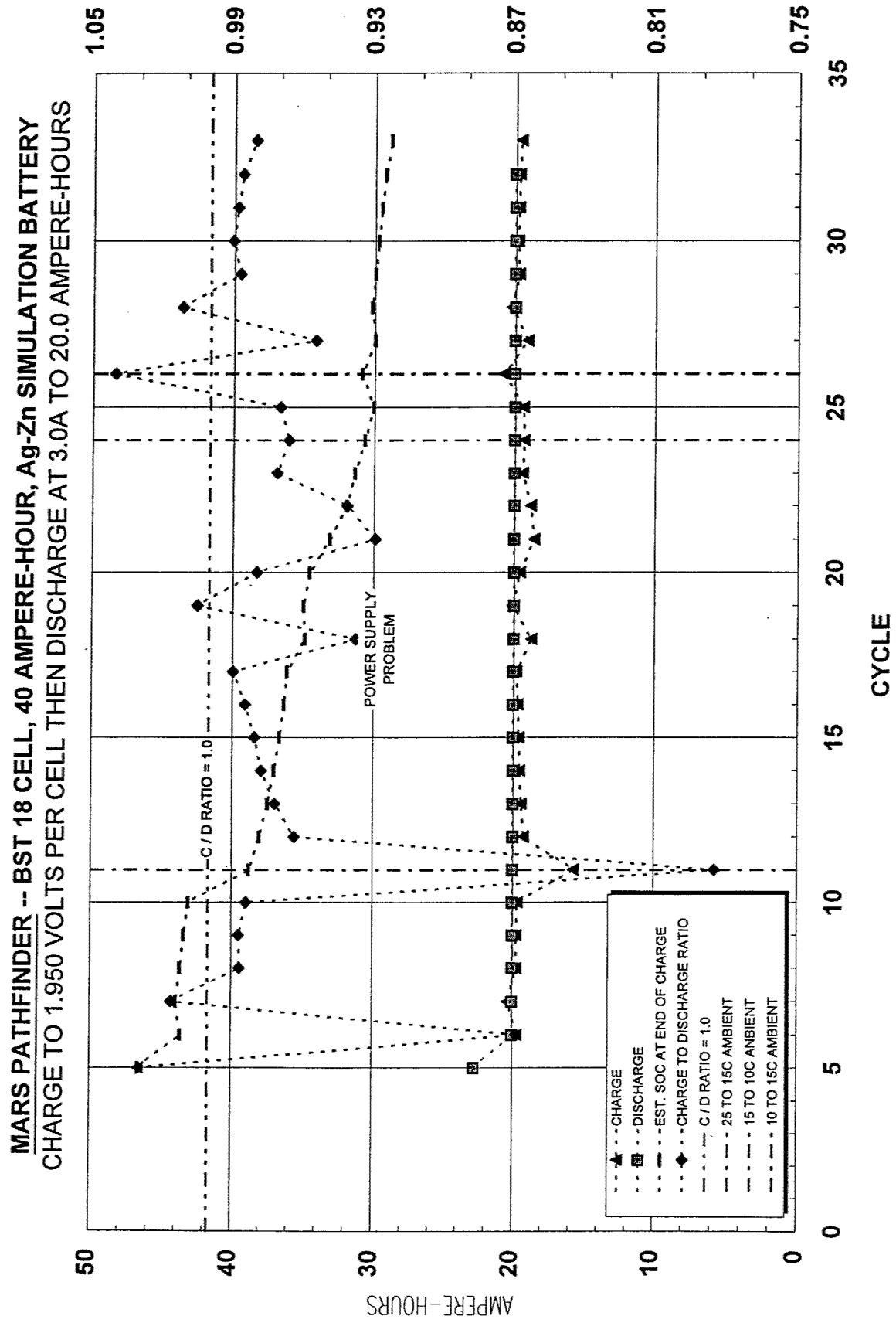

D. PERRONE 12/5/96 3:48 PM

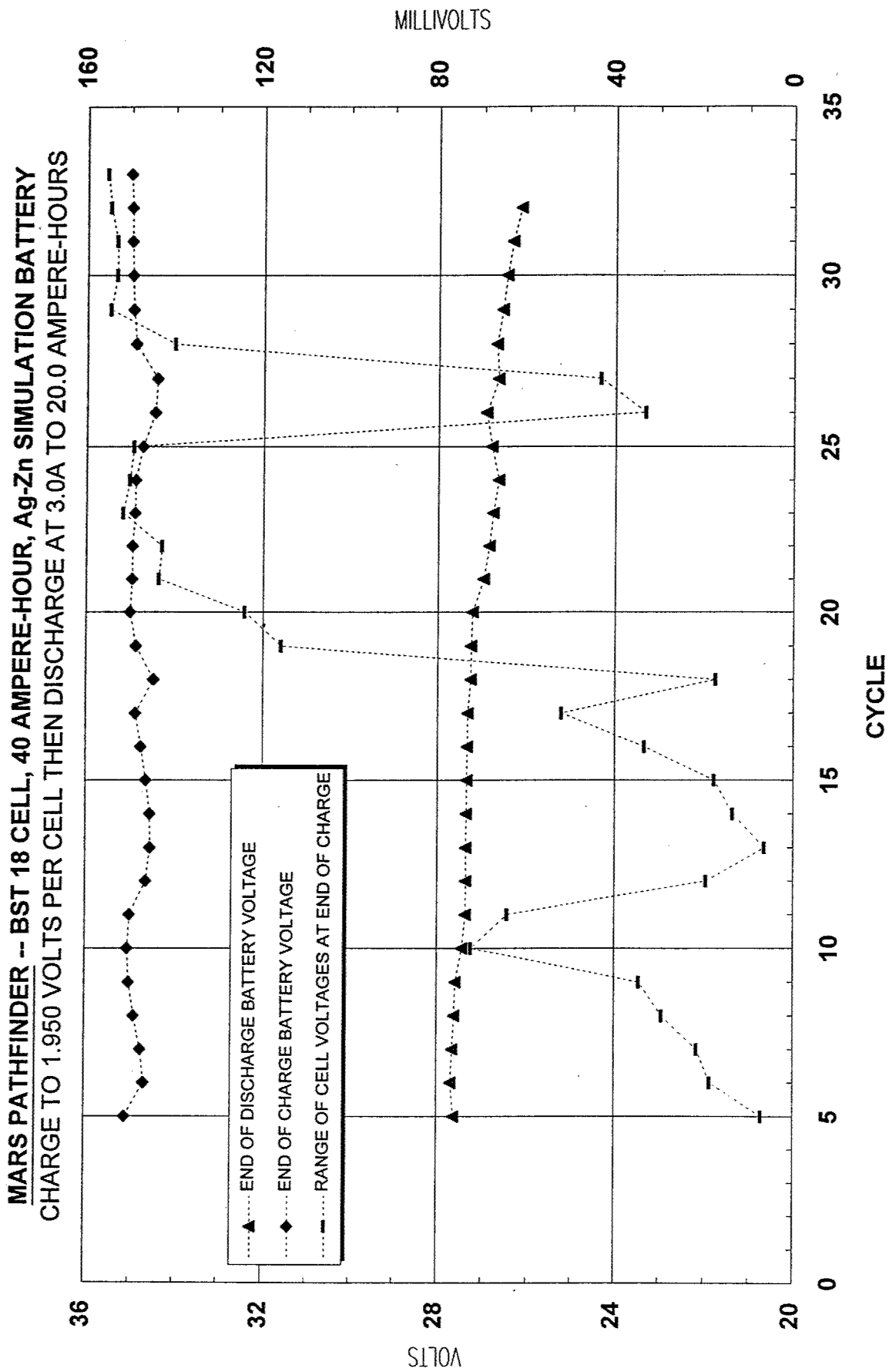

D. PERRONE 12/5/96 3:49 PM

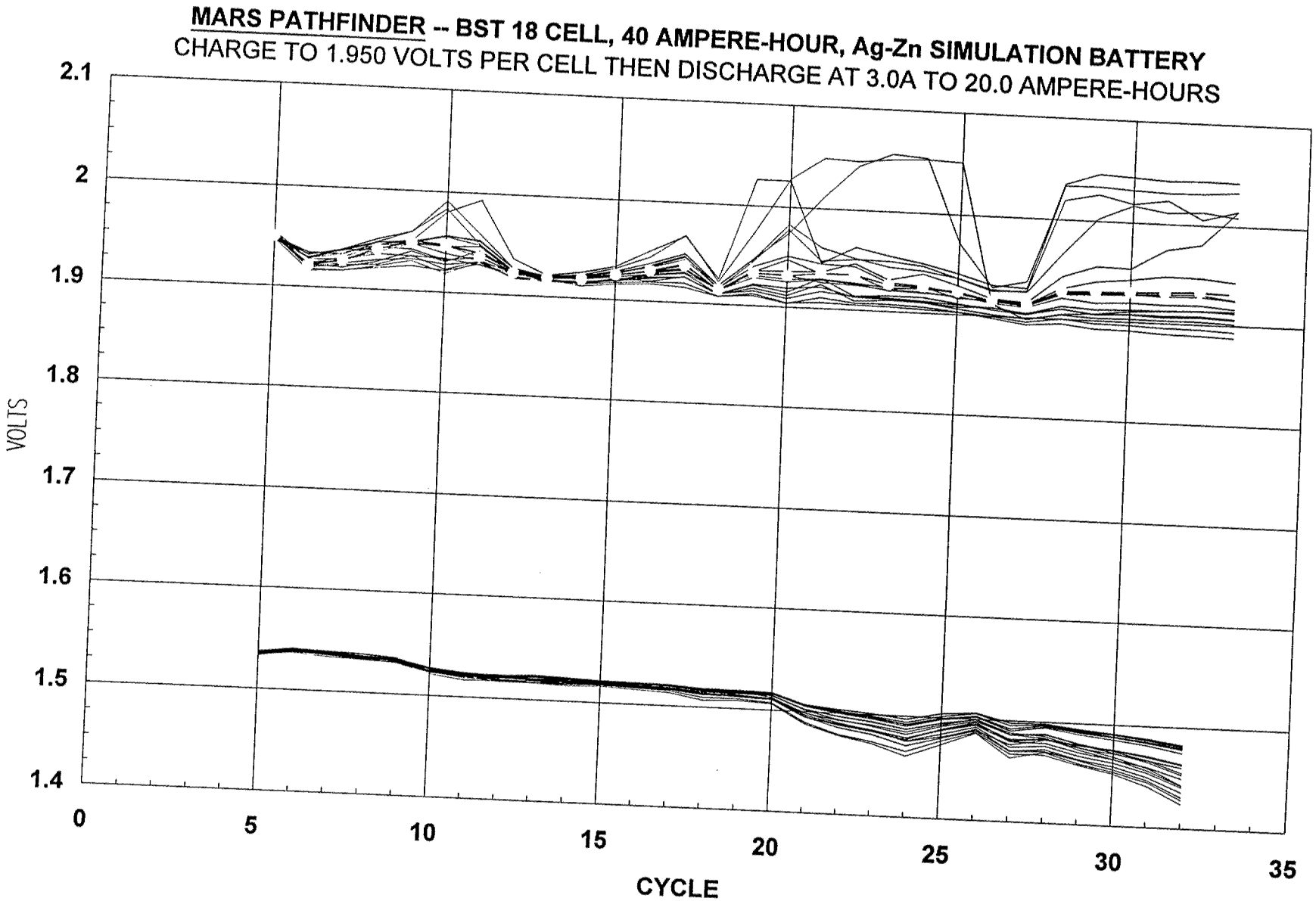

D. PERRONE 12/5/96 3:49 PM

Mars Pathfinder Battery - Conclusions

- Battery survived 47 days at 25°C and supported launch loads
- Battery survived a 7 month stand at 10 to -5°C
- Battery met and exceeded 40 ampere-hour capacity for EDL
- Battery met the 30 cycle minimum for Mars surface operation
- The projected power profile for Mars surface operation does not yield energy balance

Acknowledgment

- This work was performed at the Jet Propulsion Laboratory, California Institute of Technology under contract with the National Aeronautic and Space Administration.
- This work was sponsored by the Mars Pathfinder Project and the NASA office of the Chief Engineer (Code AE)
- Thanks to Zoe Adamedes and Mike Solis of BST Systems for battery engineering and manufacture.
- Thanks to Steve Dawson, Mike Shirbacheh, Burton Otzinger, and Subbarao Surampudi of JPL.

Page
114
Blank

INVESTIGATION OF AN ABERRANT CELL VOLTAGE DURING THE FILLING OF A LARGE LITHIUM THIONYL CHLORIDE CELL

By:
Lawrence H. Thaller and Michael V. Quinzio
Presented By: Margot L. Wasz
The Aerospace Corporation

For Presentation AT:
THE NASA AEROSPACE BATTERY WORKSHOP

HUNTSVILLE, ALABAMA
DECEMBER 3-5, 1996

An investigation was carried out to explain the out-of-family voltage trace associated with one of the 250 ampere hour lithium-thionyl chloride cells produced for an Air Force flight program. The voltage trace was generated during the manufacturing step where electrolyte is added to the cell while the open circuit voltage is monitored and recorded on a strip chart. Instead of recording a constant increase in cell voltage, there was a decrease in the open circuit voltage followed by a second period of increase to its expected value of greater than 3.6 volts. The intervening and unexplained drop in cell voltage was a cause of concern and an investigation into its cause was initiated. The investigation was carried out in several steps. First, discussions were held with the manufacturer. The manufacturer was able to suggest theories that were consistent with the observations that were available for review. The theories were later tested in the electrochemical laboratories of The Aerospace Corporation. Using specially constructed cells equipped with reference electrodes, the individual contributions of the anode, cathode, and cell container to the overall voltage transients associated with an interrupted cell filling process were measured. These results validated some of the manufacturers theories. What had been suggested as a minor contributor to the aberrant voltage trace was found by experimentation to be the most important one. That was the contribution of the porous carbon electrode. Our experiments added further support to the earlier conclusion that the out-of-family voltage signature seen in this cell was not indicative of a problem within the cell.

CELL DESIGN

- Manufactured by SAFT (Poitiers)
- 3.3 volts
- 250 A-hr, nominal capacity
- 300-500 Wh/kg energy density

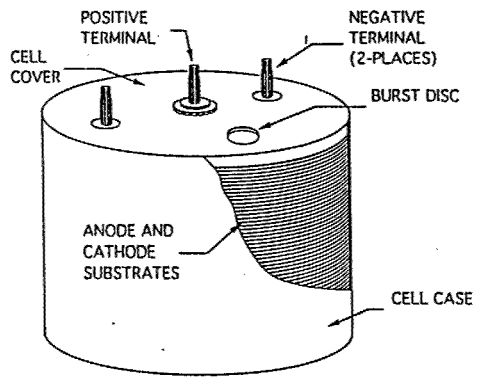

Energy Technology Department
Electronics Technology Center

THE AEROSPACE CORPORATION

SAFT manufactures large, 250 ampere hour cells using the lithium-thionyl chloride system. The cylindrical cell consists of a series of anodes, cathodes, and separators which are stacked horizontally within a stainless steel can. Electrodes are attached to bus bars located near the outer periphery which connect to two anode terminals and a single, insulated, cathode feedthrough. The cell container is held at the same potential as the lithium electrodes. The electrolyte is $SOCl_2$ with proprietary compounds added to alleviate the voltage delay. A single burst disk protects the cell against excessive internal pressure build-up.

PROBLEM: An out-of-family voltage trace was found during the filling of a production cell

- Voltages between the positive and both of the negatives are monitored during the filling process consisting of:
  - Integrity check
  - Pull vacuum
  - Electrolyte filling (1-2 minutes)
  - Settling (15-20 minutes)
- Was the out-of-family trace caused by a short that cleared? Could the short re-establish itself?

Energy Technology Department
Electronics Technology Center

THE AEROSPACE CORPORATION

An out-of-family voltage trace was discovered during the review of the strip charts recorded during the filling of a number of the lithium-thionyl chloride cells. Two strip charts are used during production to measure the voltage response during filling and settling between the anodes and cathode of the cell. Prior to filling, the integrity of the cell is measured by checking the resistance across the electrodes and a vacuum is established inside the the case. Filling is usually accomplished on the order of a few minutes and the cell is allowed to settle for 15-20 more minutes. An unexplained voltage drop was discovered in one of the traces for a cell. Although the chart showed that the voltage recovered to an acceptable open circuit voltage 25 minutes later, there was concern as to whether or not it might have been caused by a momentary short. A fully developed short can cause venting or an explosion. A short that has burned clear might be prone to reestablishing a destructive short at a later time.

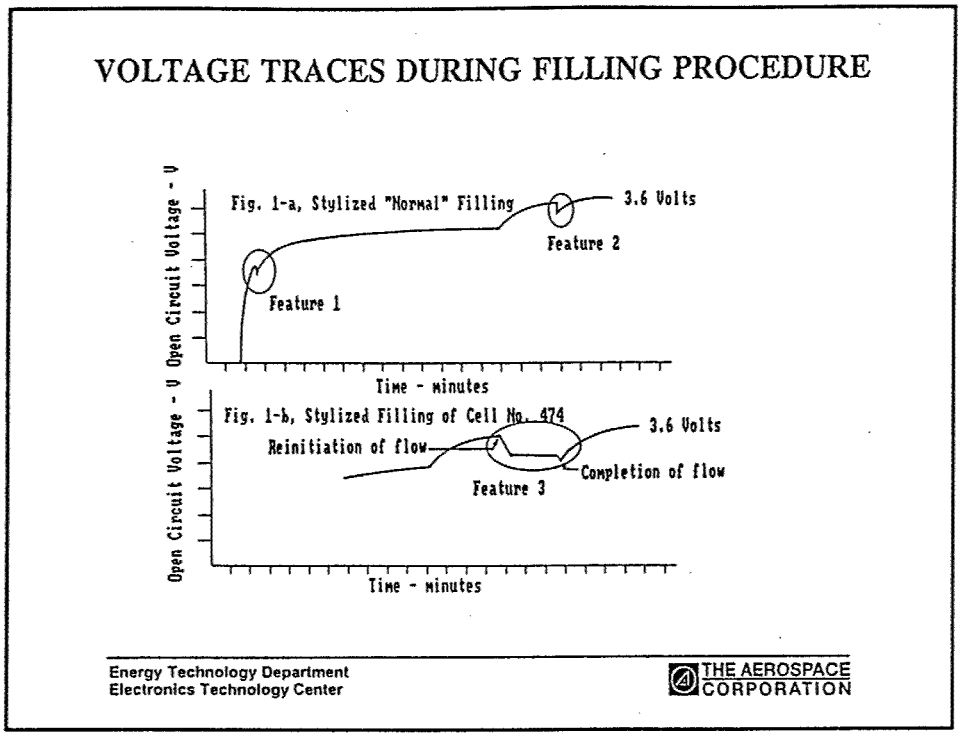

The top figure is a schematic of the typical voltage changes observed during the filling of a lithium-thionyl chloride cell with electrolyte. The two characteristic voltage dips occur just after electrolyte filling commences (Feature 1) and after the vacuum is broken when filling is complete (Feature 2). The abrupt change in slope prior to Feature 2 indicates a change in strip chart speed during settling. The lower figure is a schematic of the out-of-family voltage recorded for one of the cells. It was characterized by a steep voltage drop of about 75 millivolts, followed by a linear region which lasted about five minutes, and then another short duration voltage dip. However, after these events, the cell voltage exponentially increased to an open circuit voltage of about 3.65V. Upon review of their records, the manufacturer discovered that the filling of this cell had been interrupted to clear a blockage in the filling apparatus.

THEORIES

- SAFT records indicated that filling had been interrupted due to a line blockage. It was suggested that the voltage dip upon resumption could have been caused by:
  - Transient Mixed Potential of the Lithium Electrode
  - Passivation of the Stainless Steel Cell Container
  - Oxidation of the Cathode
- Aerospace initiated laboratory testing to verify which, if any, of these mechanisms were correct

Energy Technology Department
Electronics Technology Center

THE AEROSPACE CORPORATION

The manufacturer of the cell offered several explanations for the series of voltage dips encountered during interruption and restarting of the filling process. The lithium electrode may act as a combination lithium anode and rapidly corroding cathode as electrolyte covers its surface. During the time it takes the surface of the lithium electrode to passivate, it should display a mixed potential. The stainless steel cell case can act as a rapidly pacifying cathode when connected to the lithium electrode which might depress the open circuit voltage until passivation is complete. Finally, the porous carbon cathode could have sites which are oxidized by the thionyl chloride electrolyte upon contact. Though plausible, the magnitude of these three mechanisms, and the time scale upon which they acted, was unknown. Therefore, The Aerospace Corporation initiated a series of tests to evaluate each separately and together.

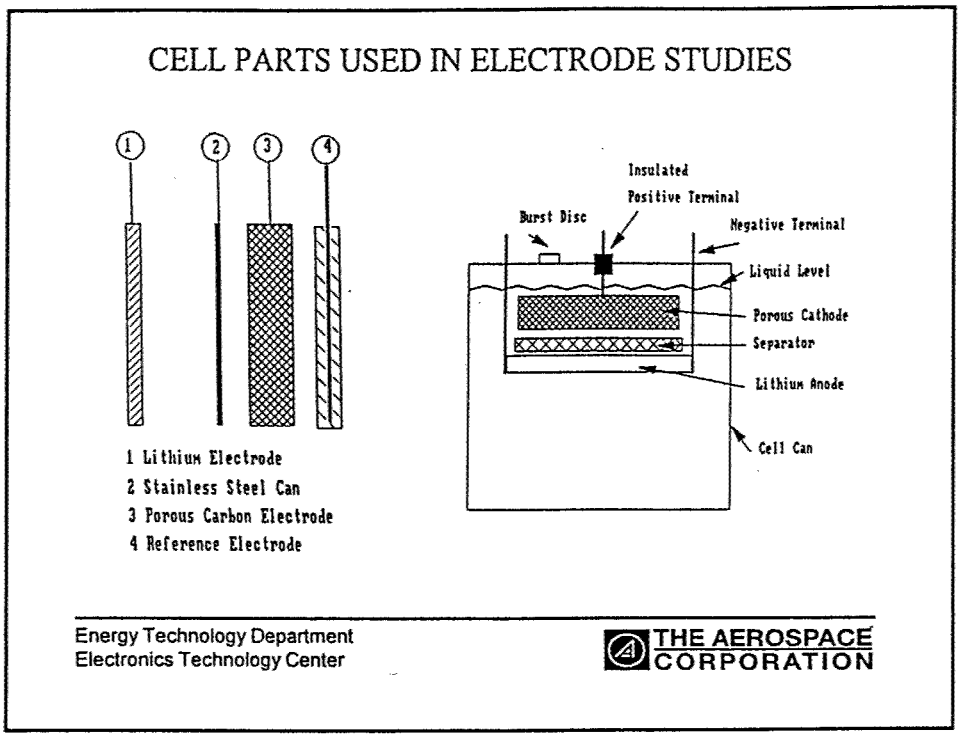

Several experiments were designed to explore the transient response of each of the three mechanisms separately. The figure above defines the schematic utilized in the following vue graphs to denote the various cell structures used in the studies. The lithium was battery grade foil from Lithcoa, the electrolyte was 1.5M tetrachloroaluminate dissolved in thionyl chloride. The cathode was a mixture of carbon black and Teflon pressed and heated on a stainless steel screen. The cell container was simulated using 304L stainless steel. The reference electrode was a strip of lithium that had been equilibrated in the electrolyte for at least five minutes to render it immune from any time dependent transients. Experiments were conducted in a glass beaker. Filling commenced using a burette and interrupted after adding 10% of the electrolyte to the test cell. After a two minute pause, the rest of the electrolyte was added.

TRANSIENT MIXED POTENTIAL OF THE LITHIUM ELECTRODE

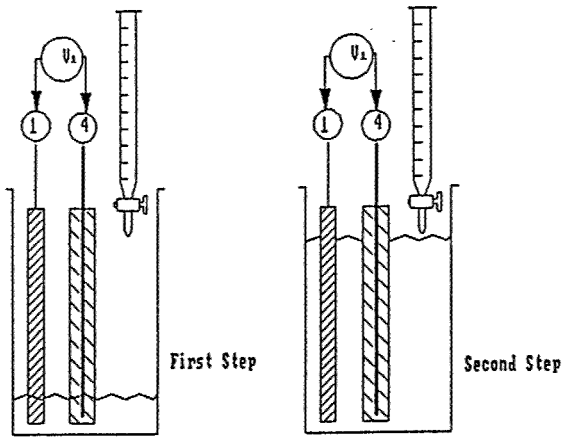

Energy Technology Department
Electronics Technology Center

THE AEROSPACE CORPORATION

This schematic shows the arrangement used to measure the transient voltage of the lithium electrode. When a fresh lithium surface is exposed to the oxidizing thionyl chloride, the surface is rapidly corroded as it forms a protective layer of lithium chloride.

$$4Li + SOCl_2 = 4LiCl + S + SO_2$$

When the second portion of electrolyte is added, the upper portion of the lithium will function as a redox cathode for a short period of time until it too has become passivated. Although most of the reaction occurs within seconds, the lithium chloride layer can continue to grow for days which contributes to the voltage delay.

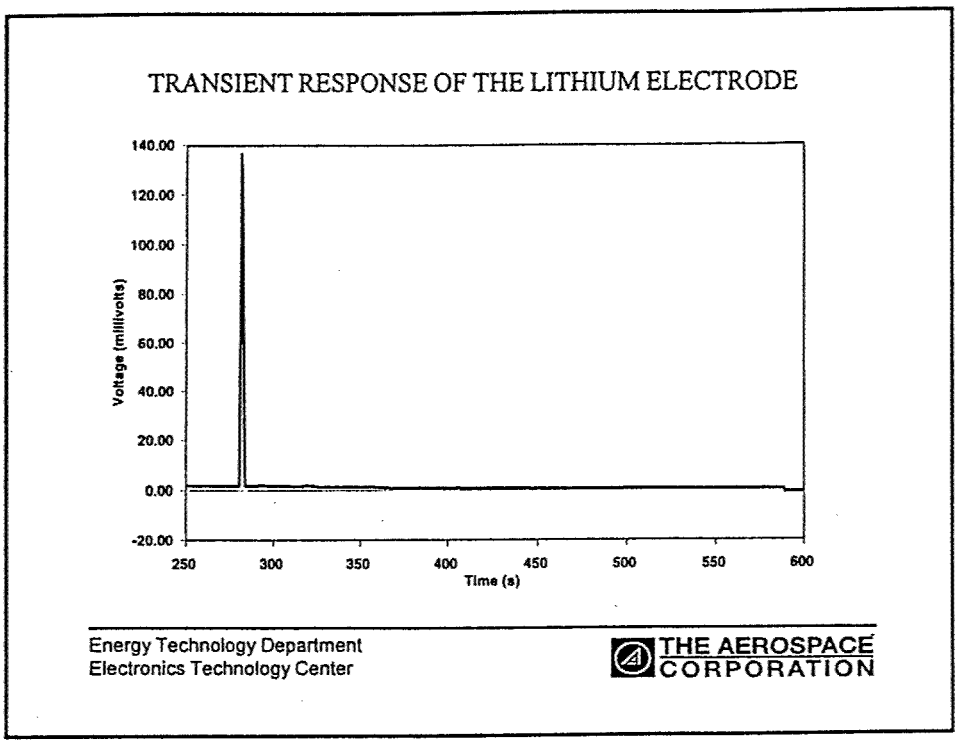

The above voltage response was measured during the final addition of the electrolyte in a cell containing just the lithium electrode. The voltage rose very sharply, about 135 millivolts above the reference electrode of passivated lithium. The transient only lasted about 5 seconds before returning very close to the potential of the reference electrode.

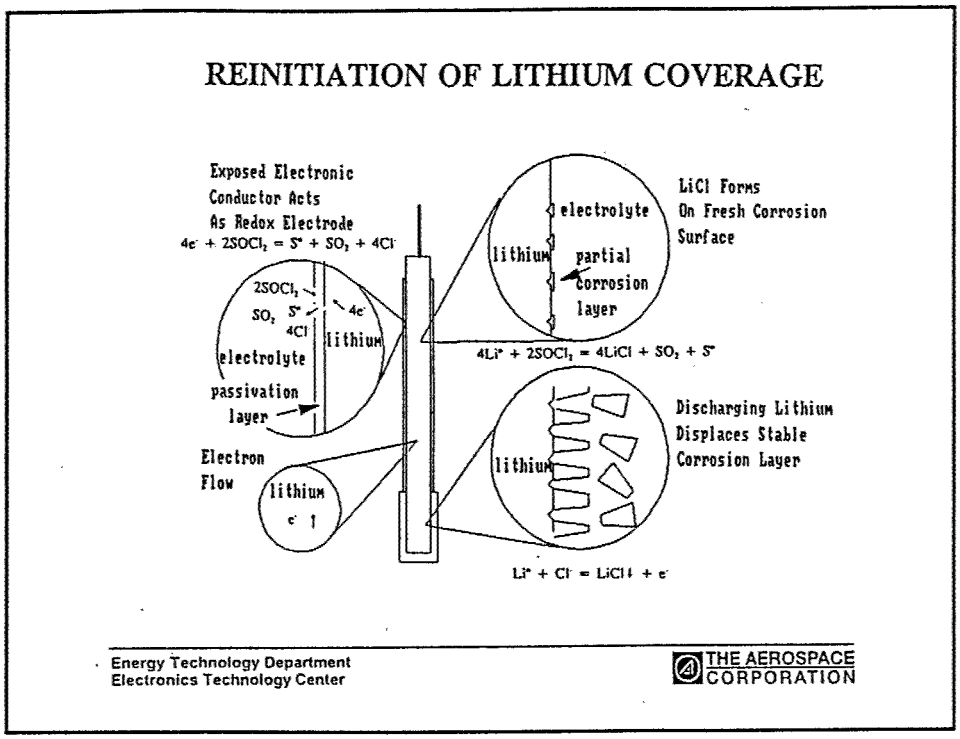

The chemical and electrochemical reactions taking place in the lithium electrode during the transient are shown schematically. Once a stable passivation layer is formed in areas that have been exposed to the thionyl chloride electrolyte, and new areas are subsequently exposed, the newly exposed areas function as an electrode for the discharge of thionyl chloride while the previously exposed areas are discharged. Electrons from the previously passivated portion of the lithium are supplied to the portion that is discharging thionyl chloride. As the passivation process progresses, the amount of current flowing between the two portions of the lithium diminishes. The reaction taking place at the lower portion of the the electrode is:

$$Li + Cl^- = LiCl + e^-$$

Thus the lithium electrode is acting as a redox electrode, and the surface functions only to interchange electrons to soluble species in the electrolyte. The reactions occurring on the newly exposed surface as it corrodes are:

$$4e^- + 2SOCl_2 = S + SO_2 + 4Cl^-$$

$$4Li + SOCl_2 = 4LiCl + S + SO_2$$

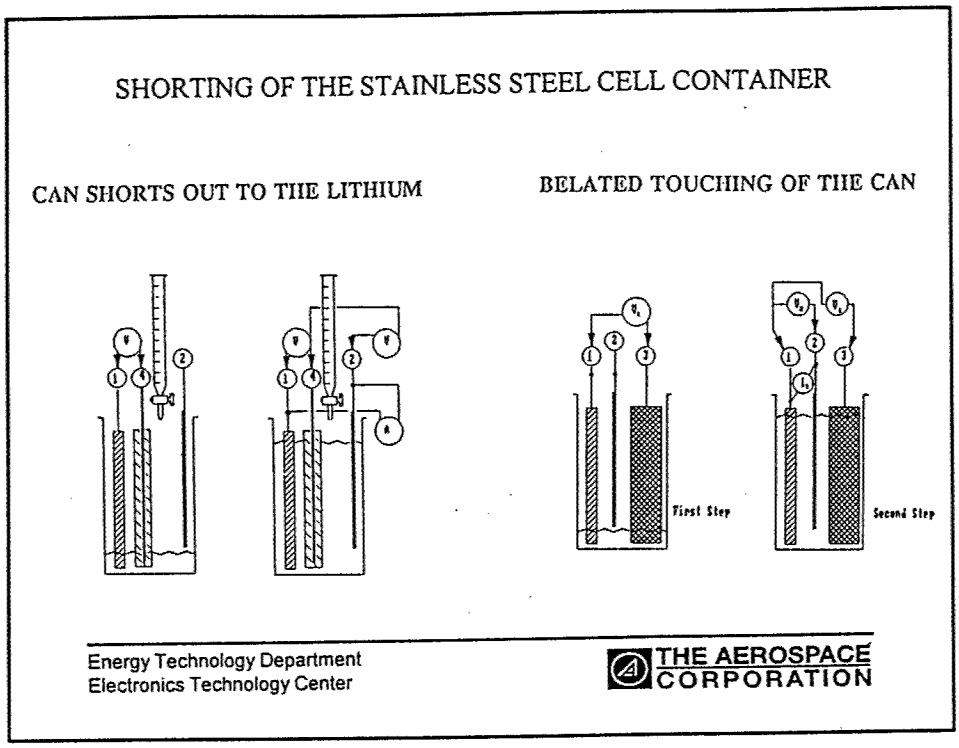

The influence of the stainless steel cell container was investigated using two different scenarios. In the first, the can is shorted to the lithium and the current measured while the stainless steel acts as a redox electrode for the the reduction of thionyl chloride until it is passivated. In the second configuration, the electrolyte does not contact the stainless steel can until after both the lithium anode and carbon cathode are wetted. When filling is resumed, both the lithium and the stainless steel act as rapidly passivating redox cathodes.

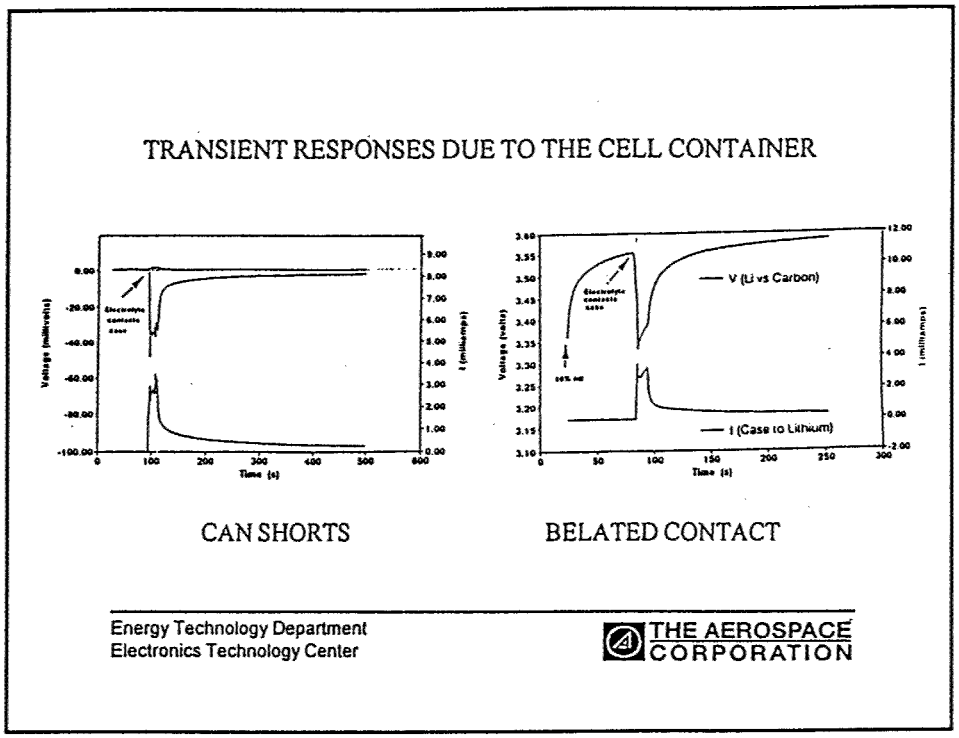

The figure on the left shows the transient of the current and voltages measured against the reference electrodes of the stainless steel shorted to the lithium electrode. The top curve shows a small voltage rise measured between the stainless steel and the lithium anode. The middle curve depicts the voltage drop as measured between the lithium anode and the reference electrode. The bottom curve is the measured current between the case and the lithium anode.

The figure on the right depicts the voltage measured following belated contact of the stainless steel to the wetted lithium and carbon electrodes. The traces shown are the voltage between the lithium anode and carbon cathode, and the current measured between the stainless steel and the lithium anode. The transients from both scenarios are rapid and last about 10-20 seconds.

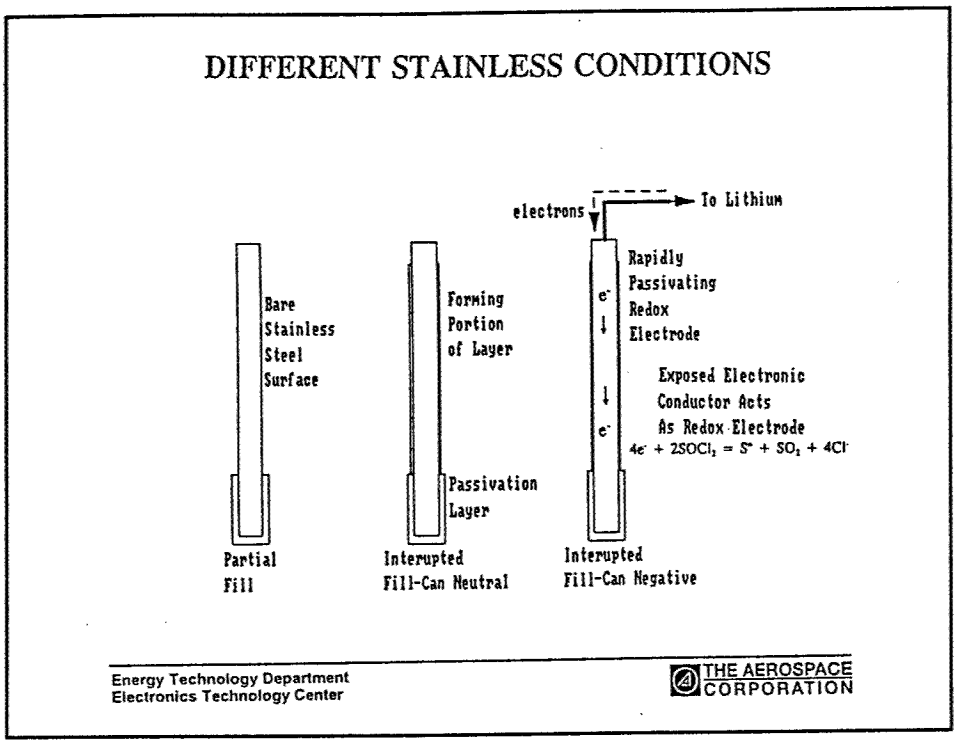

The stainless steel portions of the cell are protected by a passivation layer of chloride as a result of being oxidized by the thionyl chloride (left-hand side figure). When connected to the lithium anode, a complete electrochemical cell is formed which discharges active material until a passivation layer is formed on the stainless steel at which time the reaction falls to a negligible rate. In this case, the stainless steel acts as a redox electrode as shown in the right-hand side figure. In the case neutral position (center figure), the stainless steel still reacts with the thionyl chloride to form a passivation layer which protects the metal against further oxidation by the thionyl chloride.

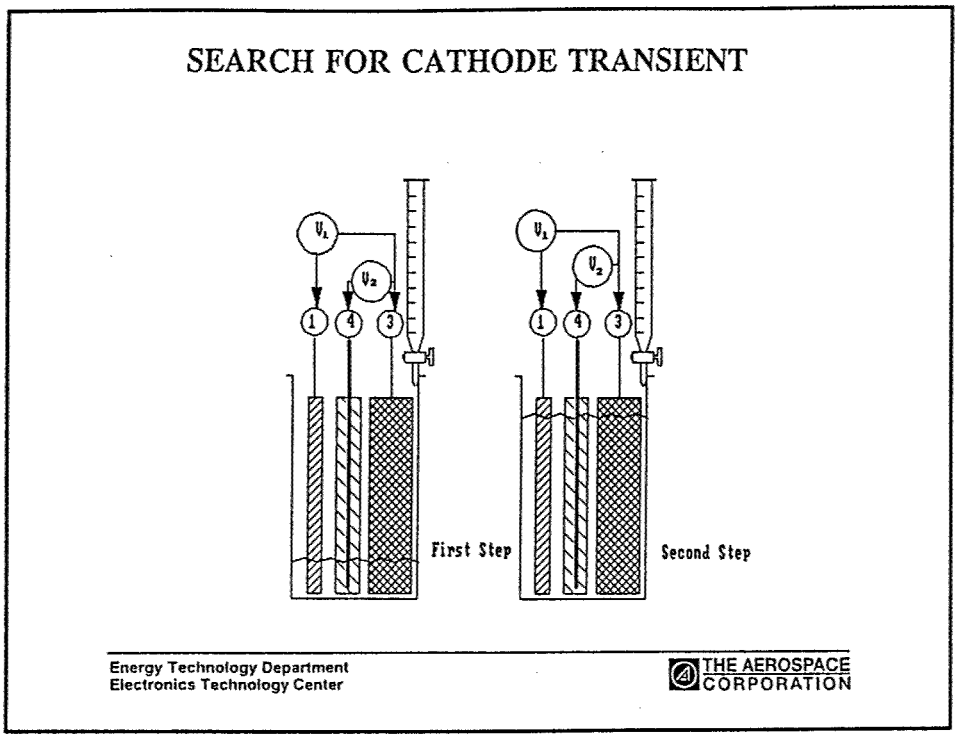

The porous carbon electrode is a candidate for the lowered voltage transients seen because it is formed in a reducing atmosphere and thus may have oxidizable surface sites that react upon exposure to the thionyl chloride. Also, the carbon electrode is partially non-wetting which could affect the rate of oxidation by the electrolyte. The above schematic shows the configuration used to measure the relative contributions of voltages from the lithium anode and carbon cathode in an interrupted filling process.

CATHODE VOLTAGE TRANSIENTS (FRESH CATHODE)

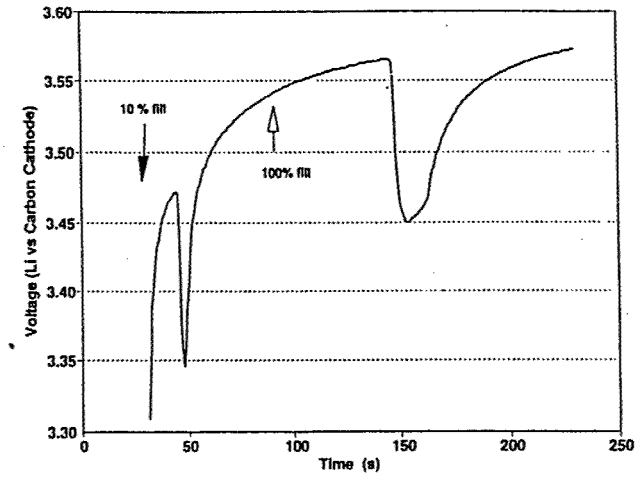

Energy Technology Department
Electronics Technology Center

THE AEROSPACE CORPORATION

This expanded voltage transient was measured between the reference electrode and the carbon electrode. It shows the characteristic initial dip (Feature 1) common to the normal filling process as well as the final dip at the end of filling.

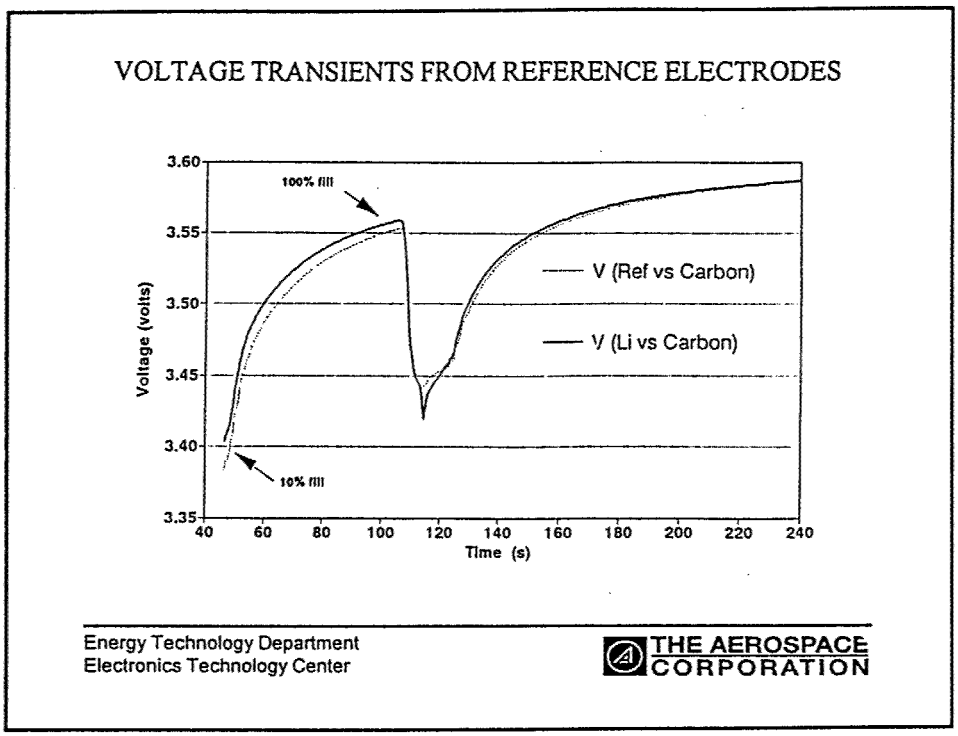

This figure shows the relative contributions of both the lithium and the carbon electrodes to the second filling transient shown on the last figure. It is evident that the majority of the response is due to the oxidation of the porous carbon electrode. Note that this voltage transient is much longer than the transients associated with the passivation of the lithium anode and the stainless steel can.

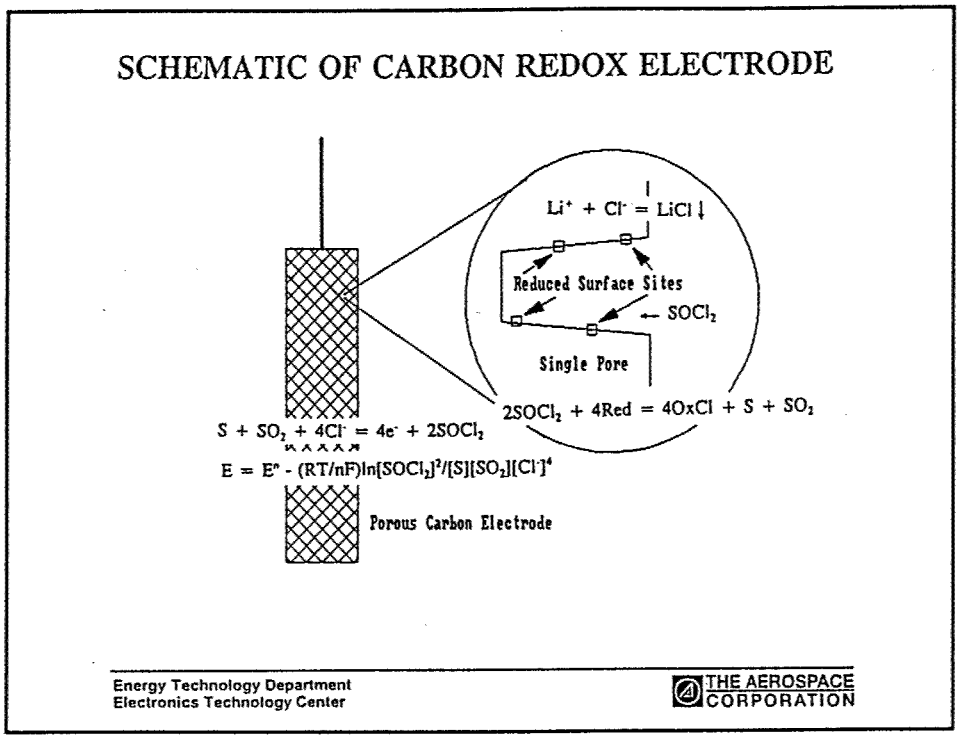

The figure above depicts the internal oxidation reaction by the thionyl chloride on the porous carbon electrode. The oxidation reaction can be described by the Nernst equation where the voltage is a function of the concentrations of species present. :

$$E = E^{o} - (nF/RT)\ \ln[SOCl_2]^2/[S][SO_2][Cl^-]^4$$

When new portions of the carbon cathode are exposed, there is a rapid drop in voltage (Feature 1), but not all interior sites are immediately oxidized. There is a slow recovery as reaction products diffuse out of the carbon electrode into the bulk electrolyte, and as a result, the voltage exponentially approaches the open circuit value. Porosity and wetting behavior also affect the rate of the oxidation of the cathode. Many of pores are at a higher pressure than the rest cell during the vacuum-filling process, and once vacuum is broken at the end of filling and the cell is exposed to atmospheric pressure, the electrolyte quickly penetrates these regions causing the final, short voltage dip identified as Feature 2 in the normal filling process.

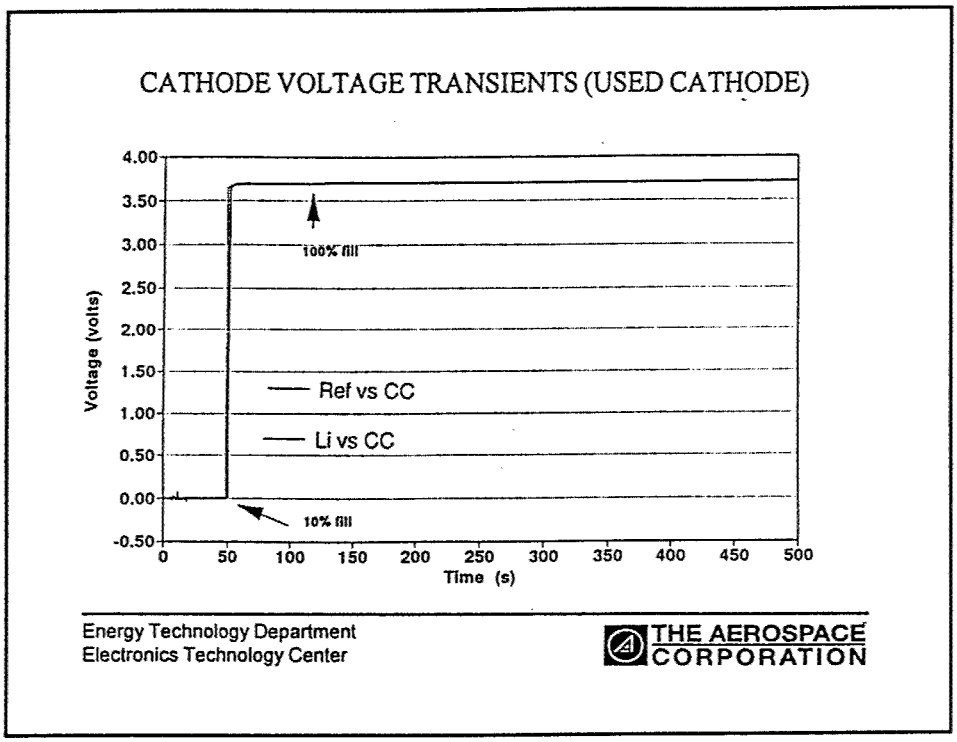

To test the hypothesis that the voltage transients were indeed caused by the oxidation of the carbon cathode by the thionyl chloride, the previous experiment was repeated with a fresh lithium anode and a used porous carbon electrode. The above voltage transients between the reference electrode and the carbon cathode, and between the lithium anode and the carbon cathode, were measured during the interrupted filling procedure. Note that there are no voltage dips, and Features 1 and 2 are absent.

SUMMARY STATEMENTS

- An aberrant voltage trace was noted during the review of cell filling data
- Incident was traced to an interruption during filling
- Experimentation suggested oxidizable sites within the carbon electrode were responsible for the drop in voltage
- The voltage anomaly could be reproduced by interrupting the filling of similar cells
- Anomalous voltage dip was not due to a short
- The battery containing this cell is scheduled for flight

Energy Technology Department
Electronics Technology Center

THE AEROSPACE CORPORATION

The out-of-family voltage signatures seen in the filling of the 250 ampere hour lithium thionyl chloride cell can be attributed to the response of the carbon electrode to interrupted filling. It is controlled by the rate of oxidation of the carbon cathode by the thionyl chloride. Both the magnitude and the time duration of the response, which were experimentally measured, were in accordance with the initial anomaly. Other interrupted filling tests of lithium-thionyl chloride batteries by the manufacturer reproduced the signature on similar cells. These studies showed that the response of the production cell was appropriate for an interrupted filling procedure and not indicative of a temporary short. The cell is now part of a nine-cell battery scheduled for flight.

NASA ARC

Galileo Probe

HUGHES

GALILEO PROBE BATTERY SYSTEM

B. P Dagarin, R. K. Taenaka, and E. J. Stofel
Hughes Space and Communications Company, El Segundo, CA 90245

Presented at the

1996 NASA Aerospace Battery Workshop

December 3-5, 1996

At the Huntsville Hilton Hotel
Huntsville, Alabama

© COPYRIGHT 1996
HUGHES ELECTRONICS

Galileo Probe

Galileo Probe Battery System

CONCLUSIONS

NASA ARC HUGHES

December 1996

- Battery performance met mission requirements, with margin
- Extensive ground-based and flight tests of batteries prior to Probe separation from Orbiter provided good prediction of actual entry performance at Jupiter
- Li-SO_2 battery was an important choice for Probe's main power:
  - good energy density,
  - established manufacturing processes,
  - excellent energy retention in extended storage,
  - acceptable limit on voltage delay at start-up

ACKNOWLEDGMENTS

- The Galileo Probe was designed and built by Hughes Space and Communications under the direction of the NASA Ames Research Center, Contract NAS 2-10000
- Li-SO_2 batteries were manufactured by Alliant Techsystem Power Sources Center (previously Honeywell PSC), with continuing technical support during entire mission
- Thermal batteries were manufactured by Eagle-Picher Industries
- Dual use of Li-SO_2 and thermal batteries was suggested by General Electric
- Supportive diagnostic measurements and helpful discussions were provided by several personnel at the Sandia National Laboratories

Galileo Probe Battery System

GALILEO PROBE MISSION

NASA ARC | HUGHES

December 1996

- Galileo Probe was the first spacecraft to enter and measure an outer planet atmosphere
- There was a 6-hour pre-entry and entry operation in addition to the 1-hour atmospheric descent on the main parachute
- 6 science instruments measured various atmospheric parameters
- Data was telemetered to the Orbiter spacecraft, which later relayed the data to Earth (in non-real time)

SCHEDULE

- 1977 - Program approved by Congress
- 1979-81 - Fabrication of principal Probe hardware
- 1982-86 - NASA made several revisions to launch schedule
- 1981-88 - Multiple rebuilds of Li-SO_2 batteries
- 1989(Oct) - Launch by Shuttle, with Probe attached to Orbiter
- 1989-95 - Cruise, via Venus+Earth+Earth Gravity Assist (VEEGA)
- 1995(Jul) - Probe separated from Orbiter, for trajectory divergence
- 1995(Dec) - Jupiter Encounter

The Galileo Probe required an internal source of electrical power. The source was required to remain quiescent for several years with minimum loss of stored energy, then be activated to drive the scientific instruments and the radio transmitter for a few hours as the Probe approached and then entered the Jovian atmosphere. Primary batteries were ideal for this application.

The Li/SO_2 batteries were built by Honeywell Power Sources Center, in Horsham, Pennsylvania (recently renamed Alliant Techsystems). Because the Galileo Program was very ambitious, several times during its development the launch schedule was postponed. Most of these were due to difficulties in providing an adequate launch vehicle for the mission. None of these delays were ever due to any problems with the batteries—nevertheless, with each Program delay new Li/SO_2 batteries were fabricated so that the freshest possible units would be available for the revised launch schedule. Thus, battery manufacturing and testing was repeated several times at Alliant. The first acceptable flight units were from manufacturing Lot 3, the final units, as used for the actual Galileo flight, were from Lot 10. While most of the intervening lots demonstrated adequate performance during their respective lot qualification tests, it is interesting to note that Lots 3 and 10 showed the best performance. The commonalty between these two great lots was the fact that their electrolyte was mixed by hand rather than by a mechanized batch mixer that was common to the intervening lots.

The thermal batteries were built by Eagle Picher Industries in Joplin, Missouri. Development of these had included a redesign of the header insulation. The batteries of manufacturing Lot 6 passed all qualification tests well. Because of the Galileo Program delays, there were recertification tests run on samples of these thermal batteries, but these tests showed that there was no need to rebuild fresher batteries.

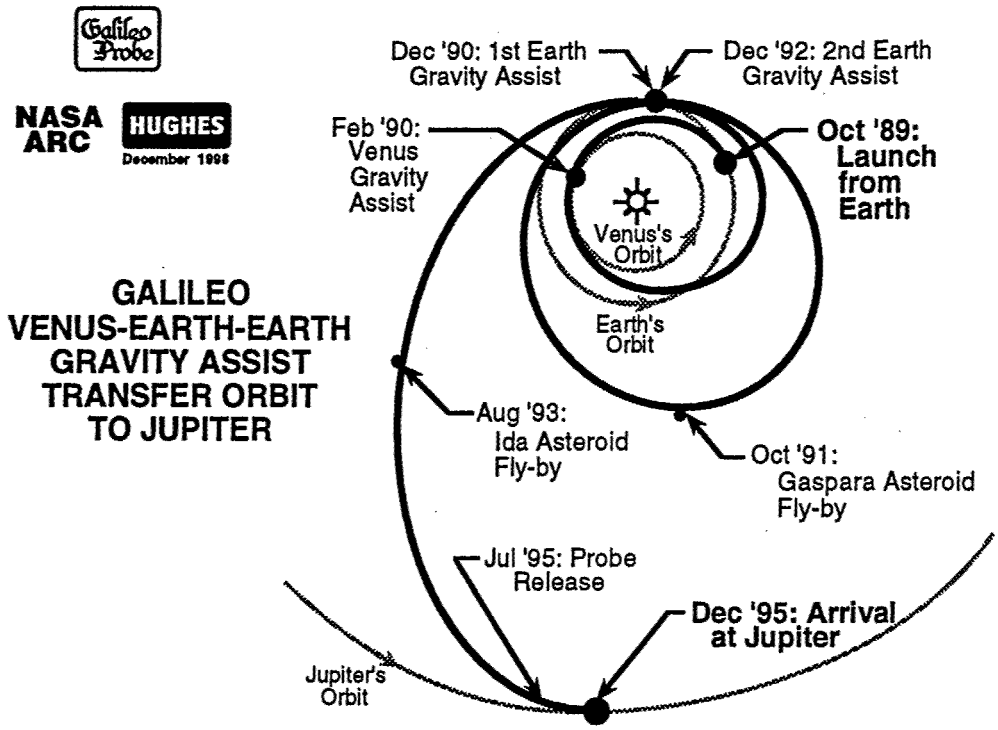

The VEEGA mission was devised by JPL in 1986 as an alternate to the originally planned direct route to Jupiter. That direct route had to be abandoned after the required Centaur upper stage was declared unsuitable for use with any future Shuttle launch—it was deemed to be potentially too dangerous by the committee that conducted the in-depth NASA safety review that had followed the disastrous launch attempt of the Challenger Shuttle in January 1986. Upon the acceptance of the VEEGA alternative, the transit time from Earth to Jupiter escalated from the 2 years that had been planned for the Centaur driven direct transit to a 6 year VEEGA journey following a circuitous route of approximately 2.4 billion miles.

The tripling of the transit duration was a real concern to the battery engineers—there were insufficient data available at that time to assure that Li/SO_2 batteries would remain fully viable for such a long duration. We initiated a life-time assessment study at Sandia National Laboratories (SNL) under the direction of Dr. Sam Levy, using representative sample cells subjected to a variety of elevated temperatures. That comprehensive and enlightening study is documented in SNL Report No. SAND88-2218•UC-94C. The shelf life changes found by the SNL work indicated a worse case loss of no more than 0.04 Ah/yr, assuming a 6 year temperature of 0°C, the temperature expected for the VEEGA transit. This was considerably more optimistic than the 0.2 Ah/yr assumption that had been used until that time. This represented a substantial reduction in the estimate of the battery capacity loss, giving the battery engineers and the Probe Program Office a great deal of confidence in the stability of our primary power system.

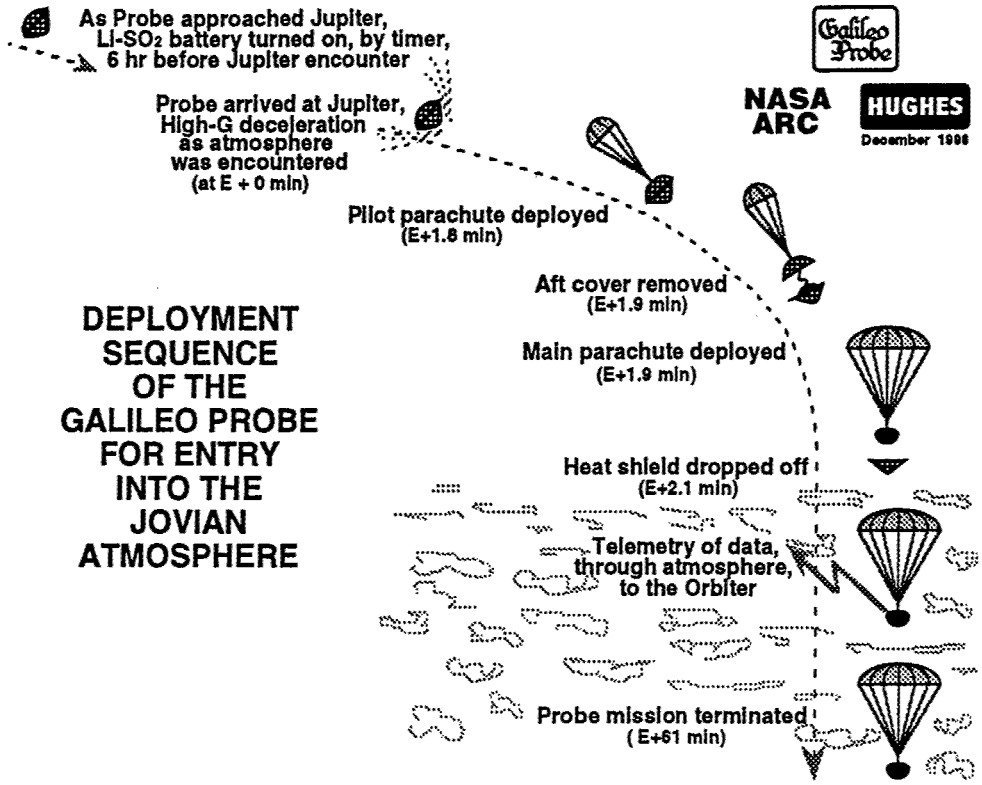

The Probe was separated from the Orbiter near midnight on July 12, 1995. The Probe was released on a ballistic trajectory toward its target zone on Jupiter at 6.57 deg ± 0.5 deg north latitude near the night-day terminator with an entry flight path angle of –8.6 deg ± 1.4 deg. We were well within the tolerance on both parameters.

Before Probe release, the modest power requirements of the Probe had been supplied by the attached Orbiter through an umbilical cord. After release, all Probe power was supplied by its on-board batteries. For the subsequent 5 month Coast phase the only significant electrical load was the on-board clock, set to awaken the Probe's electronics 6 hours prior to Encounter. The clock was set just before Probe release. It ran from only battery Module 3, leaving the other two modules undisturbed. The 5 month wake-up occurred with precision—within 18 seconds of the nominal time even though a tolerance of 8.6 minutes would have been permitted.

The Probe functioned flawlessly throughout the Coast and the Pre-Entry Periods. All of the Coast and the first 5.5 hours of the Pre-Entry period were single string operations. Initial turn-on, at Entry–6 hr, was the time at which the three battery modules underwent their battery clean-up (or depassivation) of the lithium anodes.

At the atmospheric Encounter, the Probe survived entry deceleration and its heating very nicely but was 53 seconds late in deploying the main parachute. This was due to a harness wiring error—the thermal and Li/SO_2 batteries satisfied all their Entry deployment functions properly.

The parachute controlled Descent phase operated well, with the Li/SO_2 batteries providing all required power. The Probe achieved a depth equivalent to 24 bars pressure before we lost our RF link due to extreme temperature and pressure on the RF transmitter. This Probe performance exceeded our core mission requirement, which had been merely to reach at least 10 bars.

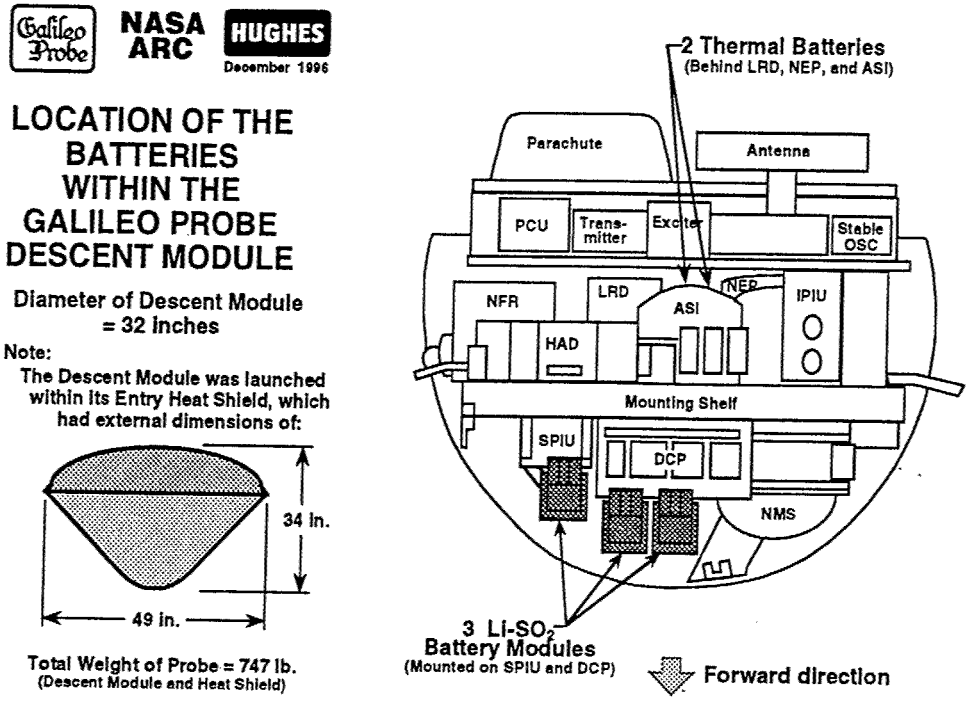

The descent module was designed and built by Hughes Space and Communication Company. A major subcontractor was the General Electric Re-Entry Systems Division (now part of Lockheed-Martin) who designed and built the deceleration subsystems, i.e., the heatshields, separation mechanisms, and the parachutes.

The descent module was designed to be as compact as possible to minimize the size and therefore the weight of the surrounding heat shield. The electronics and all other components therein were very densely packaged. The mechanical design of the battery modules provided a conformal shape to match the limited space. It also provided mechanical ruggedness to survive Entry deceleration along with thermal isolation during discharge to protect sensitive surrounding electronics.

The Probe's science instrument compliment and principle investigators are:

Neutral Mass Spectrometer: Hasso Niemann, NASA-GSFC

Helium Abundance Detector: Ulf von Zahn, Univ. of Rostock, Kühlungsborn, Germany

Atmospheric Structures Instrument: Alvin Seiff, San Jose State Univ. Foundation, San Jose, CA

Nephelometer: Boris Ragent, San Jose State Univ. Foundation, San Jose, CA

Net Flux Radiometer: Larry Sromovsky, Univ. of Wisconsin, Madison, WI

Lightening & Radio Emissions Detector: Louis Lanzerotti, Lucent Labs., Murray Hill, NJ

Energetic Particle Instrument: Harold Fischer, Univ. of Kiel, Kiel, Germany

Doppler Wind Experiment: David Atkinson, Univ. of Idaho, Moscow, ID

The science instrument package weighed 66 lb, 24% of the 278 lb descent module.

The three Li/SO_2 modules weighed a total of 16.5 lb, 6% of the total descent module. Each of these battery modules was 2.8 in. by 3.5 in. by 14.0 in.

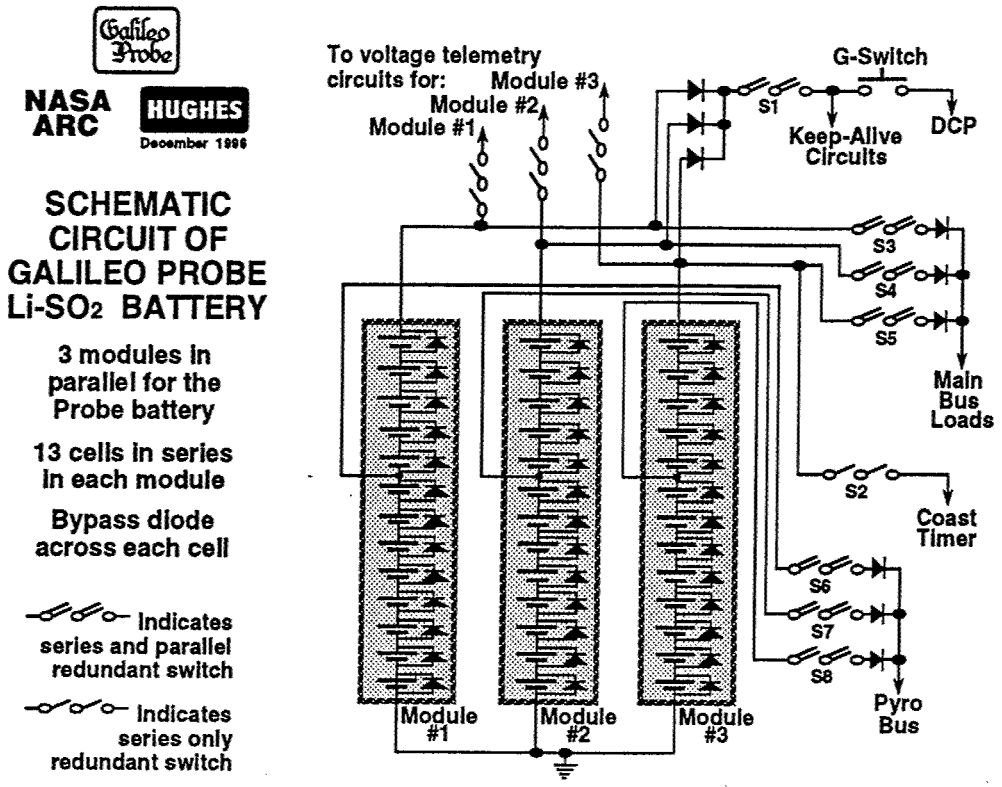

The Probe power subsystem was a simple but well planned design with careful effort put forth to assure that the Li/SO_2 battery modules were provided the utmost protection from detrimental effects of any inadvertent single part failure. Special attention was given to circuit failures that might prevent any module from being coupled to the mission loads under command or that might inadvertently drain any battery module prior to the Probe's arrival at Jupiter. The above schematic battery circuit shows locations of key redundant series+parallel switches.

The modules were also designed with internal by-pass diodes across each cell so as to prevent the loss of a complete module if any one of its constituent cells would have failed due to an open circuit, an abnormal capacity loss, or by any other means.

Each module was equipped with two sets of electrical connectors: a power connector and a test/by-pass connector. The latter permitted fusing, as a safety precaution, during all ground-based system tests. Furthermore, whenever the by-pass fused plugs were physically removed, the modules became disarmed so that it was impossible to discharge any of them even if a power switch had been closed inadvertently during any test operation. As final preparation before launch, at the launch site, the fused by-pass plugs were removed; and hard wired plugs substituted. After that time, the three module power connectors provided direct access, without fusing, to the above indicated switches leading to the Probe's power bus.

Just prior to launch, as well as multiple times during the preceding ground tests, we measured the wire harness between the modules and the power relays under applied system voltage to verify that any current leakage was less than 150 nA. This low leakage requirement was especially important for assuring that any external battery drain during the 6 year transit from Earth to Jupiter would be negligible.

Galileo Probe Battery System
THERMAL BATTERY

NASA ARC | HUGHES

December 1996

- Used as the energy source to fire the large, staging pyrotechnics for release of heat shield and parachute
- Two independent thermal batteries on Probe, each with two electrically parallel cell stacks, thus providing redundancy
- Each thermal battery activated by firing its internal squibs (two, for redundancy) using energy from Li-SO_2 battery
- Ca and $CaCrO_4$ Electrodes
- KCl+LiCl Eutectic Electrolyte
- Zr+$BaCrO_4$ Thermal Paper
- Storage Temperature = Room
- Activation Temperature > 400 C (above the melting temperature of KCl+LiCl)
- Battery Voltage = 37 V (open circuit)
- Current requirements:
  - 6 pulses, ranging from 5.3 A to 15.9 A, each 22 ms in duration, distributed sequentially within an interval of 13 s

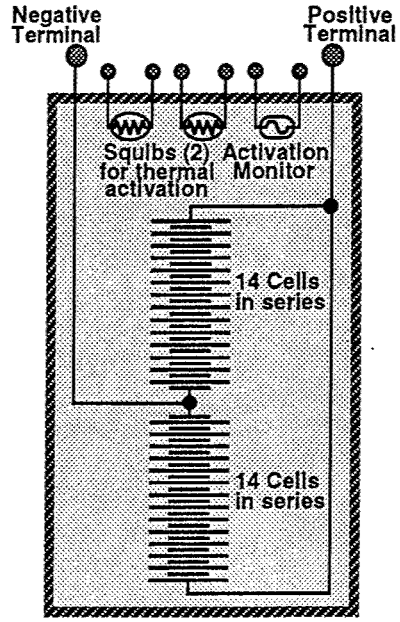

The Ca/$CaCrO_4$ thermal batteries were used for the sole purpose of supplying the few large current pulses required for firing the pyrotechnic pressure cartridges that jettisoned the heat shields and deployed the parachute. The use of these supplemental, single purpose batteries avoided placing large pulses on the main power bus which could otherwise have had a deleterious impact on the Probe's command sequencer.

The two miniature squibs within each thermal battery were redundant, fired sequentially from an 8-cell tap on each of the three 13-cell Li/SO_2 modules. The later three modules operated in parallel, for redundancy. The demand for the pulsed power to activate the large cartridges occurred within an interval of less than a minute, so thermal batteries were the logical choice for this application. They remained hot, and therefore active, for longer than was necessary to satisfy the pulsed current requirements.

Systems development tests demonstrated that a small, resistive load connected continuously across the activated thermal batteries aided the maintenance of their voltage stability during the pulsed load demands. The thermal batteries had more than enough capacity to supply that small continuous load as well as the large pulses.

The performance of the thermal batteries during the actual descent of the Probe into the Jovian atmosphere was not monitored directly—their rise in voltage and their all important current pulses would have been too rapid to have been recorded at the low data rate that had been allocated for monitoring functions within the Probe. However, from our analysis of the overall flight data we can deduce that the thermal batteries performed their required function, releasing the heat shield and parachute upon demand.

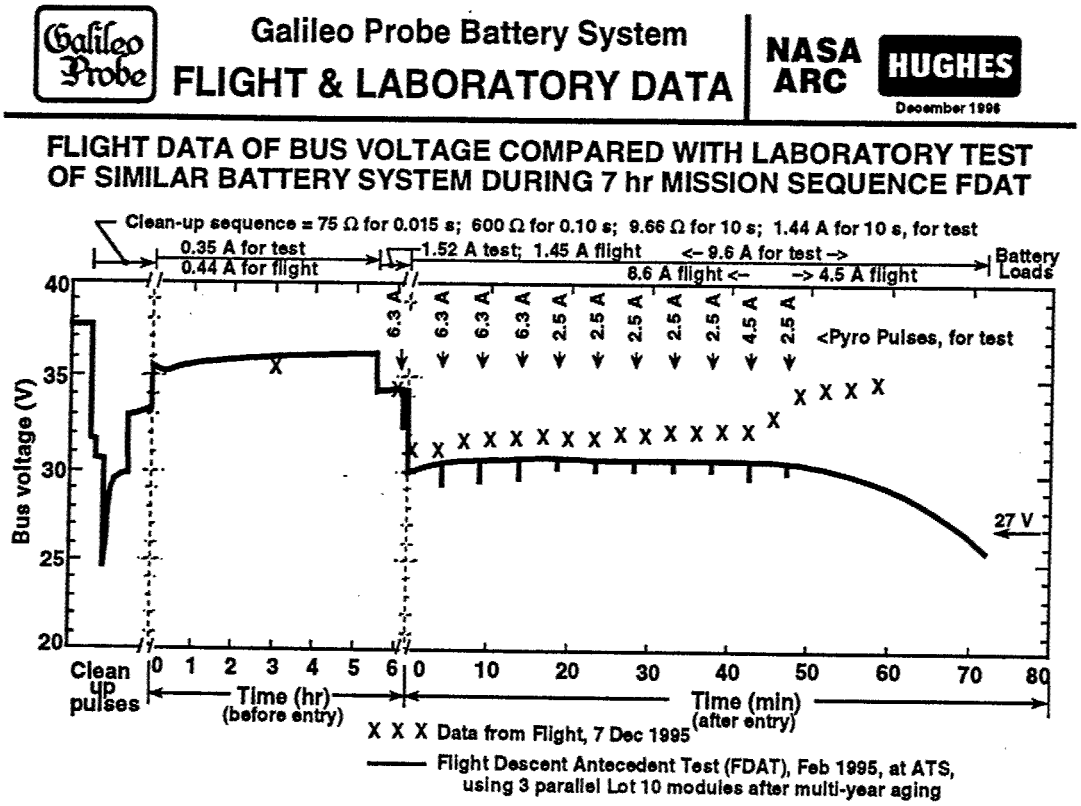

To say that we were pleased with the performance of our Li/SO_2 battery modules on December 7, 1995, would be an understatement. They performed precisely as predicted.

The solid line in the above graph represents the performance of three similar battery modules in a real-time laboratory simulation of the 6-hour Pre-entry and the hour of Descent. This was the concluding portion of the Flight Descent Antecedent Test (FDAT), a test executed to simulate total flight performance in real time as closely as practical and thereby provide a useful tool for predicting flight performance. The test modules were from the same manufacturing lot as the flight modules. Their temperature was controlled meticulously the entire time after manufacture to mimic the temperature history of the flight modules during the Launch, Cruise, Coast, Pre-entry, and Descent phases of the Probe's mission. The Coast phase simulation lasted 155 days, including a simulated clock load. The FDAT was completed on February 21, 1995—in sufficient time before the Probe's release from the Orbiter (July '95) to permit analysis of the FDAT data and to consider their systems operational implications.

Our two voltage data points from the Pre-entry flight time matched the FDAT predictions very well. The first flight point is a little low, as expected because the flight load was slightly larger than the FDAT load at the equivalent time. On the other hand, the Descent voltage profile from flight was slightly higher than that from the FDAT, due to both lighter loads in flight and a higher temperature beginning at Entry+30 minutes. The jump in flight voltage at ≈ Entry+47 minutes was due to the loss of RF String B and the resultant decrease in bus loads of 4.1 A.

We believe that the flight Li/SO_2 battery had sufficient remaining energy to have lasted, even if full load had been maintained, to reach our predicted battery operation duration of Entry+76 minutes.

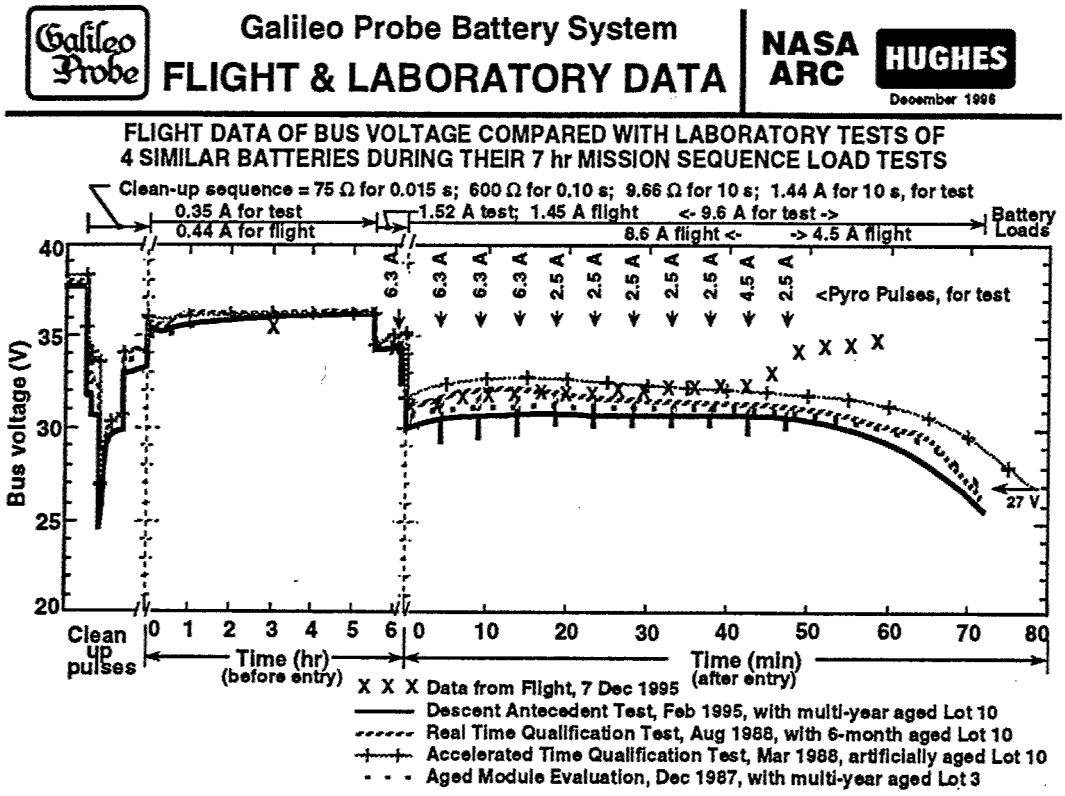

This interesting graph compares the flight data with the results of several preceding laboratory battery tests. The solid line is for the FDAT, our best ground simulation of flight conditions, as explained with the preceding graph. The line with the slanted stripe pattern is the Real Time Lot 10 Qualification Test, completed 6 months following manufacturing. It had a real time simulation of the 5 month Coast interval. However, the preceding simulation of the 5.5 year Cruise phase was highly accelerated—a 1.1 Ah discharge (over 4.5 hr) of each of the three module to approximate the capacity loss estimated for 5.5 years of quiescent storage. The line with periodic crosses depicts the result of the even faster Accelerated Lot 10 Qualification Test wherein a 60 hr, 6.0 Ah discharge of only Module 3 was used to simulate capacity loss for all modules for both the Cruise and the Coast phases. The dotted line is the result of testing Lot 3 modules which had been quiescently stored for several years as an approximation for the Cruise phase (but without the precise temperature control used for the Lot 10 FDAT). Following this Cruise approximation, the Lot 3 modules had a real time, 5 month Coast simulation with the standard clock load. No accelerated loads had been applied to those Lot 3 modules prior to the discharge depicted in the above graph.

One can clearly see the difference in voltage response (to the 9.6 A ground test simulation of the Descent load) between the Real Time and the Accelerated Lot 10 Qualification Tests. This difference was common to every lot for which their testing had included both versions of time simulations. This provides a clear justification for real-time system level testing for this electrochemical system. This 7 to 8 minute difference in time to reach the 27 V lower limit for satisfactory systems operation is significant for its importance to the mission performance prediction, as it represents 10% of the critical Descent portion of the mission.

Galileo Probe NASA ARC HUGHES December 1996

MODULE CURRENTS FOR FINAL PART OF THE LABORATORY FLIGHT DESCENT ANTECEDENT TEST
(in February, 1995)

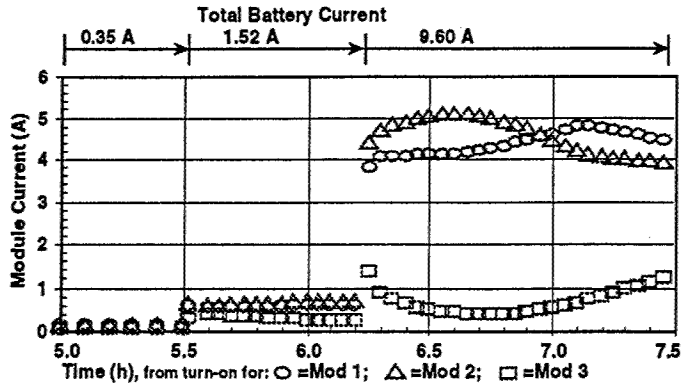

MODULE DISCHARGE FOR FINAL PART OF THE LABORATORY FLIGHT DESCENT ANTECEDENT TEST
(in February, 1995)

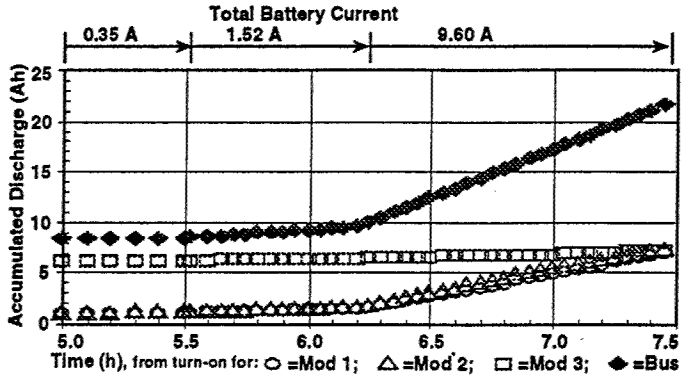

These two graphs illustrate the efficiency of our Probe battery system in terms of sharing current as well as delivering Ah capacity. The top graph depicts how Module 1 and Module 2 supplied most of the current during the 9.6 A Descent phase of the FDAT simulated mission. Module 3 had already expended more than half of its capacity supporting the clock during the real-time 155-day Coast phase, yet during the Descent phase even that module was still able to contribute all of its remaining energy to the common bus. The Descent phase of this FDAT concluded when each of three modules simultaneously reached the same limit in their capacity, as can be seen by comparing the delivered Ah results in the lower graph. This was the expected result, arising from the parallel design of the three-module battery.

The cross-over (i.e., the wave pattern in the top graph) of the currents that were supplied individually by Module 1 and Module 2 during Descent was a pattern noted throughout the several discharge tests at Honeywell (Alliant) and was also seen the during systems test on the Probe. We believe this also occurred in flight (but individual module currents were not monitored in flight)—it answers the question of why the temperatures (which were monitored in flight) of the two modules differed in their rate of change. Module 2's flight temperature initially rose at the faster rate but then slowed down. Module 1 at first rose slowly but ended with a more rapid rate. By the end of the 60 minutes of available flight Descent data, both modules had arrived at similar temperatures, indicating by that time they had supplied equal amounts of integrated Ah during their respective discharges, another aspect of the expected response for modules connected in parallel.

Galileo Probe Battery System
LESSONS LEARNED

- Command System Back-up Modes provided for variety of potential failures:
  - G-switch override—for potential coast, pre-entry failures
  - Lock-out option, at release from Orbiter, of either string A or string B
  - Option, at release from Orbiter, to use 5 month timer or G-switch mode
  - Provided early time-out shut-down, to protect remaining battery energy
- Using thermally activated batteries to provide major pyro-firing pulses was effective in preventing transient overloads on main battery
- Minimizing parasitic electrical loads on battery (by initial design, verified by preflight testing on assembled spacecraft) was vital for assuring retention of stored energy during 6 year interplanetary transit time
- Li/SO_2 Battery isolation was made adequate for the 6-year cruise by providing series-parallel switching (relays) in all paths including those for the battery module OCV telemetry measurements.

Galileo Probe

Galileo Probe Battery System

MORE LESSONS LEARNED

NASA ARC HUGHES

December 1996

- Spares and Testing Philosophy:
  Require ample spare cells and modules, with appropriate storage, to accommodate foreseen and unforeseen needs for special ground testing before and after launch

- Life Time Assessment Study Program, conducted at SNL prior to launch, proved to be a valuable tool in mission planning, both prior to and following launch

- The continuous, methodical evaluation, at NASA-ARC, of cell and module life was valuable in demonstrating high reliability of these Li-SO_2 units

- A real-time, ground-based simulation of the flight-lot battery performance preceded the schedule of the actual flight operation by 10 months, thus providing timely and precise information on how best to select the options for battery management at time of Probe separation from Orbiter

- Enthusiastic coooperation among NASA-ARC, Hughes S&C, SNL, and Alliant Techsystems contributed heavily to the success of myriad ground tests and analyses programs and was certainly responsibile for the mission success in terms of the battery performance

Nickel-Hydrogen Battery On-Orbit Reconditioning Experience Focused Session

Nickel-Hydrogen Battery Reconditioning

Erik L Levine

SPACE SYSTEMS/LORAL

12/3/96 1996 NASA Aerospace Battery Workshop

Outline

- SS/L Reconditioning Implementation
- Reconditioning Conclusions
- Superbird Reconditioning - Pressure/Capacity Growth
- INTELSAT VII/VIIA Reconditioning - Cell Voltage Plateaus and Life Testing
- N-Star Reconditioning - Cell Voltage Plateaus (Capacity Fading and Recovery)
- Questions and Answers

SS/L Battery Reconditioning Implementation

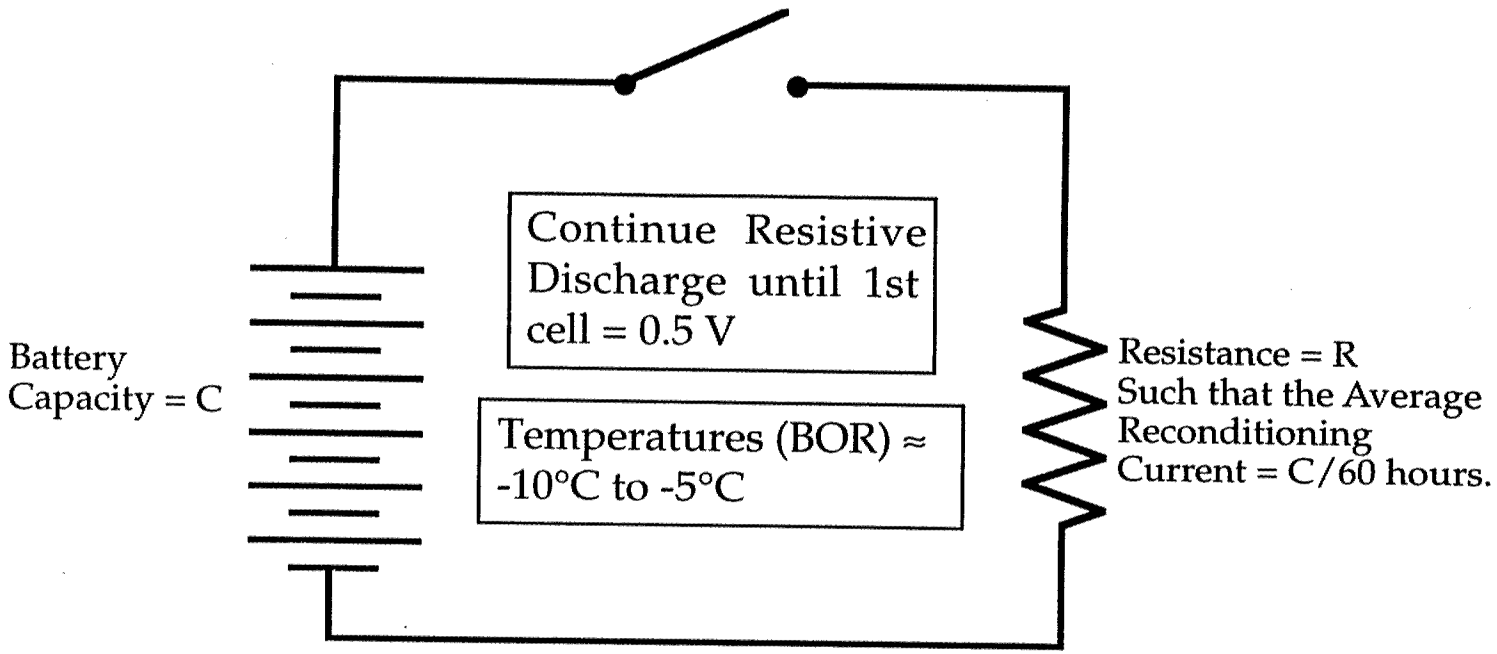

Performed ≈ 2 - 3 weeks prior to each eclipse season

(i.e. early February and late August)

Reconditioning Conclusions

- Provides no appreciable increase in performance

but, provides an excellent way for ...

- Measurement of pressure/capacity growth.
- Correlation with Life Test Data
- Verification of Capacity Fade and Recovery

and is therefore recommended when possible, but not required.

12/3/96 1996 NASA Aerospace Battery Workshop 4

- Battery performance being amp-hour capacity and cell voltages.
- Used mainly as a diagnostic tool and for trending data to observe any capacity reductions during life and to observe the presence and reduction any capacity fading / voltage second plateau.
- Only way to perform a consistent battery test since length of eclipses vary through the season and spacecraft power needs may change from season to season. Remember, the satellite is nothing more than a two terminal battery test station (right?) !
- Therefore on single bus satellites, anomalies in orbit, or LEO applications, it is not required to maintain performance.

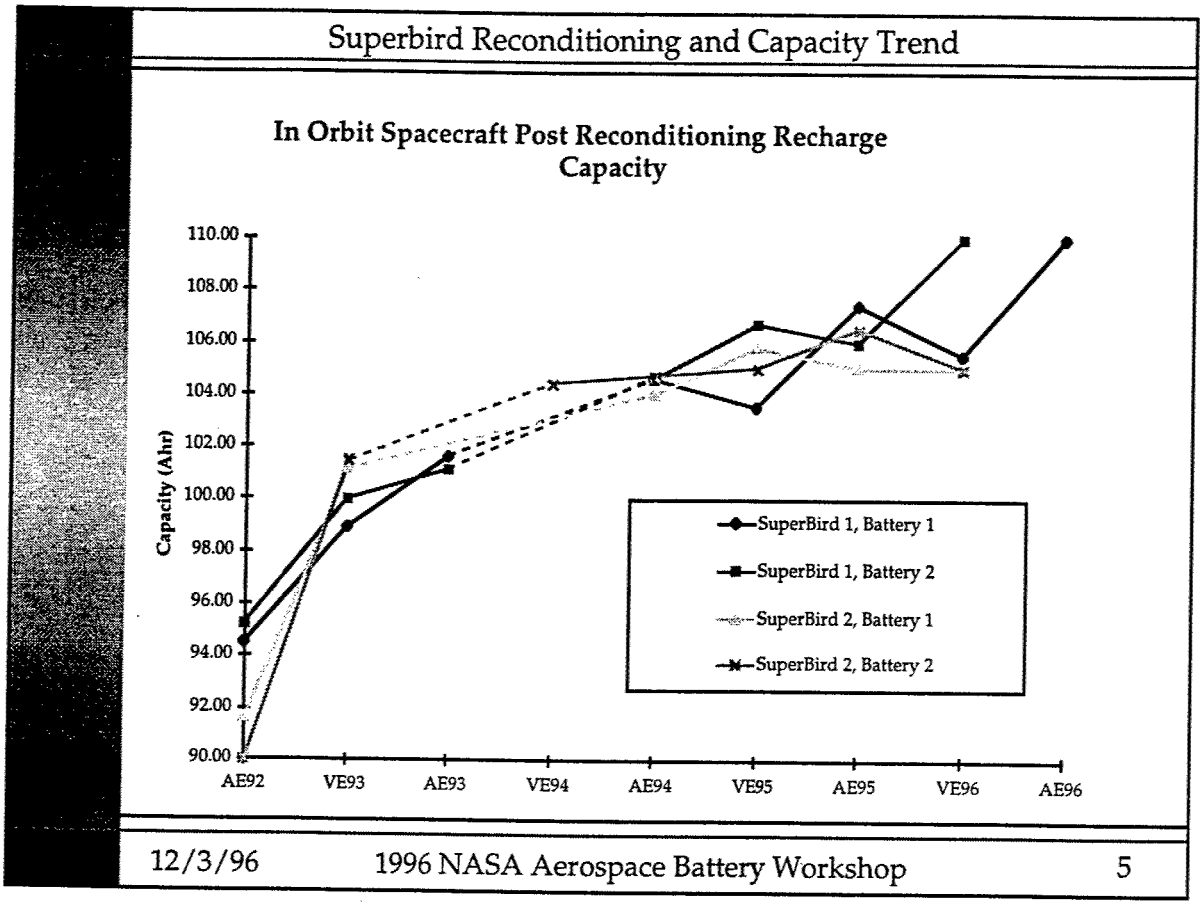

- Superbird capacity growth chart. Note that increase in end of charge pressure corresponds almost exactly with the capacity increase (i.e. no pressure increase due to degradation of cell components). Capacity shown here is the pressure reading (via a strain gage on the battery cell) compensated for the cell temperature to get amp-hours.
- Trending to flatten out per predictions.
- Note that at times some of the batteries were not reconditioned but performance still increases.

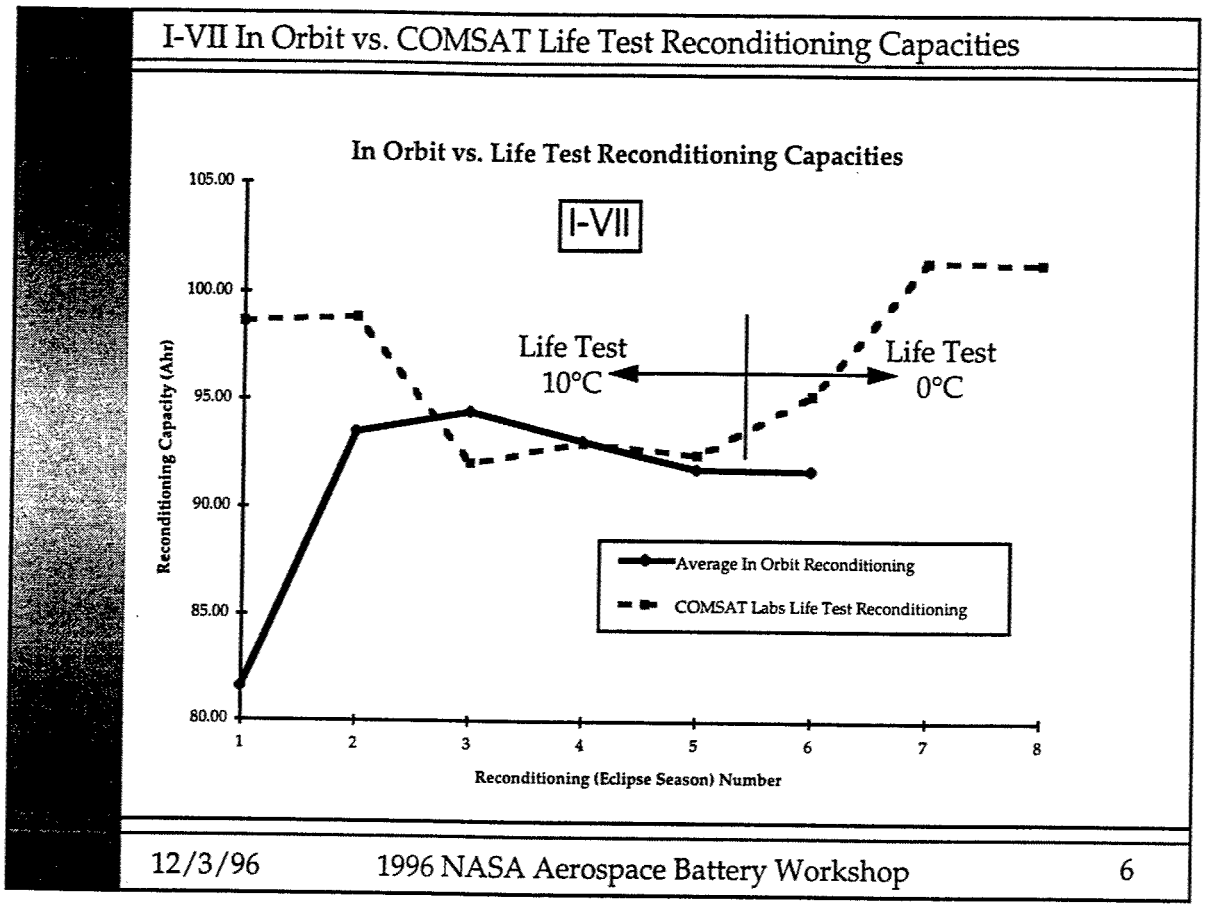

- I-VII Life Test vs. In Orbit Reconditioning.
- Note that the life test batteries have more seasons than the actual orbit.
- Scale is quite zoomed up, so the data is actually pretty tight with a few percent.
- The life test battery was tested extensively before the the first reconditioning, so all of its capacity building was already done. Therefore the reconditioning data is constant (except for effect of changing temperature). The flight batteries however go through minimal acceptance testing only and thus still has potential for capacity building in orbit, which is shown by the increase in reconditioning capacities.
- Note effect of decrease in life test temperature on the COMSAT reconditioning.

I-VIIA In Orbit vs. COMSAT Life Test Reconditioning Capacities

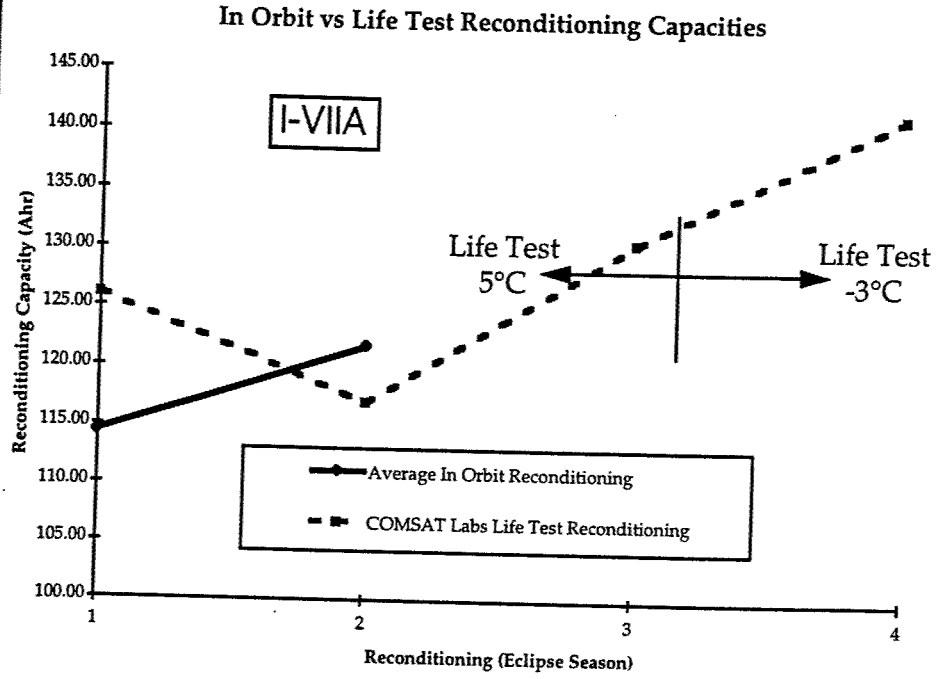

12/3/96 1996 NASA Aerospace Battery Workshop 7

- I-VIIA Life Test vs. In Orbit Reconditioning.
- Note that the life test batteries have more seasons than the actual orbit.
- Scale is quite zoomed up, so the data is actually pretty tight with a few percent.
- Note effect of decrease in life test temperature on the COMSAT reconditioning.

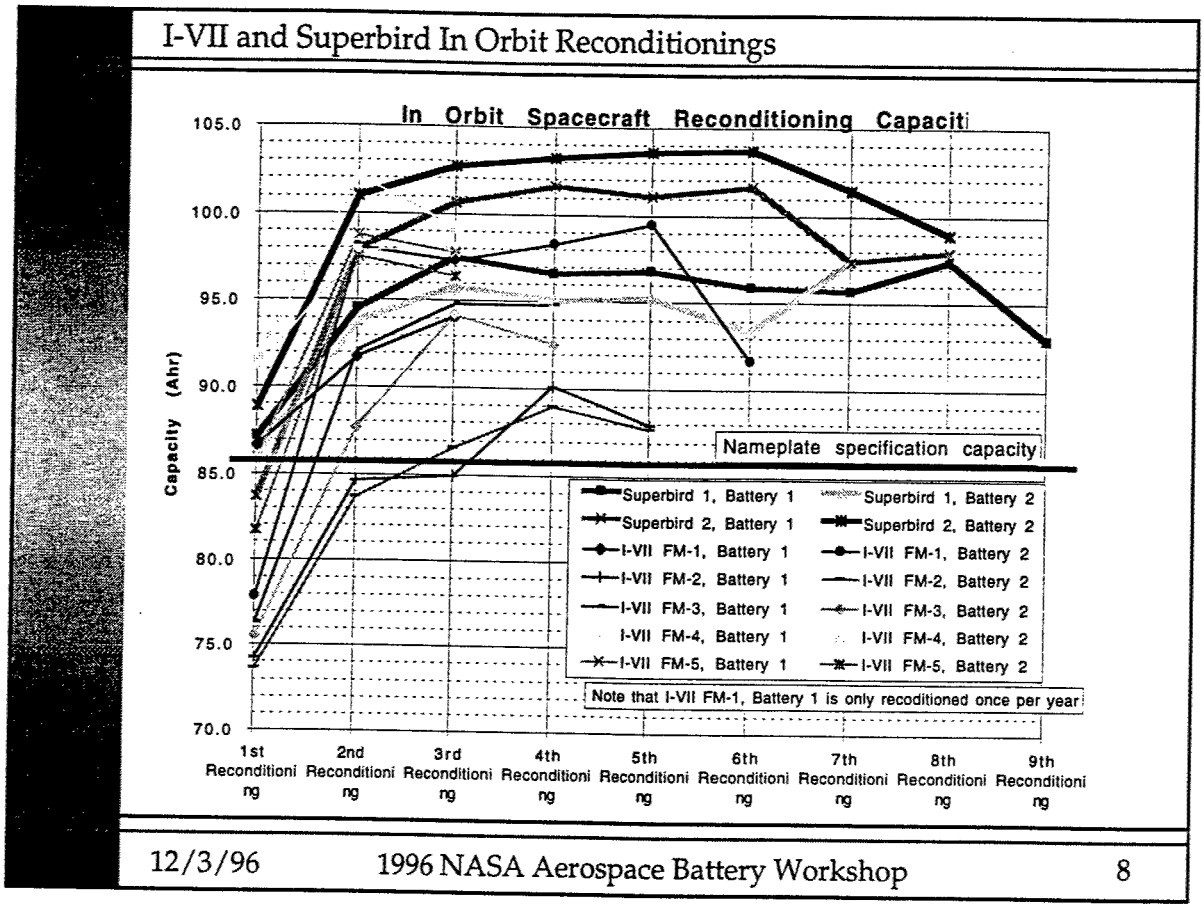

- This chart shows the reconditioning capacities in reconditioning order (not necessarily chronological).
- Note the great capacity increase between the first and second reconditionings, on the order of 10% to 20%.
- Also note the nameplate capacity is 85.5.
- This chart includes Superbird and I-VII, both are 27-cell batteries with the same cell (Superbird has no diodes, though)
- Note decrease in capacity between last two reconditioning on the I-VII spacecraft is due to an in orbit change of the battery heater setpoint points (battery temperatures were increased).

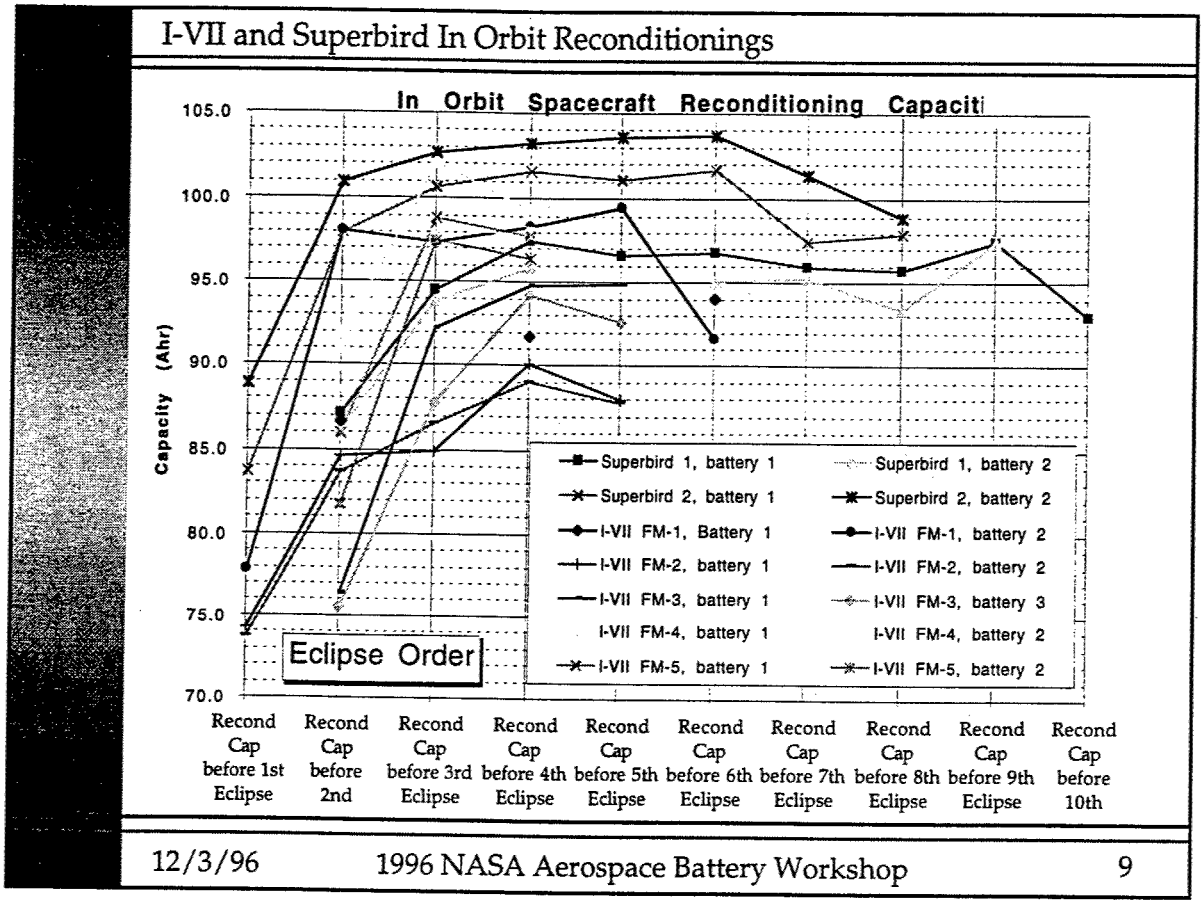

- This chart shows the reconditioning capacities in order of eclipses. Mostly to show that some batteries were not reconditioned until after the 1st eclipse season, while others had one after launch before the 1st eclipse season.
- Of particular note is 701, battery 1 which is only reconditioned once per year (due to an anomaly). Its first reconditioning was between 1st and 2cd eclipses but its 1st reconditioning was similar to the 2cd reconditioning of battery 2 on the same spacecraft.

- The following graphs show the last 4 to 5 hours of reconditioning and up to the first hour of recharge from several spacecraft (I-VII FM1 and FM2, I-VIIA FM6, and N-Star FM-a and FM-b).
- This representation is an excellent way to monitor second voltage plateaus (capacity fading) and their recovery.

I-VII FM1, Battery 1, 1994 Autumnal Reconditioning Cell Profiles

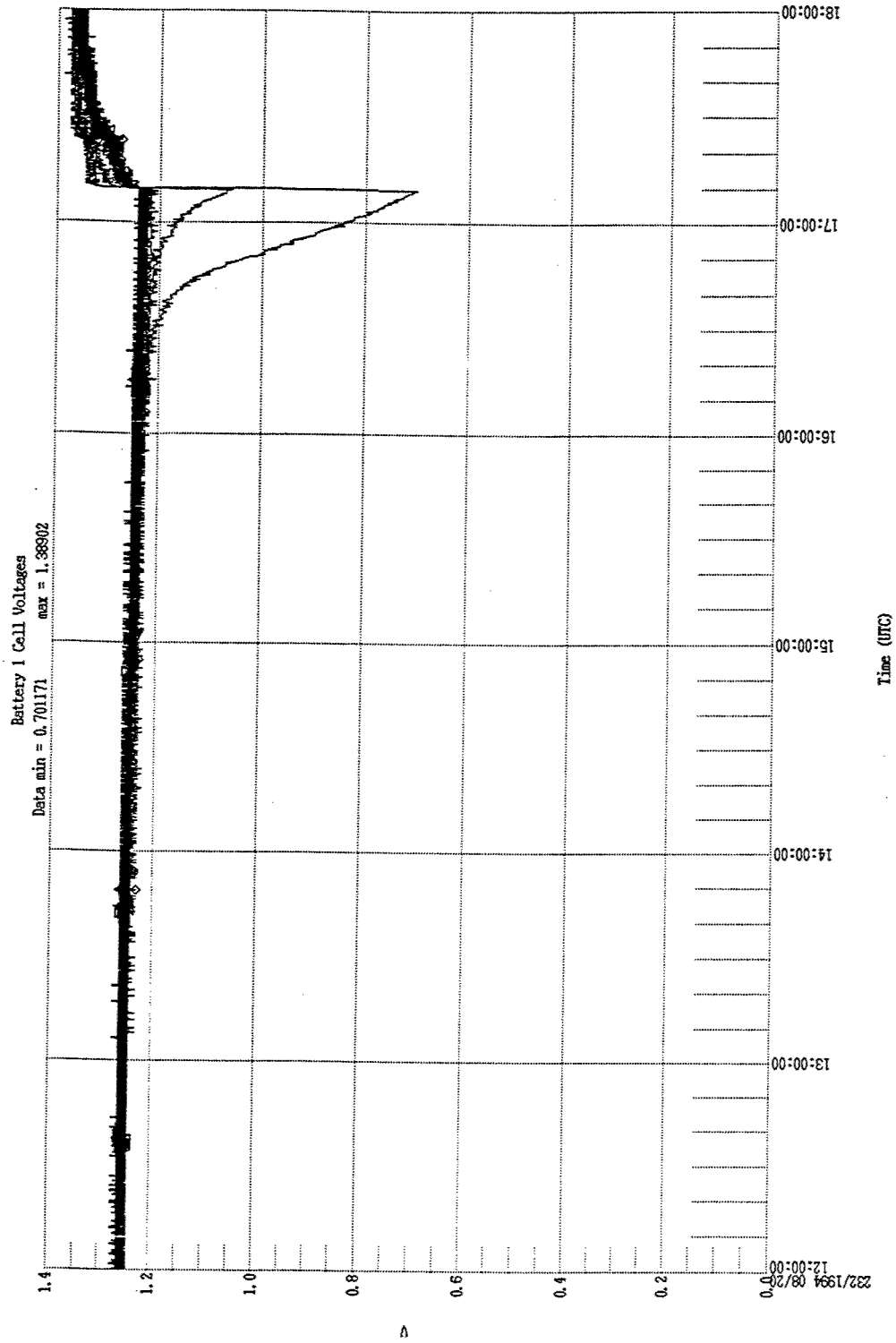

12/3/96

1996 NASA Aerospace Battery Workshop

I-VII FM1, Battery 1, 1995 Autumnal Reconditioning Cell Profiles

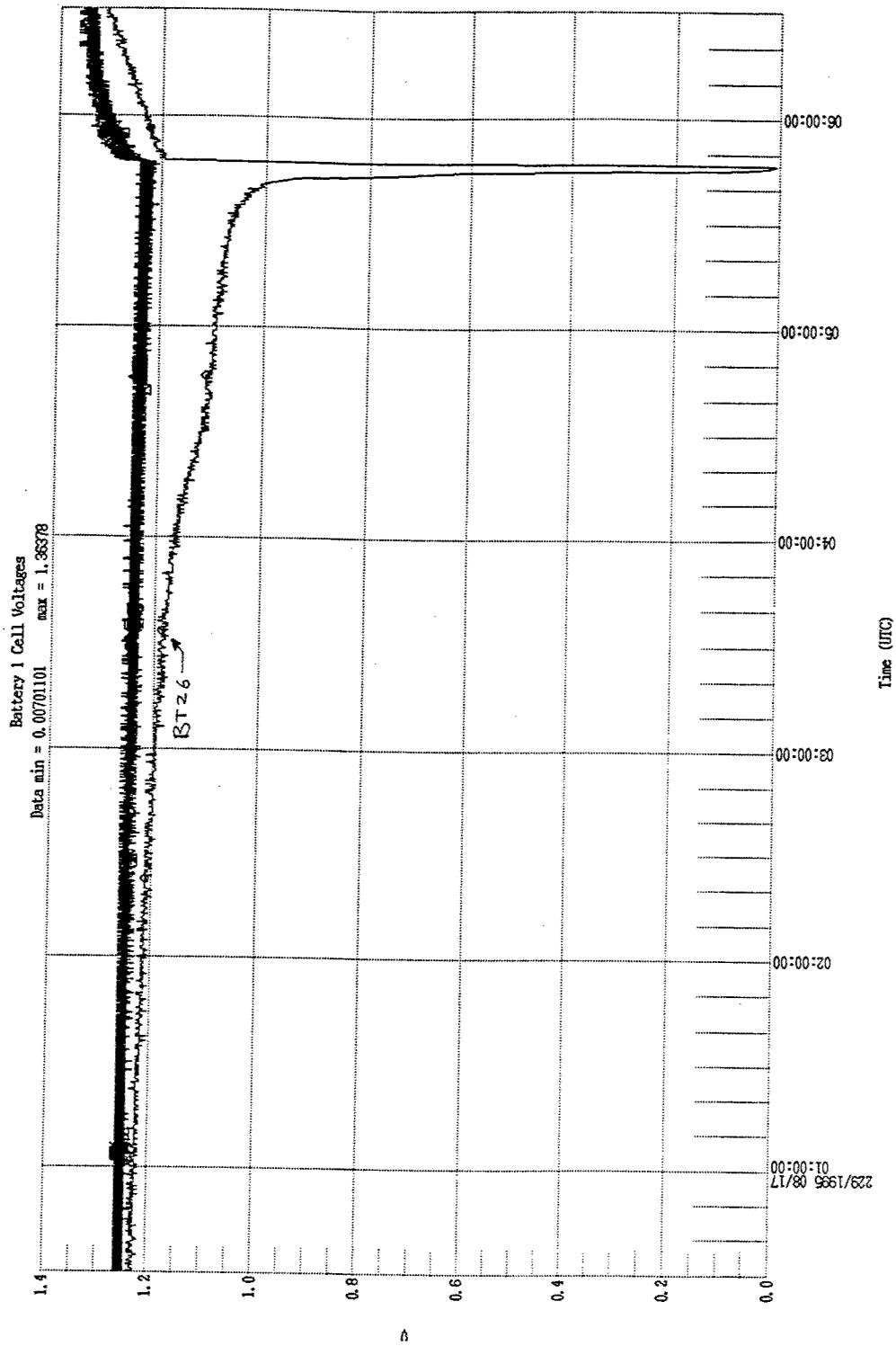

12/3/96

1996 NASA Aerospace Battery Workshop

I-VII FM1, Battery 1, 1996 Autumnal Reconditioning Cell Profiles

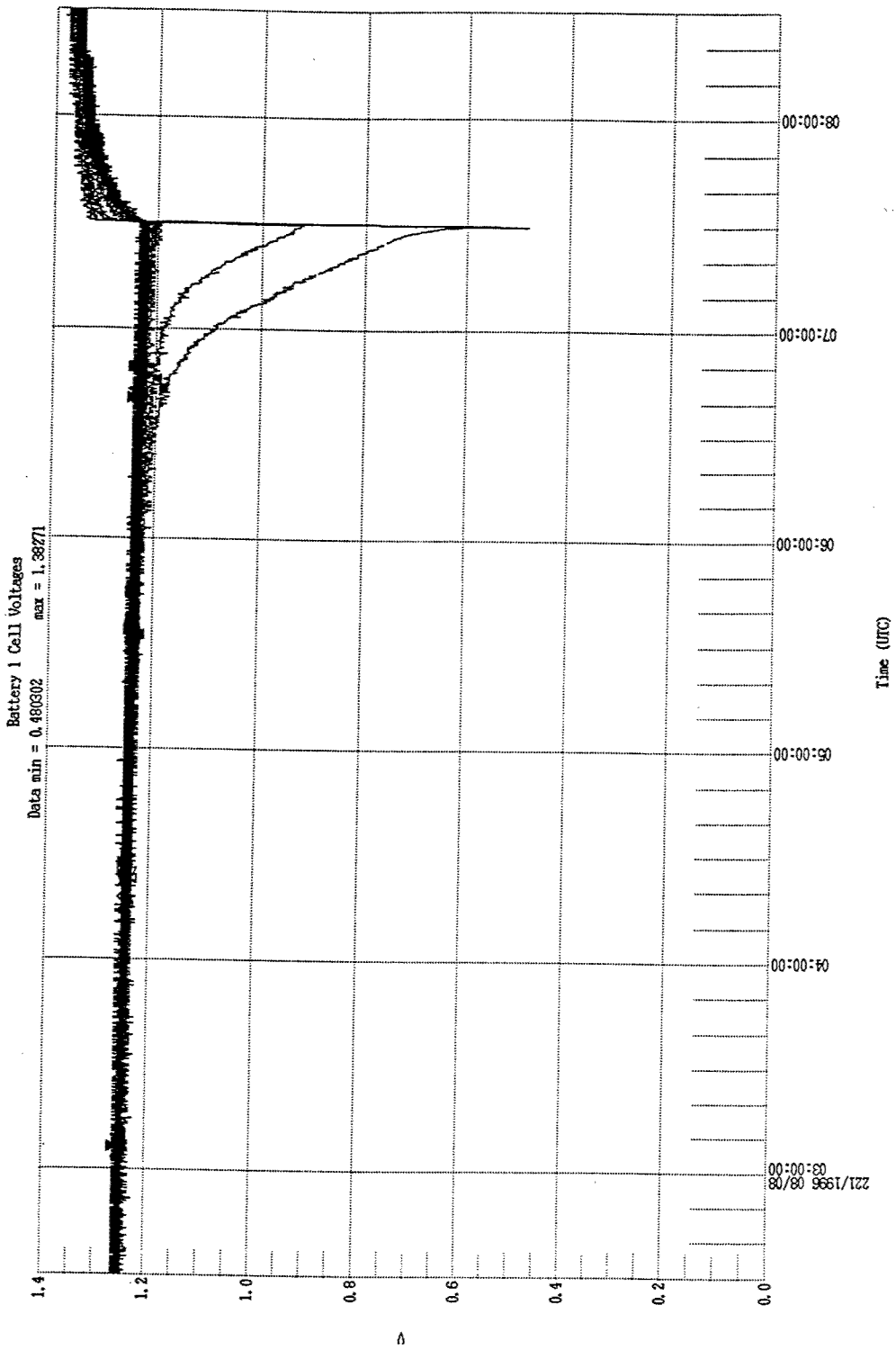

12/3/96

1996 NASA Aerospace Battery Workshop

I-VII FM1, Battery 2, 1994 Vernal Reconditioning Cell Profiles

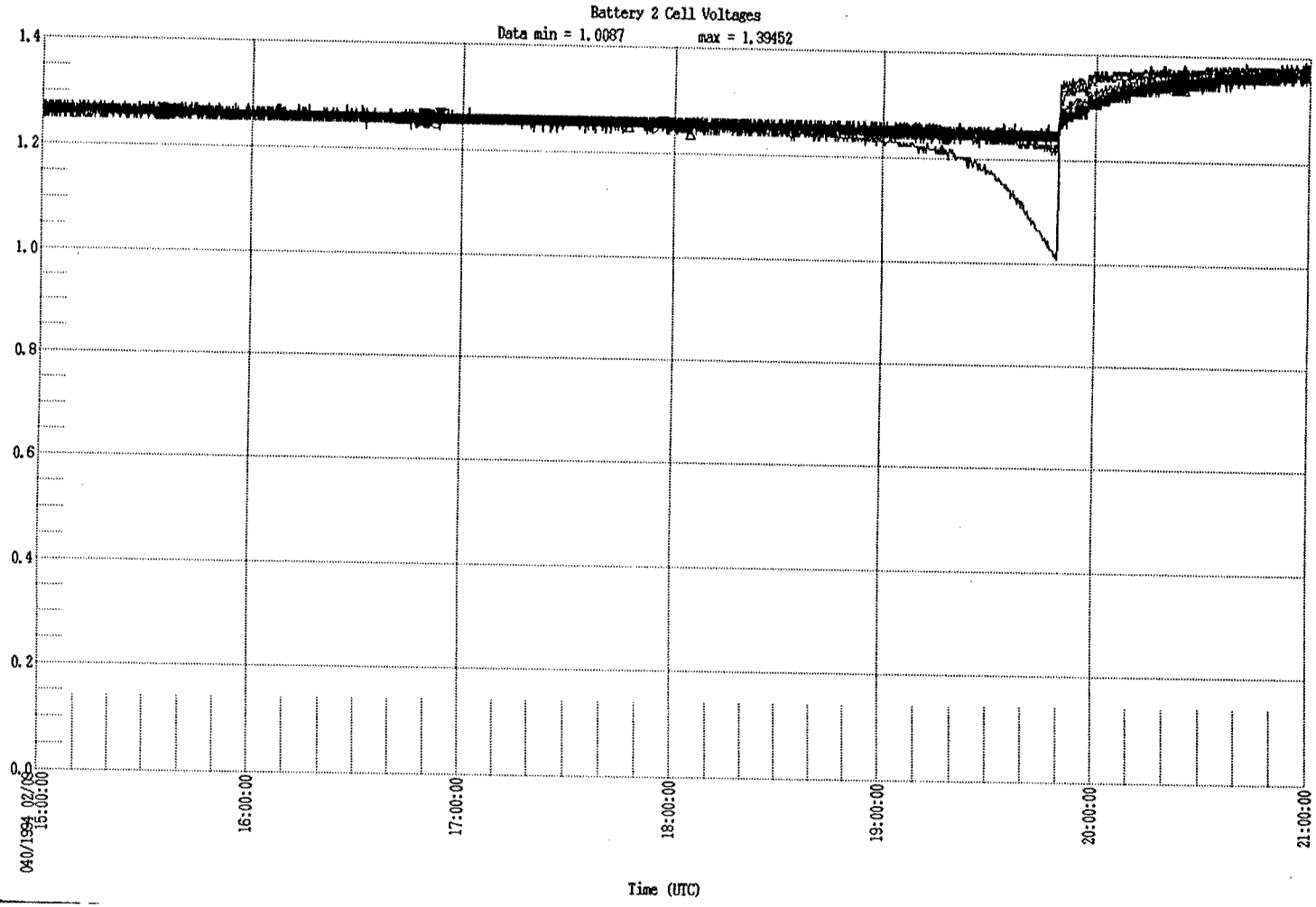

I-VII FM1, Battery 2, 1995 Vernal Reconditioning Cell Profiles

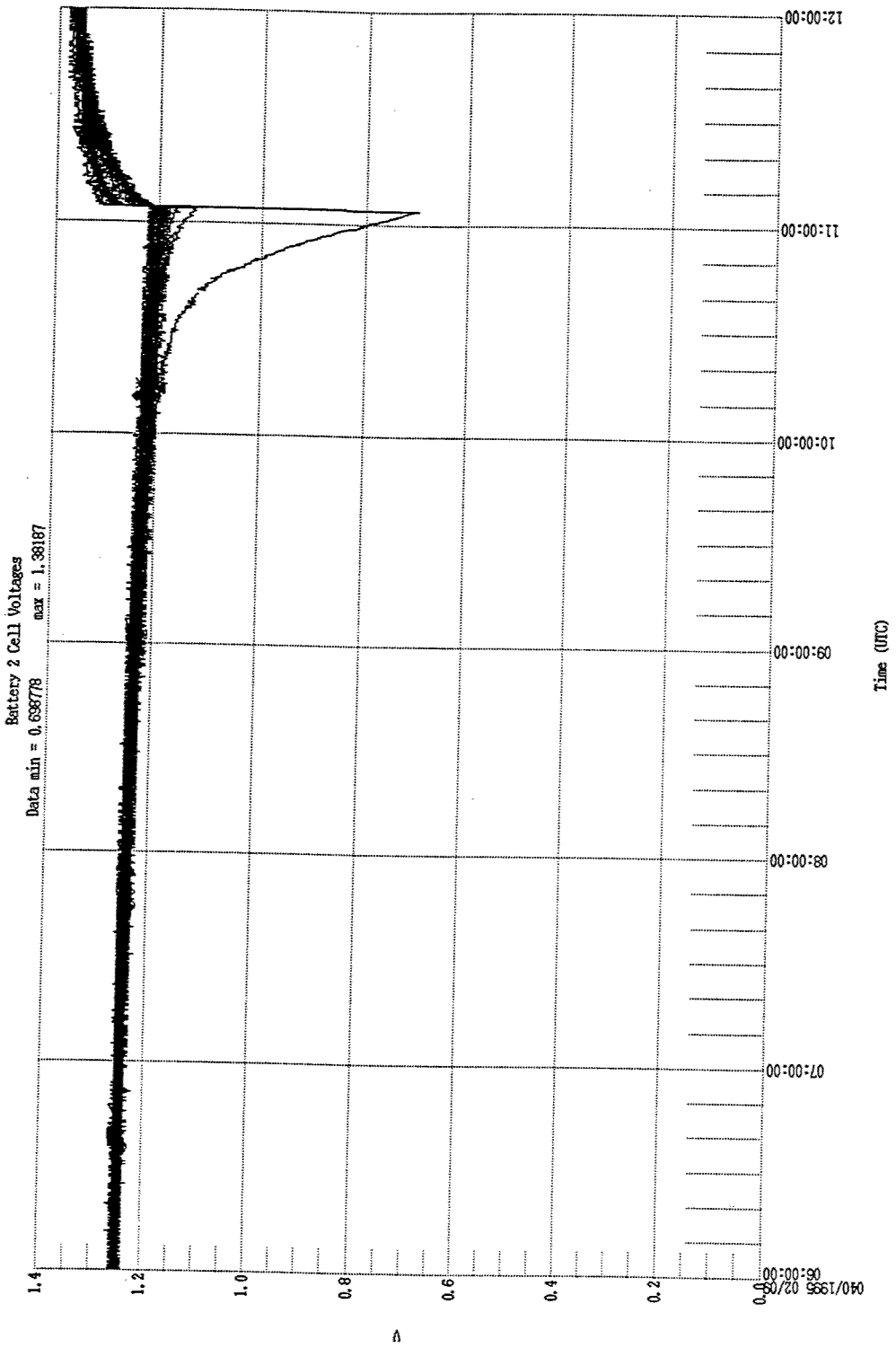

12/3/96

1996 NASA Aerospace Battery Workshop

I-VII FM1, Battery 2, 1995 Autumnal Reconditioning Cell Profiles

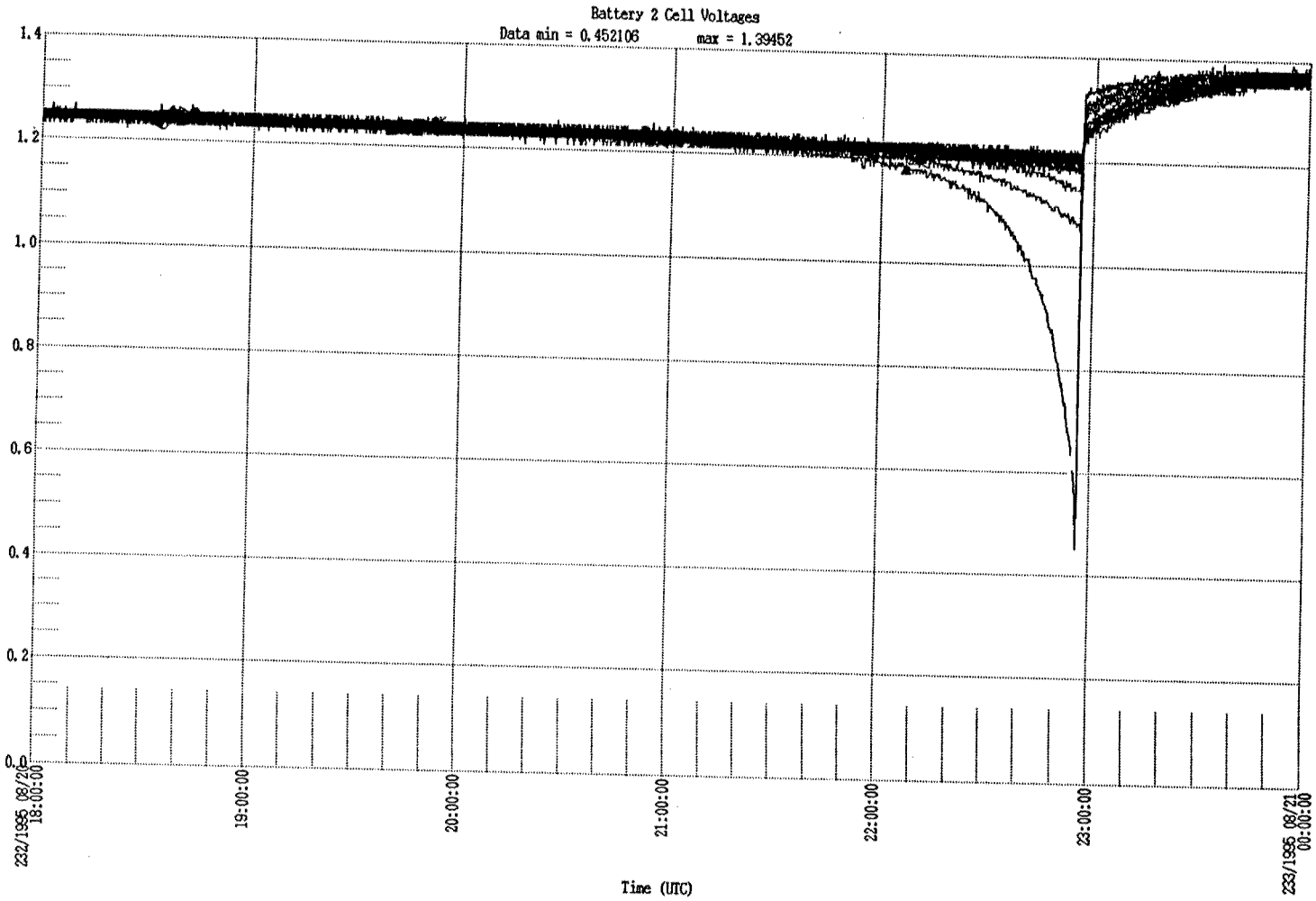

I-VII FM1, Battery 2, 1996 Vernal Reconditioning Cell Profiles

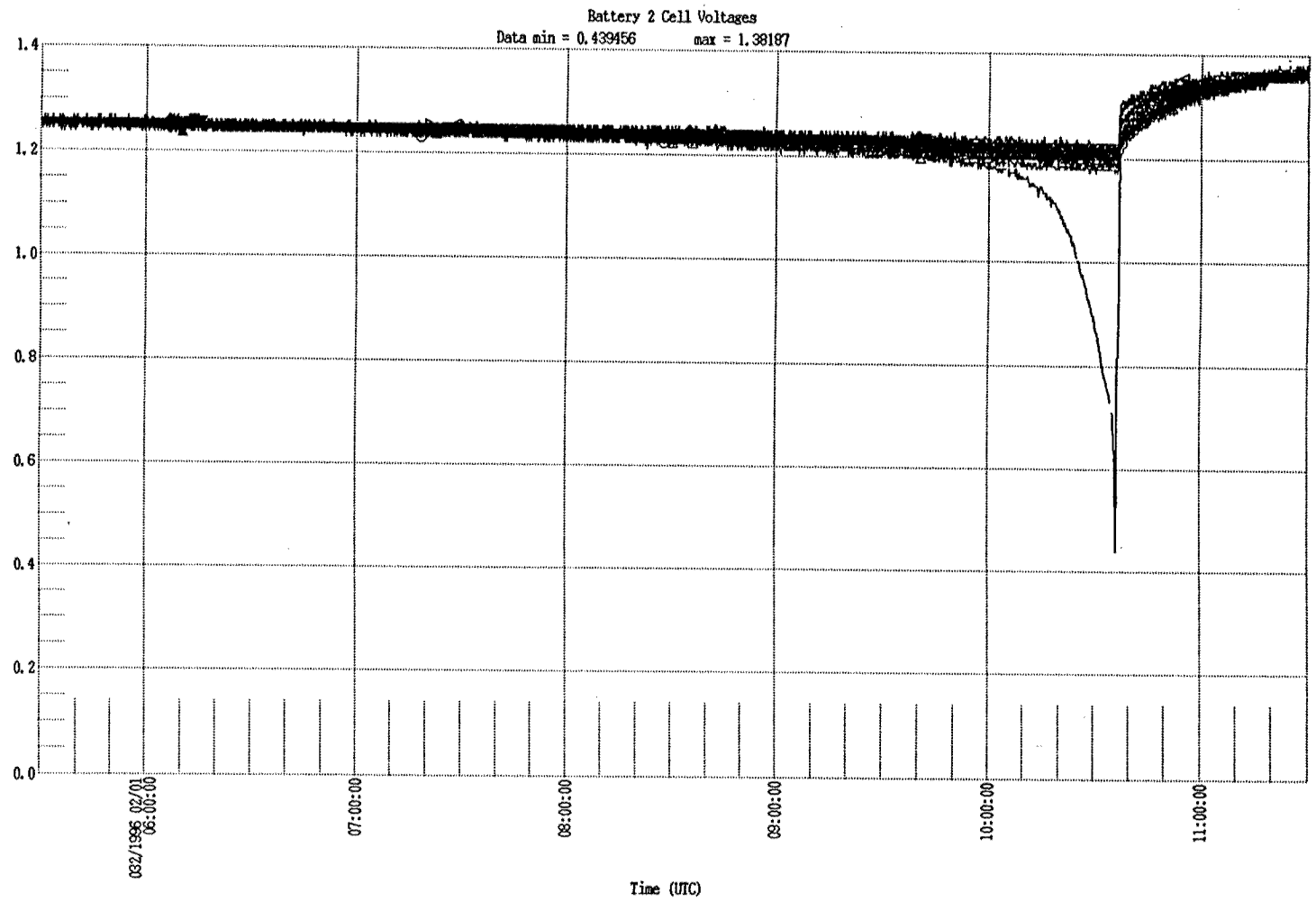

I-VII FM1, Battery 2, 1996 Autumnal Reconditioning Cell Profiles

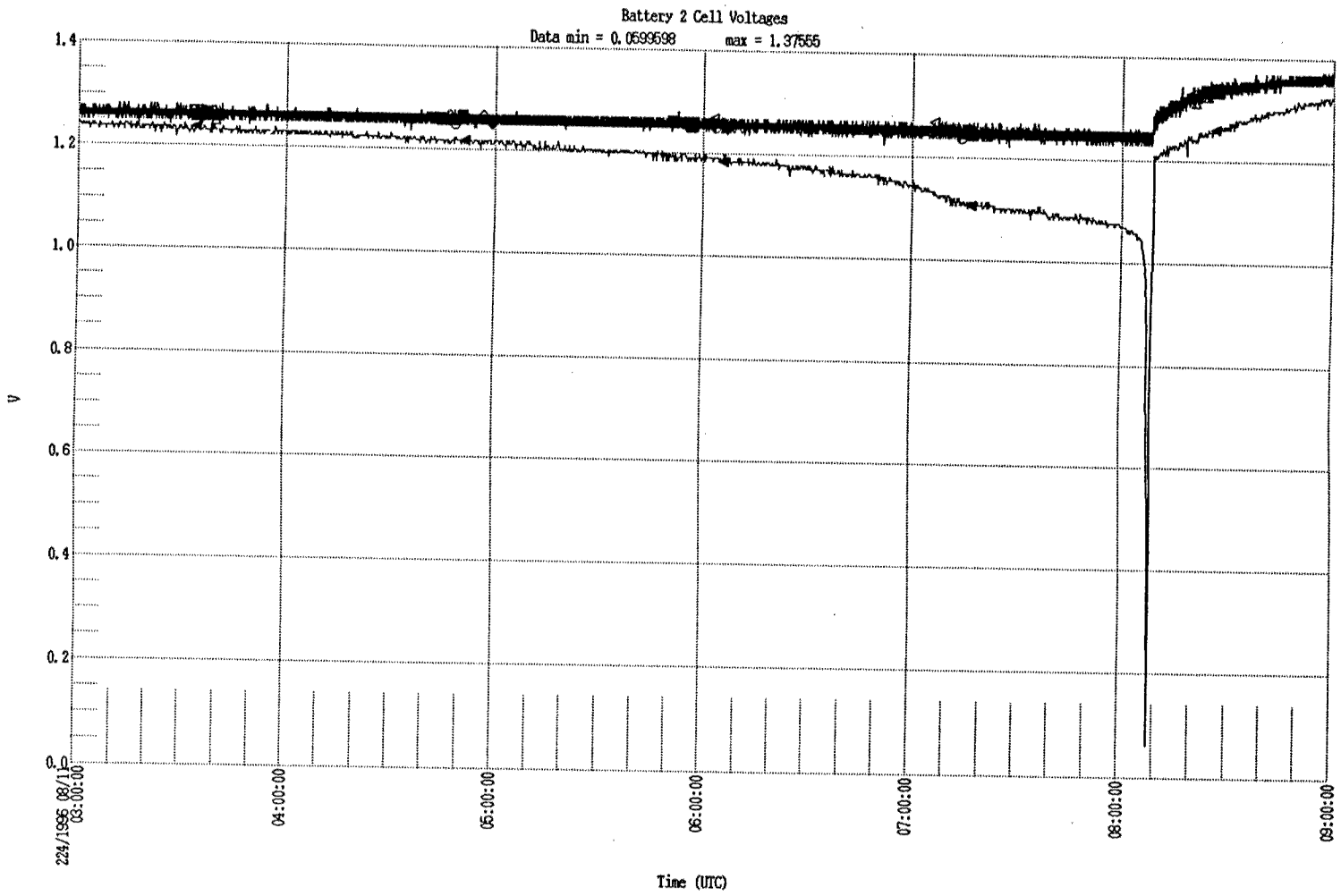

12/3/96 1996 NASA Aerospace Battery Workshop

I-VII FM2, Battery 1, 1995 Vernal Reconditioning Cell Profiles

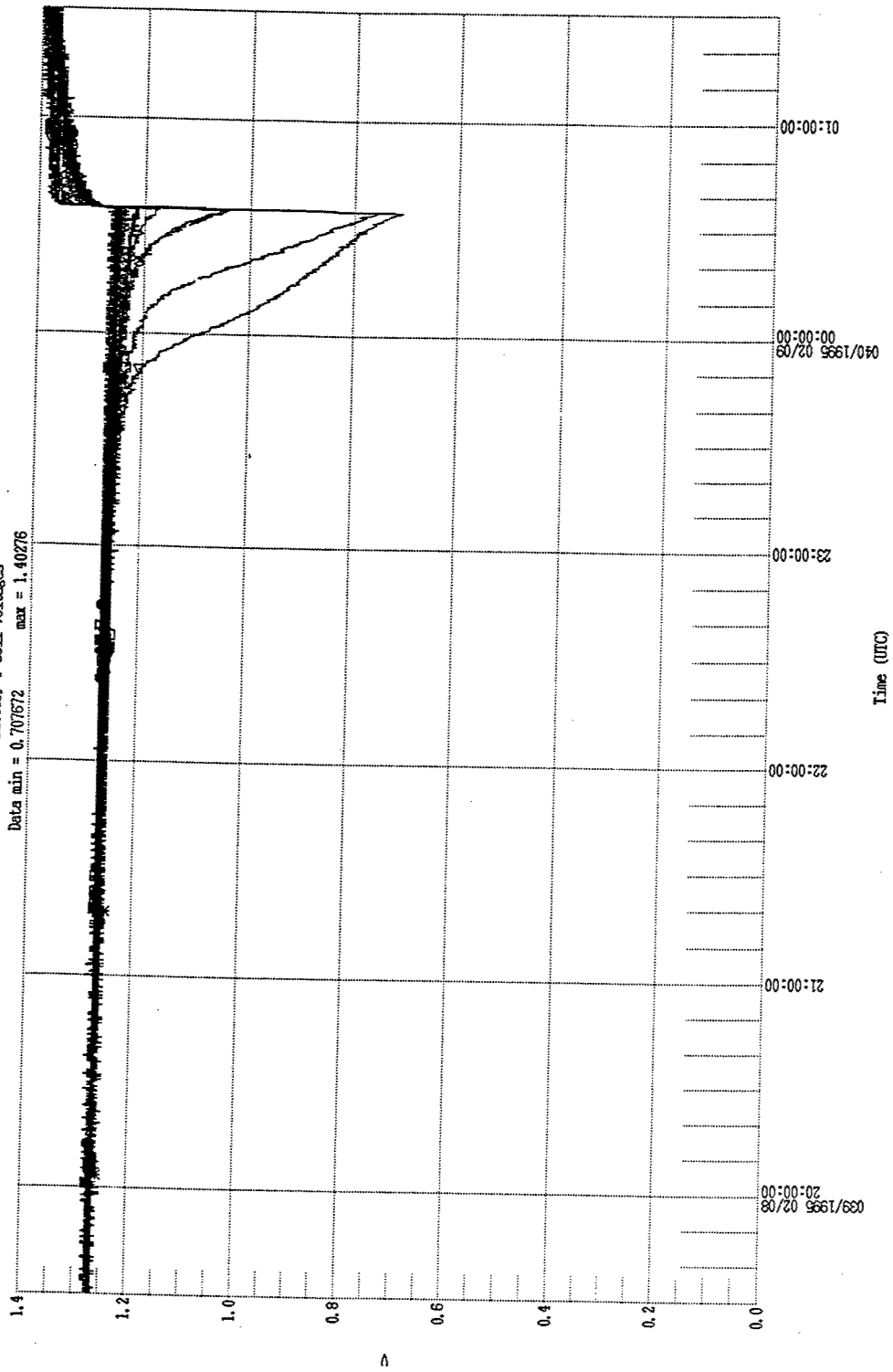

12/3/96

1996 NASA Aerospace Battery Workshop

I-VII FM2, Battery 1, 1996 Vernal Reconditioning Cell Profiles

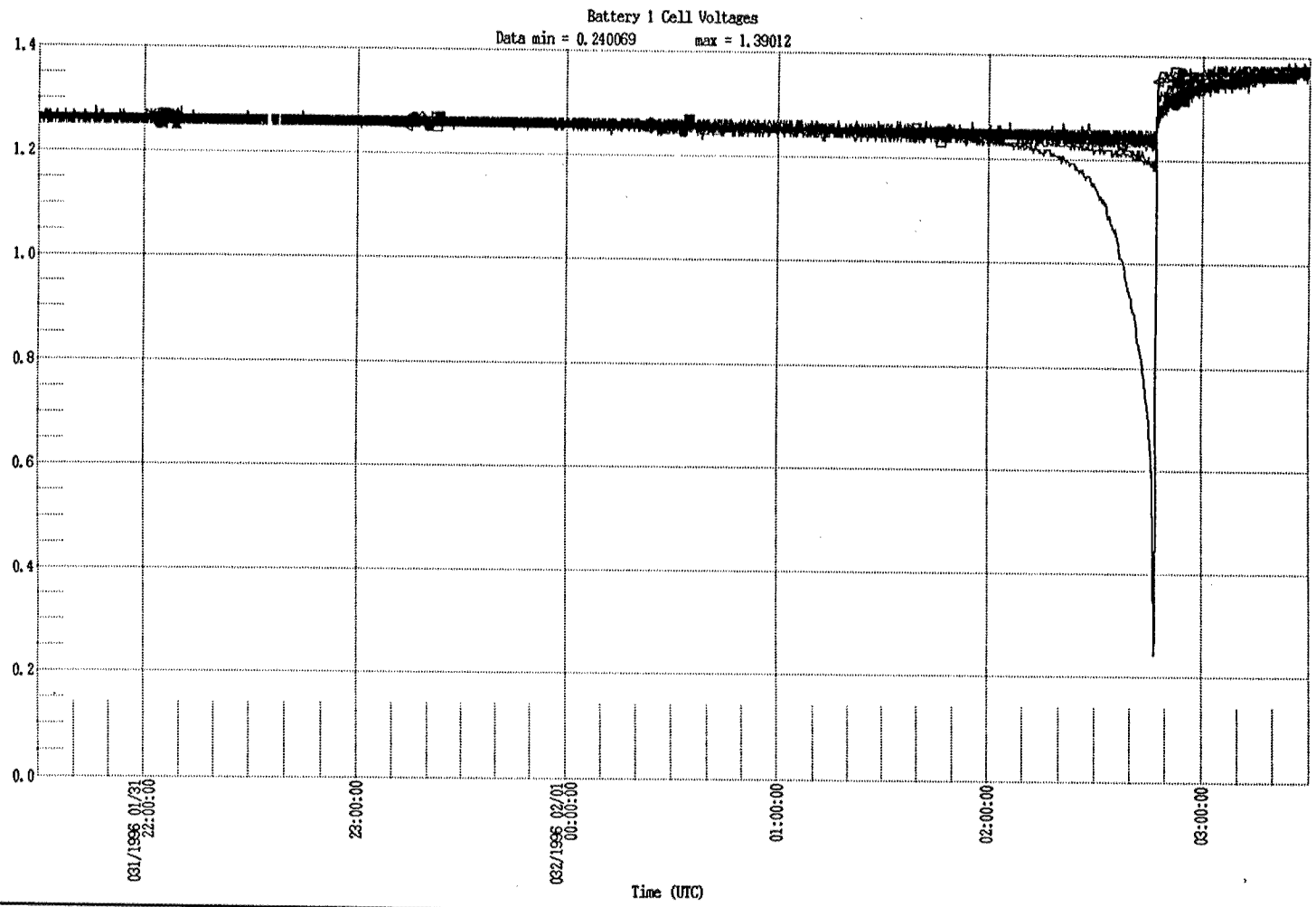

I-VII FM2, Battery 1, 1996 Autumnal Reconditioning Cell Profiles

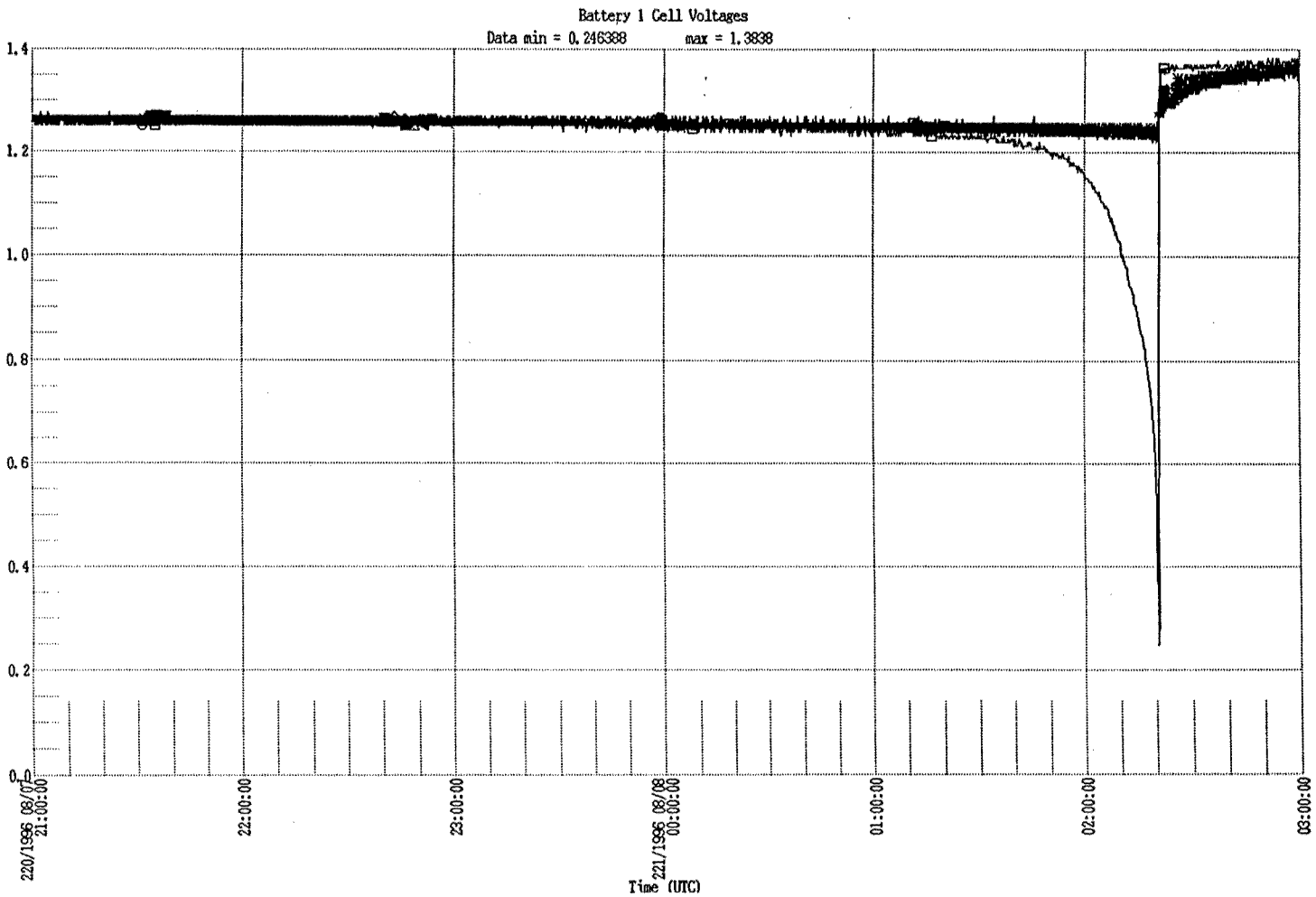

I-VII FM2, Battery 2, 1995 Vernal Reconditioning Cell Profiles

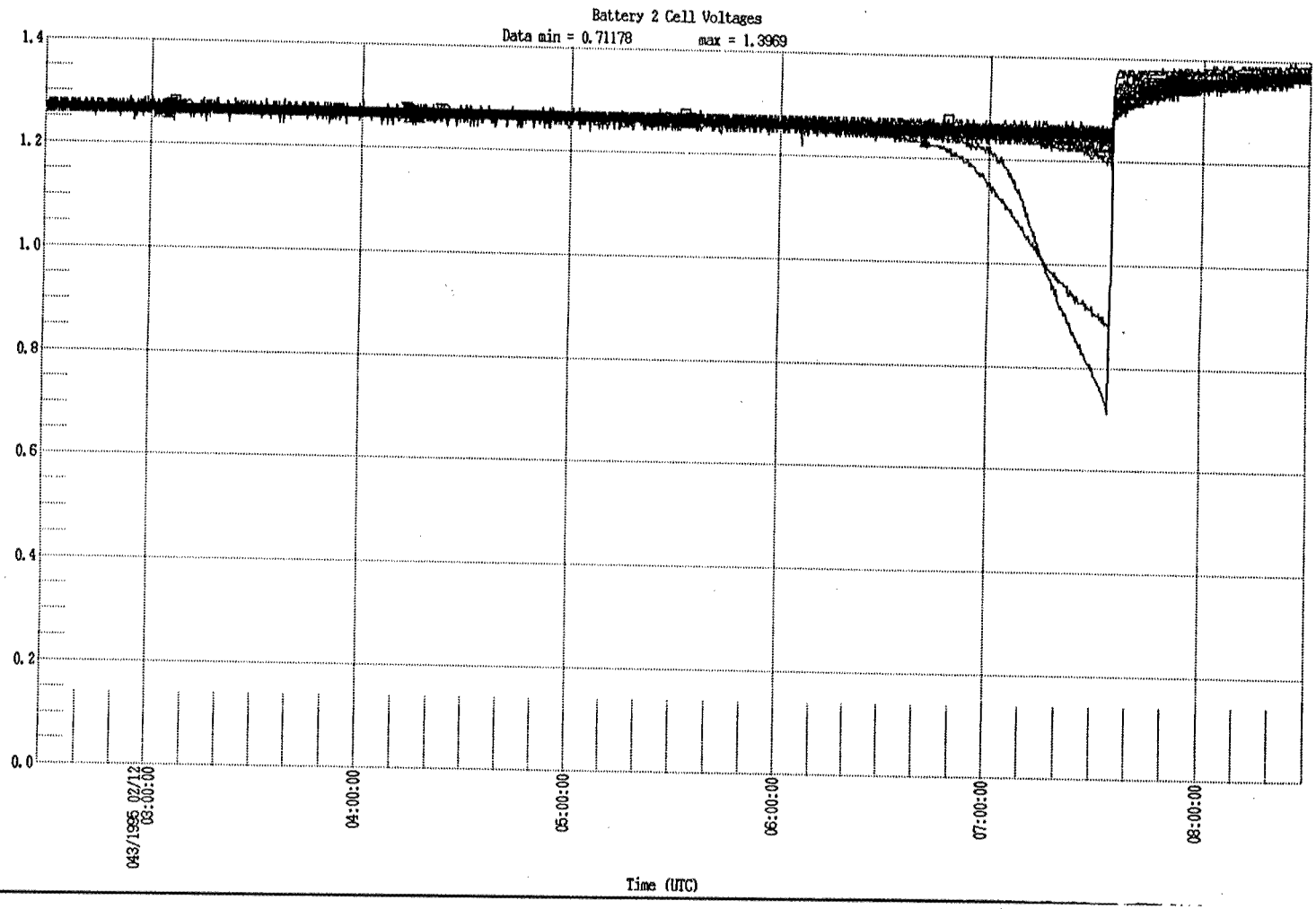

I-VIIA FM6, Battery 1, 1995 Autumnal Reconditioning Cell Profiles

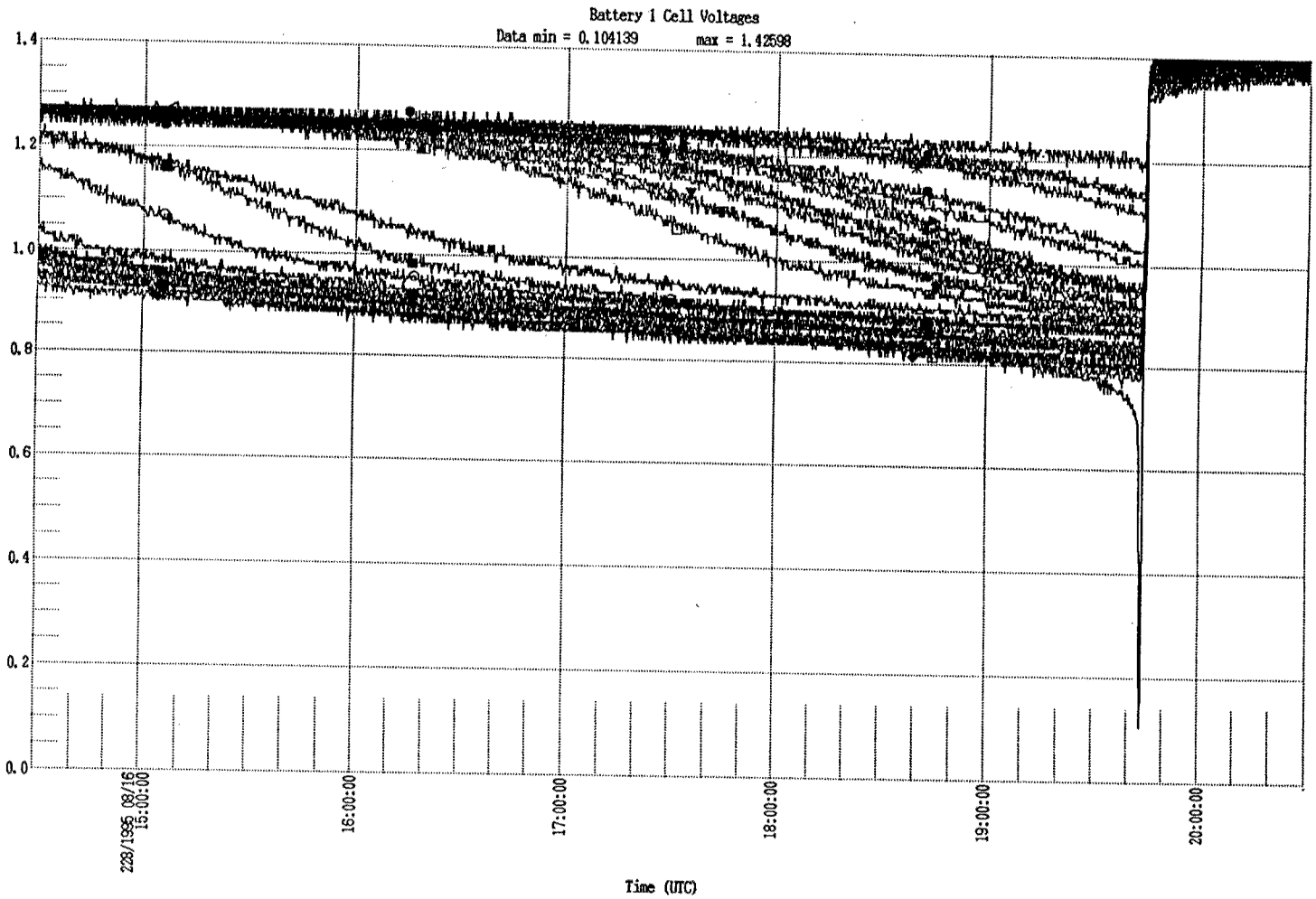

I-VII FM2, Battery 2, 1996 Autumnal Reconditioning Cell Profiles

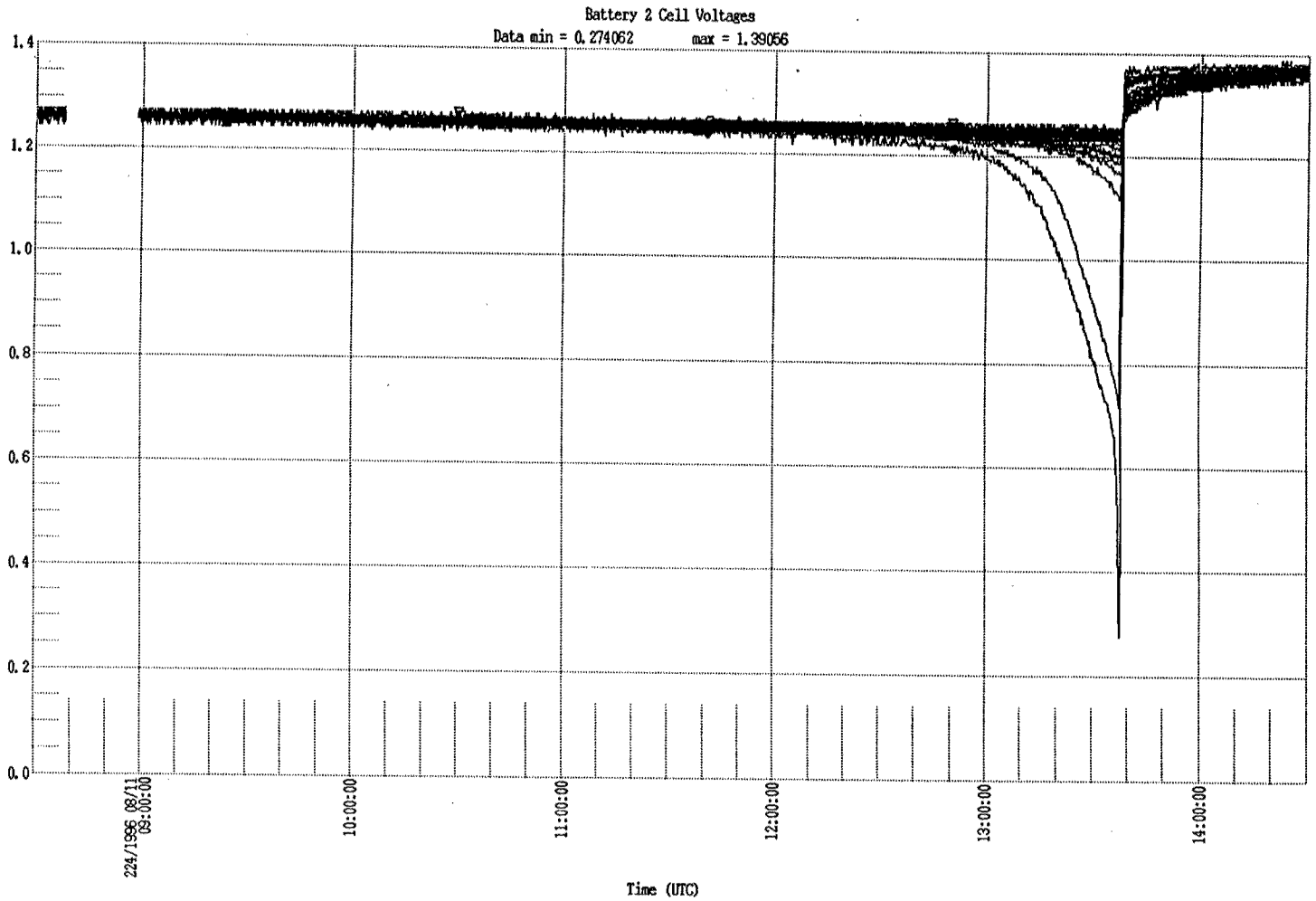

I-VII FM2, Battery 2, 1995 Autumnal Reconditioning Cell Profiles

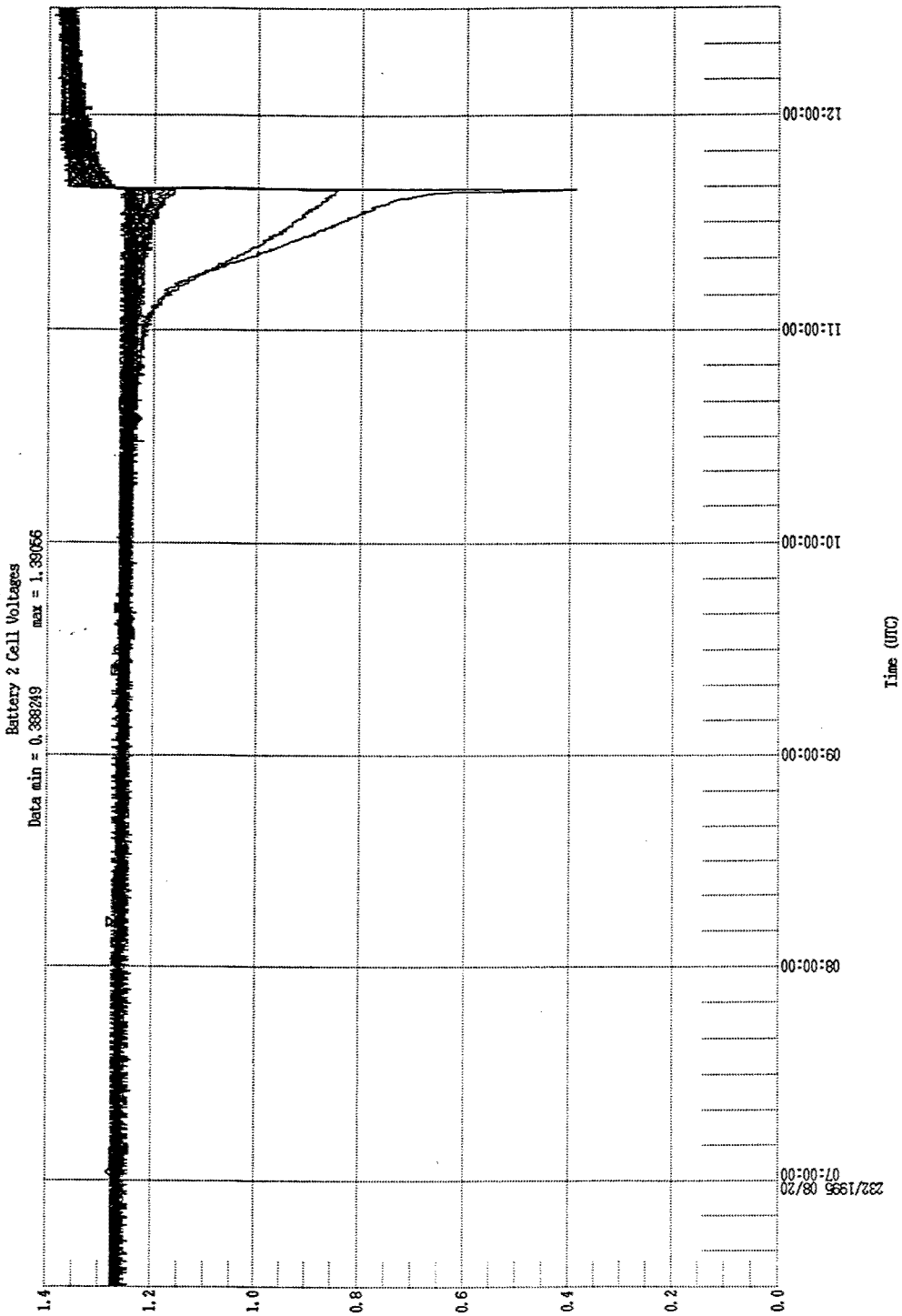

12/3/96

1996 NASA Aerospace Battery Workshop

I-VII FM2, Battery 2, 1996 Vernal Reconditioning Cell Profiles

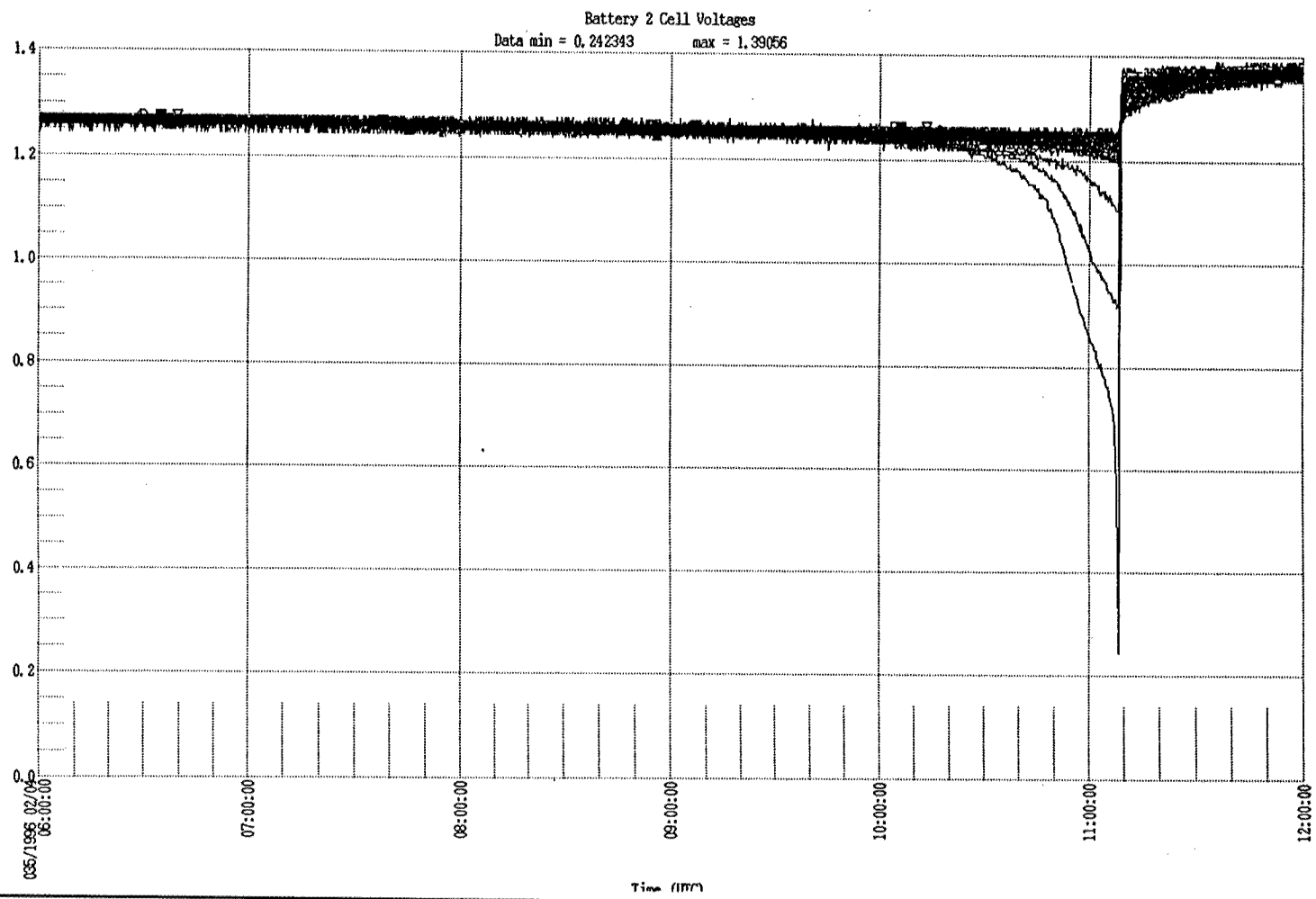

12/3/96 1996 NASA Aerospace Battery Workshop

I-VIIA FM6 , Battery 1, 1996 Vernal Reconditioning Cell Profiles

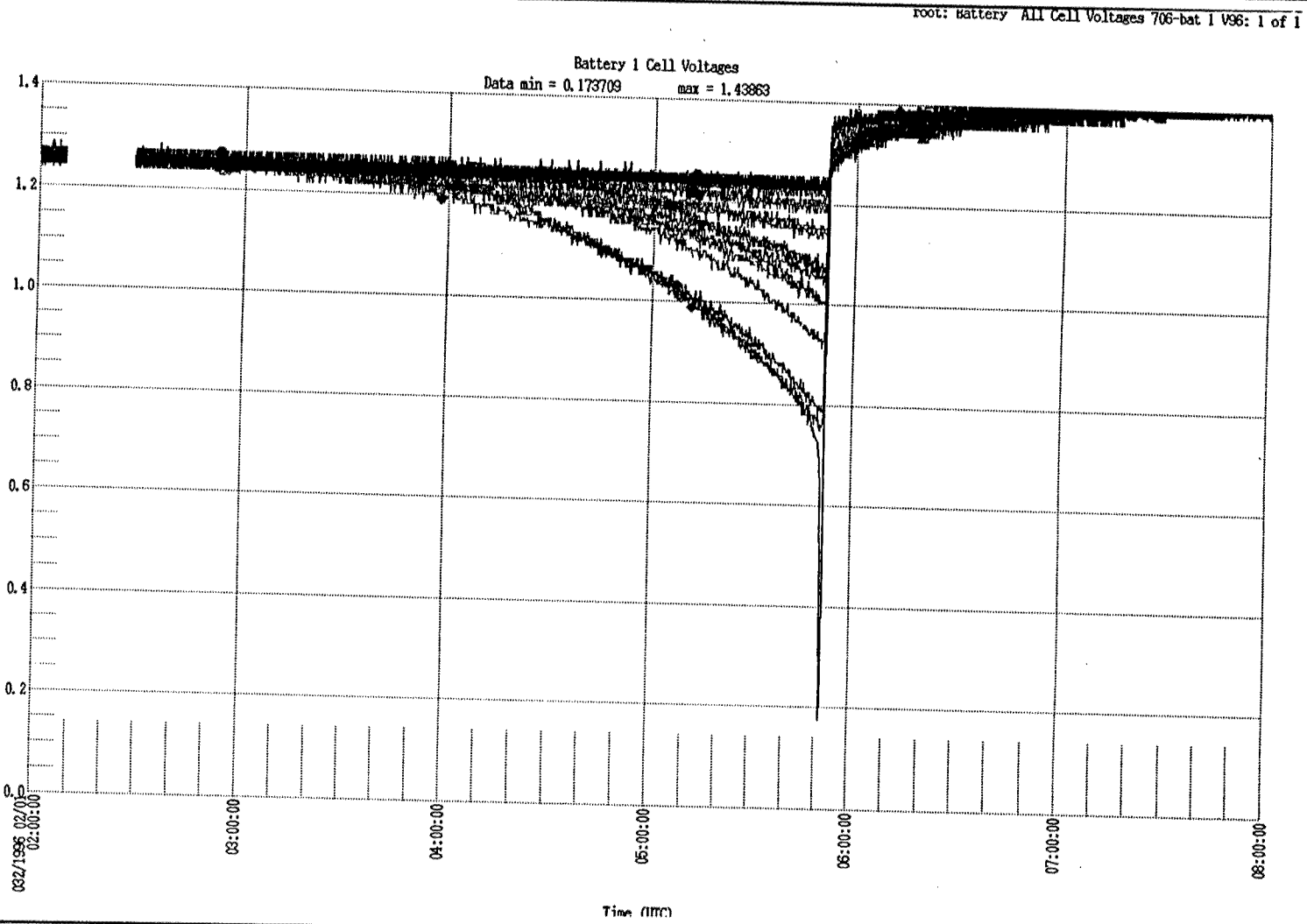

12/3/96 1996 NASA Aerospace Battery Workshop

I-VIIA FM6 , Battery 1, 1996 Autumnal Reconditioning Cell Profiles

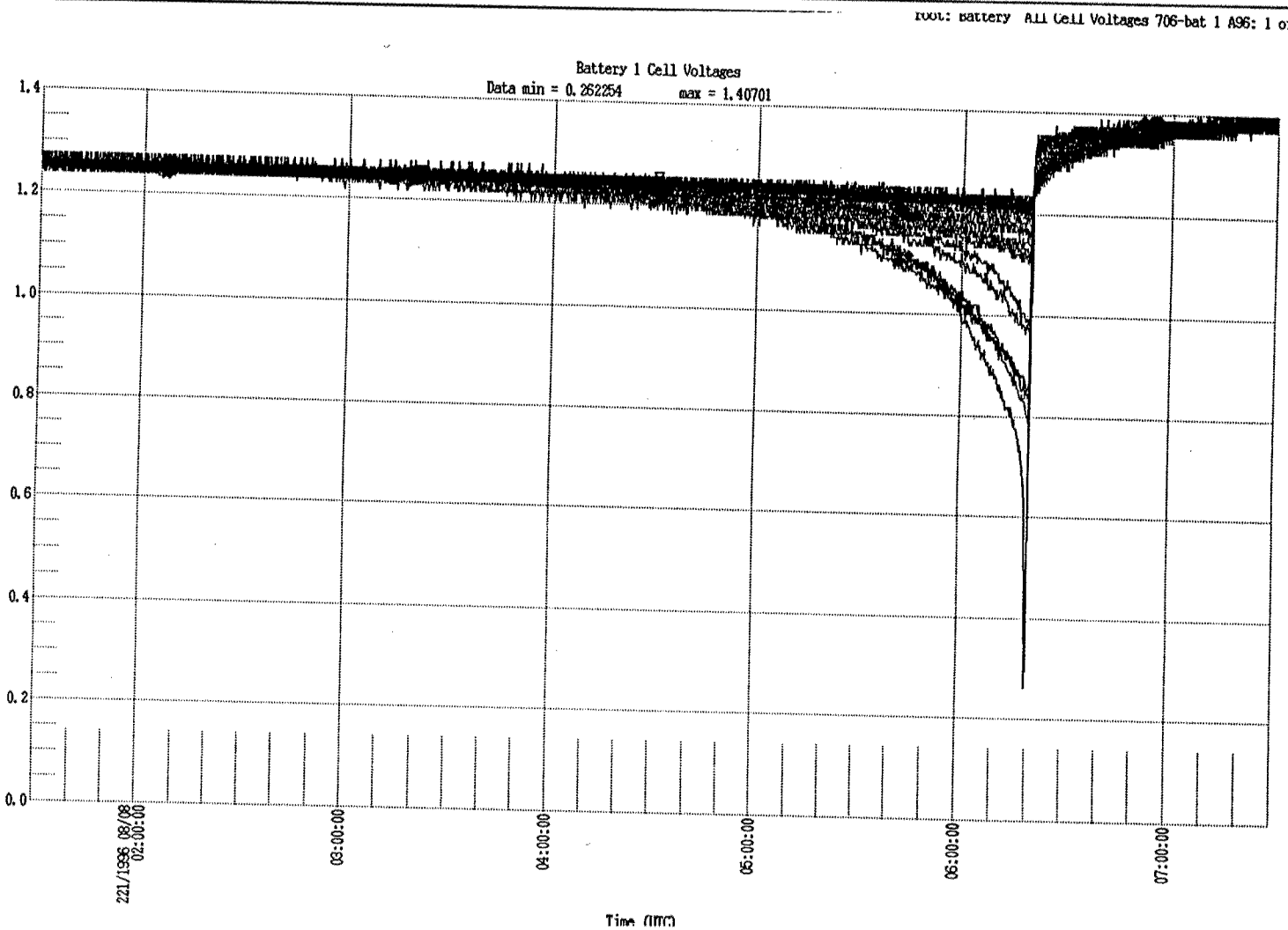

I-VIIA FM6 , Battery 2, 1995 Autumnal Reconditioning Cell Profiles

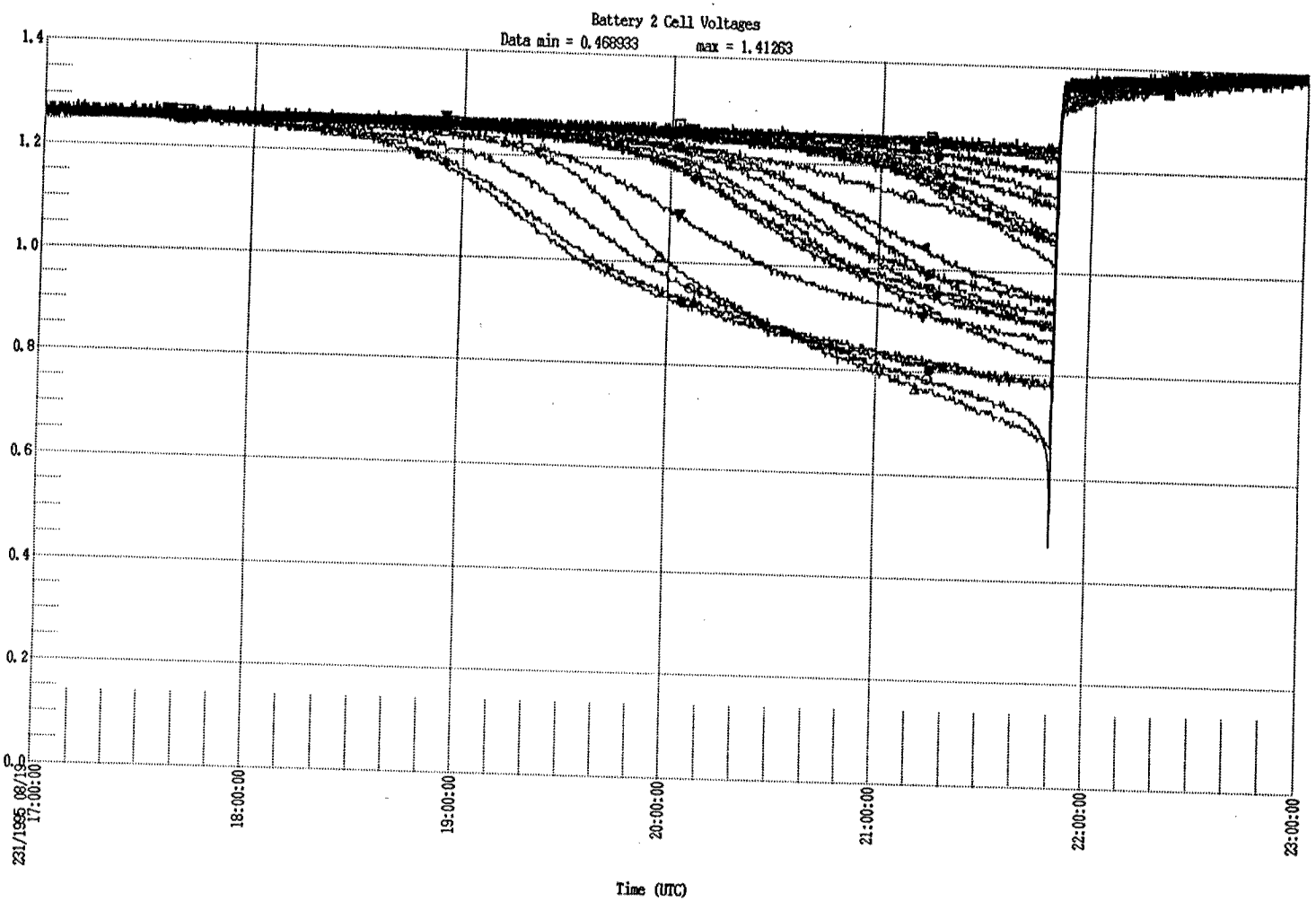

I-VIIA FM6 , Battery 2, 1996 Vernal Reconditioning Cell Profiles

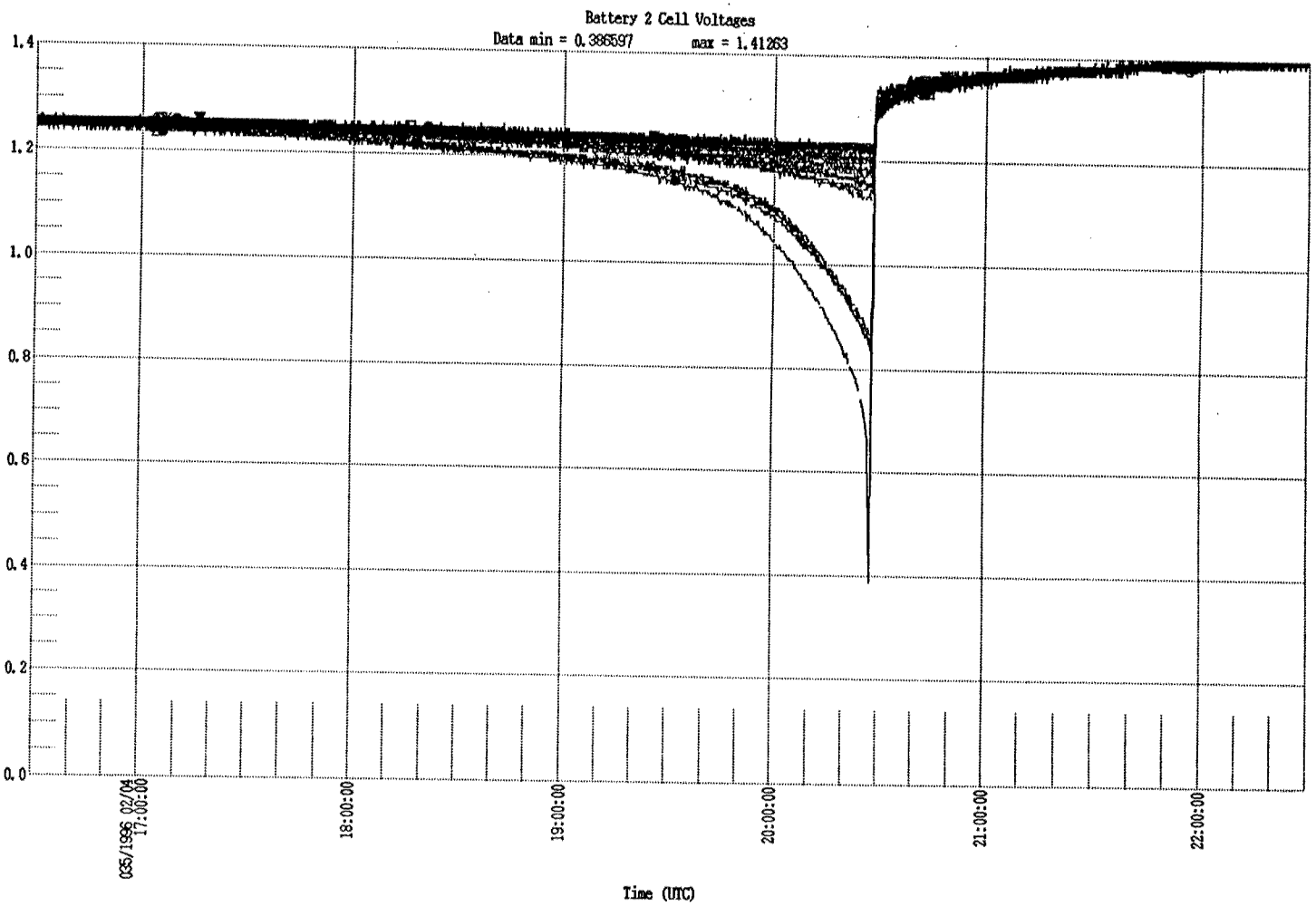

I-VIIA FM6 , Battery 2, 1996 Autumnal Reconditioning Cell Profiles

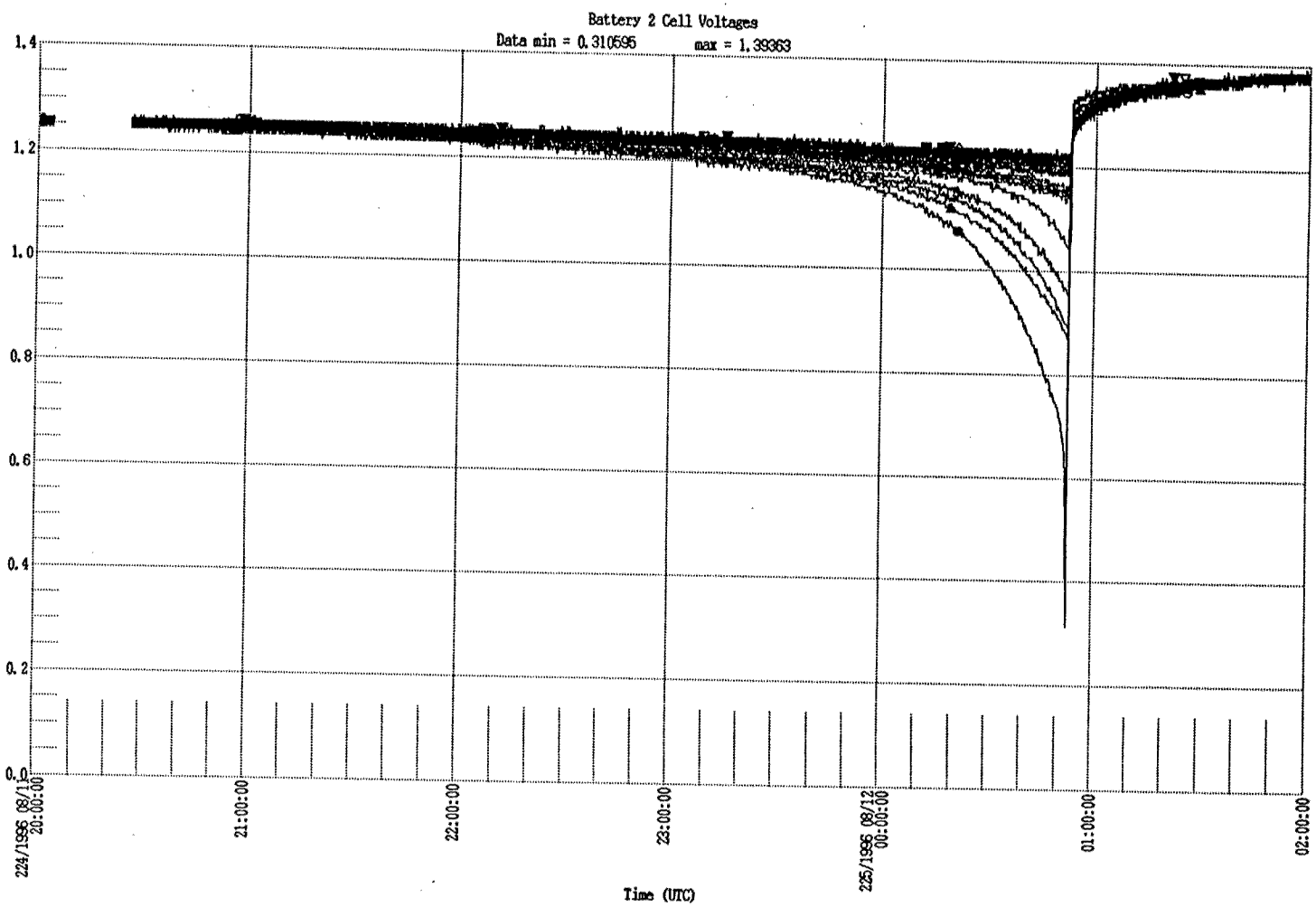

N-Star FMa Battery 1, 1996 Autumnal Reconditioning Capacity

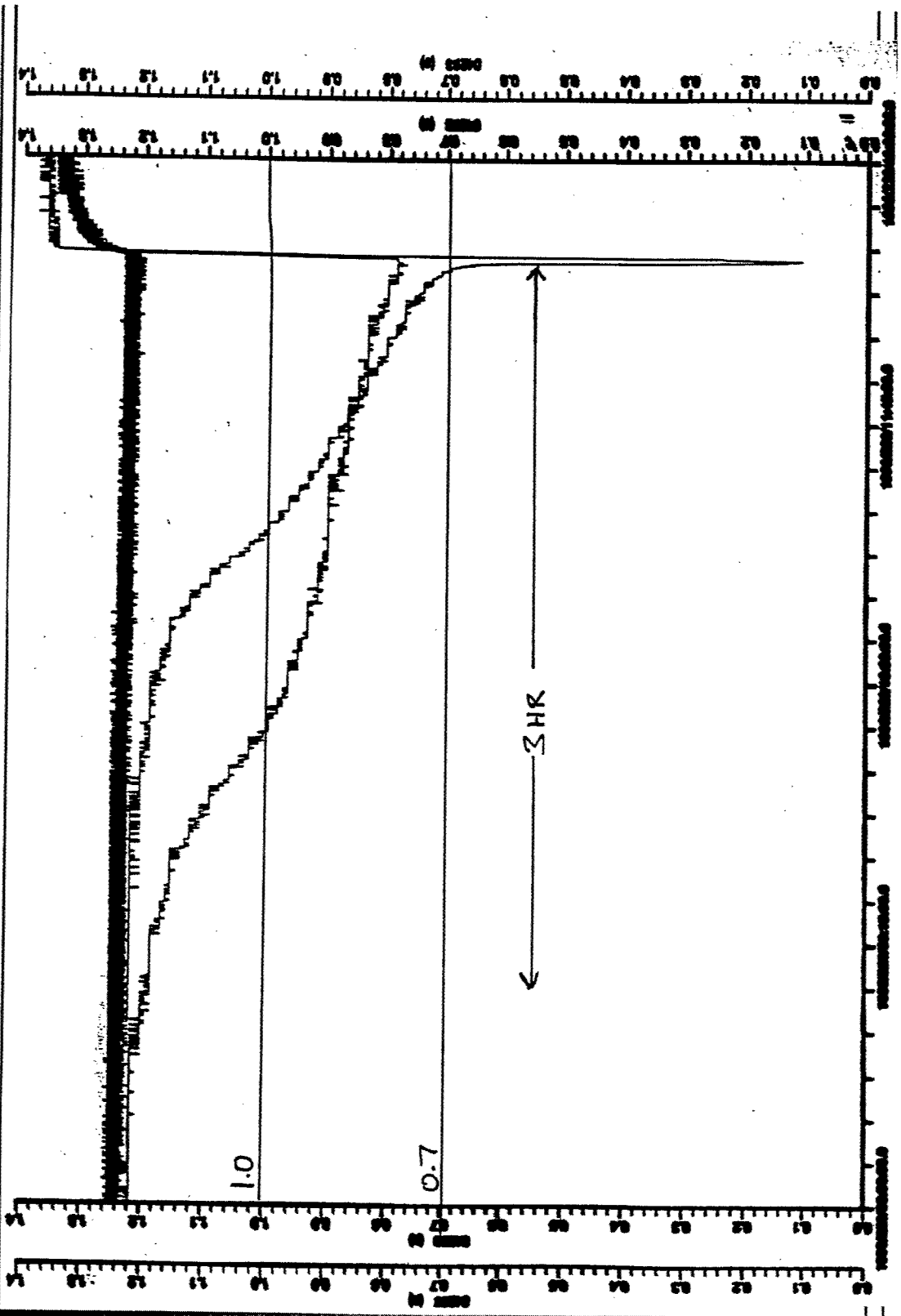

12/3/96

1996 NASA Aerospace Battery Workshop

N-Star FMa Battery 2, 1996 Vernal Reconditioning Capacity

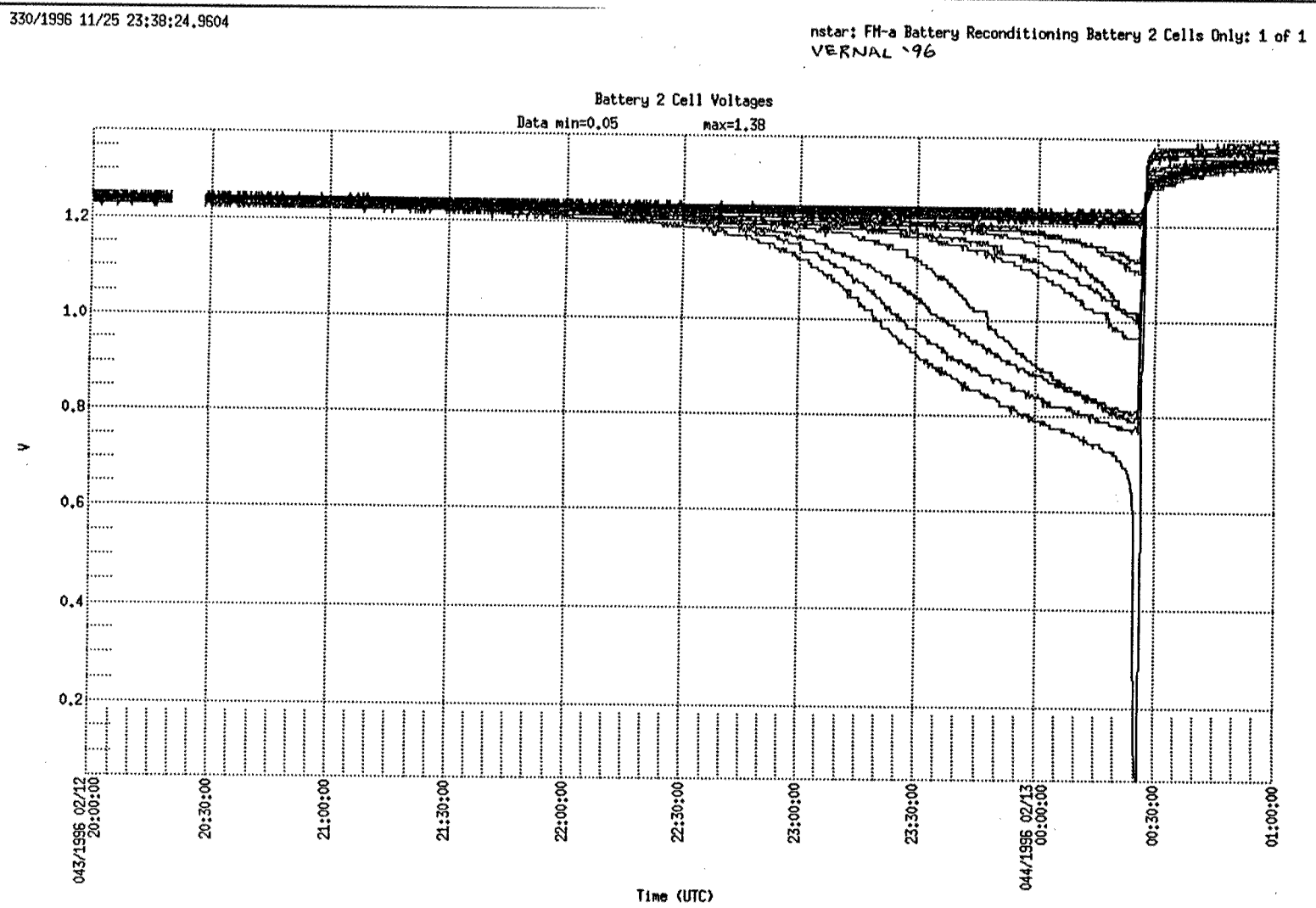

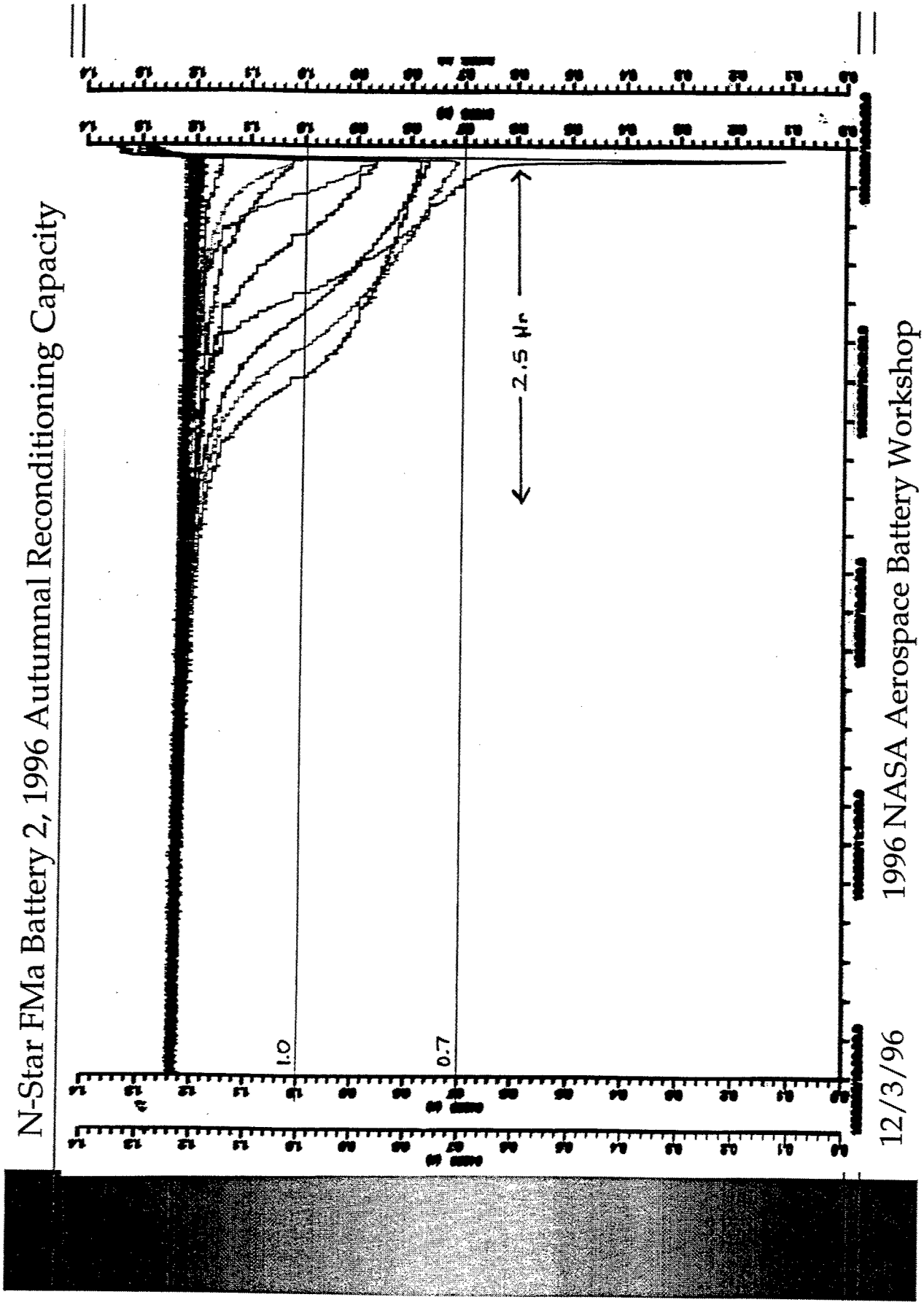
N-Star FMa Battery 2, 1996 Autumnal Reconditioning Capacity
1.0
0.7
2.5 Hr
12/3/96
1996 NASA Aerospace Battery Workshop

N-Star FMb Battery 1, Post 1996 Vernal Equinox Reconditioning Capacity

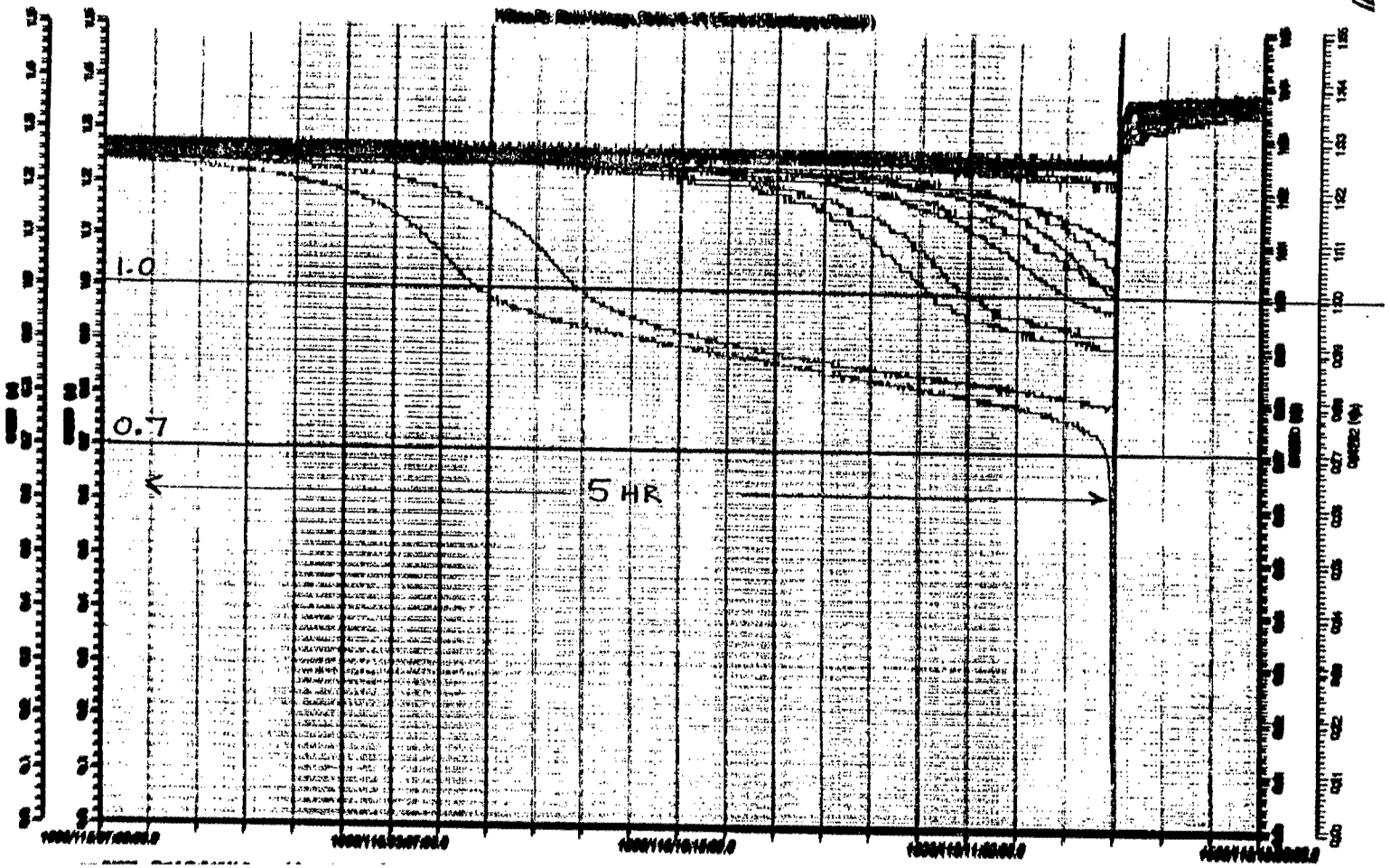

N-Star FMb Battery 1, 1996 Autumnal Reconditioning Capacity

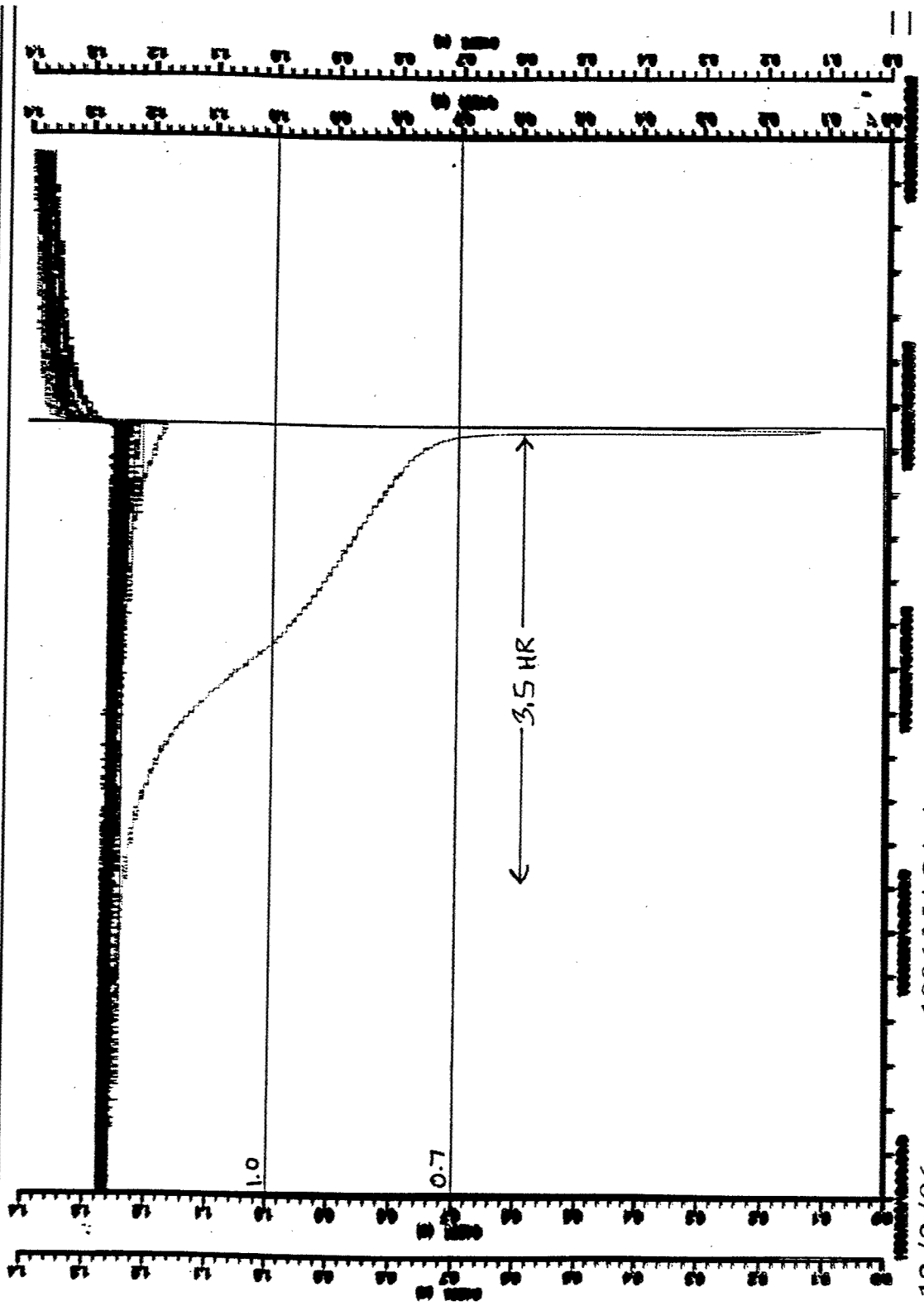

12/3/96

1996 NASA Aerospace Battery Workshop

N-Star FMb Battery 2, Post 1996 Vernal Equinox Reconditioning Capacity

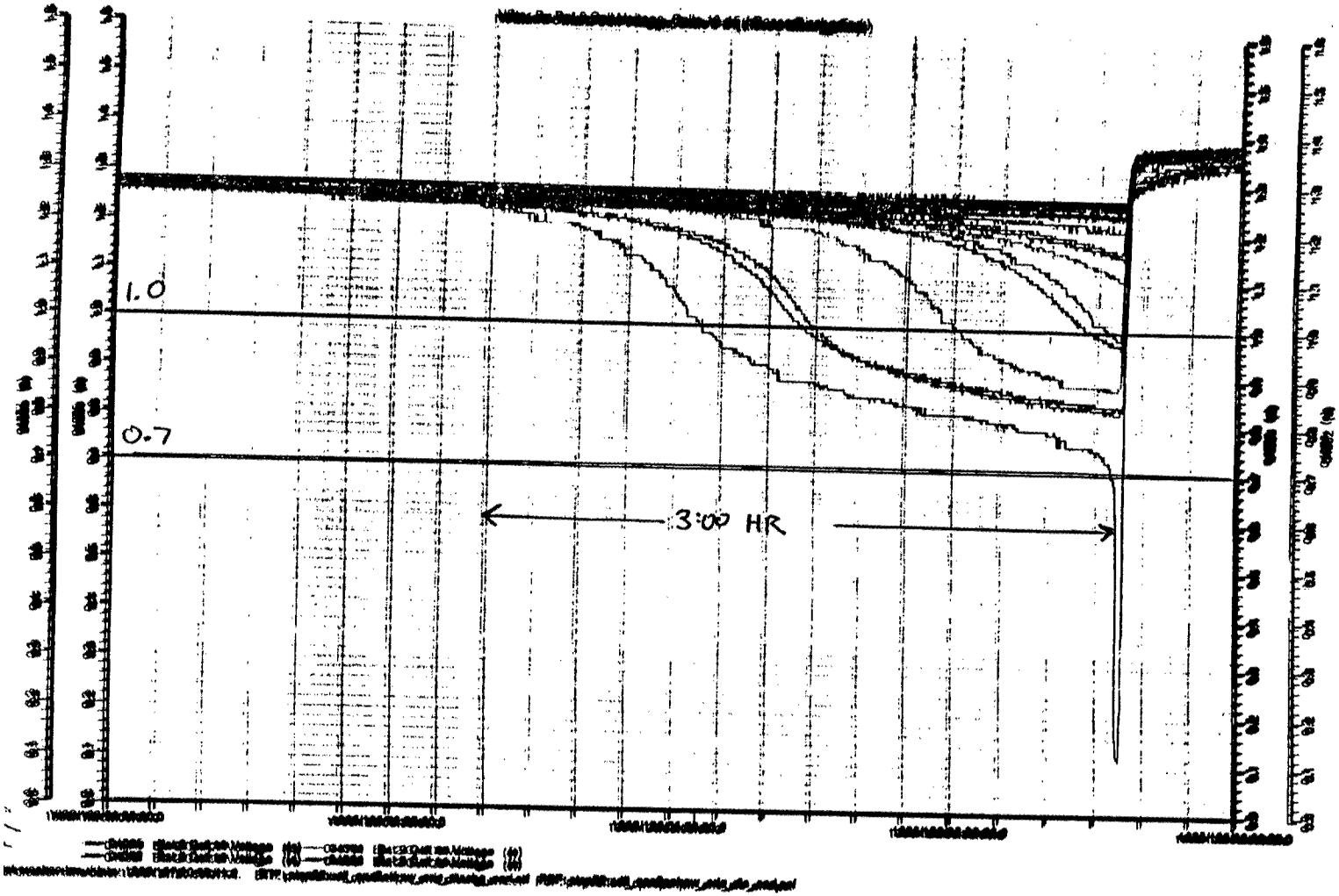

12/3/96 1996 NASA Aerospace Battery Workshop

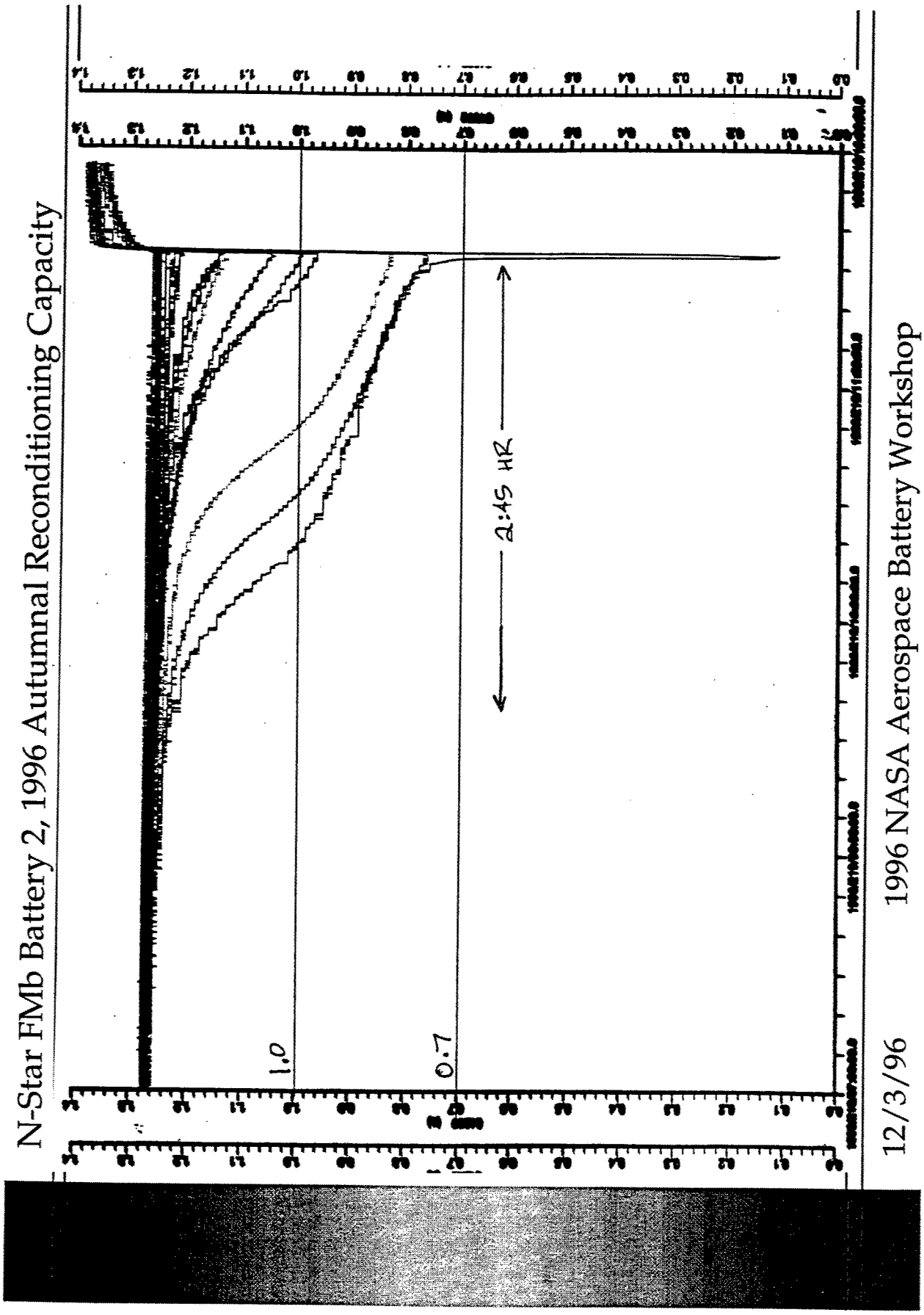
N-Star FMb Battery 2, 1996 Autumnal Reconditioning Capacity
1.0
0.7
2:45 HR
12/3/96
1996 NASA Aerospace Battery Workshop

Acknowledgments

- Marty Earl - COMSAT
- Steve Grippando - Lockheed Martin Aerosys
- Rick Hayden - Space Systems / LORAL
- Steve Lenhart - Space Systems / LORAL
- Jim Lemon - INTELSAT

Page
186
Blank

1996 NASA AEROSPACE BATTERY WORKSHOP

THE IN-ORBIT BATTERY RECONDITIONING EXPERIENCE ON BOARD THE ORION 1 SPACECRAFT

S. A. Hoover and S. Daughtridge
ORION SATELLITE CORPORATION
ROCKVILLE, MARYLAND

P.J. Johnson and S. T. King
MATRA MARCONI SPACE UK LTD.
STEVENAGE, ENGLAND

The Orion 1 spacecraft is a three-axis stabilized geostationary earth orbiting commercial communications satellite which was launched on November 29, 1994 aboard an Atlas II launch vehicle. The power subsystem is a dual bus, dual battery semi-regulated system with one 78 Ampere-hour nickel-hydrogen battery per bus. The batteries were built and tested by Eagle Picher Industries, Inc., of Joplin, MO and were integrated into the spacecraft by its manufacturer, Matra Marconi Space UK Ltd.

This paper presents the results obtained during the first four in-orbit reconditioning cycles and compares the battery performance to ground test data. In addition, the on-station battery management strategy and implementation constraints are described. Battery performance has been nominal throughout each reconditioning cycle and subsequent eclipse season.

Orion Satellite Corporation

Overview

- Battery Specifications
- Power Requirements
- Cell and Battery Characteristics
- Power Subsystem Block Diagram
- Power Subsystem Capabilities
- Objectives for Reconditioning
- Reconditioning Procedure
- Data
- Conclusion

This paper will discuss the battery specifications and power requirements that Orion Satellite Corporation presented to Matra Marconi Space for the Orion 1 satellite design. The selected cell and battery characteristics which satisfy the requirements will be identified. A brief description of the Eurostar 2000 power subsystem and its capabilities will be presented.

Following the objectives for reconditioning and procedure outline, the in-orbit results will be displayed and compared to ground test data. Finally, the achieved objectives will conclude the presentation.

Orion Satellite Corporation

Orion 1 Battery Specifications (1)

- Capable of supplying power to support launch, transfer orbit, and on-station eclipse operations (worst case: one failed cell per battery)
- Maximum depth of discharge < 70% (no cell failure) of nameplate capacity, DOD < 75% (one failed cell)
- Adequate charging system to recharge between eclipses
- Automatic end of charge control based on charge/discharge ratios or battery voltage/temperature limits
- Ability to override and/or inhibit the automatic end of charge control by ground command

The specifications that Orion Satellite Corporation (OSC) presented to Matra Marconi Space (MMS) for the Orion 1 satellite design were basically industry standard. The specifications were written to ensure that the power subsystem and all appropriate units of the subsystem were designed, manufactured, and demonstrated to meet the worst case power requirements during the various phases of the spacecraft mission over the entire designed orbital life-time of 10.5 years.

Orion Satellite Corporation

Orion 1 Battery Specifications (2)

- Sufficient telemetry to assess battery performance (voltage, current, temperature, pressure, etc.), including individual cell voltages
- Each battery shall be equipped with battery cell by-pass diodes for charge/discharge protection
- Capability to reconditioning each battery independently
- High and low discharge rates shall be selectable by ground
- No single point failure of the Power Subsystem shall inhibit the ability to charge and/or recondition either battery

In addition, the specifications were written to ensure that the battery performance can be monitored and protected automatically or by ground control. These requirements allow autonomous operation as well as operator intervention, if necessary, in the event of a failure. The power subsystem was designed such that no single point failure would affect the normal operation of the spacecraft; thus, all requirements of the Orion 1 spacecraft technical specification were satisfied.

Orion Satellite Corporation

Orion 1 Power Requirements

- Based on power estimates from unit manufactures
- The 75% DOD limit yielded a 78 Ah capacity battery
- Selected Eagle-Picher Industries, Inc. Ni-H_2 RNH-78 cell

	Solstice (Watts)	Equinox (Watts)	Eclipse (Watts)
Payload	2465	2465	2500
Platform	199	200	182
Thermal	230	393	142
Charging	66	336	0
Total	2960	3394	2824
Margin	460	360	>25% SOC

The total power budget was derived from the power requirements estimated by the unit manufactures. The batteries must support 2824W of power for the eclipse season. An average battery terminal voltage of 31.2 V (27 cells at 1.2 V per cell, with 1 failed cell) and a 700 mV drop across the battery diodes were used to calculate the minimum voltage. In addition, a maximum 5% imbalance between the two buses was also factored in the battery eclipse analysis.

$$2842\ \text{W} \div 2 \times 1.05 \div (31.2 - 0.7)\text{V} \times 1.2\ \text{hr} = 58.3\ \text{Ah}$$

Therefore to meet the 75% depth of discharge specification, a battery with a capacity of 78 Ah was selected for this mission.

Orion Satellite Corporation

Orion 1 Cell Characteristics

- Manufacturer: Eagle-Picher Industries, Inc.
- Type: Mantech design, Slurry-asbestos dual stack, Axial terminals, Hydrogen pre-charge
- Capacity (10°C): 78 Ampere-hours
- Dimensions: Length = 12.6", Diameter = 3.51"
- Mass: 1.87 ± 0.06 kg
- Heritage: Telecom 2 and Hispasat

The EPI (Eagle-Picher Industries, Inc.) nickel-hydrogen RNH-78 cell was an established design with in-orbit heritage on MMS' (Matra Marconi Space) Telecom 2 and Hispasat programs. The standard EPI "Mantech" design is a dual back-to-back stack of pineapple sliced plates with axial terminals. The electrode stack geometry provides optimal thermal characteristics for heat rejection capability.

Orion Satellite Corporation

Orion 1 Battery Characteristics

- Manufacturer: Eagle-Picher Industries, Inc.
- Type: 27 series connected 78 Ah cells,
  By-pass diode network
  4 heater circuits,
  Voltage, current, temperature, and pressure sensors
  Individual cell voltage monitoring
- Dimensions: Length=39.8", Width=18.8", Height=12.9"
- Mass: 67.4 kg
- Heritage: Telecom 2 and Hispasat

One battery pack consists of 3 rows of 9 cells with all 27 connected in series. Each cell has a by-pass diode network for failure protection. The network consists of 3 diodes in series for by-passing the cell during charge and 1 diode in parallel for the discharge case. In addition, each battery has individual cell voltage telemetry which is sequentially scanned approximately once a minute (i.e., every other format).

Each battery has one terminal voltage, one pressure, two current, and three temperature sensors for telemetry monitoring. Two of the thermistors are located on the top (i.e., the dome of the cell that points towards the interior of the spacecraft) of two separate cells. The third thermistor is located on the bottom (i.e., the dome near the radiator panel) of one of the two previous cells. This thermistor configuration provides a cell-to-cell gradient as well as a cell temperature delta to calculate radiator panel efficiency.

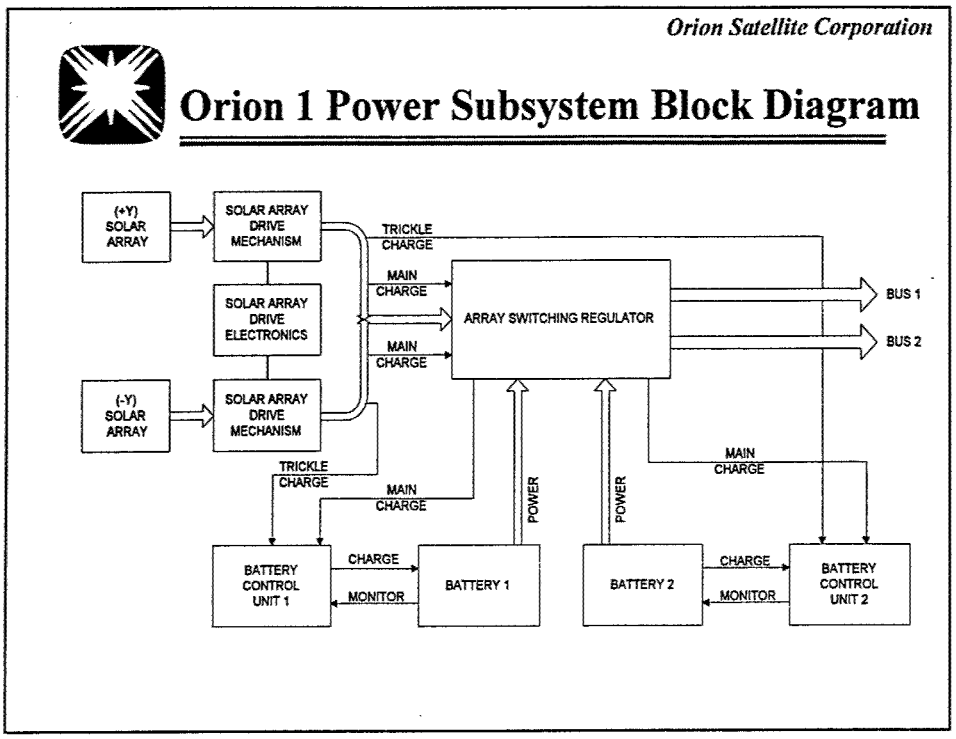

The power subsystem (PSS) provides electrical power to the spacecraft subsystems and payload for all phases of the mission. The power supply is regulated in sunlight and unregulated in eclipse. A functional block diagram of the PSS is shown above. The PSS may be described as a twin bus, twin battery, semi-regulated system. The power is generated from silicon n-on-p solar cells which are mounted on two solar array wings, each wing consisting of four panels. Power is transferred to the array switch regulator (ASR) by the solar array drive mechanism slip-rings. The wings are independent rotated about the pitch axis of the spacecraft to maintain sun pointing.

During periods when solar power is not available, the satellite is powered from energy stored in two nickel-hydrogen batteries. The batteries are recharged in sunlight from dedicated solar array sections. These sections provide a constant current source for charging. Trickle chargers are also available to assist main charge; however, the chargers are primarily used to maintain the battery state of charge. There are four such chargers, two in each battery control interface unit (BCIU).

Each battery provides a supply voltage of nominally 27 to 42 V at the PSS output interface. Battery 1 supports main bus 1 and battery 2 is dedicated to main bus 2.

Orion Satellite Corporation

Orion 1 Power Subsystem Capabilities

- Solar array main charge sections to either battery (C/17)
- Flexibility to charge with both main charge sections (C/9)
- Trickle chargers can be set to variable rates (0 to C/65)
- All 4 trickle chargers can be configured to assist main charge
- Automatic EOC, EOD, over-temperature, and under-voltage protection provided
- Independent battery reconditioning, discharge at high or low rate (C/39 or C/105)

The MMS Eurostar 2000 power subsystem provides various capabilities and configurations for flexible operations. The numerous charge rates which can be selected by ground control combined with the autonomous protection functions allow the user to optimize the power subsystem. However, minimizing the configuration changes reduces the number of variables in the battery capacity analysis and produces comparable results.

Orion Satellite Corporation

Objectives for Reconditioning

- To provide a health check of the battery
- To measure cell performance and characteristics
- To provide a bi-annual assessment of the "usable" capacity
- To help decrease or remove the capacity "fade" due to pre-launch storage
- To increase capacity and maintain the battery at the highest level of performance

Reconditioning provides an opportunity to assess and status the health of the each battery twice a year. The procedure also allows the operator to trend the performance of the cells and identify any end of life concerns regarding power margin. It should be noted that the battery capacity "fade" due to pre-launch storage may be reduced or even eliminated by in-orbit reconditioning. However, reconditioning allows one to identify and track the useful capacity of each battery and maintain the batteries at the highest performance level.

Orion Satellite Corporation

Reconditioning Procedure (1)

- Initial discharge
  - Trickle charger switched off (1 per battery)
  - Battery connected to primary and secondary loads of 36 ohms each
  - Discharge current of approximately 2.0 Amps
  - Discharge until minimum cell voltage reaches 1.05 Volts
- Reduced rate discharge
  - Secondary load disconnected
  - Discharge current of approximately 1.0 Amps
  - Discharge until minimum cell voltage reaches 0.5 Volts

In order to maintain the highest level of performance, each battery is sequentially reconditioned. One battery remains fully charge to optimize satellite safety. The reconditioning battery is connect to both the primary and secondary loads and discharged until the minimum cell voltage reaches 1.05 V. After disconnecting the secondary load, the battery is further discharged until the minimum cell voltage reaches 0.5 V. The reconditioning loads are located on the battery radiator panels.

Orion Satellite Corporation

Reconditioning Procedure (2)

- Recharge
  - K-factor (C/D ratio) set to 1.25
  - Charge via main charge (approx. 4.5A, C/17) until 700 psi is reached
  - Update K-factor to 1.15
  - Set Amperehour meter to derived parameter value (P/T)
  - Charge via main charge until Amperehour meter reaches 82 Ahrs
  - Monitor battery voltage < EOC voltage threshold (42.45 V)
  - Monitor battery temperature profile (rate of increase < 4°C/hour)
    - The over-temperature threshold is 26 °C
- End of charge
  - Trickle charger switched on
  - Set trickle charge rate to 0.48A (C/163)

The battery is recharged to 700 psi with a C/D ratio of 1.25. At 700 psi, the on board integrated coulometer is updated to the ground derived amperehour value. The derived parameter value is based on the actual battery pressure and temperature from telemetry with correction factors determined from ground tests. Following the amperehour update, the battery is recharged with a C/D ratio of 1.15 to 82 Ahrs. Charge is terminated manually. The 82 Ahrs is the maximum battery capacity value set by ground command. This value was also determined during ground testing. While approaching end of charge, the battery voltage and temperature are closely monitored to ensure that the hardware logic threshold for EOC is not violated. In addition , the exothermic characteristics of the Ni-H_2 battery are monitored for over temperatures. Finally, the battery is placed on trickle charge using the nominal on-station electronic trickle charger configuration and rate. Once the exothermic characteristics taper off, the trickle charger provides the remaining charge to the battery in order to approach 100% state of charge.

Orion Satellite Corporation

Orion 1 Reconditioning Data (1)

- Four cycles completed with nominal results
- Capacity increase has stabilized

		BATTERY 1 (N)				BATTERY 2 (S)			
		#1 WS 95	#2 SS 95	#3 WS 96	#4 SS 96	#1 WS 95	#2 SS 95	#3 WS 96	#4 SS 96
Start		12/25/94	7/17/95	2/12/96	7/29/96	1/6/95	7/31/95	1/29/96	8/12/96
End		12/28/94	7/21/95	2/15/96	8/2/96	1/10/95	8/4/95	2/2/96	8/16/96
Duration (hr)	High Rate	39:52	45:23	46:15	46:32	39:44	45:51	46:39	46:55
	Low Rate	52:56	57:12	59:10	58:01	55:57	58:34	59:08	58:54
	Charge	19:15	26:09	24:41	25:36	19:48	26:21	25:41	26:18
Discharge (Ahr)	High Rate	81.59	91.95	96.25	96.95	83.45	93.40	97.24	97.60
	Low Rate	11.90	9.76	11.00	9.55	12.89	10.67	10.03	9.51
	Total	93.49	101.71	107.25	106.50	96.34	104.07	107.27	107.11
Stop Discharge	High Rate	Cell 10	Cell 10	Cell 10	Cell 10	Cell 1	Cell 1	Cell 1	Cell 2
	Low Rate	Cell 10	Cell 10	Cell 10	Cell 10	Cell 5	Cell 5	Cell 5	Cell 16
	Charge	82 Ahr	82 Ahr	82 Ahr	82 Ahr	82 Ahr	82 Ahr	82 Ahr	82 Ahr
Pressure (psi)	High Rate	242	230	230	219	200	188	188	188
	Low Rate	150	150	150	150	100	100	100	112
	Charge	956	967	978	967	923	969	969	992
Min Voltage (V)	High Rate	33.42	33.13	33.13	32.93	33.59	32.73	32.33	31.52
	Low Rate	24.74	23.85	24.09	24.30	23.46	23.29	23.29	22.93
	Charge	42.3	42.12	41.76	42.12	42.30	42.12	41.96	41.96
Charge (Ahr)	Total	106.50	111.04	112.67	111.15	112.30	115.18	115.87	116.31

The first reconditioning cycle was performed by MMS prior to acceptance. Due to timing constraints, the procedure used during the first cycle was modified to expedite the activities. The subsequent cycles have been performed by Orion Satellite Corporation with consistent procedures. By the fourth cycle, both batteries have exhibited an increase in end of discharge (EOD) capacity of approximately 10-12% compared to the first reconditioning cycle. The increase was expected as the capacity "fade" due to pre-launch storage decreases during the first few cycles.

It should be noted that cell 10 on battery 1 has consistently been the driving cell for terminating discharge. Cell 10 also demonstrated weaker characteristics compared with the other battery 1 cells during ground testing. The battery 2 cells, on the other hand, are more closely matched. The discharge termination cell on battery 2 has varied.

The return capacities have increased by 3-5% compared to the first cycle. The minimum battery voltages and pressures have been consistent throughout the first four cycles. However, due to the location of the batteries and the thermal influence of solar input, it is believed that a season to season comparison provides an improved assessment of the results.

Orion 1 Reconditioning Data (2)

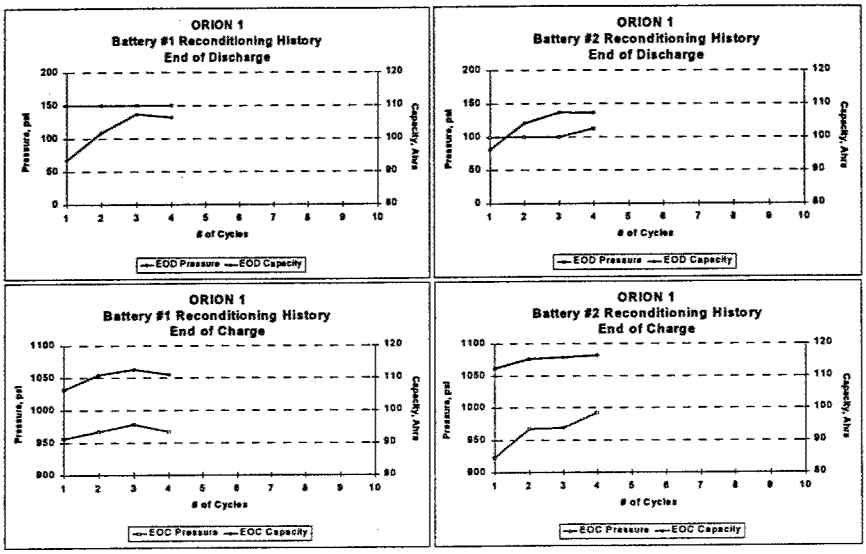

The end of discharge capacity increase provides evidence that the capacity "fade" due to pre-launch storage has decreased during the first few cycles. The "knee" shown in the EOD curves indicates that the capacity increase may have stabilized for both batteries. In addition, the end of charge capacities have increased by 3-5% from the first cycle and appear to have also stabilized. The EOD and EOC pressures have remained relatively constant (± 1-2 telemetry bits, where 1 bit = 12 psi) throughout the first four cycles.

The following graphs illustrate and compare the actual in-orbit discharge and charge cycles performed by Orion Satellite Corporation. Both batteries have exhibited consistent results.

Orion Satellite Corporation

Orion 1 Reconditioning Data (3)

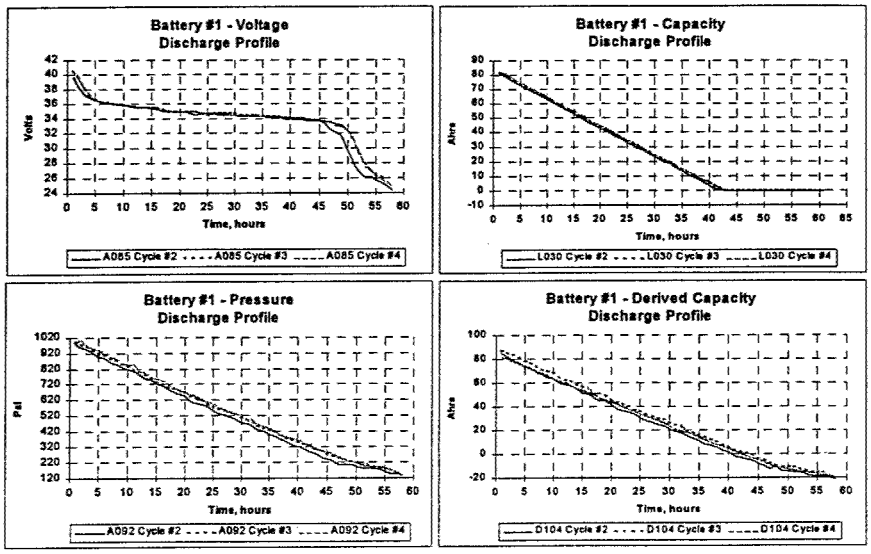

Orion Satellite Corporation

Orion 1 Reconditioning Data (4)

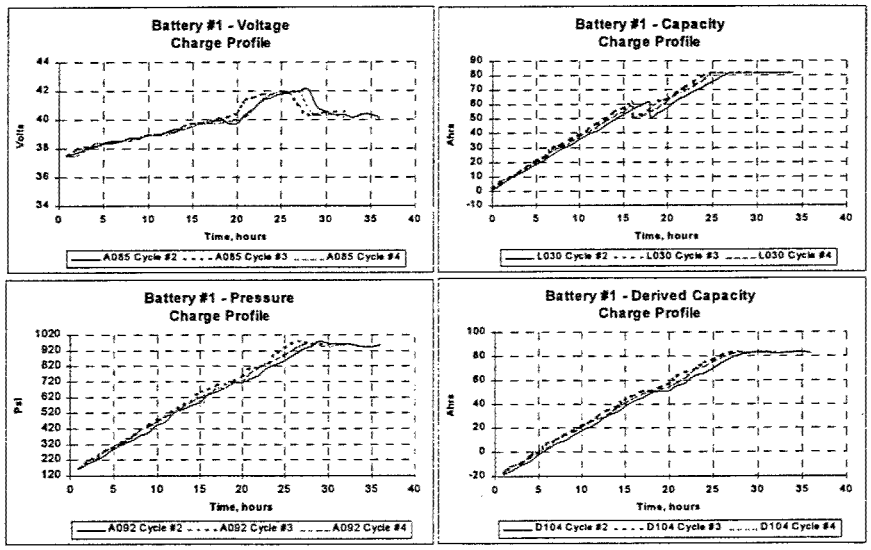

Orion Satellite Corporation

Orion 1 Reconditioning Data (5)

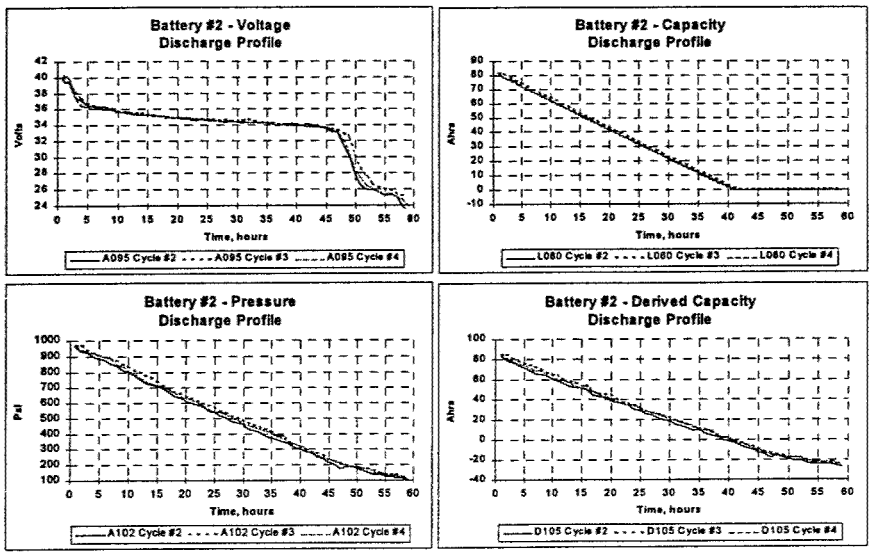

Orion Satellite Corporation

Orion 1 Reconditioning Data (6)

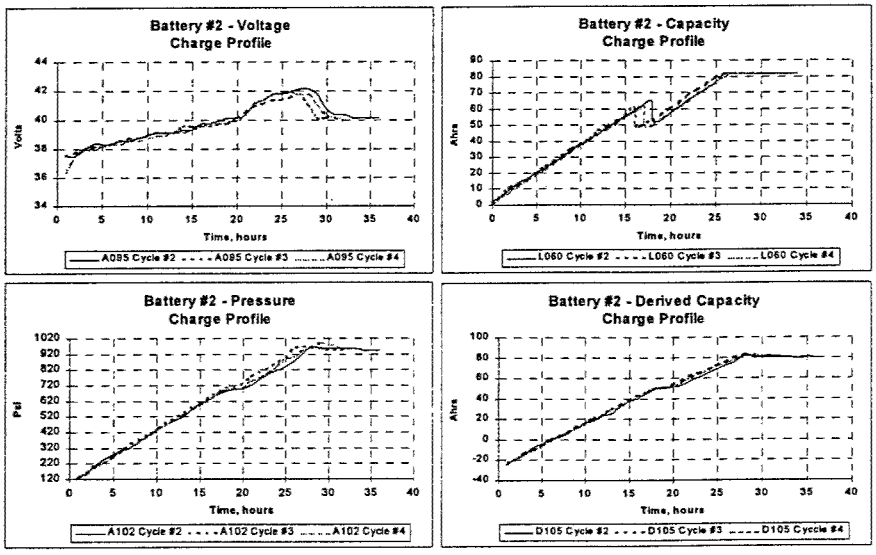

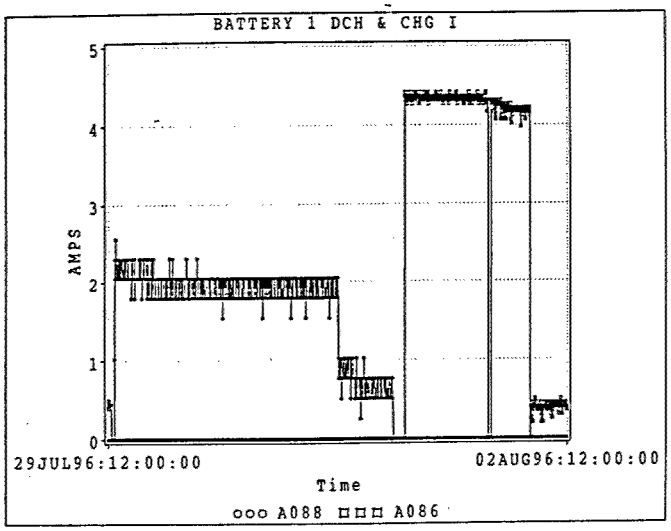
BATTERY 1 DCH & CHG I
AMPS
29JUL96:12:00:00
02AUG96:12:00:00
Time
ooo A088 □□□ A086

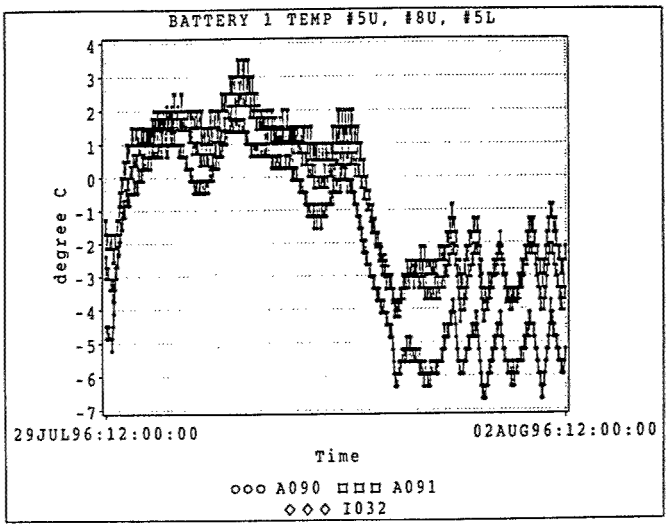
BATTERY 1 TEMP #5U, #8U, #5L
degree C
29JUL96:12:00:00
02AUG96:12:00:00
Time
ooo A090 □□□ A091
◇◇◇ I032

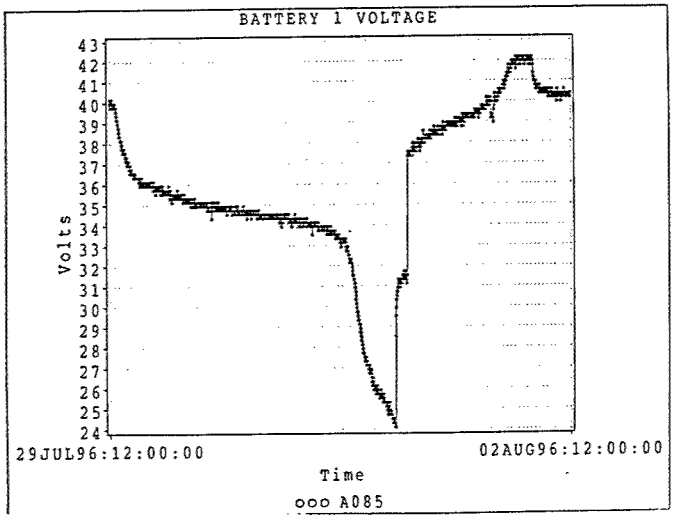
BATTERY 1 VOLTAGE
Volts
29JUL96:12:00:00
02AUG96:12:00:00
Time
ooo A085

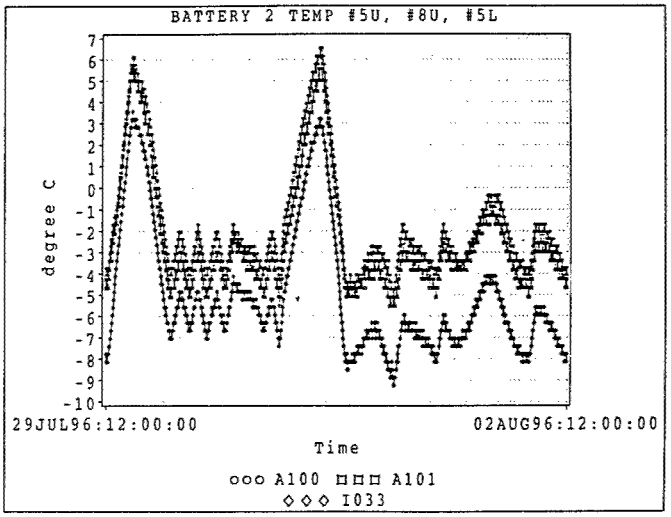
BATTERY 2 TEMP #5U, #8U, #5L
degree C
29JUL96:12:00:00
02AUG96:12:00:00
Time
ooo A100 □□□ A101
◇◇◇ I033

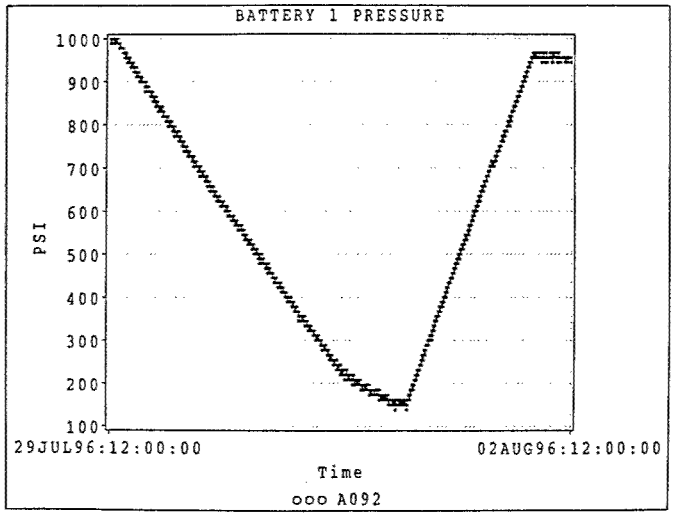
BATTERY 1 PRESSURE
PSI
29JUL96:12:00:00
02AUG96:12:00:00
Time
ooo A092

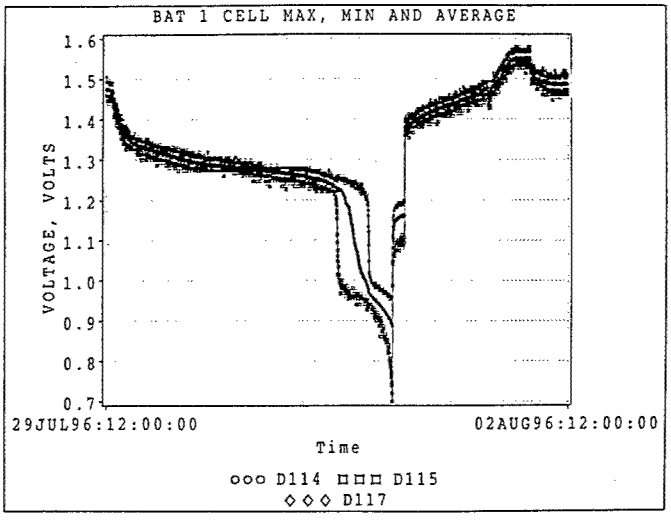
BAT 1 CELL MAX, MIN AND AVERAGE
VOLTAGE, VOLTS
29JUL96:12:00:00
02AUG96:12:00:00
Time
ooo D114 □□□ D115
◇◇◇ D117

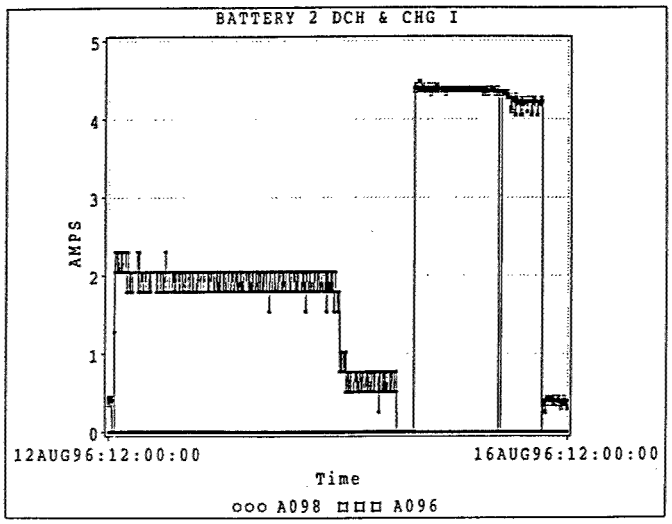
BATTERY 2 DCH & CHG I
AMPS
12AUG96:12:00:00
16AUG96:12:00:00
Time
ooo A098 □□□ A096

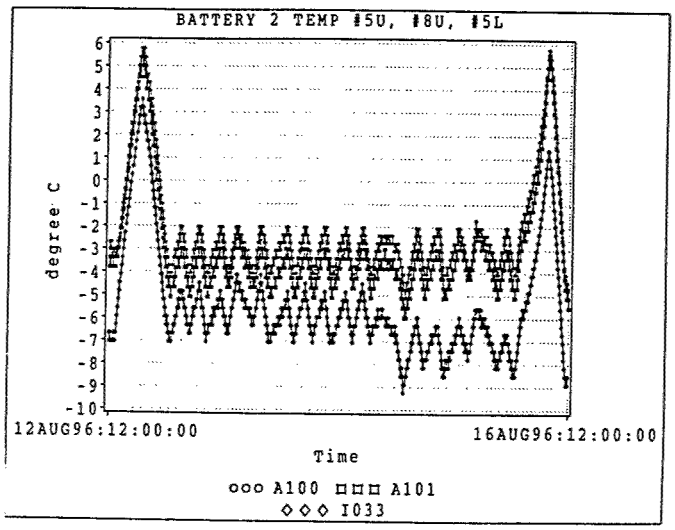
BATTERY 2 TEMP #5U, #8U, #5L
degree C
12AUG96:12:00:00
16AUG96:12:00:00
Time
ooo A100 □□□ A101
◇◇◇ I033

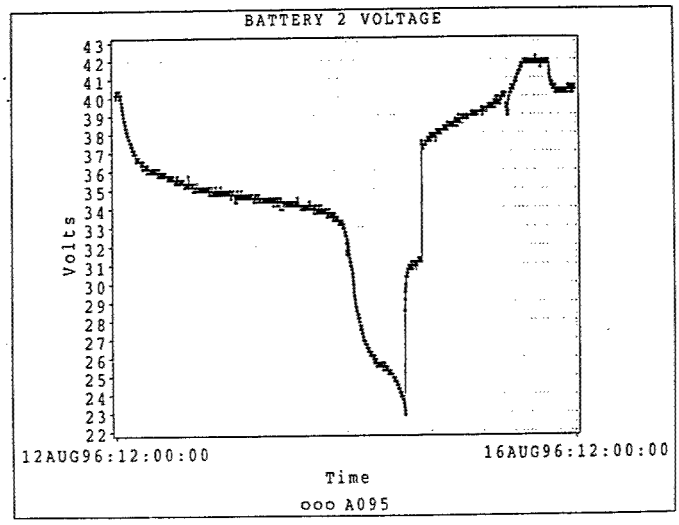
BATTERY 2 VOLTAGE
Volts
12AUG96:12:00:00
16AUG96:12:00:00
Time
ooo A095

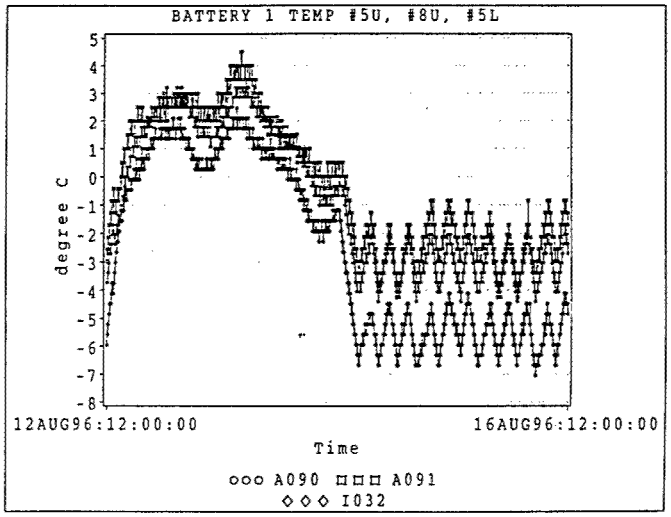
BATTERY 1 TEMP #5U, #8U, #5L
degree C
12AUG96:12:00:00
16AUG96:12:00:00
Time
ooo A090 □□□ A091
◇◇◇ I032

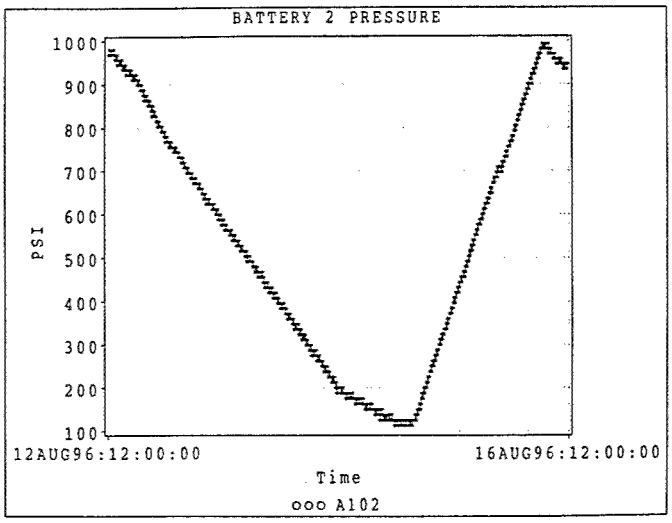
BATTERY 2 PRESSURE
PSI
12AUG96:12:00:00
16AUG96:12:00:00
Time
ooo A102

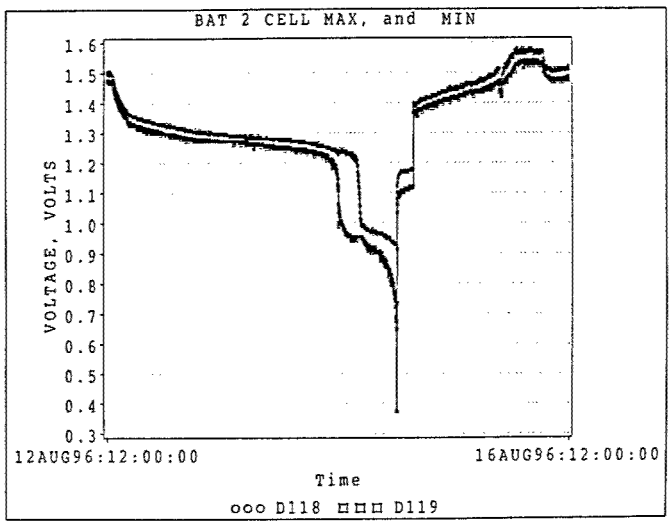
BAT 2 CELL MAX, and MIN
VOLTAGE, VOLTS
12AUG96:12:00:00
16AUG96:12:00:00
Time
ooo D118 □□□ D119

Orion 1 Reconditioning Data (7)

- Reconditioning was performed by MMS during spacecraft solar simulation (SST) and simmer (TVT) tests
- In-orbit data is consistent with ground test results

		BATTERY 1 (N)		BATTERY 2 (S)	
		SST	TVT	SST	TVT
Start		4/27/94	8/11/94	4/27/94	8/11/94
End		5/1/94	8/16/94	5/1/94	8/16/94
Discharge (Ahr)	High Rate	95.1	93.1	94.9	92.4
	Low Rate	12.5	11.9	12.9	12.6
	Total	107.6	105.0	107.8	105.0

During spacecraft ground tests, reconditioning was performed on each battery by Matra Marconi Space. The results are shown above. These results have been compared to the in-orbit data and found to be consistent. The discharge and charge profiles have also been compared to the in-orbit profiles and found to be satisfactory.

Orion Satellite Corporation

Conclusion

- Four cycles completed with nominal results
- In-orbit data is consistent with ground test results
- "Usable" capacity has been assessed
- Capacity increase appears to have stabilized
- Battery performance has been satisfactory during subsequent eclipse seasons

The Orion 1 satellite has satisfactorily completed the first four in-orbit battery reconditioning cycles. Both batteries have exhibited consistent and nominal results compared to ground test data. Battery reconditioning has provided a bi-annual assessment of the "usable" capacity, established an in-orbit performance baseline, and furnished an opportunity to trend the current performance which may identify any end of life power margin concerns. After two years on-station, the Orion 1 batteries have performed nominally with no present concerns.

The INTELSAT Experience with Reconditioning of NiH_2 Batteries

Frank Scalici, Andrew Dunnet, and Daphne Xu
International Telecommunications Satellite Organization
Washington, D.C.

INTRODUCTION

INTELSAT has been reconditioning NiH_2 batteries since 1983 when the INTELSAT V F-6 geosynchronous communications satellite was launched. This was the first commercial use of NiH_2 batteries. INTELSAT has continued this practice on all 46 NiH_2 batteries it has operated in-orbit. The batteries are of several types including the classic INTELSAT cell, the HAC re-circulating design, and the Gates Mantech design.

Reconditioning is performed twice each year, prior to the Eclipse Season. At this time Water Migration problems, if present, are dealt with. Temperature limits are imposed for the discharge and charge cycles as a safety precaution.

In support of in-orbit operations, it is INTELSAT's practice to perform ground based life tests. In-orbit data and ground tests results are presented and the benefits of reconditioning noted.

PROCESS

Prior to each eclipse season the Power subsystem is configured such that half the batteries aboard can maintain the satellite in an emergency while the remainder are placed on the reconditioning load until a preset cell voltage limit is met or, in cases where cell voltage telemetry is unavailable, until a battery voltage limit is met. Where available, automated systems calculate amp hours removed by comparing battery voltage and the size of the load and then integrating over the period of the discharge. On the INTELSAT K and INTELSAT VI, the average voltage over time is used to integrate the amp hours removed. All other series use the average voltage method as a backup to the automated processes. The batteries are then recharged to a pre-determined Charge/Discharge (C/D) ratio. When these batteries have completed the cycle, the remaining batteries are then started.

The C/D is intentionally set 5% less than would be used for a typical eclipse recharge in keeping with INTELSAT policy of avoiding overcharge whenever possible. The schedule allows a sufficient amount of time spent at trickle charge to return to a full state of charge prior to the first eclipse. In addition to voltage limits, temperature limits are set to ensure safety. Table 1 lists the various types of cells used.

REASONS TO RECONDITION

There are several reasons INTELSAT continues to recondition NiH_2 batteries in-orbit and require a reconditioning capability on its future satellites. INTELSAT's position is that reconditioning NiH_2 batteries provides for:

- an assessment of state of health prior to each eclipse season .

- a method for dealing with water migration within NiH_2 cells should it occur.

- an evaluation of pressure increase to establish whether the increase is due to capacity gain or corrosion.

- an enhancement of performance in EODV and cell voltage matching during discharge.

- a correlation between life test data and in-orbit performance.

- a source of flexibility for battery operations.

RESULTS

1. Assessment of State of Health.

A assessment of state of health is derived during the reconditioning by collecting and tabulating various data (see Table 2). The total capacity to the voltage limit, battery EODV, cell EODV, and delta pressure or capacity are analyzed. These data are then compared to previous seasons to identify net changes. Particular attention is paid to the total capacity which should only vary seasonally and cell voltage spread on discharge. Recently, capacity below 1.0 volts to the voltage limit has been characterized to assess whether or not the amount of capacity below 1.0 volts is changing. This is of particular interest on new INTELSAT VII or VIIA batteries which tend to have larger capacities below 1.0 volts when launched then, with cycling, recover useful capacity.

2. Method for Dealing with Water Migration

The use of reconditioning as a method for dealing with water migration was documented in reference 1. Each eclipse season "Frank Plots" are made for the longest eclipse day for each battery in-orbit. Frank Plots show each cells minimum and maximum voltage over 24 hours referenced to the average voltage at either end of discharge or end of charge. These plots are analyzed for changes in cell impedance which is thought to be symptomatic of water migration from the stack. If problematic cells are identified the battery is subjected to the COMSAT/INTELSAT developed procedure to rejuvenate the cell.

As an example (see Figures 1 and 2), the plots for Spring 1996 longest eclipse indicated problematic cells on both INTELSAT V-F6 (506) Battery 1, (Cell 22) and INTELSAT V-F15 (515) Battery 2, (Cells 4 and 26) . Both batteries were subjected to the procedure prior to the Fall 1996 eclipse season as part or the normal pre-eclipse reconditioning.

506 Battery 1 Cell 22 EODV increased 0.026 volts with a 0.6 amp greater load and the cell voltage spread (minimum to maximum) decreased from 0.051 volts in Spring to 0.025 volts in Fall. 515 Battery 2 Cell 26 EODV increase 0.063 volts with a 0.6 amp lighter load and the cell voltage spread decreased from 0.102 volts in Spring to 0.045 volts in Fall.

3. Evaluation of Pressure Increase

An accurate measure of pressure increase due to the effects of corrosion can be made by tracking the pressure at the end of reconditioning discharge. This is especially important on the INTELSAT VI which has a dry powder sintered positive and used the alcohol EC impregnation. These positive plates tend to corrode.

A study of INTELSAT VI-F2 in-orbit reconditioning data revealed that BOD pressure increased each season with cycling while EOD pressure remained essentially constant for the first five seasons in orbit. This rise in BOD pressure without a corresponding increase in EOD pressure shows up as increased useful capacity during the reconditioning. Beginning in sixth season the EOD pressure begins to ramp up and becomes the major component of the increase noted in the BOD pressure while a corresponding leveling and gradual decrease in capacity takes place. This increase in EOD pressure can only be excess hydrogen which has been liberated by the consumption of oxygen in the corrosion reaction. The data gained at end of reconditioning discharge is a measure of pressure growth due to corrosion.

4. Enhancement of Performance in EODV

The INTELSAT VI batteries were the first for INTELSAT with a Nickel pre-charge, the INTELSAT V's all having been Hydrogen pre-charged. In 1985 INTELSAT commissioned HAC, the prime contractor on INTELSAT VI program, to perform a series of life tests on flight representative packs of battery cells. Four packs were built up, two were the standard 16 cell design but with Hydrogen pre-charge. The other two packs contained 16 Hydrogen pre-charged cells and two Nickel pre-charged cells which were fitted into the growth area of the pack structure. It should be noted that at this time HAC had not yet made the decision to use Nickel pre-charge cells. The tests subjected one

16 cell pack to real time simulated life test which was terminated after six seasons. The second 16 cell pack was placed in cold storage with capacity checked every six months. The two 18 cell packs were put into a semi-accelerated life test, real time eclipse, with a solstice varied by the time necessary to recondition one of the packs. The eclipse season simulation was a daily 27.4A discharge for periods starting at 15 minutes, increasing to 70 minutes, with a corresponding DOD of 69.2%, and then tapering back to 15 minutes over a 46 day period. The recharge was at the standard C/10 for a return of 110%. Following each eclipse season Pack Q004 was put on trickle charge while Pack Q003 was reconditioned. The reconditioning involved a let-down of the pack using a 20 ohm, 35 watt resistor across the pack terminals until 5 volts was reached. The capacity to 1.0 volts was noted Following the reconditioning, the pack was recharged at 4.8A for 18 hours in an attempt to match the capacity of the two packs, a practice which stopped after Season 13 being replaced by a C/10 recharge to 115%.

Comparison of the data after season 30 shows that the EODV for reconditioned Ni pre-charge cells was 42mV higher than those not reconditioned (see Figure 4), an EODV increase of 1.34 volts on a standard INTELSAT VI 32 cell battery. For the H_2 pre-charge pack the EODV was 21mV higher or 0.67 volts for the standard INTELSAT VI battery. In addition, across the 18 cells in each of the two test packs the EODV spread for reconditioned cells was 26mV at BOL and 24mV at EOL. The spread for non-reconditioned cells was 26mV at BOL and 42mV at EOL. Review of the INTELSAT VI-F2, which has completed 14 seasons in-orbit, shows a cell voltage spread of 25mV on Battery 1 and 26mV on Battery 2. INTELSAT V satellites which have completed more than 22 seasons in-orbit show similar results with a 25mV spread on both batteries.

5. Correlation Between Life Test Data and In-Orbit Performance

All INTELSAT sponsored life testing is run in real time, including solstice. The tests are started several seasons ahead of the first in-orbit use. All operational requirements and environmental elements are simulated as closely as possible.

The INTELSAT VI life test at COMSAT Labs has completed over 20 real-time seasons, while the oldest INTELSAT VI in orbit, 602, has completed 14 seasons. Similar testing at HAC ran for 30 accelerated seasons. Both life tests simultaneously test(ed) identical cells with a Hydrogen and Nickel pre-charge.

The first concern to arise on these cells was a significant pressure increase. The initial assumption was that the batteries were being subjected to an excessive amount of overcharge thus contributing to corrosion of the positives. Examination of the first five reconditioning cycles showed that while the BOD pressure of the cells was increasing the EOD pressure was essentially constant (see Figure 5). Analysis of the reconditioning data showed this to be an increase in useful capacity due to cycling and not a deleterious effect. In season six the capacity peaked and has remained essentially constant on the Hydrogen pre-charge cells and slowly decreased on the Nickel pre-charge cells. A corresponding increase in EOD pressure has occurred over the same period on the Nickel pre-charge cells. The in-orbit data from 602 agrees well with the Nickel pre-charge line (see Figure 6).

When first launched INTELSAT VII/VIIA batteries experienced a capacity fade which showed up as reconditioning capacities that were lower than the battery nameplate. INTELSAT was unsure at this point as to the high rate useful capacity of the batteries. The correlation between reconditioning capacity and high rate capacity is of great importance to the satellite operators but a C/2 discharge capacity measurement to 1.0 volts is not feasible in orbit. In order to resolve this problem the real time life testing, that COMSAT Labs perform for INTELSAT, incorporates a C/2 discharge capacity measurement in each odd eclipse season. As cycling continued the in-orbit capacities increased until the reconditioning capacity exceeded nameplate, as expected, and closely matched the results from the life test. When the in-orbit reconditioning capacities were of the same order as those of the life test

battery, the assumption was made that the high rate capacities were also similar.

6. Source of Flexibility

The reconditioning circuitry has proved valuable to satellite operators for purposes other than reconditioning. INTELSAT VII/VIIA has the reconditioning resistors configured as a backup battery heater, a feature which is now in use on one of the batteries.

Another use involved electro-thermal thrusters which run directly from the batteries. The process, which was developed by Lockheed Martin allows the thruster start-up transients to be minimized by offsetting the battery voltages for the first few seconds of the maneuver. This is achieved by charging one battery to elevate the voltage and using the reconditioning load to suppress the voltage of the other battery.

Conclusion

The INTELSAT position on reconditioning of NiH_2 batteries has been stated. It is beneficial to the health and operation of the batteries in-orbit. Further, the availability of the circuitry has proven to be helpful for dealing with anomalous situations.

Reference:

1. "Method for Rejuvenating NiH_2 Battery Cells" by Earl, Burke, and Dunnet, 27th IECEC 1992

Table 1

INTELSAT NiH_2 Batteries					
	INTELSAT V	INTELSAT VI	INTELSAT K	INTELSAT VII	INTELSAT VIIA
Manufacturer	EPI	HAC/EPI	EPI	Gates	Gates
Cell Diameter (cm.)	8.9	8.7	8.9	8.7	11.8
Total Length (cm.)	21.2	28.0	29.1	29.3	20.2
Cell Mass (gm.)	890	1460	1413	1840	2640
Cap (AH) to 1V @ 10 °C	36	56	55	96	130
Nameplate CAP (AH)	32	44	50	85	120
Stack Design					
Plate Shape	Truncated Disk	Pineapple Slice	Truncated Disk	Pineapple Slice	Pineapple Slice
Configuration	Single Stack	Single Stack	Single Stack	Single Stack	Single Stack
Arrangement	Back-to-Back Pos.	Recirculating	Back-to-Back Pos.	Back-to-Back Pos.	Back-to-Back Pos.
Terminal Design	Ziegler/Axial	Teflon/Axial	Ziegler/Axial	Ceramic/Axial	Ceramic/Rabbit Ear
Positive Electrode					
Plaque	Wet Slurry	Dry Powder	Wet Slurry	Dry Powder	Dry Powder
Impregnation	Aqueous EC	Alcohol EC	Aqueous EC	Aqueous EC	Aqueous EC
Thickness (mm.)	0.775	0.880	0.762	0.920	0.920
No. of Plates	24	40		48	38
Separator	Asbestos	2 Layer Zircar	Asbestos	2 Layer Zircar	2 Layer Zircar
% Electrolyte by wt. dischgd.	38	31	38	31	31
Negative Electrode					
No. of Plates	24	41	40	48	38
Thickness (mm.)	0.137	0.148	0.178	0.116	0.116
Reconditioning					
Began	Fall 1983	Spring 1990	Fall 1992	Spring 1994	Spring 1994
Cell Voltage Limit	1st Cell to 0.9 V	1st Cell to 1.0 V	1st Cell to 0.5 V	1st Cell to 0.5 V	1st Cell to 0.5 V
C/D Ratio	110%	100%	110%	110%	110%
Change	Fall 1987	N/A	Fall 1994	Spring 1996	Spring 1996
Cell/Battery Limit	1st Cell to 0.5 V	N/A	Batt to 25 V (2&4)	N/A	N/A
C/D Ratio	N/A	N/A	N/A	105%	105%

TABLE 2
BATTERY RECONDITIONING
CAPACITY AND MINIMUM VOLTAGE
INTELSAT V F-6 (506)

BATTERY 1									BATTERY 2								
RECONDITIONING			ETT	TOTAL	BATT	CELL	CELL	S/G	RECONDITIONING			ETT	TOTAL	BATT	CELL	CELL	S/G
SEASON	HRS	MINS	A*H	A*H	EODV	EODV	#	CAP	SEASON	HRS	MINS	A*H	A*H	EODV	EODV	#	CAP
F83	52	30		35.70	25.40	0.896	27		F83	56	8		38.1	25.0	0.901	5	
S84	32	54	16.00	36.30*	26.80	0.896	27		S84	52	5		35.4	27.2	0.895	5	
F84	48	17	8.10	40.00	26.40	0.889	6		F84	55	30		37.7	27.8	0.895	5	
S85	52	38		35.80	30.00	0.896	27	41.6	S85	55	20		37.6	34.0	0.895	5	48.6
F85	56	32		38.40	27.00	0.896	6	44.3	F85	55	12		37.5	30.8	0.895	5	48.5
S86	49	27		33.70	31.80	0.889	27	39.9	S86	55	46		37.9	29.2	0.895	1	47.6
F86	57	5		38.80	26.60	0.180	27	42.1	F86	55	17		37.6	28.6	0.220	5	48.6
S87	51	51		35.30	30.00	0.230	27	37.4	S87	46	55	7.3	38.3	27.8	0.260	5	39.2
F87	55	20		37.60	28.40	0.200	27	38.0	F87	54	43		37.2	28.8	0.310	5	38.8
S88	51	40		35.20	30.00	0.240	27	35.6	S88	56	59		38.8	26.2	0.270	5	39.9
F88	54	3		38.80	28.20	0.260	5	41.0	F88	55	37		37.8	26.8	0.230	5	39.0
S89	54	16		36.90	29.80	0.240	27	38.0	S89	54	16		36.9	28.8	0.340	5	38.0
F89	59	0		40.10	27.00	0.380	5	41.0	F89	59	3		40.2	25.6	0.220	13	42.0
S90	56	3		38.10	29.60	0.240	27	41.0	S90	56	42		38.6	29.0	0.410	5	40.0
F90	58	40		39.90	27.40	0.100	27	41.0	F90	52	59		36.0	29.8	0.290	5	37.0
S91	53	38		36.50	29.00	0.230	27	38.0	S91	58	6		39.5	28.2	0.310	5	41.0
F91	60	0		40.80	27.40	0.220	5	44.0	F91	57	20		39.0	28.6	0.290	5	41.0
S92	57	21		39.00	30.00	0.240	27	42.0	S92	58	9		39.6	28.6	0.310	5	41.0
F92	63	27		43.10	28.00	0.240	5	45.0	F92	57	0		38.8	29.4	0.320	5	41.0
S93	57	0		38.80	29.80	0.220	27	41.0	S93	59	26		40.4	27.6	0.360	1	43.0
F93	61	35		41.90	28.00	0.210	5	44.0	F93	60	52		41.4	26.8	0.950	5	43.4
S94	55	58		38.00	30.00	0.090	27	41.0	S94	59	43		40.6	28.4	0.350	5	42.5
F94	61	54		42.10	29.00	0.140	27	43.6	F94	58	9		39.5	29.2	0.490	5	41.5
S95	56	55		38.70	30.20	0.200	27	41.6	S95	59	21		40.4	28.2	0.490	5	42.5
F95	61	0		41.50	29.00	0.000	27	42.1	F95	61	55		42.1	26.2	0.460	5	43.5
S96	57	19		39.00	30.20	0.220	27	42.3	S96	59	24		40.4	29.6	0.320	5	40.4
F96	61	0		41.50	32.30	0.000	27	40.3	F96	62	57		42.8	25.9	0.170	5	43.6

Figure 1

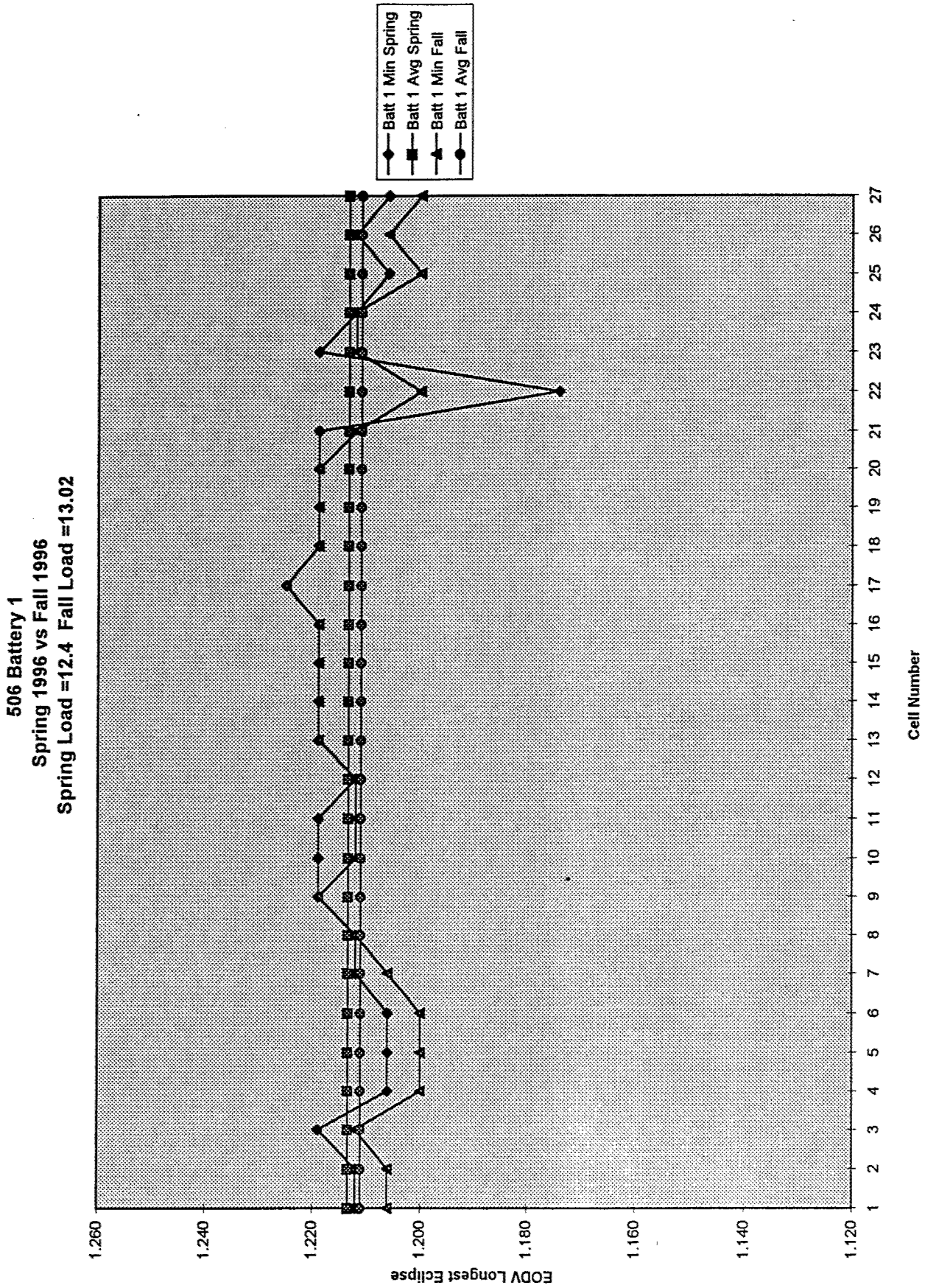
506 Battery 1
Spring 1996 vs Fall 1996
Spring Load =12.4 Fall Load =13.02
Batt 1 Min Spring
Batt 1 Avg Spring
Batt 1 Min Fall
Batt 1 Avg Fall
EODV Longest Eclipse
1.260
1.240
1.220
1.200
1.180
1.160
1.140
1.120
Cell Number
1 2 3 4 5 6 7 8 9 10 11 12 13 14 15 16 17 18 19 20 21 22 23 24 25 26 27

Figure 2

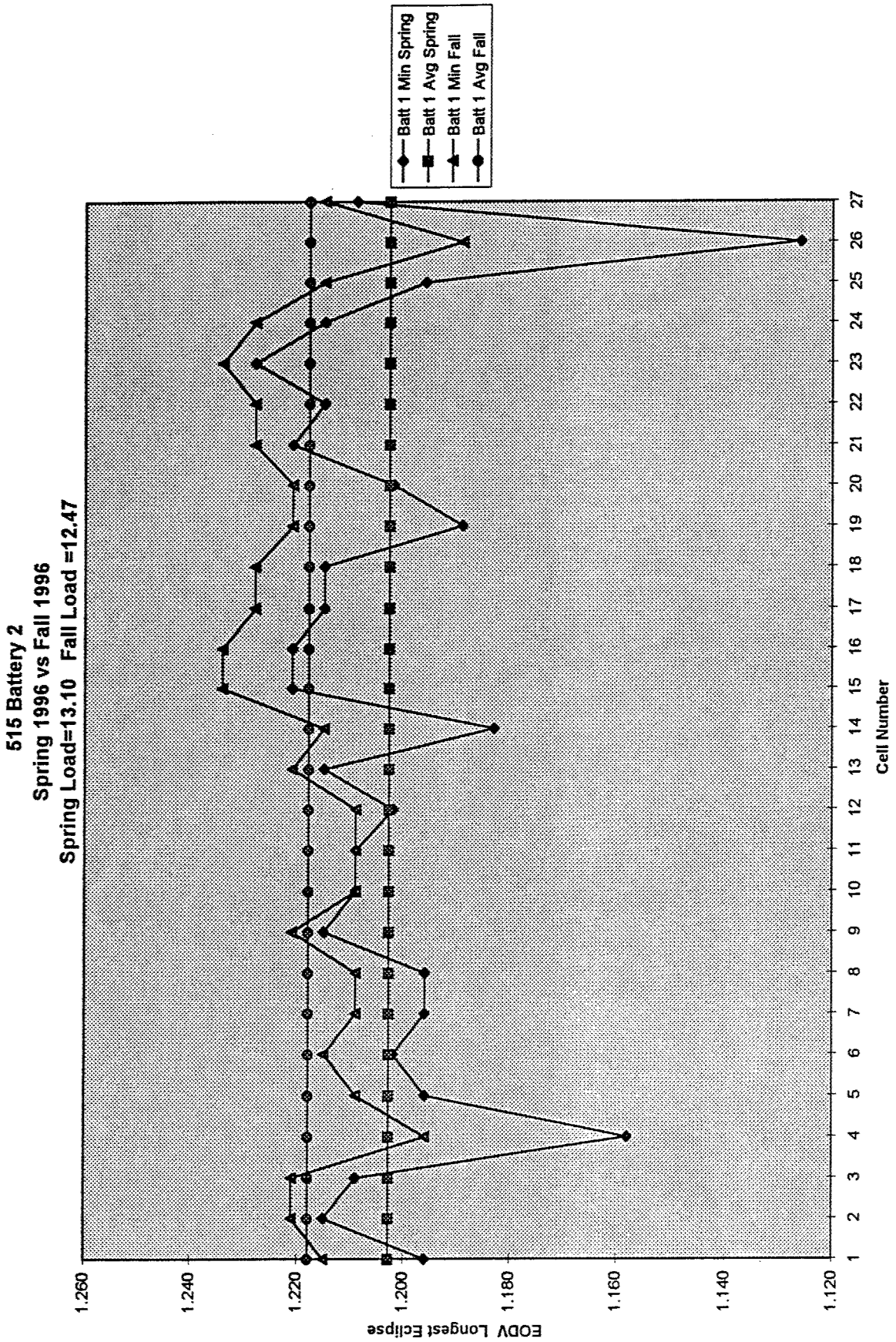
515 Battery 2
Spring 1996 vs Fall 1996
Spring Load=13.10 Fall Load =12.47
Batt 1 Min Spring
Batt 1 Avg Spring
Batt 1 Min Fall
Batt 1 Avg Fall
EODV Longest Eclipse
1.260
1.240
1.220
1.200
1.180
1.160
1.140
1.120
Cell Number
1 2 3 4 5 6 7 8 9 10 11 12 13 14 15 16 17 18 19 20 21 22 23 24 25 26 27

Figure 3

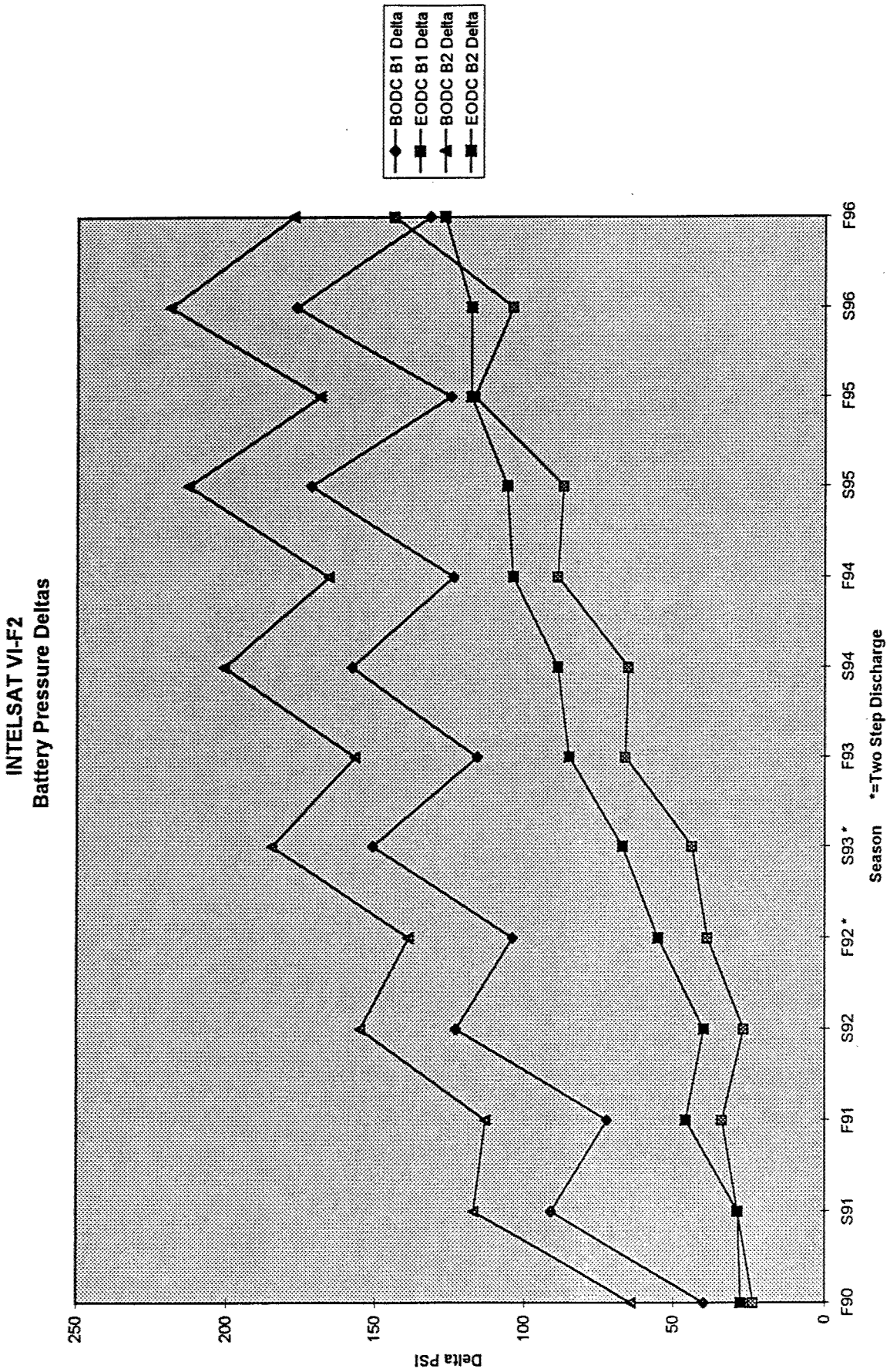
INTELSAT VI-F2
Battery Pressure Deltas
BODC B1 Delta
EODC B1 Delta
BODC B2 Delta
EODC B2 Delta
Delta PSI
250
200
150
100
50
0
F90
S91
F91
S92
F92 *
S93 *
F93
S94
F94
S95
F95
S96
F96
Season
*=Two Step Discharge

Figure 4

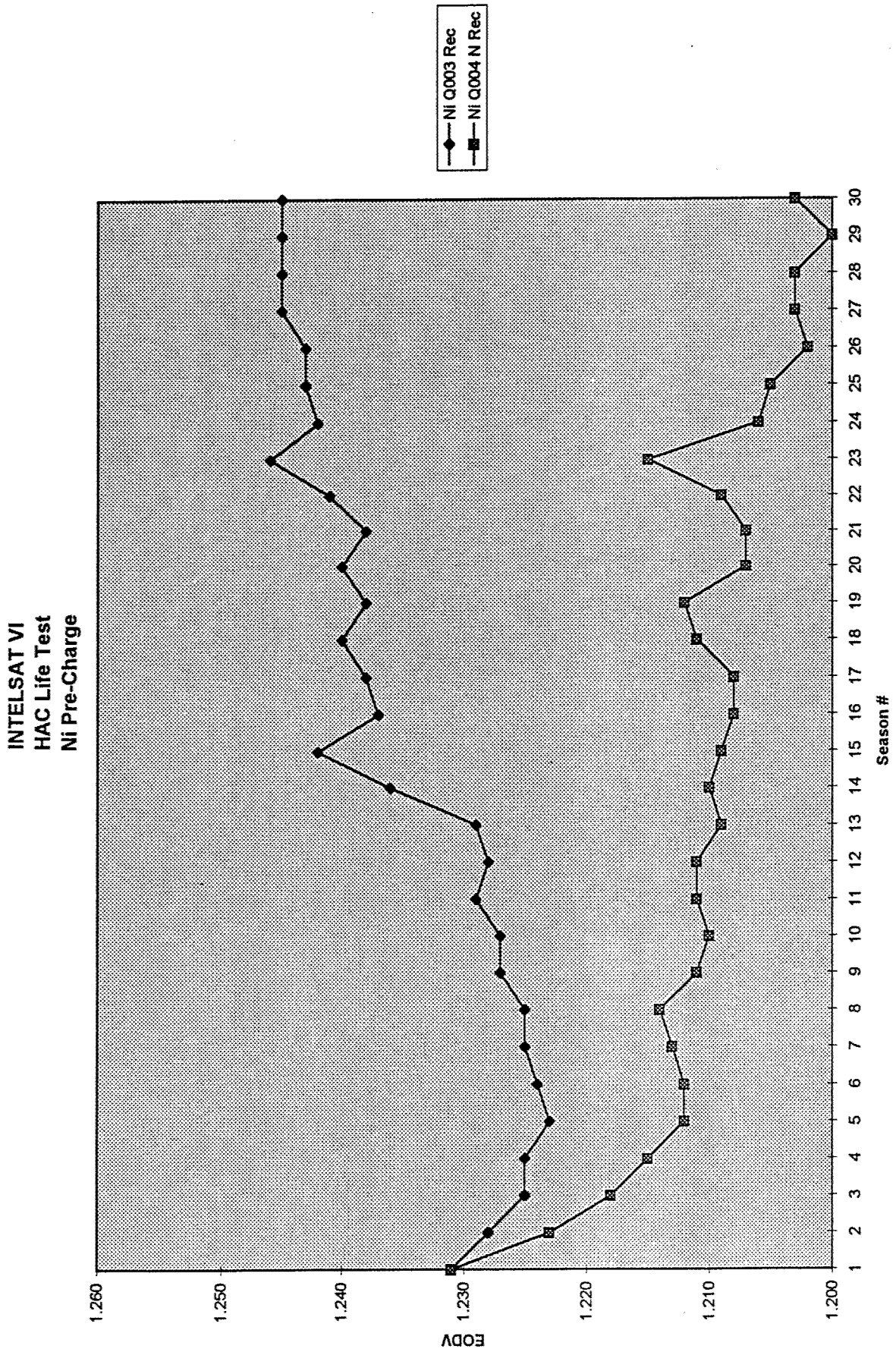
INTELSAT VI
HAC Life Test
Ni Pre-Charge
Ni Q003 Rec
Ni Q004 N Rec
EODV
1.260
1.250
1.240
1.230
1.220
1.210
1.200
Season #
1 2 3 4 5 6 7 8 9 10 11 12 13 14 15 16 17 18 19 20 21 22 23 24 25 26 27 28 29 30

Figure 5

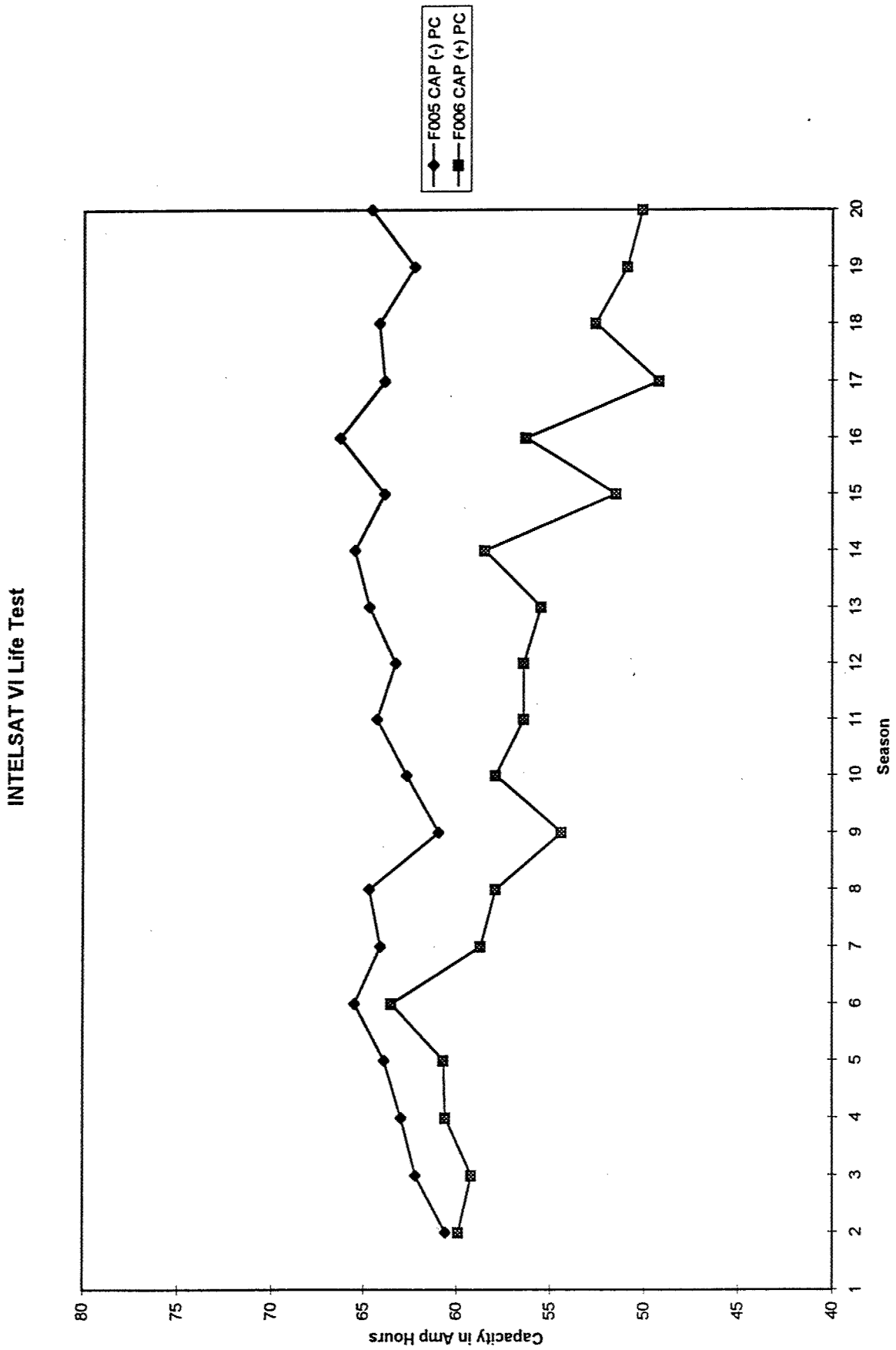
INTELSAT VI Life Test
F005 CAP (-) PC
F006 CAP (+) PC
Capacity in Amp Hours
80
75
70
65
60
55
50
45
40
Season
1
2
3
4
5
6
7
8
9
10
11
12
13
14
15
16
17
18
19
20

Figure 6

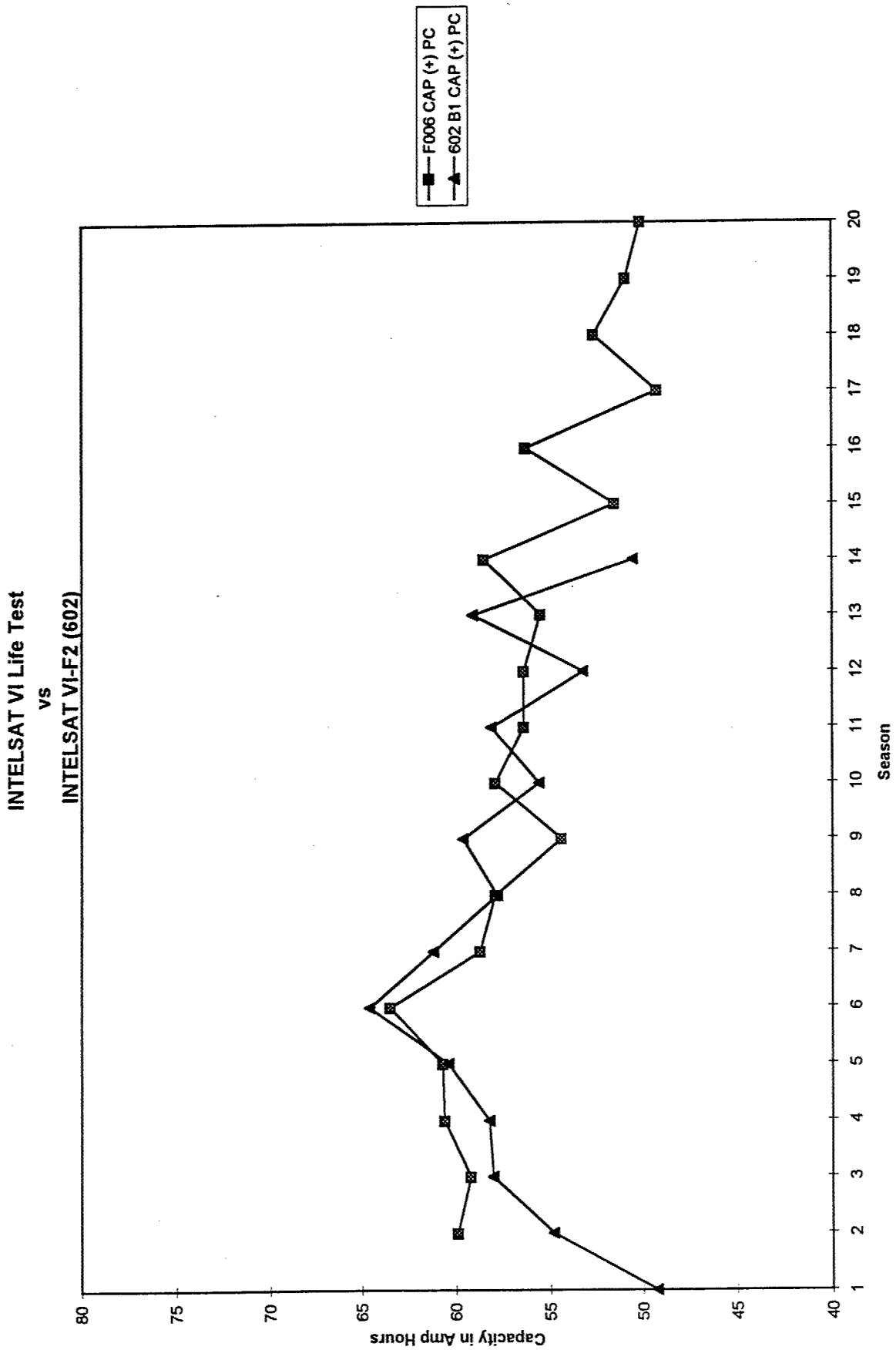
INTELSAT VI Life Test
vs
INTELSAT VI-F2 (602)
F006 CAP (+) PC
602 B1 CAP (+) PC
Capacity in Amp Hours
80
75
70
65
60
55
50
45
40
Season
1
2
3
4
5
6
7
8
9
10
11
12
13
14
15
16
17
18
19
20

Telstar 401 Reconditioning Experience

Dr. Dean W. Maurer
McKnight Associates Inc.
292 Johnston Dr.
Watchung, NJ, 07060
(908) 753-4457
or (908) 949-6690
Fax (908) 949-8082

Telstar 401 was launched December 15, 1993. It has two 58 cell 50 AH Nickel Hydrogen batteries of the Comsat design. Reconditioning is carried out with relay selected resistors across the entire battery for rates of approximately C/50 and C/100. There are individual cell voltage monitors and the discharge is carried out until the first cell reaches 0.8 volts.

Figure 1 is a composite plot to the maximum and minimum battery voltage and pressure by day since the beginning of the Spring '94 eclipse. Note that the minimum pressure is a uniform "smile" curve for each season; the minimum battery voltage is similar except for the Spring '95 season when it has become a "smirk" Note also that there is no reconditioning before the latter season. (Seen most clearly in the pressure plot). The variable depth discharges that occur between the eclipse seasons are for Arc Jet firings for station keeping.

Figures 2 & 3 are the Fall '94 and Spring '95 seasons respectively in close up. The "smirk" has been attributed to the effects of silicate poisoning for reasons beyond the scope of this talk, however, what follows is some Figures generated in ground tests at our Murray Hill laboratory on cells from the same manufacturing lot as the flight cells which show what is occurring. The silicate poisoning effect shows up most clearly in a depressed voltage in the discharge following an open circuit stand such as in the "charge retention" test.

Figure 4 shows the discharges following an open circuit stand of various duration at a temperature of -5^0 C typical of flight.

Figure 5 shows the same experiment plotted as the minimum voltage reached for the best and worst cell in the study as a function of open circuit time. Included are measurements of the internal resistance of the cells

Figure 6 shows the same type of test except that the charge time is varied keeping the open circuit and discharge the same. The worst effect is seen in the most fully charged case.

Figure 7 shows the effect of discharge temperature for the charge retention test run at $+10^0$ C. The resistive effect is seen to be very temperature dependent.

Figure 8 shows the surprising effect of the temperature of the open circuit stand period on the subsequent discharge at -5^0 C. The *warmer* the open circuit stand the worse the effect!

Figure 9 shows that a brief (3 hour) excursion to 30^0 C during an otherwise -5^0 C, 72 hour stand has a large effect on the voltage depression

Finally Figure 10 shows the effect of a prolonged trickle charge on the discharge of a -5^0 C cycle. Thus trickle charge has an effect similar to the open circuit stand.

In all cases the voltage depression is wiped out by the discharge itself and subsequent cycles will have normal appearance Therefore the data suggest that the "smirk" is a result of the prolonged trickle charge of the solstice period interspersed with the shallow (15%) discharges of the arc jets coupled with no reconditioning. Later eclipse seasons which have reconditioning are more normal but some deleterious effect is seen from the 2 to 3 week period between reconditioning and the start of the eclipse season.

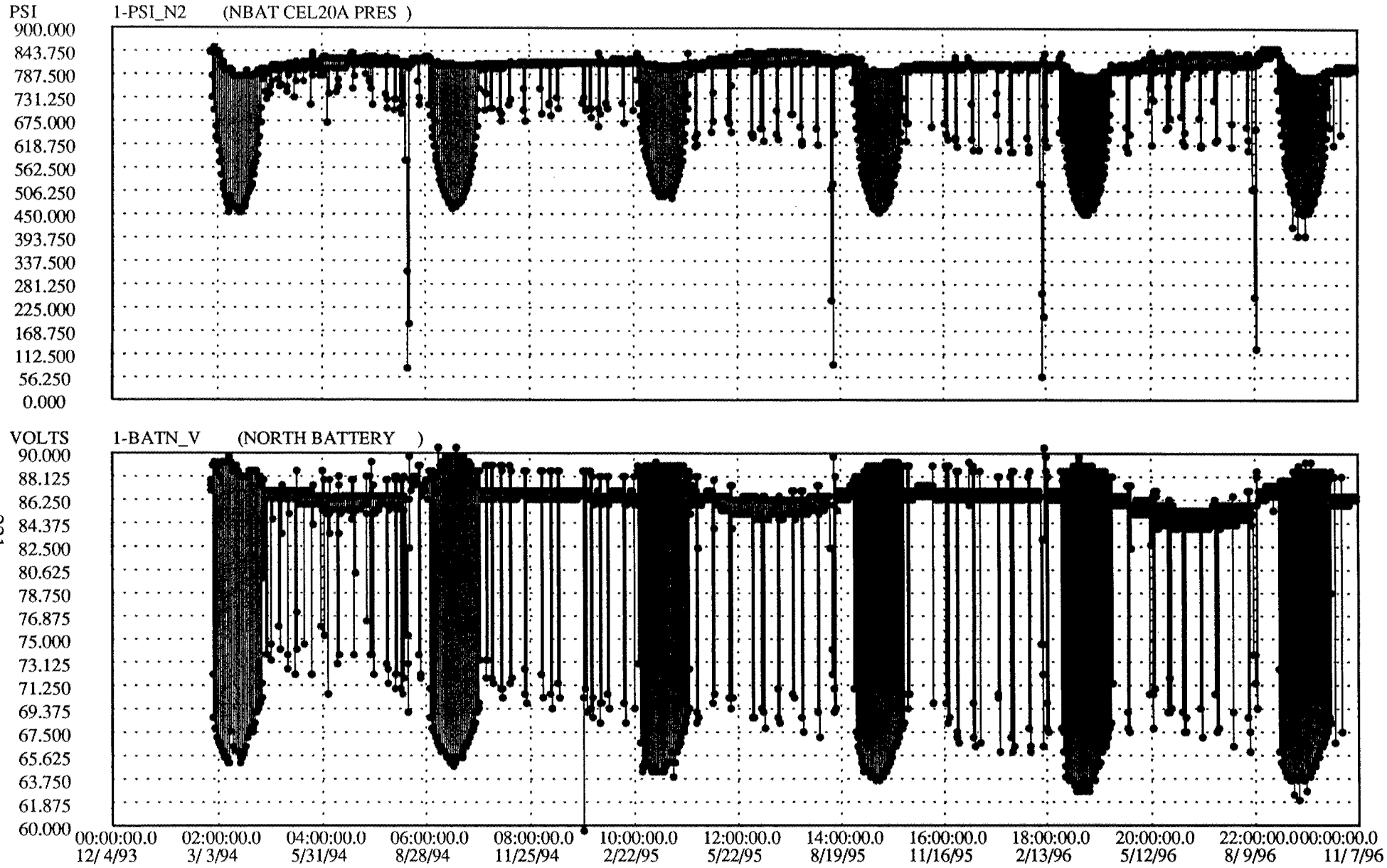
PSI
1-PSI_N2 (NBAT CEL20A PRES)
900.000
843.750
787.500
731.250
675.000
618.750
562.500
506.250
450.000
393.750
337.500
281.250
225.000
168.750
112.500
56.250
0.000
VOLTS
1-BATN_V (NORTH BATTERY)
90.000
88.125
86.250
84.375
82.500
80.625
78.750
76.875
75.000
73.125
71.250
69.375
67.500
65.625
63.750
61.875
60.000
00:00:00.0 12/ 4/93
02:00:00.0 3/ 3/94
04:00:00.0 5/31/94
06:00:00.0 8/28/94
08:00:00.0 11/25/94
10:00:00.0 2/22/95
12:00:00.0 5/22/95
14:00:00.0 8/19/95
16:00:00.0 11/16/95
18:00:00.0 2/13/96
20:00:00.0 5/12/96
22:00:00.0 8/ 9/96
00:00:00.0 11/ 7/96

Fig 1

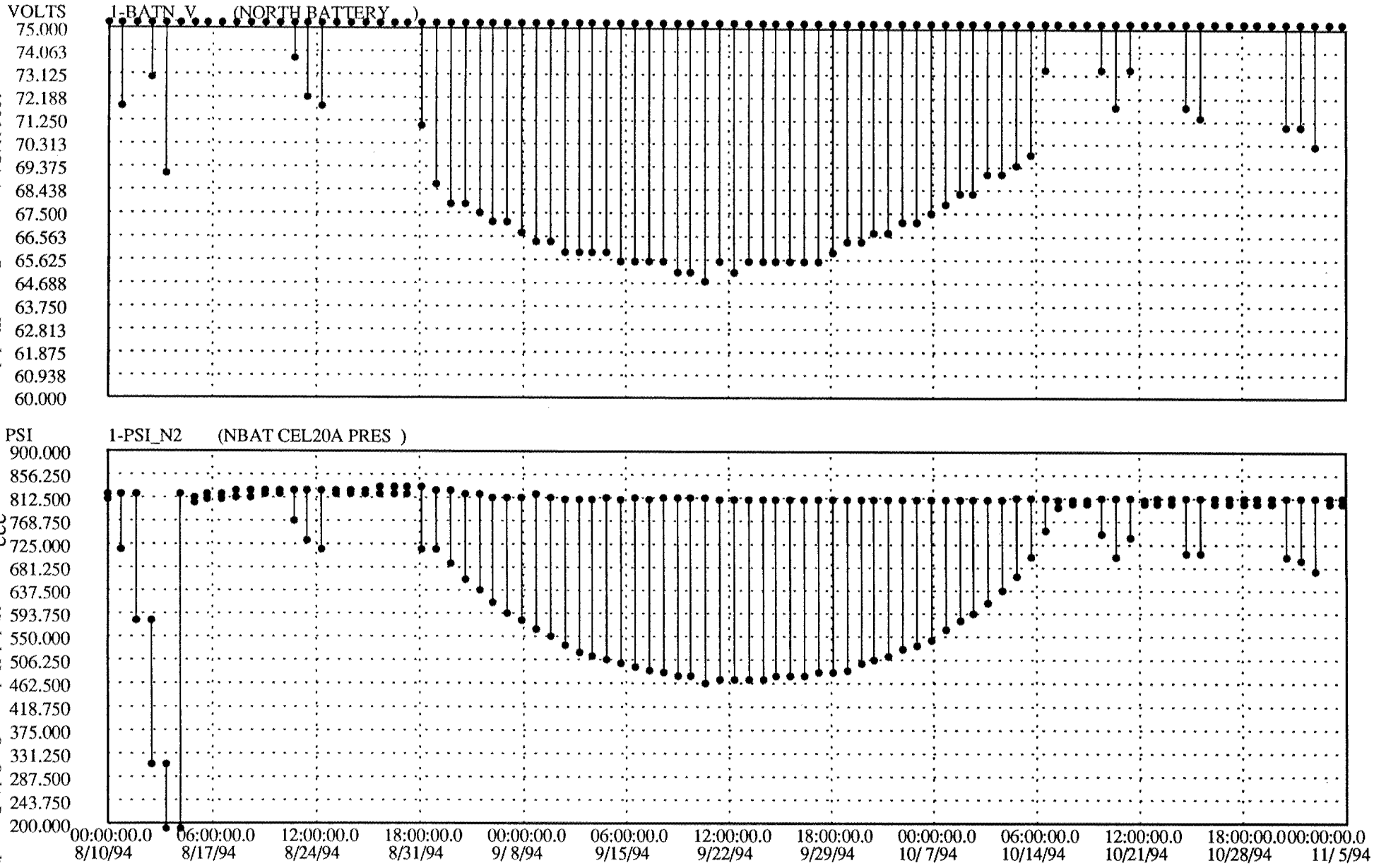
VOLTS
1-BATN_V (NORTH BATTERY)
75.000
74.063
73.125
72.188
71.250
70.313
69.375
68.438
67.500
66.563
65.625
64.688
63.750
62.813
61.875
60.938
60.000
PSI
1-PSI_N2 (NBAT CEL20A PRES)
900.000
856.250
812.500
768.750
725.000
681.250
637.500
593.750
550.000
506.250
462.500
418.750
375.000
331.250
287.500
243.750
200.000
00:00:00.0 8/10/94
06:00:00.0 8/17/94
12:00:00.0 8/24/94
18:00:00.0 8/31/94
00:00:00.0 9/ 8/94
06:00:00.0 9/15/94
12:00:00.0 9/22/94
18:00:00.0 9/29/94
00:00:00.0 10/ 7/94
06:00:00.0 10/14/94
12:00:00.0 10/21/94
18:00:00.0 10/28/94
00:00:00.0 11/ 5/94

Fig 2

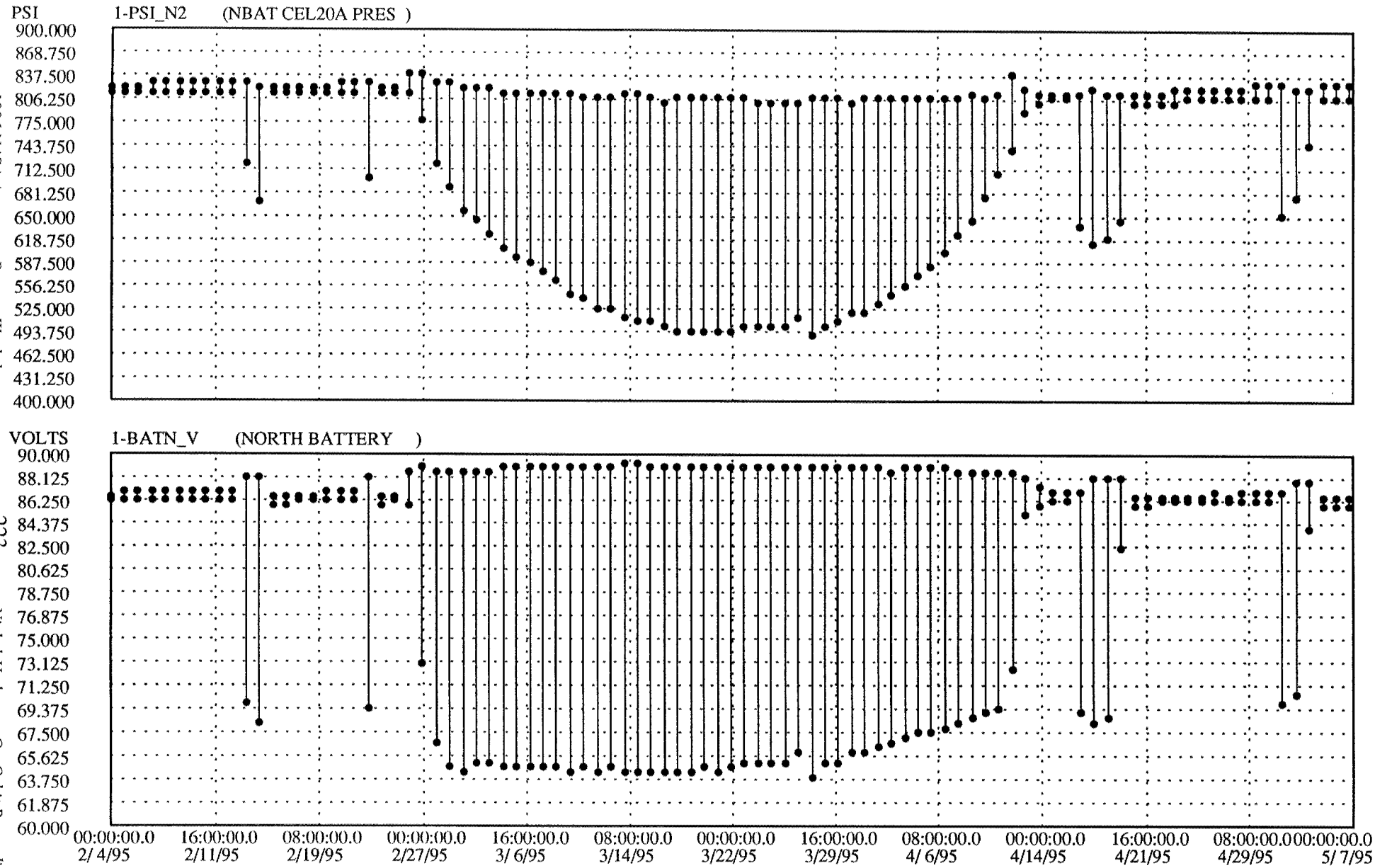
PSI
1-PSI_N2 (NBAT CEL20A PRES)
900.000
868.750
837.500
806.250
775.000
743.750
712.500
681.250
650.000
618.750
587.500
556.250
525.000
493.750
462.500
431.250
400.000
VOLTS
1-BATN_V (NORTH BATTERY)
90.000
88.125
86.250
84.375
82.500
80.625
78.750
76.875
75.000
73.125
71.250
69.375
67.500
65.625
63.750
61.875
60.000
00:00:00.0 2/ 4/95
16:00:00.0 2/11/95
08:00:00.0 2/19/95
00:00:00.0 2/27/95
16:00:00.0 3/ 6/95
08:00:00.0 3/14/95
00:00:00.0 3/22/95
16:00:00.0 3/29/95
08:00:00.0 4/ 6/95
00:00:00.0 4/14/95
16:00:00.0 4/21/95
08:00:00.0 4/29/95
00:00:00.0 5/ 7/95

Fig 3

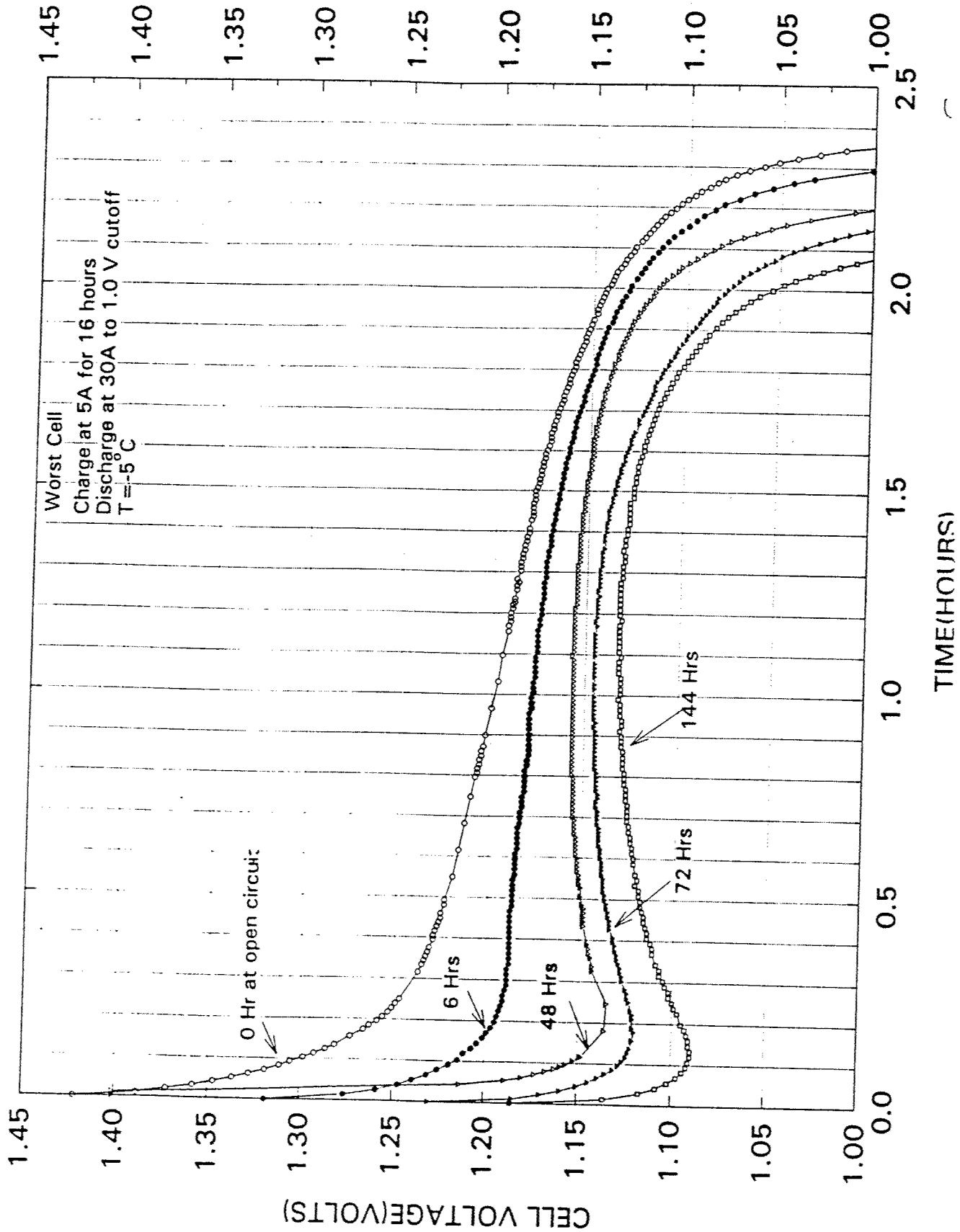
Worst Cell
Charge at 5A for 16 hours
Discharge at 30A to 1.0 V cutoff
T=-5°C
0 Hr at open circuit
6 Hrs
48 Hrs
72 Hrs
144 Hrs
CELL VOLTAGE(VOLTS)
TIME(HOURS)
1.45
1.40
1.35
1.30
1.25
1.20
1.15
1.10
1.05
1.00
0.0
0.5
1.0
1.5
2.0
2.5

Fig 4

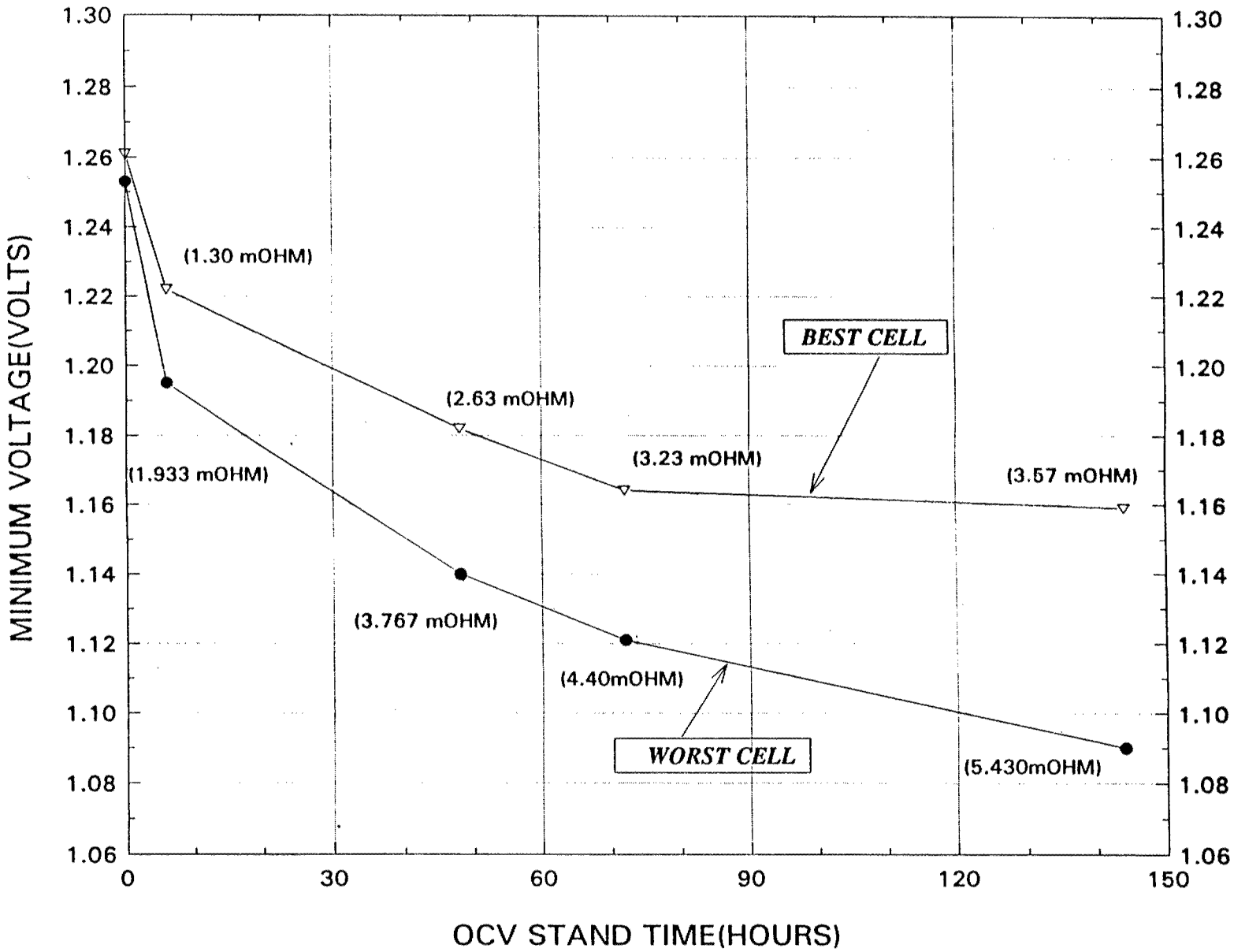
MINIMUM VOLTAGE(VOLTS)
OCV STAND TIME(HOURS)
1.30
1.28
1.26
1.24
1.22
1.20
1.18
1.16
1.14
1.12
1.10
1.08
1.06
0
30
60
90
120
150
(1.30 mOHM)
(2.63 mOHM)
(3.23 mOHM)
(3.57 mOHM)
BEST CELL
(1.933 mOHM)
(3.767 mOHM)
(4.40mOHM)
(5.430mOHM)
WORST CELL

Fig 5

minV-t

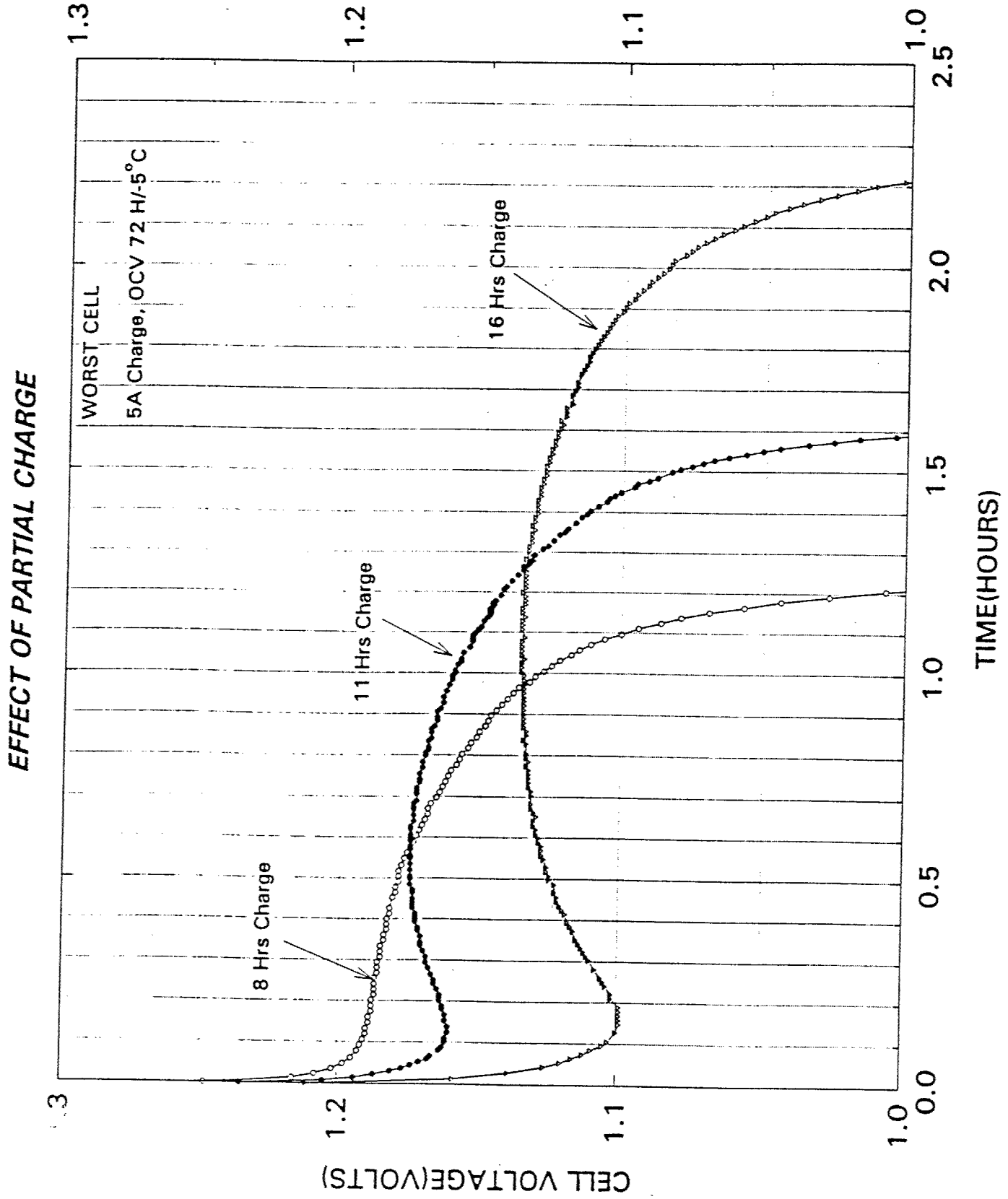
EFFECT OF PARTIAL CHARGE
WORST CELL
5A Charge, OCV 72 H/-5°C
16 Hrs Charge
11 Hrs Charge
8 Hrs Charge
CELL VOLTAGE(VOLTS)
TIME(HOURS)
1.3
1.2
1.1
1.0
0.0
0.5
1.0
1.5
2.0
2.5

Fig 6

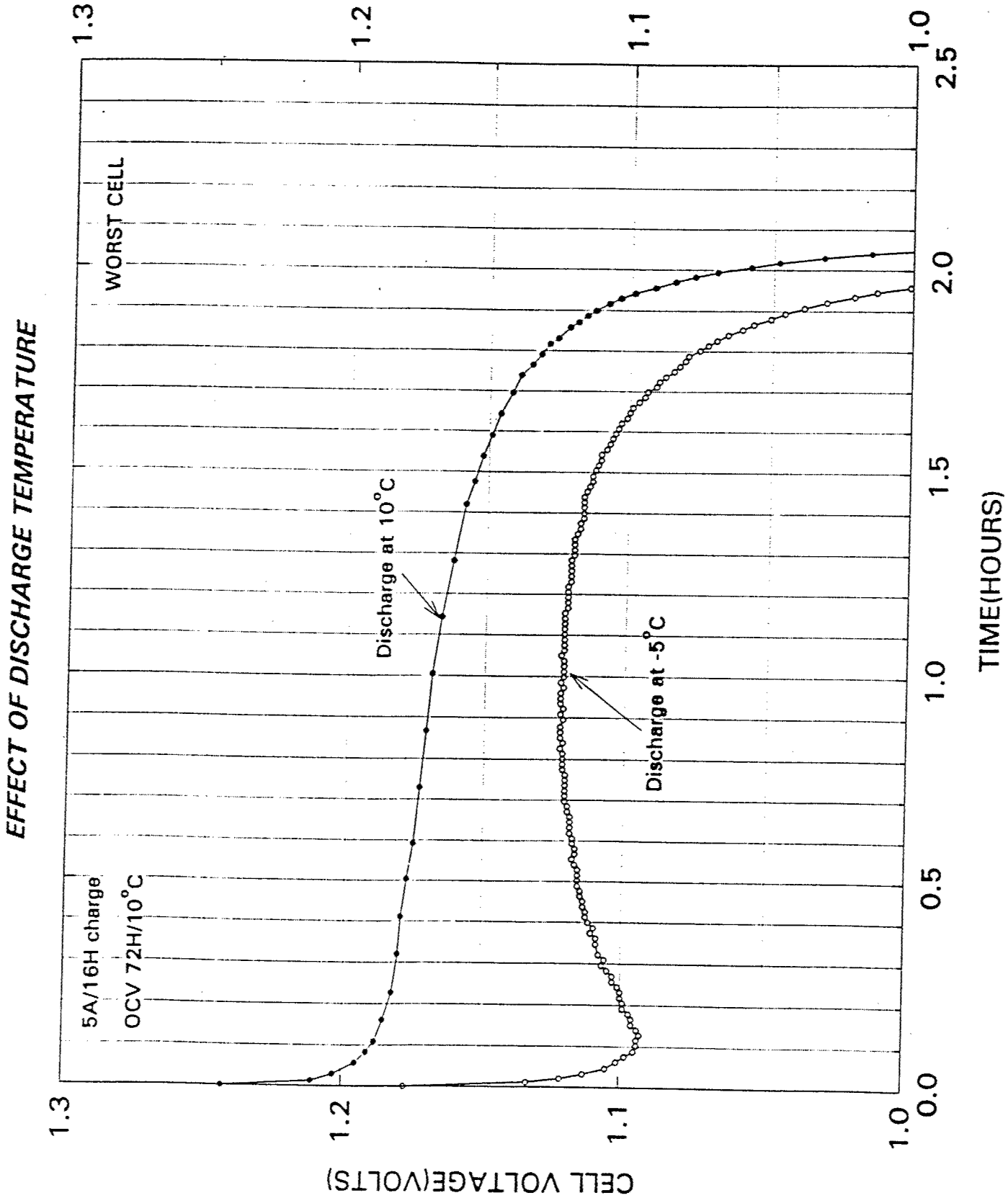
EFFECT OF DISCHARGE TEMPERATURE
WORST CELL
5A/16H charge
OCV 72H/10°C
Discharge at 10°C
Discharge at -5°C
CELL VOLTAGE(VOLTS)
TIME(HOURS)
1.3
1.2
1.1
1.0
0.0
0.5
1.0
1.5
2.0
2.5

Fig 7

OCV STAND FOR 72 HOURS AT DIFFERENT TEMPERATURES

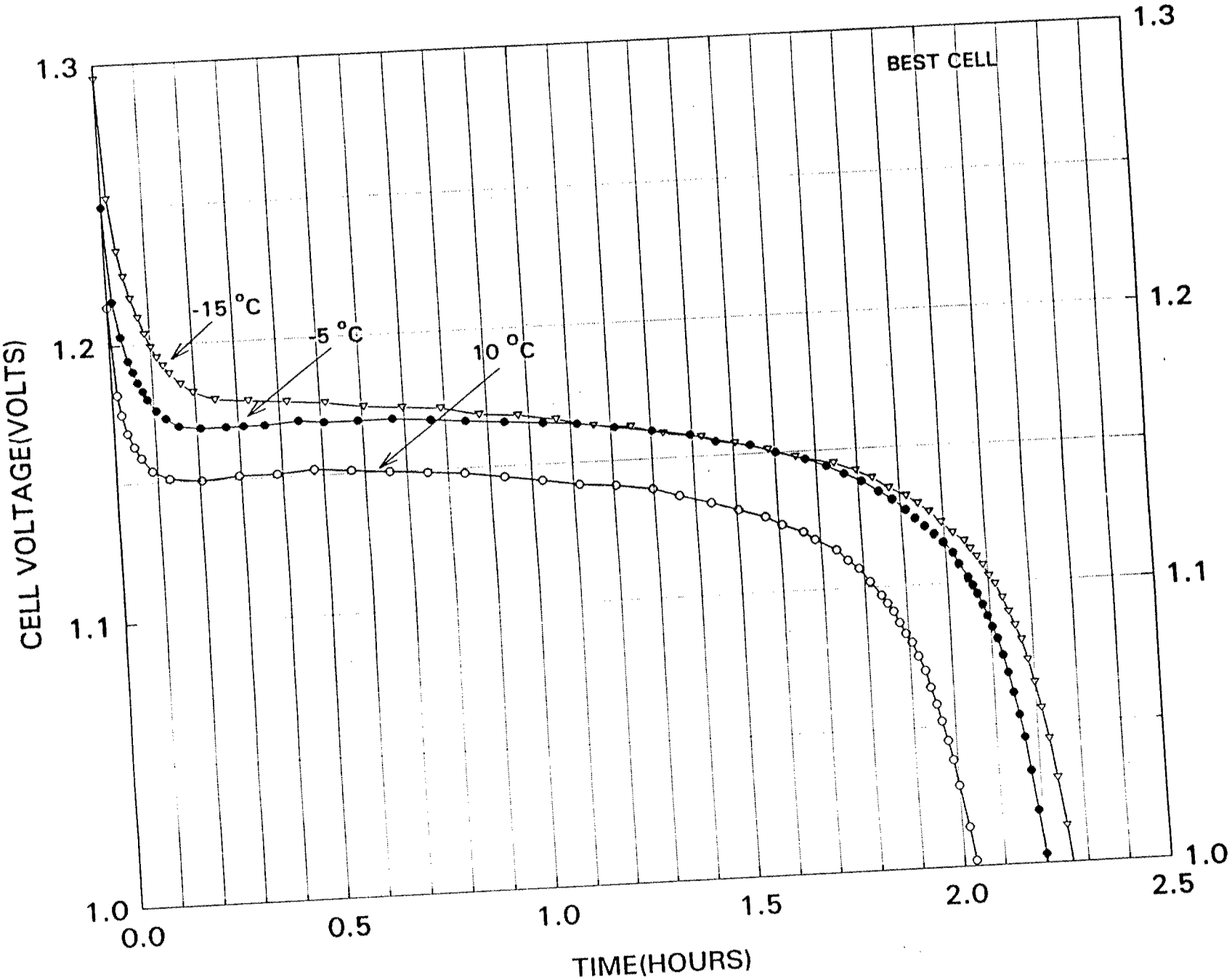

#1-TEMP

Fig 8

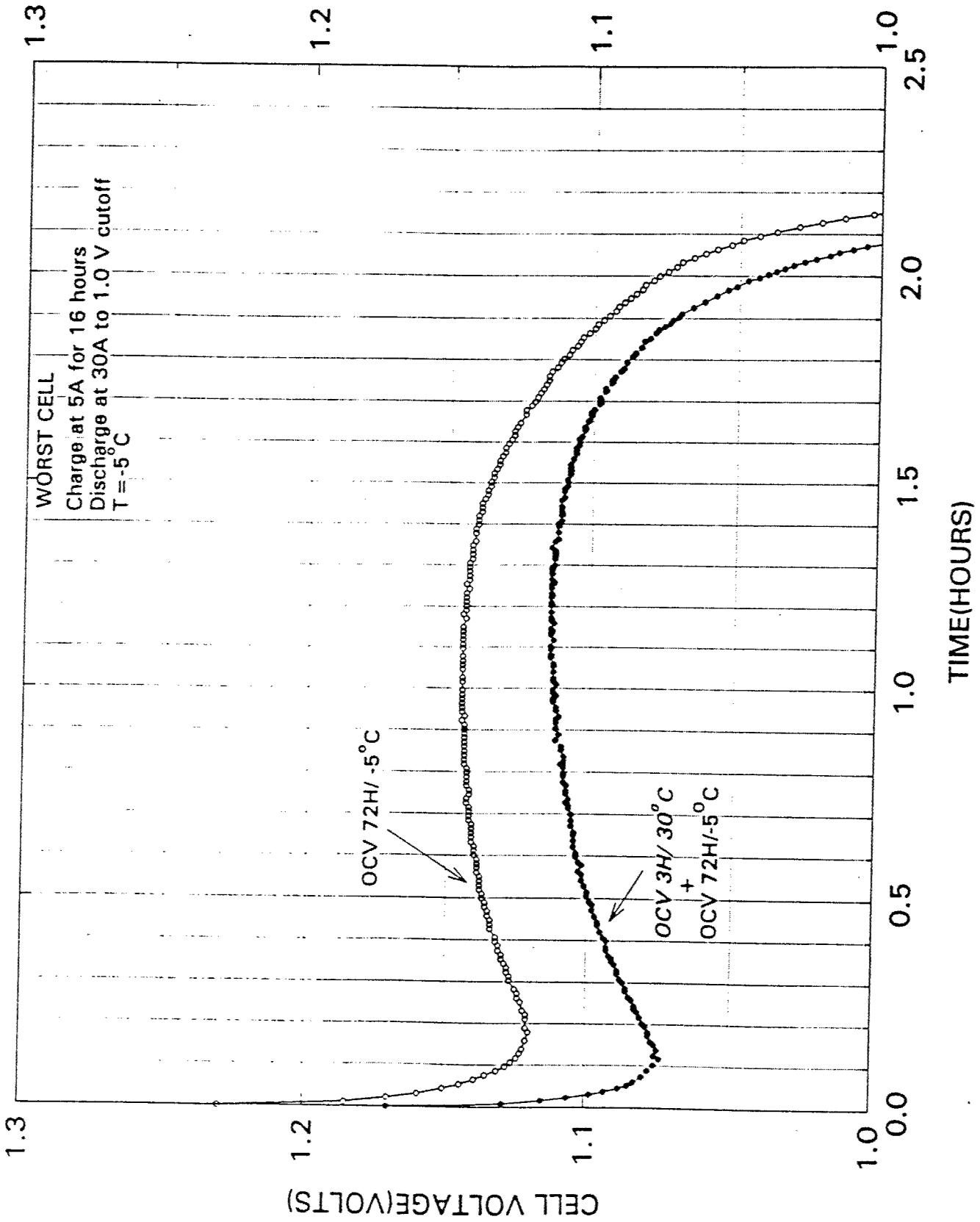
WORST CELL
Charge at 5A for 16 hours
Discharge at 30A to 1.0 V cutoff
T = -5°C
OCV 72H/ -5°C
OCV 3H/ 30°C
+
OCV 72H/-5°C
CELL VOLTAGE(VOLTS)
TIME(HOURS)
1.3
1.2
1.1
1.0
0.0
0.5
1.0
1.5
2.0
2.5

Fig 9

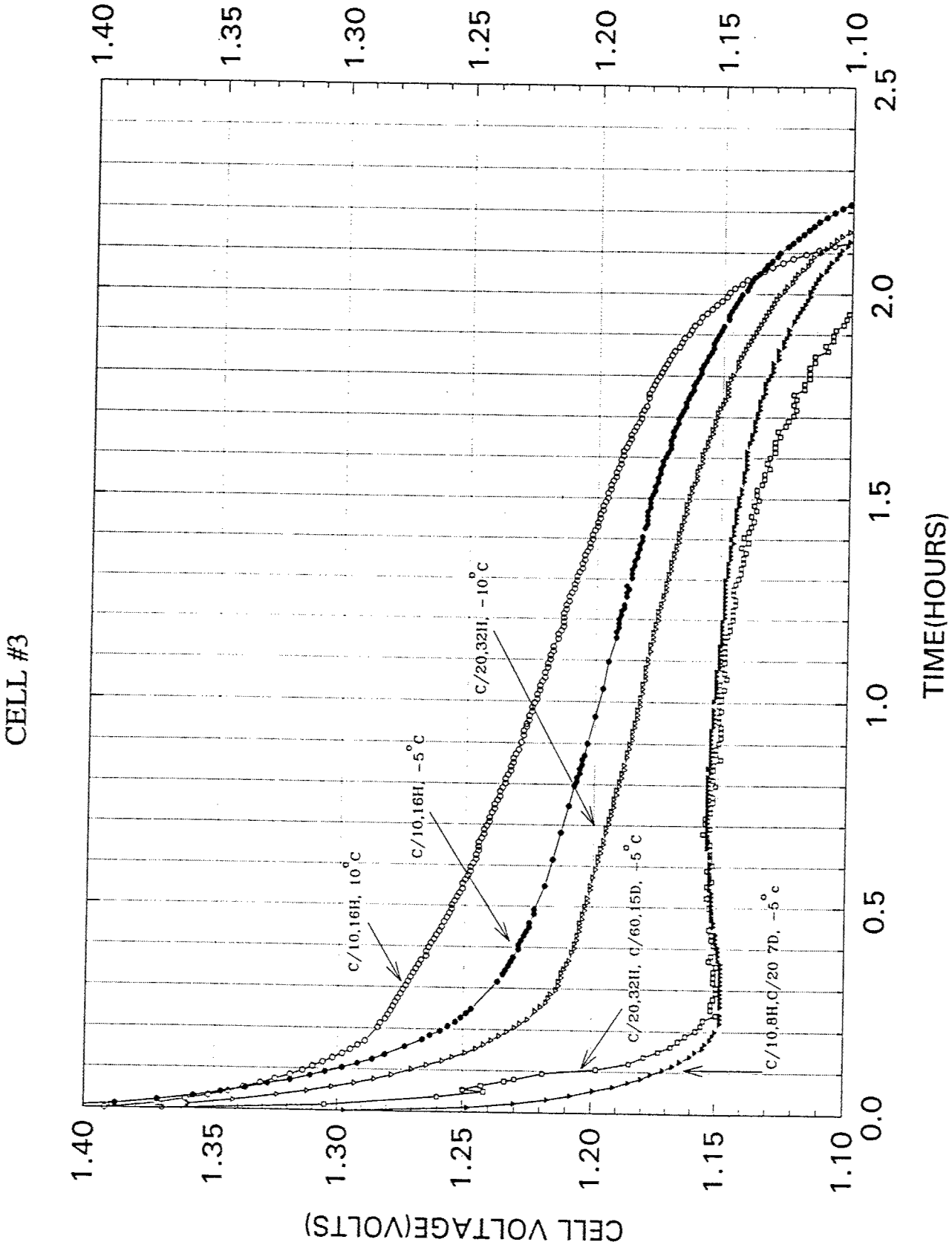
CELL #3
C/10,16H, 10°C
C/10,16H, -5°C
C/20,32H, -10°C
C/20,32H, C/60,15D, -5°C
C/10,8H,C/20 7D, -5°c
CELL VOLTAGE(VOLTS)
TIME(HOURS)
1.40
1.35
1.30
1.25
1.20
1.15
1.10
0.0
0.5
1.0
1.5
2.0
2.5

Fig 10

On-Orbit Health Check of Hubble Space Telescope Nickel-Hydrogen Batteries

Gopalakrishna M. Rao and Harry Wajsgras

Space Power Applications Branch

NASA / Goddard Space Flight Center

Stanley J. Krol Jr.

HST, EPS System Engineer

Lockheed Martin Technical Operations Inc.

Betty Colhoun

HST, Data Systems Engineer

Computer Sciences Corp.

NASA AEROSPACE BATTERY WORKSHOP

Dec. 3 - 5, 1996

Introduction

- Background
- Objective of Capacity Check/Reconditioning
- Battery Reconditioning Circuitry
- Reconditioning Procedure
- Results of Reconditionings
- Conclusions

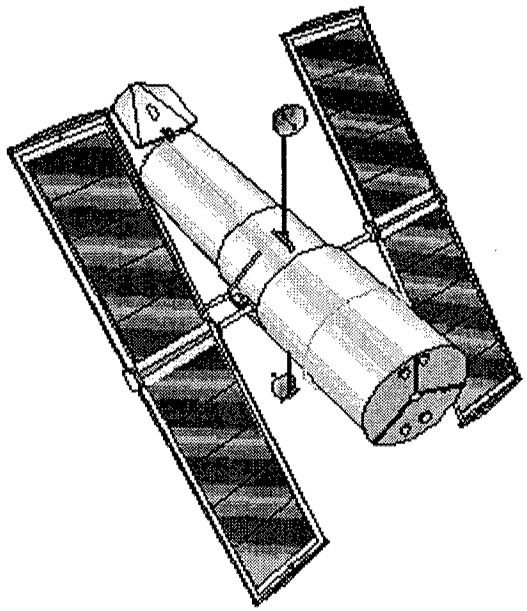

Background

- The Hubble Space Telescope is a one-of-a-kind spacecraft that pushes technology to its limits. Housing an 8-foot (2.4 meter) mirror and several sophisticated cameras and detectors, the telescope is the largest orbital astronomy observatory ever placed in space.
  - Launch date - April 24, 1990
  - Deployment - April 25, 1990
  - First Servicing Mission - December 4, 1992
  - Second Servicing Mission - February, 1997

Background

- Battery Design
  - Two Modules Each Containing Three 88 Ah NiH_2 Batteries (Six total)
    - Manufactured by: Eagle Picher / Lockheed
    - 23 Cells in Each, Only 22 Cells Are Electrically Connected (Position #22 Inactive)
      - Dry sintered nickel positive electrodes stacked with the platinum negative electrodes, zirconium oxide cloth separators and gas screens on a polysulfone core.

Background

- Positive Plate Fabrication
  - Flight Spare Module (FSM) in Feb. - June, 1988
  - Flight Module 2 (FM2) in June - Nov. 1988
- Cell Activation
  - FSM in Jan. 1989
  - FM2 in Mar. 1989

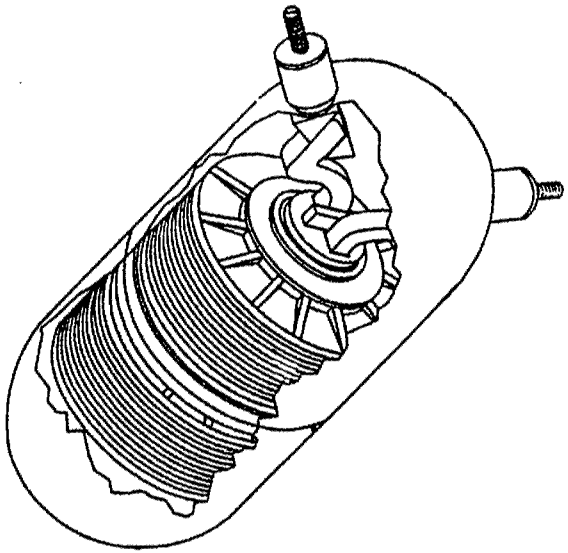

Background

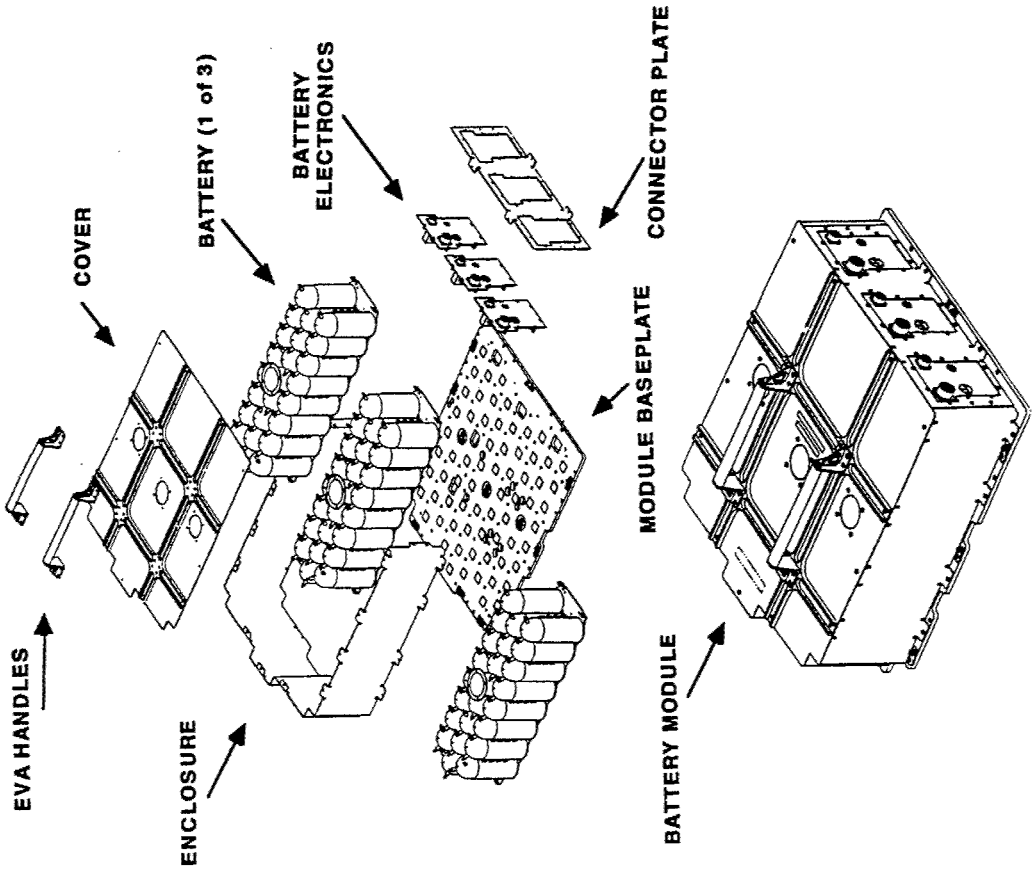
EVA HANDLES
COVER
ENCLOSURE
BATTERY (1 of 3)
BATTERY ELECTRONICS
MODULE BASEPLATE
CONNECTOR PLATE
BATTERY MODULE

Background

- Each Battery Has the Following Dedicated Monitors and Controls:
  - One Temperature Monitor for Telemetry
  - Four Charge Control Thermistors
  - One Primary and One Backup Heater System With Controllers
  - One Current Monitor (-25 to +25 Amps)
  - Two Cell Pressure Monitors (0 to 1500 PSI)
    - One telemetered through the Data Interface Unit (DIU) A side, the other through the DIU B side
      - Only one read at a time

Background

- Charge System
  - Charge Managed for Each Battery by Charge Current Controllers (CCC)
    - Provide Multilevel Control of Battery Charging Based on Voltage and Temperature Characteristics
    - Control Relays Inside the Power Control Unit (PCU)
  - Charge Modes
    - Hardware Charge Control
      - Utilizes CCC "K" relays to remove Solar Panel Assemblies (SPA's) from batteries
      - Relays open based on battery voltage & temperature (Taper Charge)

Background

- Software Charge Control
  - DF-224 controlled
  - Initiated when two CCC "K" relays open
  - Commands SPA Trim Relays open to drop charge current down to the database defined level (Trickle Charge)

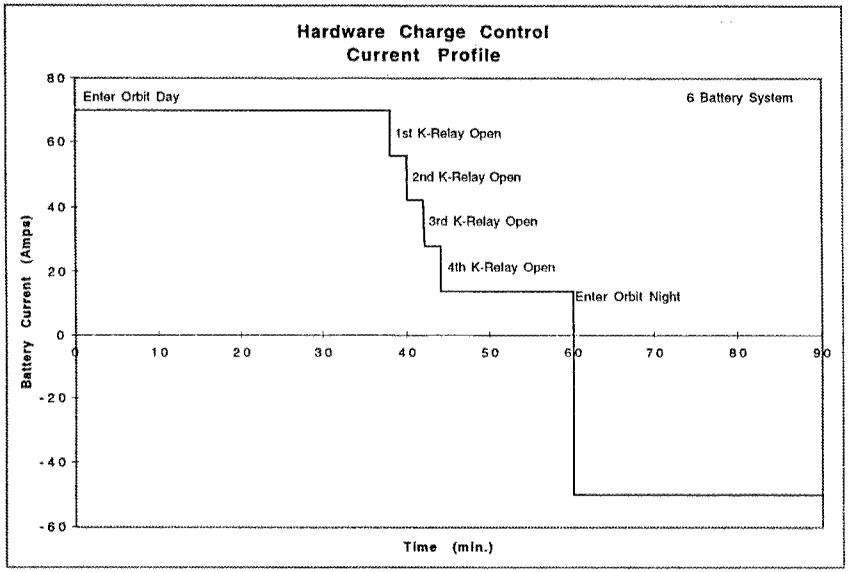

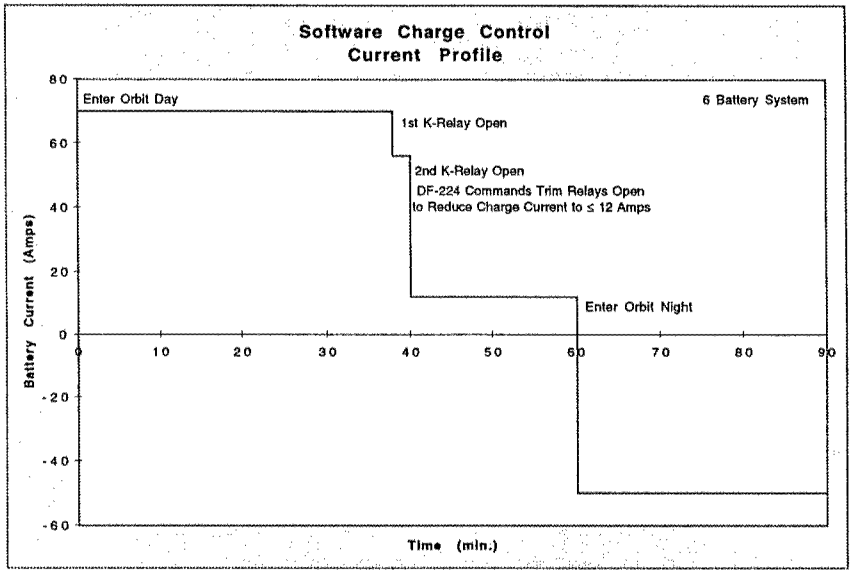

Background

- Battery History
  - Batteries were Charged and Installed Prior to Transfer to Launch Pad
    - Standard Baseline Charge used During Development and Testing of Cells and Batteries
      - Charge 10 Hours @ 9 amp rate (~C/10)
      - Charge 14 Hours @ 4 amp rate (~C/24)
  - Launch Delay
    - Batteries Removed for Reconditioning and Recharge
    - At Time of Release in Orbit, Pressure-based Capacity $\approx$ 61.7Ah / battery

Background

- Current Status
  - Six and One Half Years of Nominal Performance
  - Hardware Charge Control Operation Mode @ K1L4, K2L3
  - Completed 35982 Eclipse Orbits
  - Depth of Discharge Ranges Between 5 and 8.5%
  - System Capacity ≈ 461 Ah
  - Average Recharge Ratio ≈ 1.05
  - Last Reconditioning - March 25, 1996
    - Battery 3, Coulombic Capacity to 26.4V ≈ 74.7 Ah

Objective of Reconditioning

- The Reconditionings:
  - Determine Actual Battery Capacity for Trend Analysis and Mission Planning
  - Provide Verification of the Accuracy of the Pressure Transducers
  - Provide Data to Assess Battery Health
  - Reduce Battery Pressure
  - Restore Cell Balance

Battery Reconditioning Circuitry

- Switching Circuitry
  - Contained in the HST Power Control Unit
    - Two Parallel 25 Amp Latching Relays Isolate the Test Battery by Connecting the Solar Array (SA) Section Directly to the Diode Bus
    - Two 15 Amp Latching Relays Connect the Battery to Either the "High Rate" or "Low Rate" Reconditioning Resistor
      - SA section must be switched from the battery first
      - Discharge is autonomously terminated if HST enters safemode

Battery Reconditioning Circuitry

- Reconditioning Resistors
  - Constructed Using Heater Elements
  - "Low Rate" 50.7Ω ±3%
  - "High Rate" 5.1Ω (10 X 50.7Ω ±3% in parallel)

Battery Reconditioning Circuitry

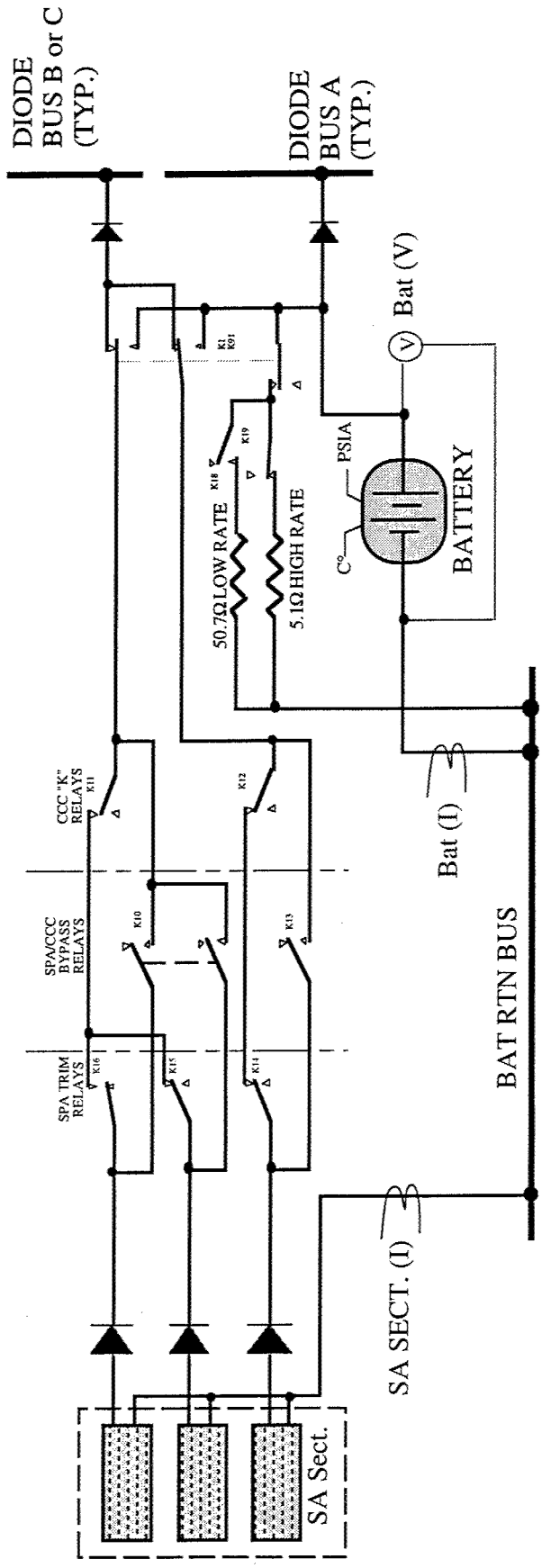

Reconditioning Procedure

- Test Preparation
  - Normalize Test Conditions to Previous Test of the Specified Battery
    - Sun-to-Orbit Ratio (within ±2 minutes)
    - SA / Sun Incidence angle (±10°)
  - Other Preparations
    - Schedule TDRSS Support to Configure, Initiate, Monitor and Reconfigure HST for the Test

Reconditioning Procedure

- Schedule At Least One 15 min. Forward Link / Orbit During Discharge for Contingency Test Termination.

– "Go For Test" Conditions

- Two Orbits of Charge In Which Full Charge Cut-off Attained
- **DO NOT Interrupt Science!**

Reconditioning Procedure

- Test Procedure
  - The Battery is Reconditioned to 15V
    - Autonomously Terminated by the "Special Hardware Limit Test"
    - Battery is Discharged "High Rate" Through the 5.1Ω Resistor
      - Average current = 5.4 Amps
      - Duration of discharge is about 15 to 18 hours
  - Data is Monitored and Collected During Discharge
    - Current, Voltage, Temperature and Pressure

Reconditioning Procedure

- Criteria For Test Termination
  - Flight Software State of Charge (SOC) Below 275 Ah for the 5 Battery System *
    - Benchmark SOC for 5 Battery System = 345 Ah
  - -8.0C° > Test Battery Temperature > 7.0°C **
  - 15.0V > Test Battery Voltage > 33.5V **
  - HST Safemode Entry ***

* Terminated Manually
**Terminated by Special HW Limit Test
***Terminated by Safemode Macro

Reconditioning Procedure

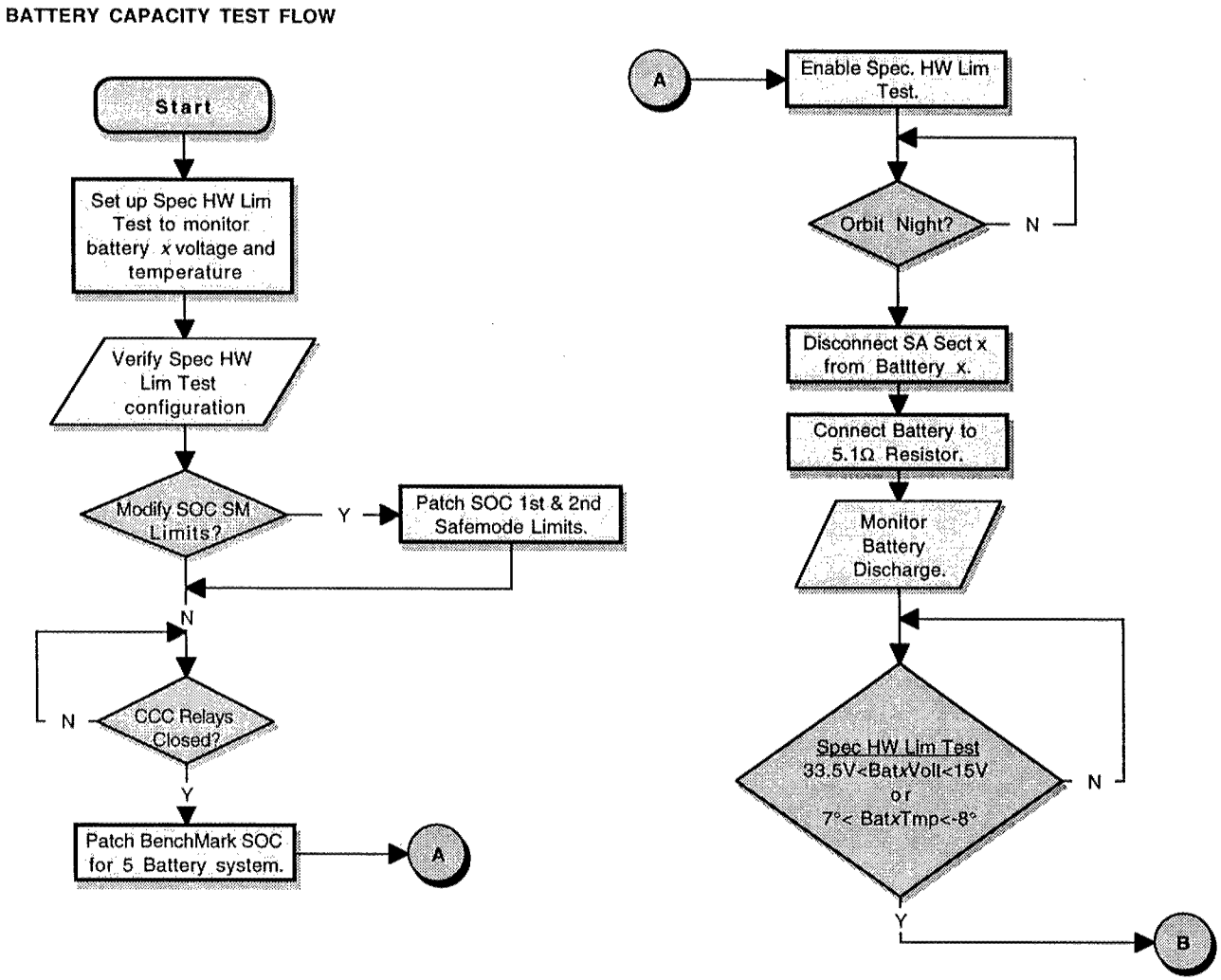

Reconditioning Procedure

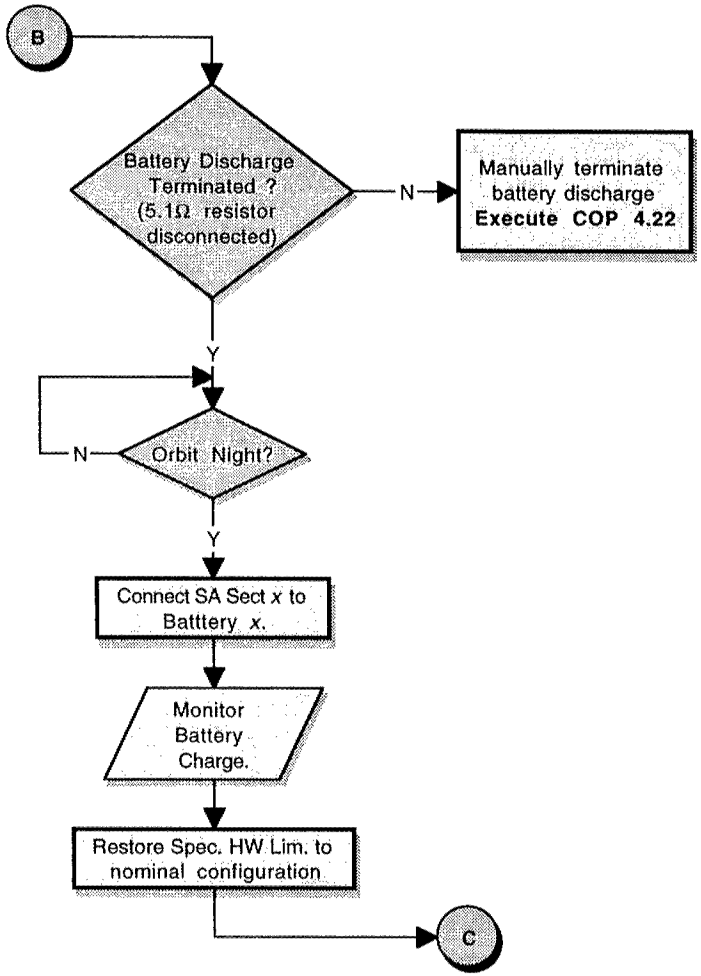

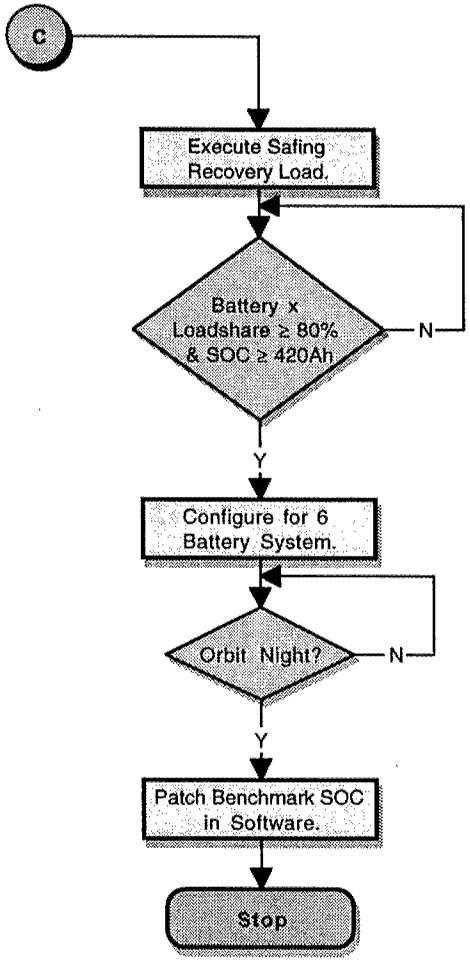

Results of Reconditionings

- Capacity
  - Batteries Reconditioned During April 1990 through Sept. 1992 Yielded (Current Integrated) Capacity Between 85.6 and 94.2 Ah
    - Indicated (Pressure Based) Capacity Prior to Reconditioning Ranged Between 88 and 102.6 Ah
      - Pressure transducers are recalibrated following each battery reconditioning
  - Capacity Recovery Very Gradual, Never Reached Original Level
    - Average Loss of $\approx$ 4.8 Ah/bat/year

Results of Reconditionings

- Decrease in Capacity Led to Disabling Primary Battery Heaters, Nov. 1995
  - Two Battery Reconditionings Since Heaters Disabled
    - Battery #5, yielded a decrease of 4.6 Ah in capacity, Jan. 1996 (previously tested Feb. 1995)
    - Battery #3, yielded an increase of 1.2 Ah in capacity, Mar. 1996 (previously tested April 1995)

Results of Reconditionings

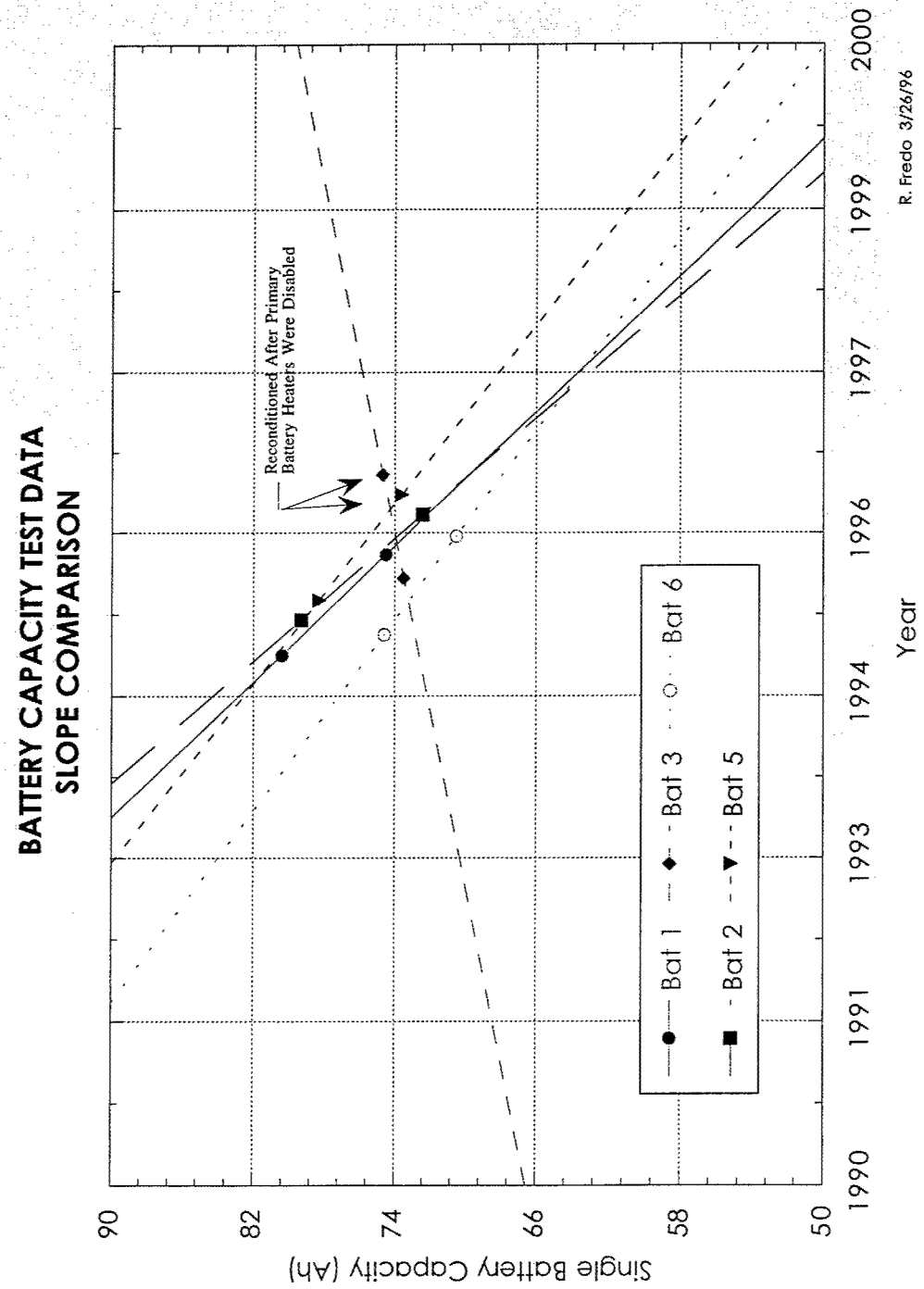

Results of Reconditionings

- Cell Balance
  - Reconditionings Following the Lowering of Charge Levels (Dec. 1993) Exhibit a Sluggish Voltage Knee in Contrast to an Earlier Sharp Knee
    - Indicates Cell Imbalance in the Battery
- Residual Pressure
  - Increases in Residual Battery Pressure @ 15V Typically Range Between 6 and 19 PSI
    - Most Recent Data Yielded an Increase of 0 PSI

Results of Reconditionings

Battery #	Date of Test (MM/YY)	Battery Pressure min - max (psi)	Pre-test Cap Pressure Based (A-h)	Post-test Cap Current Integrated (A-h)
Launch - CCC 1-6 K2 V-T level 2, CCC 1-6 K1 V-T level 3, Software Charge Ctrl; 4/28/90 - CCC 1-6 K2 V-T level 3				
1	Dec-90	980 - 1115	93	94.2
4	Dec-90	937 - 1044	88	93.4
5	Aug-92	991 - 1101	102.6	94
2	Aug-92	1053 - 1163	94	88.5
6	Aug-92	977 - 1094	93.9	88.3
3	Aug-92	951 - 1071	92.3	85.6
3/25/93 - CCC 1-6 K1 V-T level 4, Hardware Charge Ctrl 12/10/93 - CCC 4 K2 V-T level 2; 1/31/94 - CCC 4 K2 V-T level 1 4/5/94 - CCC 5 K1 level 3 (short between +E hot and +B return.)				
1	Aug-94	1017 - 1136	94.4	80.4
6	Oct-94	979 - 1079	86.5	74.6
2	Dec-94	895 - 1046	82.2	79.3
1/8/95 - SA Slew minimization 1/20/95 - CCC 5 K1 level 4 (healed short between +E hot and +B return.)				
5	Feb-95	1036 - 1032	94.8	78.3
3	Apr-95	956 - 1035	82.1	73.5
1	Jul-95	1011 - 1119	81.5	74.5
4	*	999 - 1085	100.1	80.4
6	Sep-95	979 - 1052	74.2	70.5
2	Nov-95	885 - 962	76.4	72.4
11/27/95 - Pri Battery heaters disabled				
5	Jan-96	863.9 - 1094	78.7	73.7
3	Mar-96	945 - 1029	74.5	74.7

* The Battery 4 Capacity is an estimate based on the other 5 battery tests.
No test of battery 4 was conducted due to PCU relay failures.

Results of Reconditionings

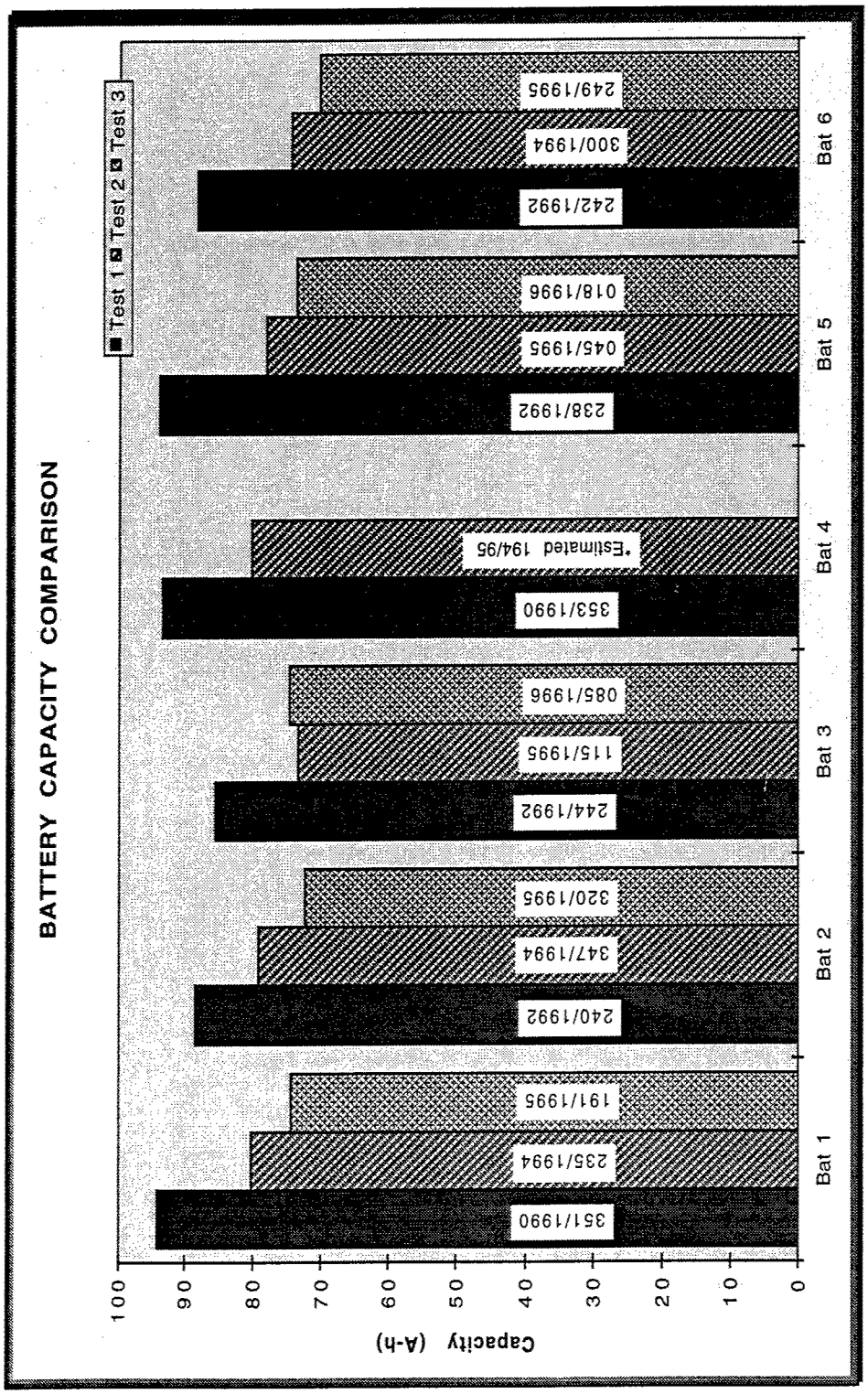

Results of Reconditionings

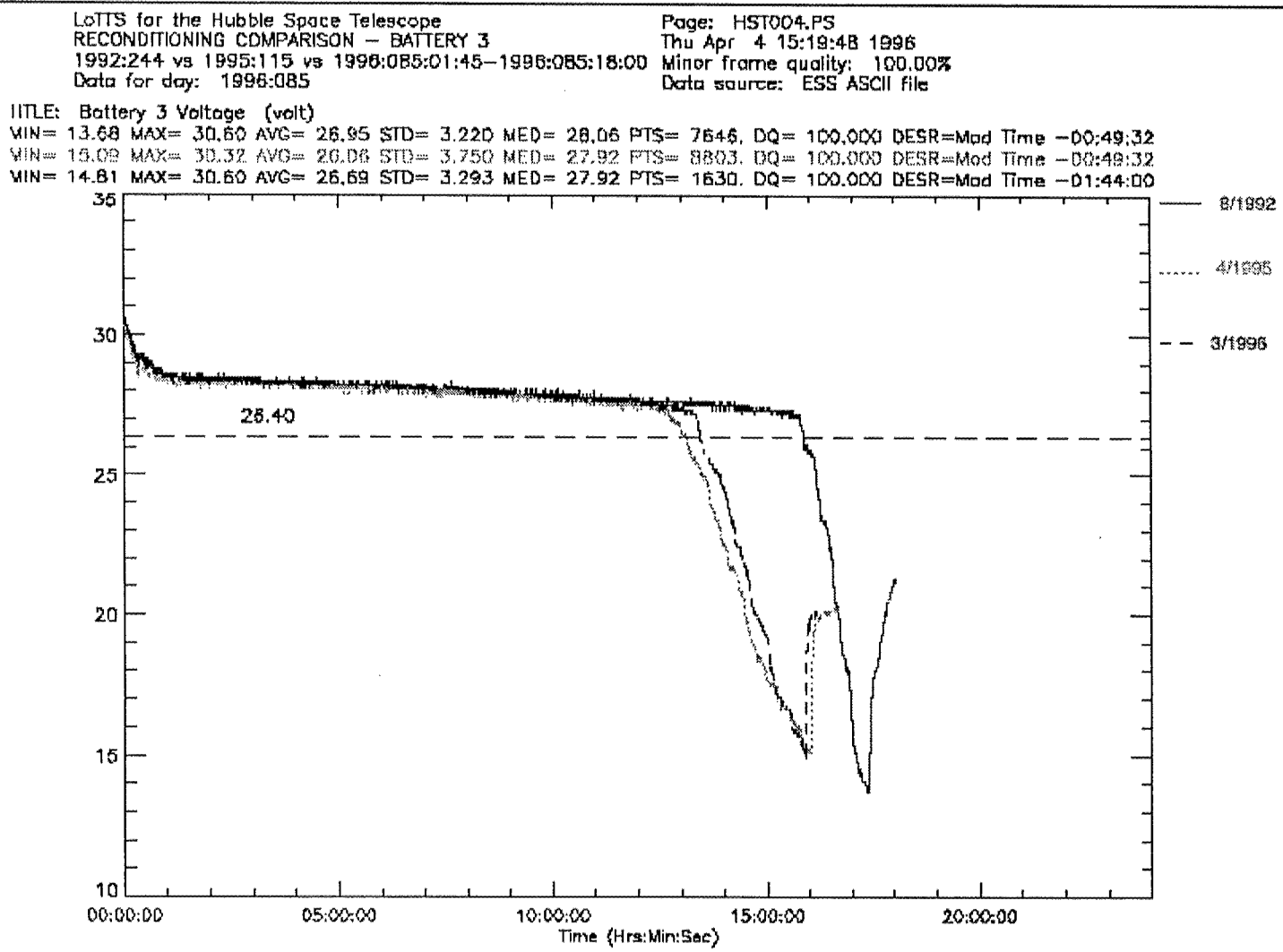

Results of Reconditionings

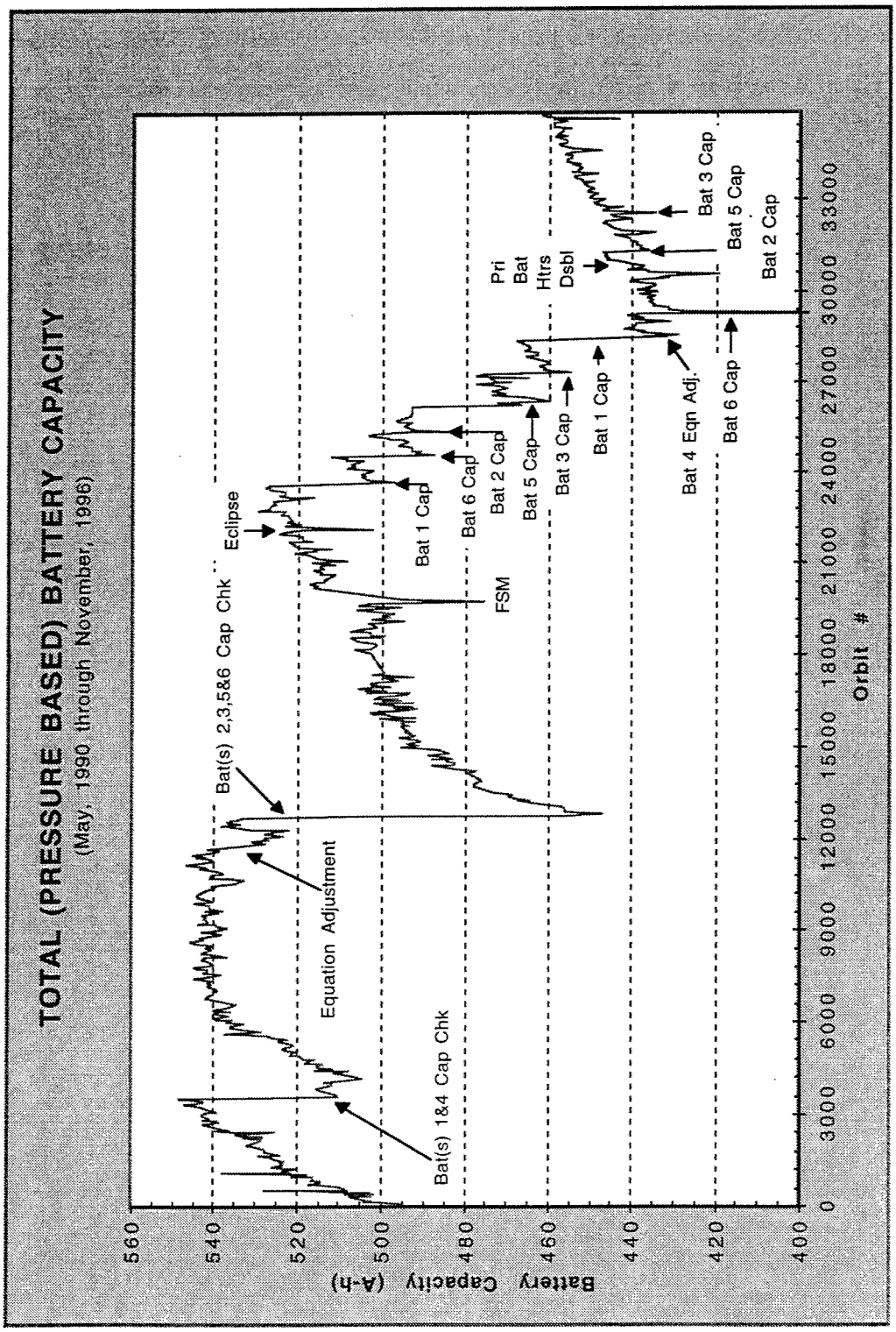

Conclusions

- Battery Capacity, From Reconditioning Data, Decreased Over Time (1990 - 1996)
  - Battery Temperatures Were Decreased by Disabling Primary Heaters, Nov. 1995
    - Allows Batteries to be Charged to Higher Voltage
    - Last Reconditioning Indicated Improvement, Mar. 1996
  - Development of New Charge Scheme is in Progress to Mitigate the Battery Degradation

Conclusions

- Health-Check, Capacity Data Indicated no Need to Refurbish Batteries in the Second Servicing Mission - Feb. 1997
- Reconditioning Decreased the Battery Operating Pressures
- Calculated Battery Capacity, Based on the Pressure Transducers, was Found to be Inaccurate
  - Recalibrated Pressure the Transducers

Page
262
Blank

1996 NASA AEROSPACE BATTERY WORKSHOP

NiH_2 BATTERY RECONDITIONING FOR LEO APPLICATIONS

J. D. Armantrout & D. P. Hafen
Lockheed Martin Missiles & Space
1111 Lockheed Martin Way
Building 149, 0/E6-01
Sunnyvale, CA 94089-3504

ABSTRACT

This paper summarizes reasons for and benefits of reconditioning nickel-hydrogen (NiH_2) batteries used for Low Earth Orbit (LEO) applications. NiH_2 battery cells do not have the classic discharge voltage problems more commonly associated with nickel-cadmium (NiCd) cells. This is due, in part, to use of hydrogen electrodes in place of cadmium electrodes. The nickel electrode, however, does have a similar discharge voltage signature for both cell designs. This can have an impact on LEO applications where peak loads at higher relative depths of discharge can impact operations. Periodic reconditioning provides information which can be used for analyzing long term performance trends to predict usable capacity to a specified voltage level. The reconditioning process described herein involves discharging NiH_2 batteries at C/20 rates or less, to an average cell voltage of 1.0 volts or less. Recharge is performed at nominal C/5 rates to specified voltage/temperature (V/T) charge levels selected to restore required capacity with minimal overcharge. Reconditioning is a process of restoring reserve capacity lost on cycling, which is commonly called the memory effect in NiCd cells. This effect is characterized by decreases in the discharge voltage curve with operational life and cycling. The end effect of reconditioning NiH_2 cells may be hidden in the versatility of that design over the NiCd cell design and its associated negative electrode fading problem. The process of deep discharge at lower rates by way of reconditioning tends to redistribute electrolyte and water in the NiH_2 cell electrode stack, while improving utilization and charge efficiency. NiH_2 battery reconditioning effects on life are considered beneficial and may, in fact, extend life based on NiCd experience. In any case, usable capacity data obtained from reconditioning is required for performance evaluation and trend analysis. Characterization and life tests have provided the historical data

base used to determine the need for reconditioning in most battery applications. The following sections briefly describe the background of NiH_2 battery reconditioning and testing at Lockheed Martin Missiles & Space (LMMS) and other aerospace companies.

BATTERY RECONDITIONING BACKGROUND

Reconditioning is a discharge-charge sequence normally applied to NiCd batteries to minimize degradation of the battery electrical performance, specifically capacity measured to a nominal voltage of 1.1 volts per cell. The process involves discharge of the battery at C/20 rates or less, to an average cell voltage of 1.0 volts or less. The subsequent charging process must be sufficient to restore rated, or actual measured capacity, whichever is greater, in order to compensate for charge efficiency. Reconditioning is a process of restoring reserve capacity lost on cycling, which is commonly called the memory effect in NiCd cells. It is characterized by decreases in the voltage of the discharge curve with operational life and cycling. Although NiH_2 battery cells do not have the classic voltage degradation problems that NiCd cells have, the nickel electrode has a similar discharge voltage signature during cycling for both cell designs. The effects of reconditioning on NiH_2 cells may be hidden in the versatility of that system over the NiCd system and its associated negative electrode fading problem. Water loss from the electrode stack can occur in NiH_2 cells by evaporation from the stack and condensation at the pressure vessel wall. This is normally compensated for in MANTECH NiH_2 cell designs by a wall wick inside the pressure vessel which returns any electrolyte loss or water loss from the stack by way of the separator in contact with the wall wick. COMSAT cell designs do not have a wall wick and therefore are more subject to adverse effects of electrolyte loss or water loss from the cell stack. Such losses are usually encountered during cell overcharge, which must be minimized in COMSAT battery cells. Hydrogen gas is oxidized to water during discharge and reformed to gas during charge for both COMSAT and MANTECH NiH_2 cell designs. COMSAT cell designs have teflonated pressure vessel walls that are not hydroscopic which tends to repel any water loss from the stack back into the stack in a zero G environment. The process of deep discharge by way of reconditioning tends to redistribute electrolyte and water in the cell stack, and improve utilization and charge efficiency. Reconditioning effects on life are considered beneficial and may, in fact, extend life based on NiCd experience. In any case, the capacity data

obtained from reconditioning can be used for performance evaluation and trend analysis. This has been documented in Reference (1) for GEO applications for COMSAT cell designs. In-orbit performance of batteries is normally judged by the minimum end-of-discharge voltage (EODV) during peak loading. GEO batteries are usually reconditioned prior to each eclipse season to verify capacity to an end voltage. LEO batteries are reconditioned as required to verify long term capacity fading trends such as described for HST MANTECH NiH_2 batteries in Reference (2). Capacity tests at nominal reconditioning rates have shown a trend of decreasing capacity with cycle life for the HST mission. Extrapolation of that data has provided a basis for determining the useful life of the HST batteries beyond the specified design life of seven years. Recondition discharge of the HST batteries is performed through a 25 ohm resistor to an end voltage of 15 volts (0.7 volts per cell). This voltage limit minimizes the potential for cell reversal at end of discharge when actual discharge rates approach a C/150 rate. It also allows for more complete redistribution of electrolyte for improved utilization and charge efficiency. The following section summarizes testing background which has provided the historical data base for determining the need for reconditioning NiH_2 batteries.

BATTERY TESTING BACKGROUND

Battery test facilities for characterizing and life testing cells and batteries exist at most aerospace companies. TRW's battery test facilities were established in the 1960's following battery problems associated with various NASA programs. TRW performed extensive characterization tests for NASA on NiCd cells in the 1960's and 1970's as documented in Reference (3). GSFC began characterization testing of various cell and battery designs at NWSC in Crane, Indiana, during the same time period. Ford Aerospace Company (now Loral) and Hughes Aircraft Company (HAC) established battery test facilities in the 1970's for the Intelsat IV, V and VI satellite programs. Martin Marietta, GE Valley Forge and RCA battery test facilities were also established in the same time period for other military and commercial satellite applications utilizing NiH_2 batteries. Development and test history for these and other NiH_2 designs are documented in Reference (1). As NiH_2 and other advanced battery designs have been integrated into more sophisticated spacecraft programs at LMMS (HST, Milstar and Iridium), increased battery test costs have forced descoping of tests to reduce costs. The trend to reduce overhead

costs of long term battery and cell performance characterization testing by descoping tests requires some risk assessment analysis. Battery problems usually drive the need for more extensive development and test programs, such as happened in the 1960's when battery failures affected end item operations, as documented in Reference (4) for the Orbiting Astronomical Observatory (OAO) satellite. Batteries normally fail gracefully and in a predictable manner which can be reliably quantified based on a relatively large test data base as reported in Reference (5). The need to maintain battery test facilities can only be determined by an assessment of whether or not the existing data base can be used to predict battery life for particular spacecraft power requirements. The following section summarizes results of NiH_2 battery life testing for a specific LEO application which uses reconditioning to predict usable capacity to a specified voltage level.

BATTERY RECONDITIONING

A series of tests were initiated at Eagle Picher Industries (EPI) to evaluate effects of reconditioning on long term performance of RNH-76-3 NiH_2 cells. The testing consisted of cycling at 41°F to a maximum depth-of-discharge (DOD) of 33 Ah. Test articles included a 9-cell pack and a 20-cell battery. The objective of the 9-cell pack reconditioning test was to evaluate the reconditioning effectiveness for a battery configuration between a 25 ohm discharge to 15V and a 5.3 ohm discharge to 25V, then 25 ohm to 15V. The following tests were completed on the 9-cell pack:

TASK NUMBER	RECONDITION RATE
4A	2.2 Ohm to 6.14V
4B	2.2 Ohm to 6.14V
4C	2.2 Ohm to 10.64 V
	10.2 Ohm to 6.14V
4D	2.2 Ohm to 10.64V
	10.2 Ohm to 6.14V

The actual recondition discharge tests performed did not significantly change the discharge voltage stabilization levels for Tasks 4A, 4B or 4C as shown in Figure 1. However, a significant improvement in the discharge voltage level occurred during performance of Task 4D following one week of discharged open circuit stand after reconditioning, also shown in Figure 2. A reconditioning sequence designated D2 was then performed according to the same test procedure as the reconditionings for Tasks 4C and 4D. The comparison of reconditionings D and D2 plotted in Figure 3 show very stable voltage performance to 10.64V. The reduced capacity after removal of approximately 86Ah was due to lower capacity of one cell in the pack during the D2 reconditioning discharge. The significant voltage improvement during performance of Task 4D was attributed to redistribution of electrolyte and water in the cell electrode stack following one week open circuit stand after reconditioning at the lower discharge rate (10.2 Ohm to 6.14V).

The objective of the 20-cell battery test was to verify long term battery performance under similar test conditions as imposed on the 9-cell pack. Figure 4 illustrates improvements in minimum daily voltages after 12,000 cycles following capacity checks or partial reconditionings. The capacity checks consisted of discharging at 15A to 13.6V, or until the first cell reached 0.7V. Figure 5 shows voltage performance versus cycles experienced since reconditioning events shown in Figure 4. A trend in decreasing EODV with cycle life similar to the 9-cell pack test was observed for the battery test. The following section summarizes conclusions reached from analysis of data presented herein.

CONCLUSIONS

The end effect of reconditioning NiH_2 cells provides usable capacity data for performance evaluation and trend analysis. NiH_2 battery reconditioning effects on life are considered beneficial and may, in fact, extend life based on NiCd experience. Characterization and life testing have provided a historical data base to determine the need for reconditioning to improve voltage performance to a specified voltage level. Although NiH_2 battery cells do not have the classic voltage degradation problems that NiCd cells have, the nickel electrode has a similar discharge voltage signature during cycling for both cell designs. The process of deep discharge by way of reconditioning tends to redistribute electrolyte and water in the NiH_2 cell stack, and

improve utilization and charge efficiency. In-orbit performance of batteries is normally judged by the minimum EODV reached during peak loading. GEO batteries are usually reconditioned prior to each eclipse season to improve voltage performance and verify capacity to an end voltage. LEO batteries are reconditioned as required to verify long term capacity fading trends such as summarized herein. Extrapolation of reconditioning discharge data provides a basis for predicting cycle life performance for both NiCd and NiH_2 batteries.

REFERENCES

1. J.D. Dunlop, G.M. Rao and T.Y. Yi, **NASA Handbook for Nickel Hydrogen Batteries**, NASA Reference Publication 1314, September 1995.

2. G.M. Rao and J.D. Armantrout, **Hubble Space Telescope Program Battery Experience**, 1996 Space Power Workshop.

3. W.R. Scott and D. W. Rusta, **Sealed-Cell Nickel-Cadmium Battery Applications Manual**, NASA Reference Publication 1052, December 1979.

4. F.E. Ford, G.M. Rao, and T.Y. Yi, **Handbook for Handling and Storage of Nickel-Cadmium Batteries: Lessons Learned**, NASA Reference Publication 1326, February 1994.

5. D.P. Hafen, **Comparison of Nickel-Hydrogen and Nickel-Cadmium Reliability**, IECEC Paper 929257, August 1992.

LOCKHEED MARTIN
Missiles & Space

NiH_2 BATTERY RECONDITIONING FOR LEO APPLICATIONS

Jon D. Armantrout
Douglas P. Hafen
Lockheed Martin Missiles & Space

Presented at

The 1996 NASA Aerospace Battery Workshop
Focused Session on NiH_2 Battery On-Orbit Reconditioning Experience

December 3, 1996

LOCKHEED MARTIN
Missiles & Space

NiH_2 Battery Reconditioning in LEO

OBJECTIVE

- RESTORE RESERVE CAPACITY LOST ON CYCLING
- IMPROVE VOLTAGE PERFORMANCE AND CYCLE LIFE
- REDISTRIBUTE ELECTROLYTE AND WATER IN CELL STACKS
- IMPROVE ELECTRODE UTILIZATION AND CHARGE EFFICIENCY
- ESTABLISH DATA BASE FOR LONG TERM PERFORMANCE EVALUATION

LOCKHEED MARTIN
Missiles & Space

NiH_2 Battery Reconditioning in LEO

PROCEDURE

- DISCHARGE AT C/20 OR LESS TO 1.14 V/CELL NOMINAL
- DISCHARGE AT C/100 OR LESS TO 0.7 V/CELL NOMINAL
- RECHARGE AT C/5 TO TEMPERATURE-COMPENSATED VOLTAGE LIMIT
- REPEAT AS NECESSARY TO STABILIZE CELL CAPACITY AND VOLTAGE
- COLLECT DATA FOR PERFORMANCE EVALUATION AND TREND ANALYSIS

LOCKHEED MARTIN
Missiles & Space

NiH_2 Battery Reconditioning in LEO

LIFE TESTING

- SERIES OF TESTS CONDUCTED TO EVALUATE EFFECTS OF RECONDITIONING
- TEST ARTICLES INCLUDED 9-CELL PACK AND 20-CELL BATTERY
- TEST CONDITIONS BASED ON 90 Ah NOMINAL CAPACITY
  - 96 MINUTE CYCLING AT 41°F (5°C)
  - 33 Ah MAXIMUM DOD ONCE PER DAY
  - 15 A NOMINAL LOAD / 25 A PEAK LOAD
  - 15 A CHARGE TO TEMPERATURE COMPENSATED VOLTAGE LIMIT

LOCKHEED MARTIN
Missiles & Space

NiH_2 Battery Reconditioning in LEO

9-CELL PACK TESTING

- RECONDITION PERFORMED FOLLOWING SEVERAL TEST CONDITIONS
  - 2.2 OHM TO 6.14V (AFTER TASKS 4A AND 4B)
  - 2.2 OHM TO 10.64V
    10.2 OHM TO 6.14V (AFTER TASKS 4C AND 4D)

- MINIMUM EODV CHANGED FOLLOWING RECONDITIONING AFTER TASK 4C
  - IMPROVED VOLTAGE PERFORMANCE ATTRIBUTED TO REDISTRIBUTION OF ELECTROLYTE AND WATER IN CELL STACK DURING ONE WEEK OPEN CIRCUIT STAND FOLLOWING RECONDITIONING AFTER TASK 4C
  - FIGURE 1 SHOWS IMPROVEMENT IN EODV DURING CYCLING
  - FIGURE 2 SHOWS LESS EODV IMPROVEMENT WITHOUT OPEN CIRCUIT STAND FOLLOWING RECONDITIONING AFTER TASK 4D
  - FIGURE 3 SHOWS VOLTAGE PERFORMANCE DURING 15 A DISCHARGES

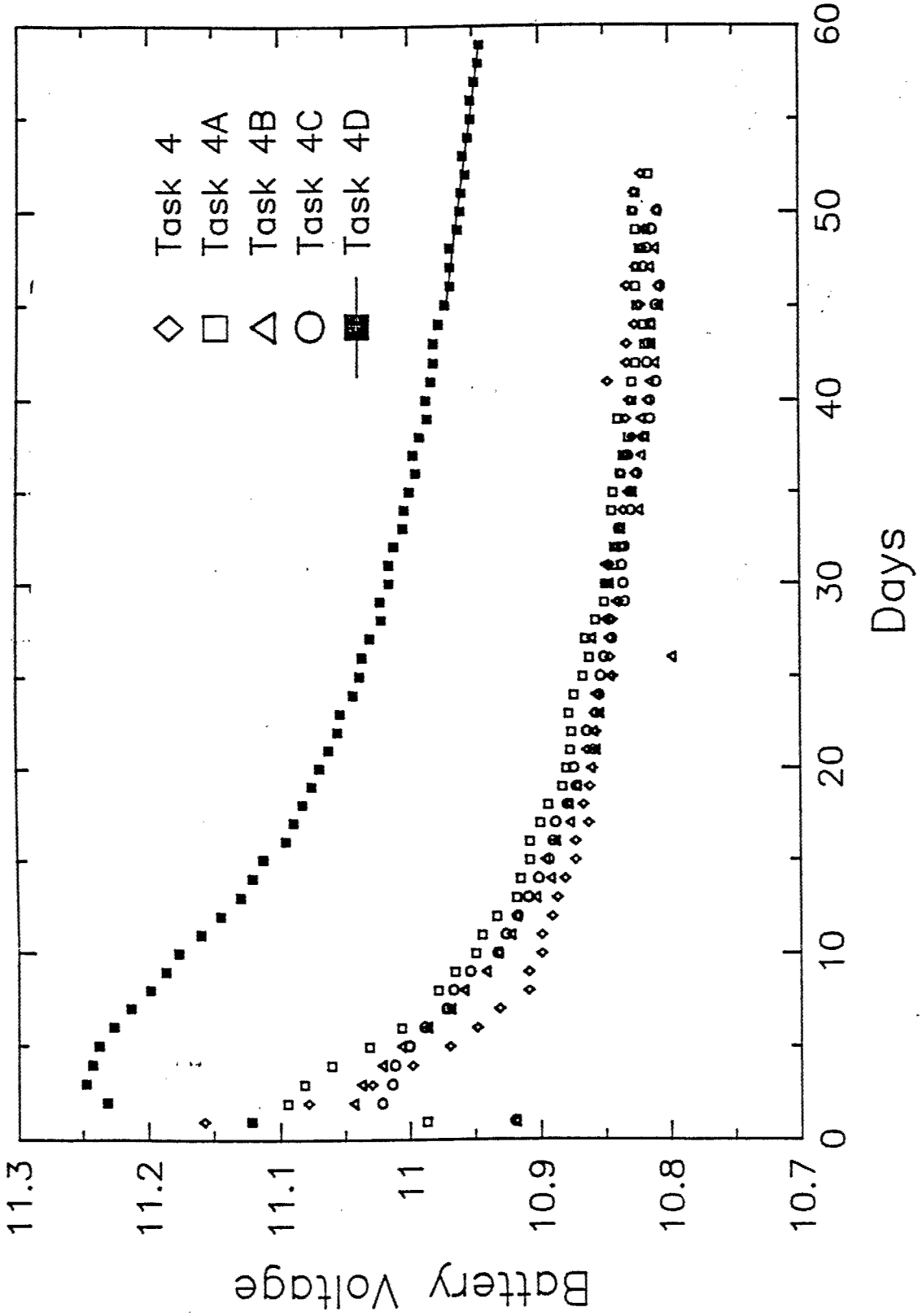

Figure 1. End of Discharge Voltage Comparisons

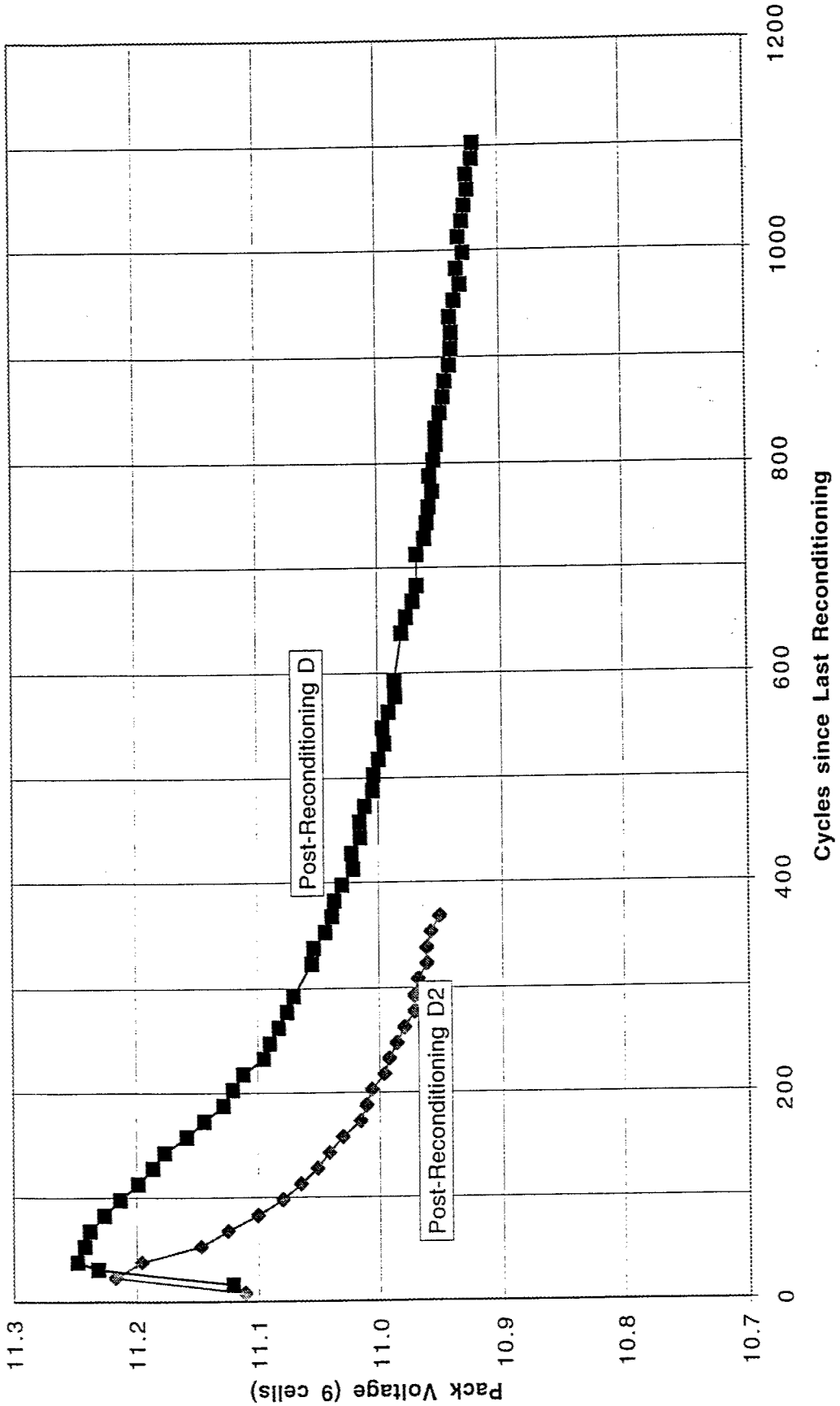

Figure 2. Comparision of Cycle 8 EODV after Reconditioning For Reconditionings D and D2

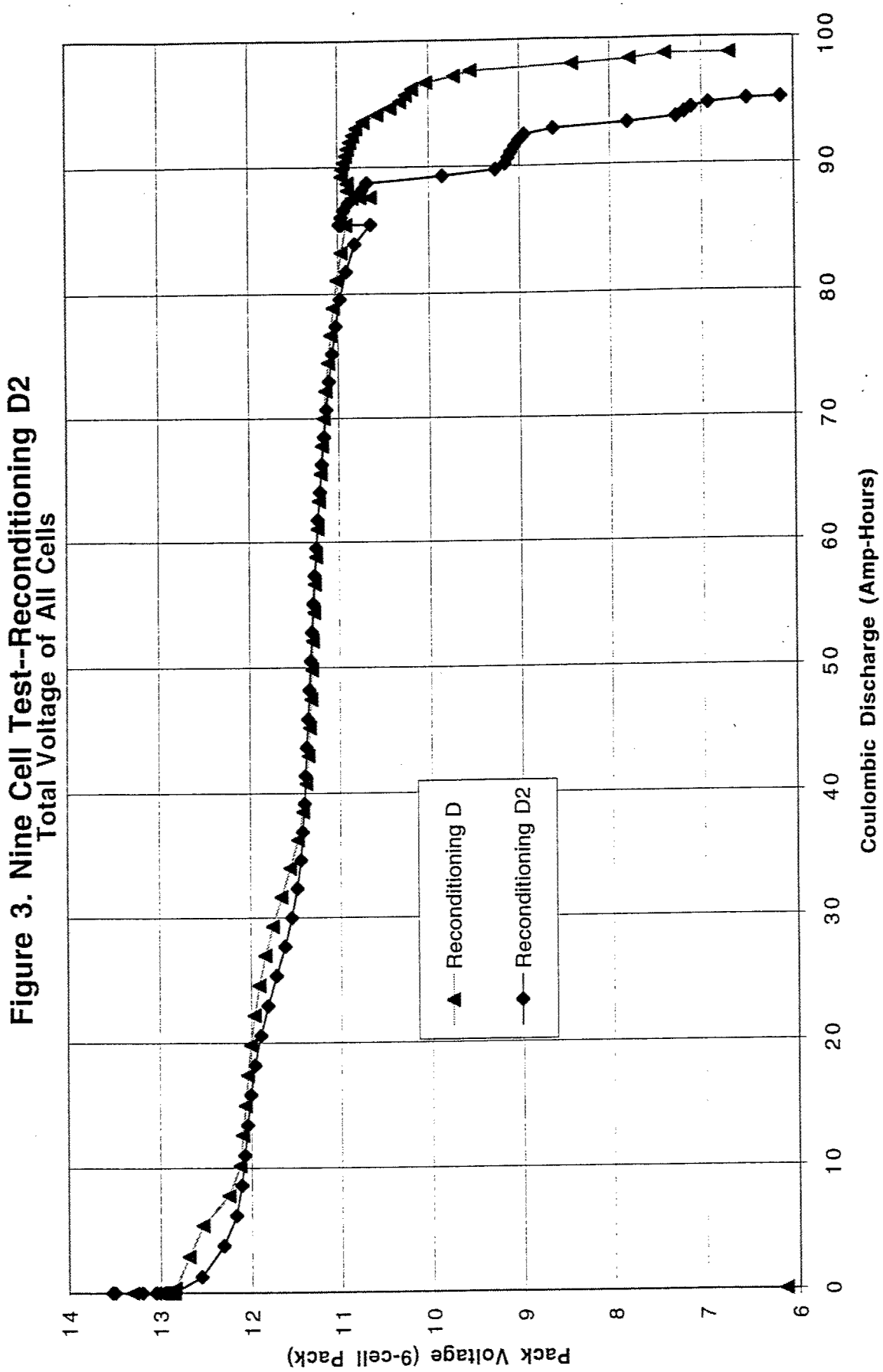
Figure 3. Nine Cell Test--Reconditioning D2
Total Voltage of All Cells
Pack Voltage (9-cell Pack)
14
13
12
11
10
9
8
7
6
Coulombic Discharge (Amp-Hours)
0
10
20
30
40
50
60
70
80
90
100
Reconditioning D
Reconditioning D2

NiH_2 Battery Reconditioning in LEO

20-CELL BATTERY TESTING

- CAPACITY CHECKS OR PARTIAL RECONDITIONINGS IMPROVED MINIMUM EODV AS SHOWN IN FIGURE 4
  - CAPACITY MEASUREMENTS MADE AT 15 A RATE TO 13.6V OR FIRST CELL TO 0.7V
  - PARTIAL RECONDITIONINGS DUE TO TEST EQUIPMENT PROBLEMS

- TREND IN DECREASING EODV WITH CYCLING OBSERVED
  - FIGURE 5 SHOWS VOLTAGE PERFORMANCE VERSUS CYCLES
  - TREND SIMILAR TO 9-CELL PACK DATA SHOWN IN FIGURE 1

Figure 4. Qual Battery Performance

S/N -1005R, RNH76-3 Cells

20-cell configuration

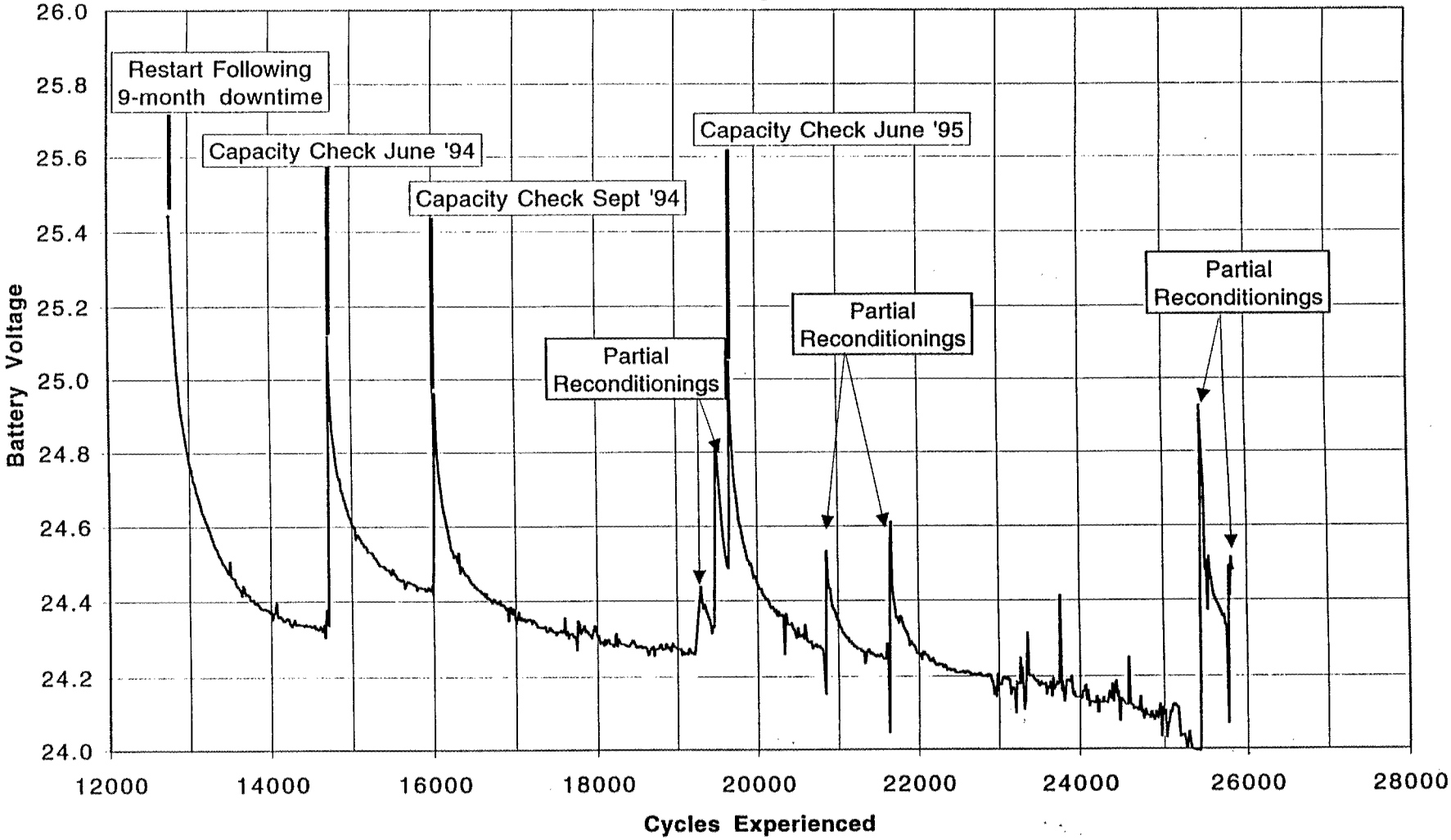

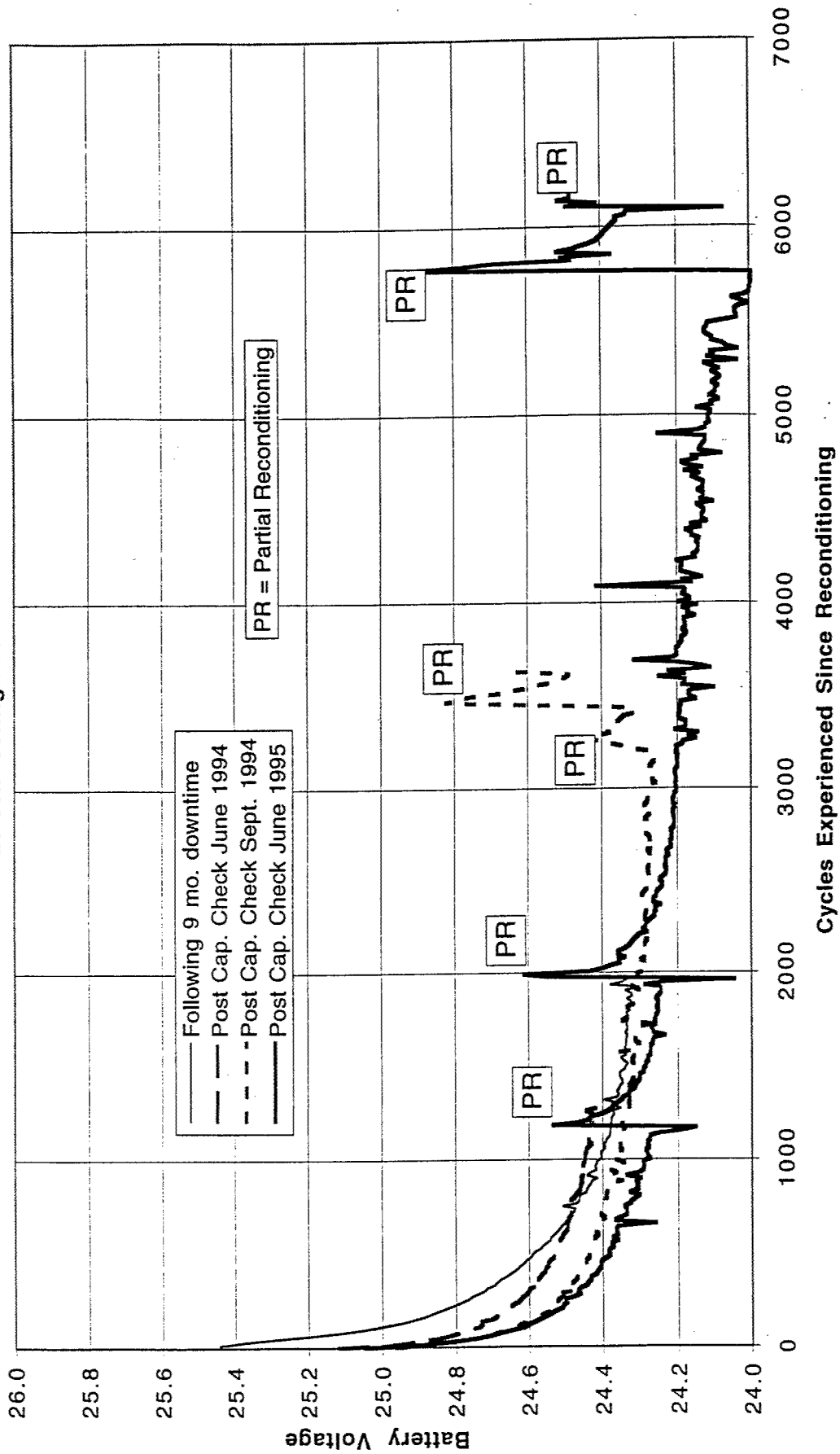

Figure 5. Qual Battery Performance

S/N -1005R, RNH76-3 Cells

20-cell configuration

LOCKHEED MARTIN
Missiles & Space

NiH_2 Battery Reconditioning in LEO

CONCLUSIONS

- RECONDITIONING PROVIDES USABLE CAPACITY DATA FOR PERFORMANCE EVALUATION AND TREND ANALYSIS
- DEEP DISCHARGE BY WAY OF RECONDITIONING TENDS TO REDISTRIBUTE ELECTROLYTE AND WATER IN CELL STACKS
- RECONDITIONING RESTORES RESERVE CAPACITY LOST ON CYCLING AND IMPROVES VOLTAGE PERFORMANCE

Nickel-Hydrogen Session

Page
282
Blank

Development of Sintered Fiber Nickel Electrodes For Aerospace Batteries

Jennifer Francisco, Dennis Chiappetti, Jack Brill
Eagle-Picher Industries, Inc.
Joplin, Missouri 64801

ABSTRACT

The nickel electrode is the specific energy limiting component in nickel battery systems. A concerted effort is currently underway to improve NiH_2 performance while decreasing system cost. Increased performance with electrode specific energy (mAh/g) is the major goal of this effort. However, cost reduction is also an important part of the overall program, achieved by reducing the electrode weight. A lightweight, high energy density nickel electrode is being developed based on a highly porous, sintered fiber, nickel substrate. This developing technology has many applications, but is highly applicable to the military and aerospace industries.

Introduction

The aerospace industry has used the nickel-hydrogen battery system for more than 20 years developing both an extensive history and a large database. The aerospace industry demands a high degree of performance and reliability in which the nickel hydrogen battery is able to maintain. Advances in technology are constantly being made. The focus of the present work is to develop an aerospace flight qualified nickel electrode. Rapid growth in earth orbital satellite applications, including small satellites, and increasing spacecraft power system performance requirements, have created a need for improved flight qualified nickel hydrogen (NiH_2) battery technology. However, these performance improvements must not compromise the inherent safety or reliability of the NiH_2 battery. A concerted effort is currently underway to improve the NiH_2 performance while decreasing system cost. This effort involves work at the component, cell and full battery level. Component level development work includes performance enhancement and cost reduction at the basic electrode level. Increased performance, with electrode specific energy (mAh/g) as figure of merit, is the major goal of this effort. However, cost reduction is also an important part of the overall program.

Electrode Substrate Material

Eagle-Picher Ind., Inc. currently manufacture the sintered carbonyl nickel powder electrode substrate. This forms a rigid, highly porous matrix into which the nickel-hydroxide active material may be introduced. Sintered nickel powder is very strong and dimensionally stable, but it contributes adversely to the overall electrode weight. This type of electrode may account for more than 50% of the total weight in a typical aerospace nickel electrode. A lightweight substrate would greatly improve the electrode specific energy. The approach used in this development effort has been to utilize fiber based nickel electrode substrates, prepared using proprietary micro-diameter metal fiber technology. This material is superior to prior fiber substrates based on the small fiber diameter, smaller equivalent pore size and dimensional stability. Two vendors which produce such substrates are Memtec America Corp. and Ribbon Technology Corp. Due to proprietary reasons, the data will not specify to which company it refers.

The active material loading obtained typically with fiber based substrates has been relatively low. An additional problem is that the active material utilization has also been typically low. This results in an electrode with a relatively low specific energy (in terms of milliampere-hours per gram), even though the fiber is lighter in weight than sintered nickel powder.

In general, the electrochemical impregnation method deposits the nickel hydroxide active material directly into the pores of the electrode substrate from the "inside out". Nickel hydroxide is produced inside the pore structure of the electrode by the nitrate reduction process. Since the outer pores near the electrode surface are filled last with active material, the entire electrode structure is used. This technique provides for much more intimate contact between the active material, and the current collector, which results in a lower effective current density during electrode operation. The resultant electrode has lower impedance, increased rate capability, higher electrochemical utilization based on theoretical energy density and improved cycle life.

The small pore structure retains active material much better than a corresponding larger pore size material, which con-

tributes significantly to charge/discharge cycle life. As the electrode is cycled, the active material undergoes significant changes in phase, oxidation state, state of hydration, structure, crystallinity, and density. These changes in the active material cause the gradual extrusion of the active material out of the substrate and into the electrolyte/separator matrix in the cell. The smaller pore size in the electrochemically impregnated substrate and the more intimate contact between the active material and the substrate minimizes this active material extrusion loss during cycling.

Electrode Active Material Impregnation/Formation

The highly porous substrate material allows the nickel hydroxide active material to be inserted into the electrode. This work is being performed primarily for aerospace applications. Therefore, the nickel hydroxide active material insertion method primarily being investigated is a close variation of the aerospace electrochemical impregnation method.

In general, the porous electrode substrate is cathodically polarized in a bath of aqueous nickel-nitrate. The charge/discharge cycle then forms the active material, creating a working nickel electrode. The basic chemical reactions are listed in Table I. The electrochemical reactions at the catalytic electrode are similar to basic alkaline fuel cell chemistry. When the nickel electrode is charged, the nickel active material is oxidized to a higher oxidation state at the nickel electrode. This is typically shown as a charge from nickel (II) to nickel (III). The reaction at the gas electrode is essentially the alkaline electrolysis of water, in the presence of a catalyst, to produce molecular hydrogen gas. This is essentially a reduction reaction. When the electrode is discharged, the nickel active material is reduced to its original state and the hydrogen gas is oxidized to form water, producing two electrodes per molecule of gas that reacts.

Table I. Electrochemical Reactions Experienced by the Electrodes

Water and Ion Balanced Reactions

Positive: $NiO(OH) + H_2O + e \Rightarrow Ni(OH)_2 + (OH)^-$

Negative: $\frac{1}{2}H_2 + (OH)^- \Rightarrow H_2O + e$

Net Reaction: $\frac{1}{2}H_2 + NiO(OH) \Rightarrow Ni(OH)_2$

Unlimited Overcharge Capability

Positive: $2(OH)^- \Rightarrow 2e + \frac{1}{2}O_2 + H_2O$

Negative: $2H_2O + 2e \Rightarrow 2(OH)^- + H_2$

$\frac{1}{2}O_2 + H_2 \Rightarrow H_2O$

High Cell Reversal Tolerance

Positive: $H_2O + e \Rightarrow (OH)^- + \frac{1}{2}H_2$

Negative: $\frac{1}{2}H_2 + (OH)^- \Rightarrow H_2O + e$

Process parameters such as temperature, current, pH, and others are precisely controlled with specific limits.

Electrochemical Impregnation Results

A number of electrodes were tested within nine separate groups.

Individual results were obtained, however, Table II shows all 80 electrodes averaged according to the category from which they belong.

The column labeled "Standard" is similar data for a standard aerospace grade electrode. The initial substrate thickness for the R&D substrate was measured using a dial micrometer. The average initial substrate thickness is indicated along with the standard deviation, which is a measure of substrate uniformity. Table III shows the calculations used for each electrode and how the information was derived.

Electrode Parameters after the Electrochemical Impregnation

The sample area is constant since there is no measurable change with the length and width of the substrate. The thickness, however, does increase during the impregnation process. This is the result of filling substrate voids with nickel-hydroxide active material. The substrate is dimensionally stable in the length and width because of the way the that the fibers are randomly oriented within the electrode during the layering process. They are essentially interwoven in interlocking layers. The substrate is much less stable in the thickness direction. Even though the substrate is sintered to provide additional strength in this direction, the forces involved in the active material changes that occur cannot completely overcome. One of the major factors effecting ultimate electrode performance is this tendency towards thickness growth. Minimizing this effect is essential, particularly for a long life aerospace application, and is one of the major goals of the current study.

As can be seen from Table II, the impregnated electrode thickness increases from 63.5% to 181.91%. This is considerably more than the corresponding increase observed in aerospace sinter powder electrodes. Growth occurs mainly during impregnation due to the addition of the nickel. Growth also occurs - although not as much - during formation as the result of active material expanding during the charge/discharge cycle. Considerable progress has been made in optimizing fiber substrate parameters to minimize growth. While excessive thickness increase is not desirable, it is not necessarily prohibitive in an electrolyte starved compressed cell stack design, such as a NiH_2 cell design. Figures 1 & 2 show

Table II A Listing of the Average of All 80 Electrodes Used in the Study

	STANDARD	*Group A*				*Group B*				
		1	2	3	4	1	2	3	4	5
	AVGS	AVGS	AVGS	AVGS	AVGS	AVGS	AVGS	AVGS	AVGS	AVGS
Approximate size (in^2)	7.900	4.000	4.000	4.000	4.000	4.000	4.000	4.000	4.000	4.000
Substrate Weight (g)	8.610	1.599	1.782	2.254	2.337	2.295	2.371	3.056	3.242	3.221
Raw Weight with Tab (g)		6.950	6.768	7.269	7.670	7.739	7.858	8.550	8.923	8.538
Initial Thickness Average (in)	0.030	0.045	0.050	0.059	0.061	0.044	0.047	0.053	0.062	0.066
Initial (thickness) Porosity (%)	80.000	93.958	93.883	93.490	93.441	90.988	91.249	89.810	91.010	91.605
Initial Volume (cc)	3.880	2.975	3.278	3.894	4.016	2.870	3.050	3.446	4.052	4.311
Initial Void Volume (ccvv)	2.940	2.795	3.078	3.641	3.754	2.612	2.784	3.102	3.687	3.949
Number of Impregnation Cycles		2	2	2	2	2	2	2	2	2
Final Thick Average (in)	0.031	0.076	0.080	0.104	0.094	0.088	0.088	0.090	0.106	0.117
Final (thickness) Porosity (%)	80.000	96.372	96.147	96.263	95.697	95.454	95.284	93.908	94.742	95.174
Final Volume (cc)		4.984	5.221	6.798	6.136	5.773	5.784	5.919	6.949	7.663
Final Void Volume (ccvv)	3.050	4.805	5.021	6.544	5.873	5.515	5.525	5.575	6.585	7.301
Final Weight (g)	13.640	11.072	12.074	16.150	12.217	15.314	12.307	9.109	17.282	18.090
Finished Raw Weight (g)		5.721	7.088	11.135	6.884	9.869	6.820	14.603	11.602	12.773
Finished Pick-up (g)	5.030	4.122	5.306	8.881	6.915	7.575	6.885	6.053	8.359	9.551
Total Thick Increase (in)	0.001	27.791	33.855	42.311	33.930	79.407	69.868	55.141	39.988	62.588
Total Thick Increase (%)	5.880	63.569	68.040	71.412	56.111	181.910	149.097	109.629	65.195	94.980
Final (thickness) Load (g/ccvv)	1.650	0.851	1.048	1.359	1.163	1.377	1.245	1.091	1.271	1.306
Flood Capacity* (Ah)	1.740	0.737	1.159	1.780	1.330	1.719	1.685	1.630	1.653	2.021
Theoretical Capacity (Ah)	1.450	1.191	1.533	2.567	1.998	2.189	1.990	1.749	2.416	2.760
Utilization (%)	120.000	61.411	76.634	70.260	67.739	79.206	86.231	93.629	68.450	75.519
mAh/in^2		184.286	290.079	444.893	332.921	429.643	421.587	408.190	413.214	505.714
Ah/in^3		2.404	3.621	4.304	3.529	4.906	4.825	4.521	3.908	4.421
mAh/cm^2		28.564	44.962	68.959	51.603	66.595	65.346	63.270	64.048	78.386
mAh/cm^3		146.687	220.937	262.608	215.337	299.313	294.406	275.850	238.409	269.743
Active mass (%)	36.870	71.466	74.056	79.596	73.916	76.528	73.835	65.521	72.060	74.311
Inactive mass (%)	63.130	14.543	19.496	14.003	20.545	15.024	20.571	25.885	18.751	21.601
Specific Energy (mAh/g)	127.850	127.029	163.517	161.061	144.171	174.928	183.065	176.605	142.469	160.941

Table III A Listing Of The Mathematical Formulas Used

	SAMPLE
	0.06
Approximate size (in²)	9
Substrate Weight (g)	3.63
Raw Weight with Tab (g)	9.2101
Initial Thickness Average (in)	AVERAGE OF THICKNESS
Initial (thickness) Porosity (%)	100*INITIAL VOID VOLUME/INITIAL VOLUME
Initial Volume (cc)	APPROXIMATE SIZE*INITIAL THICKNESS AVERAGE*16.39
Initial Void Volume (ccvv)	(INITIAL VOLUME)-(SUBSTRATE WEIGHT/8.9)
Number of Impregnation Cycles	2
Final Thick Average (in)	AVERAGE OF THICKNESS
Final (thickness) Porosity (%)	100*FINAL VOID VOLUME/FINAL VOLUME
Final Volume (cc)	APPROXIMATE SIZE*FINAL THICKNESS AVERAGE*16.39
Final Void Volume (ccvv)	(FINAL VOLUME)-(SUBSTRATE WEIGHT/8.9)
Final Weight (g)	22.4668
Finished Raw Weight (g)	SUBSTRATE WEIGHT+GREEN WEIGHT
Finished Pick-up (g)	FINAL WEIGHT-RAW WEIGHT WITH TAB
Final (thickness) Load (g/ccvv)	FINISHED PICKUP/FINAL VOID VOLUME
Flood Capacity* (Ah)	3.1177
Theoretical Capacity (Ah)	FINISHED PICKUP*0.289
Utilization (%)	100*FLOOD CAPACITY/THEORETICAL CAPACITY
mAh/in²	1000*FLOOD CAPACITY/APPROXIMATE SIZE
Ah/in³	FLOOD CAPACITY/(APPROXIMATE SIZE*FINAL THICKNESS AVERAGE)
mAh/cm²	1000*FLOOD CAPACITY/(APPROXIMATE SIZE*2.54*2.54)
mAh/cm³	1000*FLOOD CAPACITY/ (APPROXIMATE SIZE*16.39*FINAL THICKNESS AVERAGE)
Active mass (%)	100*FINISHED PICKUP/FINISHED RAW WEIGHT
Inactive mass (%)	100*SUBSTRATE WEIGHT/FINAL WEIGHT
Specific Energy (mAh/g)	1000*FLOOD CAPACITY/FINISHED RAW WEIGHT

the percentage of weight and thickness gained and lost. This shows the greatest thickness occurring at the final formation and the most weight at the last impregnation.

The electrode flooded capacity is determined by cycling in KOH. The electrode is charged at a constant C/2 rate until 150% overcharge is reached. The electrode is then discharged at constant current at the C/2 rate and the time measured relative to an end voltage (typically -1.7VDC verses the nickel counter electrode). The electrical capacity is then expressed in milliampere-hours. The electrode theoretical capacity is calculated from the finished active material weight in grams multiplied by 0.289 Ah/g, which is the theoretical energy density of the nickel-hydroxide electrochemical reaction, based on a one electron reaction (Ni++/Ni+++). State-of-the-art aerospace electrodes manufactured by Eagle-Picher typically yield about 120% of theoretical capacity under these test conditions. This attests to the efficiency of the electrochemical impregnation process. Low utilization has typically been one of the major disadvantages of fiber substrates in the past (along with excessive active material bleeding and the thickness growth). The utilization problem has been essentially solved during the development phase of this program.

Active material weight is typically lost during the formation process due to simple extrusion and expulsion through vigorous gas). Also, any surface loading is easily lost during this step. In some respect, the measure of weight loss during formation is indicative of the efficiency of the impregnation step. A lower weight loss in formation indicates that the active material is more tightly held in the substrate pores and is not easily lost during electrical cycling in KOH. The active material weight loss during formation (expressed as a

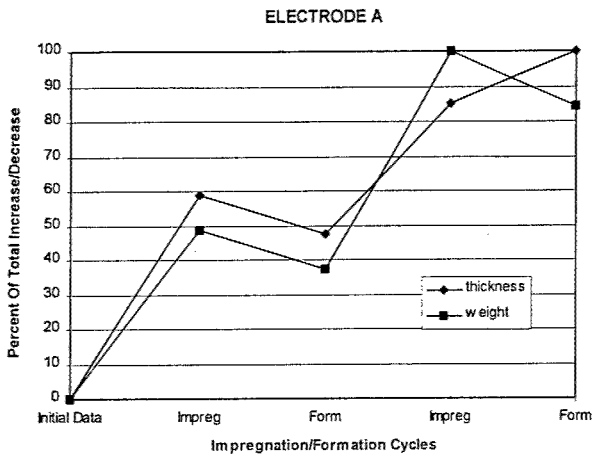

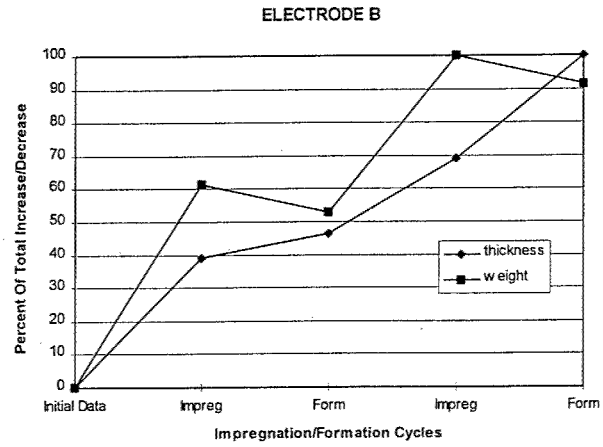

Figures 1 and 2
Electrode A is the electrode with the lowest specific energy. Electrode B has the highest specific energy.

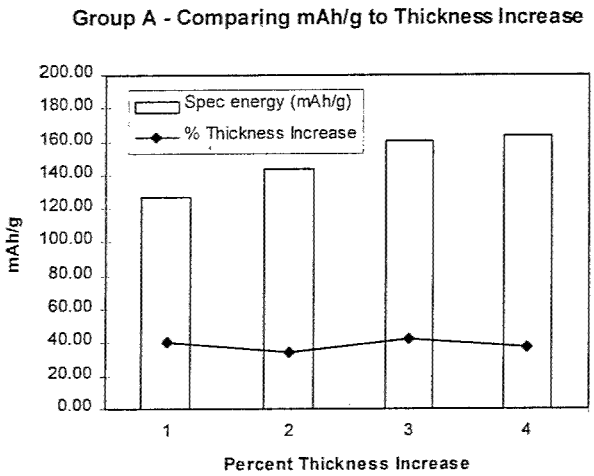

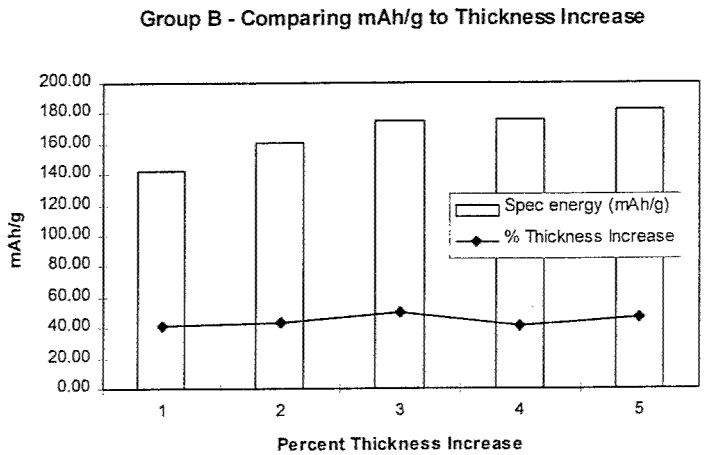

Figures 3 and 4
Comparing the specific energy to the % thickness increase.

percentage of the impregnated pick-up) varies from 5.823% to 12.055%.

The final active material loading (grams of active material per cubic centimeter of electrode void volume) is calculated from the difference in the substrate weight and the final weight after formation. The actual grams of active material loaded into the substrate can be very accurately determined on an analytical balance. Finished loading ranged from 0.851 g/ccvv to 1.377 g/ccvv. Electrode specific energy is the energy storage capacity per weight of the electrode and is figured by watt-hours per gram (converted to mAh/g). Specific energy ranges from 127.029 mAh/g to 183.065 mAh/g. In general, one group has higher specific energy, utilization, and flooded capacity, but also have higher thickness swelling.

In general, the single biggest disadvantage of the nickel electrode can be conveniently expressed in terms of the ratio of active material in the electrode to inactive material in the electrode. In a state-of-the-art sintered nickel powder aerospace electrode, about 63% of the total weight of the nickel electrode is electrochemically inactive. This weight is comprised of the sintered nickel powder substrate and the nickel wire mesh current collector. These components provide no energy storage capacity in the electrode. Correspondingly,

only 37% of the electrode weight is electrochemically active material. This is the reason that although the active material has a theoretical energy density of 289 mAh/g, the nickel electrode is much lower e.g. 120mAh/g, which is about 42% of theoretical. By comparison, fiber nickel electrodes are up to 60% active mass. This corresponds to an electrode specific energy of 180 mAh/g of the theoretical specific energy of pure nickel active material. An increase of specific energy from 120 to 180 mAh/g, 42% to 62% of theoretical, makes a very significant increase in overall specific energy at the full cell and battery level. The fiber based electrode, therefore, has the potential of significantly increasing the specific energy of the nickel hydrogen cell.

Conclusions

Most of the specific work done was primarily directed towards aerospace nickel hydrogen batteries. However, the nickel electrode technology developed is usable in a wide range of applications. Optimized electrode substrate microstructure, micro-fiber diameters and small equivalent pore size have greatly improved the fiber electrode substrate. The electrochemical impregnation process allows more efficient active material loading into the substrate and yields higher active material utilization. Specific energy was increased and overall weight was decreased, both being the major goals of this project. Electrodes yielding up to 180 milliamphere-hours per gram, with high utilization, have been prepared on a laboratory scale. Scale-up to full flight weight nickel hydrogen cells is underway.

There is a considerable amount of literature available on the nickel electrode in general. Several papers have been published on fiber type nickel electrodes specifically *(1-5)*. Eagle-Picher has done substantial work in the past on fiber nickel electrodes *(5-7)* and in conjunction with specific battery Research and Development programs *(8)*.

REFERENCES

1. Kohler, D.A., et.al., *Metal-Carbon Composite Electrodes From Fiber Precursors,* 24th IECEC, 1989, p.1441.

2. D.L. Britton, *Characterization and Cycle Tests of Lightweight Nickel Electrodes, ECS Proceedings* Volume 90-4, 1990.

3. W. Taucher, et.al., *Development of Lightweight Nickel Electrodes for Zinc/Nickel Oxide Batteries,* 186th ECS Meeting, 1994.

4. R. Rouget, et.al., *Connection of the Charge Efficiency and Self-Discharge of the Fibrous Electrode With the Structure of the Support,* ESC Proceedings Volume 90-4, 1990.

5. M.J. Vanderpool, et.al., *Development of the Fiber-Based Nickel Hydroxide Electrodes for Nickel-Iron Batteries, ECS Proceedings* Volume 90-4, 1990.

6. D.K. Coates, et.al., *Advances in Lightweight Nickel ElectrodeTechnology,* Space Electrochemical Research and Technology, NASA Lewis, 1988.

7. J.M. Francisco, et.al., *High Energy Density Microfiber Based Nickel Electrode for Aerospace Batteries,* 11th Annual Battery Conference, 1996.

8. D. Coates, et.al., *Advanced Dependent Pressure Vessel (DPV) Nickel Hydrogen Spacecraft Battery Design,* 19th International Power Sources Symposium, 1995.

Studies of the Codeposition of Cobalt Hydroxide and Nickel Hydroxide

C. H. Ho, M. Murthy, and J. W. Van Zee

Center for Electrochemical Engineering
Department of Chemical Engineering
University of South Carolina
Columbia, SC 29208

J. W. Van Zee, University of South Carolina
Presented at the NASA Battery Workshop
Dec. 4, 1996

Center of Electrochemical Engineering
Department of Chemical Engineering
University of South Carolina
Columbia, SC 29208

Outline

- Chemistry
- Experimental Measurements
- Planar Film Model Development
- Impregnation Model Development
- Results & Conclusions
  - Effect of $Ni_4(OH)_4^{4+}$
  - Effect of Cobalt Concentration on Deposition / Loading
  - Effect of Current Density on Loading Distribution
- Acknowledgment

J. W. Van Zee, University of South Carolina
Presented at the NASA Battery Workshop
Dec. 4, 1996

Center of Electrochemical Engineering
Department of Chemical Engineering
University of South Carolina
Columbia, SC 29208

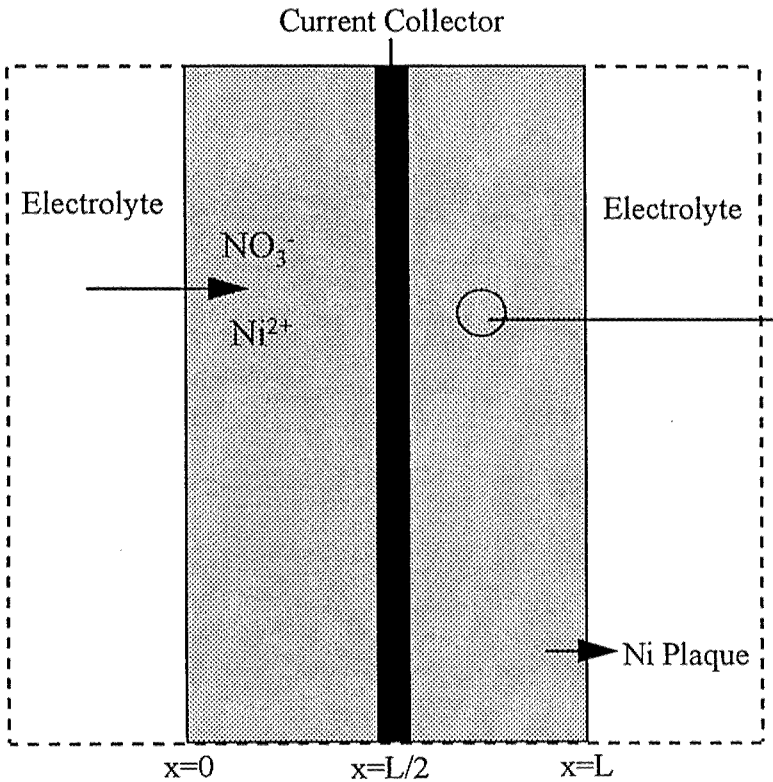

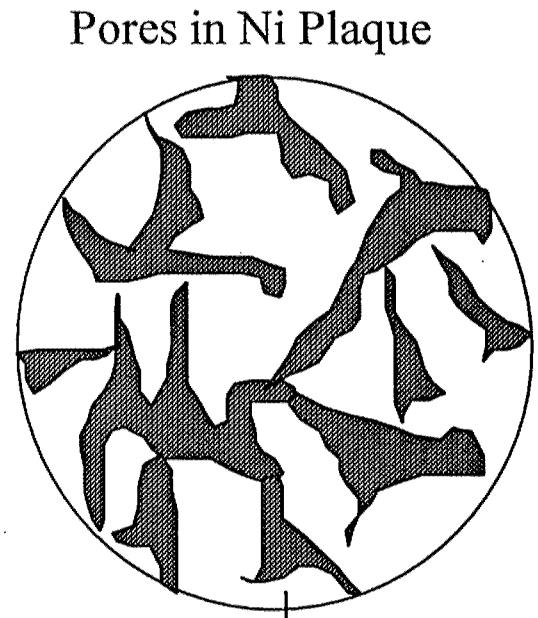

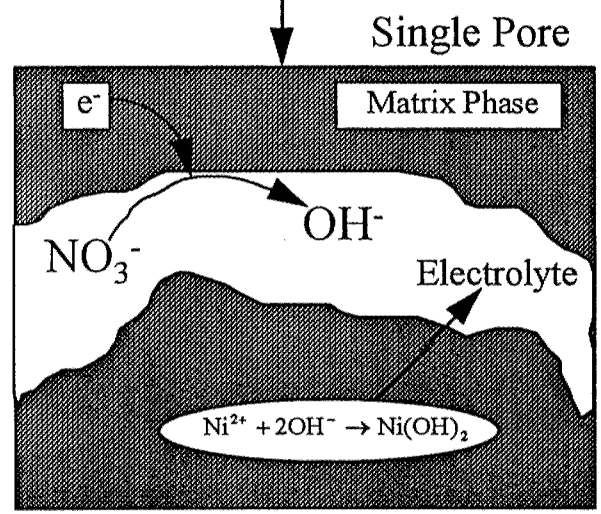

Electrode Reaction

$$\frac{1}{8}NO_3^- + \frac{3}{4}H_2O + e^- \rightarrow \frac{1}{8}NH_3 + \frac{9}{8}OH^-$$

Precipitation Reactions

$$Ni^{2+} + 2OH^- \rightarrow Ni(OH)_2$$

$$Co^{2+} + 2OH^- \rightarrow Co(OH)_2$$

Nickel Chemistry

- Dilute Solutions ($Ni^{2+} < 0.1$ M, pH < 7)

$$Ni^{2+} + H_2O \Leftrightarrow NiOH^+ + H^+$$

- Concentrated solutions ($Ni^{2+} > 0.1$ M, 5 < pH < 7)

$$4Ni^{2+} + 4H_2O \Leftrightarrow Ni_4OH_4^{4+} + 4H^+$$

References: Baes & Mesmer (1976), Kawai et al. (1973), Burkov et al. (1965), Kolski et al. (1969)

J. W. Van Zee, University of South Carolina
Presented at the NASA Battery Workshop
Dec. 4, 1996

Center of Electrochemical Engineering
Department of Chemical Engineering
University of South Carolina
Columbia, SC 29208

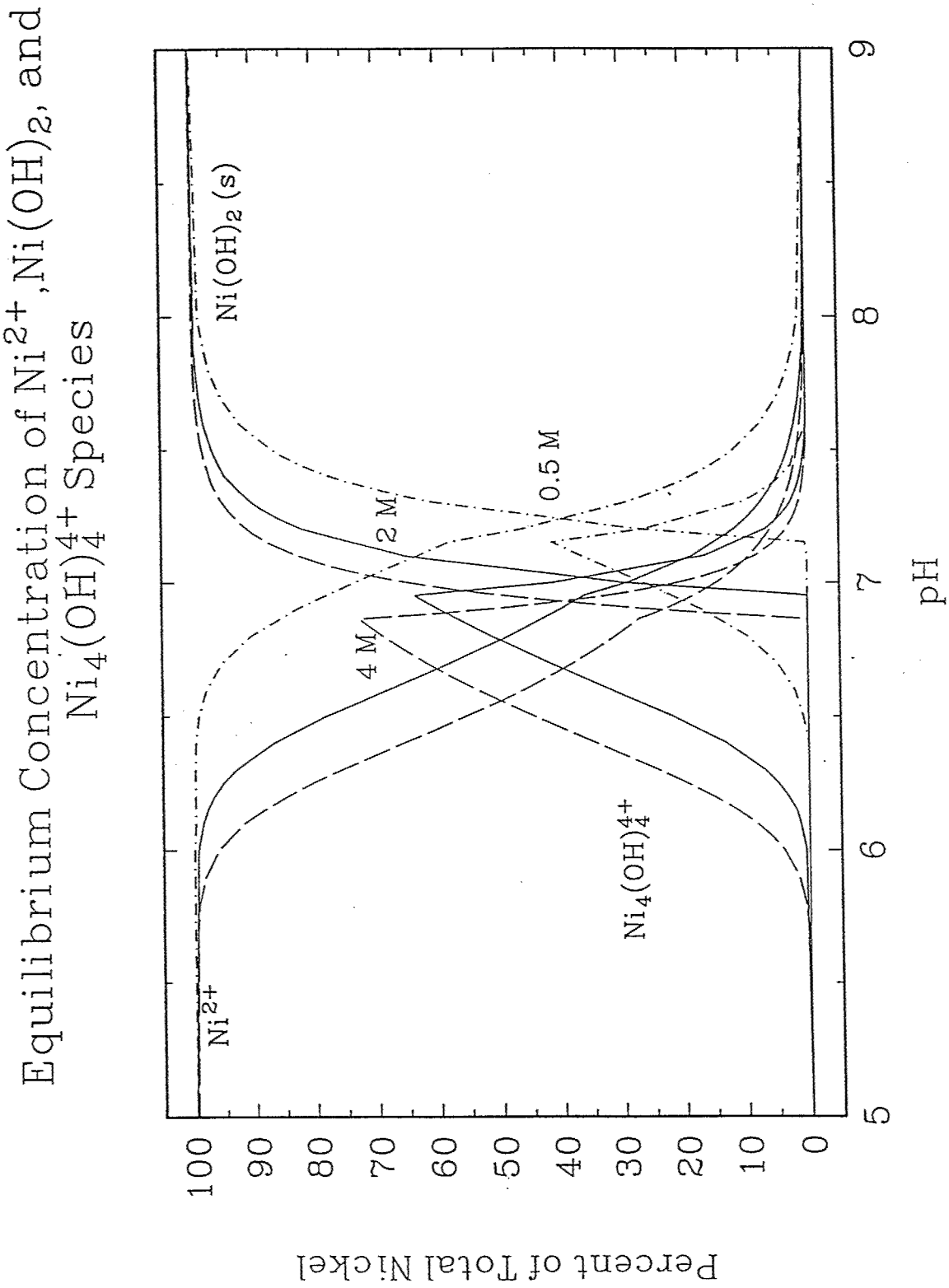
Equilibrium Concentration of Ni^{2+}, $Ni(OH)_2$, and $Ni_4(OH)_4^{4+}$ Species
Percent of Total Nickel
pH
100
90
80
70
60
50
40
30
20
10
0
5
6
7
8
9
Ni^{2+}
$Ni_4(OH)_4^{4+}$
4 M
2 M
0.5 M
$Ni(OH)_2$ (s)

Cobalt Chemistry

- Dilute solutions ($Co^{2+} < 0.1$ M, pH < 7)

$$Co^{2+} + H_2O \Leftrightarrow CoOH^+ + H^+$$

- Concentrated solutions ($Co^{2+} > 0.1$ M, 5 < pH < 7)

$$4Co^{2+} + 4H_2O \Leftrightarrow Co_4(OH)_4^{4+} + 4H^+$$

- Cobalt $K_{eq} \approx 0.1\ K_{eq}$ of nickel species
  Reference : Baes & Mesmer (1976)

- Ionic strength important

J. W. Van Zee, University of South Carolina
Presented at the NASA Battery Workshop
Dec. 4, 1996

Center of Electrochemical Engineering
Department of Chemical Engineering
University of South Carolina
Columbia, SC 29208

Equilibrium Chemical Reactions

- Two Step Deposition Mechanism *(Streinz et al. 1995)*

$$Ni^{2+} + OH^- \Leftrightarrow \frac{1}{4} Ni_4(OH)_4^{4+}$$

$$\frac{1}{4} Ni_4(OH)_4^{4+} + OH^- \Leftrightarrow Ni(OH)_2 \downarrow$$

- Cobalt Deposition Mechanism (*Baes and Mesmer 1976*)

$$Co^{2+} + OH^- \Leftrightarrow \frac{1}{4} Co_4(OH)_4^{4+}$$

$$\frac{1}{4} Co_4(OH)_4^{4+} + OH^- \Leftrightarrow Co(OH)_2 \downarrow$$

J. W. Van Zee, University of South Carolina
Presented at the NASA Battery Workshop
Dec. 4, 1996

Center of Electrochemical Engineering
Department of Chemical Engineering
University of South Carolina
Columbia, SC 29208

Equilibrium Chemical Reactions(Contd.)

- Reactions for Nickel Nitrate Complexes (*Fedorov et al. 1976*)

$$Ni^{2+} + NO_3^- \Leftrightarrow Ni(NO_3)^+$$

$$Ni^{2+} + 2NO_3^- \Leftrightarrow Ni(NO_3)_2 \text{ (aq)}$$

- Reactions for Cobalt Nitrate Complexes (*Fedorov et al. 1976*)

$$Co^{2+} + NO_3^- \Leftrightarrow Co(NO_3)^+$$

$$Co^{2+} + 2NO_3^- \Leftrightarrow Co(NO_3)_2 \text{ (aq)}$$

J. W. Van Zee, University of South Carolina
Presented at the NASA Battery Workshop
Dec. 4, 1996

Center of Electrochemical Engineering
Department of Chemical Engineering
University of South Carolina
Columbia, SC 29208

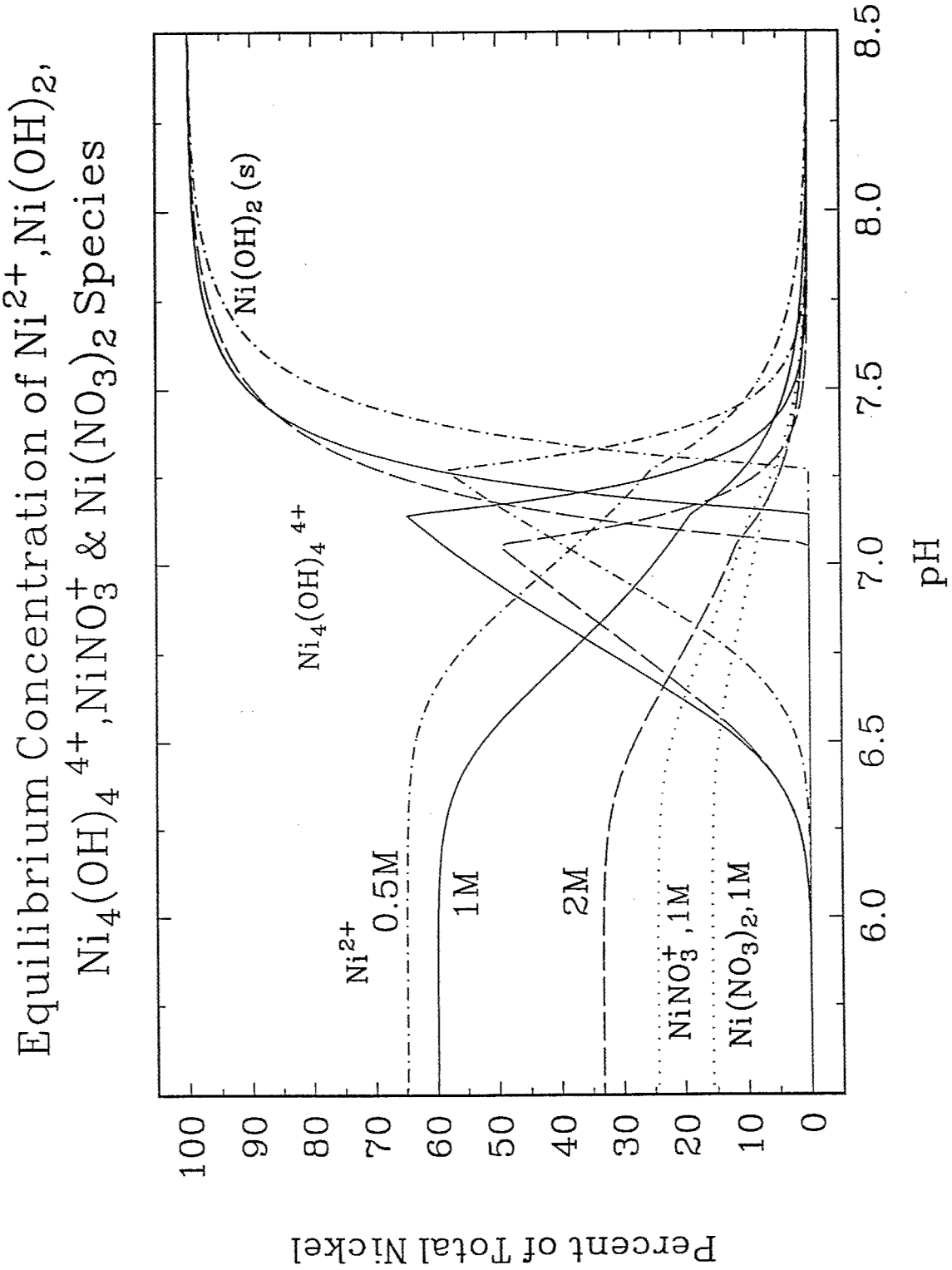
Equilibrium Concentration of Ni^{2+}, $Ni(OH)_2$, $Ni_4(OH)_4^{4+}$, $NiNO_3^+$ & $Ni(NO_3)_2$ Species
Percent of Total Nickel
pH
100
90
80
70
60
50
40
30
20
10
0
6.0
6.5
7.0
7.5
8.0
8.5
$Ni(OH)_2$ (s)
$Ni_4(OH)_4^{4+}$
Ni^{2+} 0.5M
1M
2M
$NiNO_3^+$, 1M
$Ni(NO_3)_2$, 1M

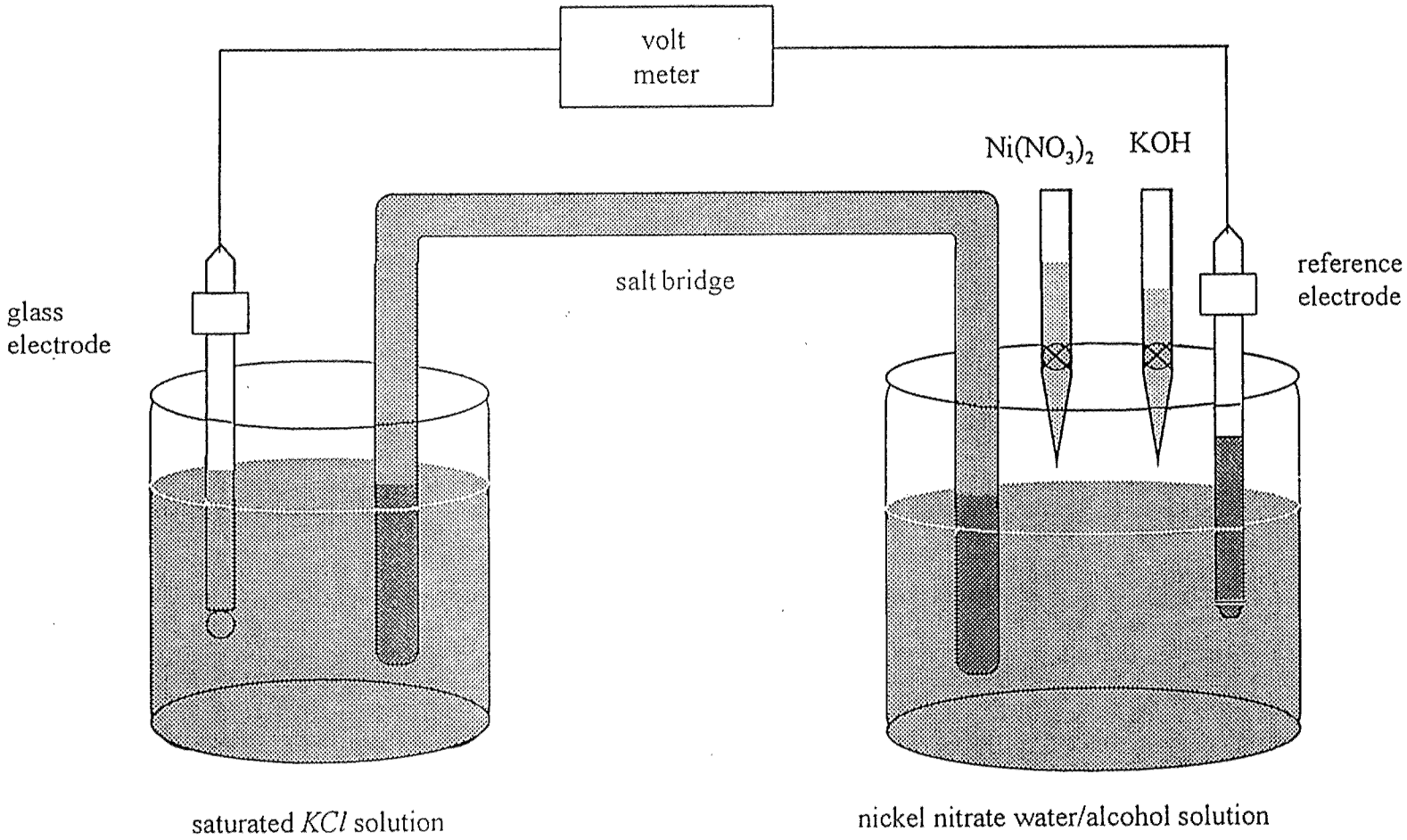

Schematic Diagram for Nonaqueous pH Measurement

J. W. Van Zee, University of South Carolina
Presented at the NASA Battery Workshop
Dec. 4, 1996

Center of Electrochemical Engineering
Department of Chemical Engineering
University of South Carolina
Columbia, SC 29208

Experimental Measurement

- Hydrolytic reaction

$$qNi^{2+} + pH_2O = Ni_q(OH)_p^{(2q-p)+} + pH^+$$

$$Q_{p,q} = \frac{\left[Ni_q(OH)_p^{(2q-p)+}\right]\left[H^+\right]^p}{b^q}$$

- Material Balance

$$B^\circ = B^N + B + b$$

$$[(B+b)]\,Z = h - H + K_W h^{-1}$$

$$= (Q_{1,1}bh^{-1} + 4Q_{4,4}b^4h^{-4} + Q_{1,2}b^2h^{-1})$$

J. W. Van Zee, University of South Carolina
Presented at the NASA Battery Workshop
Dec. 4, 1996

Center of Electrochemical Engineering
Department of Chemical Engineering
University of South Carolina
Columbia, SC 29208

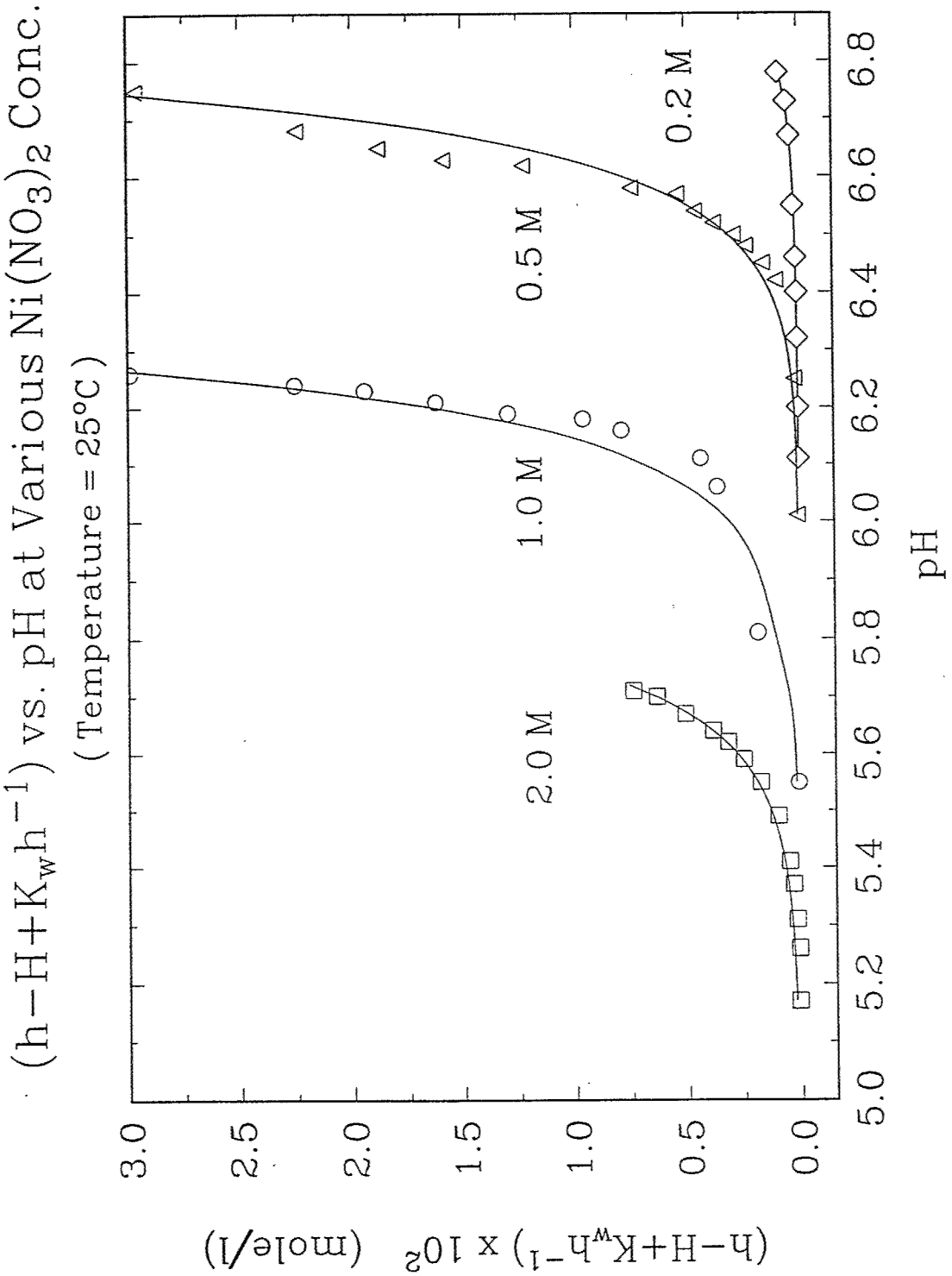
(h−H+K_w h^−1) vs. pH at Various Ni(NO3)2 Conc.
(Temperature = 25°C)
0.2 M
0.5 M
1.0 M
2.0 M
pH
(h−H+K_w h^−1) x 10^2 (mole/l)
5.0
5.2
5.4
5.6
5.8
6.0
6.2
6.4
6.6
6.8
0.0
0.5
1.0
1.5
2.0
2.5
3.0

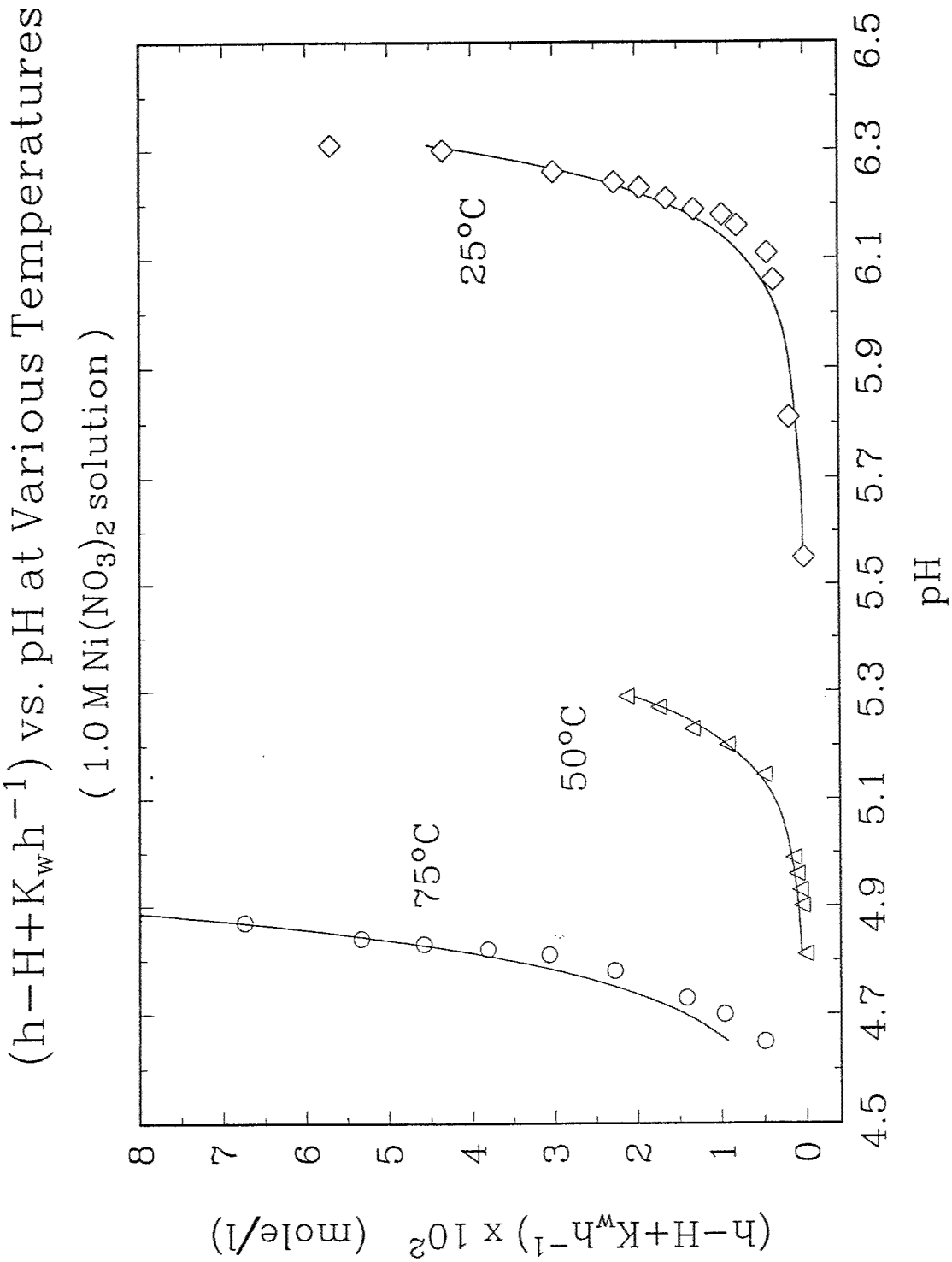
(h−H+K_w h^−1) vs. pH at Various Temperatures
(1.0 M Ni(NO3)2 solution)
25°C
50°C
75°C
(h−H+K_w h^−1) x 10^2 (mole/l)
pH
0
1
2
3
4
5
6
7
8
4.5
4.7
4.9
5.1
5.3
5.5
5.7
5.9
6.1
6.3
6.5

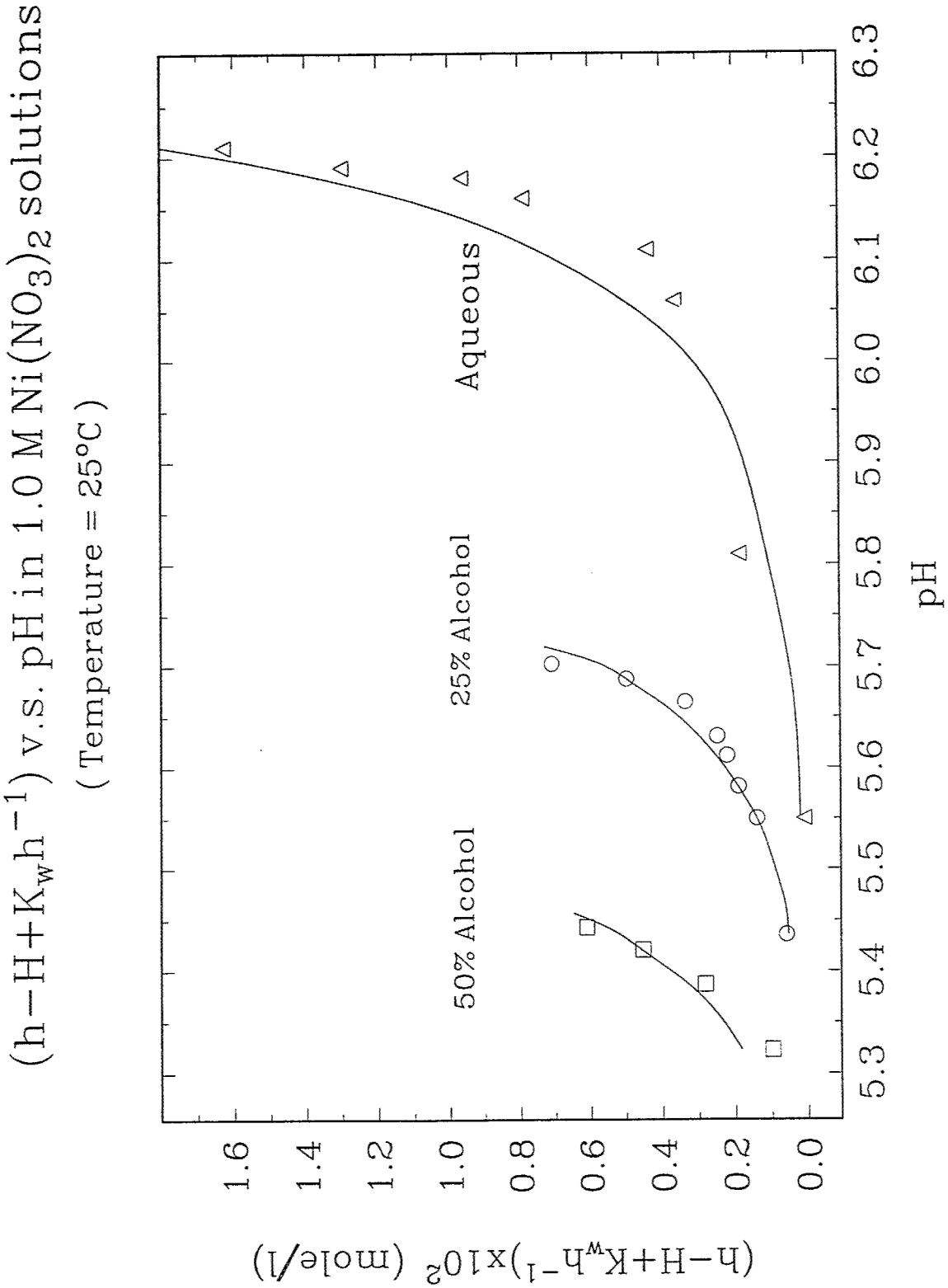
(h−H+KWh−1) v.s. pH in 1.0 M Ni(NO3)2 solutions
(Temperature = 25°C)
Aqueous
25% Alcohol
50% Alcohol
(h−H+KWh−1)x10² (mole/l)
1.6
1.4
1.2
1.0
0.8
0.6
0.4
0.2
0.0
5.3
5.4
5.5
5.6
5.7
5.8
5.9
6.0
6.1
6.2
6.3
pH

Effect of Ionic Strength

- Equilibrium reaction

$$4Ni^{2+} + 4H_2O = Ni_4(OH)_4^{4+} + 4H^+$$

$$Q_{eq} = \frac{\left[Ni_4(OH)_4^{4+}\right]\left[H^+\right]^4}{\left[Ni^{2+}\right]^4}$$

- Effect of ionic strength

$$\log\ Q_{eq} = \log\ K_{eq} + \frac{a\,I^{1/2}}{1 + I^{1/12}} + bm_X$$

J. W. Van Zee, University of South Carolina
Presented at the NASA Battery Workshop
Dec. 4, 1996

Center of Electrochemical Engineering
Department of Chemical Engineering
University of South Carolina
Columbia, SC 29208

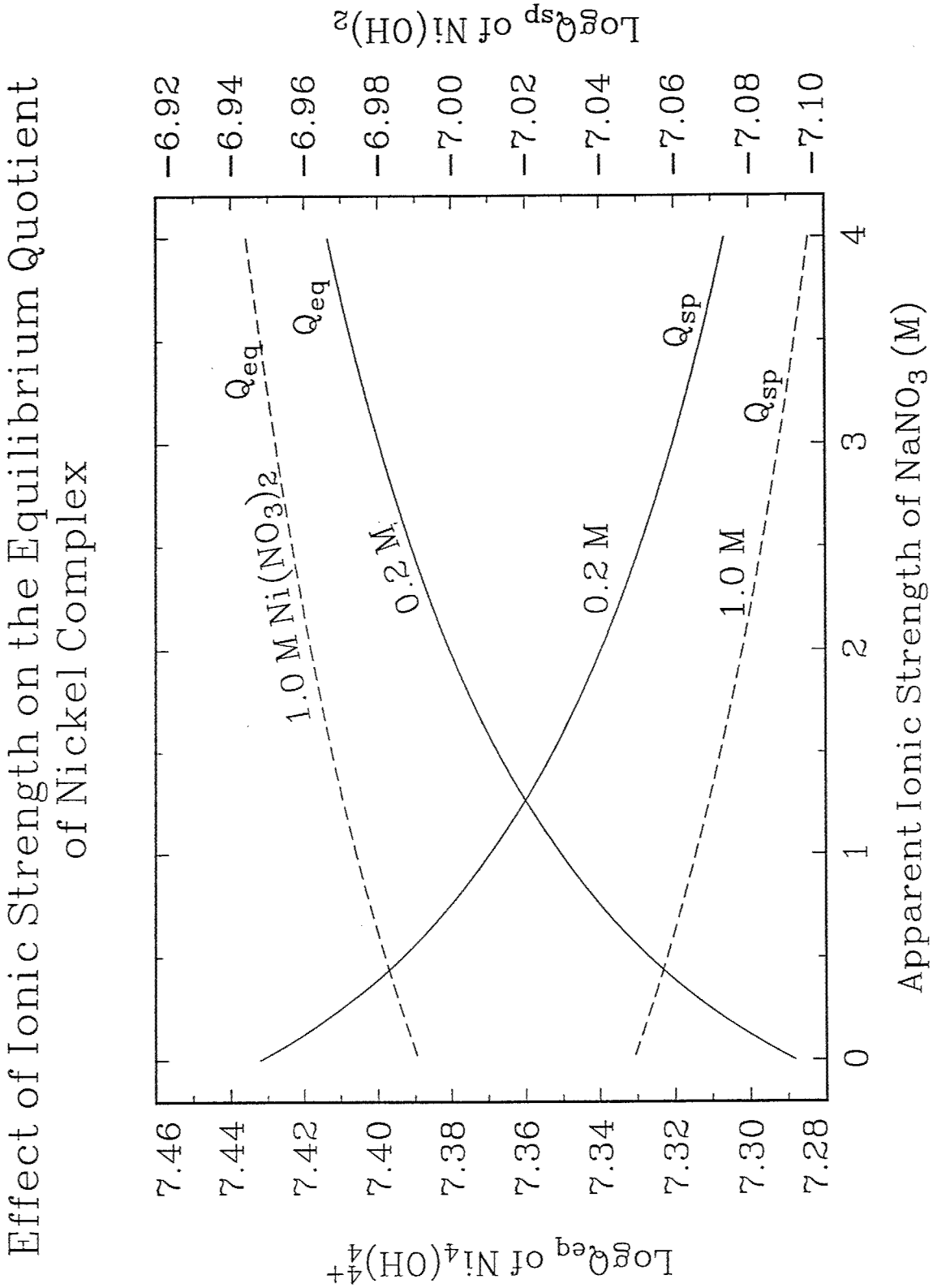
Effect of Ionic Strength on the Equilibrium Quotient of Nickel Complex
LogQ_{eq} of $Ni_4(OH)_4^{4+}$
LogQ_{sp} of $Ni(OH)_2$
Apparent Ionic Strength of $NaNO_3$ (M)
7.46
7.44
7.42
7.40
7.38
7.36
7.34
7.32
7.30
7.28
−6.92
−6.94
−6.96
−6.98
−7.00
−7.02
−7.04
−7.06
−7.08
−7.10
0
1
2
3
4
Q_{eq}
Q_{eq}
Q_{sp}
Q_{sp}
1.0 M $Ni(NO_3)_2$
0.2 M
0.2 M
1.0 M

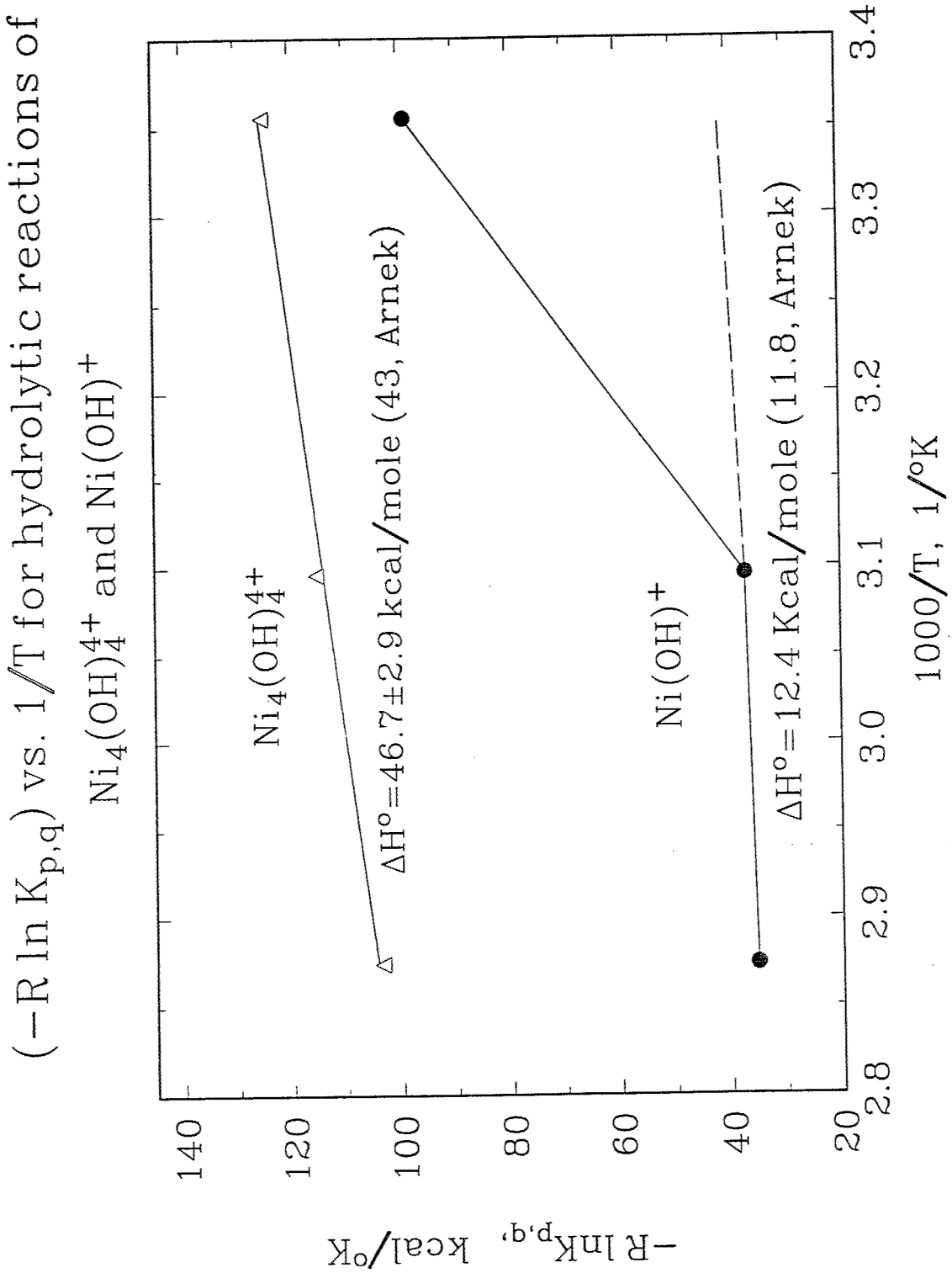
(−R ln $K_{p,q}$) vs. 1/T for hydrolytic reactions of
$Ni_4(OH)_4^{4+}$ and $Ni(OH)^+$
$Ni_4(OH)_4^{4+}$
ΔH^o=46.7±2.9 kcal/mole (43, Arnek)
$Ni(OH)^+$
ΔH^o=12.4 Kcal/mole (11.8, Arnek)
−R ln$K_{p,q}$, kcal/°K
140
120
100
80
60
40
20
2.8
2.9
3.0
3.1
3.2
3.3
3.4
1000/T, 1/°K

Schematic of an Electrochemical Quartz Crystal Microbalance

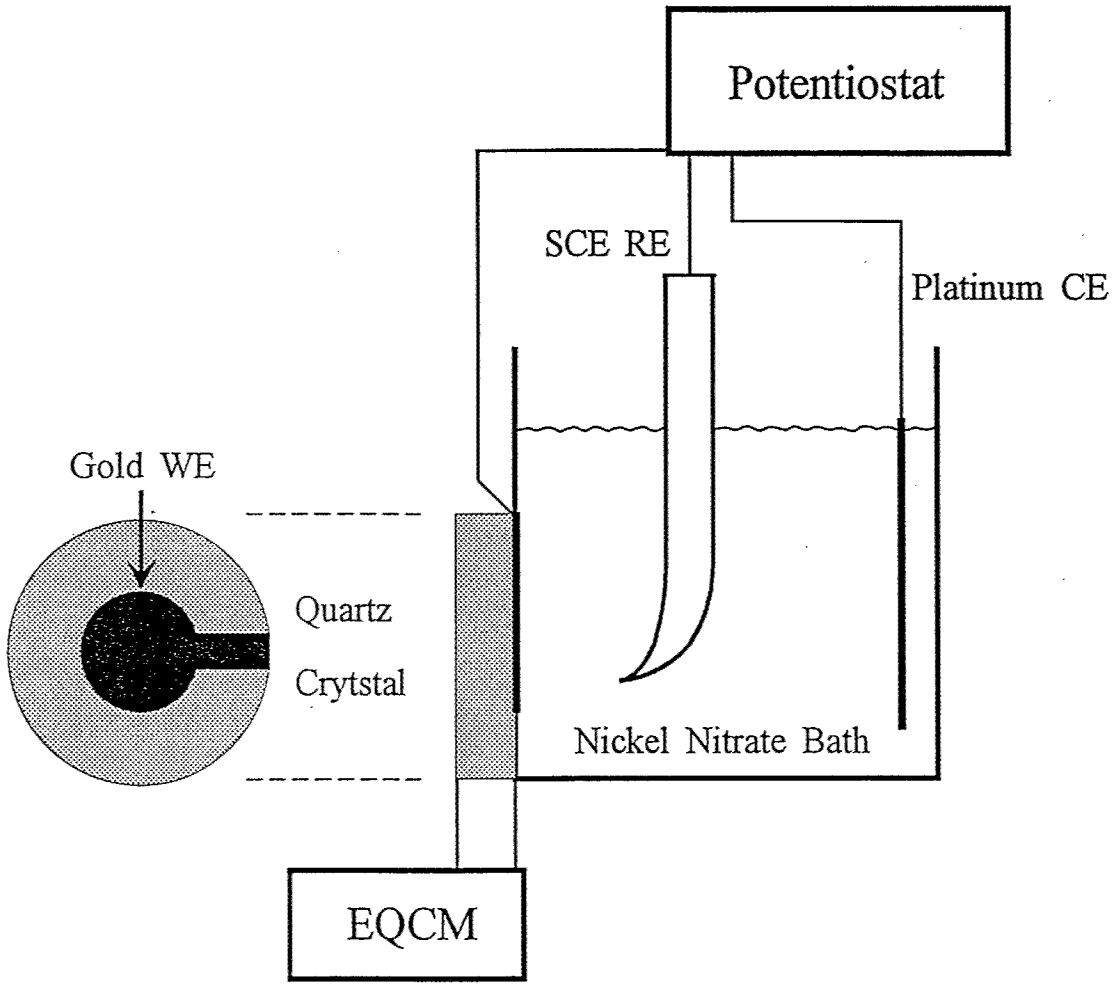

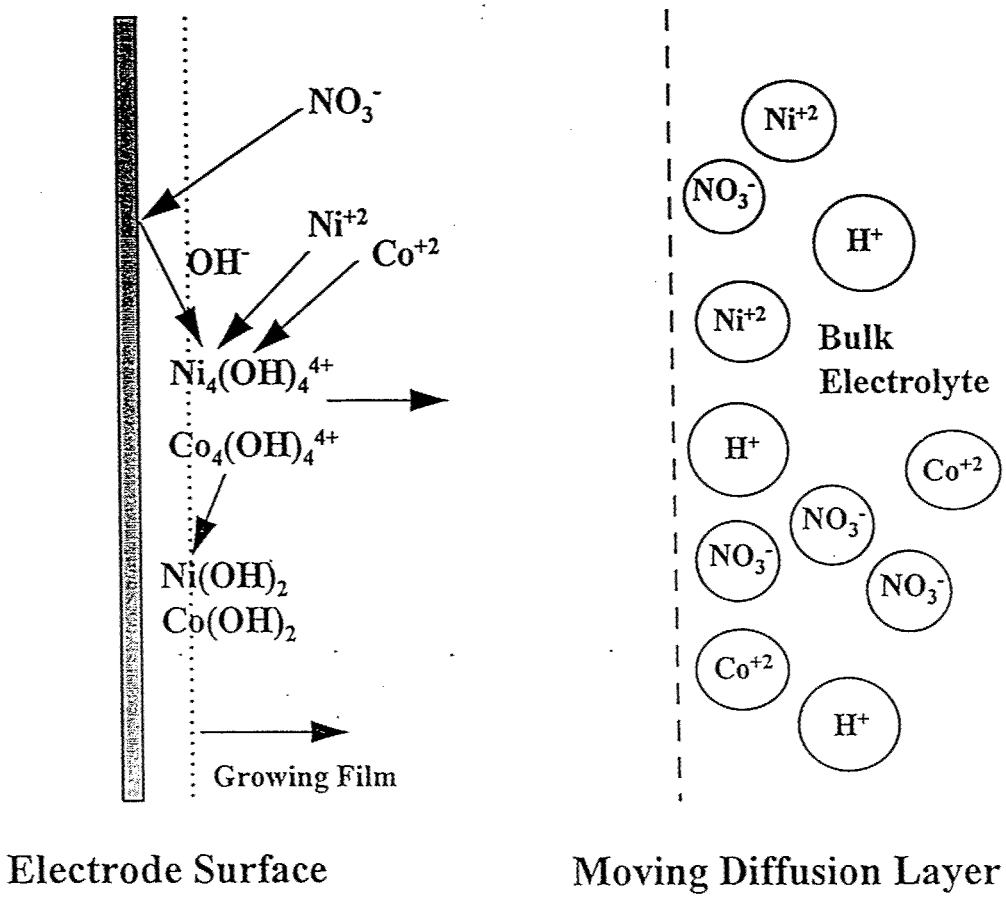

Schematic of the Deposition Process on Planar Electrodes

Governing Equations for Planar Film Model

- Mass balances for species: Ni^{2+}, Co^{2+}, NO_3^-, OH^-

$$\frac{\partial C_i}{\partial t} = -\nabla \cdot Ni + R_i$$

- Equilibrium reactions for remaining species, H^+, $NiNO_3^+$, $Ni(NO_3)_2$, $CoNO_3^+$, $Co(NO_3)_2$, $Ni_4(OH)_4^{4+}$, and $Co_4(OH)_4^{4+}$
- Electroneutrality for solution potential, ϕ
- Eleven concentrations and ϕ

J. W. Van Zee, University of South Carolina
Presented at the NASA Battery Workshop
Dec. 4, 1996

Center of Electrochemical Engineering
Department of Chemical Engineering
University of South Carolina
Columbia, SC 29208

Boundary Conditions for Planar Film Model

- Diffusion layer-electrolyte interface

$$C_i = C_{i,b}$$

$$\phi = 0$$

- Electrode surface
  - flux balances
  - equilibrium reactions
  - electroneutrality

J. W. Van Zee, University of South Carolina
Presented at the NASA Battery Workshop
Dec. 4, 1996

Center of Electrochemical Engineering
Department of Chemical Engineering
University of South Carolina
Columbia, SC 29208

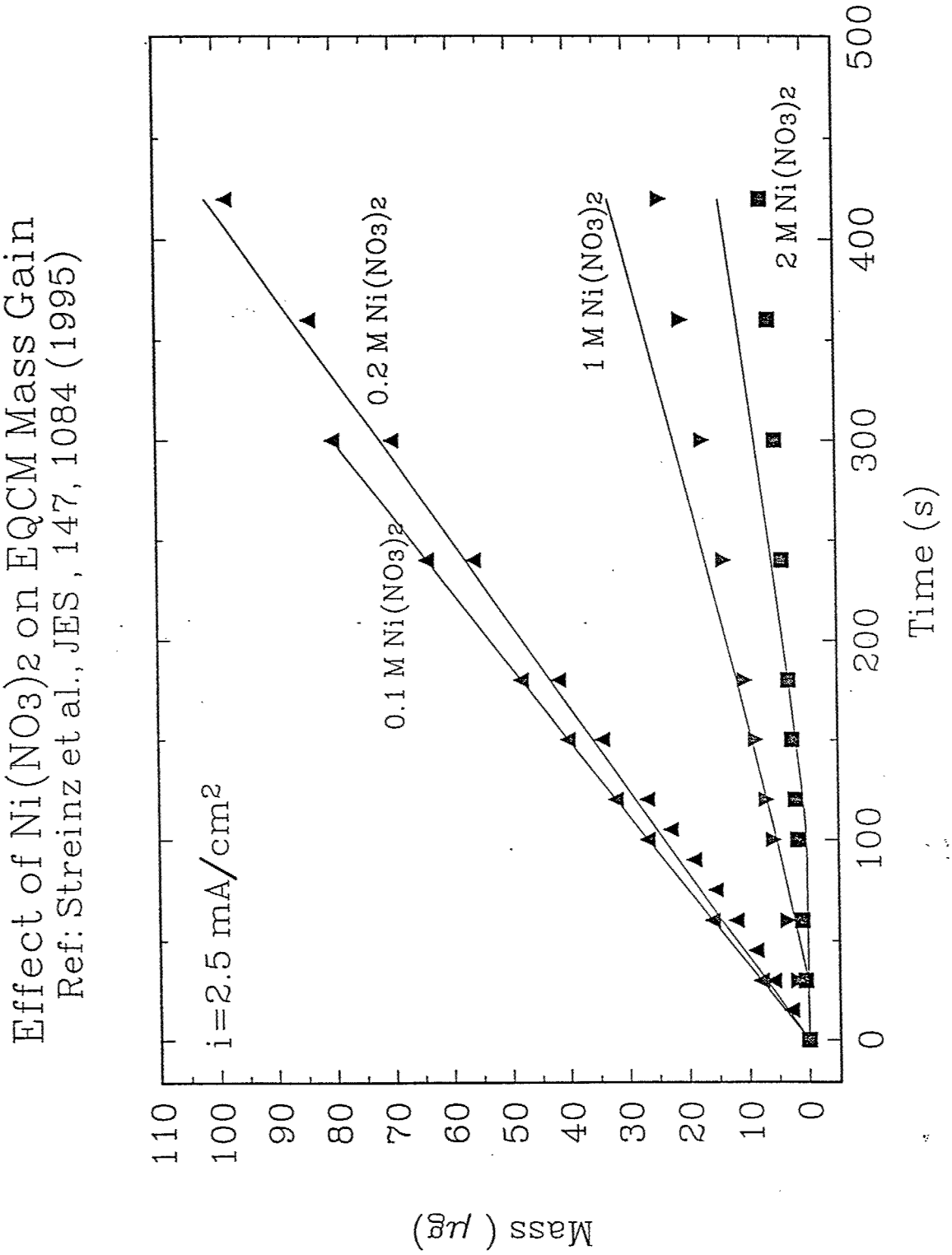
Effect of Ni(NO3)2 on EQCM Mass Gain
Ref: Streinz et al., JES, 147, 1084 (1995)
i=2.5 mA/cm2
0.1 M Ni(NO3)2
0.2 M Ni(NO3)2
1 M Ni(NO3)2
2 M Ni(NO3)2
Mass (μg)
Time (s)
0
10
20
30
40
50
60
70
80
90
100
110
0
100
200
300
400
500

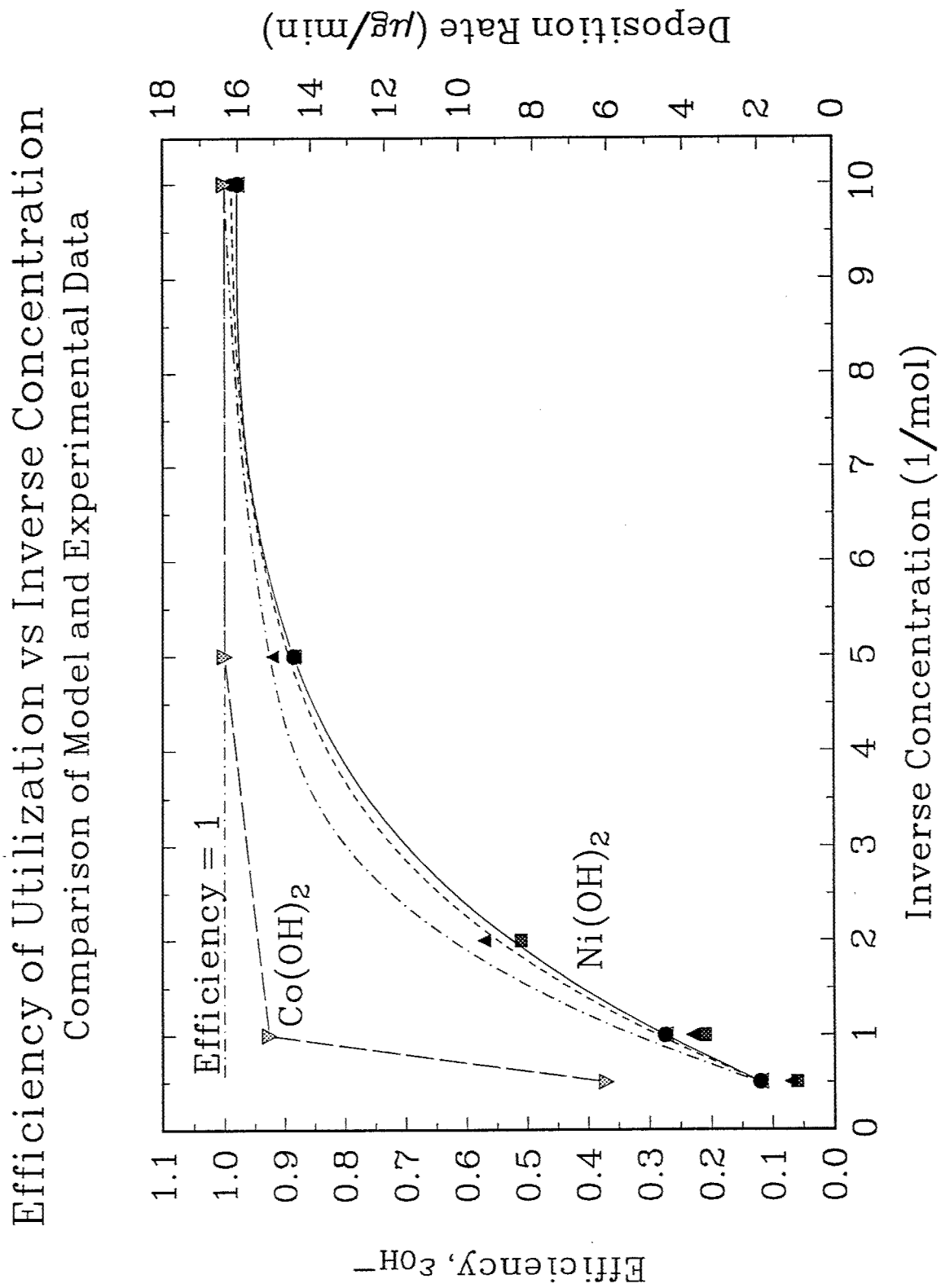
Efficiency of Utilization vs Inverse Concentration
Comparison of Model and Experimental Data
Efficiency = 1
$Co(OH)_2$
$Ni(OH)_2$
Efficiency, ε_{OH^-}
Deposition Rate (μg/min)
Inverse Concentration (1/mol)
1.1
1.0
0.9
0.8
0.7
0.6
0.5
0.4
0.3
0.2
0.1
0.0
18
16
14
12
10
8
6
4
2
0
0
1
2
3
4
5
6
7
8
9
10

Determination of K_{eq} and K_{sp} from Film Experiments

- Determine least square error between experimentally measured mass and model predictions.

$$E = \sum_{i=1}^{q} (m_{I_1}^{exp} - m_{I_1}^{pred.})^2 + \sum_{i=1}^{q} (m_{I_2}^{exp} - m_{I_2}^{pred.})^2$$

where $m = f(K_{eq}, K_{sp})$ and K_{eq}, K_{sp} correspond to zero ionic strength

$$E = E_1 + E_2$$

m: mass gain of $Ni(OH)_2$

I_1, I_2: Ionic strength of medium

q: number of experimental data

J. W. Van Zee, University of South Carolina
Presented at the NASA Battery Workshop
Dec. 4, 1996

Center of Electrochemical Engineering
Department of Chemical Engineering
University of South Carolina
Columbia, SC 29208

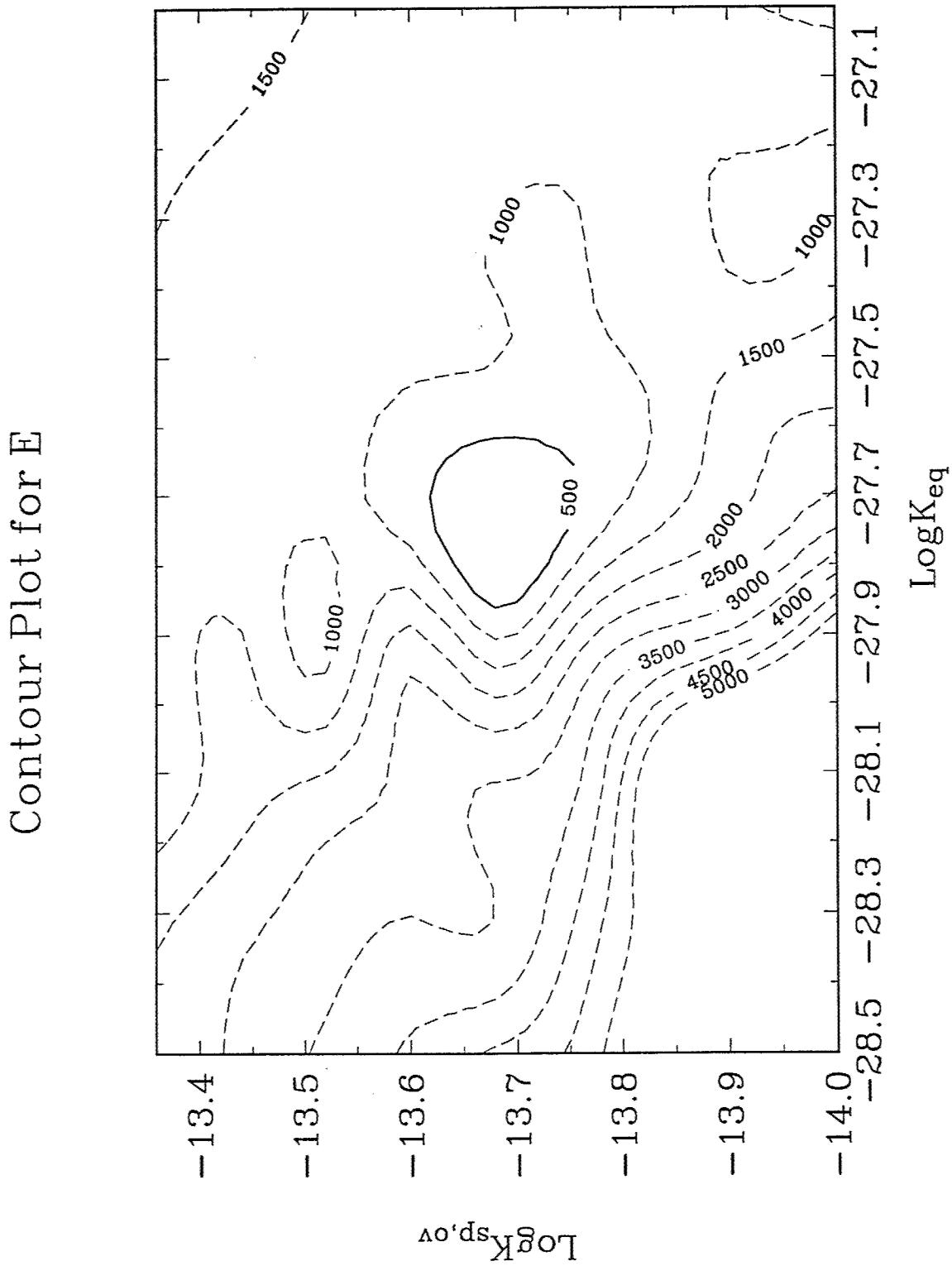
Contour Plot for E
1500
1000
1000
1000
1500
500
2000
2500
3000
3500
4000
4500
5000
−13.4
−13.5
−13.6
−13.7
−13.8
−13.9
−14.0
LogKsp,ov
−28.5
−28.3
−28.1
−27.9
−27.7
−27.5
−27.3
−27.1
LogKeq

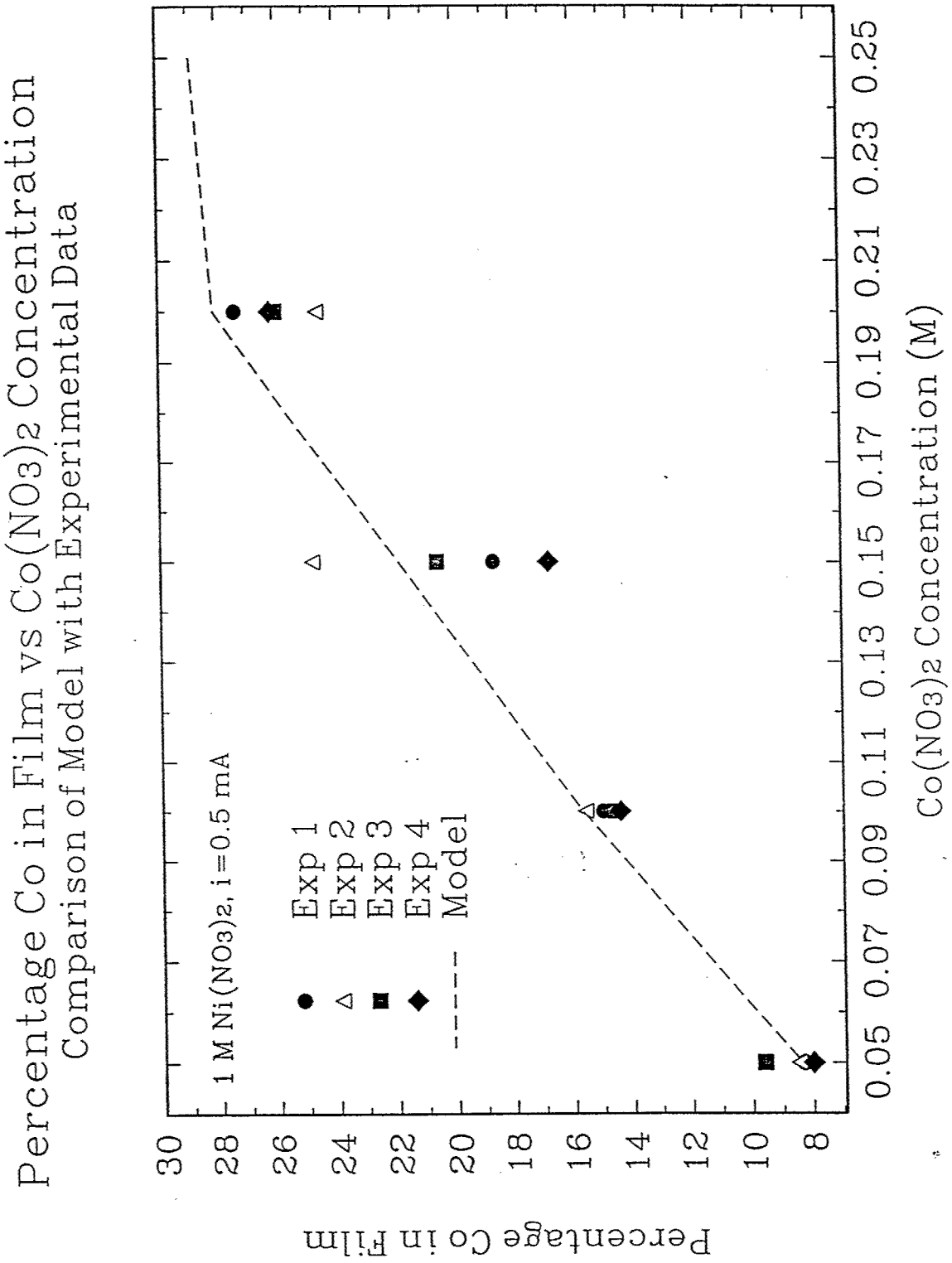
Percentage Co in Film vs Co(NO3)2 Concentration
Comparison of Model with Experimental Data
1 M Ni(NO3)2, i=0.5 mA
Exp 1
Exp 2
Exp 3
Exp 4
Model
Percentage Co in Film
30
28
26
24
22
20
18
16
14
12
10
8
0.05
0.07
0.09
0.11
0.13
0.15
0.17
0.19
0.21
0.23
0.25
Co(NO3)2 Concentration (M)

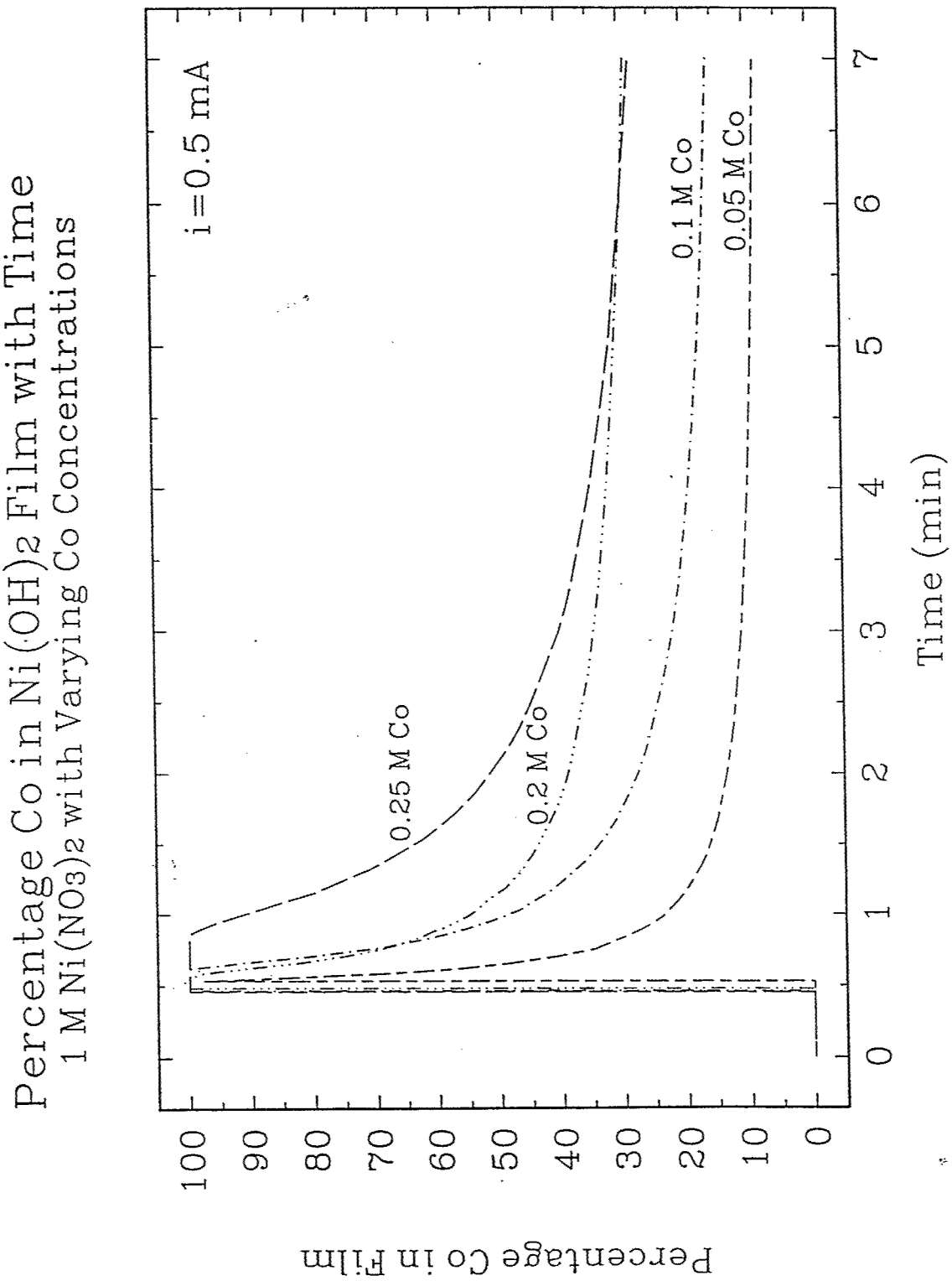
Percentage Co in Ni(OH)2 Film with Time
1 M Ni(NO3)2 with Varying Co Concentrations
i=0.5 mA
0.25 M Co
0.2 M Co
0.1 M Co
0.05 M Co
Percentage Co in Film
Time (min)
0
10
20
30
40
50
60
70
80
90
100
0
1
2
3
4
5
6
7

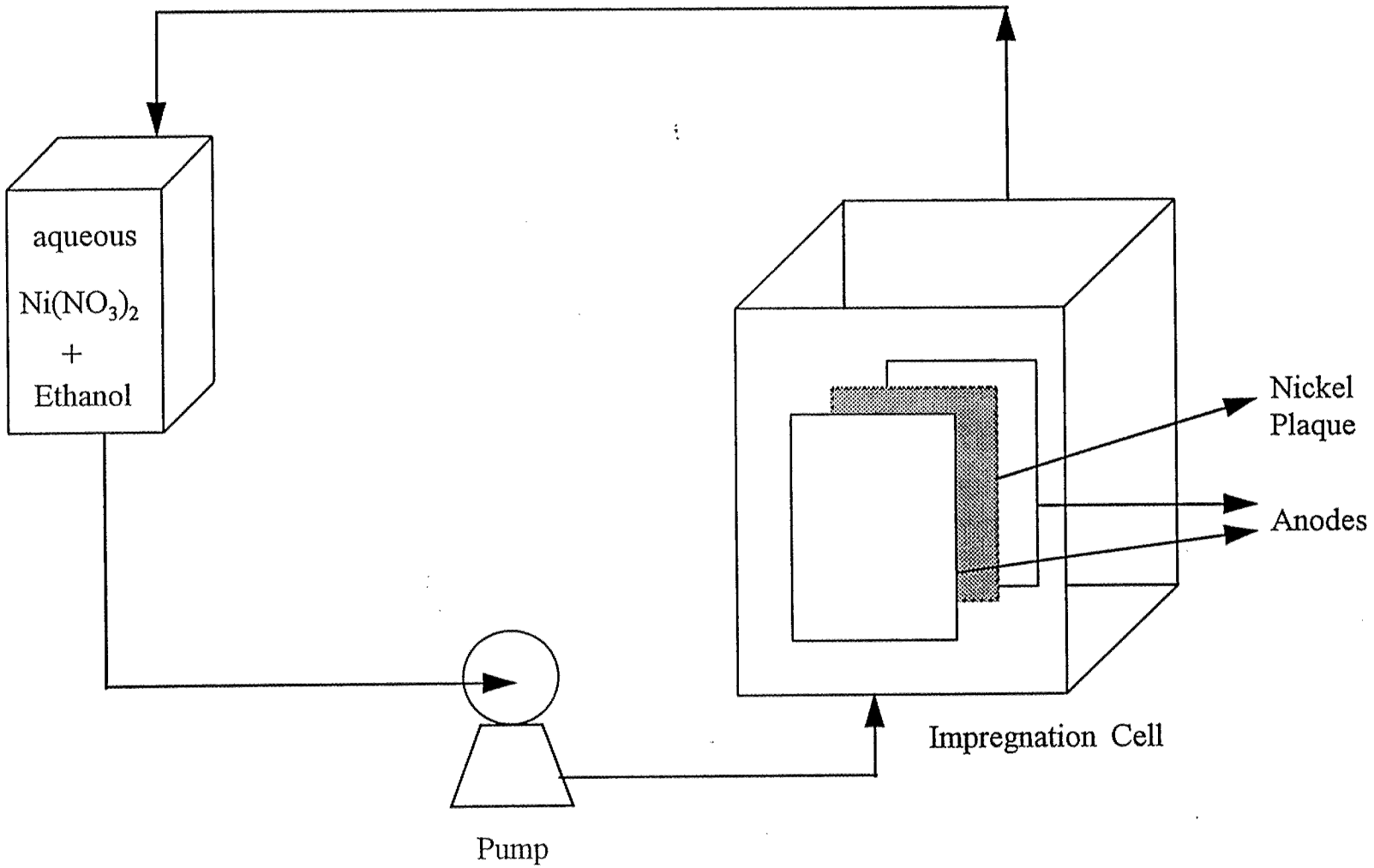

Electrochemical Impregnation System

J. W. Van Zee, University of South Carolina
Presented at the NASA Battery Workshop
Dec. 4, 1996

Center of Electrochemical Engineering
Department of Chemical Engineering
University of South Carolina
Columbia, SC 29208

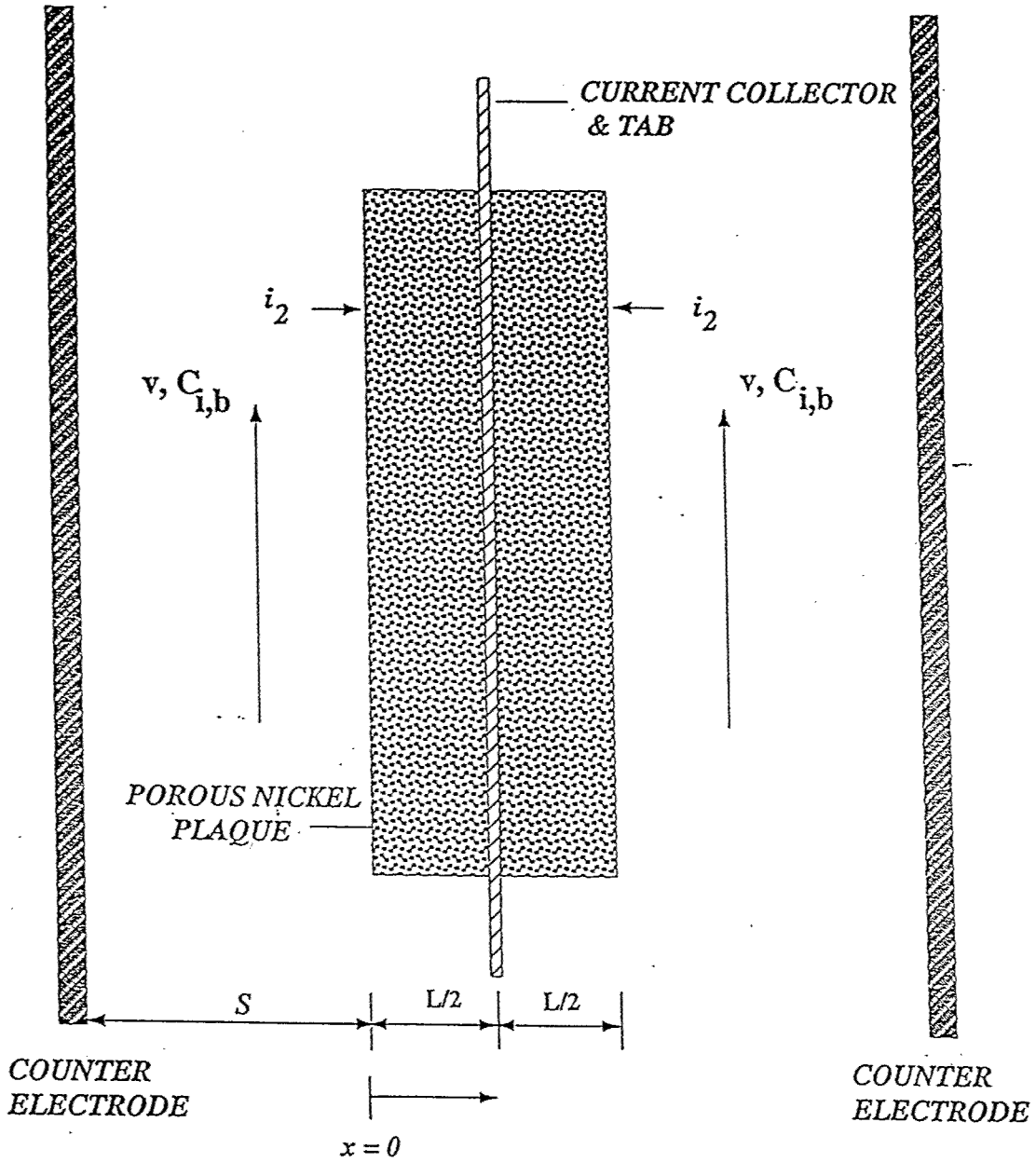
CURRENT COLLECTOR
& TAB
i_2
i_2
v, $C_{i,b}$
v, $C_{i,b}$
POROUS NICKEL
PLAQUE
S
L/2
L/2
COUNTER
ELECTRODE
COUNTER
ELECTRODE
x = 0

Governing Equations for Impregnation Model

- Mass balances for species: Ni^{2+}, Co^{2+}, NO_3^-, OH^-

$$\frac{\partial \varepsilon C_i}{\partial t} = -\frac{s_i}{nF}\frac{\partial i_2}{\partial x} - \frac{\partial N_i}{\partial x} + R_i$$

  - Flux: Diffusion and migration only

- Equilibrium equations for: H^+, $Ni_4(OH)_4^{4+}$, $Co_4(OH)_4^{4+}$, $Ni(NO_3)^+$, $Ni(NO_3)_2$, $Co(NO_3)^+$, $Co(NO_3)_2$
- ϕ_2 is governed by electroneutrality

J. W. Van Zee, University of South Carolina
Presented at the NASA Battery Workshop
Dec. 4, 1996

Center of Electrochemical Engineering
Department of Chemical Engineering
University of South Carolina
Columbia, SC 29208

Governing Equations (Cont.)

- The rates of precipitation are related to Q_{sp} of the hydroxides. (r_{ppt1}, r_{ppt2})

- Solution current: $$\frac{\partial i_2}{\partial x} = a\ j_n$$

- Porosity:

$$\frac{\partial \varepsilon}{\partial t} = -\ r_{ppt1}\left(\frac{M}{\rho}\right)_{Ni(OH)_2} - \ r_{ppt2}\left(\frac{M}{\rho}\right)_{Co(OH)_2}$$

J. W. Van Zee, University of South Carolina
Presented at the NASA Battery Workshop
Dec. 4, 1996

Center of Electrochemical Engineering
Department of Chemical Engineering
University of South Carolina
Columbia, SC 29208

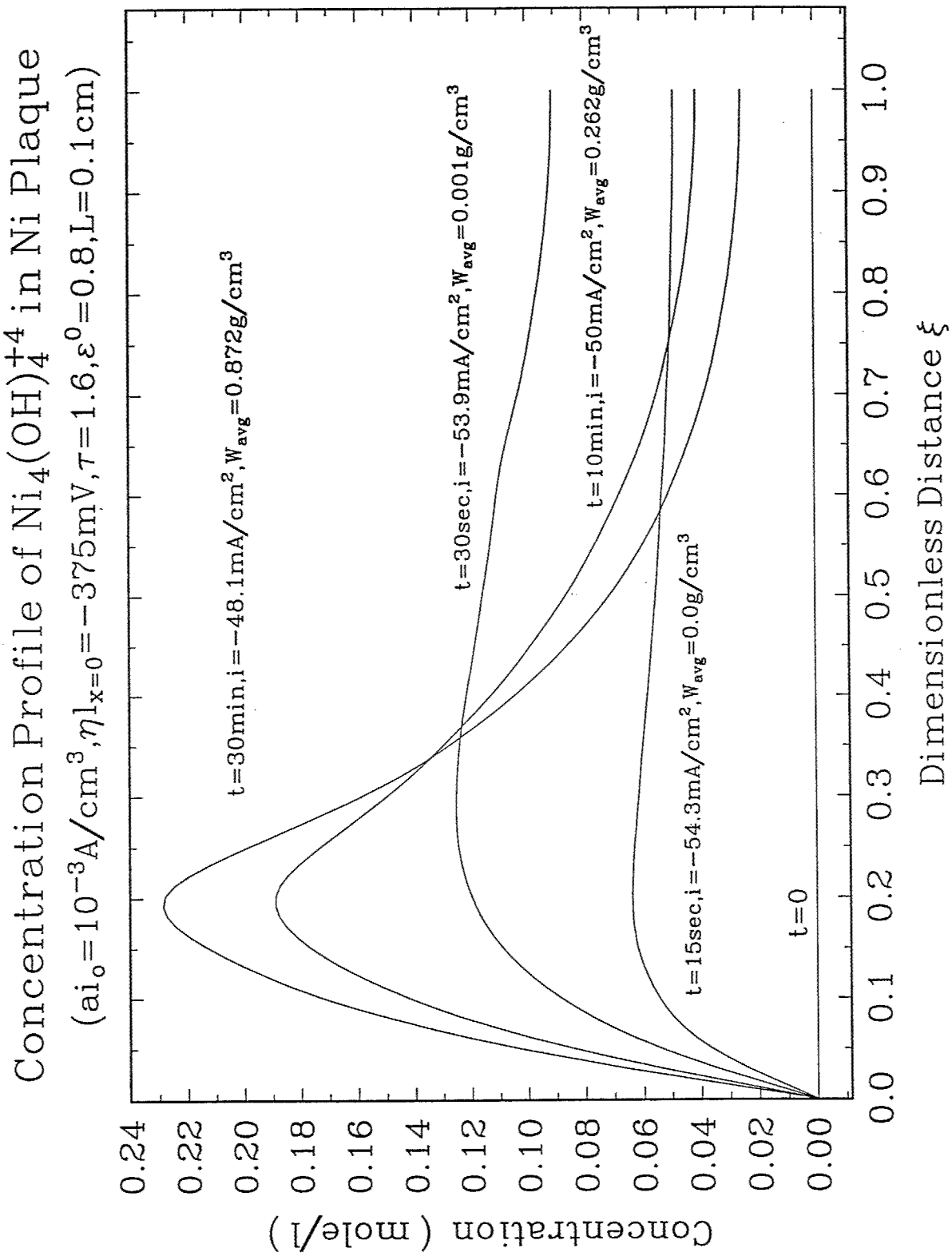
Concentration Profile of $Ni_4(OH)_4^{+4}$ in Ni Plaque
$(ai_o=10^{-3}A/cm^3, \eta|_{x=0}=-375mV, \tau=1.6, \varepsilon^0=0.8, L=0.1cm)$
t=30min,i=−48.1mA/cm²,W_avg=0.872g/cm³
t=30sec,i=−53.9mA/cm²,W_avg=0.001g/cm³
t=10min,i=−50mA/cm²,W_avg=0.262g/cm³
t=15sec,i=−54.3mA/cm²,W_avg=0.0g/cm³
t=0
Concentration (mole/l)
0.00
0.02
0.04
0.06
0.08
0.10
0.12
0.14
0.16
0.18
0.20
0.22
0.24
Dimensionless Distance ξ
0.0
0.1
0.2
0.3
0.4
0.5
0.6
0.7
0.8
0.9
1.0

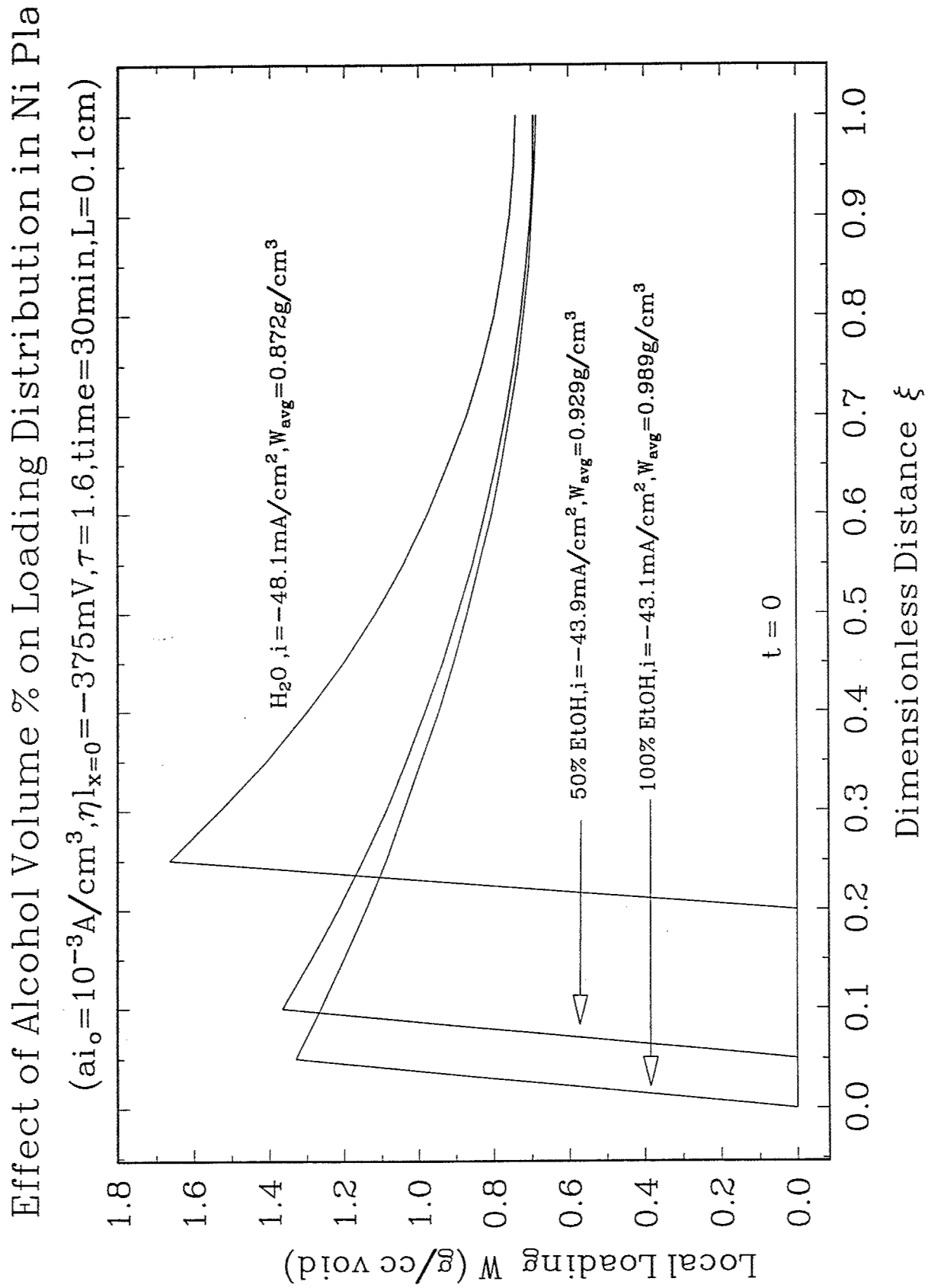
Effect of Alcohol Volume % on Loading Distribution in Ni Pla
(ai$_o$=10^{-3}A/cm^3,η|$_{x=0}$=−375mV,τ=1.6,time=30min,L=0.1cm)
H$_2$O ,i=−48.1mA/cm^2,W$_{avg}$=0.872g/cm^3
50% EtOH,i=−43.9mA/cm^2,W$_{avg}$=0.929g/cm^3
100% EtOH,i=−43.1mA/cm^2,W$_{avg}$=0.989g/cm^3
t = 0
Local Loading W (g/cc void)
Dimensionless Distance ξ
0.0
0.2
0.4
0.6
0.8
1.0
1.2
1.4
1.6
1.8
0.1
0.3
0.5
0.7
0.9

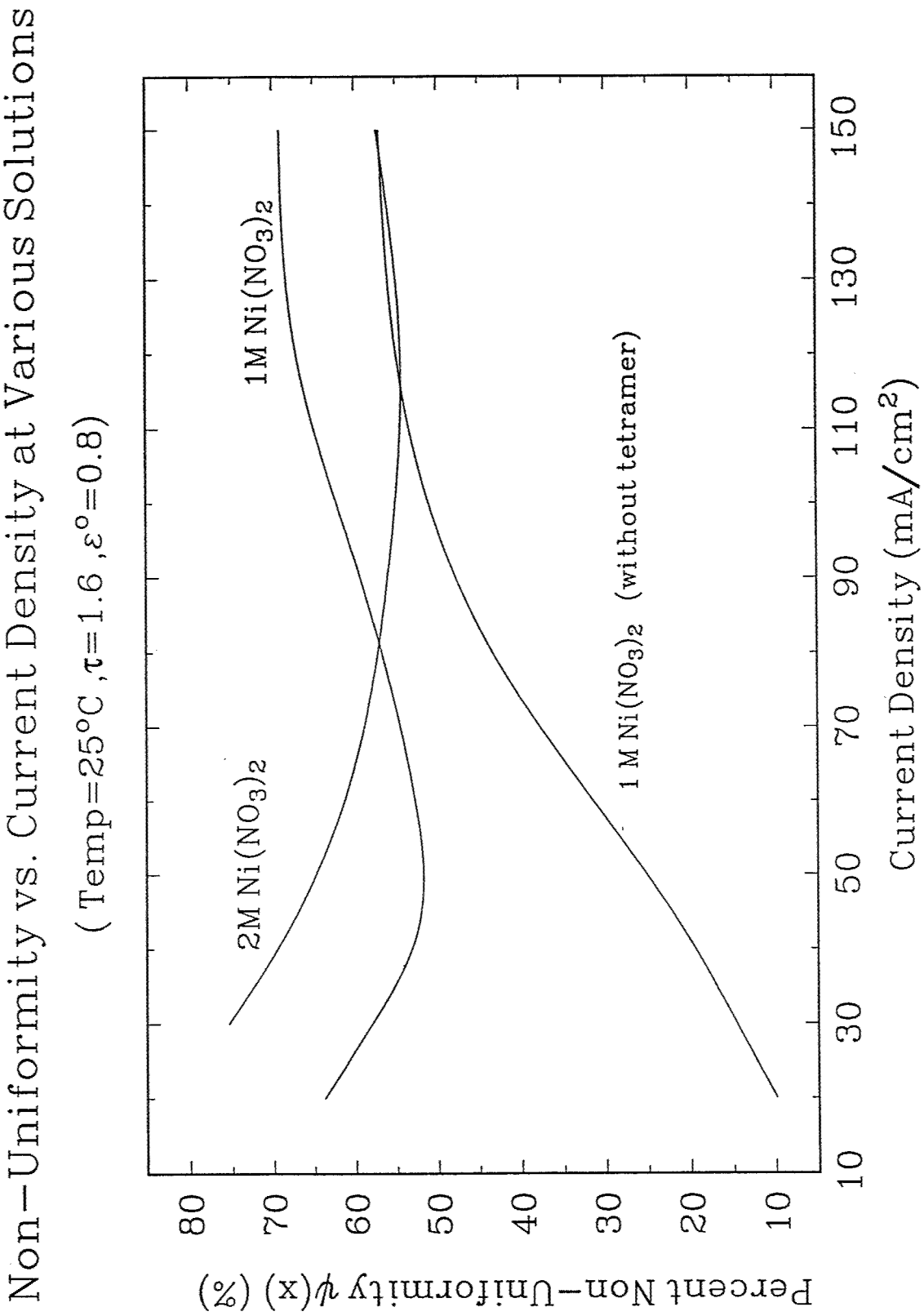
Non-Uniformity vs. Current Density at Various Solutions
(Temp=25°C ,τ=1.6 ,ε°=0.8)
2M Ni(NO3)2
1M Ni(NO3)2
1 M Ni(NO3)2 (without tetramer)
Percent Non-Uniformity ψ(x) (%)
80
70
60
50
40
30
20
10
10
30
50
70
90
110
130
150
Current Density (mA/cm2)

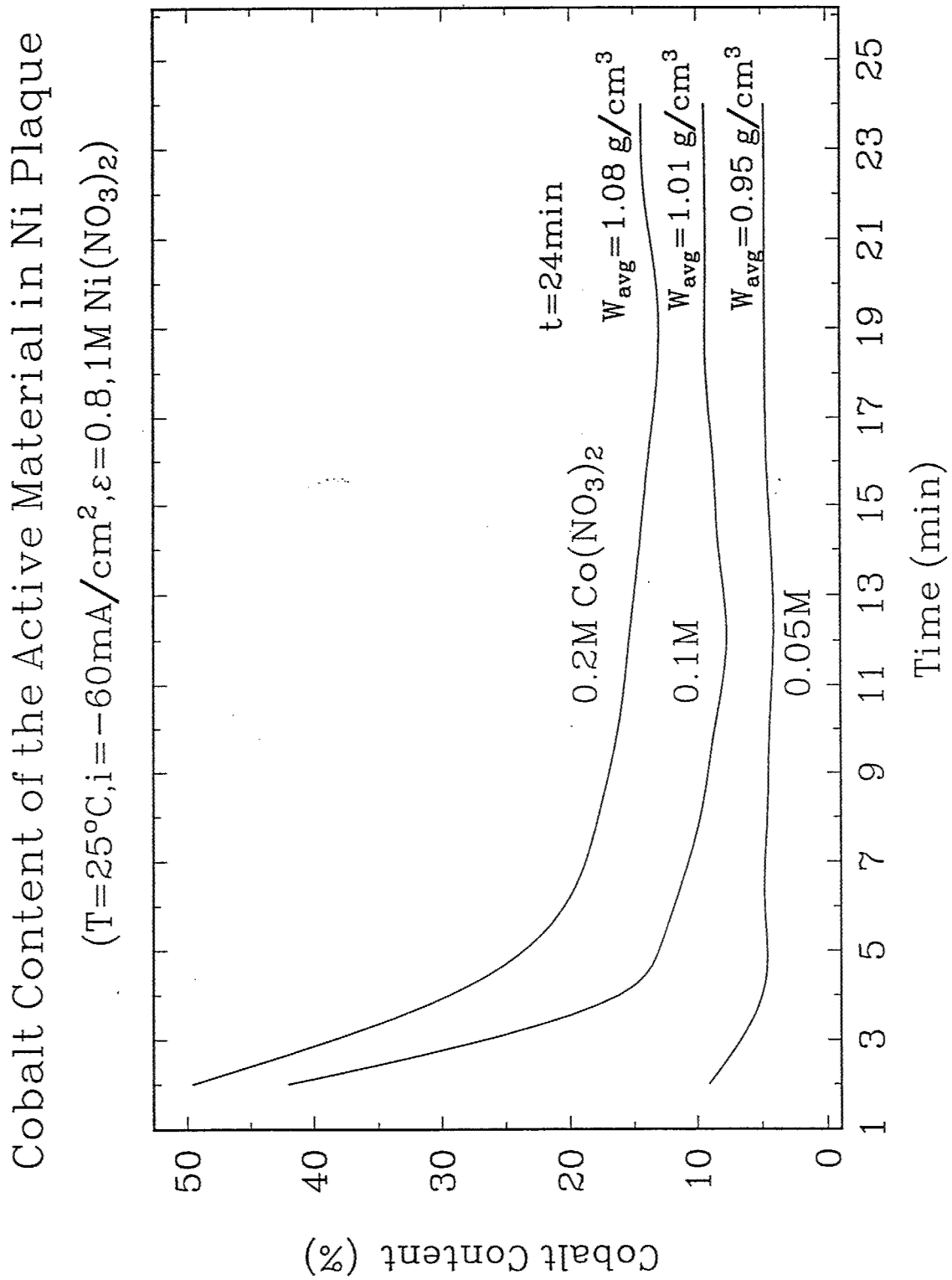
Cobalt Content of the Active Material in Ni Plaque
(T=25°C, i=−60mA/cm², ε=0.8, 1M Ni(NO3)2)
t=24min
W_avg=1.08 g/cm³
W_avg=1.01 g/cm³
W_avg=0.95 g/cm³
0.2M Co(NO3)2
0.1M
0.05M
Cobalt Content (%)
Time (min)
0
10
20
30
40
50
1
3
5
7
9
11
13
15
17
19
21
23
25

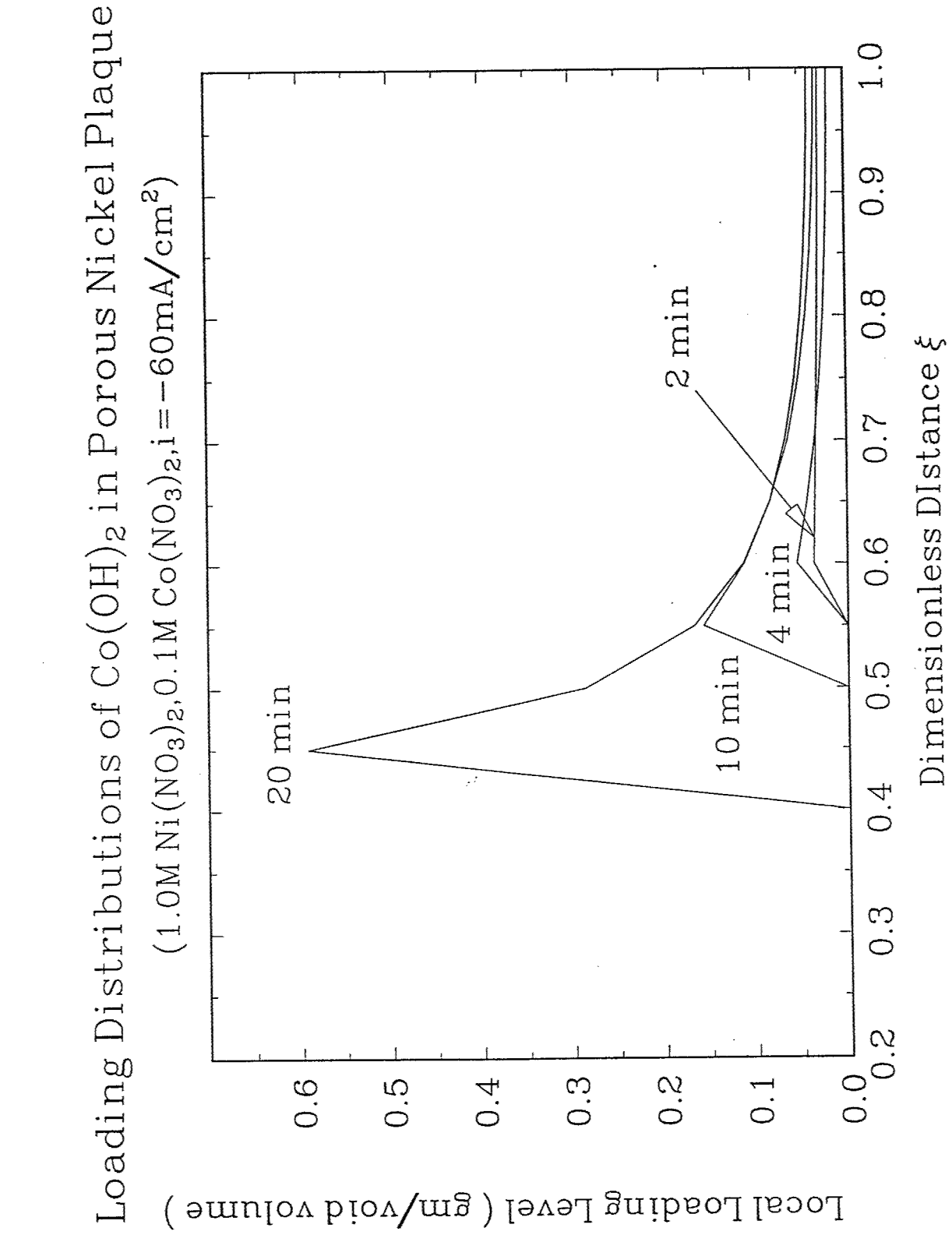
Loading Distributions of $Co(OH)_2$ in Porous Nickel Plaque
($1.0M\ Ni(NO_3)_2, 0.1M\ Co(NO_3)_2, i=-60mA/cm^2$)
Local Loading Level (gm/void volume)
Dimensionless DIstance ξ
0.0
0.1
0.2
0.3
0.4
0.5
0.6
0.2
0.3
0.4
0.5
0.6
0.7
0.8
0.9
1.0
20 min
10 min
4 min
2 min

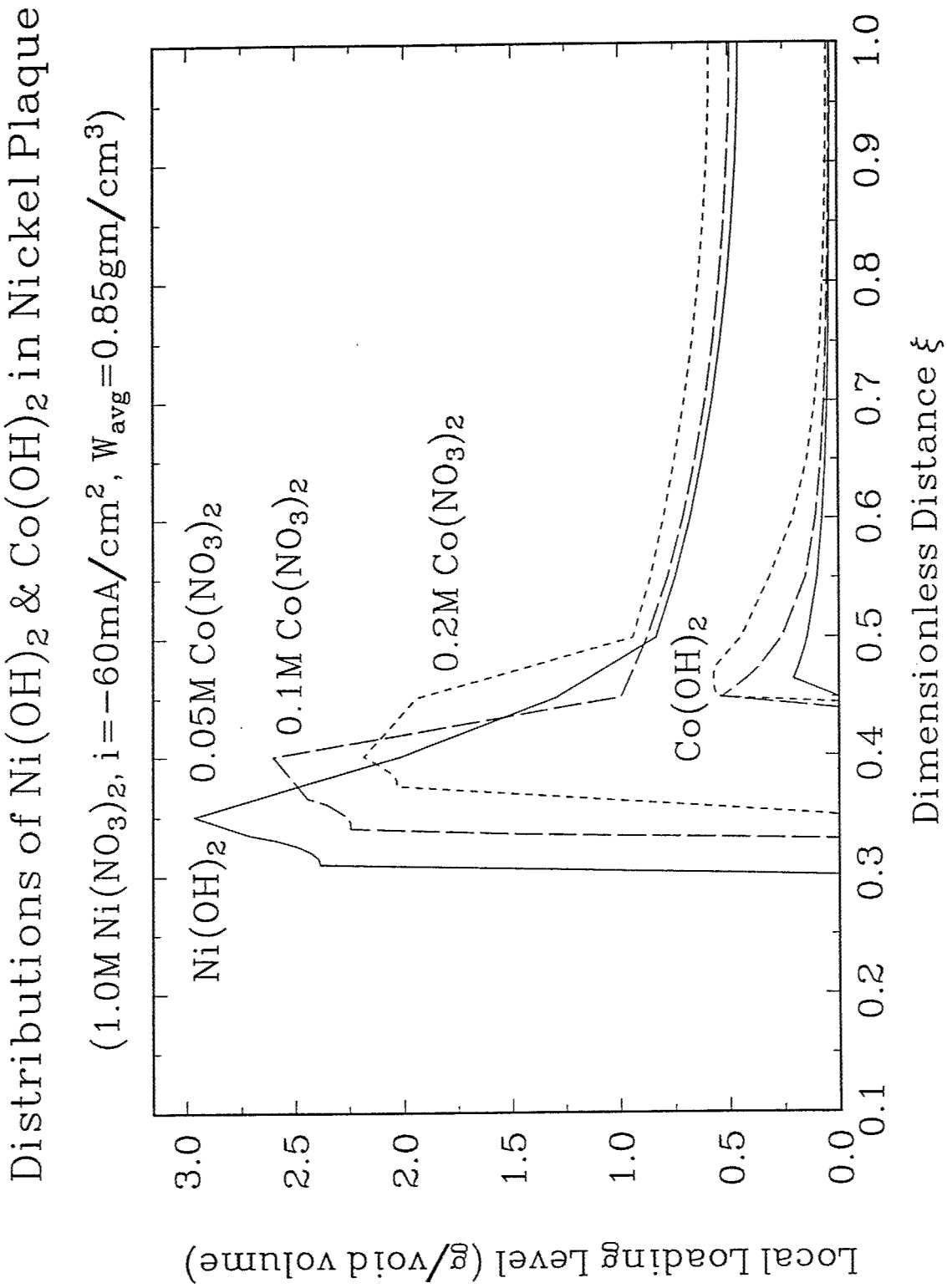
Distributions of $Ni(OH)_2$ & $Co(OH)_2$ in Nickel Plaque
(1.0M $Ni(NO_3)_2$, i=−60mA/cm^2, W_{avg}=0.85gm/cm^3)
$Ni(OH)_2$
0.05M $Co(NO_3)_2$
0.1M $Co(NO_3)_2$
0.2M $Co(NO_3)_2$
$Co(OH)_2$
Local Loading Level (g/void volume)
3.0
2.5
2.0
1.5
1.0
0.5
0.0
0.1
0.2
0.3
0.4
0.5
0.6
0.7
0.8
0.9
1.0
Dimensionless Distance ξ

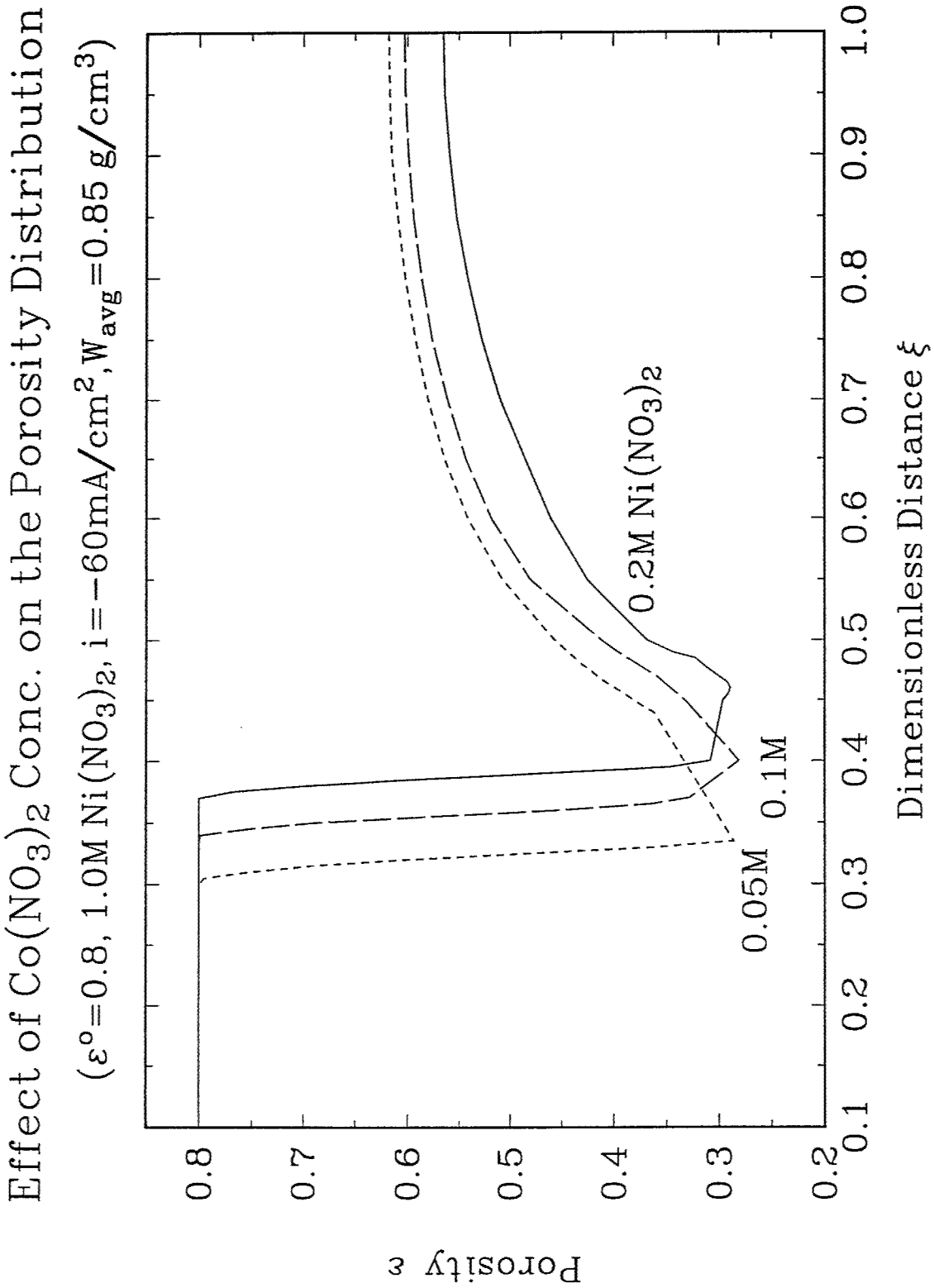
Effect of $Co(NO_3)_2$ Conc. on the Porosity Distribution
(ε^o=0.8, 1.0M $Ni(NO_3)_2$, i=−60mA/cm^2, W_{avg}=0.85 g/cm^3)
Porosity ε
0.8
0.7
0.6
0.5
0.4
0.3
0.2
0.1
0.2
0.3
0.4
0.5
0.6
0.7
0.8
0.9
1.0
Dimensionless Distance ξ
0.2M $Ni(NO_3)_2$
0.1M
0.05M

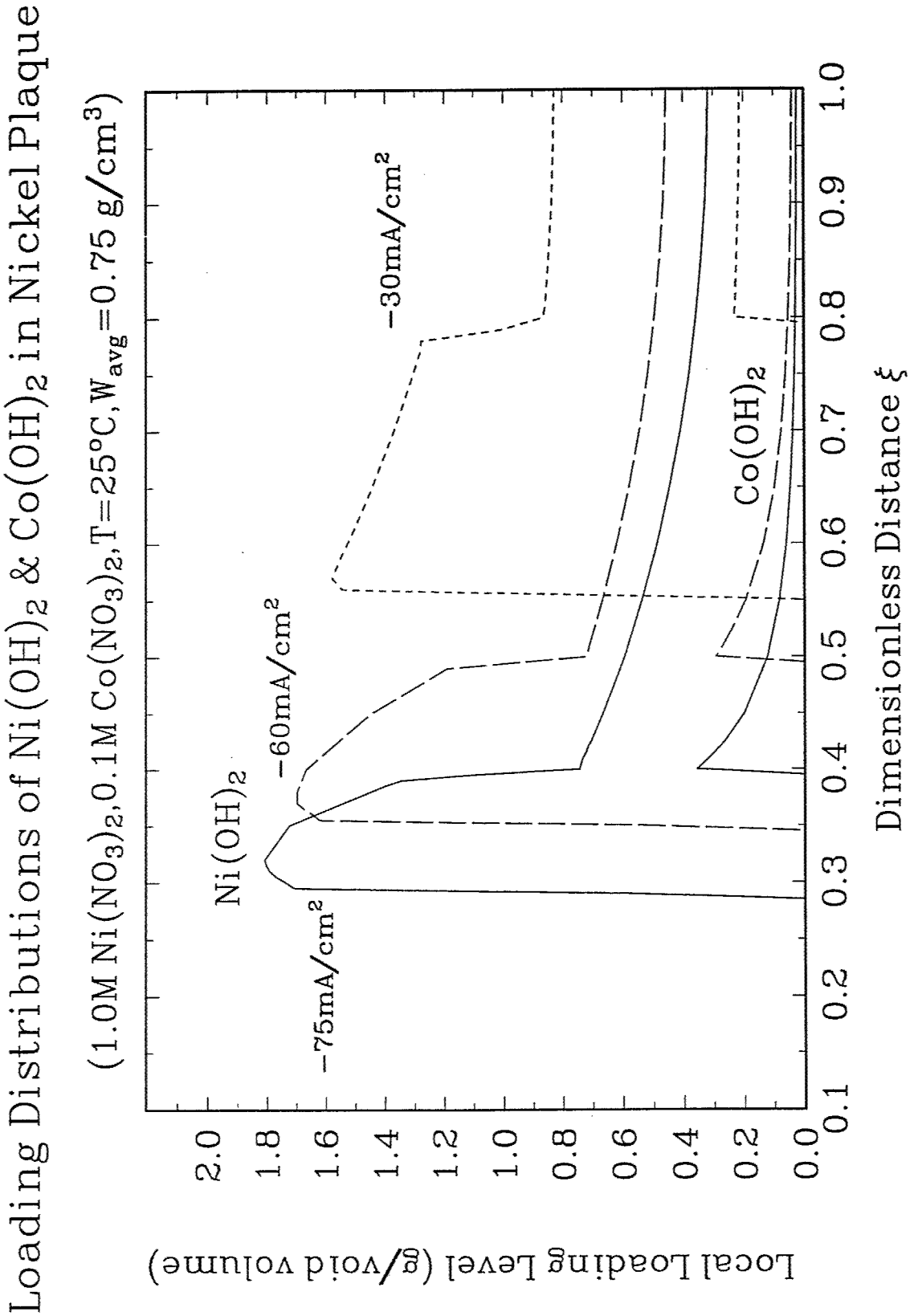
Loading Distributions of Ni(OH)2 & Co(OH)2 in Nickel Plaque
(1.0M Ni(NO3)2,0.1M Co(NO3)2,T=25°C,Wavg=0.75 g/cm3)
Ni(OH)2
−75mA/cm2
−60mA/cm2
−30mA/cm2
Co(OH)2
Local Loading Level (g/void volume)
Dimensionless Distance ξ
0.0
0.2
0.4
0.6
0.8
1.0
1.2
1.4
1.6
1.8
2.0
0.1
0.2
0.3
0.4
0.5
0.6
0.7
0.8
0.9
1.0

Summary

- Titration Experiments Determine Q_{sp}, and Q_{eq}
  - f(T, Alcohol, $[Ni(NO_3)_2]$)
- Raman Spectra Identifies $Ni_4(OH)_4^{4+}$
  - Absorbance is f(pH)
- EQCN Experiments and Film Model
  - Confirm Values of K_{eq}, K_{sp} ,and Ionic Strength Equations
- Porous Electrode Model
  - Agree with $Ni(OH)_2$ Distribution Measurements
- Porous Electrode Model Predicts Ni/Co Distributions

J. W. Van Zee, University of South Carolina
Presented at the NASA Battery Workshop
Dec. 4, 1996

Center of Electrochemical Engineering
Department of Chemical Engineering
University of South Carolina
Columbia, SC 29208

Conclusions

- For Uniform Total Deposit
  - Decrease Effect of Tetramer
    - Lower pH for deposition (decrease Q_{sp})
    - Decrease formation constant (Q_{eq})
    - Lower $[Ni(NO_3)_2]$ for fixed Q_{sp} and Q_{eq}
    - Optimum current density (low)
  - Decrease Current Density
- Quantify the Amount of Change

J. W. Van Zee, University of South Carolina
Presented at the NASA Battery Workshop
Dec. 4, 1996

Center of Electrochemical Engineering
Department of Chemical Engineering
University of South Carolina
Columbia, SC 29208

Conclusions (Cont.)

- Factors Affecting Q_{sp} and Q_{eq}
  - Increase in T yields decrease in Q_{sp} and increase in Q_{eq}
  - Increase in Alcohol conc. yields same as T
  - Increase ionic strength yields same as T

- $Co(OH)_2$ and $Ni(OH)_2$ depends on $[Co(NO_3)_2]$, Ionic Strength, $[Ni(NO_3)_2]$, T, and Alcohol Concentration

J. W. Van Zee, University of South Carolina
Presented at the NASA Battery Workshop
Dec. 4, 1996

Center of Electrochemical Engineering
Department of Chemical Engineering
University of South Carolina
Columbia, SC 29208

Acknowledgment

- Office of Research & Development of U. S. Central Intelligence Agency.
- Department of Energy by Cooperative Agreement DE-FCO2-91ER75666.

J. W. Van Zee, University of South Carolina
Presented at the NASA Battery Workshop
Dec. 4, 1996

Center of Electrochemical Engineering
Department of Chemical Engineering
University of South Carolina
Columbia, SC 29208

Tape

326

Blank

Nickel-Hydrogen Battery Fault Clearing at Low State of Charge

C. Lurie
TRW Space and Electronics Group
Redondo Beach, California 90278

The 1996 NASA Aerospace Battery Workshop
The Huntsville Hilton
Huntsville, Alabama
December 3 - 5, 1966

BACKGROUND

- **Battery fault clearing requires high rate, short duration discharges.**
- **Spacecraft batteries may be at low state of charge when a fault occurs, e.g., during reconditioning discharge to 1.0 volt per cell in a single battery power subsystem architecture.**
- **There is little relevant data available for this operating mode.**
- **Accordingly fault clearing data was obtained experimentally.**
- **The scope of the effort reported here includes determination of nickel-hydrogen battery fault clearing capability at low state of charge and comparison with capability at high state of charge.**

Battery fault clearing requires high rate discharges for a short periods of time. Fault clearing events are assumed to consist of fuse blowing and durations are typically a few milliseconds. Faults can occur at any time and battery state of charge can vary from full to very low state of charge. For example, a fault occurring at the end of a reconditioning discharge, to 1.0 volt per cell, in a single battery system, could require the fault to be cleared with little faradaic capacity in the battery.

Battery operating data describing short duration high rate discharge at low state of charge is not available. Accordingly a relevant data base was determined experimentally. Fault clearing data was obtained at high and low states of charge.

APPROACH

- **Fault clearing events are simulated by 3-millisecond discharges into resistive loads.**
- **The resistive loads are sized to provide data in the range C/2 to 3C.**
- **All testing is performed at 10° C.**

The experimental approach includes several assumptions and constraints.

Fault clearing events are simulated by 3-millisecond discharges into resistive loads. Fuse blowing generally occurs in less than 3 milliseconds and the load presented to the battery is closely approximated by a constant resistance.

The resistive loads are sized to provide data in the range C/2 to 3C (75 to 450 amperes with the 150 ampere-hour nickel-hydrogen cells used). This range provides a broad and conservative data base.

All testing is performed at 10°C. This is a "typical" battery operating temperature. A single temperature was considered adequate because fault clearing capability is a weak function of temperature over the usual spacecraft operating temperature range.

PLAN

- **Fault clearing discharges are performed at high and low states of charge.**
- **Test Sequence**
  - **Charge at the C/10 rate for 14 hours.**
  - **Discharge at the C/20 rate.**
  - **Add the fault clearing load, for 3 milliseconds, at 3 hours into the C/20 discharge. *(High state of charge event SOC = 85%)***
  - **Continue the C/20 rate discharge**
  - **Add the fault clearing load, for 3 milliseconds, at end of discharge. Three end of discharge voltages were considered: 0.9, 1.0, and 1.1 volts. *(Low state of charge event)***

Comparison of data obtained at low and high states of charge provides additional insight into the cell level processes taking place during the fault clearing events.

The test sequence is designed to provide data at a high state of charge defined by C/20 rate discharge to 85% state of charge and at three low state of charge conditions defined as C/20 rate discharge to 0.9, 1.0, and 1.1 volts per cell. The difference in capacity at 0.9, 1.0 and 1.1 volts per cell is small, but, as will be seen from the data, the difference in fault clearing parametric performance is significant.

Test Set Up

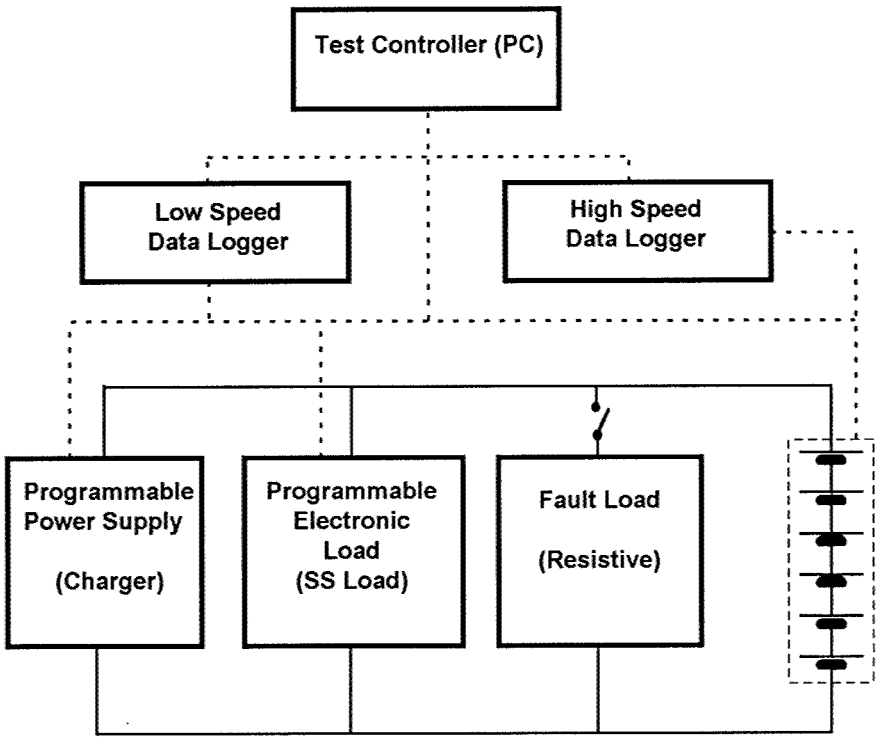

Test Cells -- 150 Ah NiH_2

- RNH 150-2
- 0.030" slurry Ni electrodes
- 2 layers of Zircar separator
- 31% electrolyte (final)
- Nickel precharge

The test equipment was designed to control all aspects of charge, discharge, thermal management, and data logging, automatically, with a PC as the primary test controller. Separate data logging was provided for the low speed requirement to provide continuous overall charge/discharge data, and the high speed requirement to provide adequate data during the millisecond fault clearing discharge pulses. The fault loads were superimposed on the C/20 steady state discharge loads at the appropriate times.

The test cells were Eagle Picher (Joplin) RNH 150-2 150 ampere-hour nickel-hydrogen cells packaged in a battery module shown on the next chart.

12-Cell 150-Ah Battery Module

- RNH 150-2 cells
- Cooling via VCHP to secondary mirror
- Fluid loop cooling capability
- Individual cell bypass
- Modular design
  - 11 or 12 cells per module
  - 110 to 210 Ah

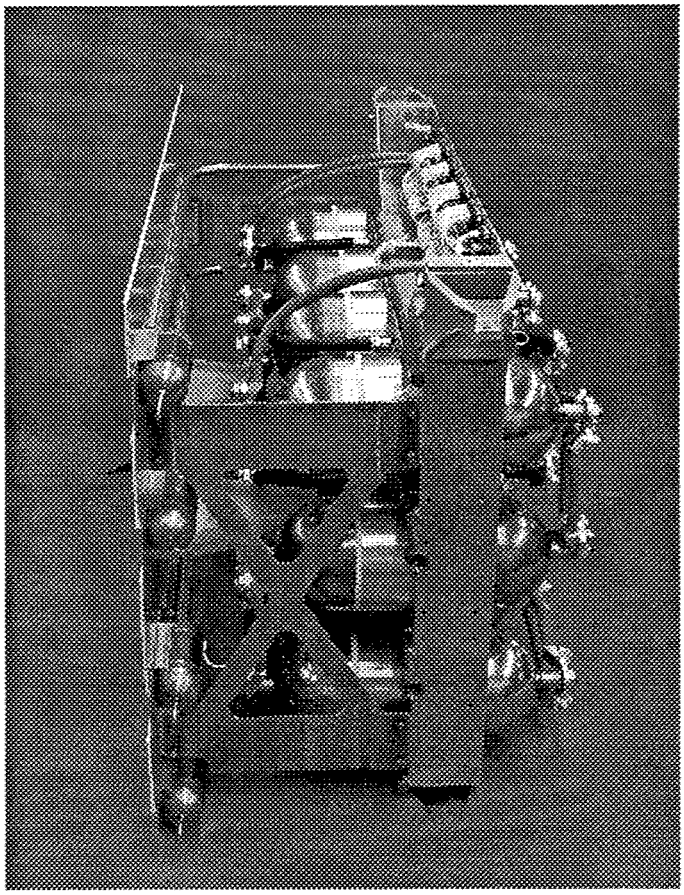

The test cells were packaged in the 150 ampere-hour battery module shown above. The packaging is modular in design and can accommodate 11 or 12 cells with capacities from 110 to 210 ampere-hours. Each cell is protected against cell open failures by individual cell bypass switches. Thermal management capabilities include cooling by moving heat from the cells to center-of-gravity mount thermal sleeves and, using variable conductance heat pipes (VCHP), to a secondary mirror for radiation to space. Fluid loop cooling capability is also provided for thermal management where active control is desired. The fluid loop cooling was utilized during the testing reported here.

120-AMPERE 3-MILLISECOND PULSE

AT HIGH STATE OF CHARGE

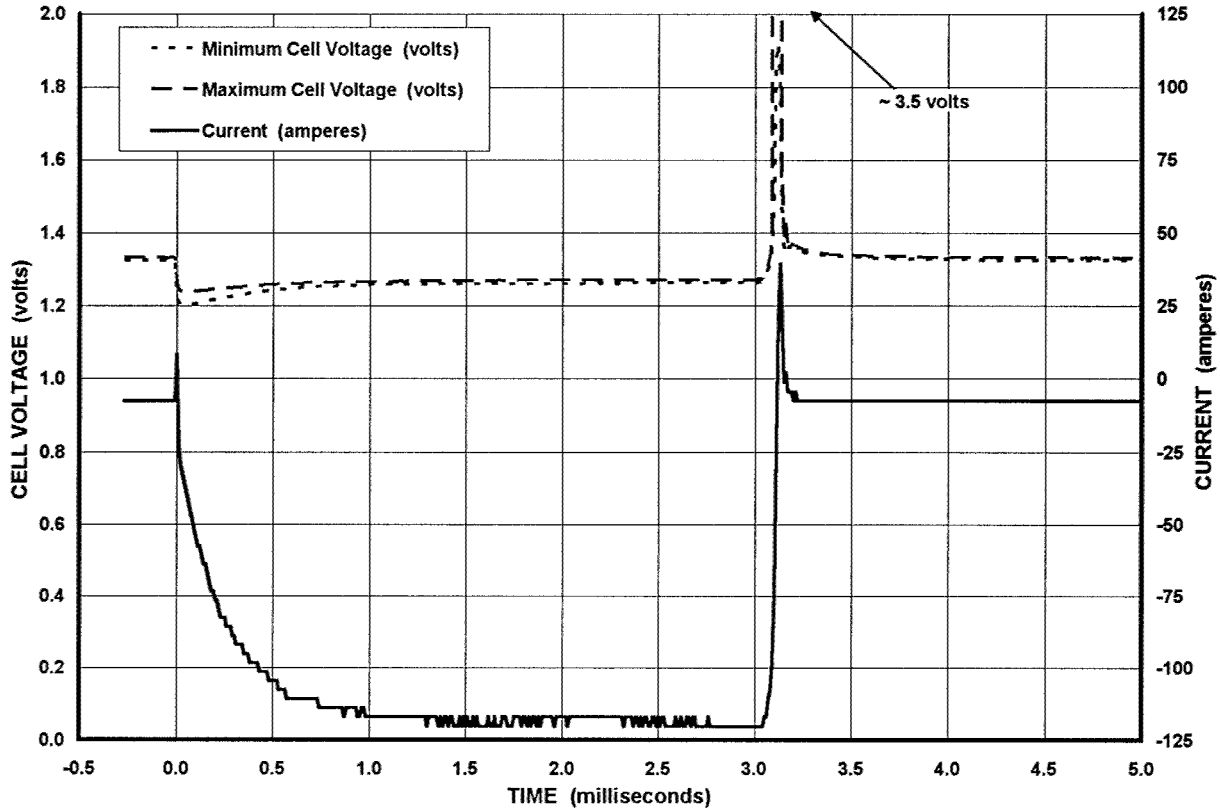

The 120-ampere discharge curve shows a typical fault clearing discharge at high state of charge. Only maximum and minimum cell voltages are plotted because the cells are well matched and the range of cell voltages is small. As can be seen from the curves the voltage is very stable during the discharge period. The dip in cell voltage at the leading edge of the pulse, as well as the "rounding" at the front end of the current trace, are due to the non-linear (inductance and capacitance) elements in the battery and test equipment. The large voltage excursion at the pulse turn-off is due, primarily, to cell inductance.

450-AMPERE 3-MILLISECOND PULSE

AT HIGH STATE OF CHARGE

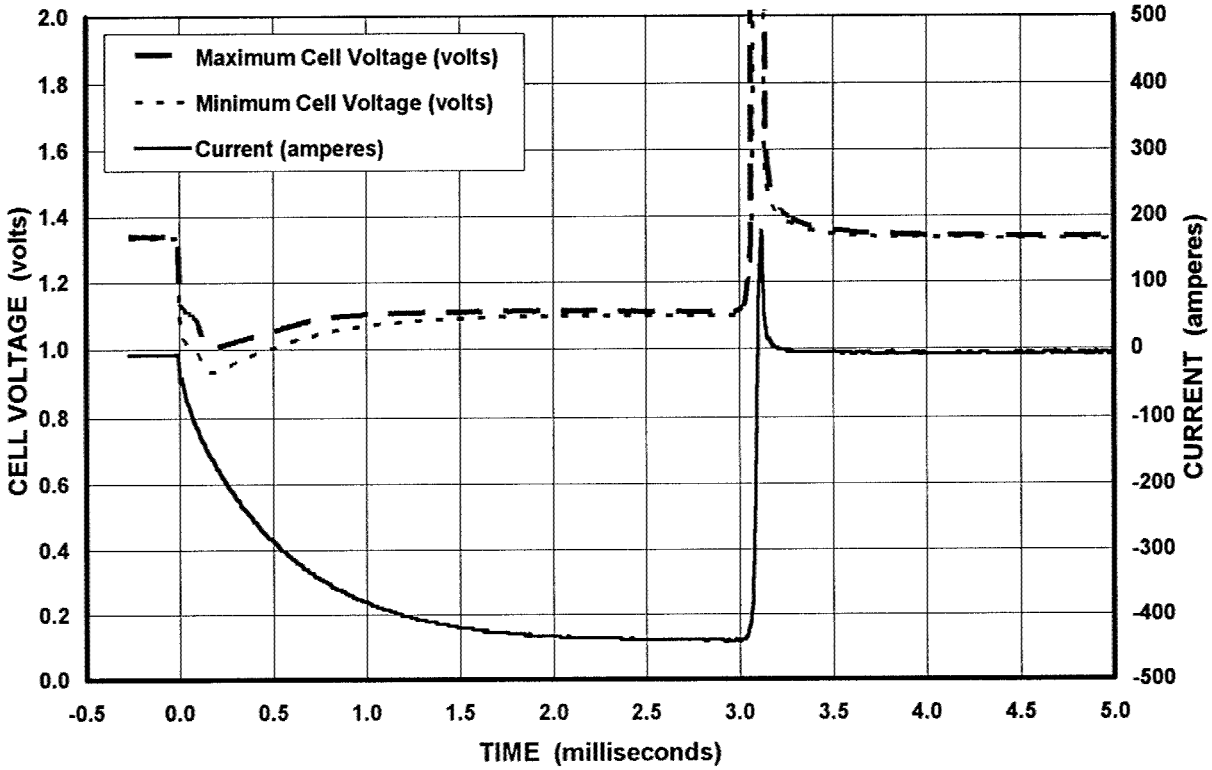

The 450-ampere discharge also shows excellent voltage "stiffness" during the fault clearing discharge. The difference between the starting voltage, e.g., the voltage prior to the fault clearing event, and the plateau voltage is greater than observed with the 150 ampere discharge. As will be seen in the succeeding charts the relationship between the initial and plateau voltages is a function of cell impedance and follows Ohms Law.

This relationship suggests that the energy expended during the fault clearing event comes from cell capacitance and that mass transfer processes do not occur to any appreciable extent.

AVERAGE PLATEAU VOLTAGE

3-MILLISECOND PULSES AT HIGH STATE OF CHARGE

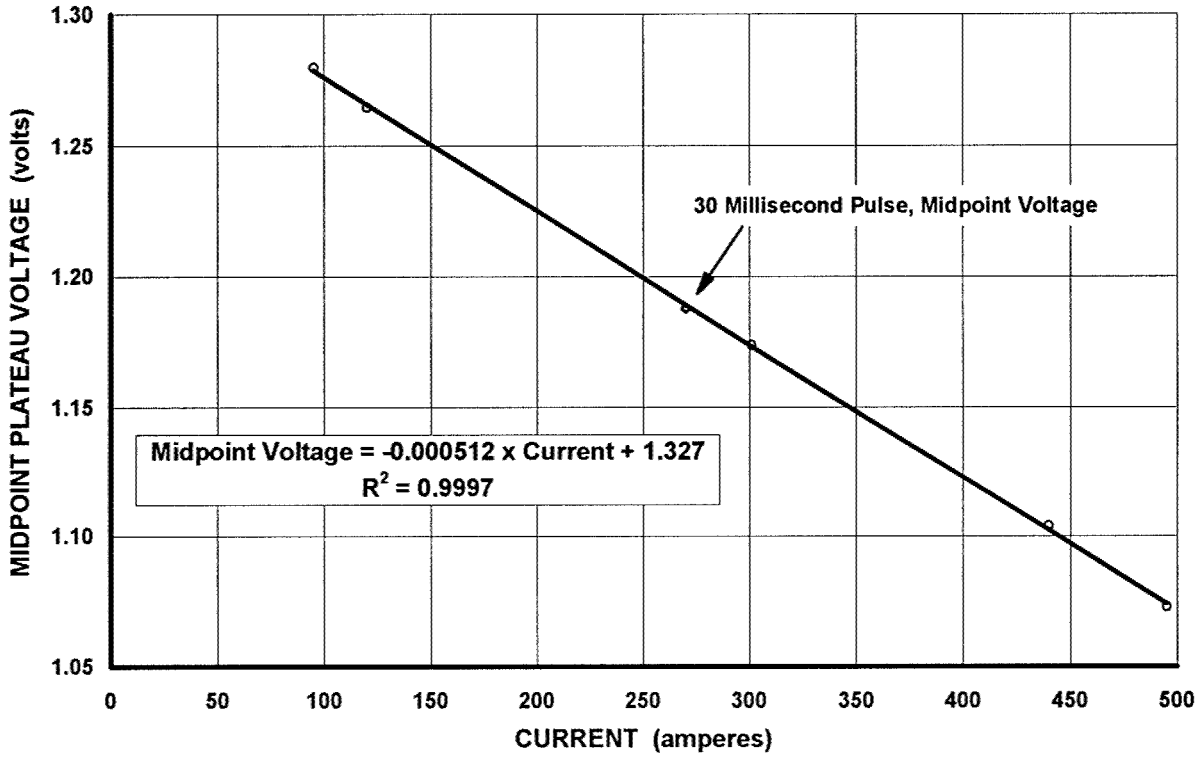

Midpoint plateau voltage data obtained at high states of charge are summarized in the plateau voltage *versus* pulse current chart. The slope of the voltage *versus* current plot is the cell resistance; the linear relationship is an expression of Ohms Law.

The 30-millisecond data point is included to demonstrate the stability of the plateau voltage. Stability in this time domain indicates that voltage decay due to faradaic and mass transfer effects require longer discharge durations at these conditions.

AVERAGE MINIMUM VOLTAGE

3-MILLISECOND PULSES AT HIGH STATE OF CHARGE

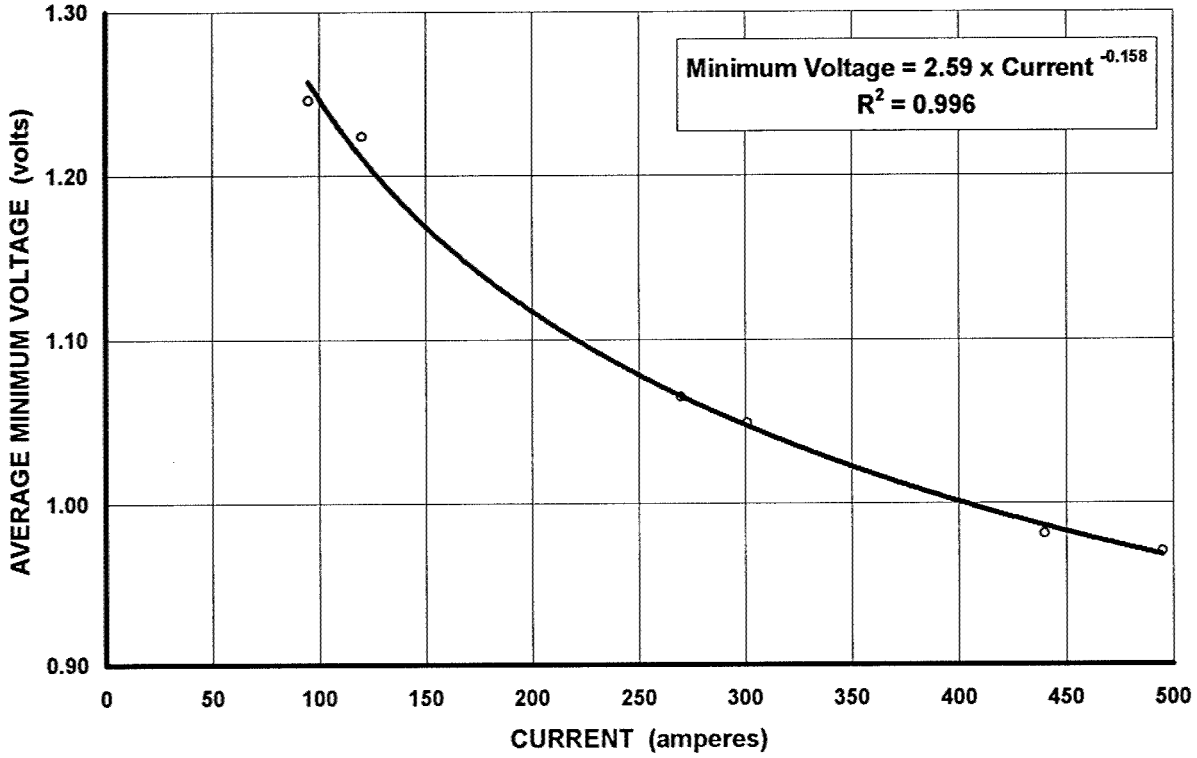

The minimum voltage observed during the fault clearing event may be of interest in terms of spacecraft bus voltage regulation. This chart shows the relationship between the average minimum voltage and the pulse current for the fault clearing data obtained at high state of charge.

It is interesting to note that an excellent fit is obtained with a power curve. If the voltage dip were due to cell inductance only the best fit would be provided by an exponential model.

75-AMPERE 3-MILLISECOND PULSE
AT LOW STATE OF CHARGE

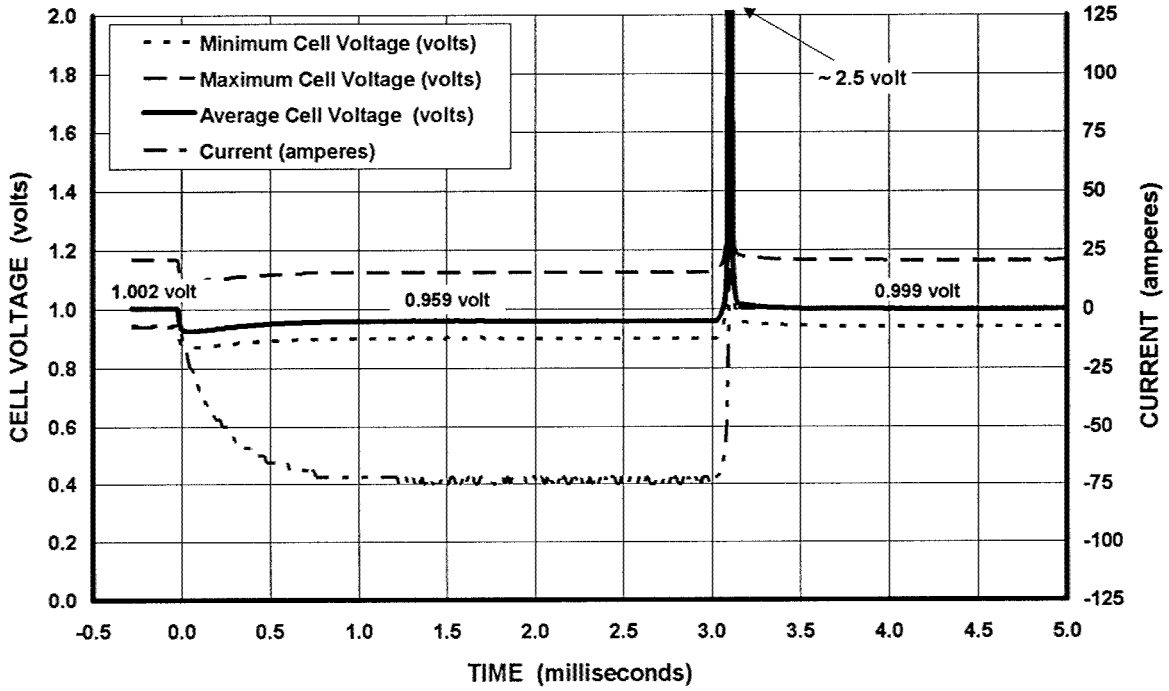

The next series of charts shows similar plateau voltage *versus* pulse current relationships obtained at low states of charge.

The 75-ampere curve shows fault clearing data following a C/20 discharge to 1.0 volt per cell. As can be seen from the chart the plateau voltage is stable and the voltage level, following the pulse, returned to within a few millivolts of the starting voltage. This is interpreted as meaning that very little mass transfer occurred.

350-AMPERE 3-MILLISECOND PULSE
AT LOW STATE OF CHARGE

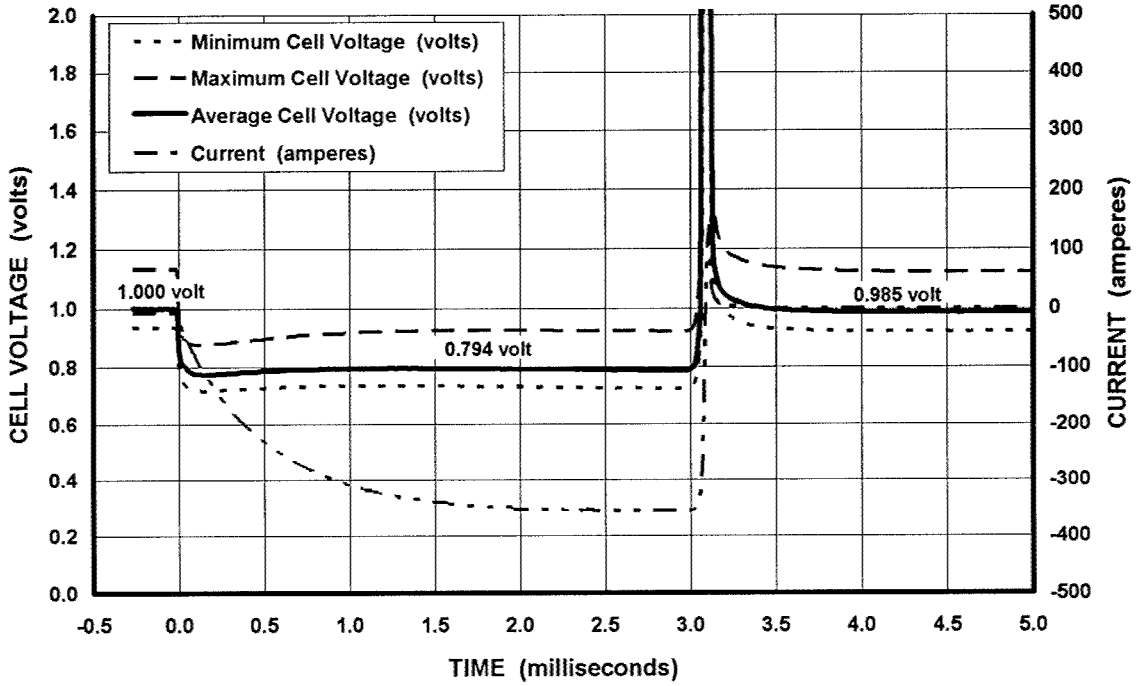

The 350-ampere curve shows data following a C/20 rate discharge to 1.0 volt per cell and is similar to the previous 75-ampere rate curve. However the plateau voltage is lower than the 75-ampere case and the post fault clearing voltage is lower than the starting voltage. The lower plateau voltage is simply a function of the higher current (Ohms Law) and the lower post fault clearing voltage is due to reduction of the cell capacitance by an amount equivalent to the energy expended during the fault clearing event.

200-AMPERE 30-MILLISECOND PULSE

AT LOW STATE OF CHARGE

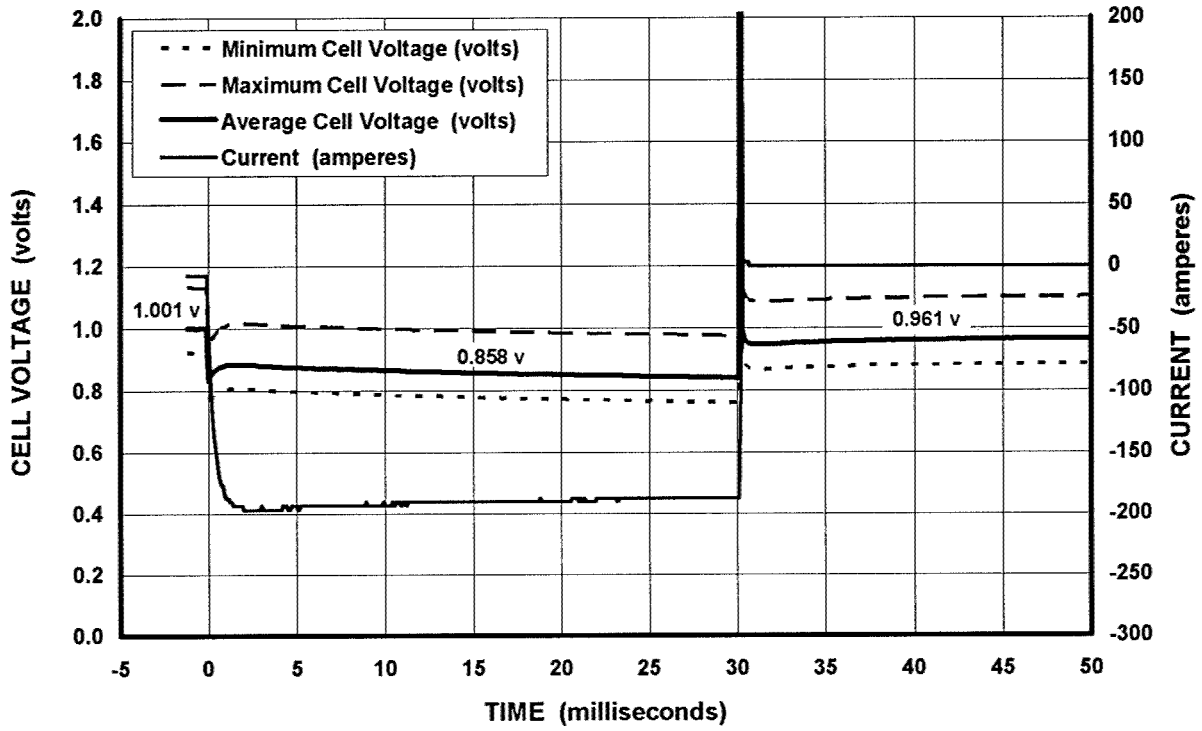

Thirty-millisecond pulse data, at low state of charge, is shown to demonstrate that the plateau voltage trajectory exhibits a negative slope as energy is removed. This slope, plus the lower post fault clearing voltage, is interpreted as indicating that the cell capacitance is changing significantly, in this time domain, at these operating conditions.

AVERAGE PLATEAU VOLTAGE

3-MILLISECOND PULSES AT LOW STATE OF CHARGE

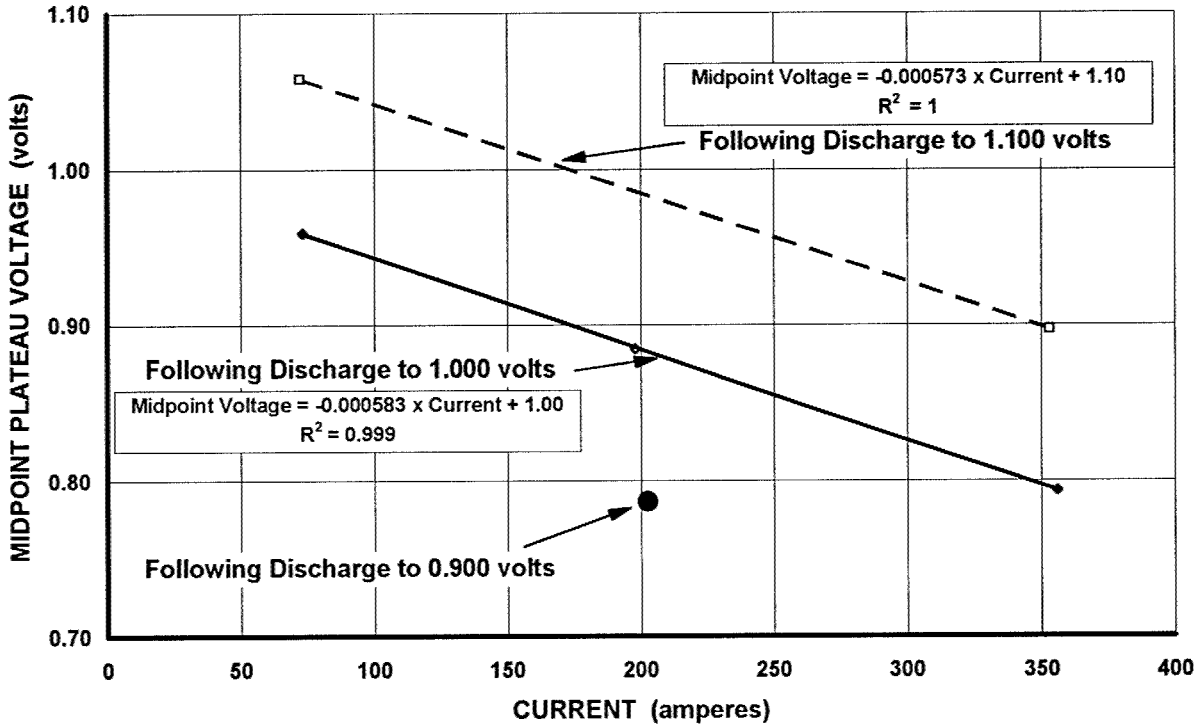

Midpoint plateau voltage data obtained at low states of charge are summarized in this plateau voltage *versus* pulse current chart. As in the case of the high state of charge data the slope of the linear relationship is cell resistance. Inspection of the chart reveals that the intercept of the regression line is the voltage at which the fault clearing pulse was started. The intercept, by definition, is the value of the plateau voltage at zero current. In fact, the C/20 discharge rate is non-zero, but is low compared to the fault clearing rates. Simple linear regression analysis yields intercept values statistically indistinguishable from the starting voltages. The slopes at low states of charge appear to larger than observed at high state of charge. It is reasonable to assume that the cell impedance is slightly higher at lower states of charge, however the statistical significance of the difference is marginal.

AVERAGE MINIMUM VOLTAGE

3-MILLISECOND PULSES AT LOW STATE OF CHARGE

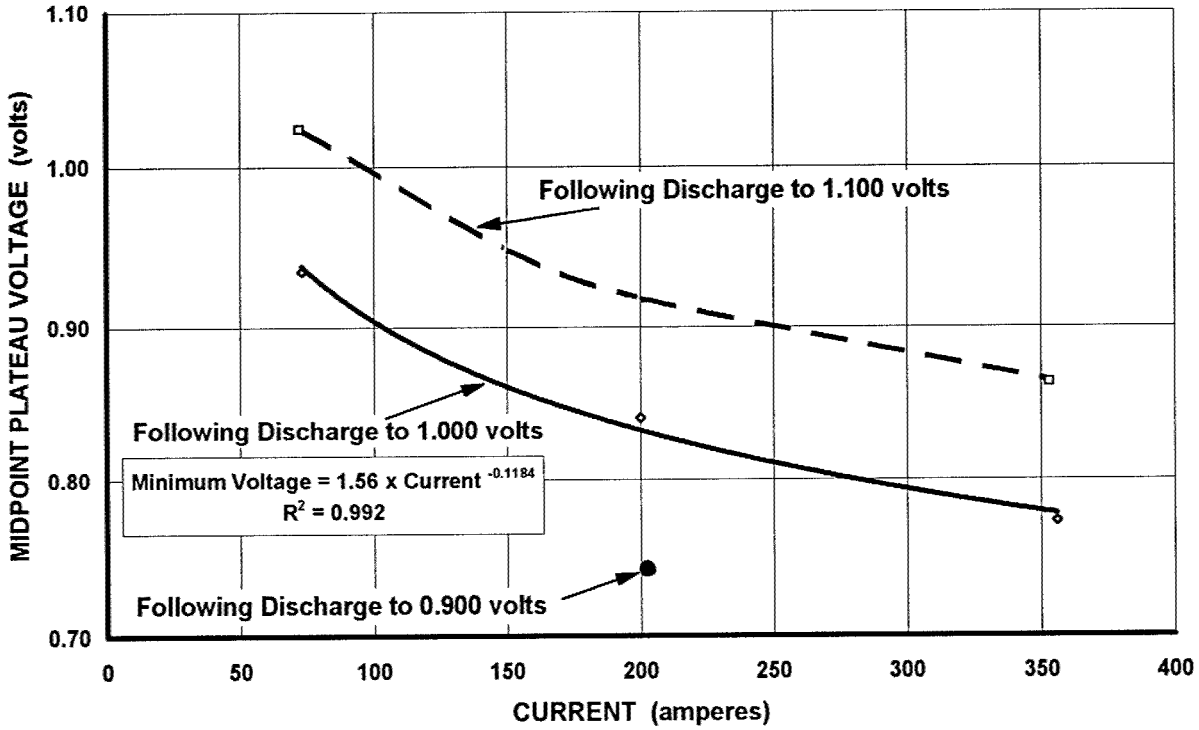

This chart shows the relationship between the average minimum fault clearing voltage and the pulse current for the fault clearing data obtained at low state of charge. As in the case of the data obtained at high state of charge, this data can be fit with a power curve.

NiH_2 Cell Equivalent Circuits
Millisecond Time Domain

- **Applicable to the 3-millisecond pulse**

- **Applicable to the 30-millisecond pulse**

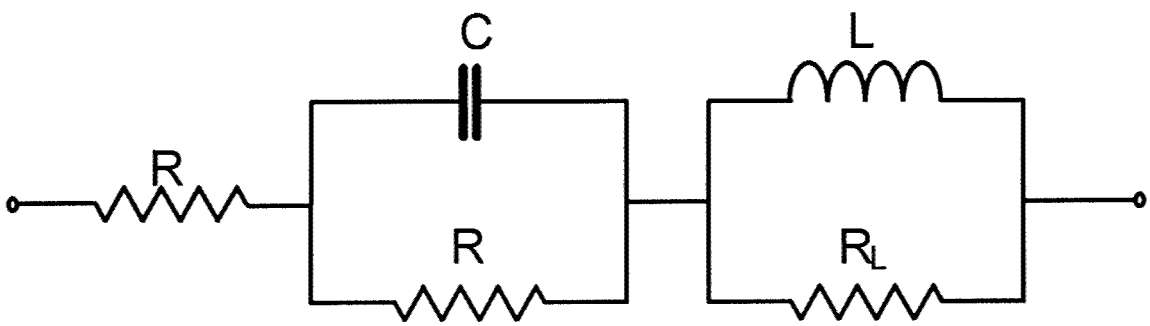

Cell performance can be described by simple equivalent circuits for the simulated fault clearing events presented here. A complete description of cell impedance includes inductive, resistive, and capacitive elements. as well as terms dealing with electrochemical phenomena. A "complete" cell equivalent circuit would contain all these elements and would be very complex. However, in the time domain, and at the operating conditions studied, significant simplifying assumptions are possible.

The "3-millisecond" data can be described simply by an inductance in series with a resistance. Cell capacitance is large enough and the time constant long enough to allow the capacitance term to be ignored. Mass transfer effects are insignificant in this time domain and are also ignored. Because the time constant for the inductive term is very short it too can be ignored if only the plateau voltage is needed.

If the pulse duration is extended, as in the 30-millisecond pulse data, a capacitance term is added to provide the proper plateau voltage trajectory.

SUMMARY

- Fault clearing currents were achieved and maintained at discharge rates from C/2 to 3C at high and low states of charge.

- The fault clearing plateau voltage is a strong function of
  - discharge current and
  - voltage-prior-to-the-fault-clearing-event

  and a weak function of state of charge.

- Voltage performance, for the range of conditions reported, is summarized as

$$= ((\quad \times \quad - \;) - (\quad \times \quad - \;) \times \quad) \times \qquad +$$

where

VMPP	=	Fault clearing midpoint voltage, volts
SOC	=	State of charge, %
IDSCHG	=	Fault clearing current, amperes
VSTRT	=	Voltage at the start of the fault clearing event, volts

Page

350

blank

COMSAT LABORATORIES

LOCKHEED MARTIN

EOS–AM1 Nickel Hydrogen Cell Interim Life Test Report

by
C.W. Bennett
Lockheed Martin Missles and Space

D.J. Keys, G.M. Rao
NASA/GSFC

H.E. Wannemacher
Jackson and Tull

H. Vaidyanathan
COMSAT Laboratories

(Performed under NASA Contracts NAS5–32500 and NAS5–32600)

Abstract

This paper reports the interim results of the Earth Observing Systen AM–1 project (EOS–AM–1) nickel hydrogen cell life test being conducted under contract to National Aeronautics and Space Administration (NASA) Goddard Space Flight Center (GSFC) at the Lockheed Martin Missles and Space (LMMS) facility in East Windsor, NJ; and at COMSAT Labs., Glarksburg, MD. The purpose of the tests is to verify that the EOS–AM–1 cell design can meet five years of real–time Low Earth Orbit (LEO) cycling. The tests include both real–time LEO and accelerated stress tests. At LMMS, the first real–time LEO simulated 99 minute orbital cycle started on February 7, 1994 and the test has been running continuously since that time, with 13000 LEO cycles completed as of September 2, 1996. Each cycle consists of a 64 minute charge (VT at 1.507 volts per cell, 1.06 C/D ratio, followed by 0.6 ampere trickle charge) and a 35 minute constant power discharge at 177 watts (22.5% DOD). At COMSAT, the accelerated stress test consists of 90 minute orbital cycles at 60% DOD with a 30 minute discharge at 60 amperes and a 60 minute charge at 40 amperes (VT at 1.54 volts per cell to 1.09 C/D ratio, followed by 0.6 ampere trickle charge).

The real–time LEO life test battery consists of seven, 50AH (nameplate rating) Eagle–Picher, Inc. (EPI) Mantech cells manufactured into three, 3–cell pack assemblies (there are two place holder cells that are not part of the life test electrical circuit). The test pack is configured to simulate the conductive thermal design of the spacecraft battery, including: conductive aluminum sleeves, 3–cell pack aluminum baseplate, and honeycomb panel all mounted to a liquid (–5°C) cold plate. The entire assembly is located in a thermal chamber operating at +3°C. The accelerated stress test unit consists of five cells mounted in machined aluminum test sleeves and is operating at +10°C.

The real–time LEO life test battery has met all performance requirements through the first 13,000 cycles, including: end of charge and discharge cell voltages and voltage gradients; end of charge and discharge cell pressures; within cell and between cell temperature gradients; discharge capacity; current and power levels; and all charge parameters. The accelerated stress test battery has completed over 5900 cycles as of 9/11/96. This paper reports both battery performances as a function of cycle life, with individual cell performance comparisons reported for selected cycles in both tests.

Battery Assembly/Spacecraft Interface

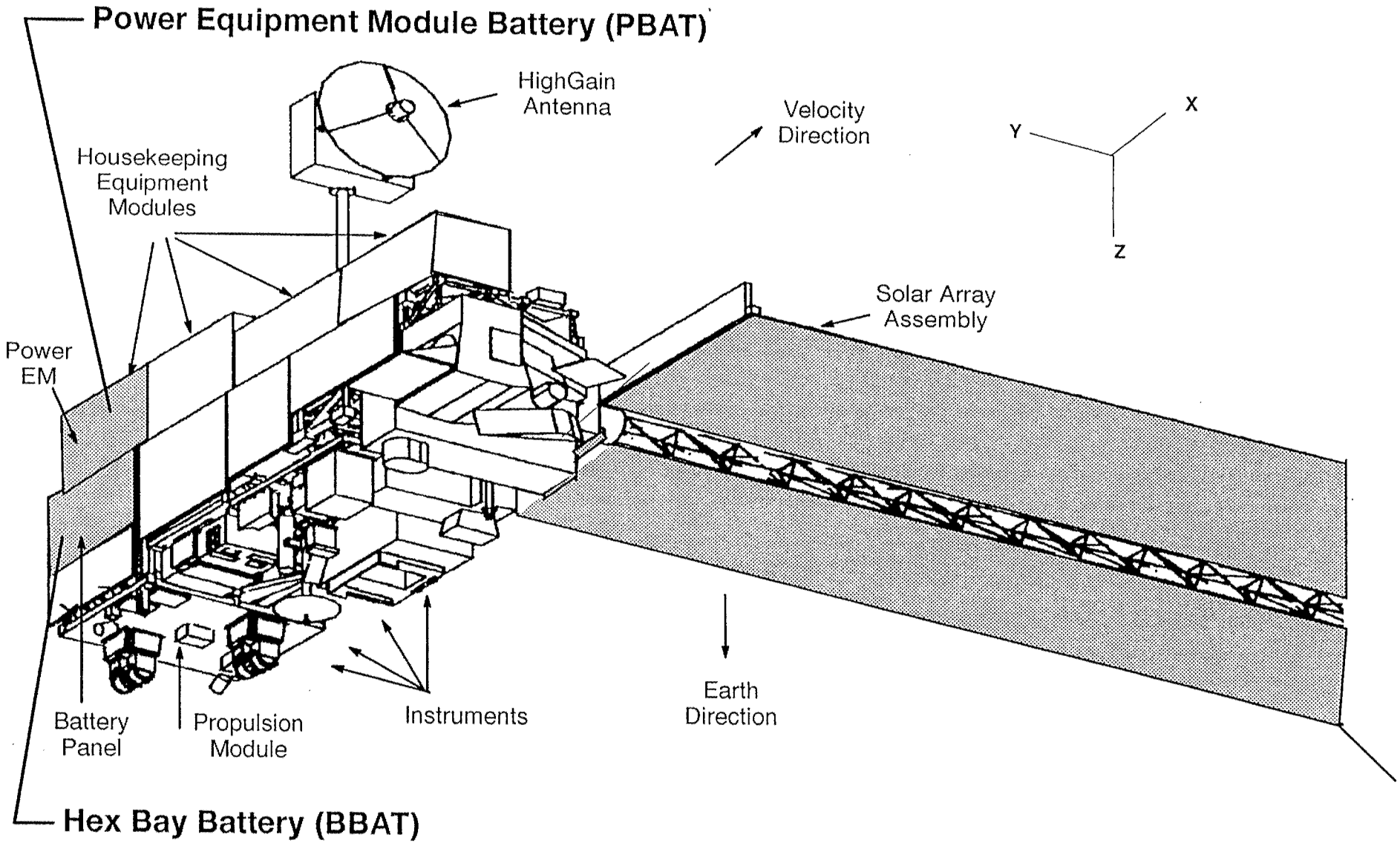

Outline

- EOS–AM cell parameters
- Real–time LEO test conditions
- Real–time LEO test results
  - Figures 1–13
- Accelerated LEO stress test conditions
- Accelerated LEO stress test results
  - Figures 14–20
- Summary and conclusions

EOS–AM Cell Parameters

LOCKHEED MARTIN

- Single stack, IPV, Mantech design
- Rabbit ear terminals
- 40, 30 mil slurry electrodes
- Back to back with double layer Zircar, catalyzed wall wick
- 31% KOH, nickel precharge
- Average cell weight = 1490 grams
- Average delivered capacity (C/2 discharge)
  - –10°C: 75 AH
  - 0°C: 71 AH
  - +10°C: 63 AH
  - +20°C: 56 AH
  - +30°C: 51 AH

Real–time LEO Test Conditions

LOCKHEED MARTIN

- Performed at LMMS, East Windsor, NJ
- Number of cells: 7
- Cell configuration:
  - Conductive thermal design with same configuration as spacecraft
  - Machined aluminum sleeves and baseplate
  - Chotherm and RTV 566 isolation
  - Mounted to spacecraft honeycomb panel with Al face sheets
  - Liquid cooled (–5°C) cold plate
- Discharge regime: 177 watts (total) constant power discharge for 35 minutes
- Depth of discharge: 22.5% nominal
- Charge regime:
  - 12.3 ampere to 1.507 V/T (per cell), taper to 1.06 C/D, 0.6 A trickle
  - 64 minute total charge time

LMMS Test Anomalies

LOCKHEED MARTIN

Table I
Schedule of Test Interruptions and Changes

Event[1]	Date	Cycle	Description
A	2/21/94	200	Charge time reached prior to VT limit. Several test aborts
B	4/26/94	1110	STE malfunction caused cells to be discharged ~ 45 AH without recharge. Charge time limit reached prior to VT limit
C	10/21/94	3500	VT changed from 10.550 to 10.626
D	10/28/94	3750	Discharge load changed from 177 watts to 88 watts
E	11/5/94	3850	Discharge load changed from 88 watts to 177 watts
F	11/7/94	3900	VT changed from 10.626 to 10.550
G	2/7/95–3/26/95	5200–5900	Data printouts not found
H	5/15/95	6600	Several short duration test aborts
I	6/30/95–7/3/95	7200	Test cells on open circuit due to STE problems
J	9/1/95–9/28/95	8100	Test cells on open circuit due to STE problems
K	11/10/95–11/1195	8700	Test cells on open circuit due to STE problems

Notes:
1. Event letters are used as markers in Figures 1–13

Fig 1

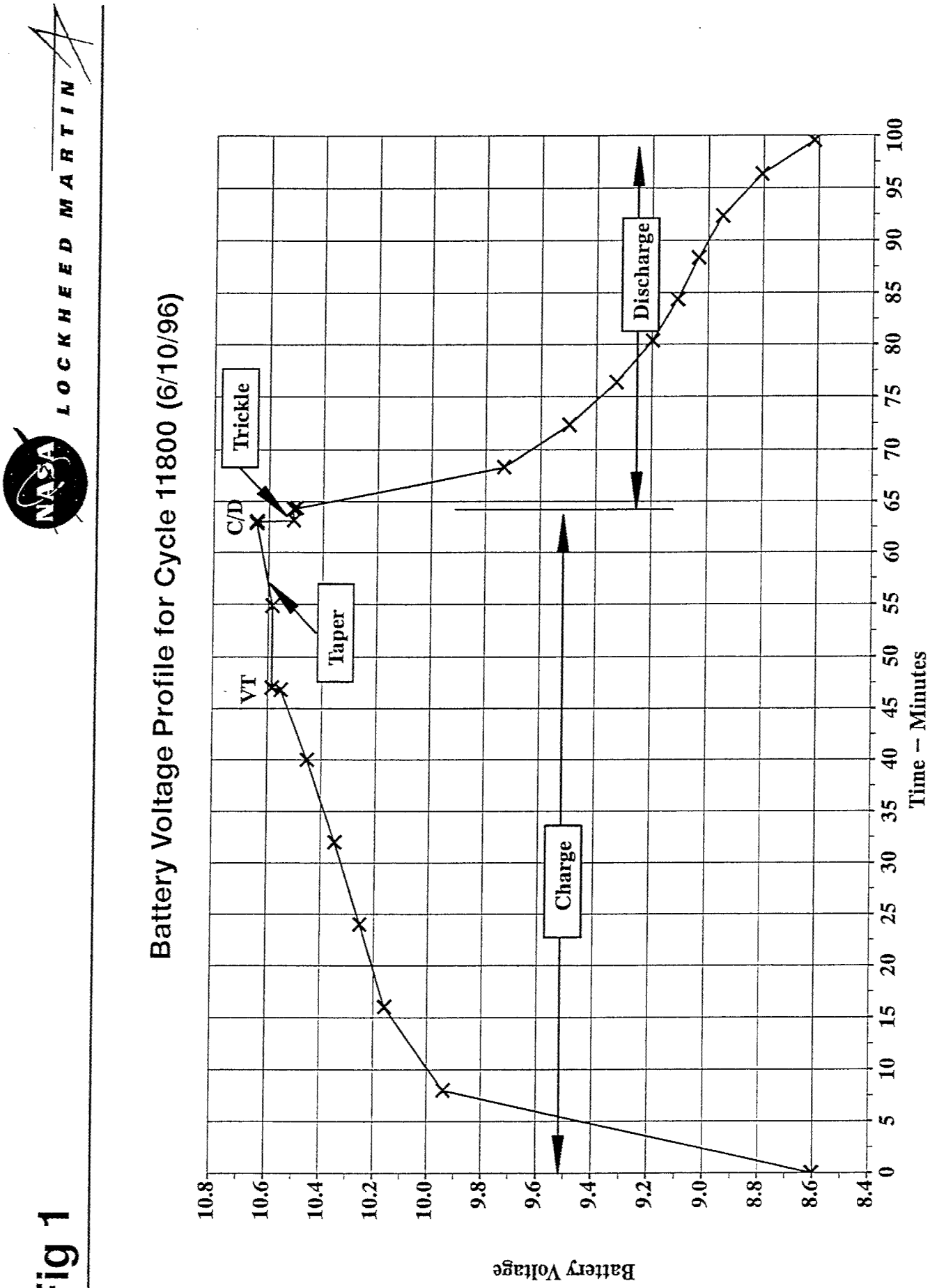
Battery Voltage Profile for Cycle 11800 (6/10/96)
Trickle
C/D
Taper
VT
Charge
Discharge
Battery Voltage
Time – Minutes
10.8
10.6
10.4
10.2
10.0
9.8
9.6
9.4
9.2
9.0
8.8
8.6
8.4
0
5
10
15
20
25
30
35
40
45
50
55
60
65
70
75
80
85
90
95
100

Fig 2

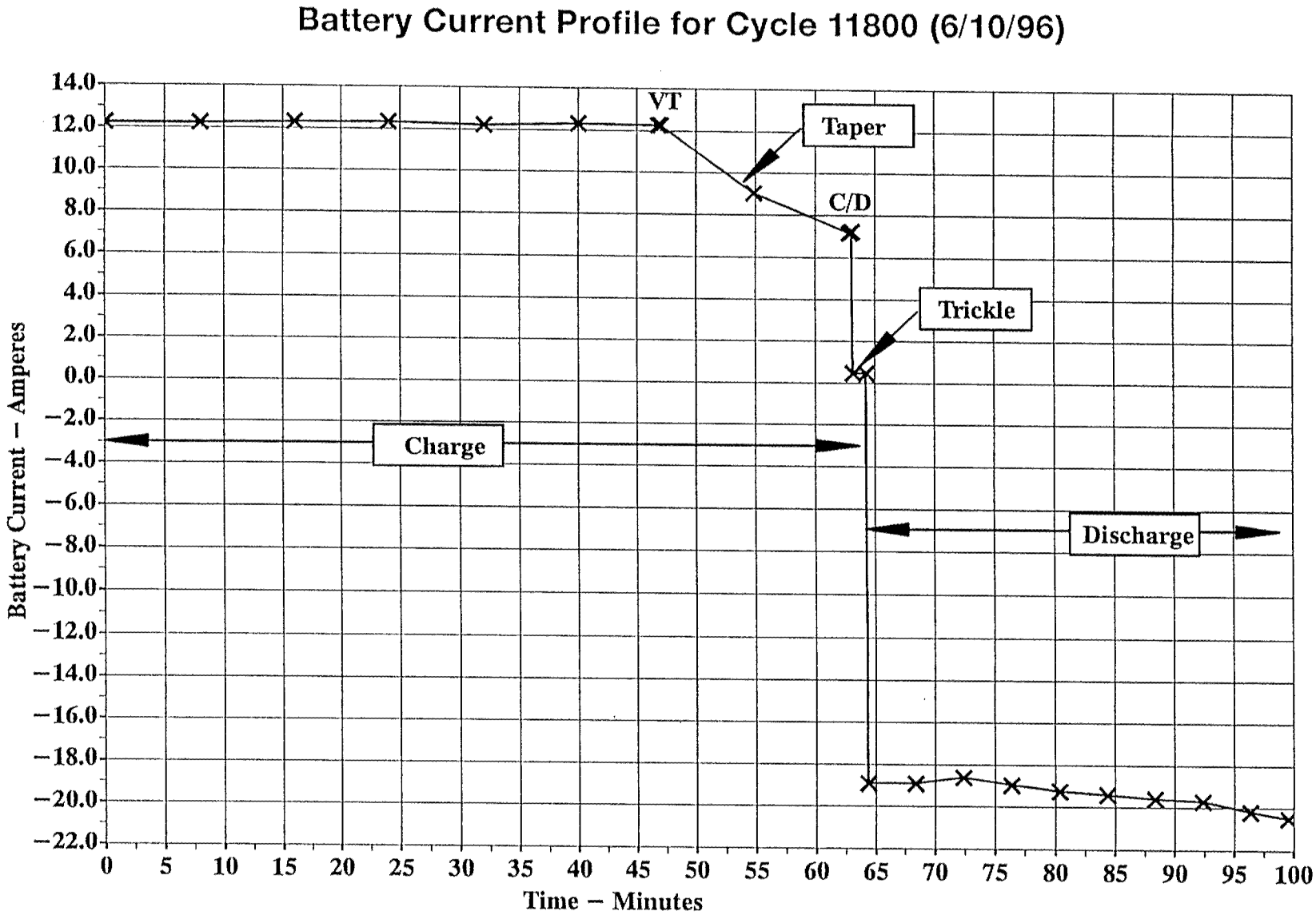
Battery Current Profile for Cycle 11800 (6/10/96)
Battery Current – Amperes
Time – Minutes
14.0
12.0
10.0
8.0
6.0
4.0
2.0
0.0
−2.0
−4.0
−6.0
−8.0
−10.0
−12.0
−14.0
−16.0
−18.0
−20.0
−22.0
0
5
10
15
20
25
30
35
40
45
50
55
60
65
70
75
80
85
90
95
100
VT
Taper
C/D
Trickle
Charge
Discharge

Fig 3

LOCKHEED MARTIN

End of Charge and Discharge Battery Voltage vs LEO Cycle

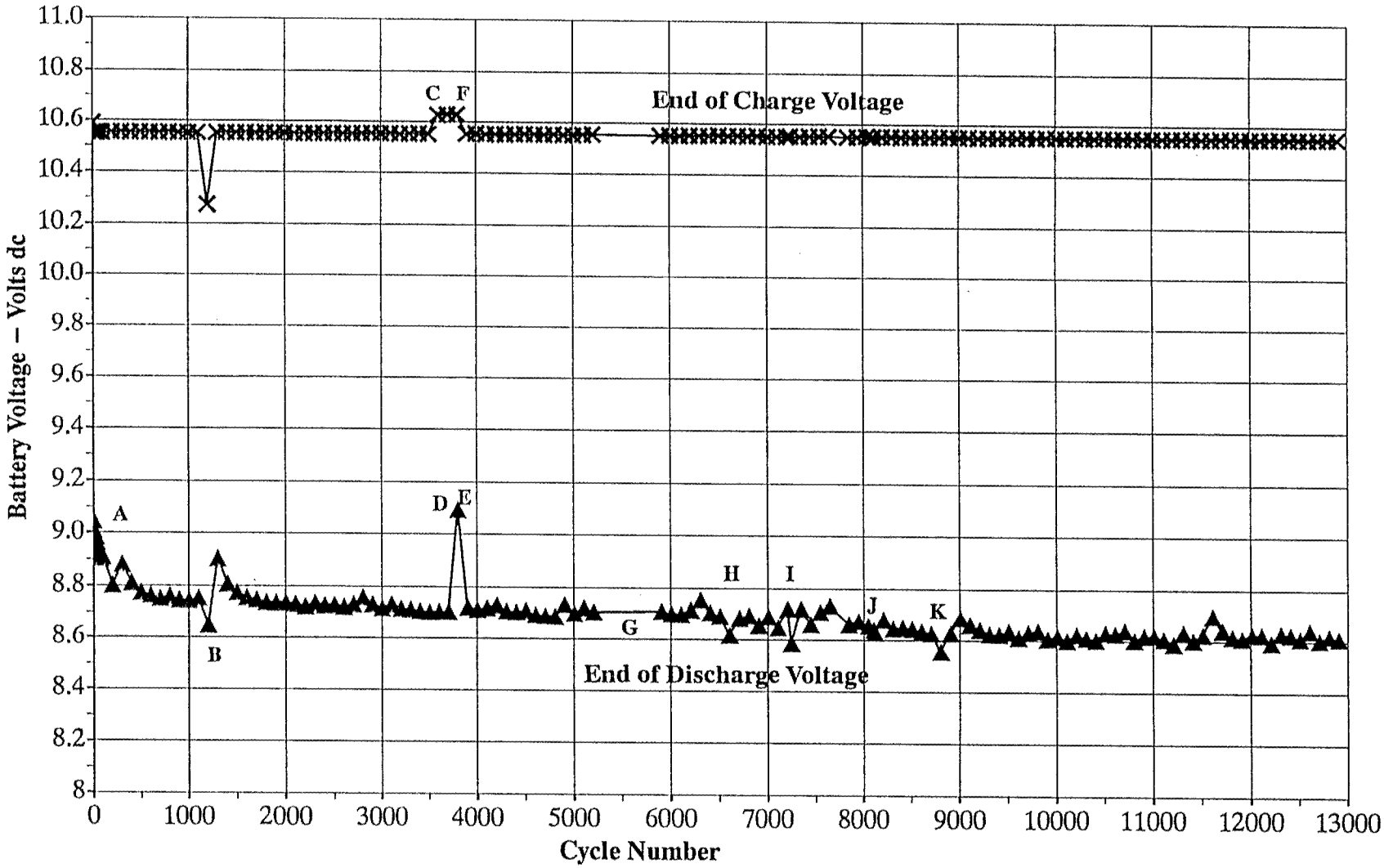

Fig 4

LOCKHEED MARTIN

Minimum and Maximum Cell End of Charge and Discharge Voltage vs LEO Cycle

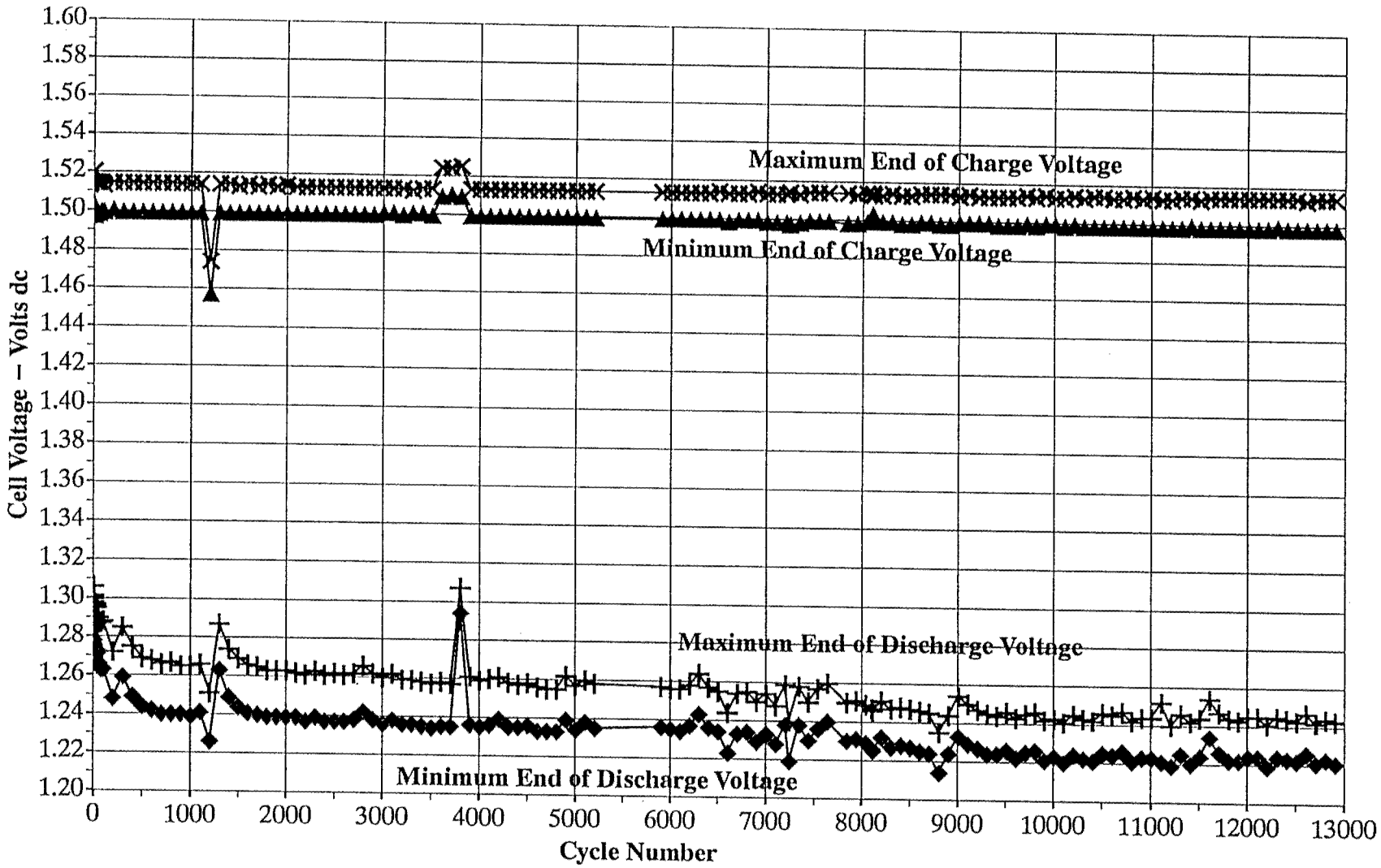

Fig 5

LOCKHEED MARTIN

Minimum and Maximum Cell End of Discharge Voltage (Expanded Scale) vs LEO Cycle

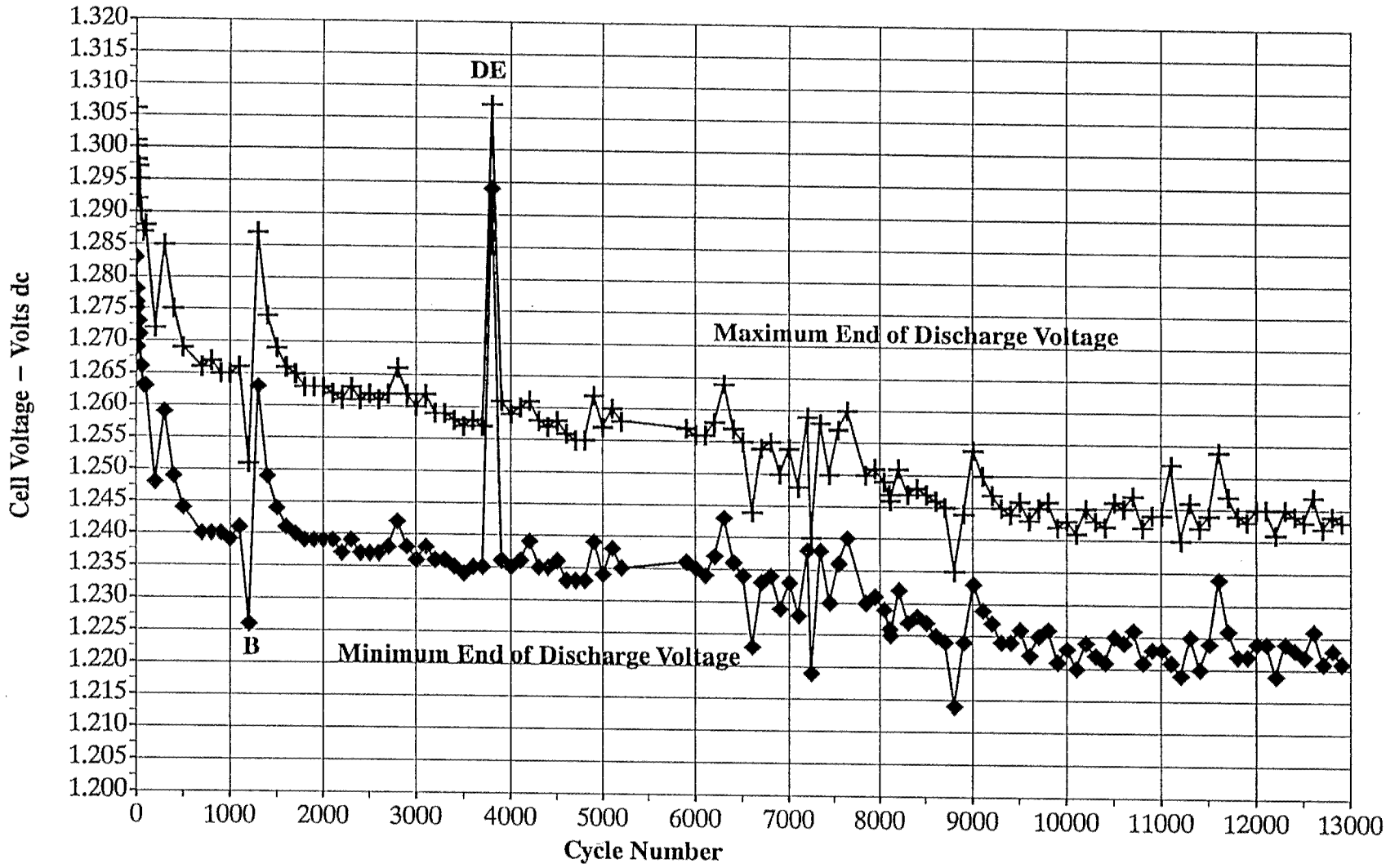

Fig 6

LOCKHEED MARTIN

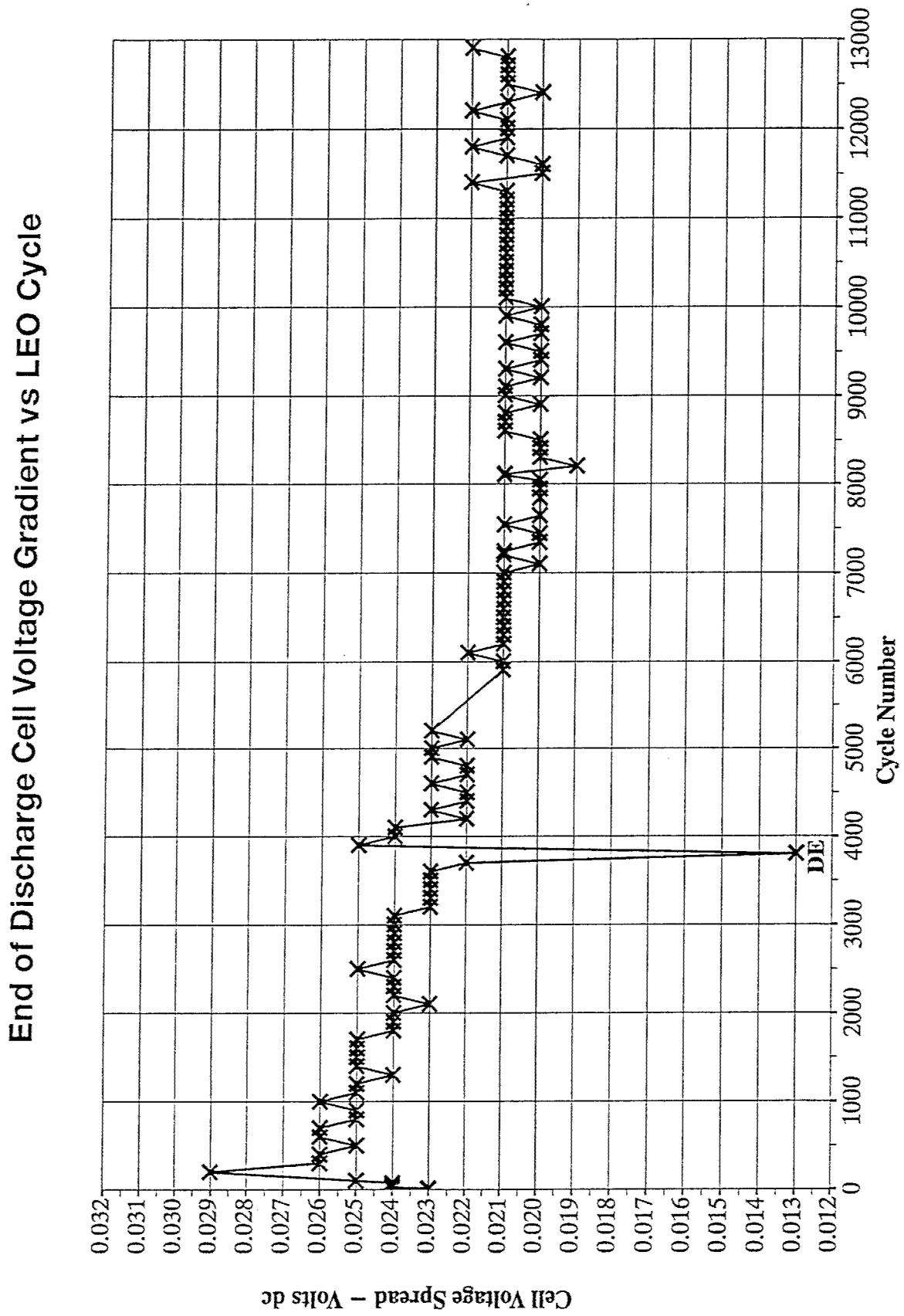

Fig 7

LOCKHEED MARTIN

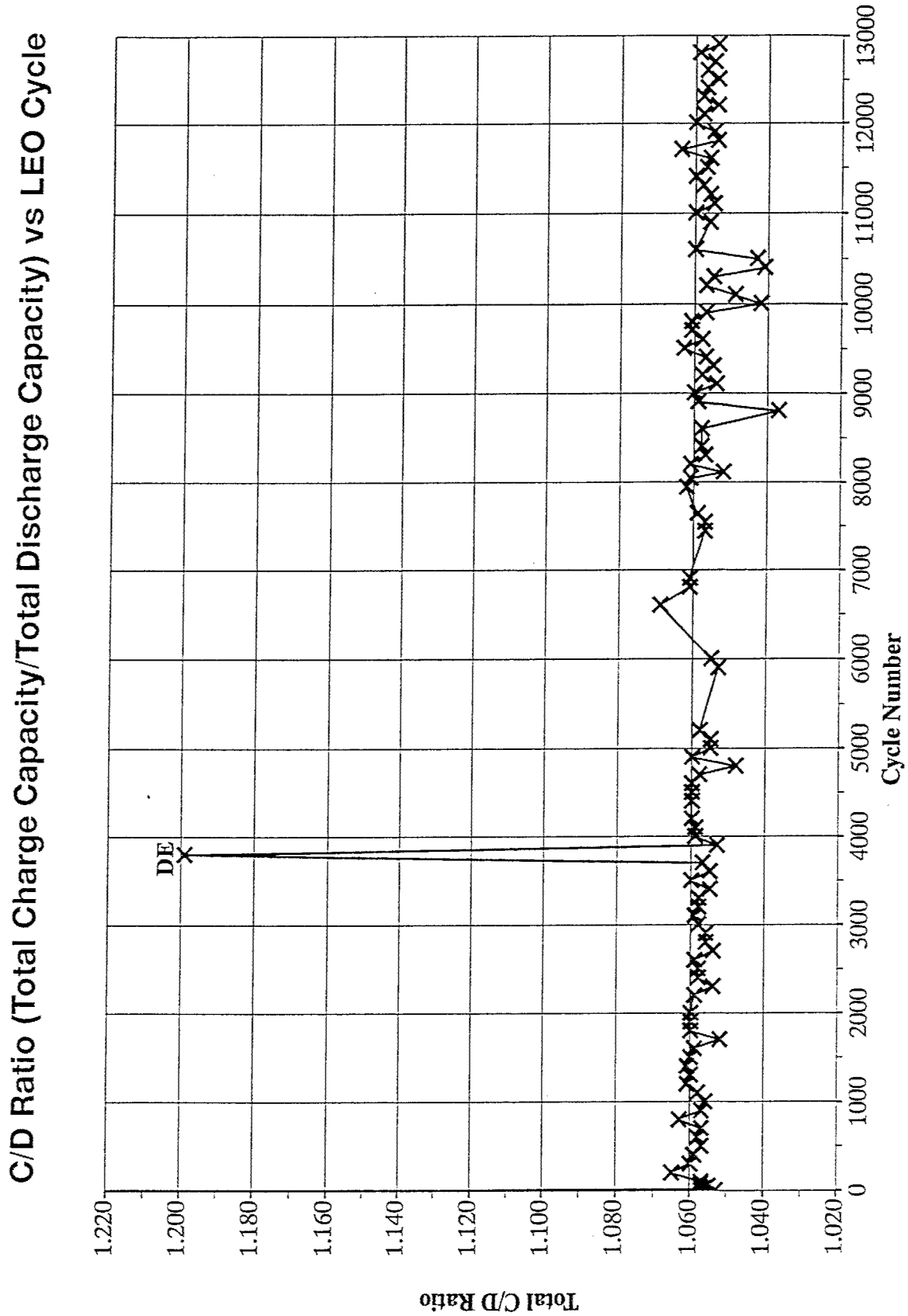

Fig 8

LOCKHEED MARTIN

Cell 1 Pressure vs LEO Cycle

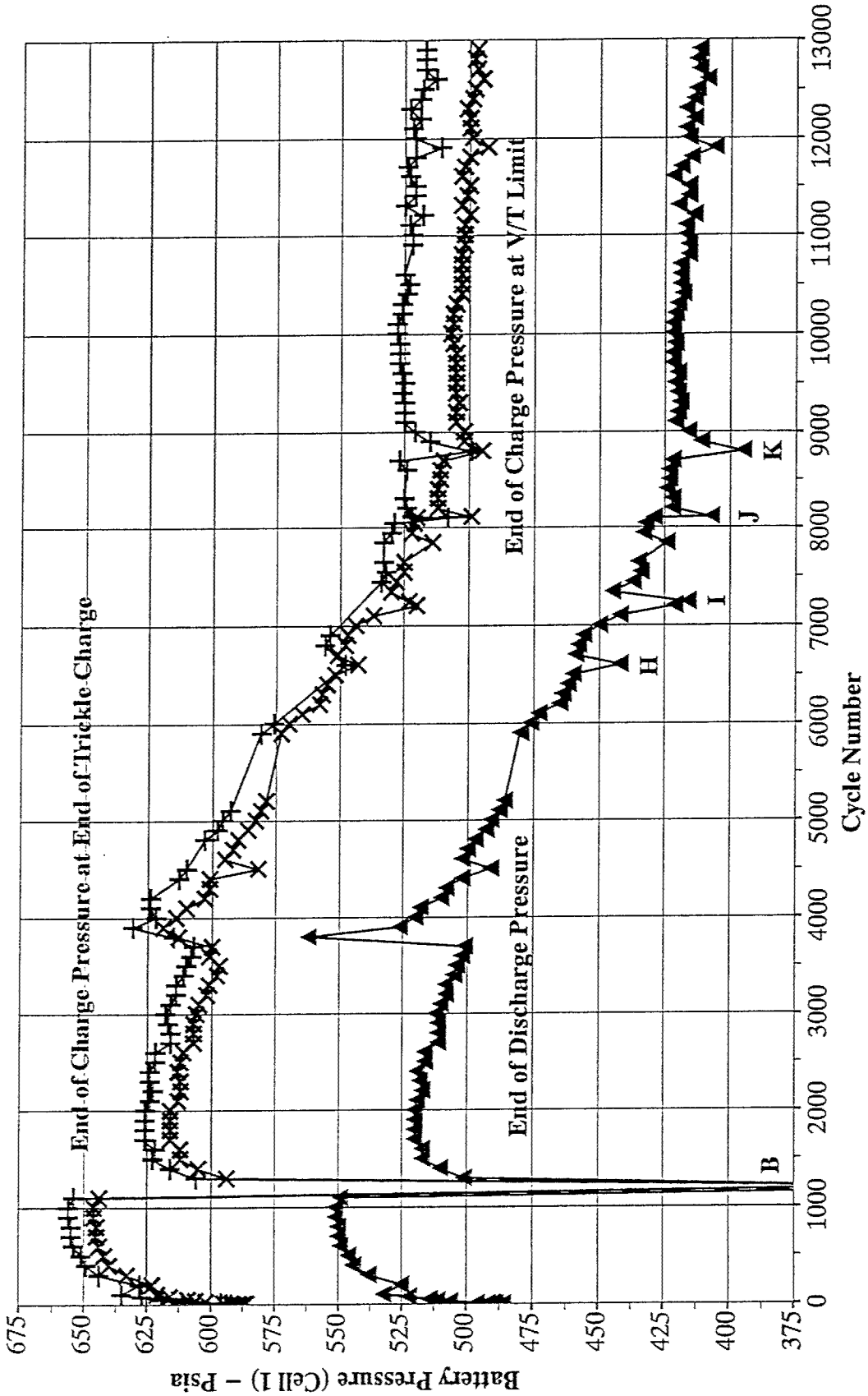

Fig 9

LOCKHEED MARTIN

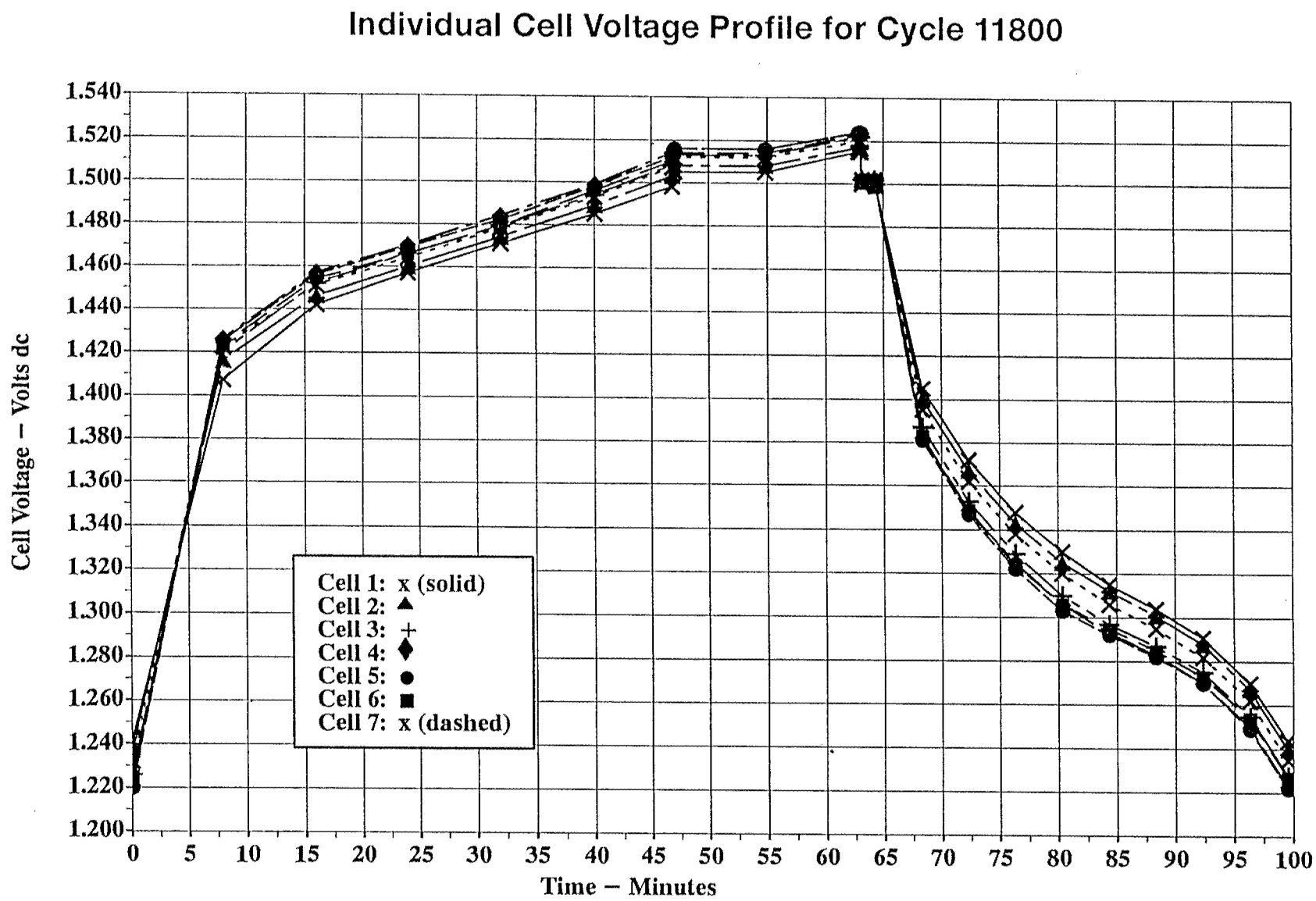

Fig 10

LOCKHEED MARTIN

Individual Cell Voltage Profile (Charge Regime) for Cycle 11800

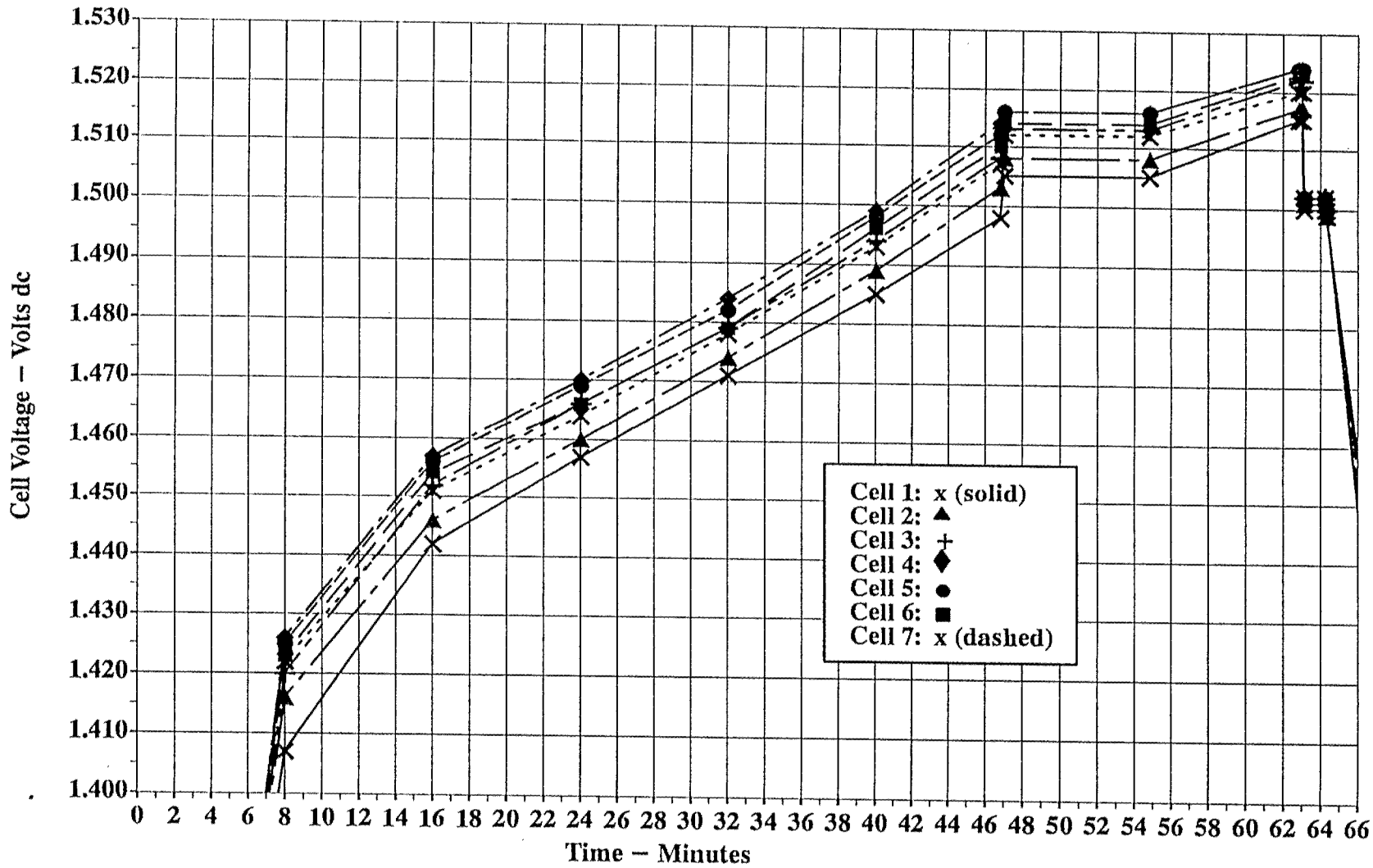

Fig 11

LOCKHEED MARTIN

Individual Cell Voltage Profile (Discharge Regime) for Cycle 11800

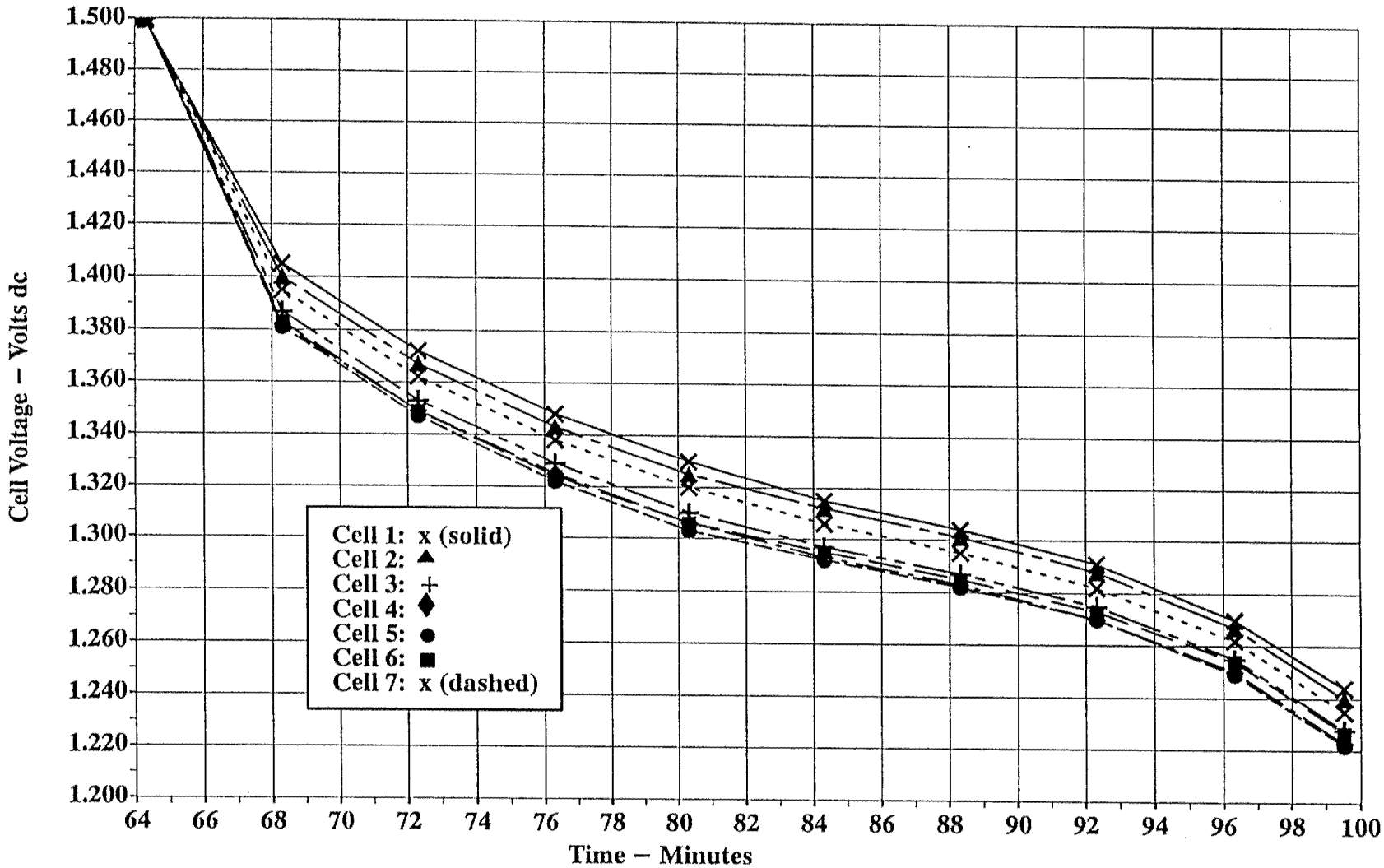

Fig 12

LOCKHEED MARTIN

Individual Cell Pressure Profile for Cycle 11800

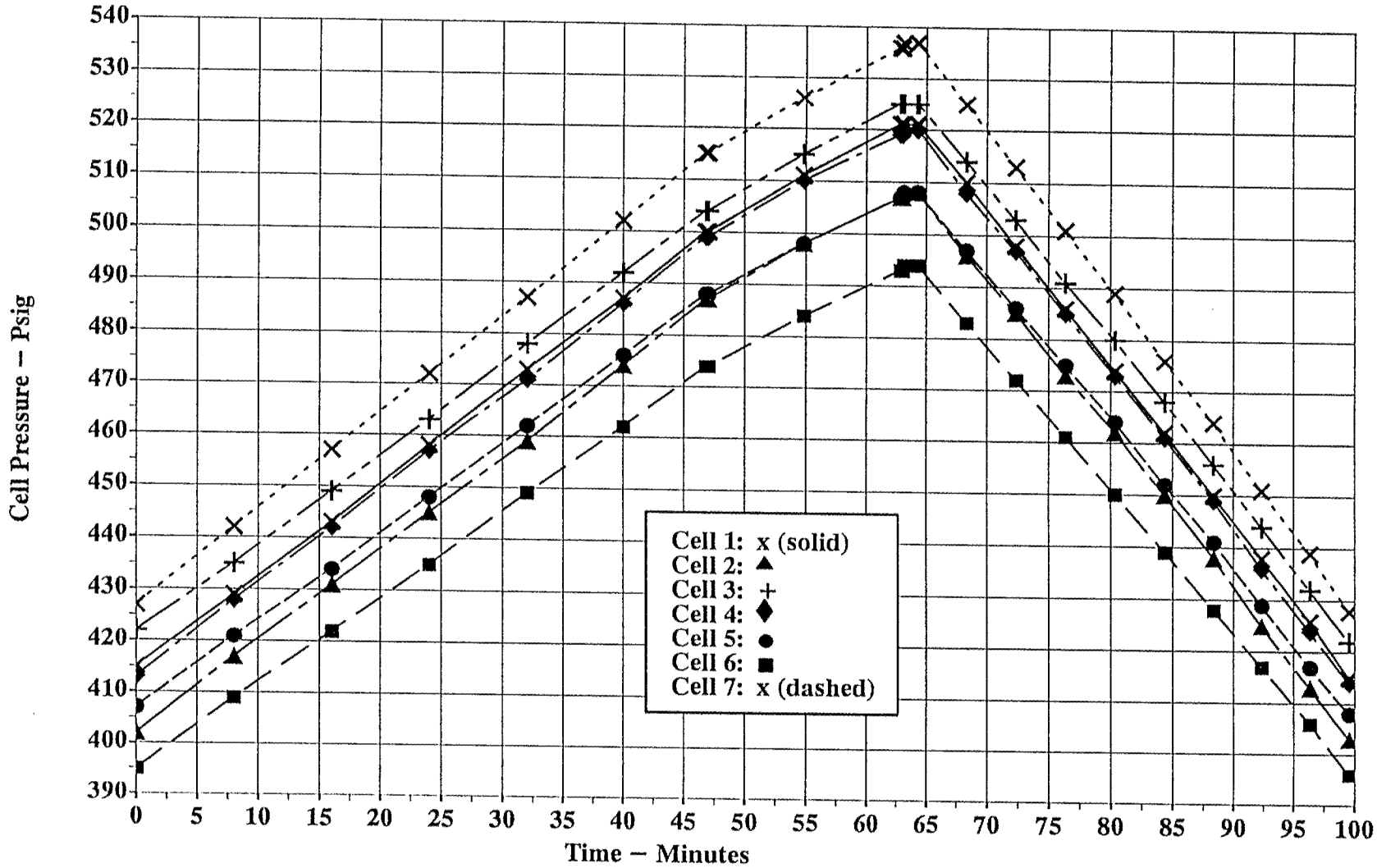

Fig 13

LOCKHEED MARTIN

Cell 1 Temperature Profile for Cycle 11800

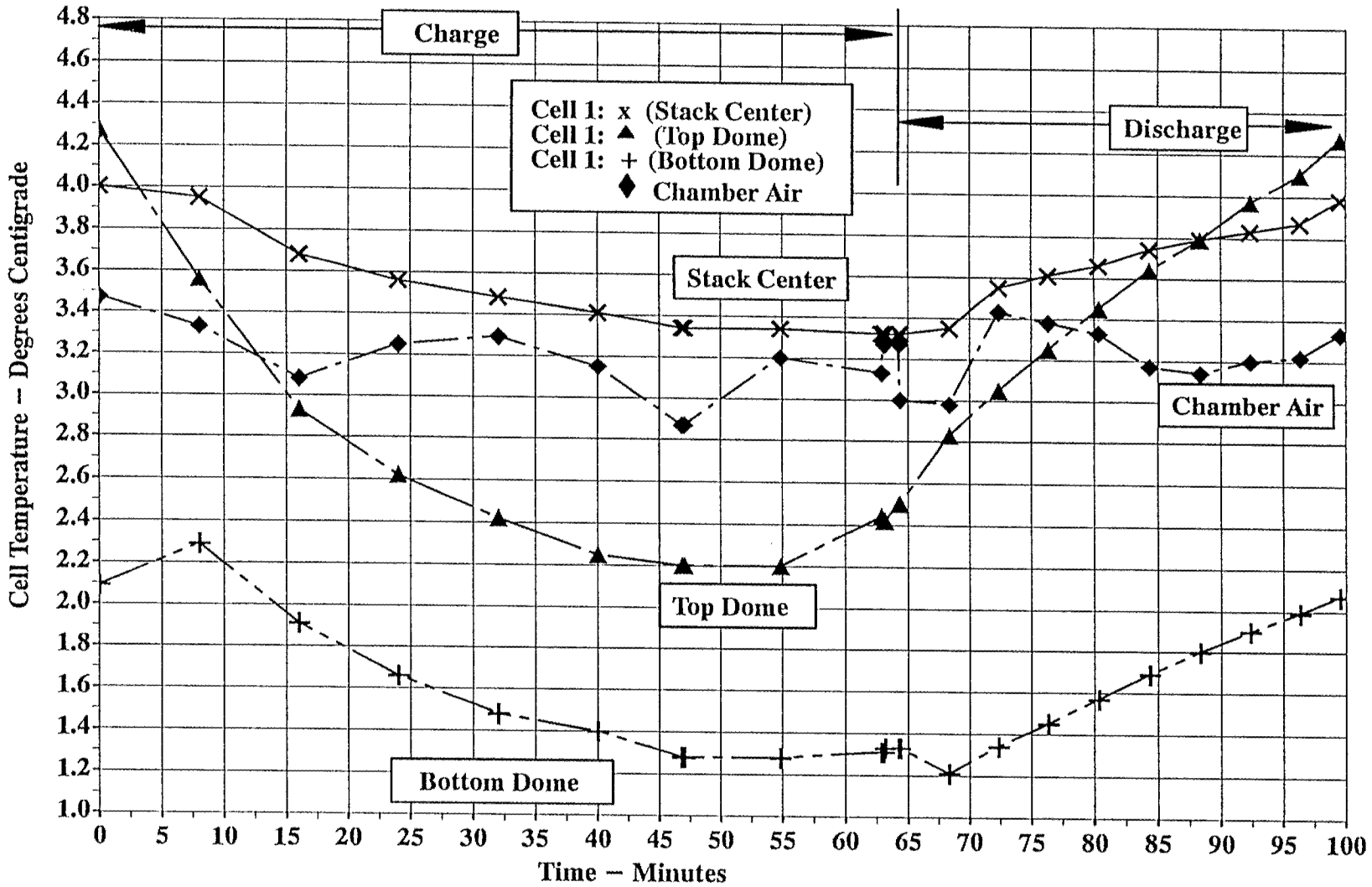

Accelerated Stress Test Conditions

COMSAT LABORATORIES

- Performed at COMSAT Laboratories
- Number of cells: 5
- Cell configuration:
  - Machined aluminum sleeves
  - Mounted on a cold plate
  - Chotherm and RTV 566 isolation
- Test temperature: 10°C
- Discharge regime: 60 amperes for 30 minutes
- Depth of discharge: 60%
- Charge regime:
  - 40 ampere to 1.54 V/T (per cell), taper to 1.09 C/D, 0.6 A trickle
  - 60 minute total charge time

Fig 14

COMSAT LABORATORIES

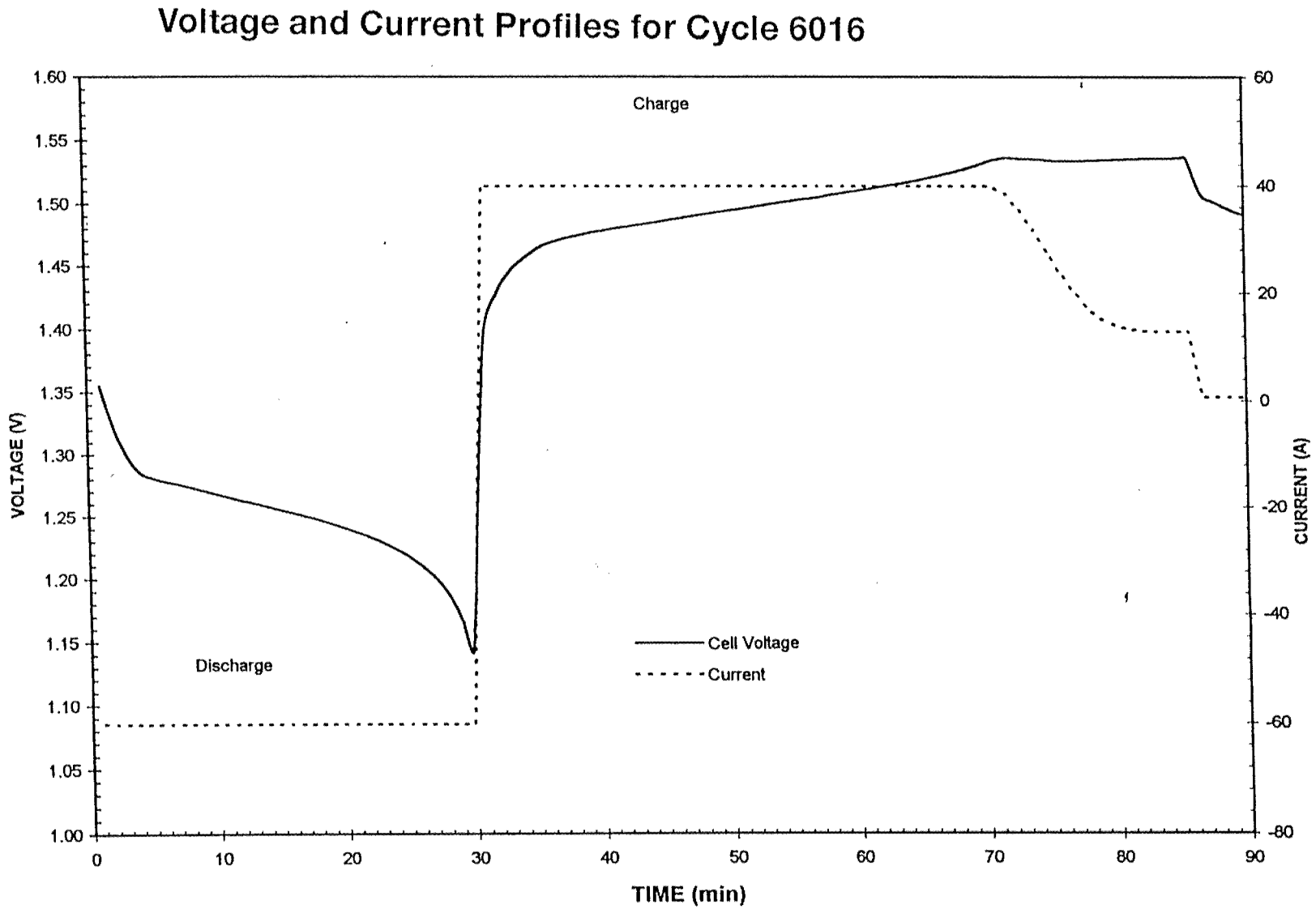

Fig 15

COMSAT LABORATORIES

Variation of C/D Ratio with Cycling

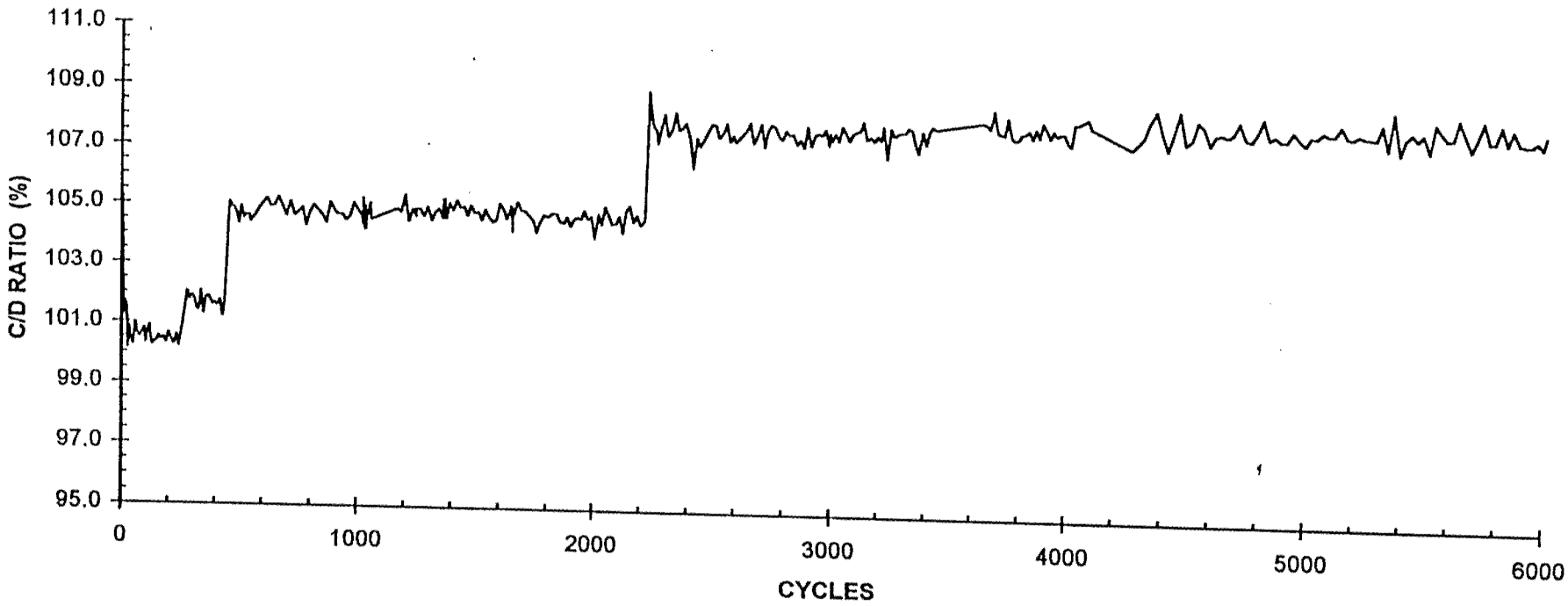

Fig 16

COMSAT LABORATORIES

Variation of Temperature with Cycling

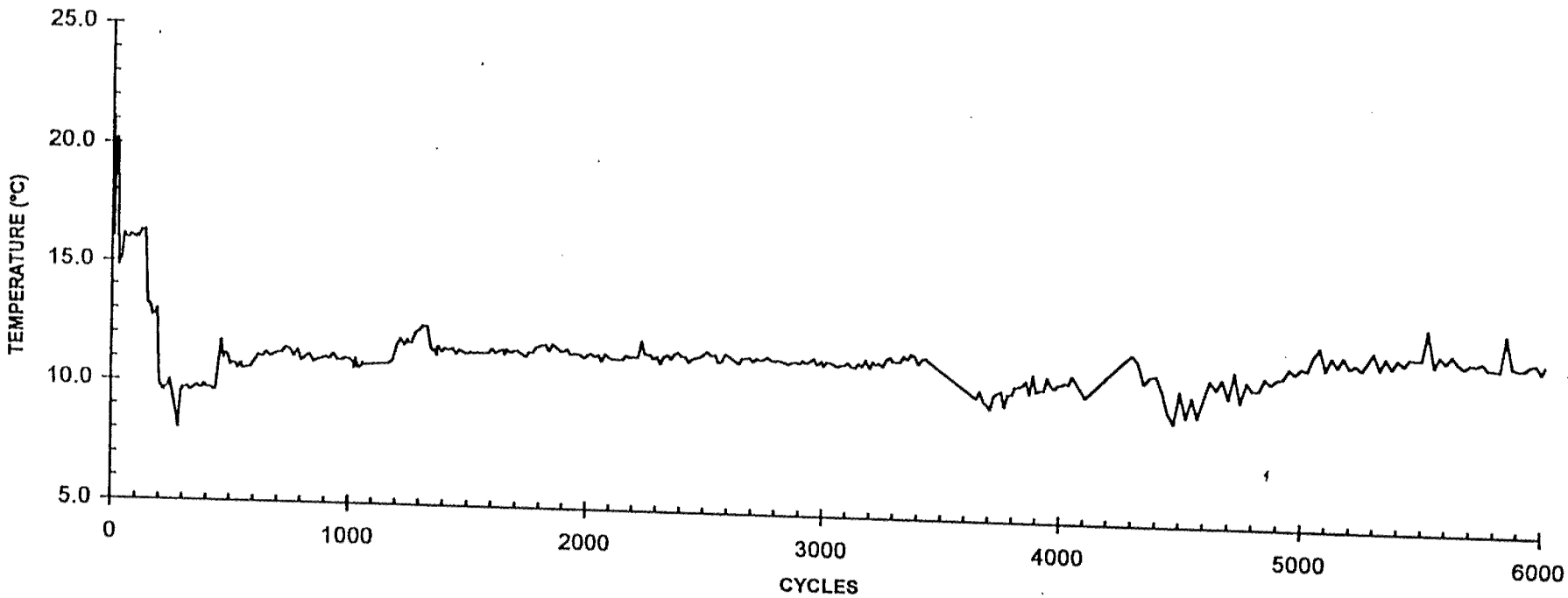

Fig 17

COMSAT LABORATORIES

Variation of End of Discharge Voltage with Cycling

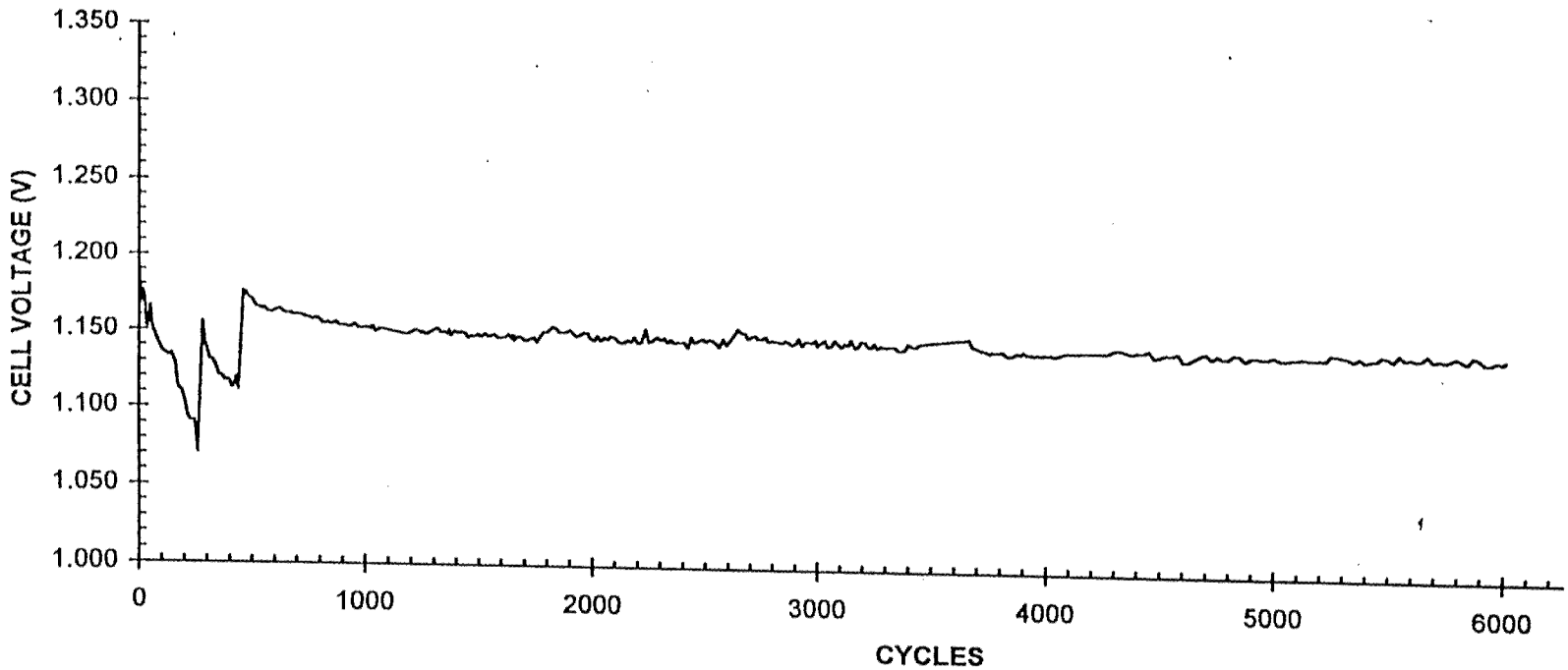

Fig 18

COMSAT LABORATORIES

Variability in the End of Discharge Voltage Among Cells

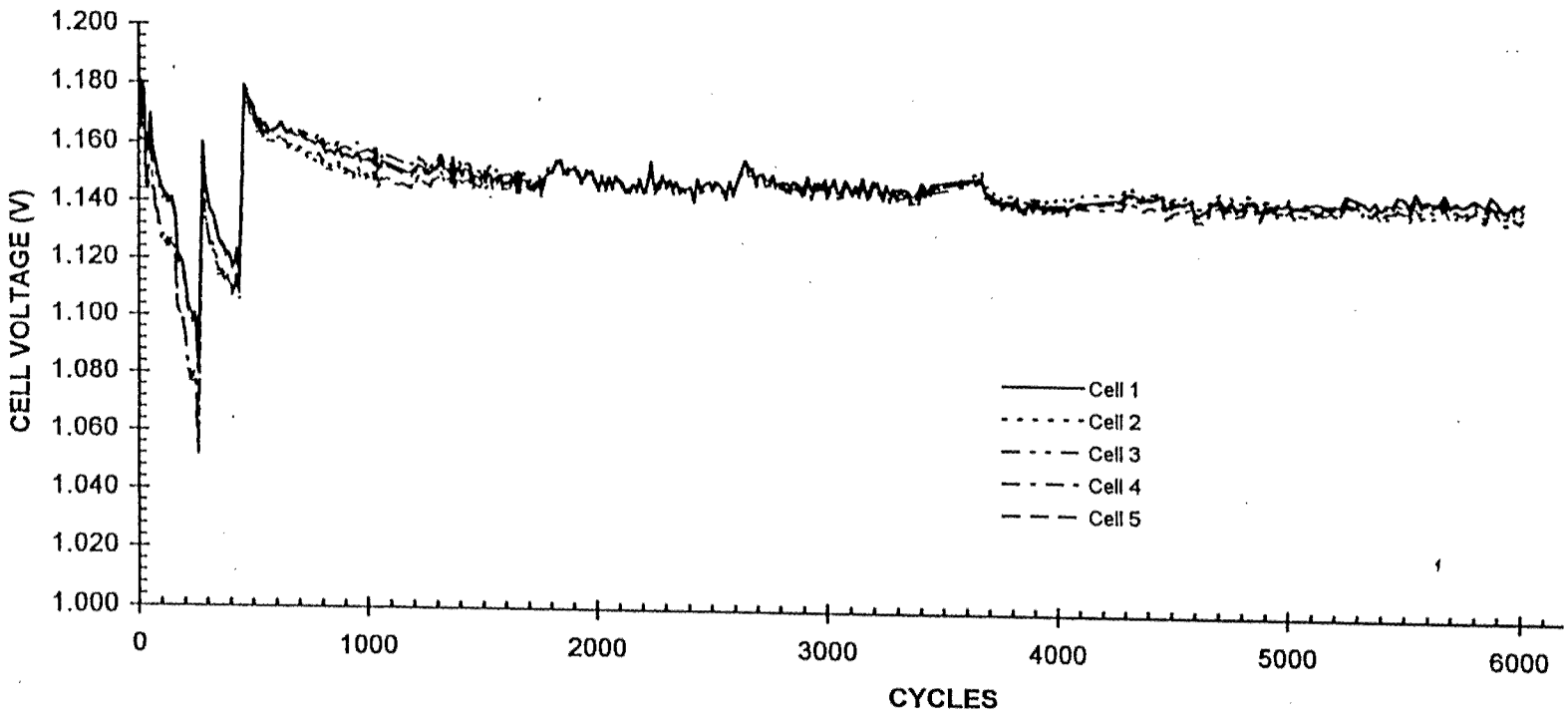

Fig 19

COMSAT LABORATORIES

Variation of End of Charge Pressure with Cycling

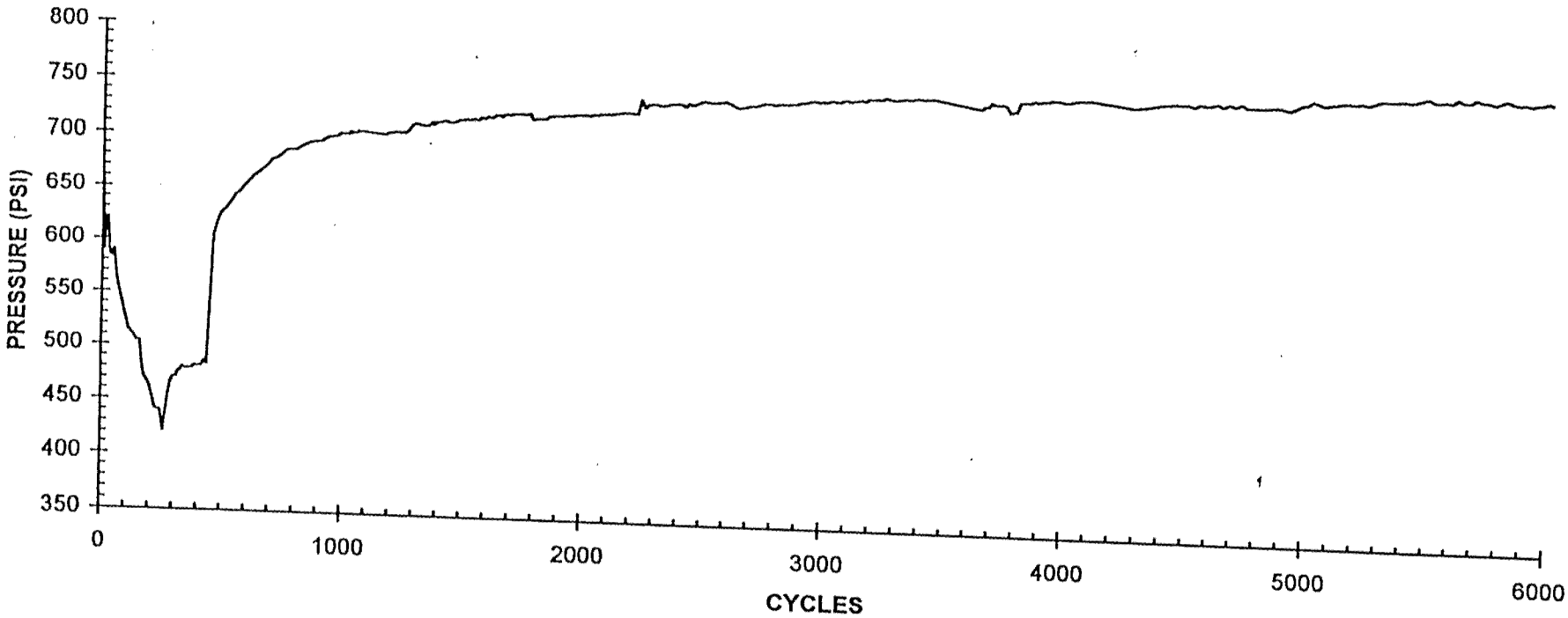

Fig 20

COMSAT LABORATORIES

Variation of End of Discharge Pressure with Cycling

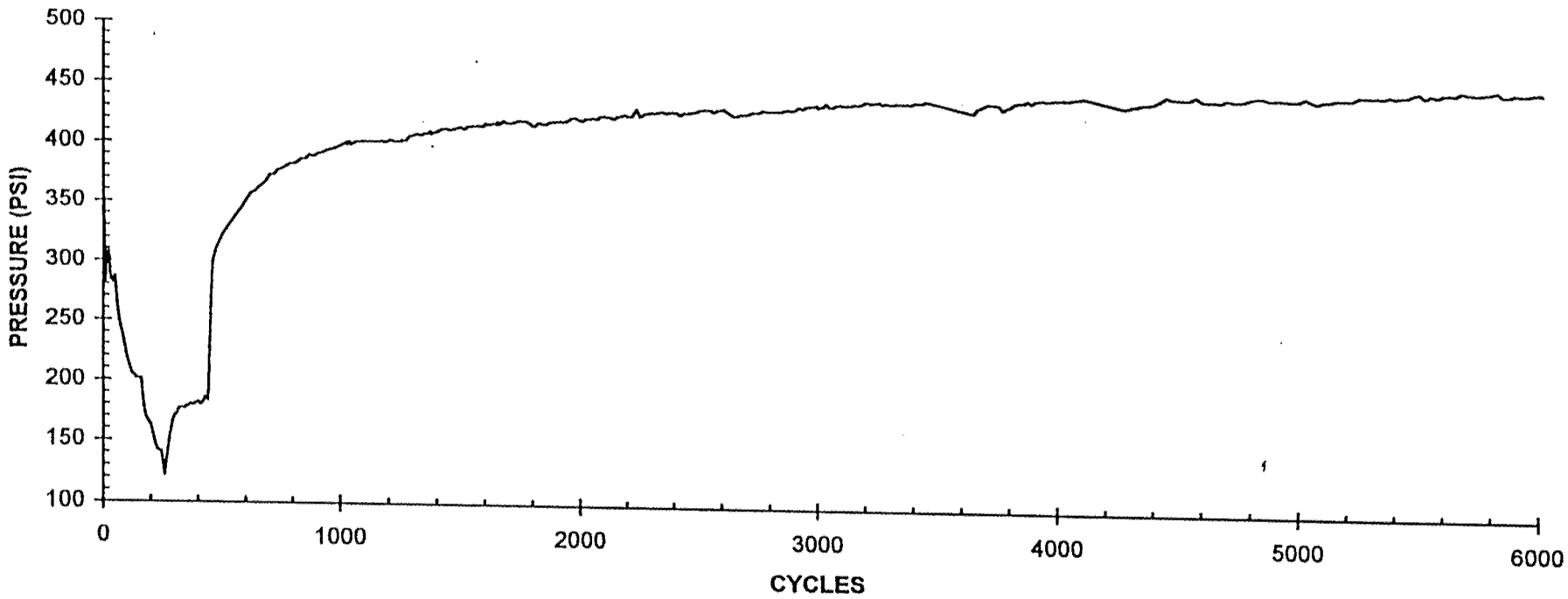

Summary and Conclusions

LOCKHEED MARTIN

- Real–time LEO life test at Lockheed Martin Missles and Space
  - Cells have completed 14300 cycles as of 12/2/96
  - End of discharge voltage decreased initially and has stabilized
  - Variation in end of discharge cell voltage has converged with cycling
  - Cell EODP and EOCP stabilized after 8000 cycles
    - 1.51 V/T limit and 1.06 C/D insufficient to makeup for early test problems (cells on open circuit during all test outages)
  - A reconditioning cycle (first cell to 1.000 volt) is scheduled to be performed
    - Sequence will replicate spacecraft operations
- Accelerated LEO stress test at COMSAT Labs.
  - Cells have completed 6015 cycles
  - End of discharge voltage decreased initially and has stabilized
  - Charge termination at 1.54 V and 1.09 C/D is appropriate for 60% DOD cycling
  - Pressure increased with cycling and has stabilized in 6000 cycles

Page
32
Blank

SSTI - LEWIS SPACECRAFT NICKEL-HYDROGEN BATTERY

R.F. TOBIAS
TRW SPACE AND ELECTRONICS GROUP
REDONDO BEACH, CALIFORNIA

THE 1996 NASA AEROSPACE BATTERY WORKSHOP
THE HUNTSVILLE HILTON
HUNTSVILLE, ALABAMA
DECEMBER 3-5, 1996

PRESENTATION OVERVIEW

- NASA SSTI OBJECTIVES
  (SMALL SPACECRAFT TECHNOLOGY INITIATIVE)
- SSTI - LEWIS OVERVIEW
- BATTERY REQUIREMENT
- TWO CELL CPV DESIGN SUMMARY
- CPV ELECTRICAL PERFORMANCE
- BATTERY DESIGN SUMMARY
- BATTERY FUNCTIONAL DESCRIPTION
- BATTERY PERFORMANCE

SSTI OBJECTIVES

- REDUCE COST AND SCHEDULE OF CIVIL SPACE MISSIONS
- PRODUCE MORE ACCESSIBLE RESULTS
- TRANSITION GOVERNMENT AND INDUSTRY TECHNOLOGY TO THE CIVIL SPACE SECTOR

SSTI - LEWIS OVERVIEW

- MAXIMIZE TECHNOLOGY TRANSFER FROM MILITARY TO CIVIL SPACE APPLICATIONS
- MORE THAN 40 NEW TECHNOLOGIES
  - NiH2 CPV INCLUDED
- 517 KM, 97.4 ° INCLINATION SUN SYNCHRONOUS ORBIT
- 5 YEAR LIFETIME GOAL
- FULLY REDUNDANT SUBSYSTEM ELECTRONICS
- 2 YEAR FAST-TRACK SCHEDULE SPAN
  - DESIGNED MAJOR MODULES SO THEY COULD BE INTEGRATED AND TESTED INDEPENDENTLY OF EACH OTHER
  - REDUCED CUSTOMER SURVEILLANCE

- THREE SCIENCE PAYLOADS WILL PROVIDE MEANINGFUL SCIENCE AND REMOTE-SENSING DATA TO A BROAD RANGE OF CIVIL AND COMMERCIAL USERS

  - EARTH OBSERVATION (TRW-HYPERSPECTRAL IMAGER)
  - COMMERCIAL REMOTE SENSING (NASA GODDARD-LINEAR ETALON IMAGING SPECTRAL ARRAY)
  - ASTROPHYSICS (UCB- ULTRAVIOLET COSMIC BACKGROUND)

BATTERY REQUIREMENTS

- LEO ORBIT- 95 MINUTE ORBIT (35.3 MINUTE ECLIPSE)
- 5 YEAR GOAL - 30,000 CYCLES
- MAXIMUM DEPTH OF DISCHARGE - 30%
- NORMAL OPERATING VOLTAGE RANGE - 24.0 TO 38.4 VOLTS
- ECLIPSE DISCHARGES AT APPROXIMATELY- 0.5 C
- BATTERY CLAMP TO THE BUS

CPV DESIGN

- EPI MANTECH DESIGN: RNHC-23-1
- DUAL-STACK: 2-23AH CELLS/VESSEL
- TERMINALS: RABBIT EARS
- POSITIVE ELECTRODE: 30-MIL, SLURRY SINTER
  36 (18 PER STACK)
  80% SINTER POROSITY
  1.65 GM/CC ACTIVE MATERIAL LOADING
- SEPARATOR: DOUBLE LAYER ZIRCAR

• PRECHARGE:	NICKEL
• PRESSURE VESSEL:	23-MIL ,INCONEL 718
• INTERNAL COATING:	ZIRCONIUM OXIDE WALL-WICK WITH Pt-CATALYST RECOMBINATION SITES
• DIMENSIONS:	3.506 INCH DIAMETER 7.60 INCH OVERALL LENGTH
• WEIGHT	MAXIMUM VESSEL WEIGHT- 1400 GM VESSEL LOT- AVERAGE 1380 GM

CPV RABBIT EAR "DUAL STACK"

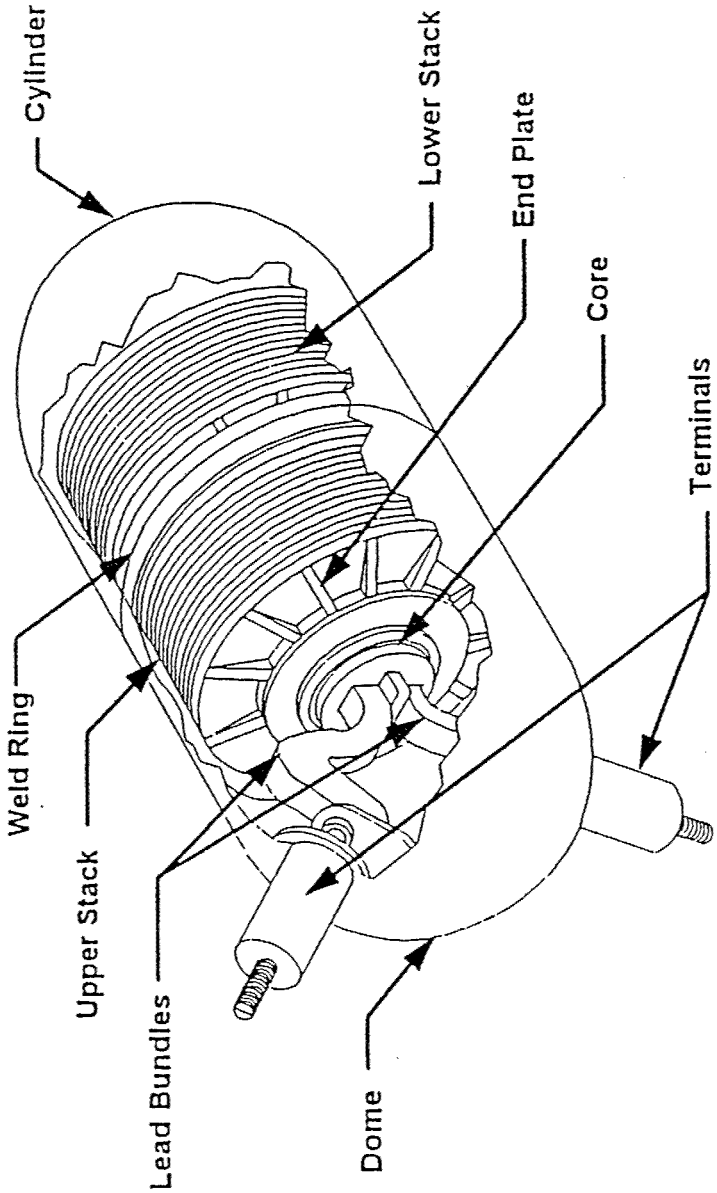

ELECTRODE STACK ASSEMBLY

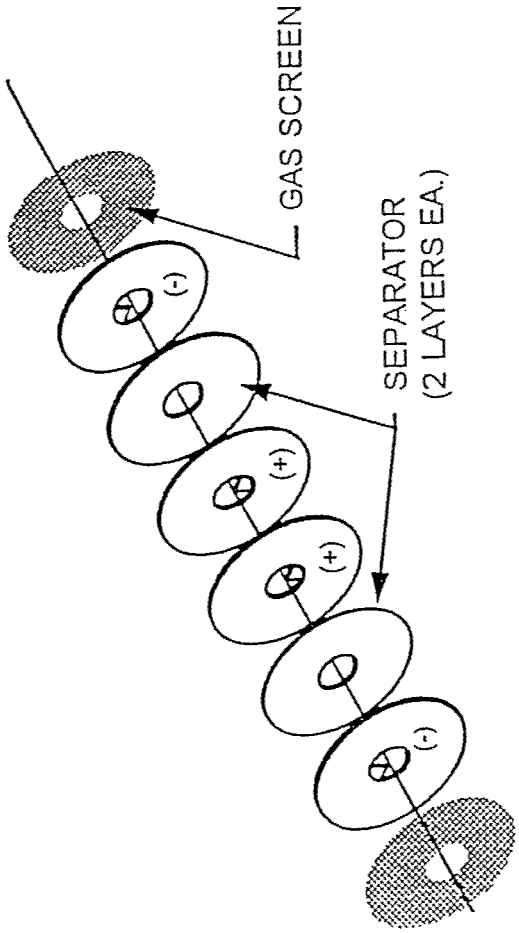

CELL ASSEMBLY CONFIGURATION

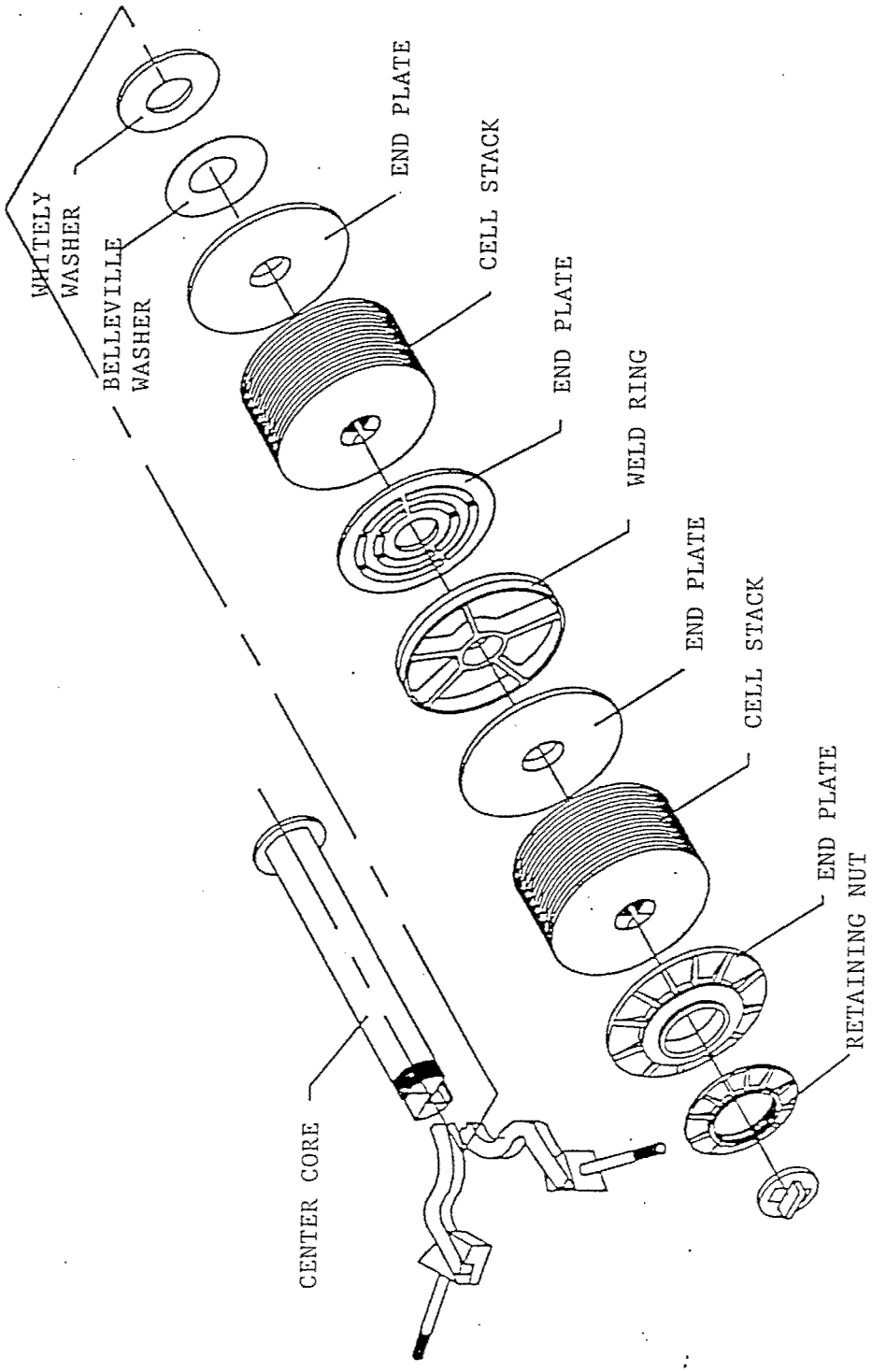

- TEFLON COATED WELD RING
  - ELECTROLYTE IMBALANCE MITIGATION

TEFLON COATED SURFACES

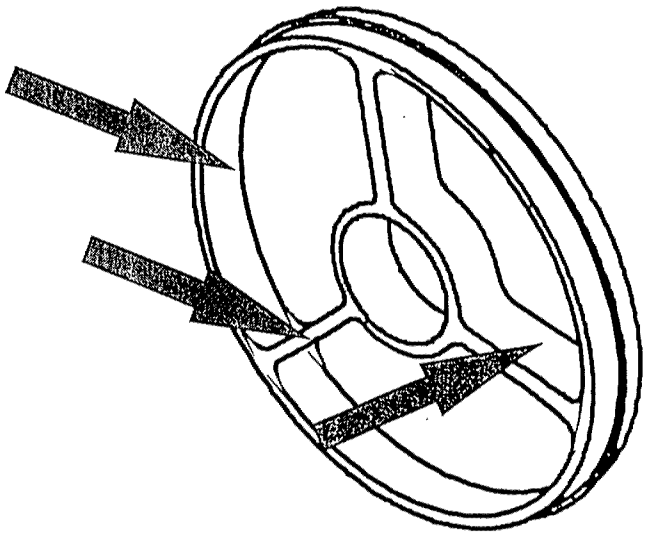

CPV PERFORMANCE DATA

- ATP TESTING PERFORMED ON 19 VESSELS
- ALL CAPACITIES DETERMINED TO 2.0 VOLTS
- TEST RESULTS

TEMPERATURE	EOCV	CAPACITY
20°C	2.996	24.2 AH
10°C	3.077	28.5
0°C	3.154	30.8

- CHARGE RETENTION CAPACITY AT 10°C = 25.7 AH (90.3%)
- OVERCHARGE AFTER 50 HOURS AT 1.5 AMPS AT 10°C = 3.075 VOLTS

BATTERY DESIGN

- TWELVE 23 AH NICKEL-HYDROGEN CPV's IN SERIES
- BATTERY CONFIGURATION CONSISTS OF SIX (6) MODULES OF TWO CPV's DISTRIBUTED AROUND INBOARD SIDE OF AFT FACING BATTERY RADIATOR
- BATTERY OCCUPIES 6 OF 7 BAYS IN BATTERY/ PROPULSION MODULE
- HEAT PIPE IS USED TO SPREAD HEAT EVENLY BETWEEN ALL 7 BPM BAYS

BATTERY LAYOUT

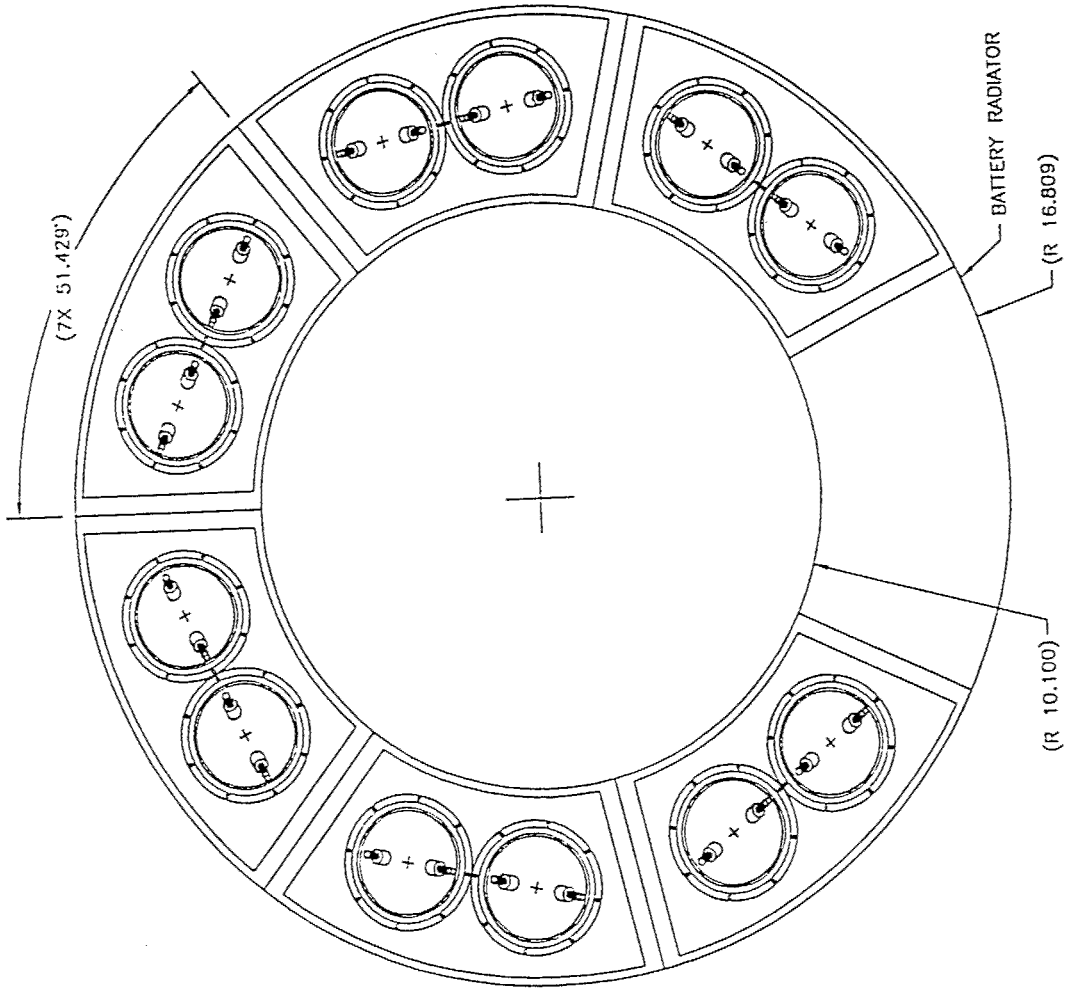

BATTERY TEMPERATURES WITHOUT HEATPIPE

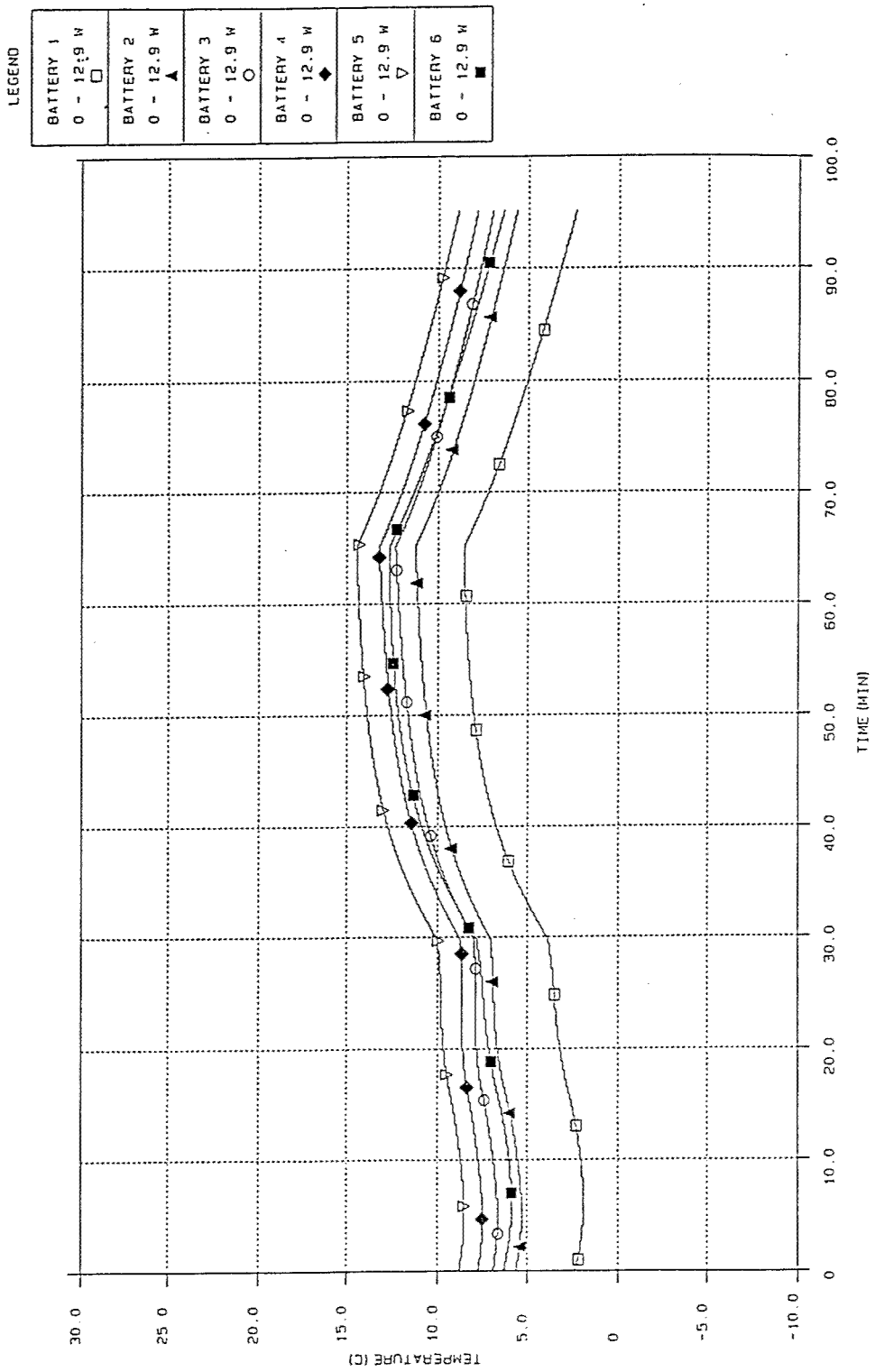

BATTERY TEMPERATURES WITH HEATPIPE

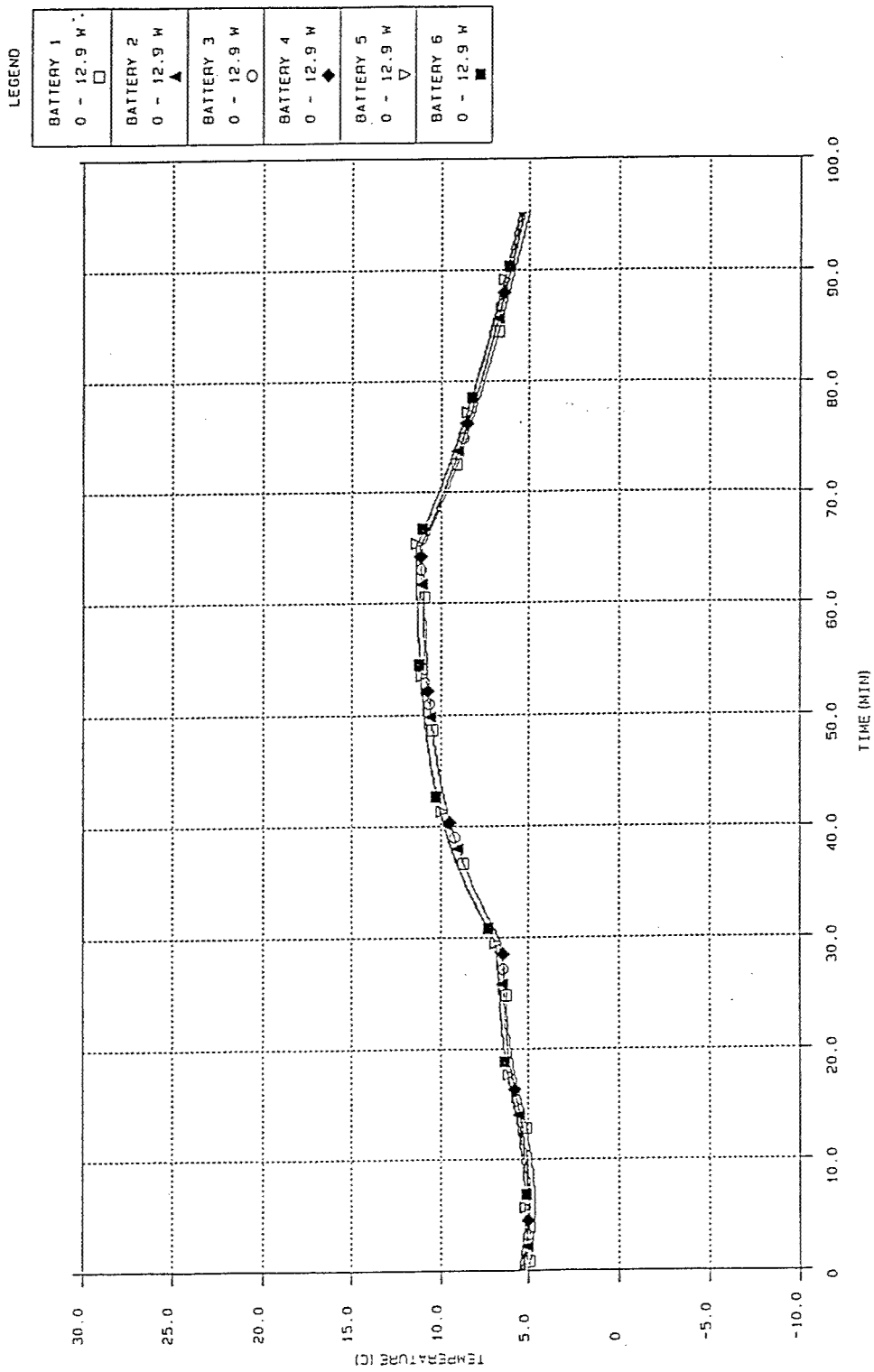

MODULE ASSEMBLY

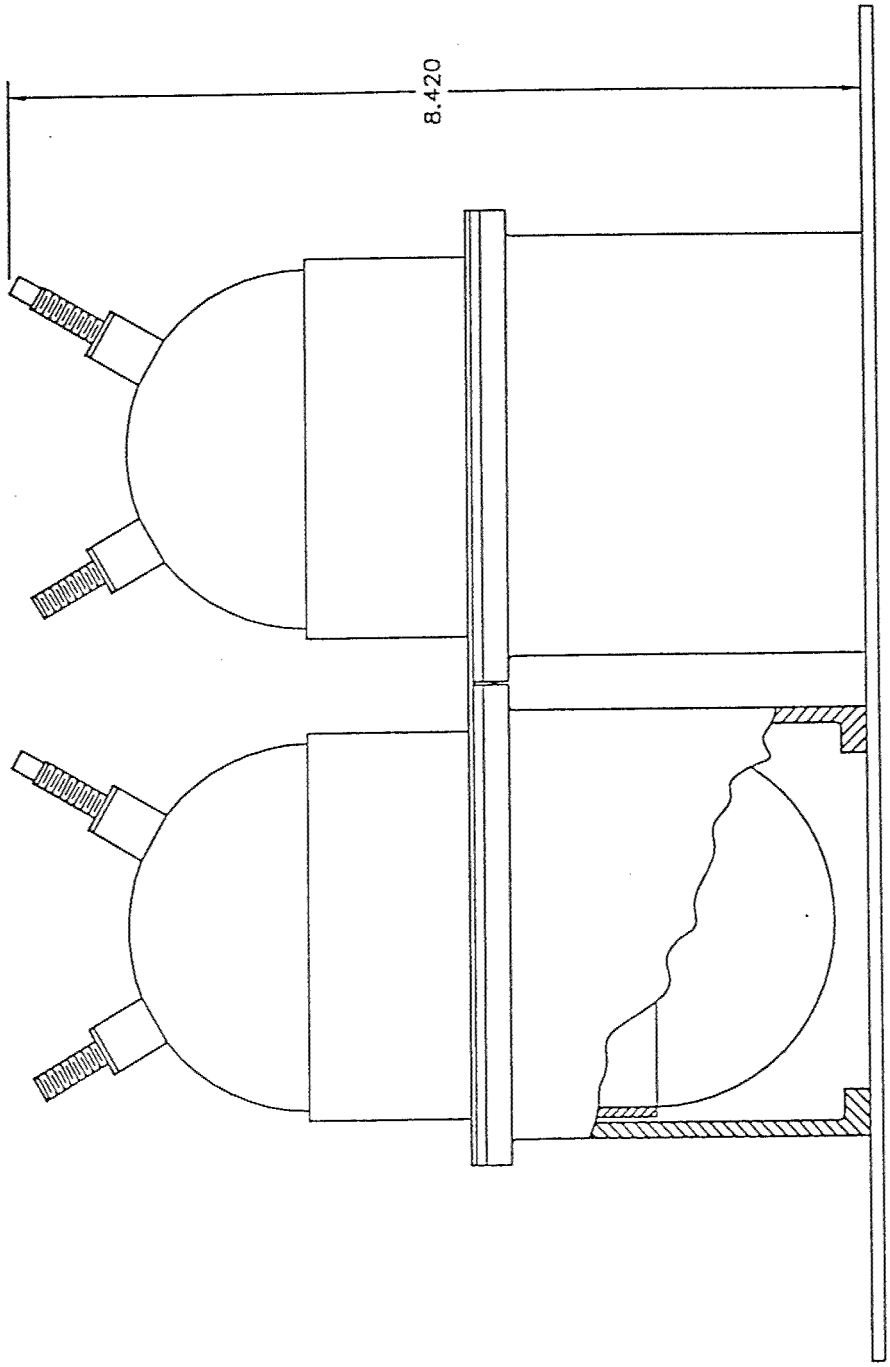

- CELL HEAT IS PASSIVELY CONDUCTED FROM THE CELL TO THE BASEPLATE WHICH RADIATES DIRECTLY TO SPACE

- EACH VESSEL IS CONTAINED WITH A THERMAL SLEEVE AND MOUNTING FLANGE WHICH IN TURN ARE MOUNTED TO ALUMINUM SLEEVES PERPENDICULAR TO THE BASE-PLATE

- BATTERY WEIGHT: 55.5 LB.

BATTERY VESSEL MOUNTING

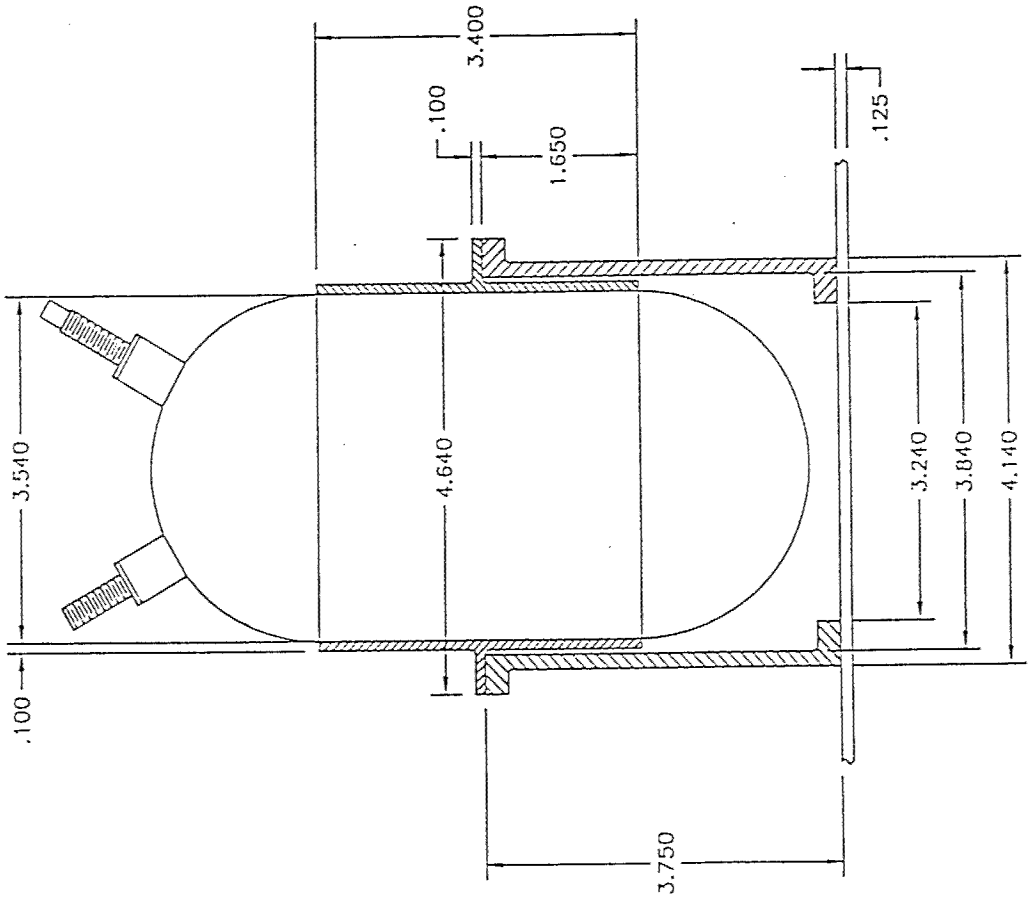

BATTERY FUNCTIONAL DESCRIPTION

- CHARGE
  - PRIMARY CHARGE CONTROL IS PROVIDED BY AH INTEGRATION PERFORMED BY THE OBC
  - CHARGE RATE IS THREE STEP PROCESS WITH RECHARGE RATIOS NOT EXCEEDING 1.10
    1. INITIAL CURRENT OF 0.4 C
    2. TAPER CURRENT
    3. FINISH CHARGE AND OVERCHARGE AT 0.2 C
  - BACKUP CHARGE CONTROL IS PROVIDED BY SENSING BATTERY TEMPERATURE TURNAROUND AT THE ONSET OF OVERVOLTAGE
  - CHARGE VOLTAGE SHALL NOT EXCEED 38.4 VOLTS

- DISCHARGE
  - BATTERY IS CAPABLE OF PROVIDING AT LEAST 325 WATTS DURING A 35.3 MINUTE ECLIPSE AT A DOD NOT EXCEEDING 30%

- RECONDITIONING
  - NOT INCLUDED IN THE BASELINE DESIGN

- THERMAL CONTROL FEATURES PERMIT OPERATION WITHIN THE FOLLOWING CONSTRAINTS
  - BATTERY ORBITAL AVERAGE TEMPERATURE SHALL BE NO GREATER THAN 10°C
  - TEMPERATURE GRADIENT BETWEEN HOTTEST AND COLDEST VESSELS SHALL NOT EXCEED 3°C
  - TEMPERATURE GRADIENT BETWEEN CELLS WITHIN A VESSEL SHALL NOT EXCEED 1°C

BATTERY PERFORMANCE

- 12 VESSELS
- VESSEL SELECTION
  - CAPACITY VARIATION AT 10°C : LESS THAN ± 1%
  - EOCV SPREAD AT 20°C: WITHIN 5 MV
- CAPACITY AT 10°C : 28.43 AH
- CHARGE RETENTION AT 10°C : 24.84 AH (87.4%)

Page
404
Blank

NEW DEVELOPMENTS IN NICKEL-HYDROGEN DEPENDENT PRESSURE VESSEL (DPV) CELL AND BATTERY DESIGN

Dwight B. Caldwell, Chris L. Fox, and Lee E. Miller
Technologies Division, Eagle-Picher Industries, Inc.
P.O. Box 47
Joplin, MO 64802
(417) 623-8333

Abstract

The Dependent Pressure Vessel (DPV) Nickel-Hydrogen (NiH2) design is being developed by Eagle-Picher Industries, Inc. (EPI) as an advanced battery for military and commercial, aerospace and terrestrial applications. The DPV cell design offers high specific energy and energy density as well as reduced cost, while retaining the established Individual Pressure Vessel (IPV) technology flight heritage and database. This advanced DPV design also offers a more efficient mechanical, electrical and thermal cell and battery configuration and a reduced parts count. The DPV battery design promotes compact, minimum volume packaging and weight efficiency, and delivers cost and weight savings with minimal design risks.

INTRODUCTION

The NiH2 battery has a number of unique features and advantages which are superior to other battery systems. Hydrogen provides a very lightweight, efficient energy storage material. Due to the unique electrochemistry, the NiH2 system is an inherently fault-tolerant design with excellent overcharge, overdischarge and deep-cycle capabilities. The battery is hermetically sealed and truly maintenance-free. The internal hydrogen pressure is a direct linear function of battery state-of-charge (SOC) and thereby provides a simple and reliable method of determining the SOC of the battery. Also, the NiH2 battery contains no toxic materials such as lead, cadmium or mercury and can be readily recycled. Projected battery costs are directly comparable with other nickel battery systems and competitive with lead-based batteries on a life-cycle cost basis.

The NiH2 battery is also the most reliable aerospace battery system available. Batteries have completed more than 180,000,000 cell-hours in orbital spacecraft operation. NiH2 batteries offer the longest cycle life of any battery system. Batteries on test have completed more than 115,000 charge/discharge cycles. Batteries have operated in Geostationary-Earth-Orbit (GEO) for more than 15 years. NiH2 batteries have low internal impedance and excellent high rate and pulse discharge capability. The many advantages and features of the NiH2 battery are the reason the system has been heavily developed for advanced critical applications such as earth-orbital spacecraft. Many of these same features and advantages are also equally desirable in terrestrial applications.

Several distinct NiH2 cell and battery designs are currently in production and under development for a wide variety of applications. These include traditional aerospace applications such as earth-orbital communications satellites, as well as terrestrial uses such as telecommunications equipment, utility load leveling and remote location power systems. Traditional IPV NiH2 technology has been supplemented by newer Common Pressure Vessel (CPV) cell designs and other cell and battery designs such as the Single Pressure Vessel (SPV) and Low Pressure Vessel (LPV) battery. The DPV battery design is the next step in the continued development and evolution of the NiH2 battery system.

DPV CELL DESIGN

A unique feature of the DPV cell design is the prismatic (rectangular) electrode stack. This stacking arrangement is more efficient than the standard cylindrical electrode stack. Also, rectangular cell components produce less waste when cut to size from the stock material which is also rectangular. Die-punching circular electrode, separator and gas screen material leaves a significant amount of unusable scrap material which must be added to the cost of the cell. The electrode stack is the electrochemically active part of the cell. It contains nickel electrodes and hydrogen electrodes interspersed with an absorbent separator material. A back-to-back stacking arrangement is used as shown in Figure 1. This stacking arrangement provides that each nickel electrode is opposed by the catalyst side of a hydrogen electrode. This puts the hydrophobic sides of the two adjacent hydrogen electrodes facing towards each other. A gas spacer is

inserted in order to facilitate hydrogen gas diffusion into and away from the hydrogen electrode during charge and discharge (Francisco 1995).

The pressure vessel geometry is another unique feature of the DPV cell. The cell case consists of two nearly identical, seamless halves. One of the halves is fitted with cell terminal bosses attached by a laser weld. The bosses are offset 15° from a central axis and elevated 30° from the plane of the girth weld as shown in the cell outline drawing in Figure 2. The DPV cell is termed "dependent" because the cell geometry requires the cell to be supported by adjacent cells or endplates in order to contain the hydrogen pressure developed inside the cell during charging. Since the pressure vessel is not required to support the full internal cell pressure, the pressure vessel can be made with a thinner wall thickness and a corresponding weight savings. The rounded edge of the pressure vessel has a relatively small radius, which is very efficient for pressure containment with minimum pressure vessel material (Coates 1995).

A metal stacking bracket holds the electrode stack in place within the cell pressure vessel. Insulation material electrically isolates the electrode stack from the pressure vessel and the stacking bracket. The electrical tabs from the electrodes emerge through a window in the stacking bracket. The lead bundles are stress relieved by introducing an "S" into the leads. This prevents mechanical stress, such as launch vibration, from being transmitted into the electrode/tab connection. Several options are available for the cell terminal/intercell connector. These are based on two types, either mechanical, such as a screw-type connection, or a solder connection between the cell terminal and intercell connector.

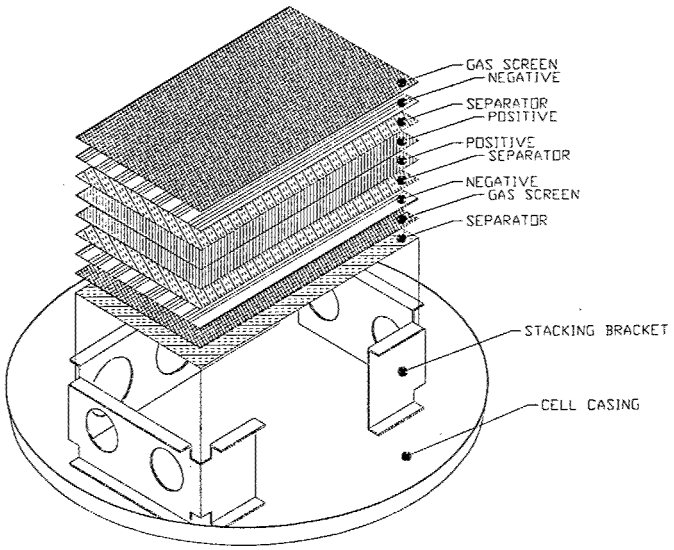

FIGURE 1. DPV Cell Stack.

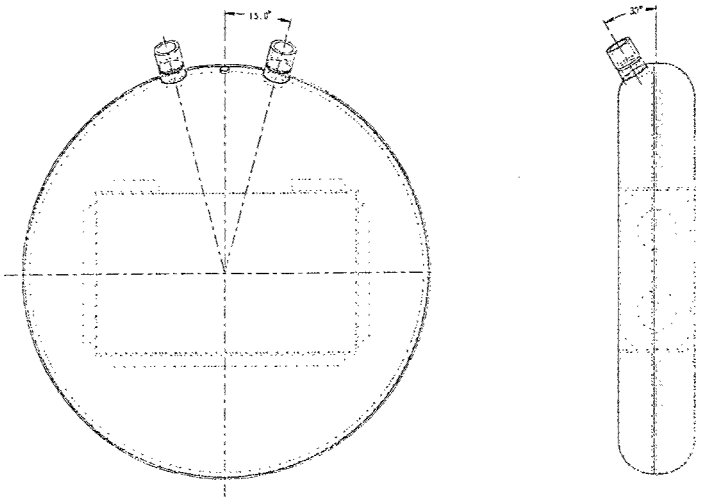

FIGURE 2. Cell Outline Drawing.

CELL DEVELOPMENT STATUS

EPI initial DPV cell development efforts began in 1973 and were first reported in the "26th Power Sources Symposium", 29-30 and 1-2 May, 1974. This effort resulted in the production of a 50 ampere-hour (Ah) rated cell lot. Although subsequent electrical testing was very successful, industry interest at that time continued to be focused in the IPV battery area and further development efforts were discontinued.

In our current development program, EPI has so far produced DPV cells of two sizes: 40 and 60 Ah cells. The first 40 Ah cells were activated in December of 1995. Figure 3 is a design summary of the 40 Ah cell. The stack contains eight positive and negative electrode pairs. Cell testing and cycling commenced in January, 1996, and the cells have consistently produced over 120% of rated capacity at 10°C. Three 40 Ah cells are currently in life-testing on a Low-Earth-Orbit (LEO) program and are doing well. Figure 4 shows charge/discharge data from that ongoing test.

Production of the 60 Ah cell was initiated in January using the same 7.75" diameter pressure vessel as the 40 Ah cell. Figure 5 is a design summary of the 60 Ah cell. Compared with the 40 Ah cell, the 60 Ah stack is longer, wider and thicker, and contains nine positive and negative electrode pairs. Similar to the 40 Ah cells during cell testing/cycling, the 60 Ah cells have consistently produced over 120% of rated capacity at 10°C. We have just commenced life-testing three 60 Ah cells in a LEO regime and will soon place three more in a GEO test profile.

FIGURE 3. 40 AH Cell Design Summary.

Cell Type	*RNHD 40-1*
Nominal Voltage	*1.25 Volts*
Rated Capacity	*40 .0 Ampere-hours*
Actual Capacity	*49.2 Ampere-hours*
No. of Positive Electrodes	*16*
Separator	*Zircar*
Weight	*1235 g.*
Specific Energy	*49.8 WHR/kg*
Diameter	*19.68 cm*
Height	*3.81 cm*
Vessel Wall Thickness	*0.038 cm*
MEOP	*500 psig*
Vessel Safety Factor	*> 2.0 X MEOP*

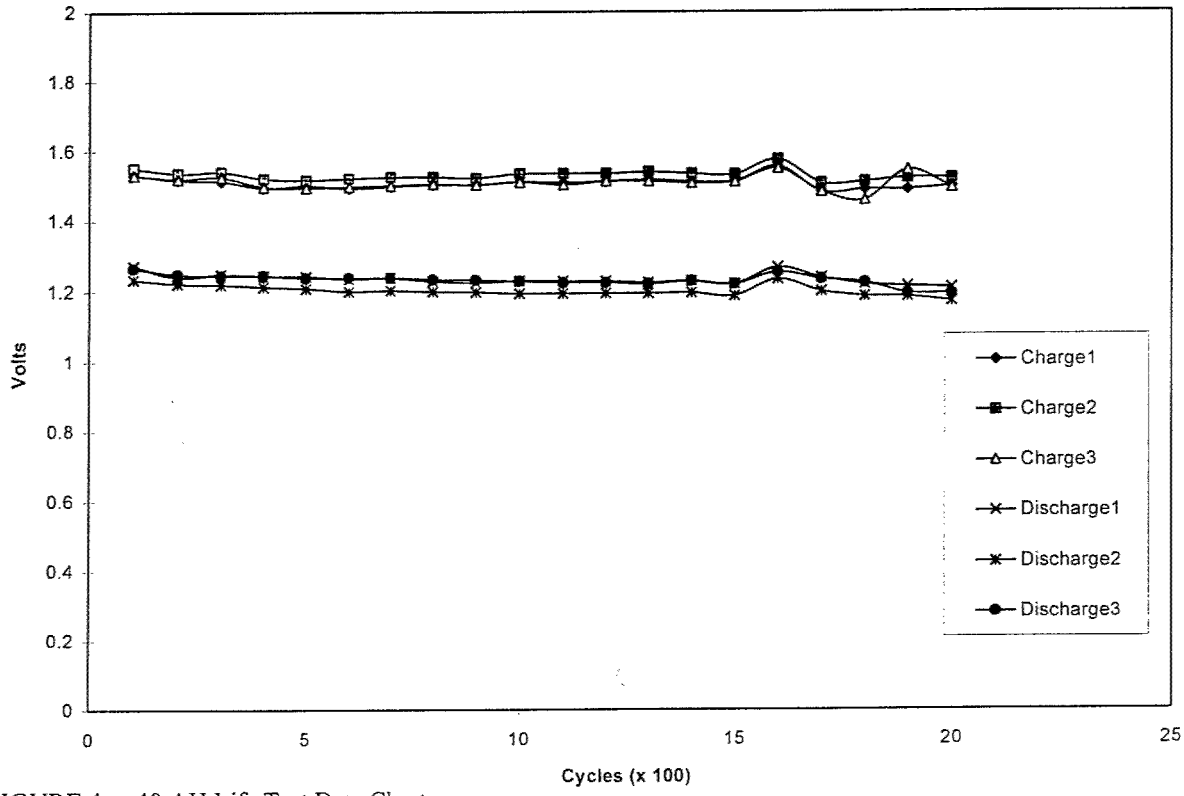

FIGURE 4. 40 AH Life Test Data Chart.

The success of this DPV development program has given EPI invaluable experience and provides a solid foundation to move ahead with further research into DPV applications examining both larger and smaller capacity cells and batteries for a variety of uses.

EPI is now under contract to produce 90 Ah DPV cells. Few changes are anticipated in the design approach for these cells as compared to the development cells described above. Briefly, these changes include: sizing the pressure vessel for a 700 psi maximum expected operating pressure (MEOP) and sizing the stack for the rated 90 Ah capacity. Figure 6 is the preliminary design summary of the 90 Ah cell.

DPV BATTERY DESIGN

The DPV cell is basically an IPV type design in that each pressure vessel contains one cell, and therefore delivers 1.25 VDC. Most applications require voltages which necessitate the connection of multiple cells in series. This is a simple, straightforward concept, however, it is a critical aspect of design for high reliability spacecraft applications. The cells must be packaged into batteries or battery modules which will meet the performance and reliability requirements of the spacecraft. This includes the mechanical, electrical and thermal design of the battery.

Mechanical Design

The mechanical design of the battery addresses primarily the physical aspects of packaging. The cells must be bound together into physically manageable units for handling and spacecraft integration. In fact, the mechanical design is primarily defined by how the battery must physically fit into the spacecraft. Standard practice for battery integration is to mount the battery to a baseplate which is not only the mechanical interface to the spacecraft but also the thermal interface as well. The dimensions of the baseplate are defined by the physical footprint of the battery, the space/volume available in the spacecraft structure and the thermal requirements of the battery/spacecraft interface. The spacecraft configuration must be considered in designing the battery and vice versa.

FIGURE 5. 60 AH Cell Design Summary.

Cell Type	*RNHD 60-1*
Nominal Voltage	*1.25 Volts*
Rated Capacity	*60 .0 Ampere-hours*
Actual Capacity	*73.0 Ampere-hours*
No. of Positive Electrodes	*18*
Separator	*Zircar*
Weight	*1510 g.*
Specific Energy	*60.43 WHR/kg*
Diameter	*19.68 cm*
Height	*3.81 cm*
Vessel Wall Thickness	*0.038 cm*
MEOP	*800 psig*
Vessel Safety Factor	*> 2.0 X MEOP*

FIGURE 6. 90 AH Cell Design Summary.

Cell Type	*RNHD 90-1*
Nominal Voltage	*1.25 Volts*
Rated Capacity	*90.0 Ampere-hours*
Predicted Capacity	*108 Ampere-hours*
No. of Positive Electrodes	*18*
Separator	*Zircar*
Weight	*2200 g. (Est.)*
Specific Energy	*61.4 WHR/kg*
Diameter	*24.41 cm*
Height	*3.81 cm*
Vessel Wall Thickness	*0.038 cm*
MEOP	*700 psig*
Vessel Safety Factor	*>2.0 X MEOP*

One of the advantages of the DPV cell design is that the mechanical battery assembly concept is much simpler than with standard cylindrical IPV cells. The DPV cells are designed to be sandwiched between two endplates, which defines the basic packaging concept for the battery design. It is simple, efficient, easily assembled and requires few parts. A multicell IPV NiH2 battery requires additional parts, such as cell mounting sleeves, which mean additional weight and cost, and additional handling and assembly work. The DPV battery packaging concept has an established heritage in the aerospace industry. The endplate/connecting rod battery design has been used with nickel-cadmium (NiCd) and silver-zinc (AgZn) cells for spacecraft applications for many years. Several battery assembly possibilities exist, which make overall DPV battery design modular and flexible. This makes the DPV battery adaptable for a variety of spacecraft designs. There is a significant advantage of the endplate battery design because the percentage of the total battery weight contributed by the battery packaging components is smaller than with the standard IPV battery.The DPV battery minimizes battery level components (Coates 1995).

The preferred (with respect to optimizing specific energy/energy density) DPV battery assembly presents the cells in a single row sandwiched between two endplates as shown in Figure 7. The endplates are tied together with threaded connecting rods. Mechanical support of the cells is provided by the endplates to support the internal hydrogen pressure developed during charging. Another basic design is shown in Figure 8, where the cells are packaged into two rows. Wiring and connectors are omitted from the figure for clarity. The advantage of two rows of cells is that the overall battery is somewhat more compact. A typical 22 cell, 28 VDC, 60 Ah battery, for example, would be approximately 22

cm wide and approximately 90 cm long for a single row of cells. With two rows of cells, the same battery would be approximately 41 cm wide and 48 cm long. The battery with two rows of cells provides a more nearly square package. A disadvantage is that the larger endplates contribute slightly more weight to the overall battery package. Therefore the single row battery will have slightly higher energy density, but the double row battery will typically be easier to integrate into a spacecraft.

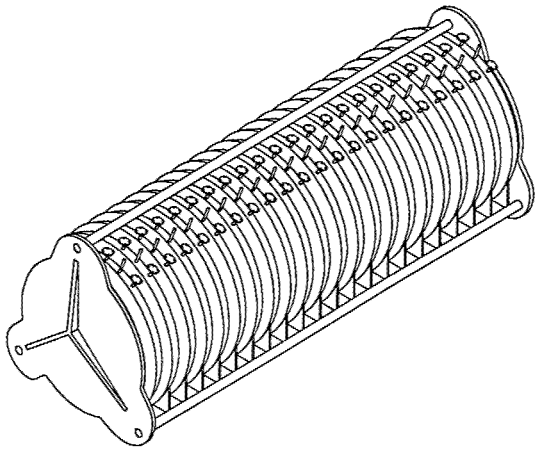

FIGURE 7. Single Row DPV Battery Design.

Electrical Design

The electrical design includes aspects and components such as intercell connection, conductor IR voltage losses, the battery electrical interface, connectors, battery monitoring, charge controllers and battery electronics such as strain gauges, strain gauge amplifiers, heaters, heater controllers, cell bypass diodes, cell voltage monitoring, current monitoring, temperature monitoring and others, depending on the specific battery design, spacecraft design and interface requirements. The battery electrical interface includes integration into the spacecraft and interface with additional batteries or battery modules on the spacecraft. Communications satellites typically carry two non-redundant batteries. Having two separate batteries, rather than a single larger one, aids in balancing the battery mass in the spacecraft and also eases the thermal interface requirements. In contrast, some small satellites may contain only a few cells wired in series with no battery electronics. The batteries have to be adaptable to a wide range of spacecraft designs, power levels and electrical requirements.

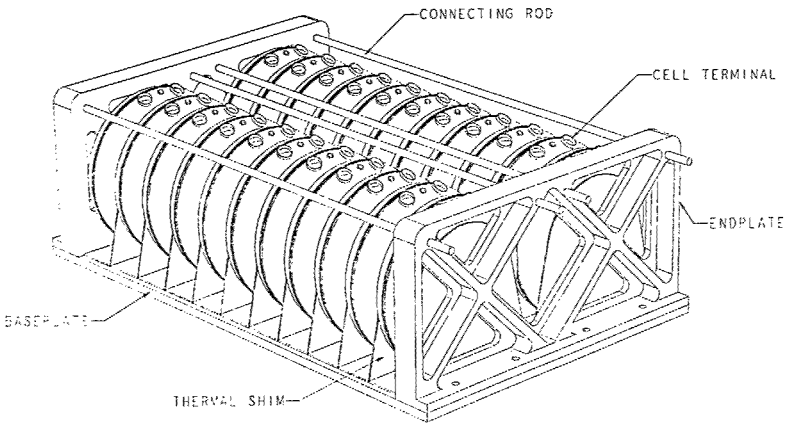

FIGURE 8. Double Row DPV Battery Design.

The battery cells are series-connected in the battery, observing cell polarity. The positive terminal of one cell is connected to the negative terminal of the next, and so on. One end of the cell string will have a remaining positive terminal open and the other end will have an unused negative cell terminal. These cell terminals are connected to the battery interface connector and provide the power connections to the spacecraft. Silver foil, nickel foil or spacecraft-rated wiring is used as the intercell connectors. It depends primarily on the length required between cell terminals and the allowable voltage losses. Batteries are generally designed to minimize the length of the intercell connection. This is done in IPV batteries by inverting every other cell such that the positive and negative cell terminals alternate at the top and bottom of the battery. This eliminates having to connect the top of one cell to the bottom of another. The DPV battery is even more efficient by aligning all of the cell terminals along a central axis running the length of the battery. Or, in the case of the dual cell, side by side battery design, two rows of cell terminals along the length of the battery (Klein 1993). Foil bus bar type intercell connectors are the most efficient method for very short connections such as in the DPV battery. Silver or nickel foil would be used, based primarily on cost considerations. The exposed portion of the intercell connector between cell terminals can be insulated with space-rated materials, though this is not typically required. The intercell connector is mechanically connected to the cell terminal. Wire, or redundant wires, are generally

used for the slightly longer connection between the two cell terminals and the battery connectors. The wire is mechanically connected to the cell terminals and soldered into the battery connector.

Strain gauge circuitry is a critical item. This component measures the microflex of the pressure vessel produced by internal pressure changes. A four bridge, active circuit is used. Two gauges are active and two gauges are null indicators. The strain gauge must be calibrated after installation on the specific cell on which it will be operated. This is done after the cell closure girth weld, but before electrolyte activation, by pressurizing the cell case with helium gas. Since the strain gauge bridge is an active circuit, an excitation voltage must be provided through the battery electronics and interface. The output signal is small, so an amplification circuit is typically supplied on the battery to boost the signal to an adequate level for spacecraft telemetry. The strain gauge output signal provides a direct indication of the cell internal pressure, and therefore the cell state-of-charge. Strain gauges are typically included on three cells in the battery for comparison and redundancy purposes. Cell heaters are usually supplied in order to closely control the battery temperature during all phases of operation. Some batteries are supplied with on-board heater controller circuitry. Heat is removed by thermal fins which contact the battery baseplate/thermal radiator. Battery temperature is monitored using thermistors. Generally, three are mounted at different locations in the battery. This provides redundancy and a measure of temperature uniformity across the battery. Battery current sensing is provided by an on-board current sensing element, usually of the non-contact, inductive type. All battery monitoring information such as voltage, current, temperature and strain gauge output are supplied to the spacecraft telemetry system through the battery electrical interface connector.

Thermal Design

Temperature control is an important aspect of battery design and spacecraft integration. Cell heaters are typically supplied to help regulate cell temperature during orbital operation. The battery is also usually mounted to a baseplate to remove excess heat when required. This baseplate normally mounts directly to a bulkhead in the spacecraft and radiates excess battery heat into space. A considerable amount of thermal analysis, calorimetry testing and thermal modeling has been done with the NiH2 system. Basically, the cell is endothermic during the bulk of charging until near the end-of-charge. At this point, as the cell goes into overcharge, oxygen gas is evolved at the nickel electrode. This oxygen gas is being generated in the presence of large excess of hydrogen gas and in the presence of a good catalyst (the hydrogen electrode). Reactions now occuring, including the reaction of hydrogen and oxygen gas, are exothermic, so excess heat is generated by the cell which must be removed. The NiH2 cell is capable of accepting extreme amounts of overcharge if this heat is removed. Even so, the cell temperature begins to rise near full state-of-charge and provides an indication, along with the pressure, that full charge has been achieved.

In an IPV battery, each cell is mounted in a thermal sleeve which serves as a heat sink to conduct excess heat from the cell into the battery baseplate. This is fairly efficient thermally, but the sleeve adds weight and cost to the battery. The approach to thermal design in the DPV battery is more direct and cost and weight efficient. A thin aluminum thermal shim is inserted between each pair of adjacent cells so each cell has a shim contacting both flat sides of the pressure vessel. The shim is electrically insulated from, and thermally coupled to, the metal pressure vessel by a thin layer of electrically insulating but thermally conductive material. The material is space-rated and is currently used for the same purpose in IPV batteries. The shim provides a large cross-sectional area through which heat can be removed from the internal electrode stack. The electrode stack has a large thermal cross-section with respect to the pressure vessel because the stack directly contacts the flat pressure vessel wall. In the IPV cell the electrode stack is perpendicular to the cylindrical pressure vessel wall with no direct contact between the electrode stack and the pressure vessel. Heat can only be rejected by the electrode stack across a narrow hydrogen gap between the electrode stack and the pressure vessel wall. The DPV provides a more direct thermal path for heat rejection by the cell (Coates 1995).

CONCLUSIONS

The NiH2 electrochemical energy storage system provides the best reliability, performance and cycle life available in an aerospace qualified battery system. The DPV design offers an important advance in this critical aerospace battery technology and will provide a substantial improvement in the mass and volume performance of the NiH2 battery system. While DPV designs are in the preliminary stages and testing and qualification is still required prior to spaceflight applications, DPV development programs are moving forward rapidly, and the cell and battery designs show great promise for military, scientific and commercial, aerospace and terrestrial uses.

References

Coates, D.K., R.D. Wright, R.S. Repplinger. (1995) "Advanced Dependent Pressure Vessel (DPV) Nickel-Hydrogen Spacecraft Cell and Battery Design," in *Proc. Fourth Space Electrochemical Research and Technology (SERT) Conference*, NASA Lewis Research Center - Office of Space Access and Technology, Cleveland, OH.

Francisco, J.M., D.K. Coates. (1995) "High Energy Density Micro-Fiber Based Nickel Electrode for Aerospace Batteries," in *Proc. Eleventh Annual Battery Conference on Applications and Advances*, California State University, Long Beach, CA.

Klein, G.C., D.F. Schmidt. (1993) "Current and Emerging Technology for Powering Small Satellites With Secondary Cells and Batteries," in *Proc. Seventh Annual AIAA/USU Conference on Small Satellites*, Utah State University, Logan, UT.

Page

412

Blank

SAFT Nickel Hydrogen Cell and Battery Update

Dr Yannick BORTHOMIEU and Annie SENNET

SAFT Advanced and Industrial Battery Group
Defense and Space Division
Poitiers France

1996 NASA Aerospace Battery Workshop
Huntsville Hilton, AL
December 3-5, 1996

OUTLINE

- CELL DESIGNS : VHS and AN TECHNOLOGIES
- BATTERY DESIGN

CELL DESIGNS

SAFT HAS TWO NICKEL HYDROGEN CELL TECHNOLOGIES :

- THE « VHS » TYPE IS THE SAFT DESIGN :
  - DEVELOPED SINCE 88
  - QUALIFIED IN 89
  - FLIGHT EXPERIENCE IN 96

- THE « AN » TYPE IS THE EX-GATES DESIGN :
  - QUALIFIED IN 87
  - IN FLIGHT OPERATION SINCE 89
  - TRANSFERRED SUCCESSFULLY FROM GAINESVILLE TO FRANCE IN 94

VHS CELL DESIGN :

CELL CONFIGURATION :

- 3'5 RABBIT EARS
- CAPACITY RANGE : 30 TO 104 AH :
- HYDROFORMED INCONEL 718 WITH ONE CENTRAL GIRTH WELD (2 PARTS)
- CERAMIC BRAZED TERMINALS
- NEGATIVE PRECHARGE

STACK CONFIGURATION :

- BACK TO BACK DESIGN
- SINGLE OR DUAL STACK
- TRUNK CIRCLE SHAPE ELECTRODES
- AGEING ACCOMMODATION SYSTEM : SPIDER SPRING
- POLYSULFONE END PLATES MAINTAINED BY A TIE ROD

VHS CELL DESIGN : (cont'd)

ELECTROCHEMISTRY :

- POSITIVE ELECTRODES :
  - WET SINTERED MATERIAL ON STEEL PERFORATED GRID
  - ACTIVE MATERIAL DEPOSITED BY AQUEOUS ELECTROCHEMICAL PROCESS

- NEGATIVE ELECTRODES :
  - ACTIVE CHARCOAL WITH PLATINUM ON EXPANDED NICKEL COLLECTOR
  - GORTEX HYDROPHOBIC LAYER WITH POLYPROPYLENE GRID

- SEPARATOR :
  3 LAYERS OF NON WOVEN POLYAMIDE FELT

- ELECTROLYTE : 31 % KOH

SAFT
Advanced and Industrial Battery Group
Defense and Space Division

SAFT Nickel Hydrogen Cell and Battery Update

VHS CELL DESIGNS : (cont'd)

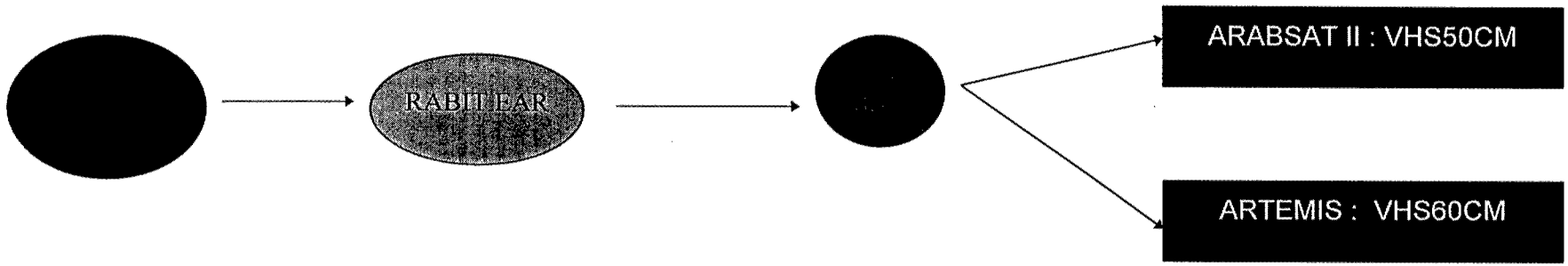

SAFT
Advanced and Industrial Battery Group
Defense and Space Division

SAFT Nickel Hydrogen Cell and Battery Update

VHS CELL DESIGN : DESIGN CHANGE

THE PREVIOUS DESIGN VHS BL HAS BEEN PROVEN 33 GEO SEASONS AT 70 % DOD
THE VHS CM HAS THE SAME ELECTROCHEMISTRY THAN THE VHS BL

RESULTS OF THE LIFE TEST PERFORMED ON VHS96CM :

- LOW END OF DISCHARGE VOLTAGES
- HIGH INTERNAL RESISTANCE
- HIGH END OF CHARGE PRESSURE

RESULTS OF DPA PERFORMED ON CELLS :

- SOME WATER AT BOTTOM OF CELL DUE TO THERMAL GRADIENT (imposed by test equipment)
- LACK OF ELECTROLYTE INSIDE THE SEPARATOR LAYERS
- INCREASE OF GLOBAL STACK ELECTROLYTE CONCENTRATION

VHS CELL DESIGN : DESIGN CHANGE (cont'd)

MODIFICATIONS :

- ADDITION OF ONE LAYER OF SEPARATOR TO ENSURE 15 YEARS AT 80 % DOD :
  INCREASE FROM 2.9 to 3.3 g of KOH /Ah
- IMPROVEMENT OF THE STACKING PROCESS (Reduction of tolerances on the applied stack preloading)

VALIDATION PLAN:

- MANUFACTURING AND TEST OF VOQ LOT
- SPECIFIC ELECTRICAL TESTING : Overcharge, Internal resistance measurements
- VIBRATIONS
- ACCELERATED CYCLING (9 cycles per day : 80 % DOD) : 2000 cycles performed without failure
  (Test discontinued at 1 V per Cell)
- DPA

VHS CELL DESIGN : DESIGN CHANGE (cont'd)

DESIGN CHANGE COMPLETELY QUALIFIED BEGINNING OF 96

ARABSAT/ARTEMIS BATTERY DESIGN REVISED PER THIS CHANGE

8 BATTERIES IN ORBIT ON ARABSAT II A and B

CONTINUED LIFE TESTING : SEMI-ACCELERATED CYCLING AT ESA
(2 cycles per day, 80 % DOD, reduced solstice)

SAFT
Advanced and Industrial Battery Group
Defense and Space Division

SAFT Nickel Hydrogen Cell and Battery Update

AN CELL DESIGNS : 4 CONFIGURATIONS

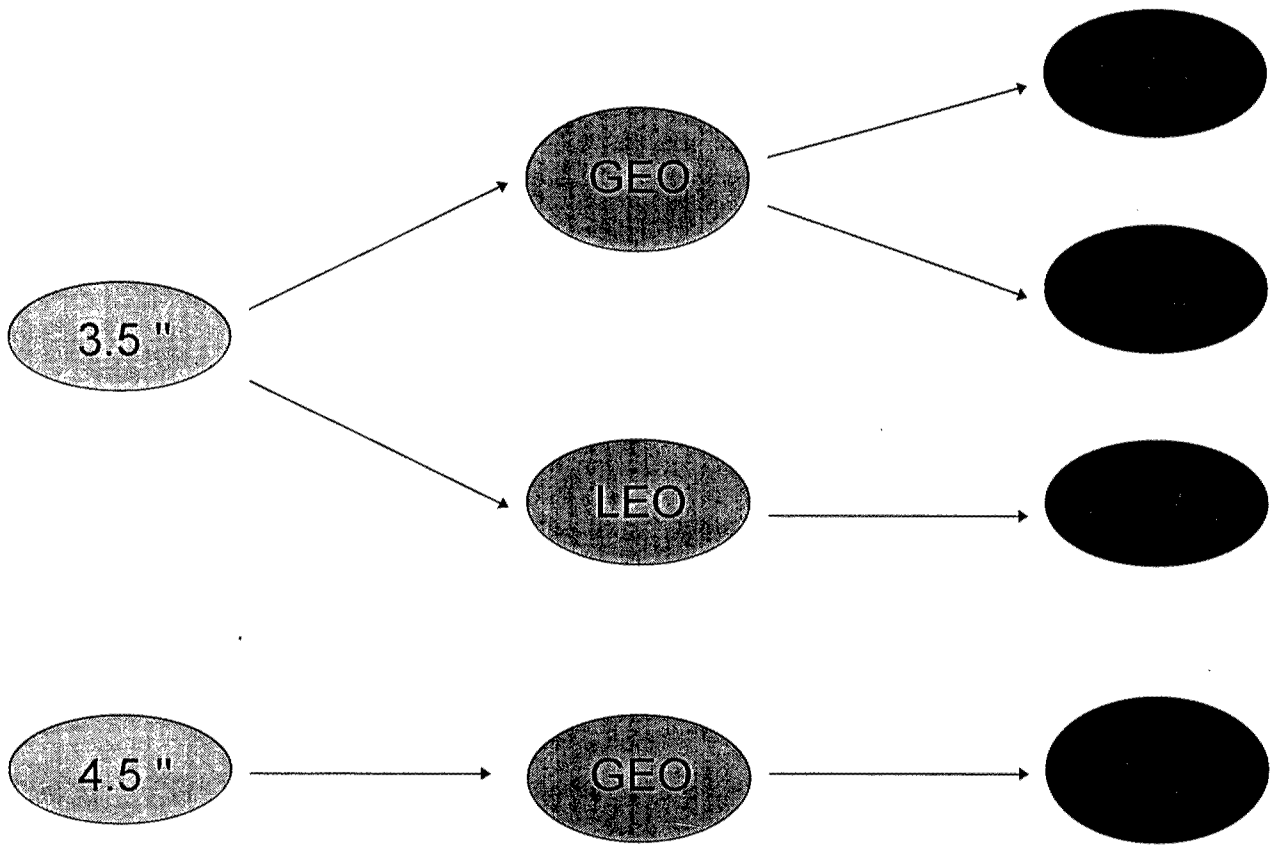

SAFT
Advanced and Industrial Battery Group
Defense and Space Division

SAFT Nickel Hydrogen Cell and Battery Update

AN CELL DESIGNS : (cont'd)

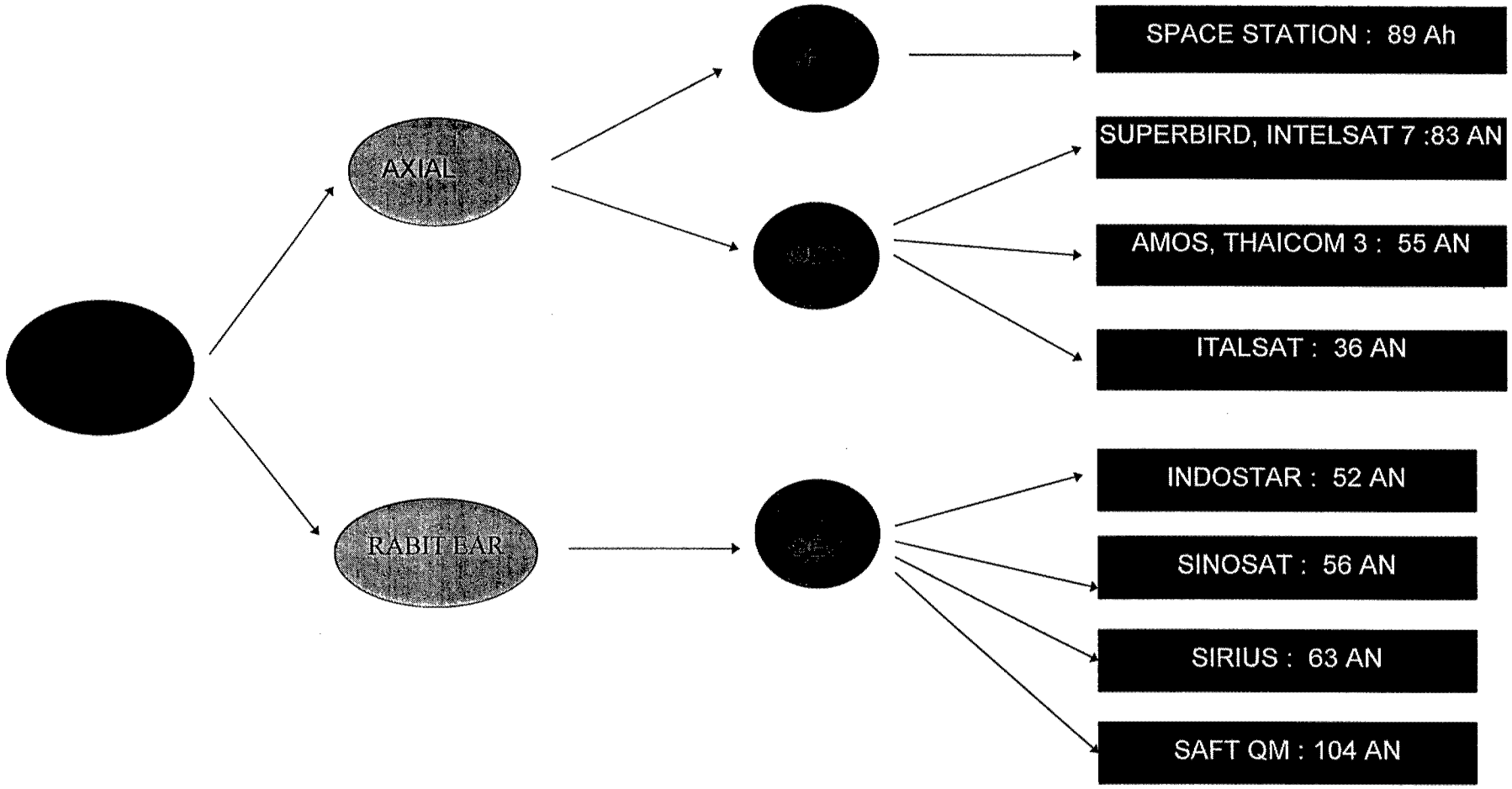

SAFT
Advanced and Industrial Battery Group
Defense and Space Division

SAFT Nickel Hydrogen Cell and Battery Update

AN CELL DESIGNS : (cont'd)

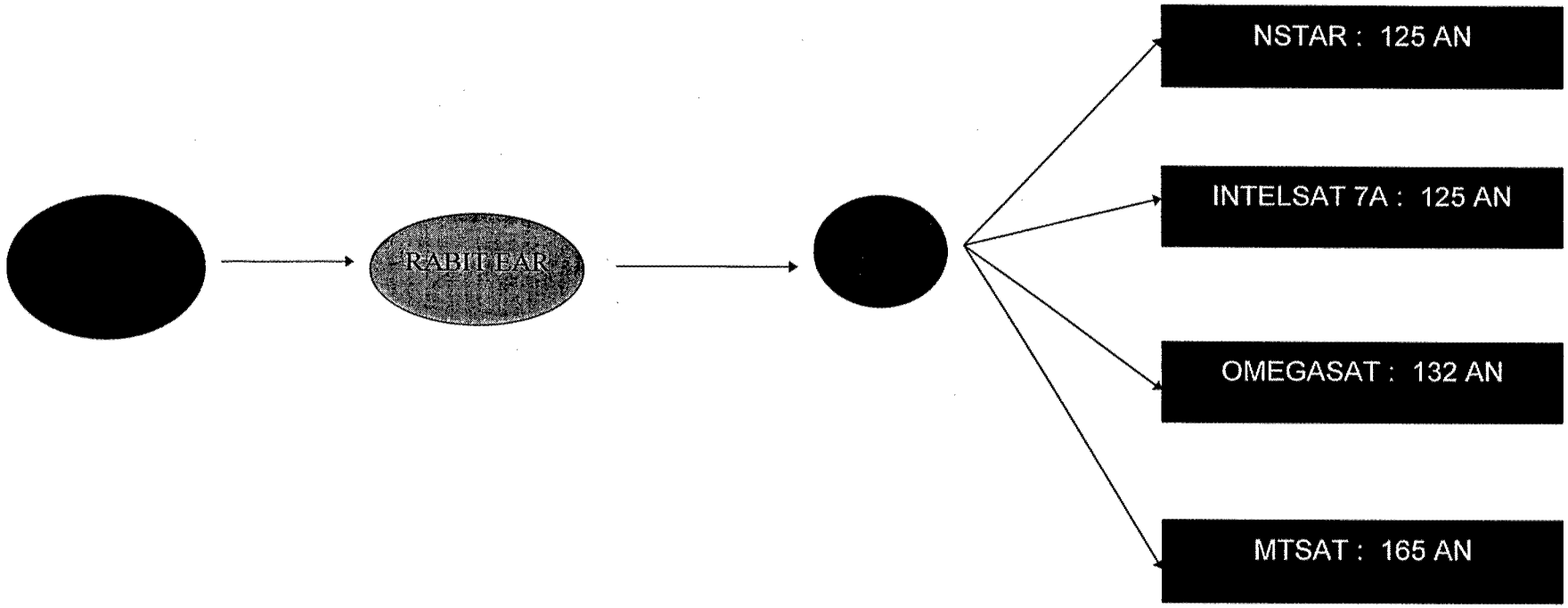

AN CELL DESIGNS : (cont'd)

CELL CONFIGURATION :

- HYDROFORMED OR ROLLED AND WELDED INCONEL 718 VESSEL (3 PARTS)
- TWO CENTRAL GIRTH TIG WELDS
- CERAMIC BRAZED TERMINALS
- POSITIVE PRECHARGE
- WALL WICK SYSTEM

STACK CONFIGURATION :

- BACK TO BACK DESIGN
- SINGLE STACK
- PINEAPPLE SLICE CONFIGURATION WITH POLYSULFONE CENTER CORE
- AGEING ACCOMMODATION SYSTEM : BELLEVILLE WASHERS
- INCONEL 718 ENDPLATES SUPPORTING STACK AT BOTH ENDS

AN CELL DESIGNS : (cont'd)

ELECTROCHEMISTRY :

- POSITIVE ELECTRODES :
  - DRY POWDER SINTERED MATERIAL ON NICKEL SCREEN
  - ACTIVE MATERIAL DEPOSITED BY AQUEOUS ELECTROCHEMICAL PROCESS

- NEGATIVE ELECTRODES :
  - PLATINUM PTFE FILM ON PHOTOETCHED GRID
  - GORTEX HYDROPHOBIC TEFLON BACKING

- SEPARATOR : 2 LAYERS OF ZIRCAR

- ELECTROLYTE : 31 % KOH WITH 3.3 G/AH

AN CELL : TRANSFER

- SAFT HAD ALREADY SOME EXPERIENCE IN TRANSFERING SPACE ACTIVITIES FROM ROMAINVILLE TO POITIERS

- AN CELL TRANSFERT BASED ON :

- TRAINING OF SAFT TEAMS ON DOCUMENTATION AND PROCESS IN GAINESVILLE

- REQUALIFICATION PLAN DEFINITION

- REQUALIFICATION AND STARTING MANUFACTURING WITH EX GATES PEOPLE IN POITIERS

SAFT Nickel Hydrogen Cell and Battery Update

AN CELL : TRANSFER (Cont'd)

GAINESVILLE

Product

- Freeze the documentation to latest revision
- Review technical documents
- Train and qualify Poitiers operators
- Establish re-qualification plan
- Fabricate qualification samples (considered as reference)

Processes

- Certify each process and equipment
- Disassemble process equipment

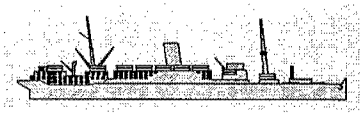

POITIERS

Processes

- Re-assemble process equipment
- Re-calibrate process equipment
- Validate each process and equipment

Product

- Fabricate requalification samples
- Compare qualification/re qualification products
- Move of some Gainesville's people to Poitiers to transfer and maintain the know-how
- Final Training and qualification of other operators
- Manufacture and test of a qualification lot (with DPA) : Comparison with Gainesville data
- Keep same suppliers

SAFT Nickel Hydrogen Cell and Battery Update

AN CELL : TRANSFER (Cont'd)

VALIDATION OF EACH PROCESS AND GOOD PERFORMANCES OF THE 6 FIRST CELLS → QUALIFICATION OF THE TRANSFER

SAFT MANUFACTURING AND DELIVERIES:

3'5

- 200 55AN Axial (Thaicom 3)
- 120 52AN RE (Indostar)
- 120 56AN RE (Sinosat)
- 250 63AN RE (Sirius 2) : In Progress

4'5

- 132AN RE (OmegaSat) delivery in 97/98
- 165AN RE (MTSat) delivery in 97

SAFT
Advanced and Industrial Battery Group
Defense and Space Division

SAFT Nickel Hydrogen Cell and Battery Update

BATTERY DESIGN

1990

BEGINNING OF THE NiH_2 BATTERY DEVELOPMENT AT SAFT

1993

QUALIFICATION OF THE GENERIC NiH_2 BATTERY WITH VHS CELLS
SELECTION OF THE 27 VHS 50 CM FOR ARABSAT II
SELECTION OF THE 23 VHS 60 CM FOR ARTEMIS

1996

LAUNCH OF 8 BATTERIES ON ARABSAT II A and B
DESIGN CHANGE TO ACCOMMODATE AN CELLS
QUALIFICATION OF AN BATTERY WITH INDOSTAR AND SB3000 PROJECTS

BATTERY DESIGN

BATTERY CONFIGURATION :

- 12 to 30 Rabbit Ear CELLS PER BATTERY
- BASE PLATE WITH ALUMINUM SLEEVE DESIGN
- INDIVIDUAL BY-PASS SYSTEM PLACED BETWEEN THE CELLS
- 2 REDUNDANT HEATER CIRCUITS
- BETWEEN 2 and 4 STRAIN GAGE EQUIPPED CELLS
- WIRING MATERIALS : COPPER OR ALUMINUM
- POWER AND MEASUREMENT CONNECTORS
- CELLS EQUIPPED WITH THERMISTORS

BATTERY DESIGN (Cont'd)

MAIN CHARACTERISTICS :

- QUALIFIED UP TO 104 Ah
- ENERGY DENSITY : 48 Wh/kg FOR 27 Cells of 63 Ah
- WEIGHT RATIO CELL/BATTERY : 80 %

VOLUME : 59*44*21 cm^3 for 27 Cells battery

- DOD max : 80 % with one failed cell
- THERMAL GRADIENT : Maximum Internal CELL : 2.5 °C
  Maximum Between 2 CELLS : 5 °C
- VIBRATION : QUALIFICATION UP TO 20 G BOTH SINE AND RANDOM

BATTERY DESIGN (Cont'd)

ACCOMMODATION OF AN CELLS:

- CHANGE OF THE DIAMETER OF THE SLEEVES (< 0.5 mm in diameter)
- CHANGE CELL CONNECTION : SCREW FOR VHS ⟶ LUG FOR AN
- NEARLY SAME BATTERY CHARACTERICS ARE MAINTAINED WITH AN CELL AS WITH VHS

CONCLUSION

SAFT NiH_2 PORTFOLIO IS :

- VHS CELLS GEO 3'5
- AN CELLS GEO 3'5/4'5
- AN CELLS LEO 3'5
- VHS AND AN 3'5 BATTERIES

CONCLUSION

FUTURE FOR SAFT :

- **NiH_2 :** - EXTEND BY-PASS SYSTEM CAPABILITY
  - HAVE 4'5 INCH BATTERY
  - OBTAIN MORE CYCLING DATA WITH AN

- **LiC :** - DEVELOP LiC TECHNOLOGY FOR SPACE

Page

436

Blank

Nickel-Cadmium Session

Page

438

Blank

NASDA
NATIONAL SPACE DEVELOPMENT AGENCY OF JAPAN

Battery Performance of ADEOS (Advanced Earth Observing Satellite) and Ground Simulation Test Results

K.Koga, Y. Suzuki, S. Kuwajima, and H. Kusawake
National Space Development Agency of Japan

NASDA
NATIONAL SPACE DEVELOPMENT AGENCY OF JAPAN

ADEOS

The Advanced Earth Observing Satellite (ADEOS) is developed with the aim of establishment of platform technology for future spacecraft and inter-orbit communication technology for the transmission of earth observation data.

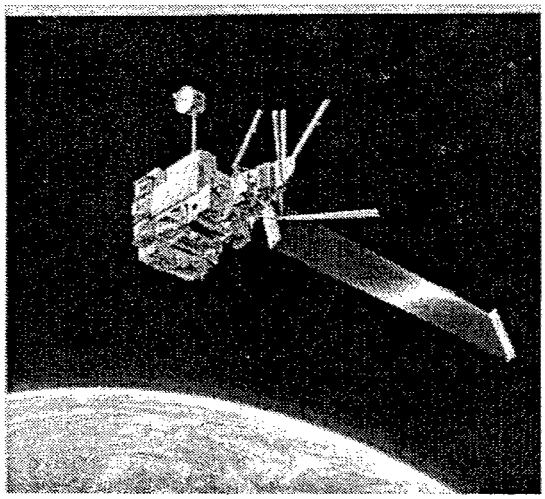

Shape : Module type with deployable paddle
- **Body**: Approx.4x4x5(m)
- **Solar Paddle**: Approx.3x26(m)
- **Weight** : Approx. 3.5 ton(at lift-off)

Launch date: 8/17/1996
Launch Vehicle :H-II
Launch Site :Tanegashima Space Center
Orbit : Sun Synchronous Subrecurrent
- **Altitude**: Approx. 800km
- **Inclination** : Approx. 98.6 deg.
- **Period** : Approx. 101 min.

NASDA NATIONAL SPACE DEVELOPMENT AGENCY OF JAPAN — Electrical Power Subsystem

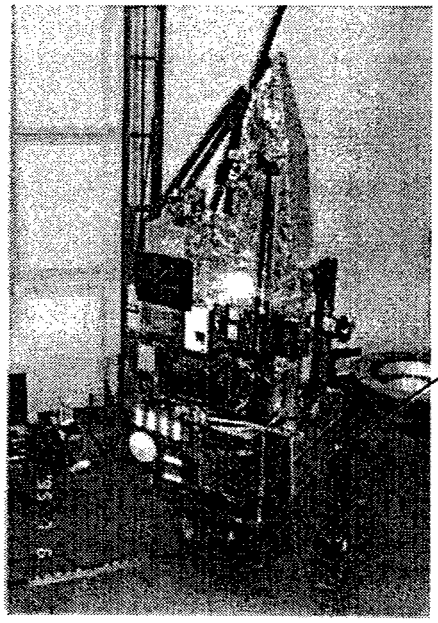

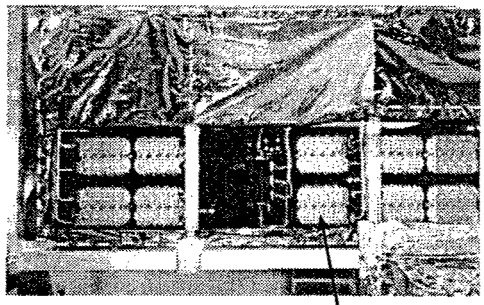

NASDA NATIONAL SPACE DEVELOPMENT AGENCY OF JAPAN — Battery Assembly

ADEOS uses 5 batteries, consists of 2 packs

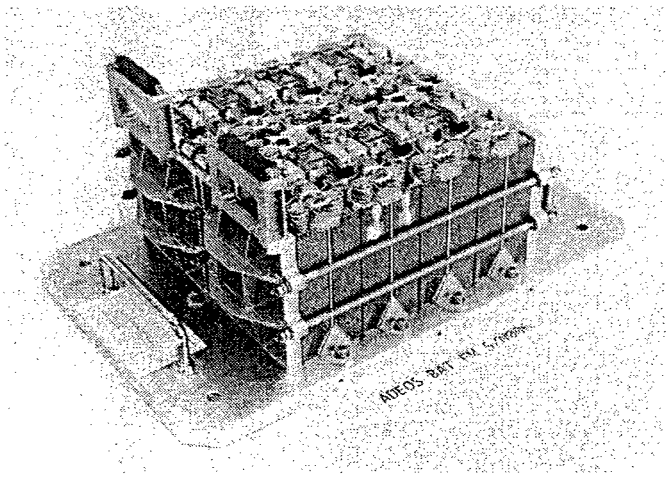

Weight : 19.3kg/pack(16cells)
Volume : 276(T) × 264(W) × 175(H)mm/pack

NASDA | 35AH SPACE Ni-Cd CELL

CELL MAJOR SPECIFICATIONS

Rated Capacity		35 AH
Mission	GEO	10Years, 1,000cycles
	LEO	3Years, 20,000cycles
Weight		max. 1050g
Energy Density		40WH/kg
Mechanical Strength	Burst Pressure	35kgf/cm^2
	Pressure Cycling	50,000cycles (0~3.5 kgf/cm^{2}G)

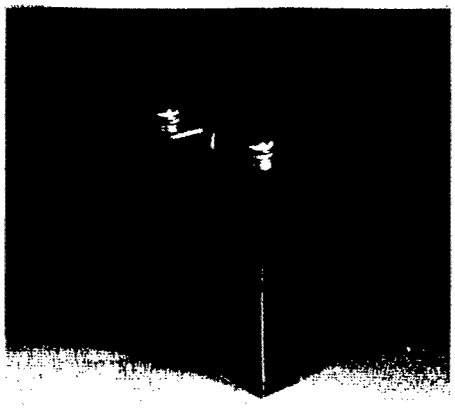

EXTERNAL VIEW OF Ni-Cd CELL

NASDA Simplified Block Diagram of the ADEOS EPS

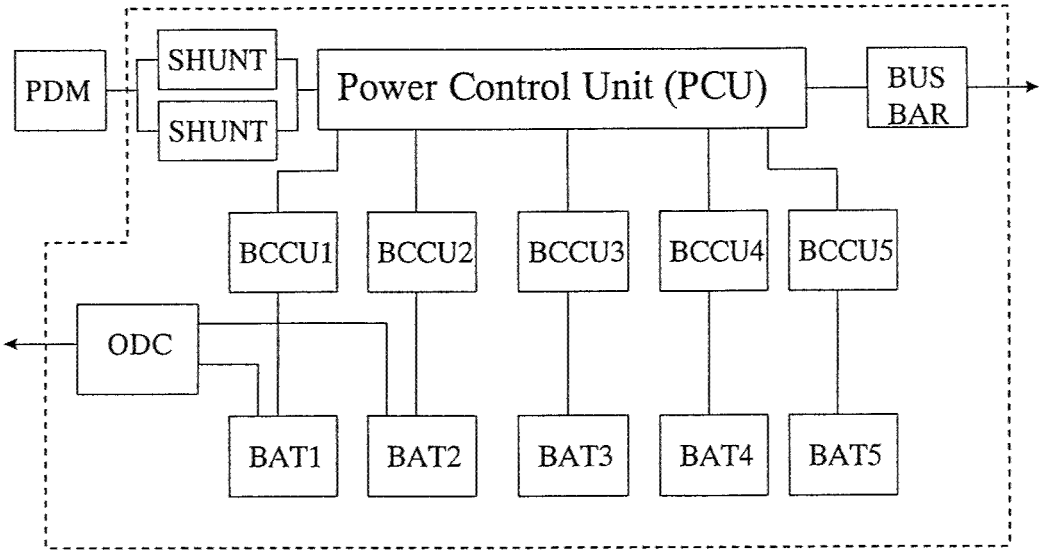

EPS

NASDA Main Specification of 35Ah Ni-Cd Battery

NATIONAL SPACE DEVELOPMENT AGENCY OF JAPAN

Cell	Ni-Cd 35Ah (Sanyo N35S)
Weight	19.3kg/pack(16cells)
Charge Scheme	V/T control
Charge Rate	0～10A±0.5A(usually)
	0～12.5A±0.5A(4 battery operation)
Depth of Discharge	20%(usually), 60%(after launch)
	25%(4 battery operation)
Operating Temp.	15℃
Mission Life	3 years (@LEO)

1996 NASA Aerospace Battery Workshop

NASDA VT Curve

NATIONAL SPACE DEVELOPMENT AGENCY OF JAPAN

ADEOS has 8 VT curves.
Initial No. is 6.

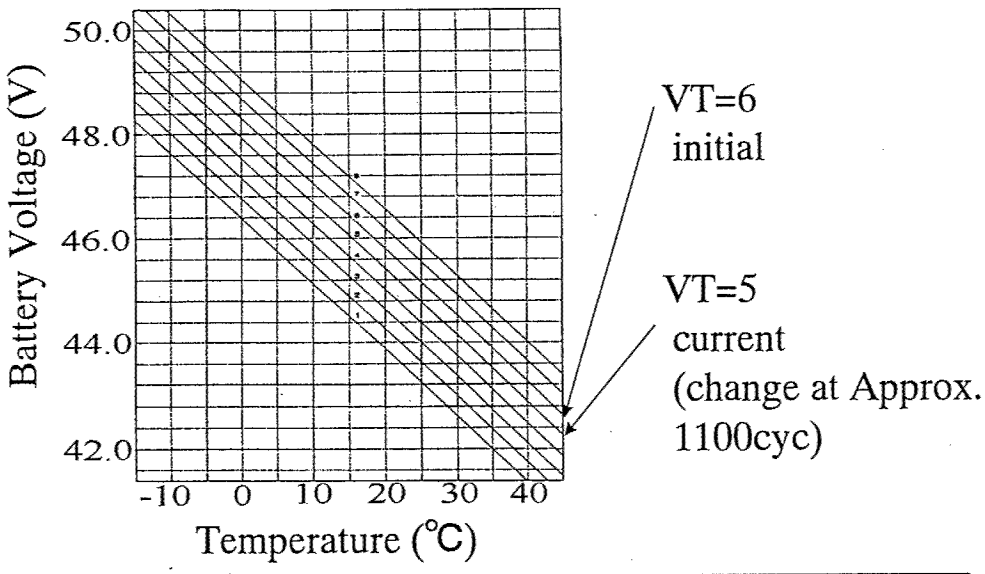

1996 NASA Aerospace Battery Workshop

NASDA Charge and Discharge of Battery #1(VT=6)

NATIONAL SPACE DEVELOPMENT AGENCY OF JAPAN

@1065Cycle
VT=6(initial)

Charge

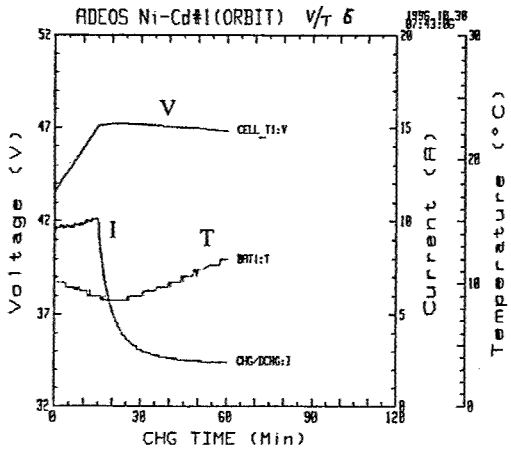

C/D=1.31

Discharge

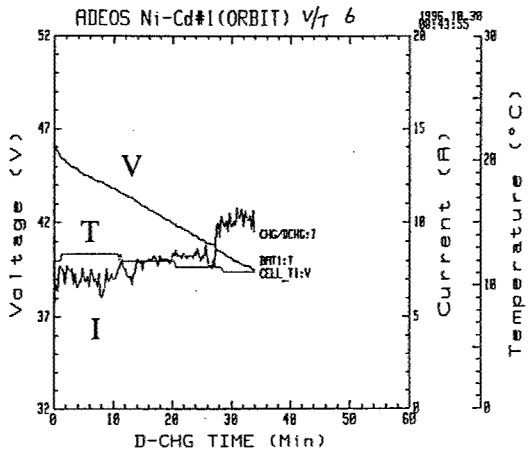

DOD=13.0 %

1996 NASA Aerospace Battery Workshop

NASDA Charge and Discharge of Battery #1(VT=5)

NATIONAL SPACE DEVELOPMENT AGENCY OF JAPAN

DOD is less than that of prediction(20%), so changed the VT level (from 6 to 5) to avoid the over charge.

Charge

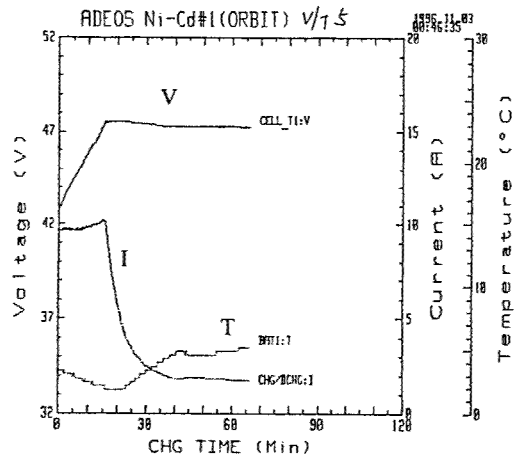

C/D=1.20

Discharge

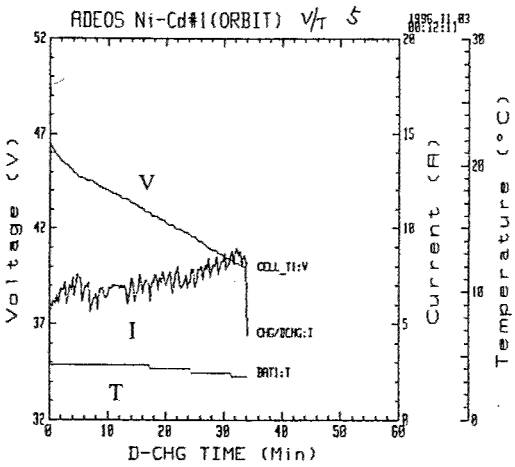

DOD=11.7 %

1996 NASA Aerospace Battery Workshop

Trend of EOCV,EODV and Temp.

EOCV and EODV

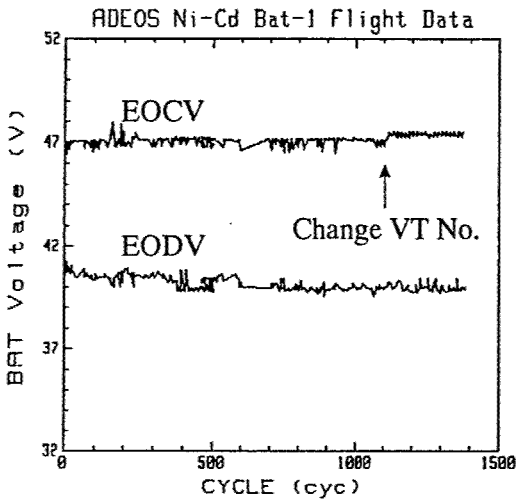

Temp.

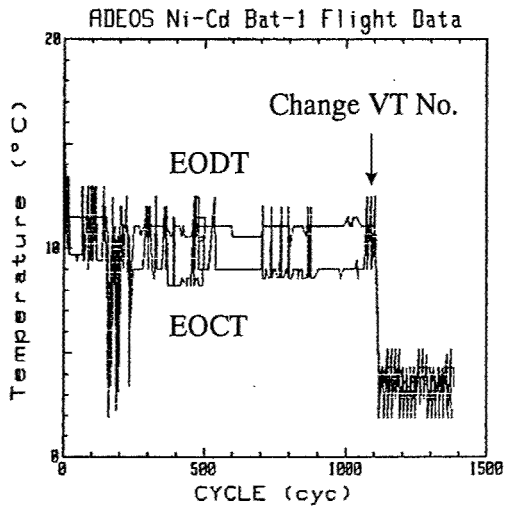

DOD Trend

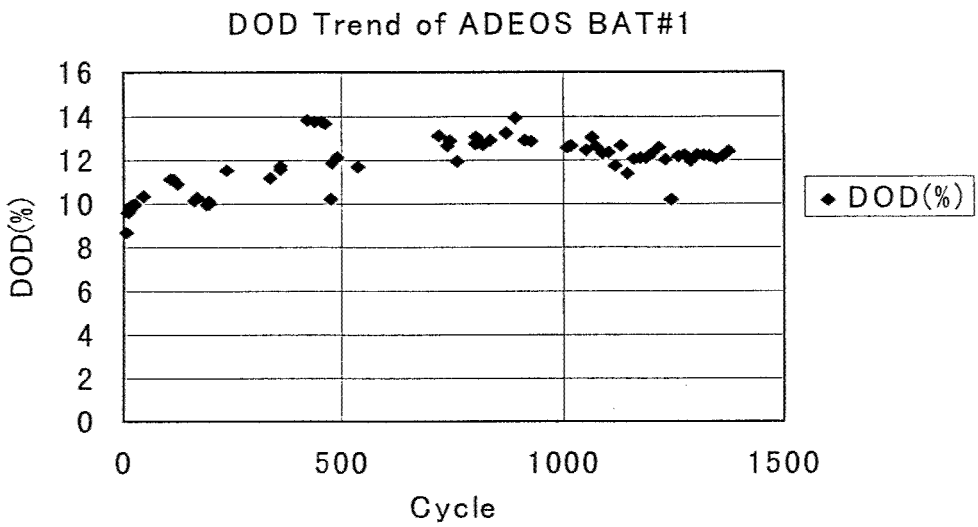

8/1996 11/1996

Simulation Test

We started the simulation test to evaluate the life cycle of ADEOS battery at April 1992.

Test material	16 cell stack (ADEOS EM cell)
Required cycle	15700cyc (3 years @LEO)
Others	measuring the tension of tie rod using strain gauge

Test Type

Normal cycle test
Contingency (simulate the reduce of solar array power)
4 battery Operation(simulate 1battery failure)
Capacity test after 15700cyc
Reconditioning

Simulation test condition

Cycle Test

Temp.	15℃
Charge	10.0A(1/3.5C), 66 min.
taper	@ 23.02V(1.439V/cell)
	(change VT level after 6478cycle)
	@ 23.15V(1.447V/cell)
Discharge	12.0A(1/2.9C), 35 min.
DOD	20 %
C/D	less than 1.15

Capacity Test (at 15700cycle)

Temp.	15℃
Charge	3.5A(1/10C), 16 hours
Discharge	17.5A(1/2C), any cell at 1 Volt

NASDA Cycle Trend of EOCV and EODV

NATIONAL SPACE DEVELOPMENT AGENCY OF JAPAN

This plot is overlapped by 16 cells.
Each cell shows the same level of voltage.

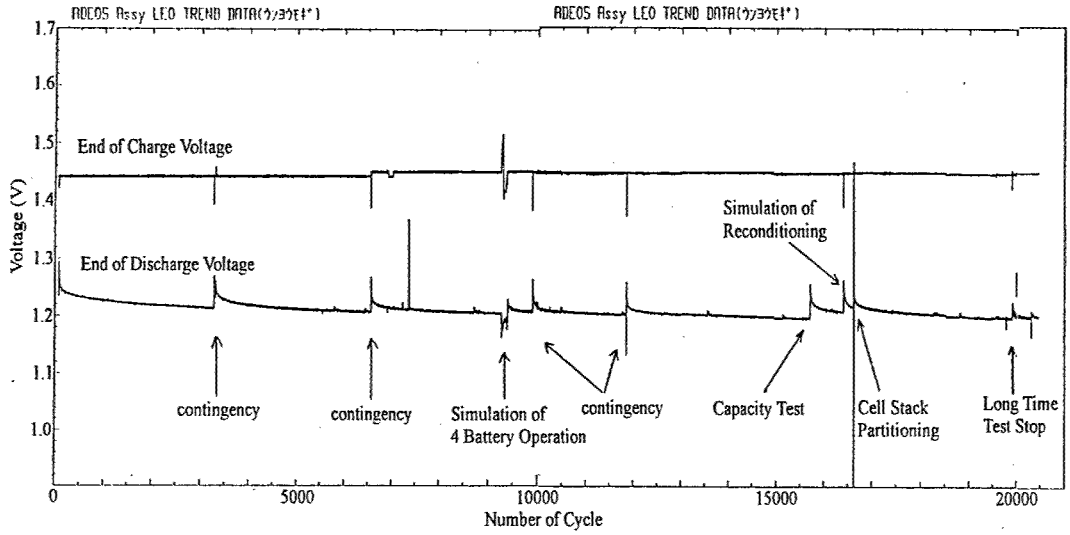

NASDA Trend of Tension

NATIONAL SPACE DEVELOPMENT AGENCY OF JAPAN

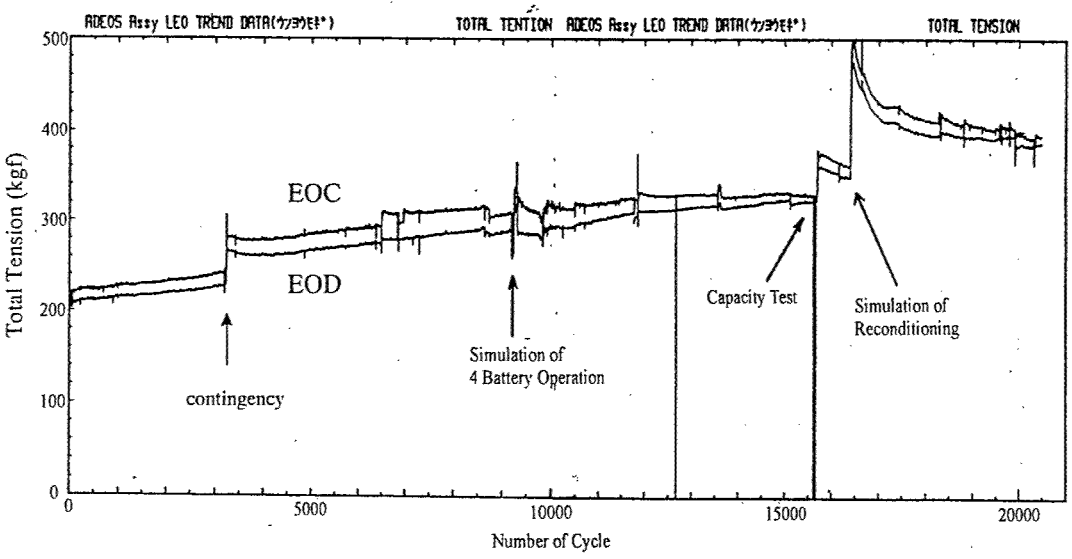

100kgf(total tension)=0.813kgf/cm^2(face pressure)

NASDA Voltage, Current and Tension at Charge

NATIONAL SPACE DEVELOPMENT AGENCY OF JAPAN

Charge characteristics at 8,1006,5202,9732,14880,19914cyc

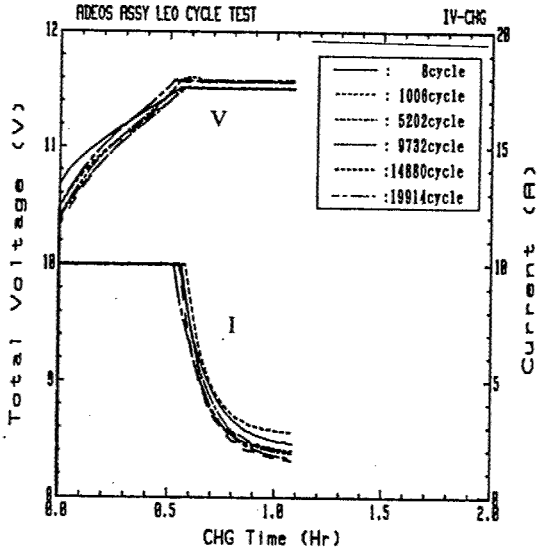

Voltage and Current

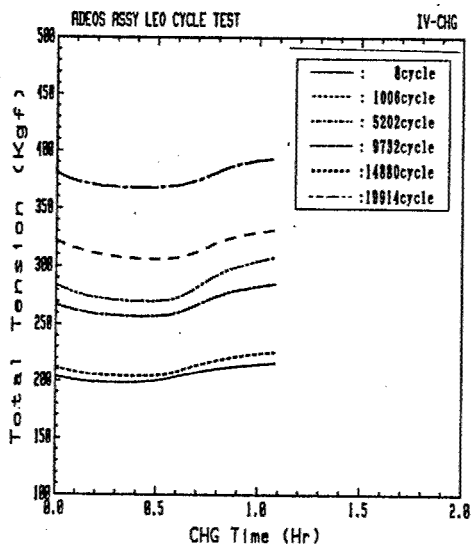

Total tension

NASDA Voltage, Current and Tension at Discharge

NATIONAL SPACE DEVELOPMENT AGENCY OF JAPAN

Discharge characteristics at 8,1006,5202,9732,14880,19914cyc

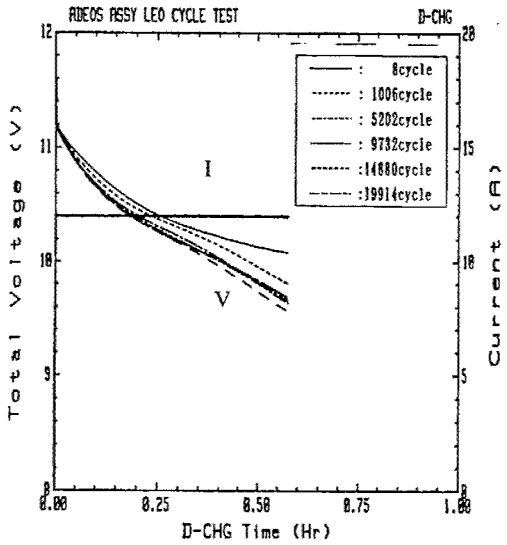

Voltage and Current

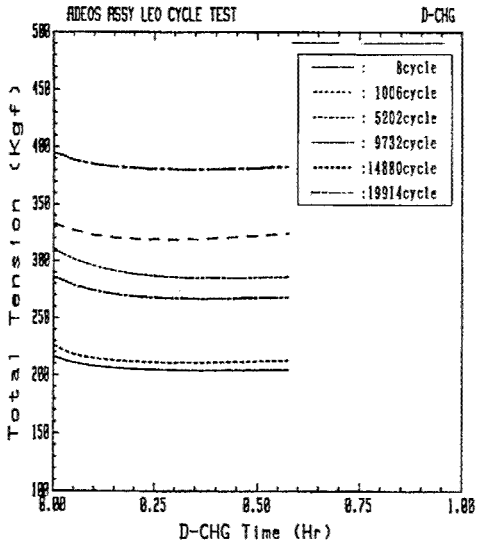

Total tension

NASDA Differences of each cell voltage

This plot is overlapped by 16 cells at 14880cyc.
Each cell shows the same level of voltage.

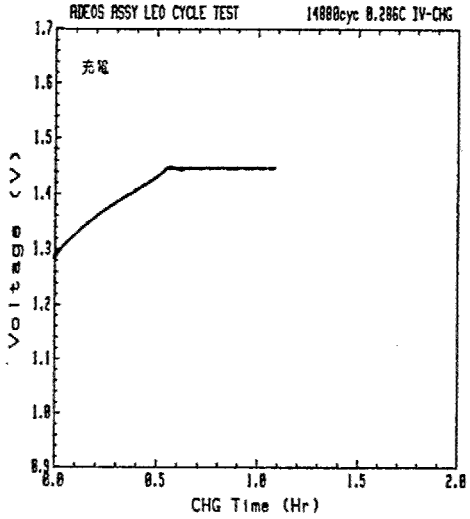

Charge

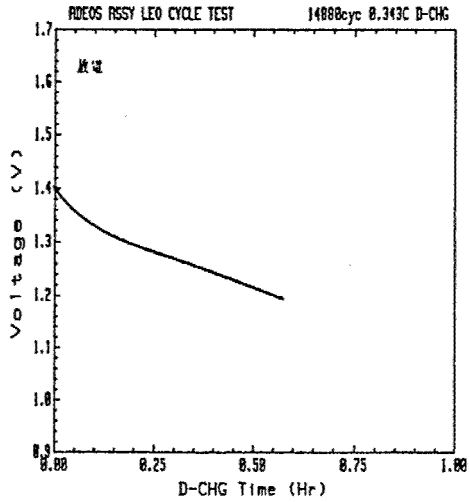

Discharge

NASDA Capacity test at 15700cycle

Capacity initial : 38.93Ah
after 15700cyc: 27.12Ah

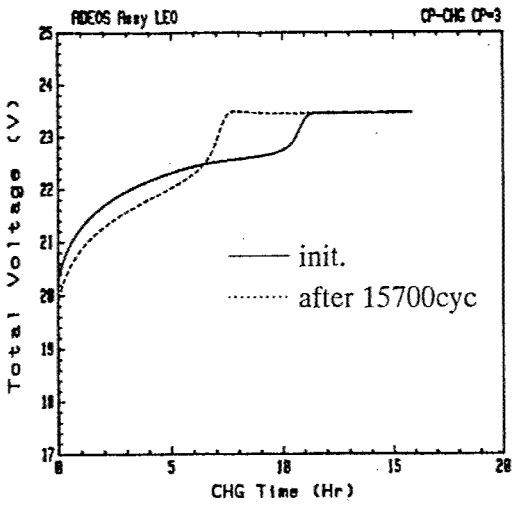

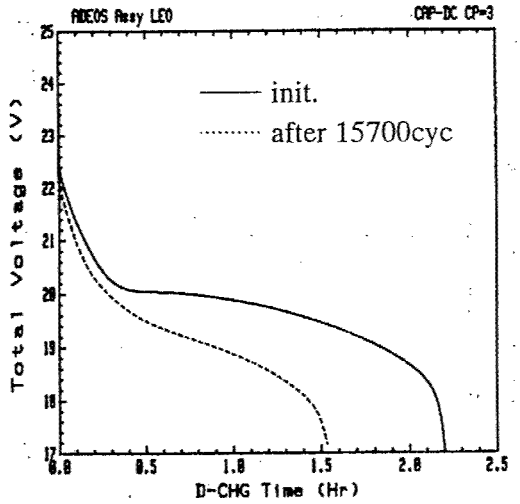

NASDA Residual and Full-Charged Capacity Test

@15700cycle

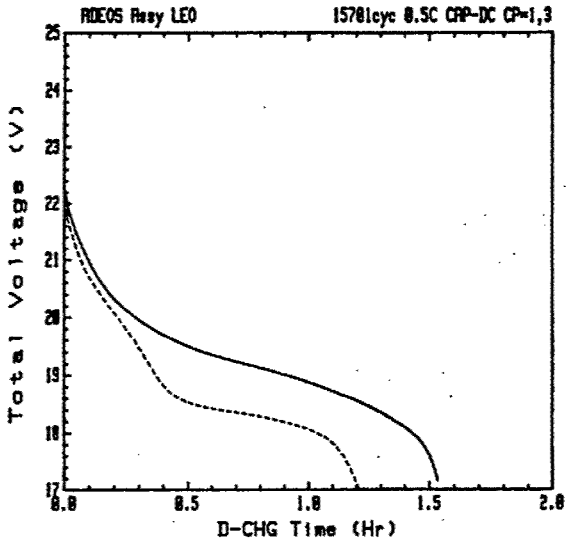

-------- Residual Capacity Test

——— Full-charge Capacity Test

Memory Effect

about 0.8V/16cells
0.05V/cell

NASDA Conclusion

ADEOS Flight Data

Each battery shows good performance.
DOD is fluctuated from 10 to 15%.
Temperature is controlled from 0 to 15℃.

ADEOS Simulation Data

Test result satisfied the required 15700 cycle.
Each cell's voltage dispersion is little.
Capacity at 15700cyc was 27.12Ah.
Test is continued over 22000 cycle(@11/1996).

Page

450

Blank

THE 1996 NASA AEROSPACE BATTERY WORKSHOP

THE IN-ORBIT PERFORMANCE OF BATTERIES ON THE SKYNET 4 SPACECRAFT FLEET: A NICKEL-CADMIUM SUCCESS STORY.

P. J. JOHNSON AND P. E. MILES

MATRA MARCONI SPACE UK LTD.,
GUNNELS WOOD ROAD, STEVENAGE,
HERTFORDSHIRE, SG1 2AS.
ENGLAND.

MATRA MARCONI SPACE

Abstract.

The SKYNET 4 constellation consists of three spacecraft which were launched between December 1988 and August 1990. The spacecraft are three-axis stabilized geostationary earth-orbiting military communications satellites with a design life of seven years on station. With the mission objective achieved all the batteries continue to give excellent performance.

This paper presents a review of the history of the six batteries from cell procurement to the end of their design life and beyond. Differences in operational strategies are discussed and the lifetime trends in performance are analyzed. The combination of procurement acceptance criteria and the on-station battery management strategy utilized are presented as the prime factors in achieving completely successful battery performance throughout the mission.

SPACECRAFT IN ORBIT VIEW

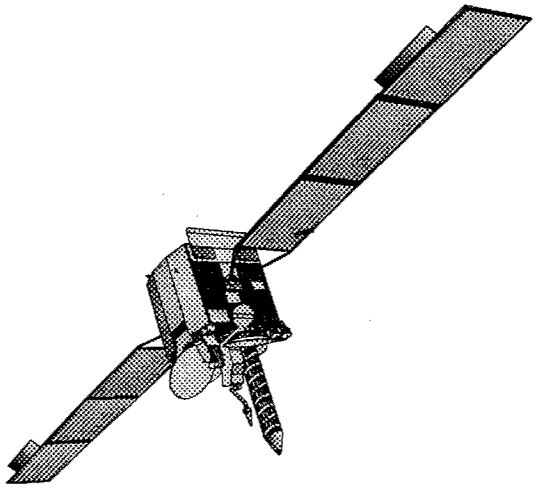

MATRA MARCONI SPACE

Introduction.

The SKYNET 4 series of three military communications satellites provide flexible tactical communications for maritime and land forces and strategic communications. They were designed, built, integrated and tested by British Aerospace Space Systems Limited (now part of Matra Marconi Space UK Limited). The spacecraft platform was derived from the platform used by the European Space Agency's (ESA) successful ECS and MARECS satellites. These are three-axis stabilized geostationary satellites which provide wide coverage. A view of one of these spacecraft as it would appear in orbit is given in the figure above.

CELL AND BATTERY STANDARDS

PARAMETER	NASA	ESA	MMS
Maximum Temperature / °C	35	30	35
Maximum Pressure / psig	80	Not Specified	60
Maximum DoD / %	70	80	50
Maximum cell volts / V	1.55	1.56	1.56
Design Life / years	8	13	7
Capacity Dispersion / %	5	3	3

MATRA MARCONI SPACE

Battery Definition.

A detailed description of the power subsystem and the battery design philosophy was given at last year's workshop [1], where spacecraft A of the SKYNET series was the focus of attention. Spacecraft B has identical batteries to spacecraft A, even having cells from the same manufacturing lots (each spacecraft had one battery built from Gates 35AB03 lot 6 cells and the other from lot 7). Spacecraft C had batteries made from cells of lot 8, which gave similar test results to the earlier lots except during the early cell level tests, when marginally lower capacities, particularly at 0°C, were recorded.

The procurement specification for the batteries was based on a combination of American [2] and European [3] standards which are compared in the above table. The maximum depth of discharge of 70% or 80% was not adopted as a result of system reliability considerations.

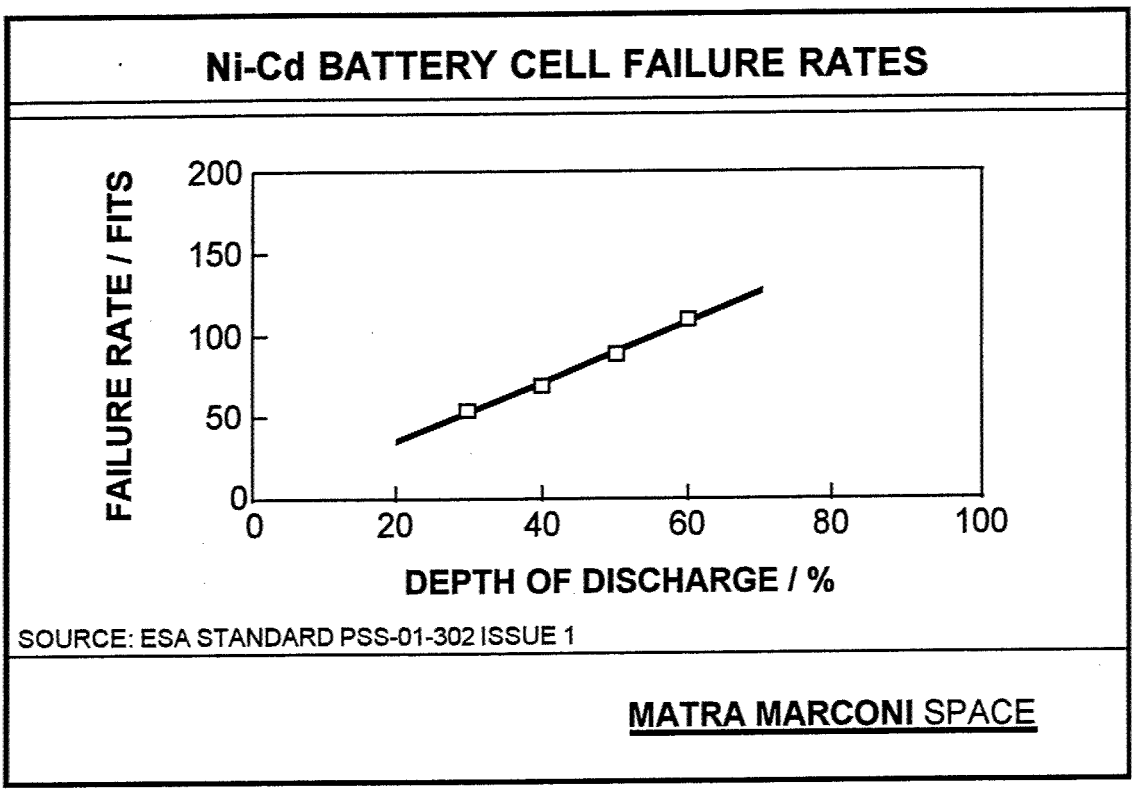

Available data at the time of the design of these spacecraft showed that cell failure rates, measured in Failure unITS (FITS), increased with depth of discharge [4], as illustrated in the above graph. Furthermore, following the work of Dawson [5], it was decided not to use cell by-pass electronics but to use the mass saving to offset the use of a larger capacity battery. Reliability analysis set the maximum failure rate for a cell at 89 FITS and consequently the design maximum depth of discharge was set to 50%.

BATTERY MANAGEMENT STRATEGY

1. The average battery temperatures are strictly maintained below 15°C.
2. Overcharge is limited in eclipse by having a k-factor goal of 105%.
3. Overcharge is limited in the hotter solstice by having trickle-charge enabled for only 50% of the time.
4. The depth of discharge is well within the design limit of 50%, with all spacecraft in the range 32-40% as they reach the latter part of their design life.

MATRA MARCONI SPACE

Battery Management Strategy.

The primary objectives were to keep the battery temperatures below 15°C throughout the mission, which has led to toggling trickle charge on and off during the solstices for the battery on the sun facing side of the spacecraft, and minimizing overcharge. The same battery management strategy is applied to all three spacecraft with two important exceptions: spacecraft A has a lower end of charge voltage limit set to terminate main charge when the recharge ratio (k-factor) is of the order of 90% and spacecraft B's batteries are only reconditioned once per year.

BATTERY CURRENTS AND RATES

PARAMETER	Current / A	C/	C_{der}/	Rate Limits
Main Charge	1.85 ± 5%	18.9	14.2	$C/10^{*} > I_{mc} > C/20$
Trickle Charge	0.3 ± 10%	116.7	87.5	$C/70 > I_{tc} > C/200$
Discharge	10.5 ± 10%	3.3	2.5	$I_d < C/2^{*}$

*Cell Manufacturer's limit

MATRA MARCONI SPACE

The secondary objective in the battery management strategy was to minimise cell current density. Although the cells had a nameplate capacity of 35 Ah the manufacturer recommended the use of a derated capacity, defining C_{der} as the capacity of the cell when discharged for one hour at a maximum current density of 20 mA cm^{-2}, in the calculation of maximum charge and discharge rates [6]. As the Gates 35AB03 cell had a positive plate total area of 1324 cm^2 this gave a derated capacity of 26.5 Ah. The above table gives the charge, discharge, and trickle charge ranges seen in orbit and compares both the rates based on nameplate capacity and on derated capacity with the limits given in the Power Standard [3]. In all cases it can be seen that the spacecraft are operating with comfortable margins on their design limits.

CHARGE TERMINATION CRITERIA

1. End of charge voltage trip level is reached.
2. Rate of temperature rise exceeds 1°C in 15 minutes.
3. The charge input exceeds 1.05 times the charge withdrawn during the preceding eclipse.
4. Average temperature of either battery reaches 15°C.
5. Battery upper temperature limit, as indicated by any thermistor, is reached.

MATRA MARCONI SPACE

Charge Termination.

Of the above charge termination criteria, numbers 1 and 5 are automatic and the remainder are manual by ground intervention. Automatic termination is preferred as the operator workload associated with the manual enabling and termination of main charge is significantly reduced, as is the real-time data analysis required to determine the manual termination criteria. Following the success of the strategy of setting a lower end of charge voltage limit on spacecraft A to ensure automatic charge termination, albeit with a lower than recommended recharge ratio, this strategy was adopted for all three spacecraft prior to the Autumn 1996 eclipse season.

The thermal limits, criteria 4 and 5, are only expected to be reached in abnormal circumstances. To date, only termination by criteria 1, 2, or 3 have been experienced.

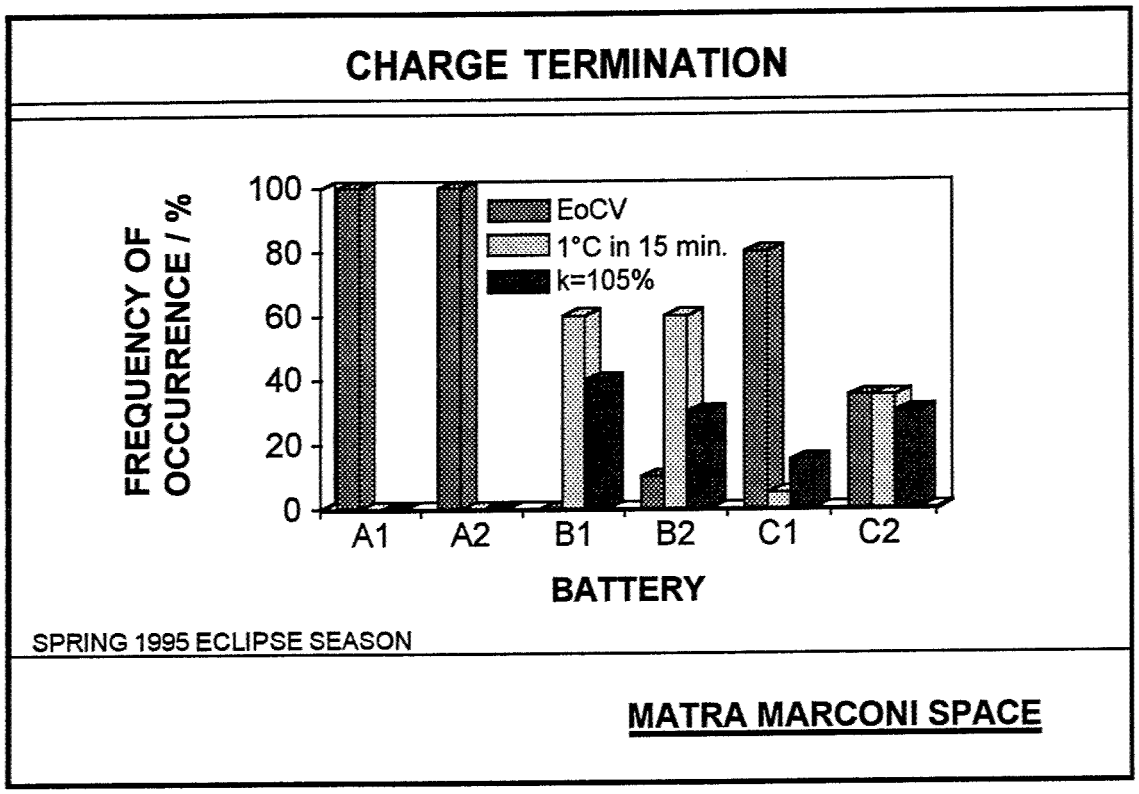

The above chart gives the frequencies of occurrence of the three charge termination criteria encountered during the Spring 1995 eclipse season. The low end-of-charge voltage (EoCV) on spacecraft A at 41.4 V ensures this criteria is always reached first. Although this results in a k-factor of ~90%, the fairly high trickle charge rate of the order of C/100 ensures the batteries are fully charged each season. Among the other batteries there is a fairly even distribution of charge termination criteria.

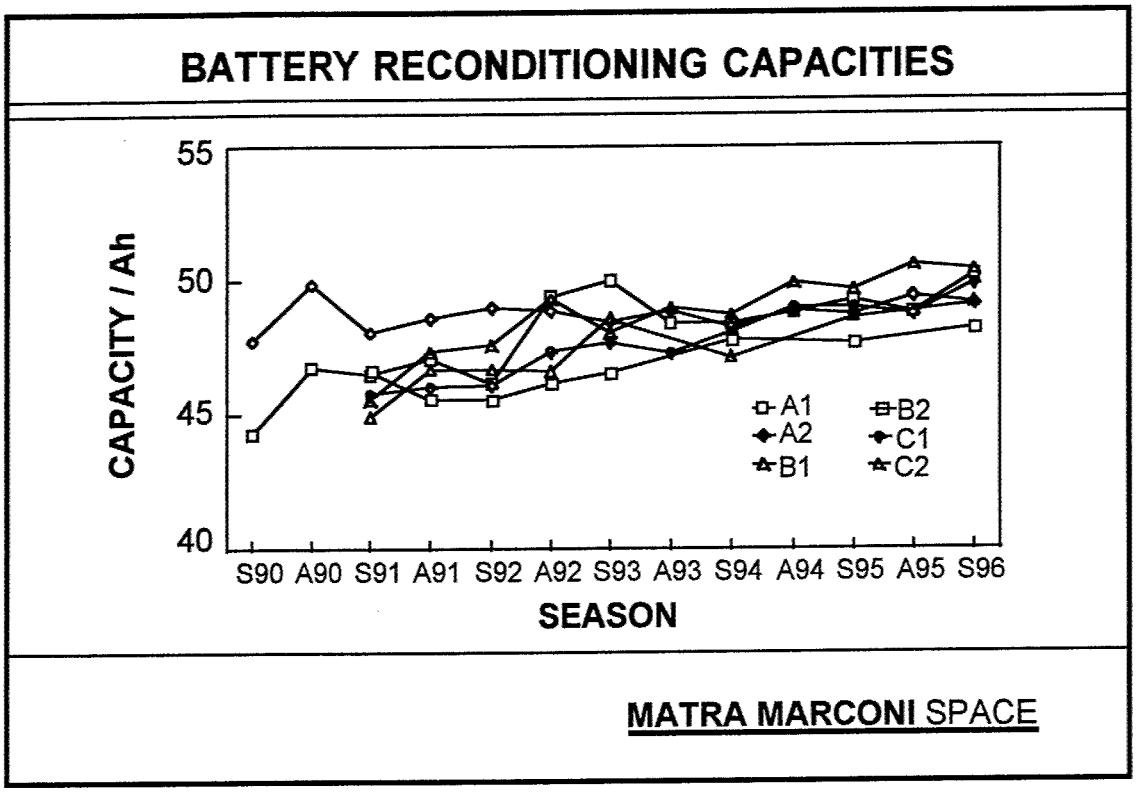

In-Orbit Performance.

1. Reconditioning.

The reconditioning cycle also serves as a battery health check. This consists of discharging the battery through a 102.5 Ω resistor until the first cell falls below 400 mV or until all cells are below 600 mV. Although it may be preferable to terminate the discharge for example when the first cell reaches 100 mV, ground station availability and "down-time" have to be taken into account. Allowing for a maximum down-time of thirty minutes, the 400 mV limit is considered a safe voltage level where a further thirty minutes of discharge would not lead to reversal.

The above figure shows the returned capacity during this cycle each time it has been performed. The 35AB03 cells used in the SKYNET batteries had a positive plate loading of 12.65 ± 0.6 g dm^{-2} of active material. This gives a theoretical capacity of 48.4 Ah on average. The gentle increase in capacity with time is considered normal and is attributed to the corrosion of the nickel substrate of the cathodes. In all cases the rate of increase in capacity is less than 1 ampère-hour per year.

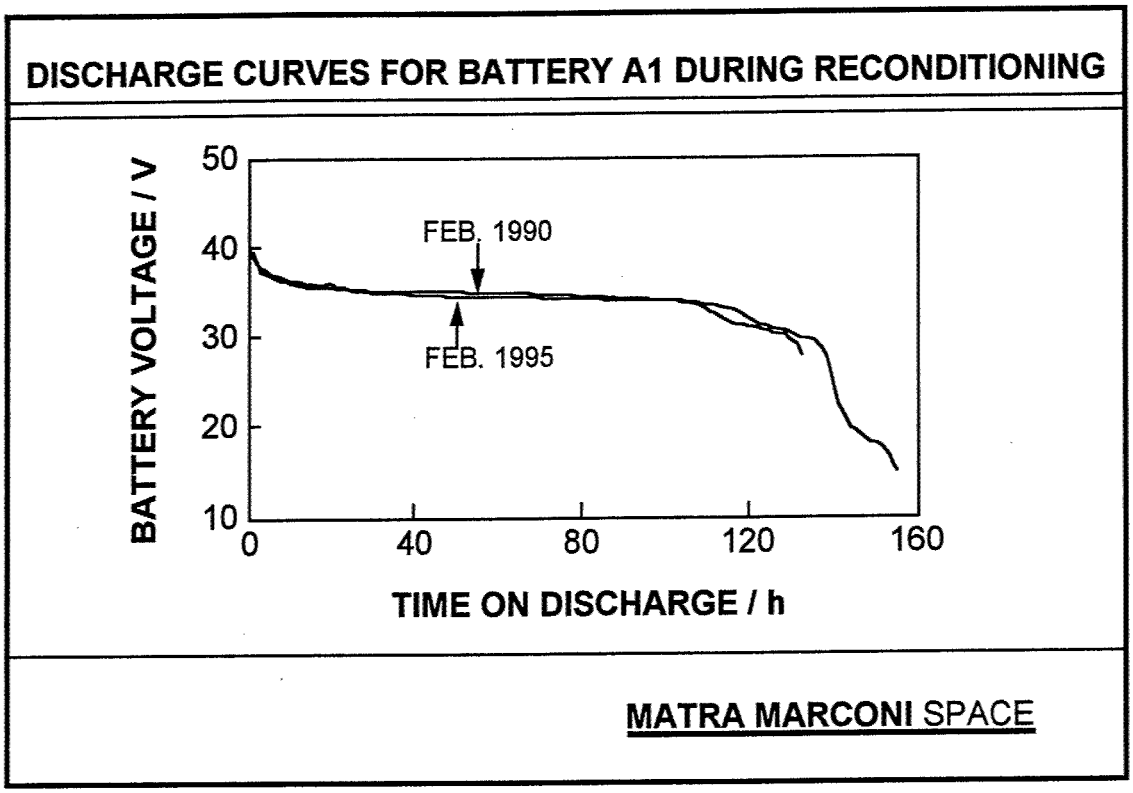

The batteries are reconditioned prior to each eclipse season, except in the case of spacecraft B which has annual reconditioning. Examination of the reconditioning discharge profile provides information on the health of the batteries. The above diagram compares the discharge profiles for spacecraft A battery 1 from 1990 with that from 1995. A second voltage plateau is evident immediately before the termination of discharge, indicating that the cells are limited by the positive electrodes. The depression of the 1995 curve by approximately 100 mV implies the internal resistance of the battery has increased by 7% over the five year period. This can be attributed to the normal electrolyte redistribution during lifetime.

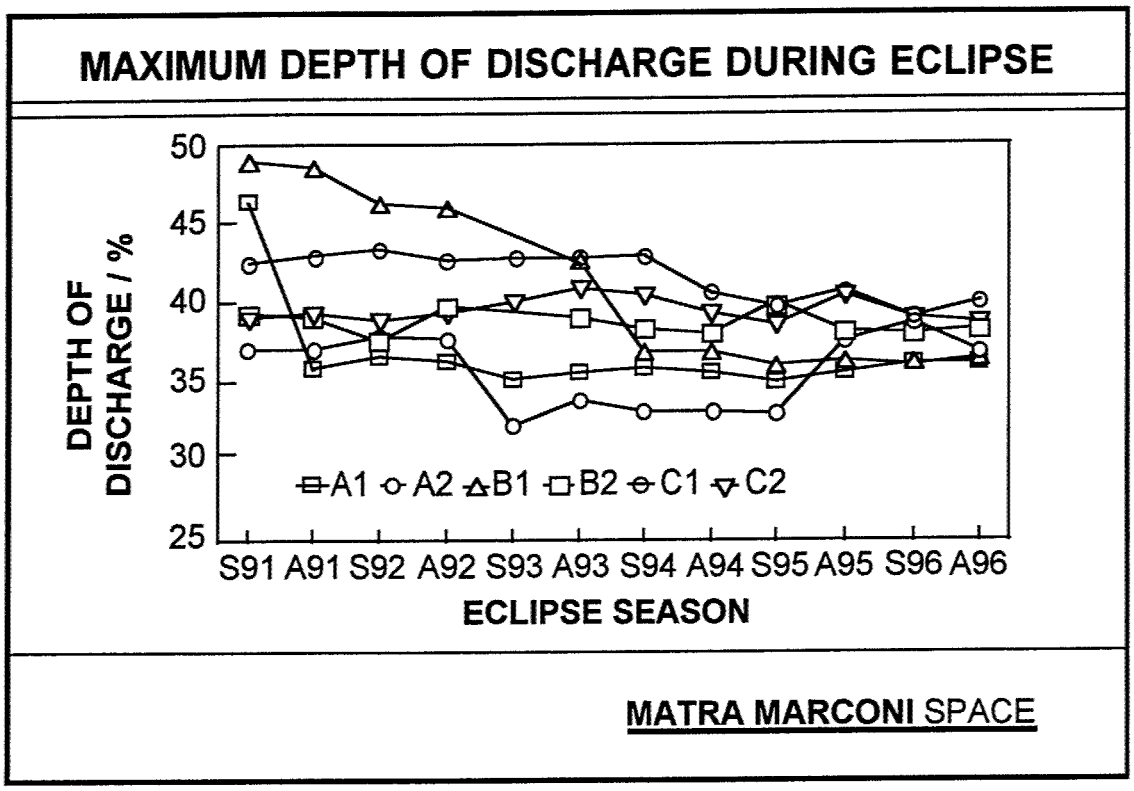

2. Eclipse Performance.

As operational demands vary the depth of discharge each battery experiences also varies from season to season, as may be seen in the above figure. The solar absorbency of the secondary surface mirrors increases with time as deposits condense from the out-gassing spacecraft, causing the spacecraft temperature to rise. Midway through the life of the spacecraft this temperature rise is compensated for by the permanent disabling of a 50 W general level heater, thereby reducing the load on battery one of each spacecraft in later years. To enable comparisons of battery voltages to be made differences in depths of discharge must be taken into account. However, from the above figure it can be seen that all six batteries have converged and are operating in the range 38 ± 2 % depth of discharge.

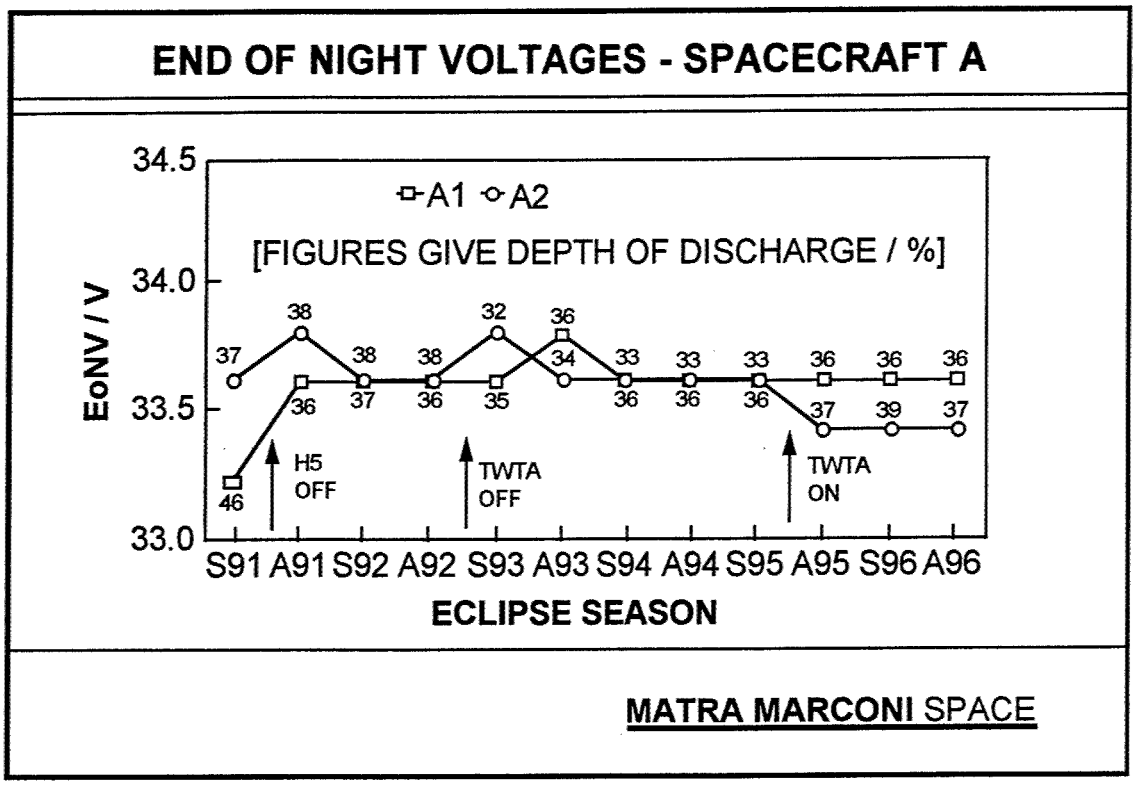

2.1 Spacecraft A.

The above figure gives the end of night voltages for spacecraft A for the peak eclipse each season. The numbers at each point indicate the depth of discharge of the battery at that eclipse. The battery voltage is measured on the spacecraft using an eight-bit analogue-to-digital converter to cover the voltage range 0-50 V, giving a resolution of 1 bit equals 194 mV. Battery 1 has had a constant peak eclipse depth of discharge after the general level heater H5 was turned off in June 1991, while battery two's depth of discharge fell by 4% during the period that one of its travelling wave tube amplifiers (TWTA) was switched off.

From the graph it can be seen that battery 2 had a depth of discharge of 37% in Spring 1991 and in the Autumn of 1995. During this period the battery voltage has decreased by 1-2 telemetry bits (~200 - 400 mV). As most of the spacecraft heaters are on bus 1 (heaters are resistive loads) and the payload is mostly on bus 2 (the payload is essentially a constant power load) this may explain the small difference in the above curves. While care must be taken with data with such limited resolution, it does appear that the battery with resistive loads is not degrading as much as the battery with constant power loads.

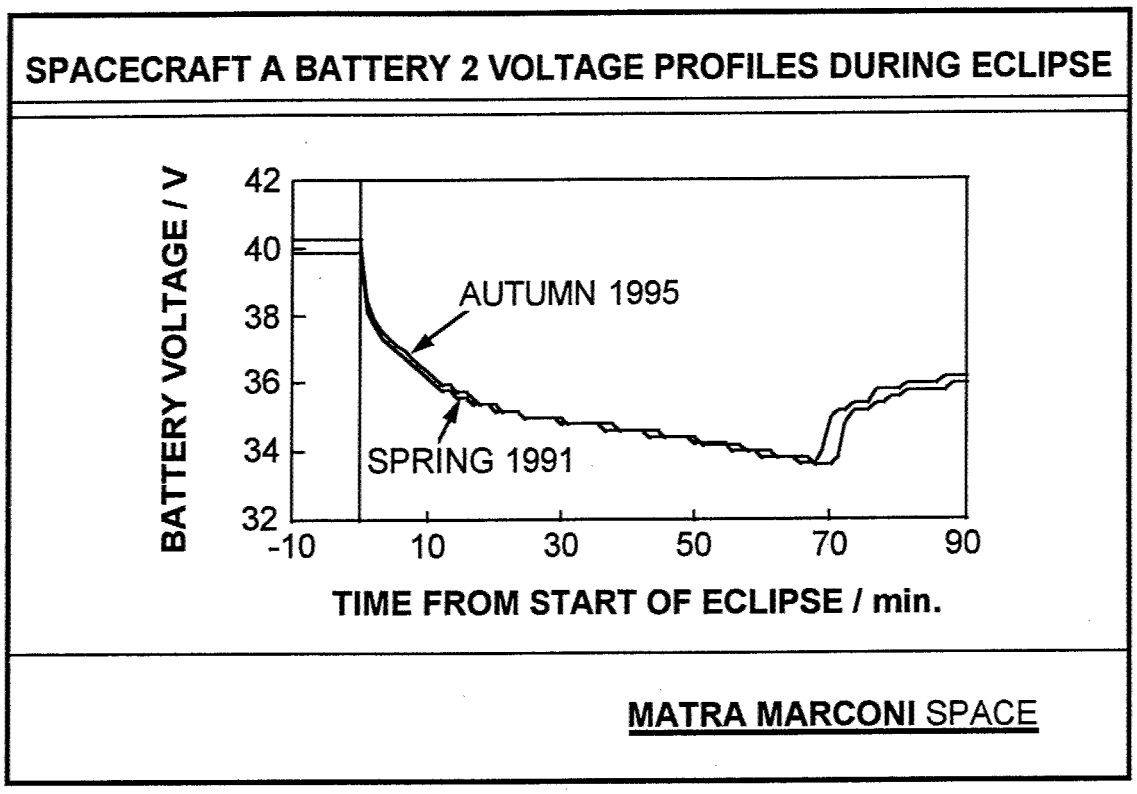

The above curves show the discharge voltage profiles during the Spring 1991 and Autumn 1995 seasons. The later curve shows a higher steady state voltage on trickle charge and a lower end-of-night voltage, though in both cases these differences correspond to one telemetry bit.

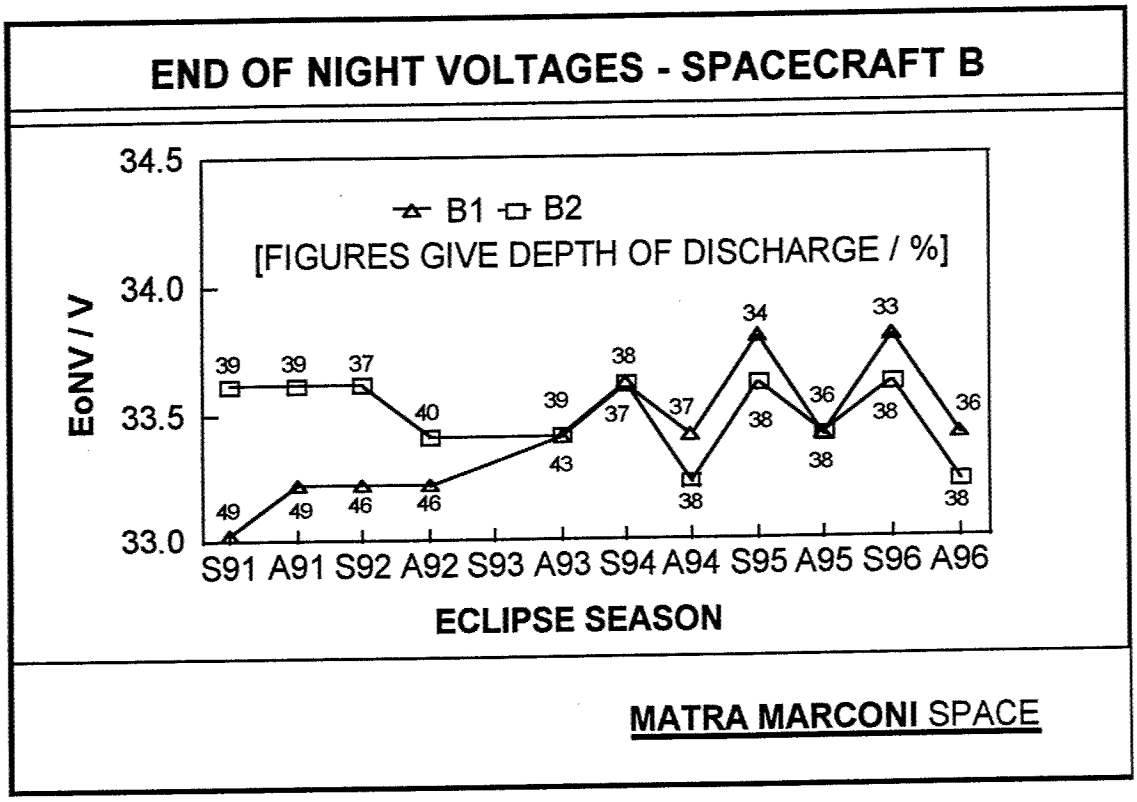

2.2 Spacecraft B.

A spacecraft is vulnerable during reconditioning when one of its batteries is fully discharged. As spacecraft B's batteries are only reconditioned once per year the effect of omitting reconditioning prior to an eclipse season can be evaluated. The option of being able to omit a reconditioning sequence may be desirable, particularly during a period of stress. The above curve shows the end-of-night voltages for the peak eclipse. Annual reconditioning, prior to the Spring eclipse season was introduced in 1994. The difference in battery voltage between the Spring and Autumn seasons is up to 400 mV. Surprisingly, the annual recondition seems more effective at restoring battery voltage than when half-yearly reconditioning was employed. However, no explanation for this phenomenon is offered.

Although battery one was more heavily discharged during the earlier part of its life, its end-of-night voltage in later life appears constant when the reconditioning effect is taken into account. Battery 2 has had a nearly constant depth of discharge throughout life with no evidence of voltage degradation.

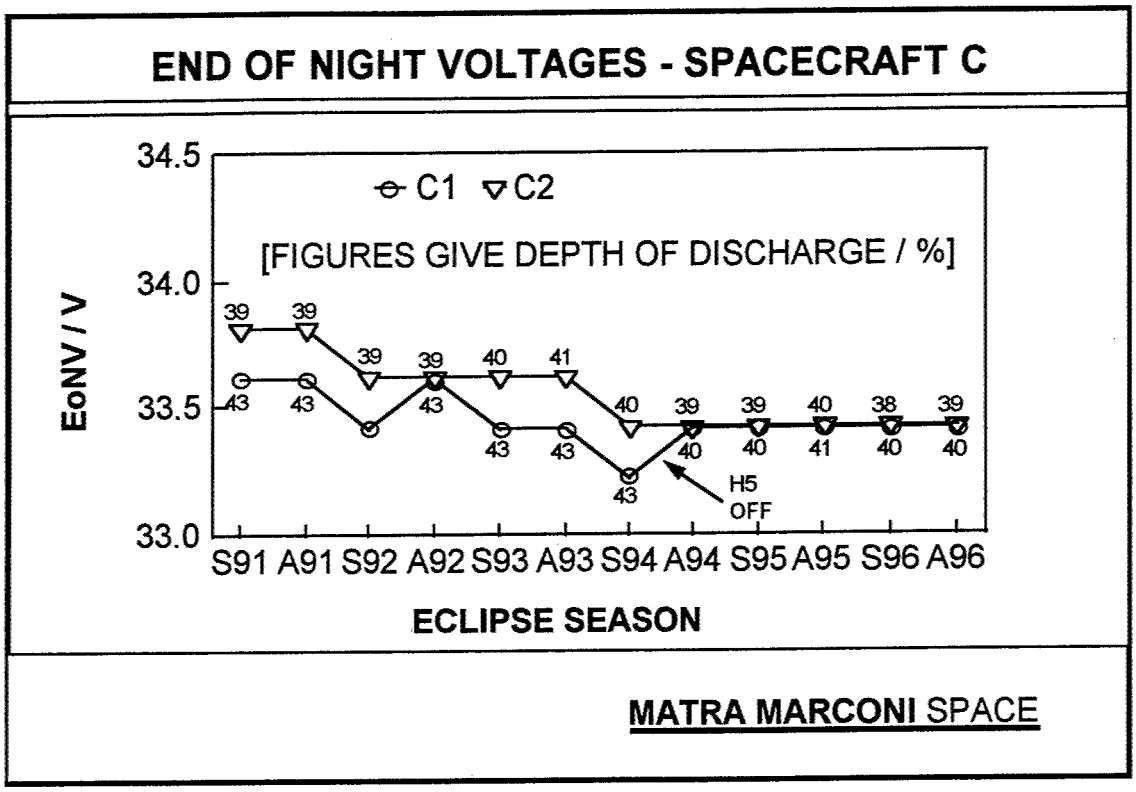

2.3 Spacecraft C.

This is the control spacecraft in the sense that the batteries are operated in accordance with established procedures. The loading on both batteries has been constant throughout life with the exception of the level heater H5 being turned off in August 1994. This gave a 3% reduction in depth of discharge. From the discharge profiles the battery voltage fall with depth of discharge, at the discharge rates used, can be determined. All spacecraft battery voltages fall within the range -65 ± 5 mV per percent depth of discharge. Thus although battery one's voltage appears to fall by one telemetry bit, when the lower depth of discharge is taken into account this is equivalent to two bits, the same as battery two.

These two batteries, while giving better than acceptable performance, are under performing the other four batteries. With hindsight this may not be surprising, as even in the cell vendor's data pack these cells were seen to have marginally lower capacities, and consequently these batteries are being worked "harder" in orbit.

SUMMARY

1. 10 387 776 cumulative cell hours in orbit with no failures.
2. Recharge ratio of 90% and a trickle charge rate of C/100 is sufficient to maintain the batteries fully charged.
3. Annual reconditioning is sufficient to fully restore battery performance.
4. The low-current, low-temperature (LILT) philosophy of battery management has resulted in better than expected battery performance over the design life.

MATRA MARCONI SPACE

Summary.

The six batteries on these three spacecraft have to date (3rd December 1996) accumulated over 10 million cumulative cell hours with no failures and continue to perform with barely detectable signs of degradation. The cell and battery specifications developed by both ESA and NASA combined with an in-orbit battery management strategy based on low temperature, low current density and low depths of discharge have resulted in a spacecraft fleet whose batteries have exceeded all expectations. The LILT approach additionally results in a simplification of the battery operational procedures. Semi-autonomous eclipse operation is possible with a single voltage limit, as temperature compensation or VT curves are not needed with the constant current charging available from the dedicated solar array strings.

ACKNOWLEDGMENTS

The authors are indebted to the following:

•The members of 1001 Space Unit, RAF Oakhanger, for their co-operation and provision of much of the data contained in this paper,

•Colleagues in the SKYNET Project Team, for many useful and informative discussions,

•The United Kingdom Ministry of Defence, for permission to publish this paper.

MATRA MARCONI SPACE

References.

1. P. J. Johnson and N. R. Francis, Proc. 1995 NASA Aerospace Battery Workshop, NASA Conference Publication 3325, (1996), 175.

2. NASA Specification NHB8073.1, "NASA Specification for Manufacturing and Performance Requirements of NASA Standard Aerospace Nickel-Cadmium Cells",(1988).

3. "Power Standard", ESA Publication PSS-02-10 Vol. 1 Issue 1 (1992).

4. "Failure Rates for ESA Spacecraft and Associated Equipment", ESA Publication PSS-01-302 Issue 1 (1985).

5. T. Dawson, "Elimination of Battery Cell Bypass Electronics on FLTSATCOM", Paper 849002, Proc. IECEC '84, (1984), 72.

6. D. F. Schmidt, General Electric Company, Private Communication, (1986).

Page

468

Blank

FAST Spacecraft Battery Design and Performance

by
David S. Jung
Gopalakrishna Rao
Anisa Ahmad

NASA/Goddard Space Flight Center
Greenbelt, Maryland 20771

Abstract

The Fast Auroral Snapshot (FAST) Explorer spacecraft is to study the physical processes that produce the aurora borealis and aurora australis. It is a unique plasma physics experiment that will take fundamental measurements of the magnetic and electrical fields. This investigation will add significantly to our understanding of the near-earth space environments and its effects. The FAST has a 1 year requirement and 3-year goal for its mission life in low earth orbit. The FAST power system topology is a Direct Energy Transfer (DET)system based on the SAMPEX design. The FAST flight battery supplies power to the satellite during pre-launch operations, the launch phase, the eclipse periods for all mission phases, and when the load requirements exceed solar array for all mission phases. The nominal orbital average load is about 50 watts. The FAST battery, 9 Ah Super nickel-cadmium (SNiCd), was designed by Hughes Aircraft Company (HAC) in Torrance, California. The cells were manufactured by Eagle Picher Industries (EPI) in Colorado Springs, Colorado. The battery assembly contains twenty-two series-connected prismatic hermetically sealed cells with dual ceramic seals. The battery weighs 11.3 Kg. The size of battery is 12.70 in x 7.26 in x 4.95 in. The cell and battery designs are presented together with the ATP data, life cycle test results, I&T operations, and in flight performance data.

OUTLINE

- MISSION OVERVIEW
- POWER SUBSYSTEM ELECTRONICS
- BATTERY DESIGN
- CELL DESIGN
- CELL ATP DATA SUMMARY
- LIFE CYCLE TEST DATA
- BATTERY BACKGROUND
- DPA SUMMARY AND RESULTS
- HANDLING AND STORAGE
- IN-FLIGHT PERFORMANCE
- SUMMARY

FAST MISSION OVERVIEW

- The second of the small-class explorer (SMEX) missions
- Investigate plasma physics of the auroral phenomena which occurs around both poles of the earth
- S/C will orbit in a near-polar, highly elliptical orbit
- One year mission duration
- Launched in August 1996

POWER SUBSYSTEM ELECTRONICS

- VT Controller

  Number of VT levels changed from 8 to 16

- Amp hour Integrator included as a key part of charge control

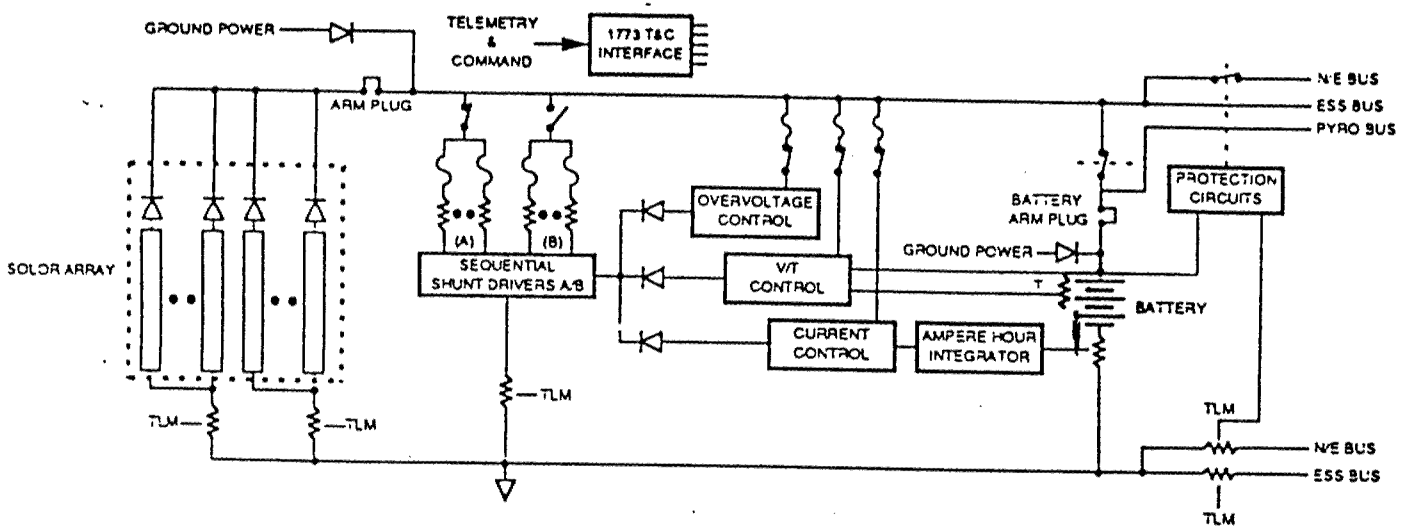

Small Explorer Power System Block Diagram

BATTERY DESIGN

- 9AH Super NiCd (S/N 002)
- 22 cells connected in series using crossed intercell connections
- 22 - 34 Volt
- Dimension: 18.3 x 32.3 x 12.6 Cm
- Mass: 10.96 Kg
- Operate in a 0 to 25 deg. C (Baseplate)
- The SAMPEX Battery connectors re-oreinted to meet FAST mechnical footprint
  - Minimum of harness re-routing
  - No re-wiring
- Capability to monitor battery & cell voltages and battery temperature
- Capability for external charging, reconditioning, and cooling of battery

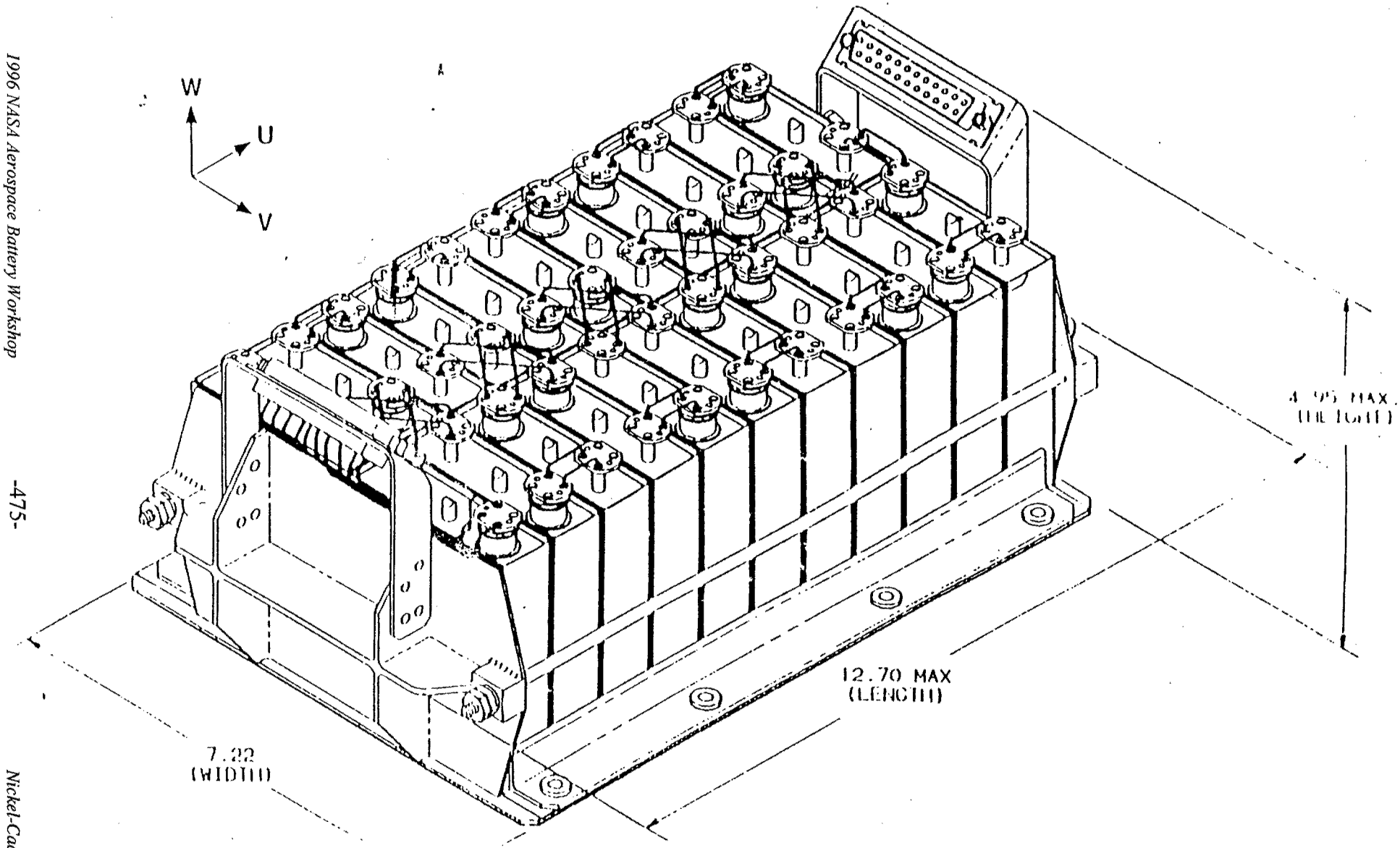

9 Amp-Hour FAST Battery Configuration

CELL DESIGN

- 11.5 AH Capacity at 10 deg. C
- Specific energy at 10 deg. C: 31Wh/Kg
- Sinter void volume for both neg. and pos. electrodes: 80%
- 11 positive, 12 negative electrochemically impregnated plates
- Zircar separator
- 31% KOH electrolyte concentration
- 35 to 40% precharge ratio

CELL ATP DATA SUMMARY

Flight Battery (S/N 002)

Cell S/N	Capacity Ah	Cell S/N	Capacity Ah
13	12.07	16	12.17
22	12.03	23	12.03
26	12.03	28	12.06
29	12.07	36	12.04
39	12.06	48	12.03
64	12.06	66	12.05
71	12.07	73	12.14
74	12.08	75	12.10
81	12.05	83	12.03
84	12.04	85	12.04
88	12.04	89	12.06

Avg. = 12.06
Avg. Cell Wt. = 442 grams
Total Cell Wt. = 21.44 LB

LIFE CYCLE TEST DATA

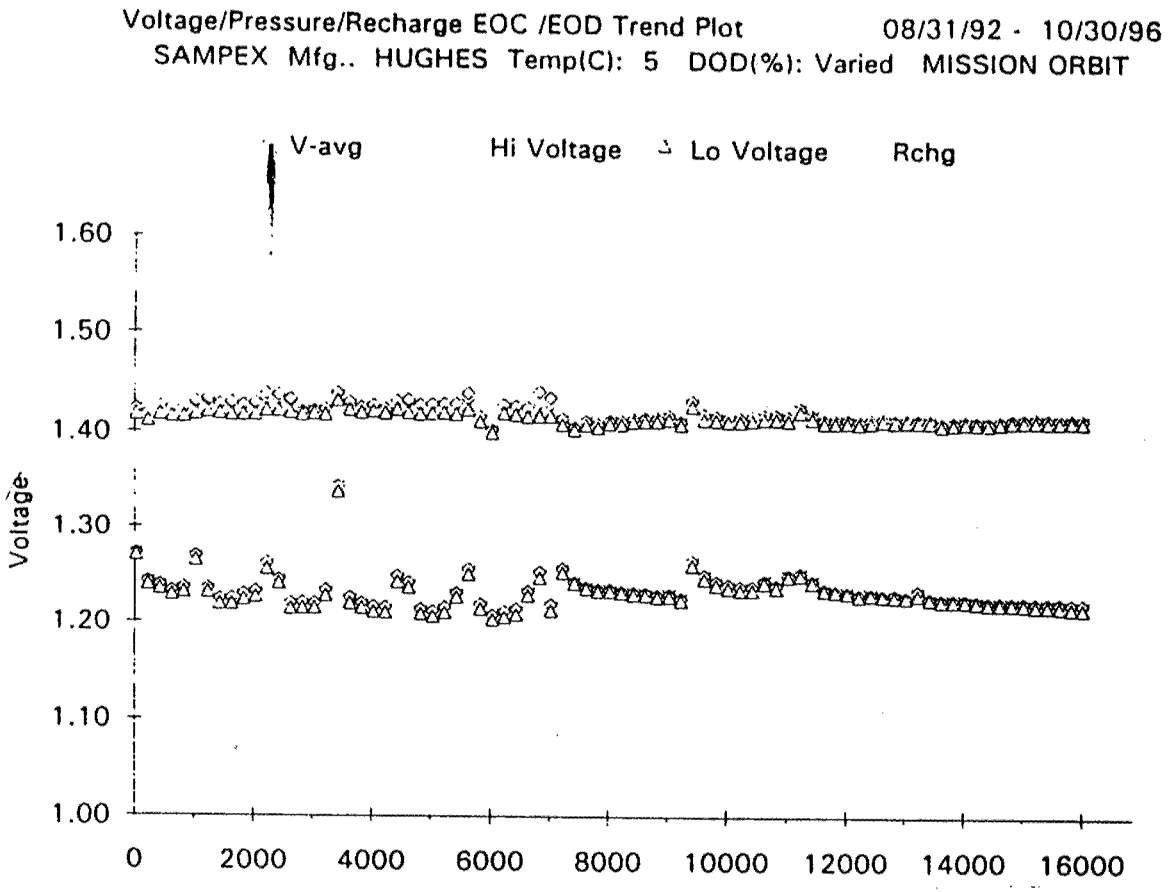

Nominal SAMPEX mission profile (7137 cycles) and nominal FAST mission profile (>9000 cycles at 12% DoD and 5 deg. C) for the FAST flight battery cell pack

BATTERY BACKGROUND

- 9 Ampere-Hour Super NiCd developed as flight Battery for SAMPEX
- Cells activated in May 1991
- Received from Hughes in January 1992
- Shipped to Hughes for rework (bent base plate) and retest in January 1992
- Hughes shipped battery back to GSFC in June 1993
- Performed magnetic testing in September 1993
- DPA one cell (LOT 1, S/N79) to extend the wet life after 3 years of storage in April, 1994
- Mechanical and electrical integration to spacecraft were performed in May 1994
- Performed thermal vac test in June 1994
- Battery moved to mag. test site for mag. testing in June 1994
- Spacecraft packed for shipment to Wallops for spin balance in July 1994
- Launch scrubbed due to Pegasus failure on August 1994
- Removed battery from S/C for storage in battery lab in September 1994

BATTERY BACKGROUND (CON'T)

- DPA another cell (LOT 1, S/N108) to extend the wet life after 4 years of storage in Mar., 1995
- Integrated battery to S/C in April 1995
- Performed T/V and S/C functional test in April 1995
- Moved battery to Battery Lab due to another Pegasus failure in August 1995
- Battery has been topped-off every 3 or 4 days intervals at Battery Lab
- Started re-integration activities in March in preparation for August, 1996
- DPA another cell (LOT 1, S/N 86) to extend the wet life after 5 years of storage in April, 1996
- Flight battery was re-integrated to S/C on April 20, 1996

DPA SUMMARY AND RESULTS

- DPA was performed on Lot 1 S/N 86 in April 1996
- The cell was removed after 5 years of open circuit and trickle charge storage to evalluate it for flight worthiness
- Nominal capacity (>10 Ah)
- Slightly lower charge and discharge voltages were observed when compared to a previous FASTcell from 3.5 years of trickle charge storage
- The same amount of electrolyte was observed for both cells (4.20 cc/Ah)
- The separators looked well wetted and the cell experienced minimal cadmium migration as evident in the separators

HANDLING AND STORAGE

- Maintained charged open circuit condition with a periodic top-off charge or trickle charged continually
- Battery was stored on trickle charge mode (C/100, 6 deg. C) at Battery Lab after receiving it from the vendor in Jan. 92
- Performed top-off charge (C/20, 0.45A, 15 deg.C, 140 min or rollover + 30 min) after 5 min. discharge at 1 Amp. every 3 or 4 days at Battery Lab when not on trickle charge
- At the launch site, performed top-off charge and battery was trickle charged continously after the final reconditioning before launch; Battery temperature was maintained at ~18 deg. C

IN-FLIGHT PERFORMANCE

- Changed VT level from 5 to 4 to acheive c/d ratio at ~110%
- Battery temperature has been stablized and is running around 5 deg. C
- The following trend plots summarize in-flight perfomance since the launch:

1. Trending delta half voltage
2. Battery voltage
3. Battery discharge volt and minimum state of charge
4. Volt and temp trending
5. Max discharge current
6. Max charge current
7. Total c/d ratio
8. C/D ratio and eclipse duration

CHART FAST DELTA

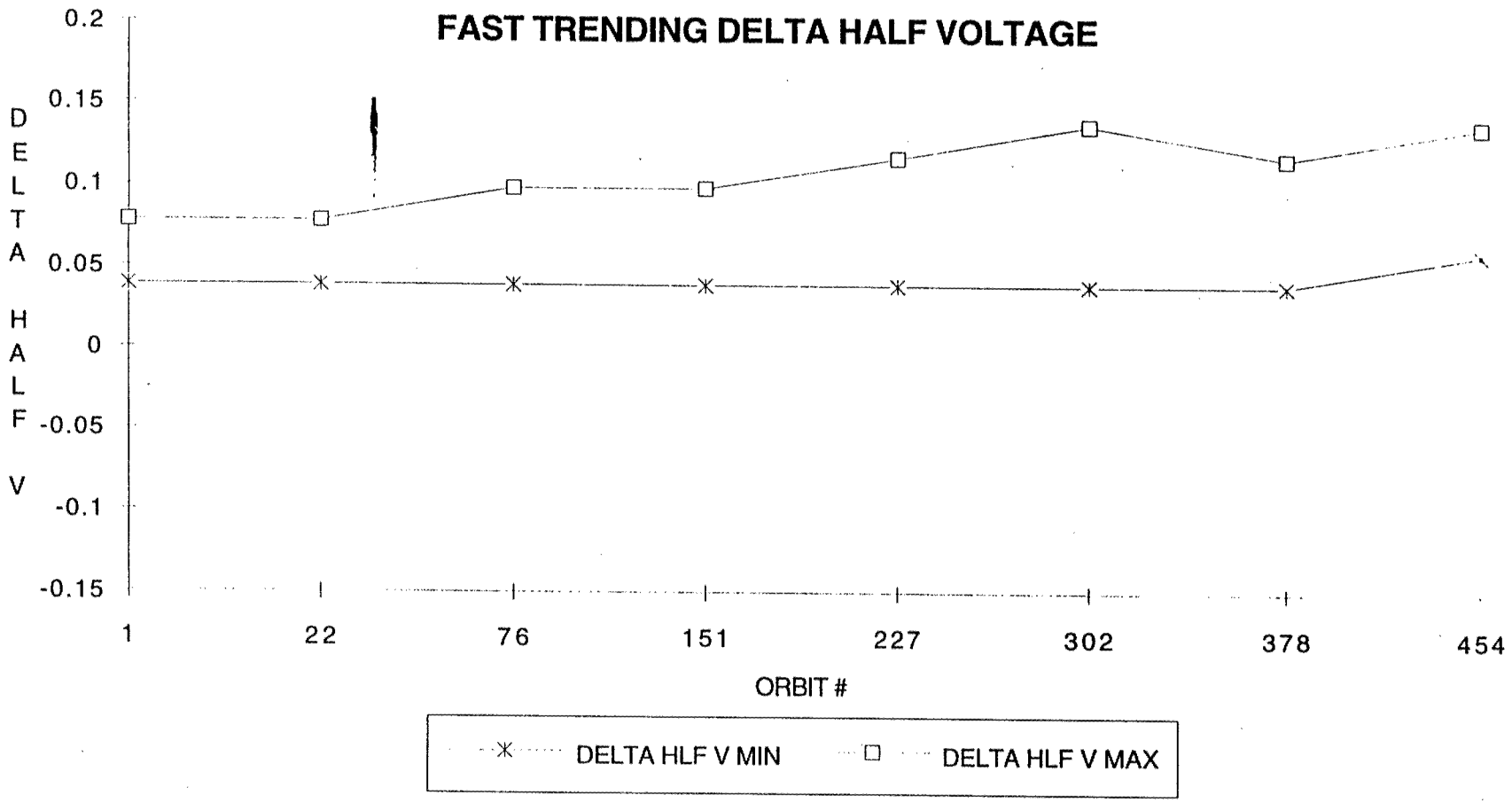

Chart FAST BAT V

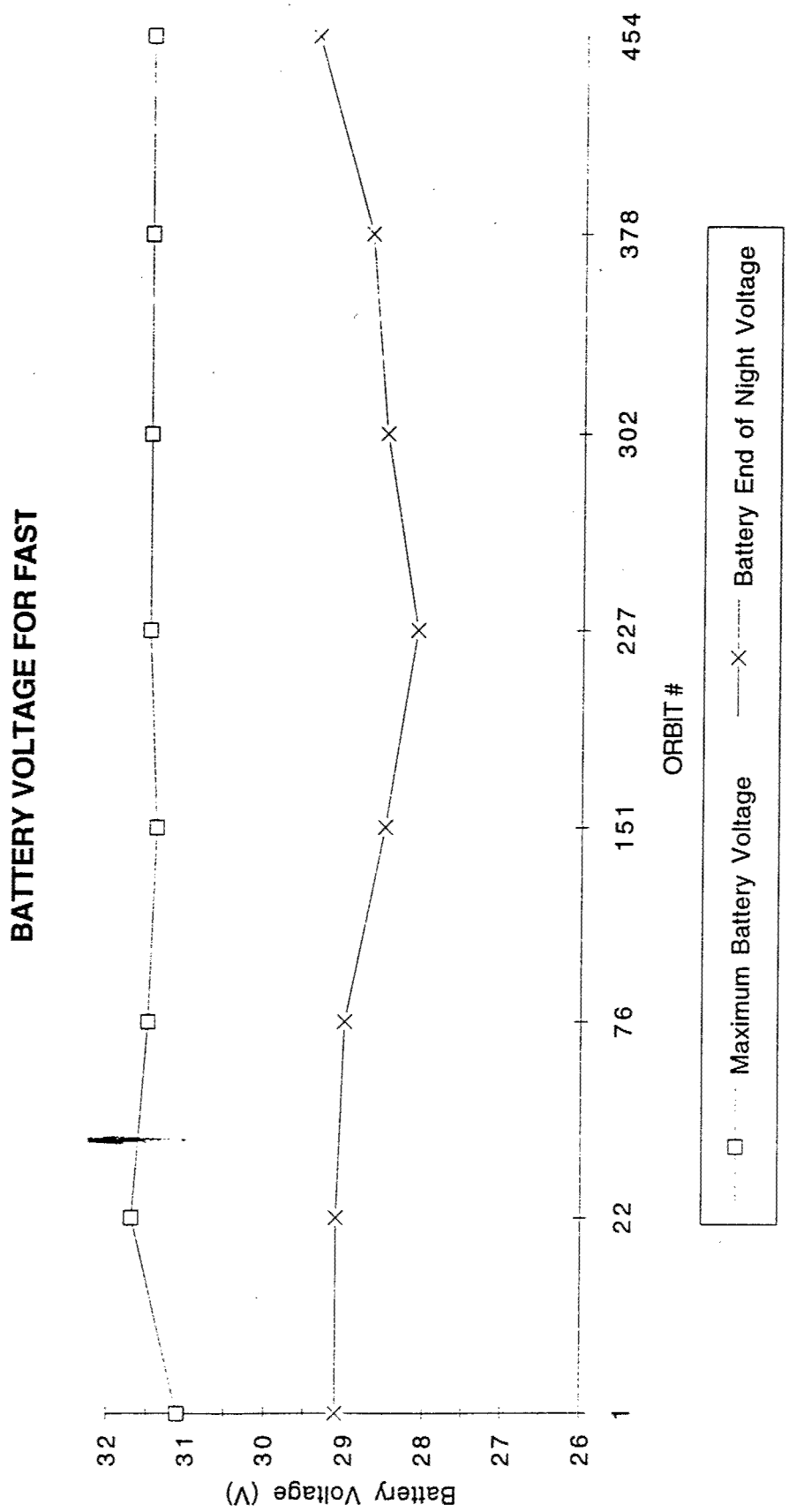

Chart FAST BAT V & SOC

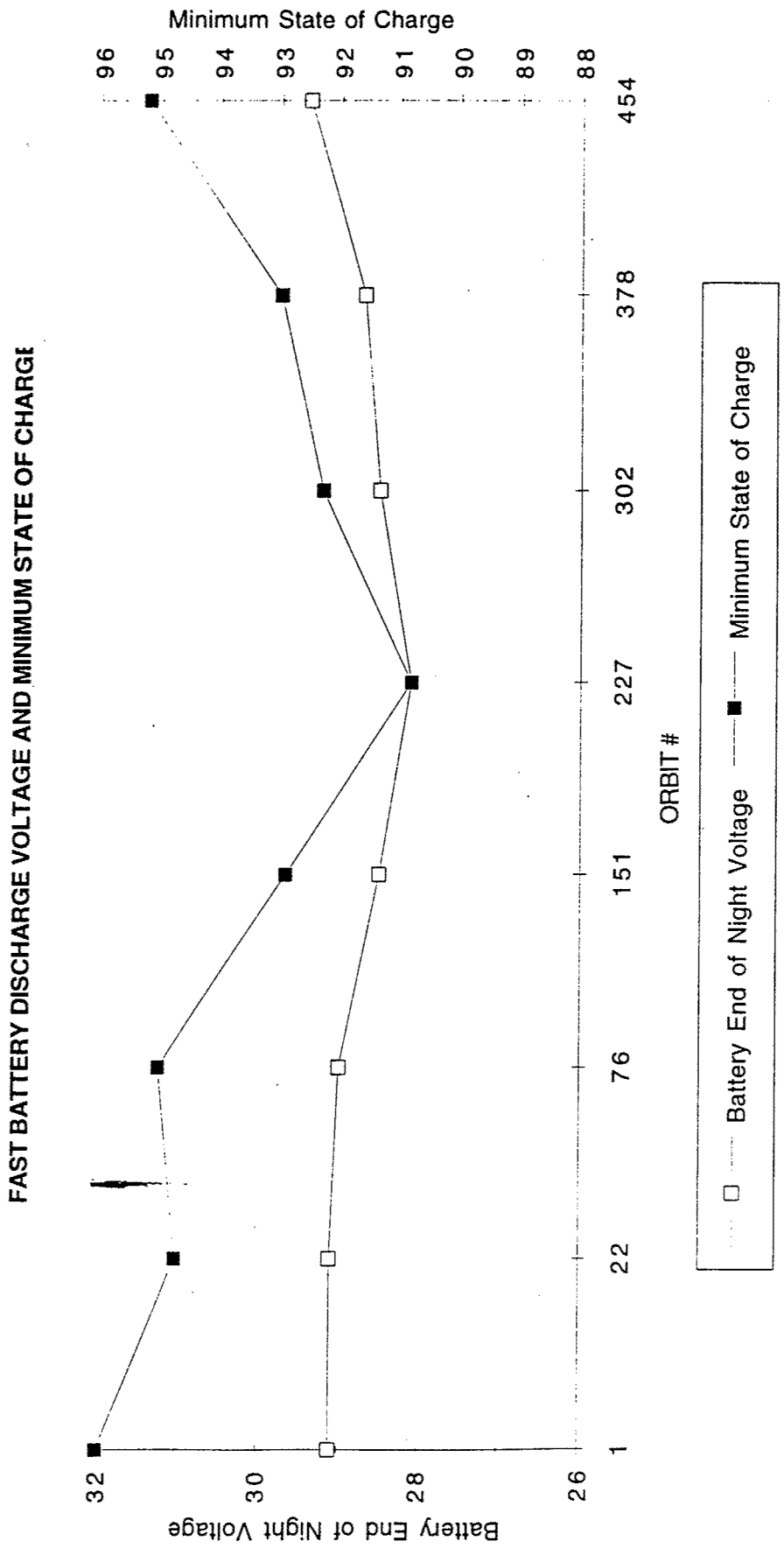

Chart FAST BAT V & T

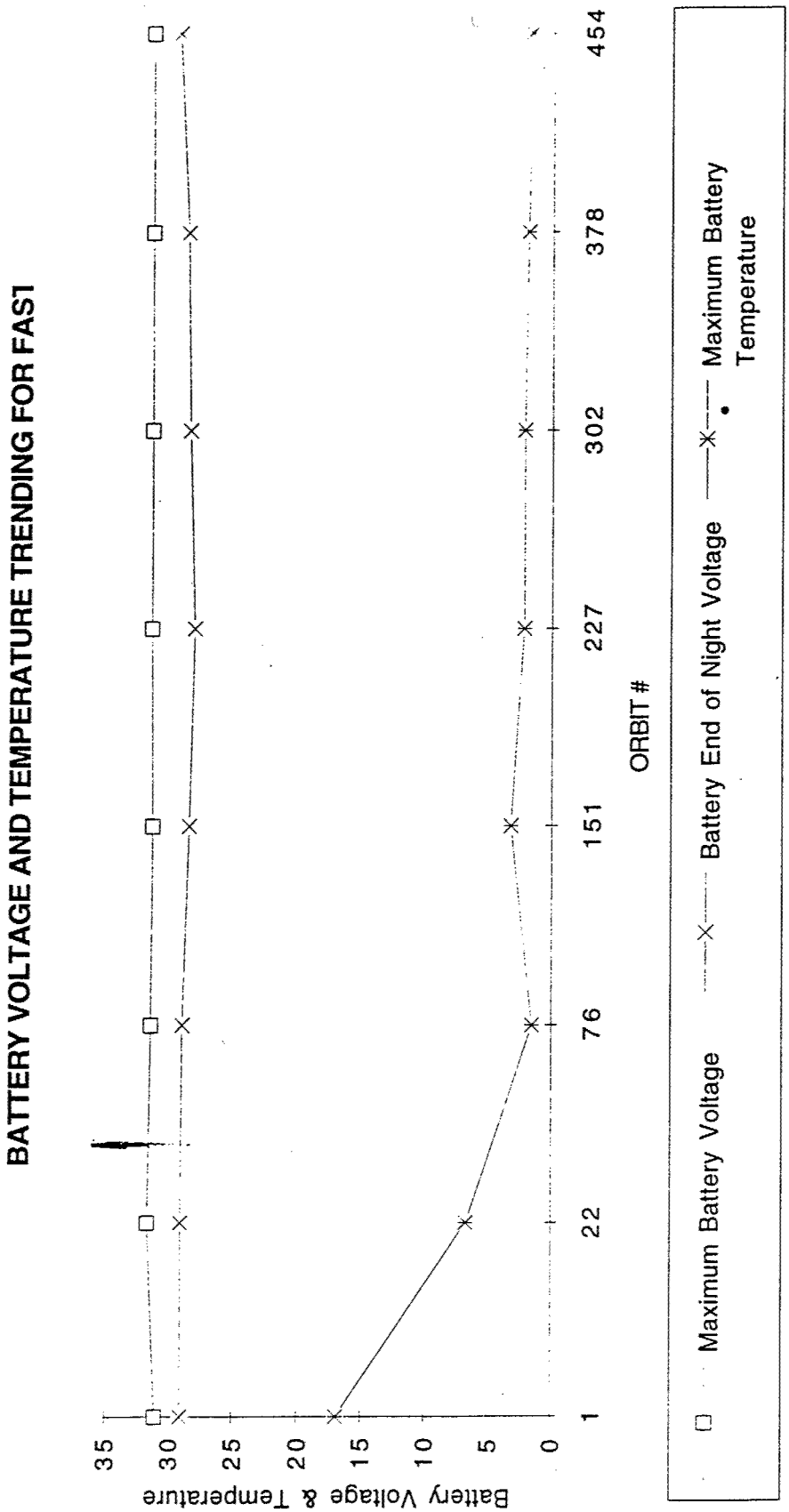

Chart FAST BAT DIS I

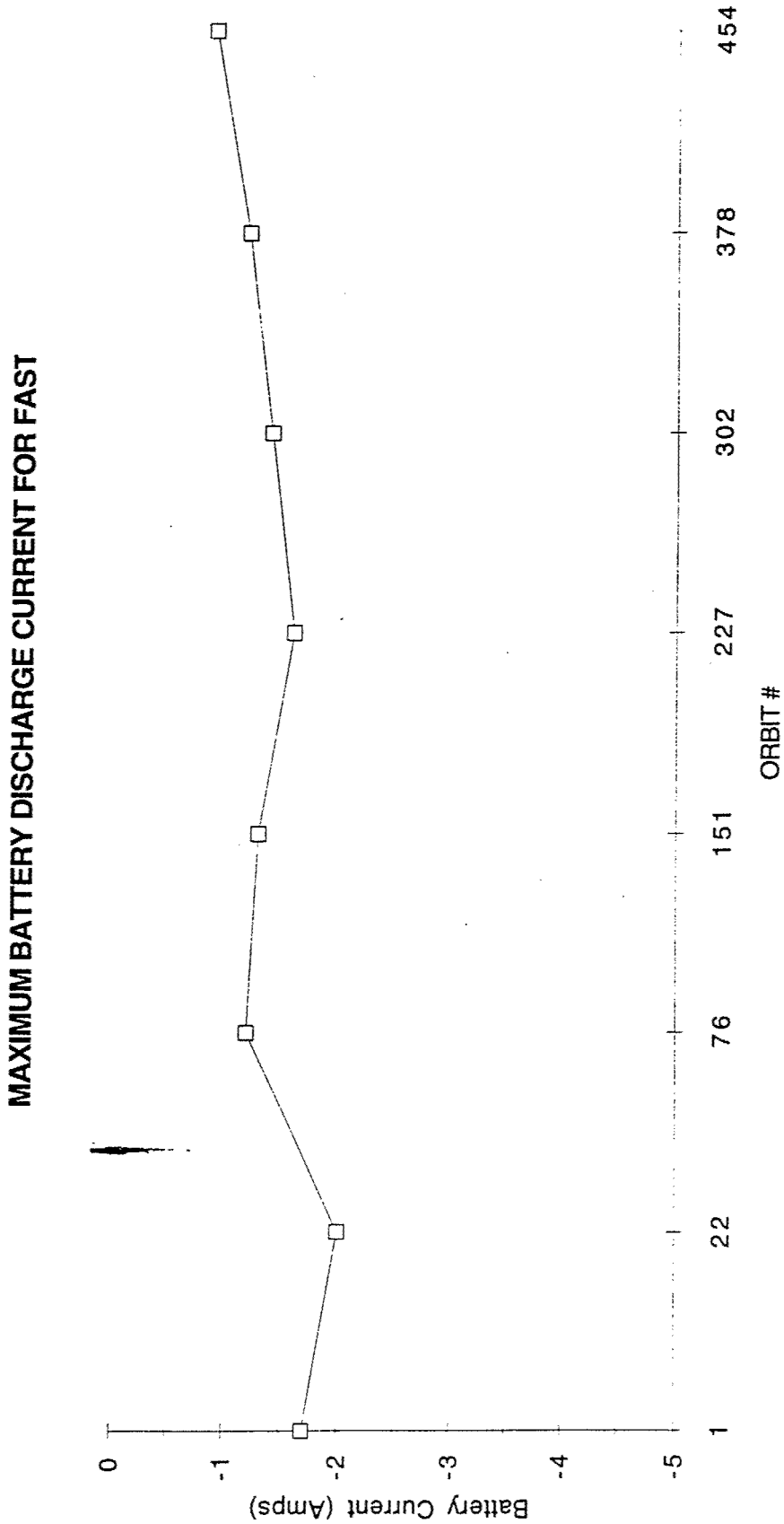

Chart FAST BAT I

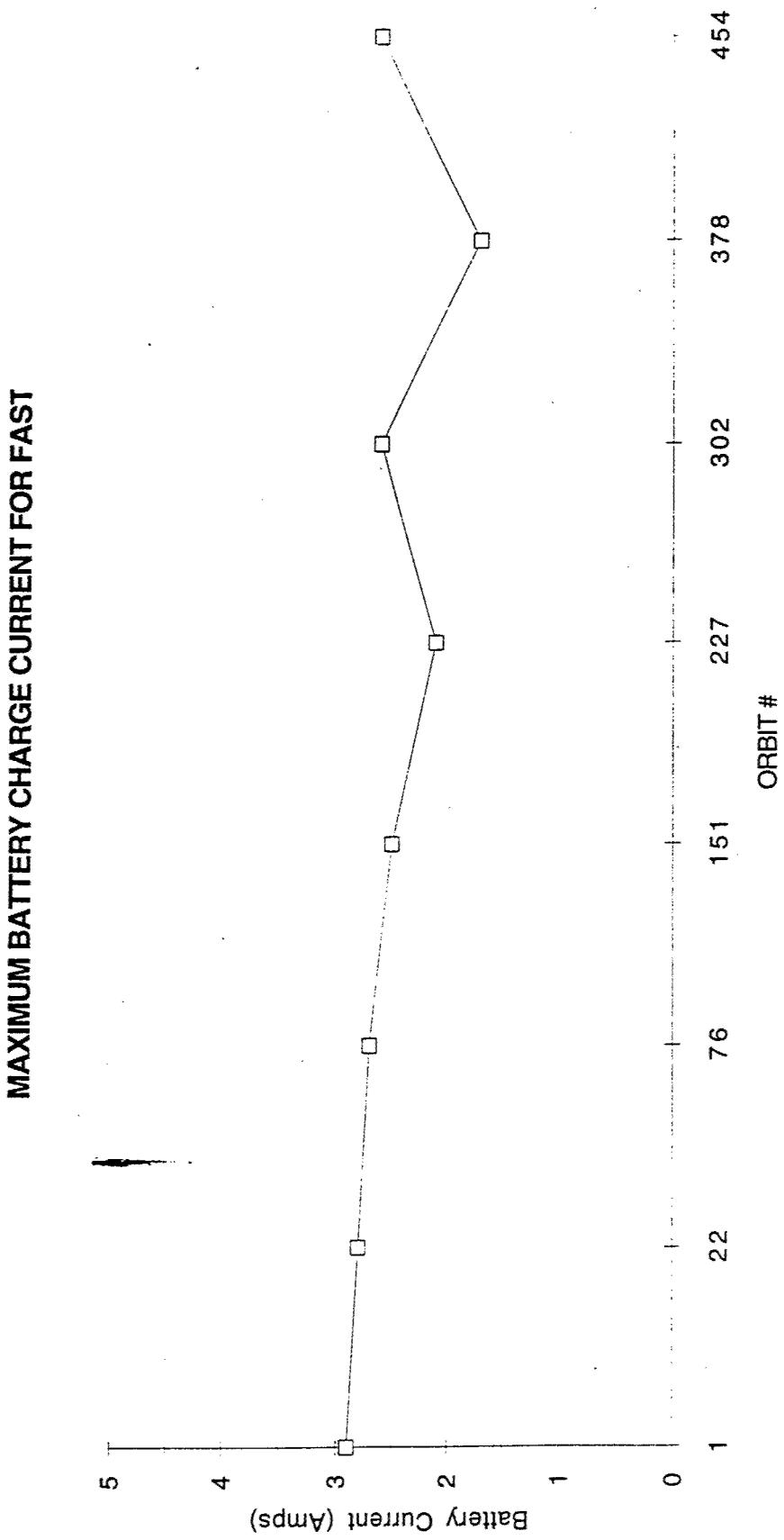

CHART FAST C/D RATIO

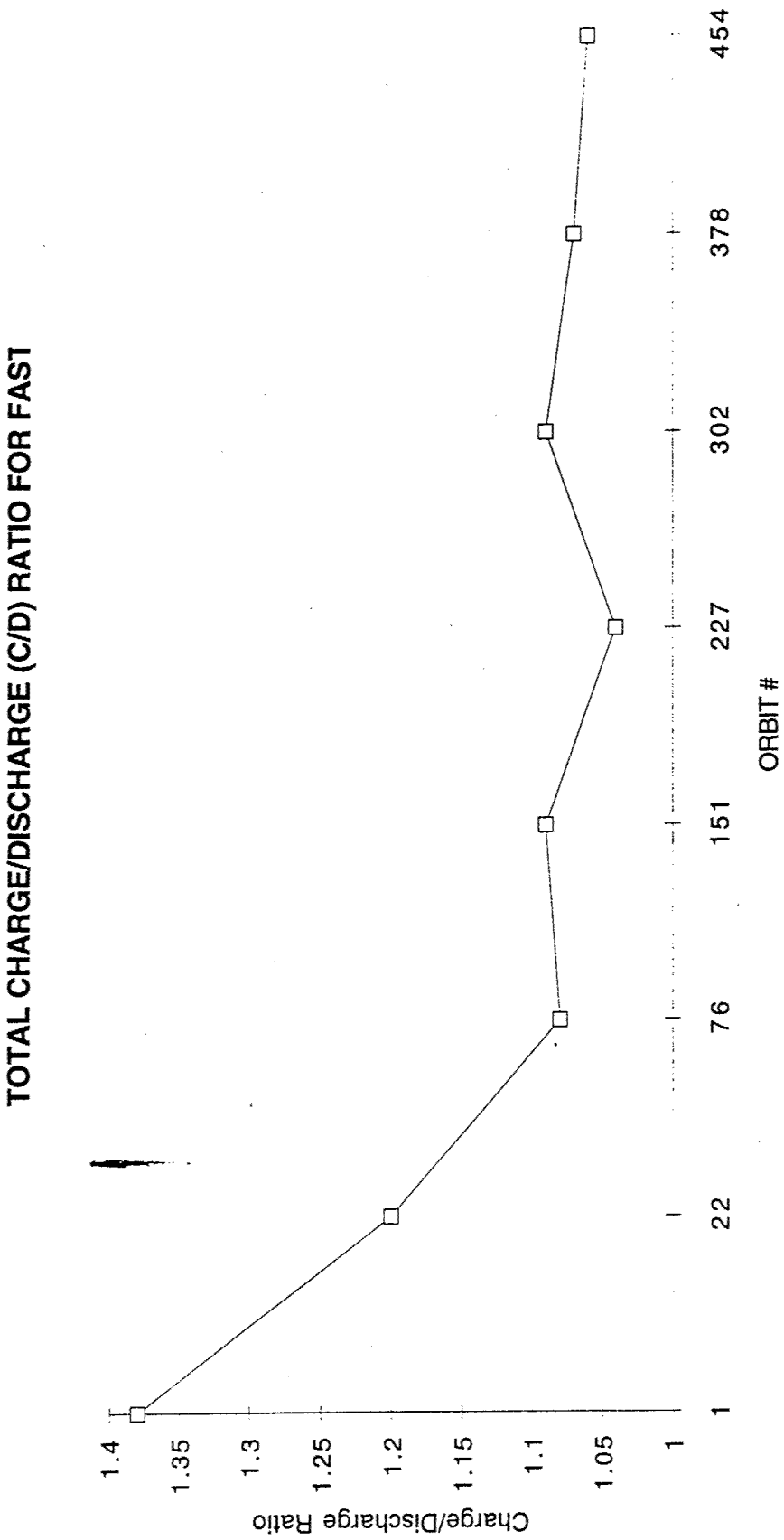

Chart FAST C/D & Eclipse

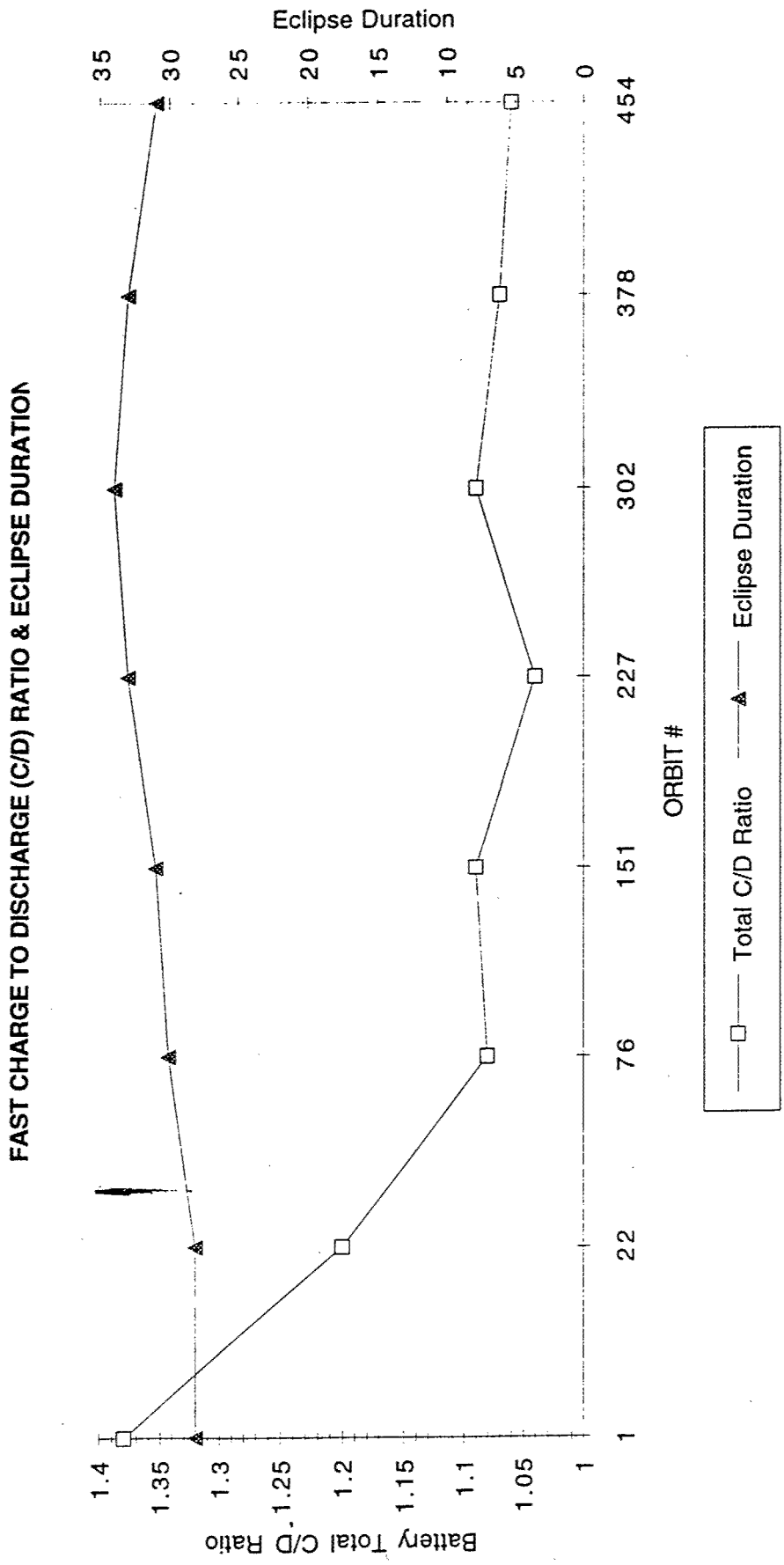

SUMMARY

- FAST S/C with 9 Ah SNiCd was launched in August 1996
- This was the fourth SNiCd mission in LEO application
- The cells were activated for 63 months prior to launch and maintained on trickle charged at 5 deg. C whenever possible
- The flight data indicates that the FAST S/C is performing nominally since Aug '96 launch

1 ## Results of V/T Verification

Steve Hall
NAVSURWARCENDIV Crane
Michelle Manzo
NASA Lewis Research Center

2 ## Program

- Evaluate various spacecraft cell designs
- Abandonment of the NASA Standard Cell design

3 ## Test Plan

- Repeat some of Manufacturers ATP test
- Perform NASA standard acceptance test
- Vibration of 1-2 cells of each cell design according to MIL-STD-1540B
- Baseline DPA performed on 1 cell each design

4 ## Test Plan Continued

- Define V/T curves for present day flight cells at 0, 20, 25 & 30 °C
- Implementation of these curves in a 40 % DoD LEO life test at 0, 20 & 30 °C
- GEO testing at 10 °C

5 ## Defining Max Voltage of Curve

- Cells cycled in 40% DoD, 90 min orbit for minimum of 500 cycles at 20 °C
- Voltage limit is increased in 10 millivolt increments
- Maximum voltage is determined when taper current begins to increase
- Repeat millivolt adjustments for remaining temperatures

6 ## Defining Min Voltage of Curve

- Voltage limit is decreased in 10 millivolt increments
- Minimum voltage at 100% recharge
- Repeat millivolt adjustments for remaining temperatures

7 ## Developing Curve

- Millivolt window = value of max-min volts
- Increment of change = Millivolt window equally divided by the remaining 6 levels

- Mid level = average volts of window

8 ❑ Types in Program

- Acme 55, 18 A/h, nylon & poly separator
- Saft 50 A/h
- Sanyo 35 A/h
- Sanyo 35 A/h, Ni-Mh
- EPI Magnum, 21 A/h
- Hughes Super Ni-Cd, 21 A/h

9 ❑ Test Conditions

- LEO Cycle 40 % DoD
  Discharge .8 C for .5 Hr.
  Charge .8C for 1 hr.
  Temperatures 0, 20 and 30 °C
- GEO Cycle 80% DoD
  Shadow period 42 days
  Orbit 24 hours.
  Temperature 10 °C
- All types except for Acme cells

10 ❑ Status

- V/T curves have been defined for Acme, Sanyo, EPI, Hughes and Saft cells
- Twenty-six packs in life cycling

11 ❑ Comments

- Recommend middle of V/T range at beginning of life
- Adjustment factor remains constant

12 ❑ Conclusions

- V/T window varies for each Manufacturer and temperature
- Maximium level increase's with cycle life
- NASA standard V/T curves not applicable

MID VOLTAGE RECHG

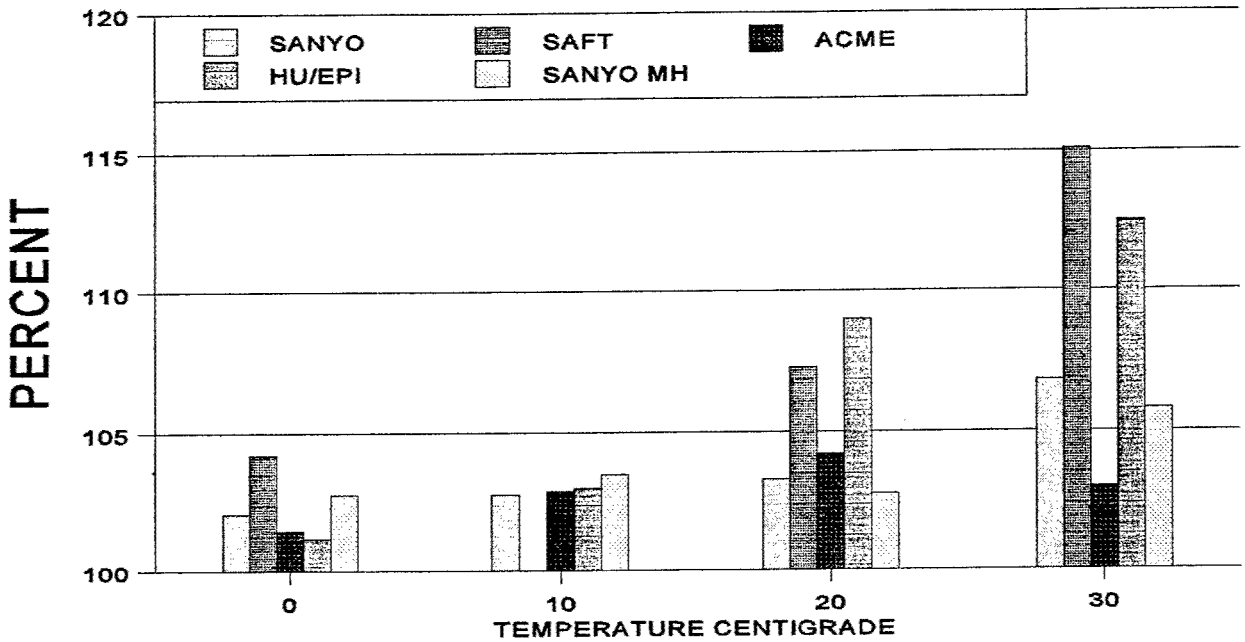

MID VOLTAGE

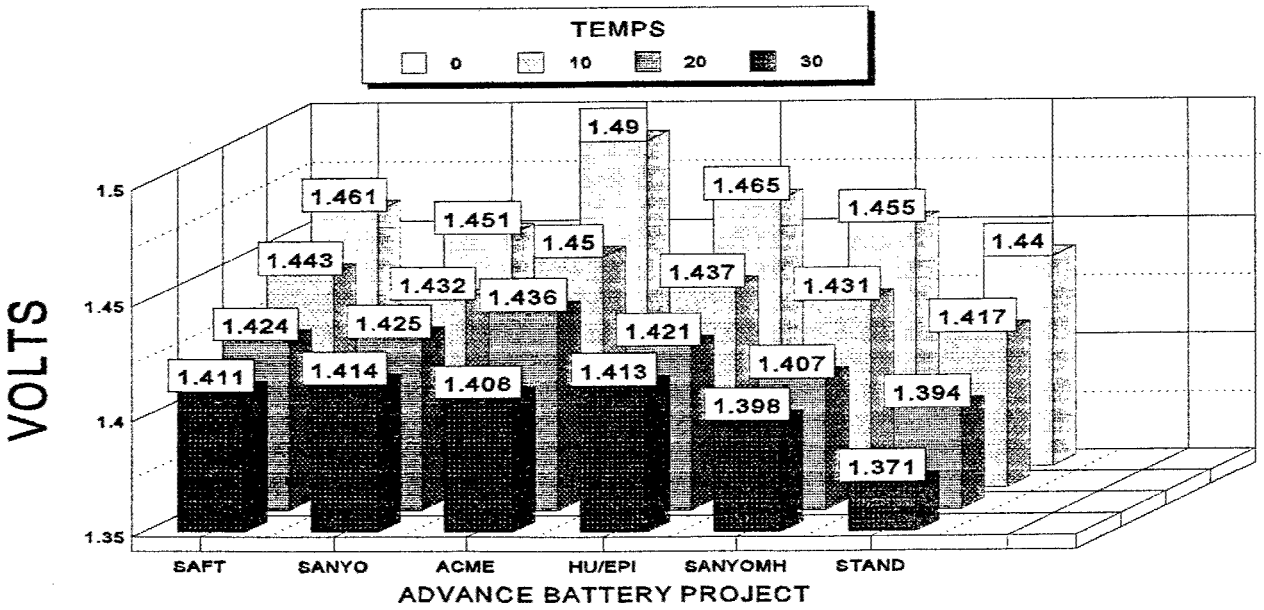

MAX - MIN VOLTS

20 DEGREES CENTIGRADE

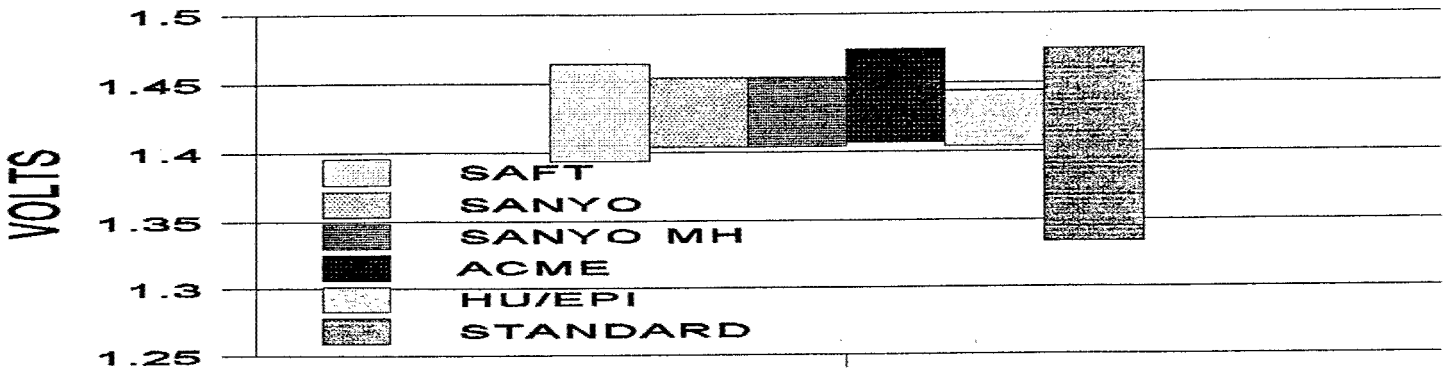

MILLIVOLT WINDOW

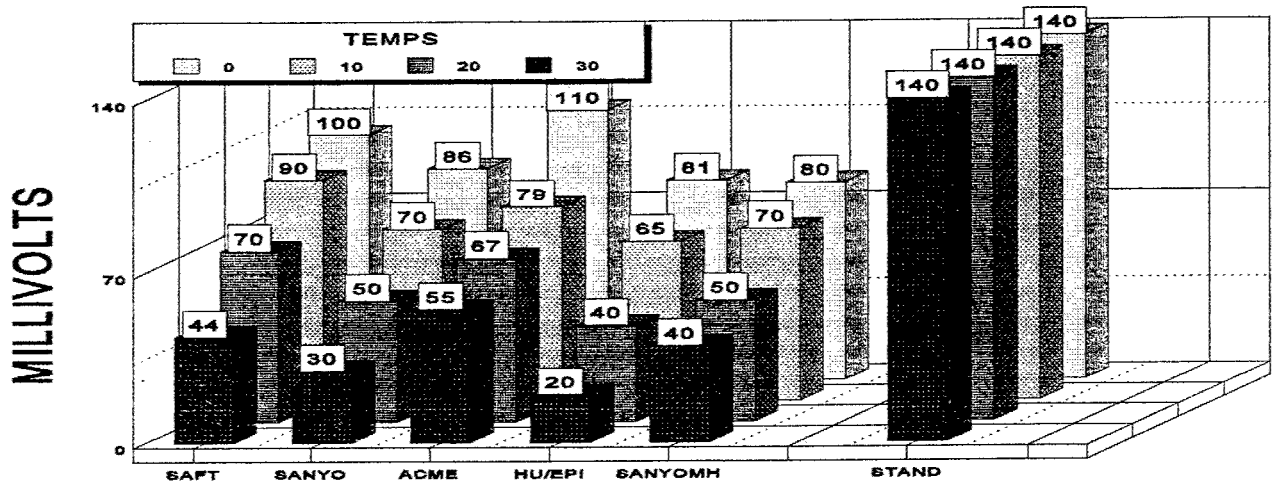

INCREMENT OF CHANGE

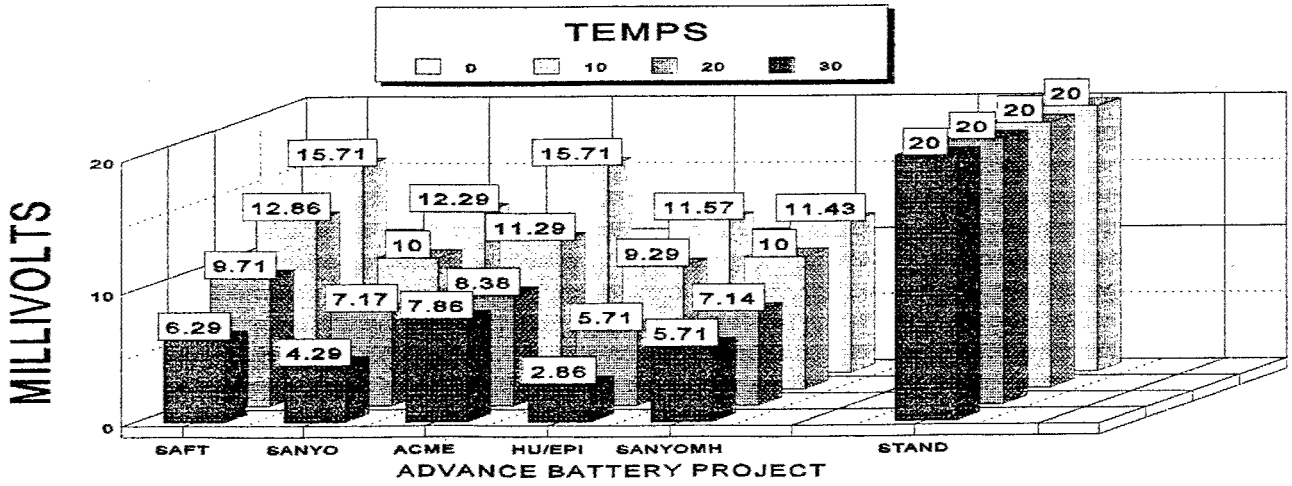

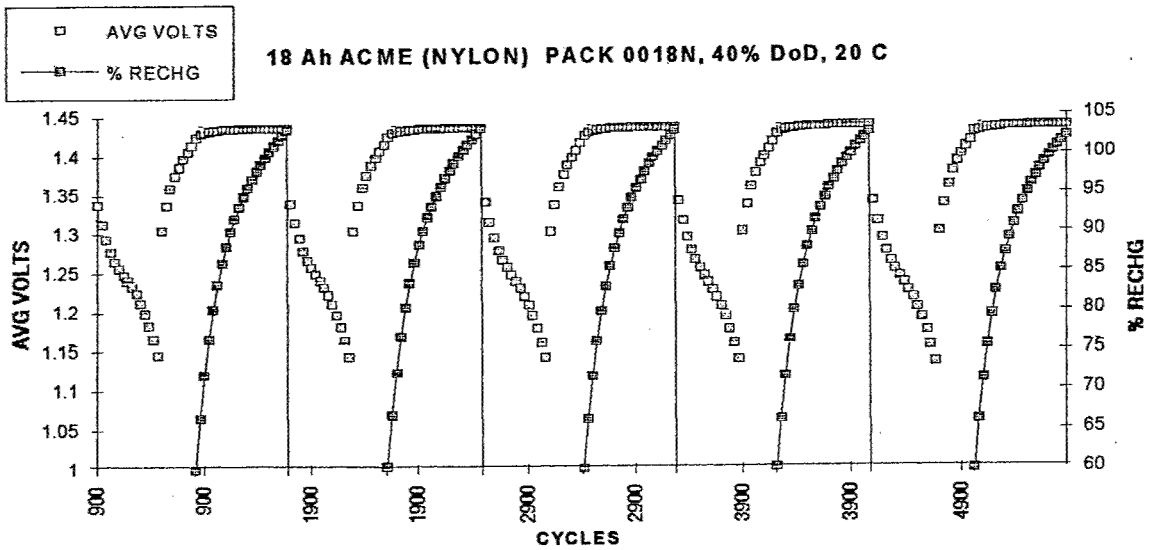
AVG VOLTS
% RECHG
18 Ah ACME (NYLON) PACK 0018N, 40% DoD, 20 C
AVG VOLTS
% RECHG
CYCLES

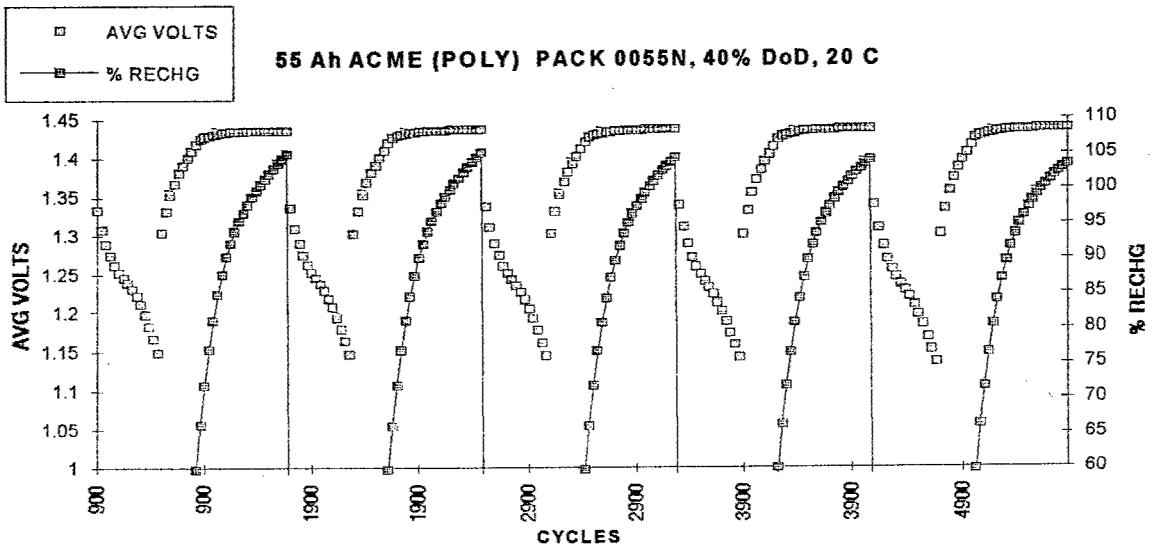
AVG VOLTS
% RECHG
55 Ah ACME (POLY) PACK 0055N, 40% DoD, 20 C
AVG VOLTS
% RECHG
CYCLES

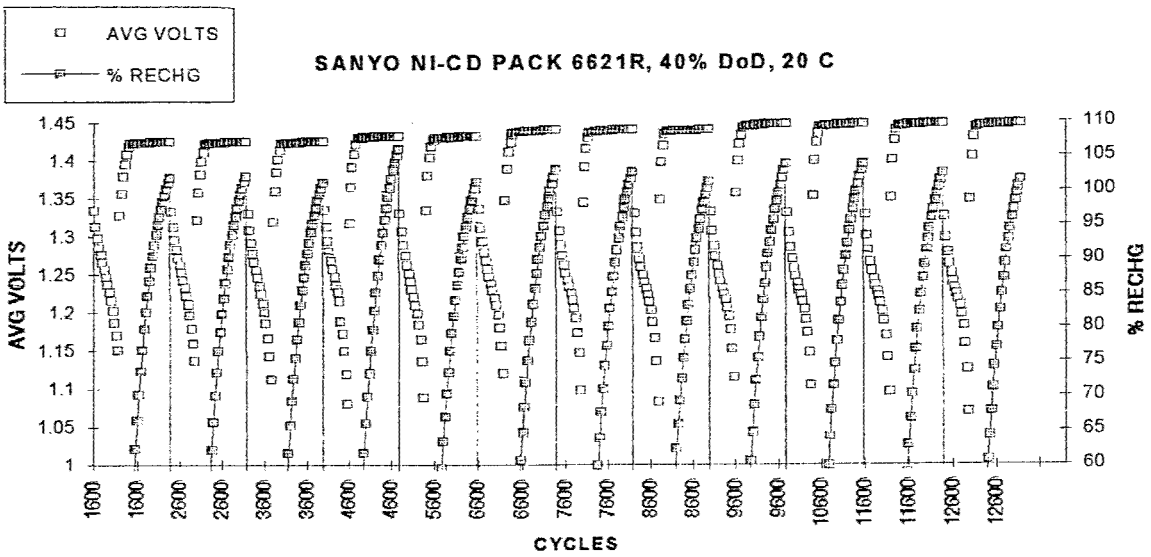
AVG VOLTS
% RECHG
SANYO NI-CD PACK 6621R, 40% DoD, 20 C
AVG VOLTS
% RECHG
CYCLES

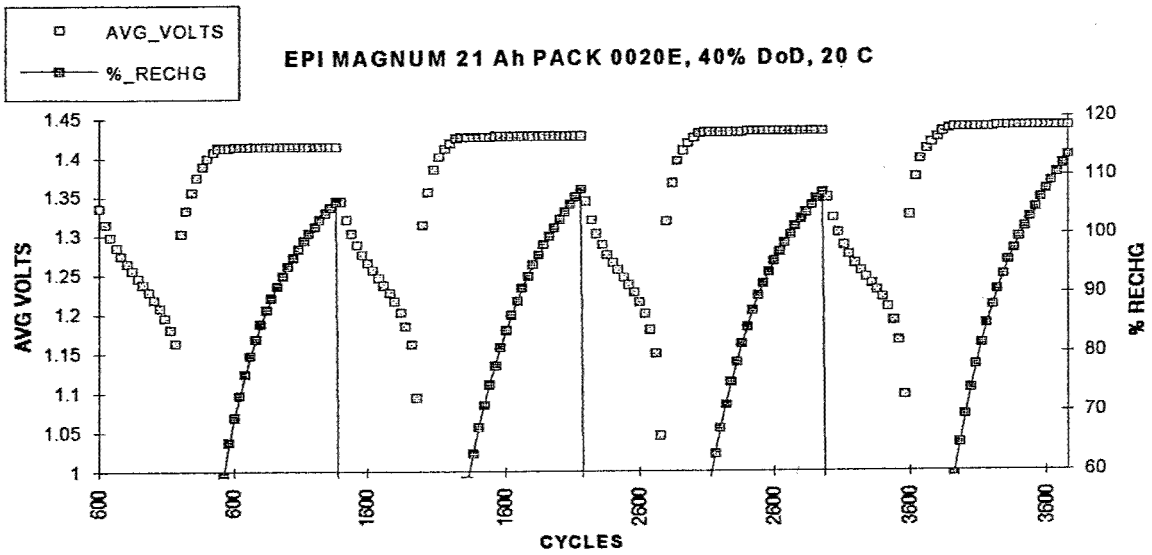
AVG_VOLTS
%_RECHG
EPI MAGNUM 21 Ah PACK 0020E, 40% DoD, 20 C
AVG VOLTS
% RECHG
CYCLES

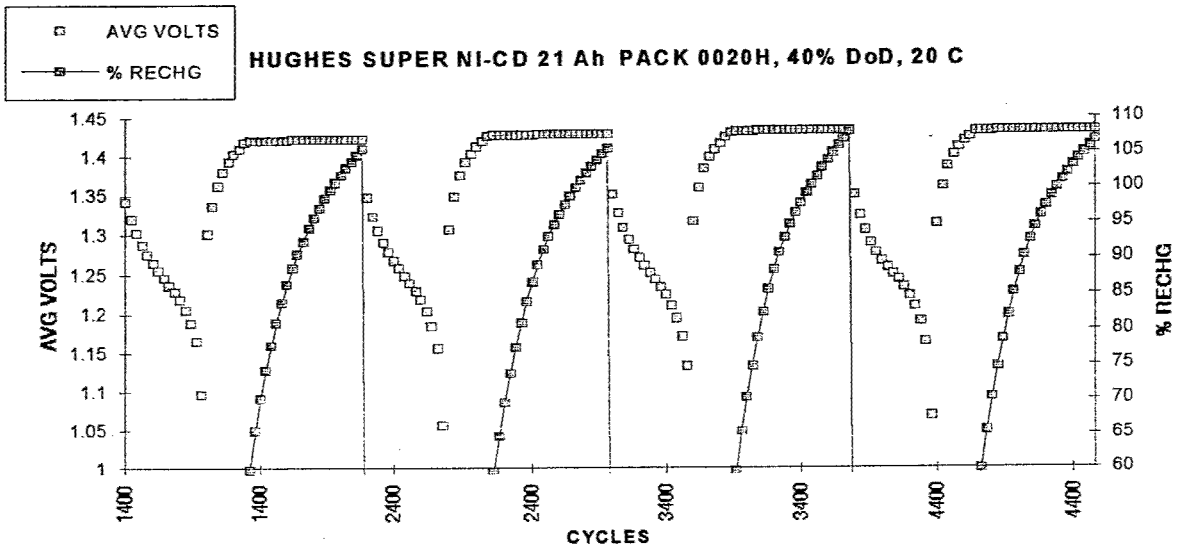
AVG VOLTS
% RECHG
HUGHES SUPER NI-CD 21 Ah PACK 0020H, 40% DoD, 20 C
AVG VOLTS
% RECHG
CYCLES

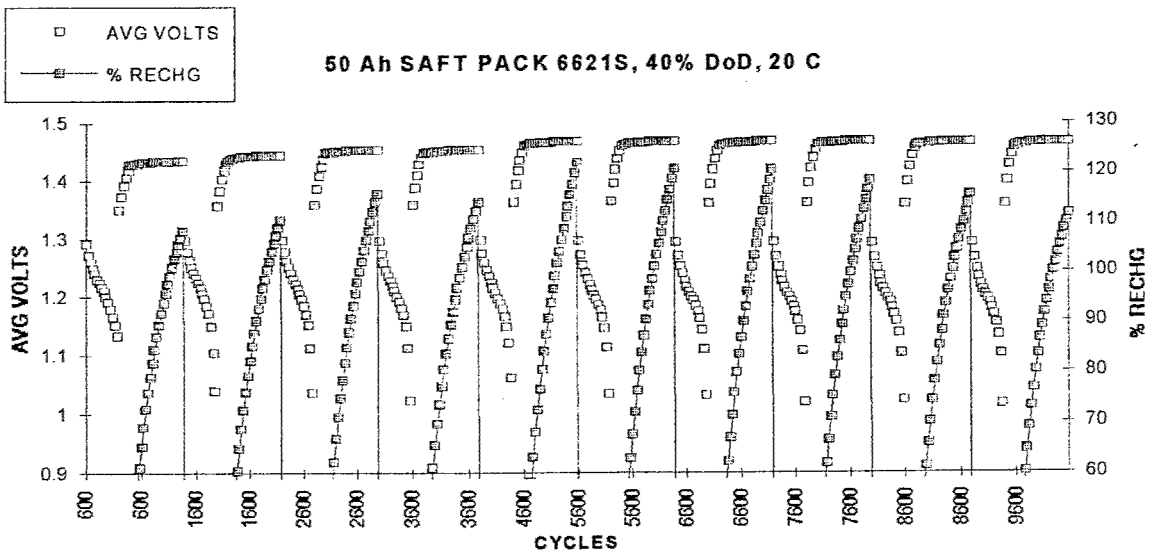
AVG VOLTS
% RECHG
50 Ah SAFT PACK 6621S, 40% DoD, 20 C
AVG VOLTS
% RECHG
CYCLES

Design and Performance Data For 81 Ah FNC Cells

F. Cohen, Rocketdyne

M. Anderman, Acme Aerospace

Presented at:

The 1996 NASA Aerospace Battery Workshop

December 3-5, 1996

Huntsville, Alabama

Background
Rocketdyne FNC Activity

- Rocketdyne contracted with Acme Aerospace in early 1994 to develop and test an 81 Ah FNC cell as a lower cost alternative to Ni-H2 cells currently targeted for the International Space Station

- Acme designed, developed, tested and initiated LEO cycle testing 8 months from receipt of contract award

- Rocketdyne has accumulated 2 years of LEO cycle test data under several accelerated test regimes

- This presentation is the first public release of Rockedyne/Acme 81 Ah FNC cell performance and cycle life data

Rocketdyne / Acme Aerospace

FNC

Background
FNC Technology

- Acme Aerospace started production of FNC cells in 1992 under license from Daug-Hoppecke in West Germany
- Several OEM contracts were secured utilizing FNC sealed cells for military and commercial aircraft
- Acme slightly modified several 7 Ah aircraft quality cells and began testing at JPL in 1992. These cells achieved 9500 LEO cycles at 40% DOD at 20 ° C
- Limited design changes were made in '93-'94 and were implemented in several battery packs subsequently put on LEO tests in '94-'95 both at Acme and at customer's laboratories.
- The Rocketdyne test is the most extensive accelerated LEO testing on FNC cells to date

Rocketdyne / Acme Aerospace

FNC

FNC Cell
Design Features

Positive Plaque	Nickel plated polyolefin fibers
Positive Impregnation	Mechanical loading @ room temperature, neutral pH, no Nitrates
Negative Plaque	Nickel plated polyolefin fibers
Negative Impregnation	Mechanical loading @ room temperature, neutral pH, and no Nitrates
Separator	Polypropylene permanently wetable Pore size less than 5 micron
Electrolyte	30% KOH
Terminals	Nickel
Terminal Seals	Ziegler Crimp Seal
Case	Welded stainless steel, hermetically sealed

Rocketdyne / Acme Aerospace

FNC

X81 Design Parameters

Theoretical Positive Capacity	96 Ah +/- 3
Theoretical Negative Capacity	275 Ah +/- 6
Theoretical Neg/Pos Ratio	2.85 +/- 0.15
Active Neg/Pos Ratio	2.1 +/- 0.1
Positive Electrode Loading	1.5 g/cc void
Seperator Thickness	12 mil
Electrolyte Volume	4.1 +/- 0.1 ml/design Ah
Weight	2860 g +/- 30 g
Mid-Design Energy Density	40 Wh/kg
Internal Impeadance @ 1 sec, 24° C	0.46 mohm

Rocketdyne / Acme Aerospace

FNC

ATP DATA

Cell Number	Ref. Capacity C/2 Ah	Impeadance 1 Sec mohm	LEO Profile
* 6	81.0	0.54	27°C Accelerated
7	85.2	0.52	"
8	84.9	0.54	"
9	85.2	0.54	-10°C Accelerated
10	84.3	0.51	"
11	84.6	0.51	"
12	85.2	0.54	10°C @ 60% DOD
13	84.7	0.54	"
14	85.2	0.54	"
* 22	89.9		10°C Accelerated
15	84.5	0.53	"
16	85.8	0.54	"
17	84.5	0.52	"
18	84.2	0.51	10°C Nominal
19	84.9	0.53	"
20	84.1	0.54	"
* 1	90.5	0.58	"
* 2	91.0	0.52	"
Average all:	86 +/- 5	0.54 +/- 0.04	
* Avg (excluding 1,2,6,22)	85 +/- 1	0.53 +/- 0.02	

Rocketdyne / Acme Aerospace

FNC

Test Matrix

Pack Number	Number of Cells	Test Temp	DOD	Disch. Rate	Cycles/ Day	Number of Cycles as of 22 Nov 96
1	3	27° C	35%	97 Amps	30	9,500
2	3	-10° C	35%	97 Amps	30	13,800
3	4	10° C	35%	97 Amps	30	15,800
4	5	10° C	35%	49 Amps	16	7,900
5	3	10° C	60%	83 Amps	16	7,780

Rocketdyne / Acme Aerospace

FNC

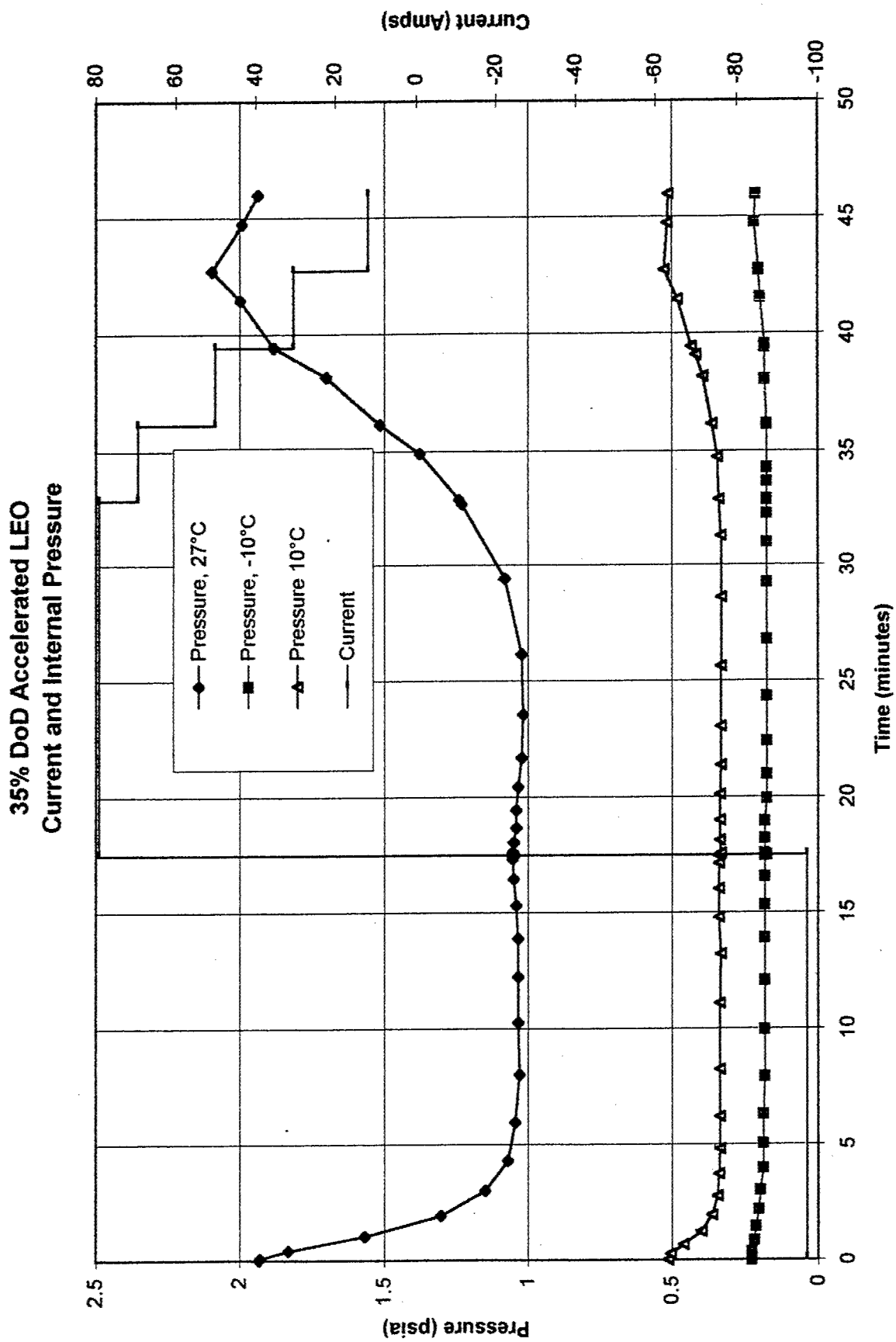

Rocketdyne / Acme Aerospace

FNC

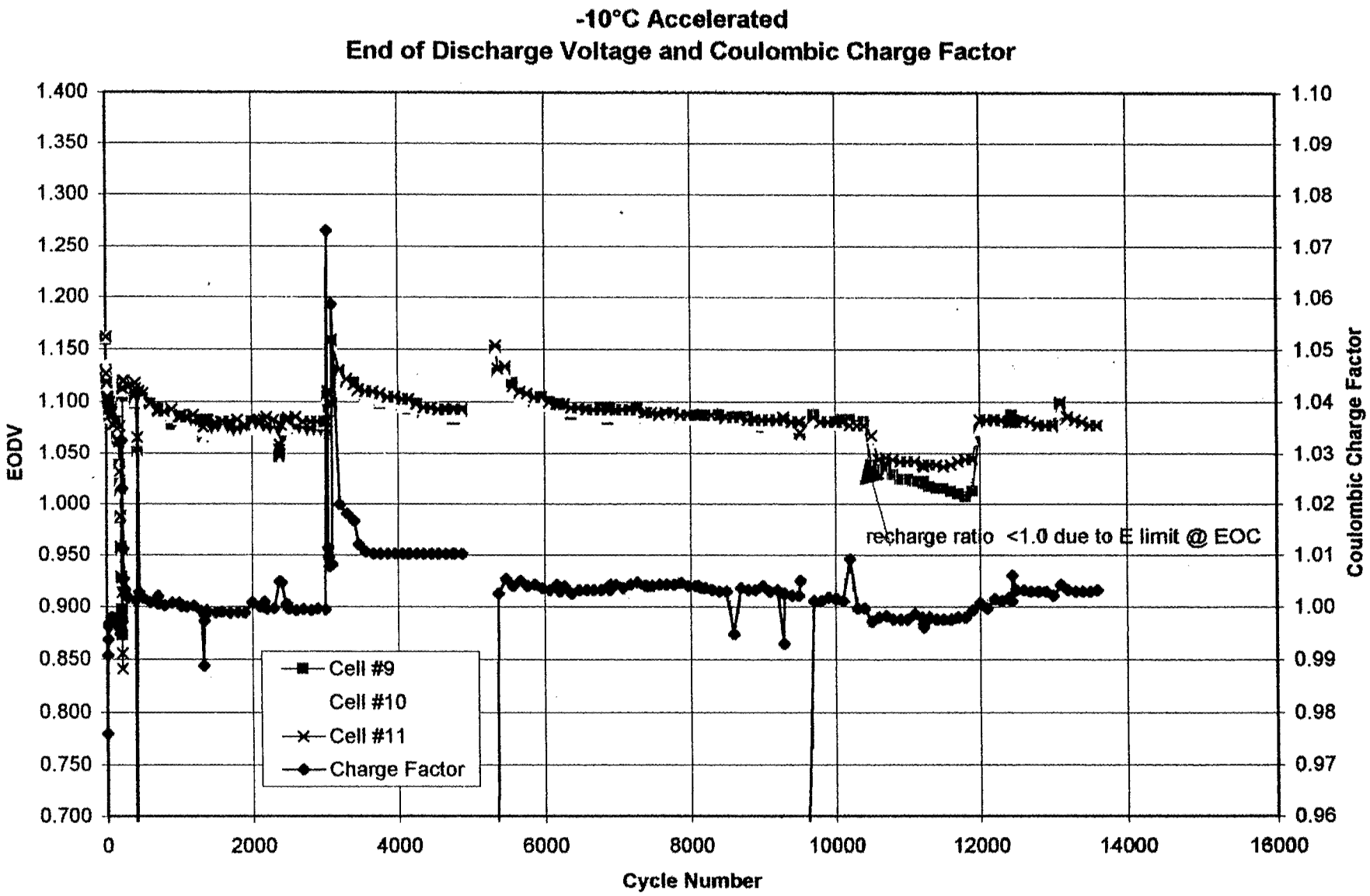

Rocketdyne / Acme Aerospace

FNC

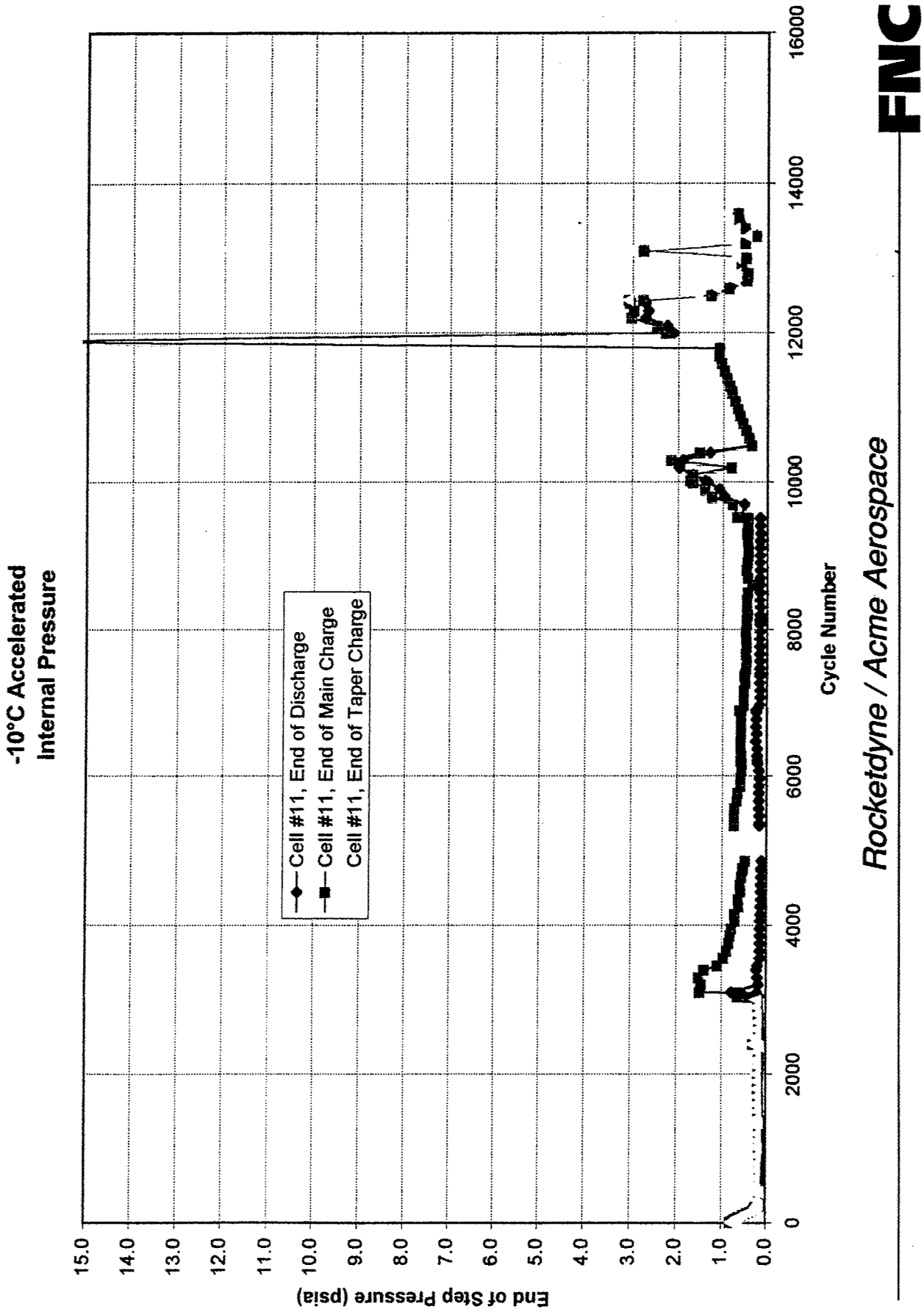
-10°C Accelerated
Internal Pressure
Cell #11, End of Discharge
Cell #11, End of Main Charge
Cell #11, End of Taper Charge
End of Step Pressure (psia)
15.0
14.0
13.0
12.0
11.0
10.0
9.0
8.0
7.0
6.0
5.0
4.0
3.0
2.0
1.0
0.0
0
2000
4000
6000
8000
10000
12000
14000
16000
Cycle Number
Rocketdyne / Acme Aerospace
FNC

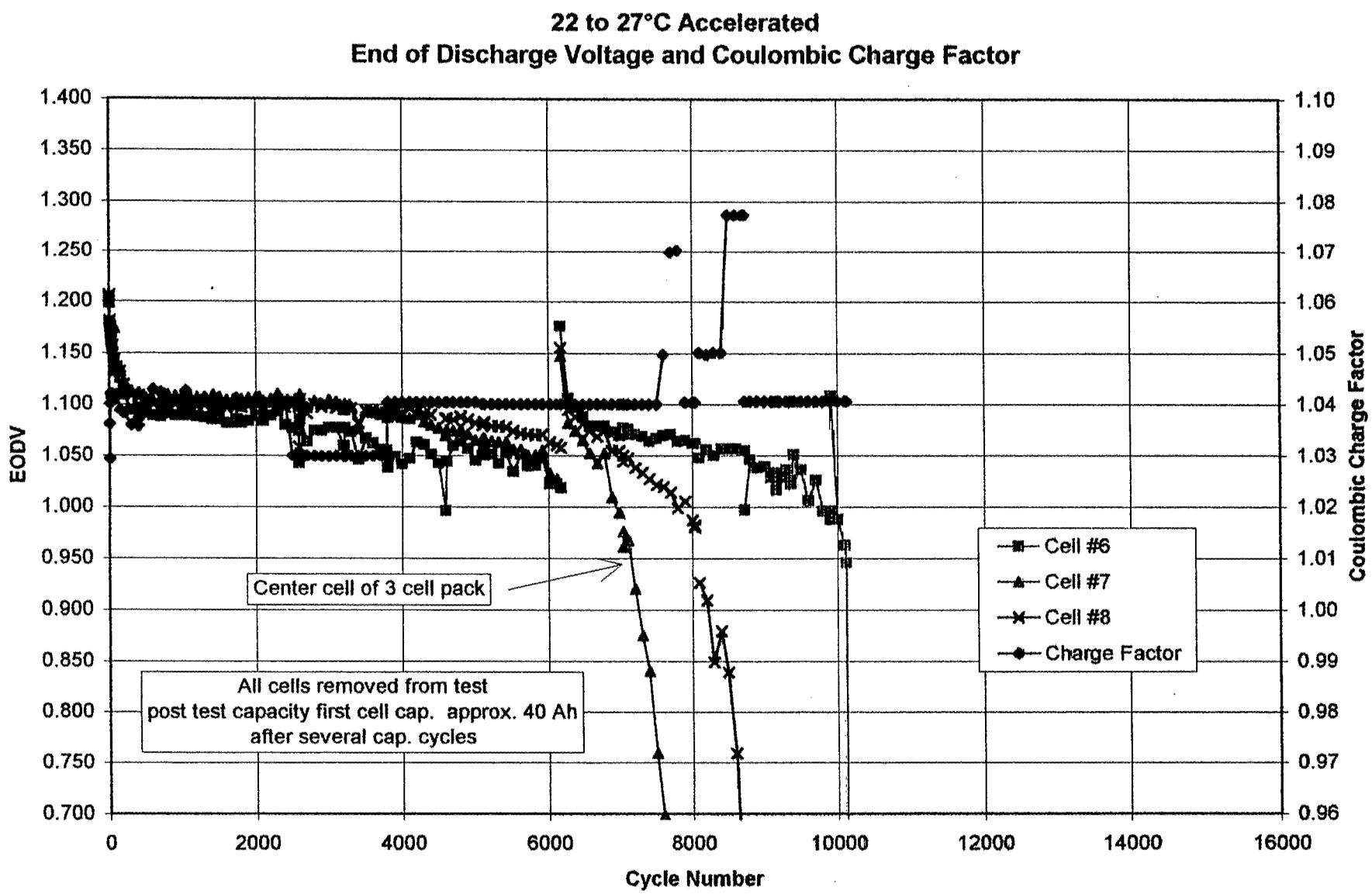

Rocketdyne / Acme Aerospace

FNC

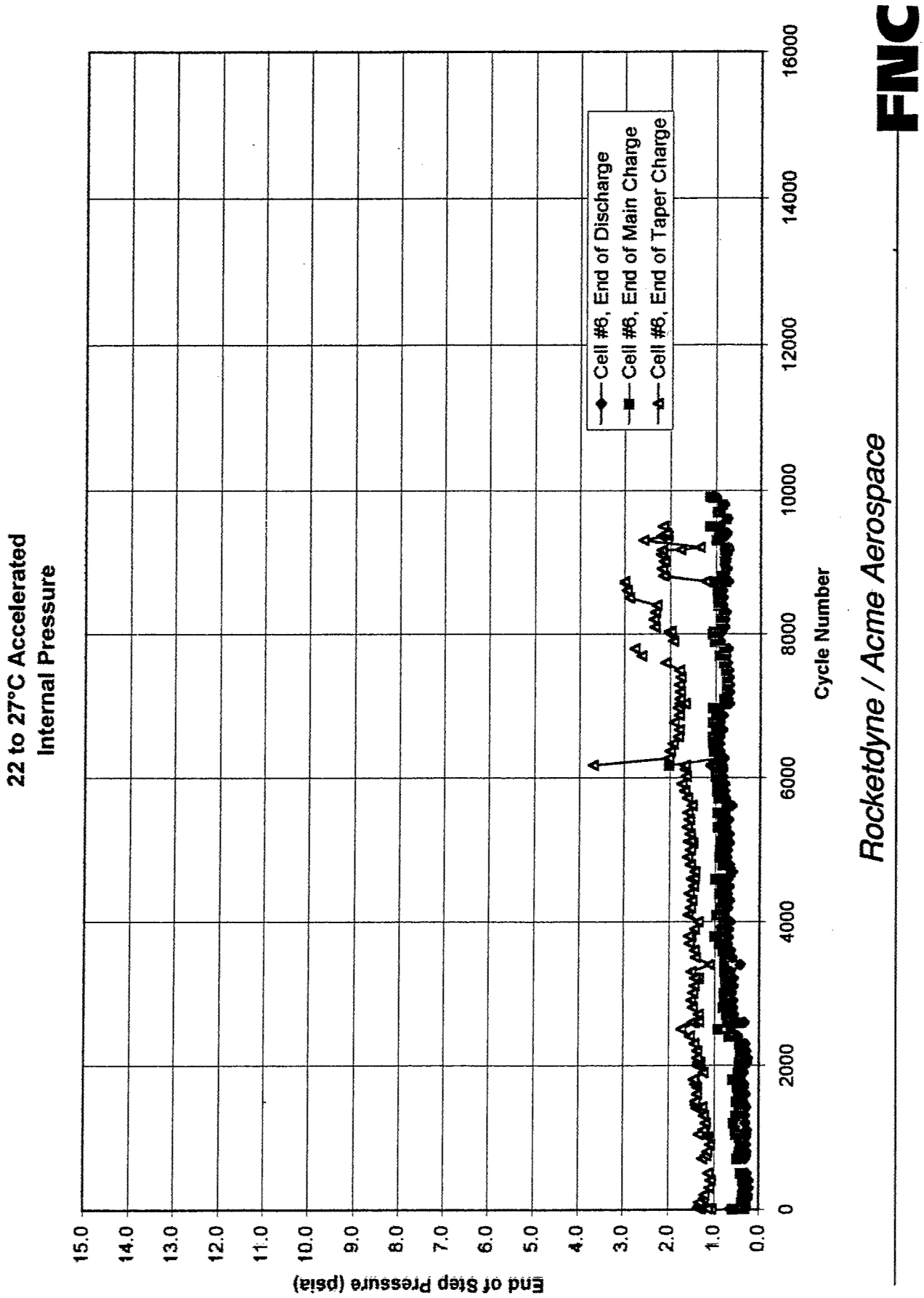
22 to 27°C Accelerated
Internal Pressure
End of Step Pressure (psia)
15.0
14.0
13.0
12.0
11.0
10.0
9.0
8.0
7.0
6.0
5.0
4.0
3.0
2.0
1.0
0.0
0
2000
4000
6000
8000
10000
12000
14000
16000
Cycle Number
Cell #6, End of Discharge
Cell #6, End of Main Charge
Cell #6, End of Taper Charge
Rocketdyne / Acme Aerospace
FNC

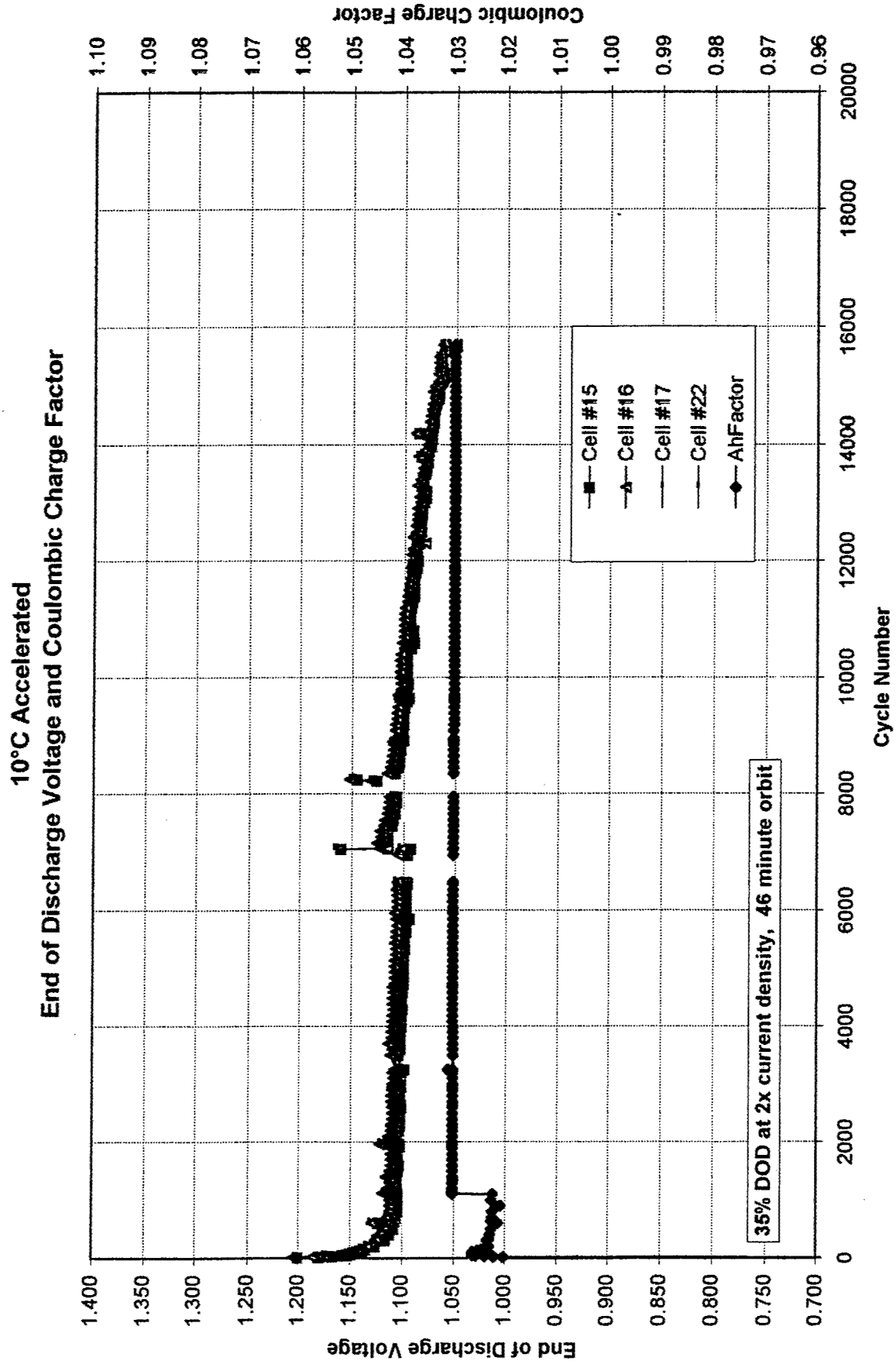

Rocketdyne / Acme Aerospace

FNC

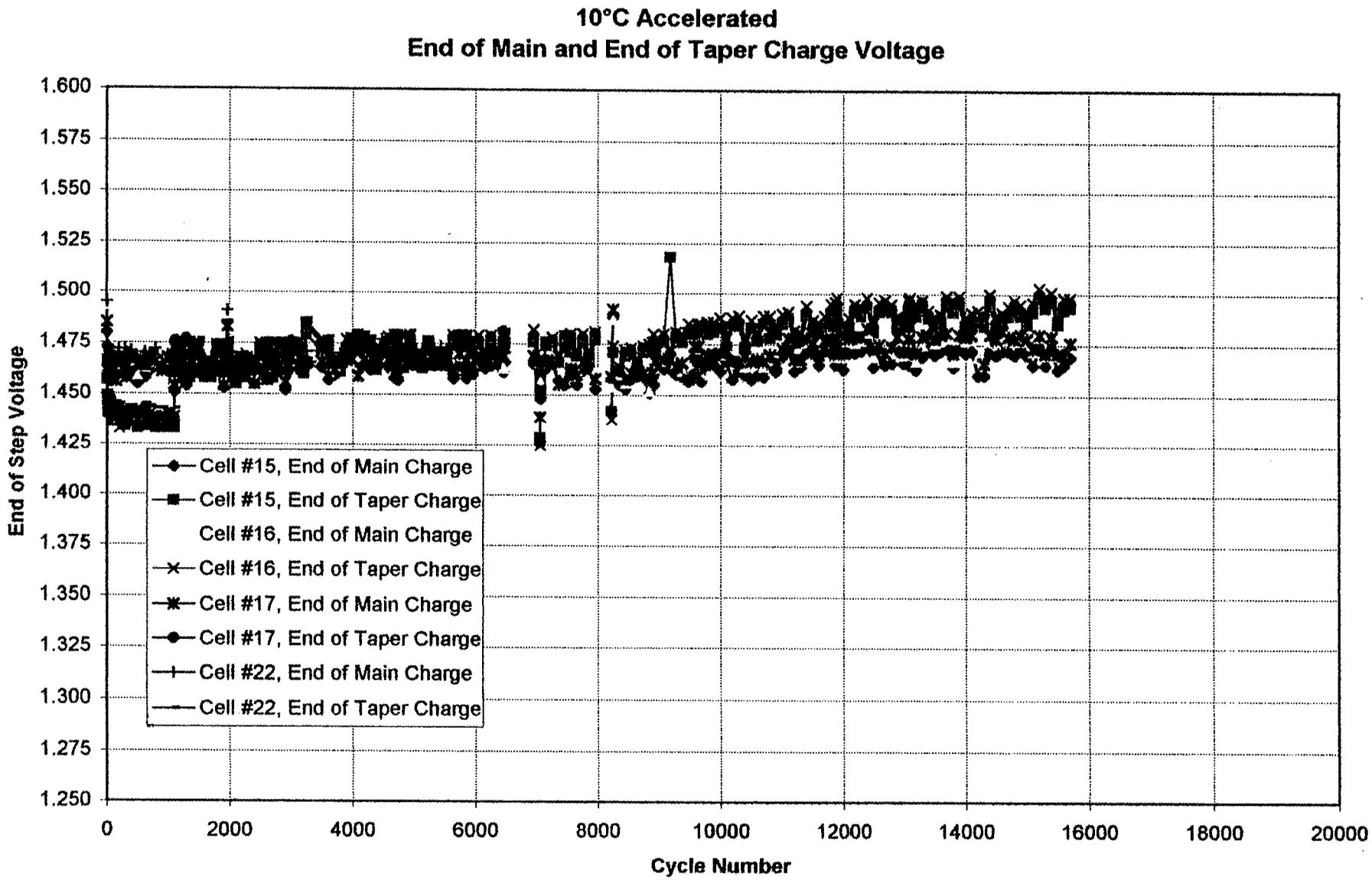

Rocketdyne / Acme Aerospace

FNC

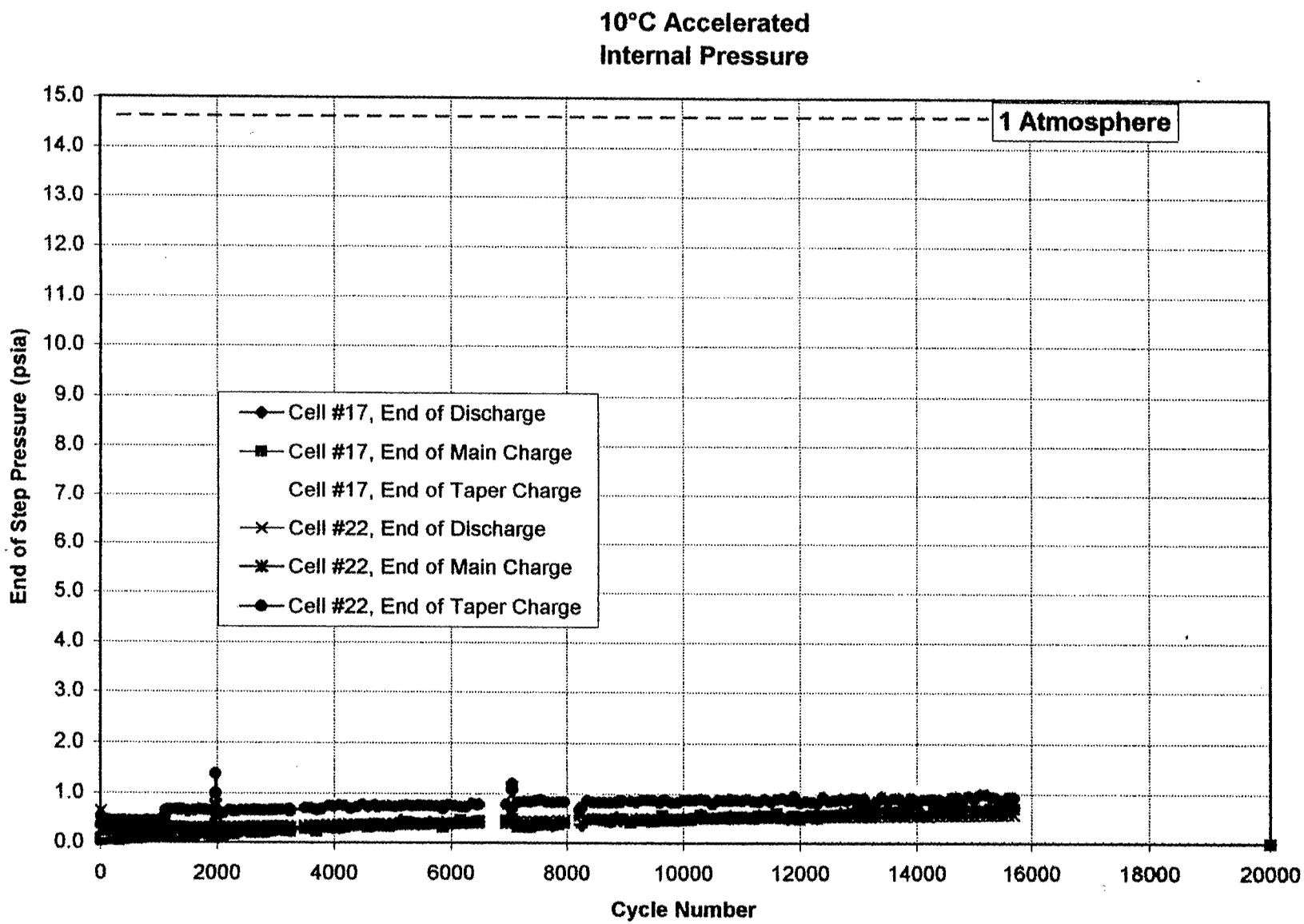

Rocketdyne / Acme Aerospace

FNC

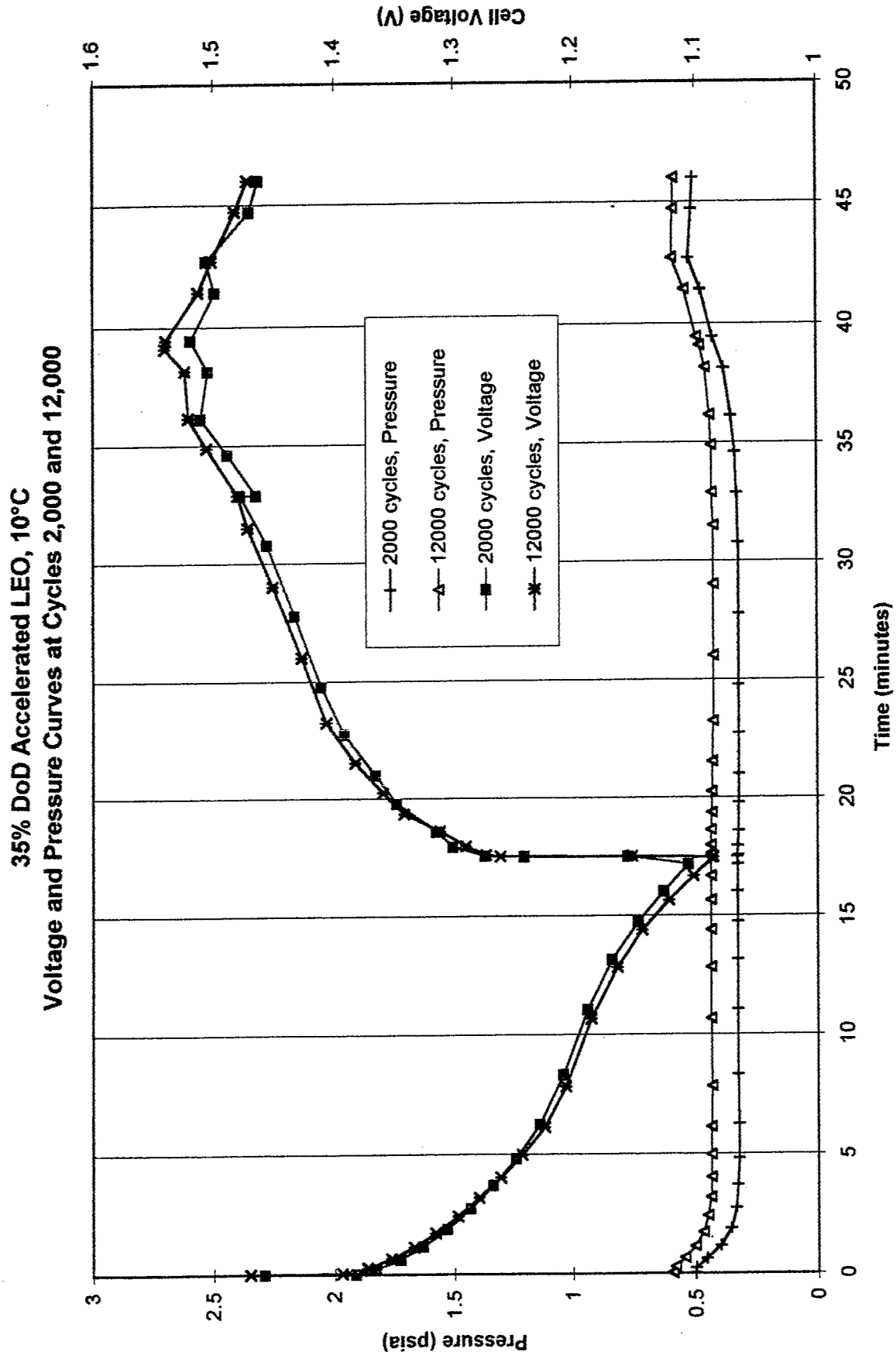

FMC

Rocketdyne / Acme Aerospace

Conclusions

- Sealed Ni-Cd cells are not limited to 50 Ah with the FNC design
- Energy Densities of 40 Wh/kg in a conservative high Cd, high electroltye design have been demonstrated
- Uniform ATP data and LEO cycling performance is being demonstrated
- Internal cell pressures remain low under all conditions
- No conditioning is necessary under any LEO profile
- Accelerated LEO cycling exhibits performance well beyond traditional Space Ni-Cd cells
- The FNC shows promise for applications at higher charge and discharge rates, wider operating temperatures and deeper DOD than has been previously possible with traditional Space Ni-Cd cells.
- FNC offers lower cost, simplified system design and operating logistics, safer operation, comparable energy density to Ni/H2, resulting in a more economical choice for many applications

Rocketdyne / Acme Aerospace

FNC

Page

516

Blank

1997 NASA BATTERY WORKSHOP

HUNTSVILLE, ALABAMA

APPLICATION OF FIRST PRINCIPLES Ni-Cd and Ni-H2 BATTERY MODELS TO SPACECRAFT OPERATIONS

Paul Timmerman, Ratnakumar Bugga, and Salvador DiStefano

OUTLINE

INTRODUCTION

REVIEW OF BI-PHASIC NICKEL ELECTRODE MODEL

EFFECTS OF AGING ON HYDROGEN PRESSURES

EFFECTS OF NICKEL ELECTRODE AGING

EFFECTS OF CADMIUM ELECTRODE AGING

SUMMARY

INTRODUCTION

PREVIOUS MODELS USE A SINGLE PHASE REACTION

CYCLED CELL BEHAVIOR CANNOT BE PREDICTED WITH A SINGLE PHASE

INTERPHASE CONVERSION PROVIDES MEANS FOR FILM AGING

AGING CELLS PREDICTIONS DISPLAY TYPICAL BEHAVIORS

- VOLTAGE FADING UPON CYCLING
- SECOND PLATEAU ON DISCHARGE OF CYCLED CELLS
- NEGATIVE LIMITED BEHAVIOR FOR Ni-Cd's
- PRESSURE CHANGES IN NiH2 CELLS

NICKEL ELECTRODE REACTION SCHEME

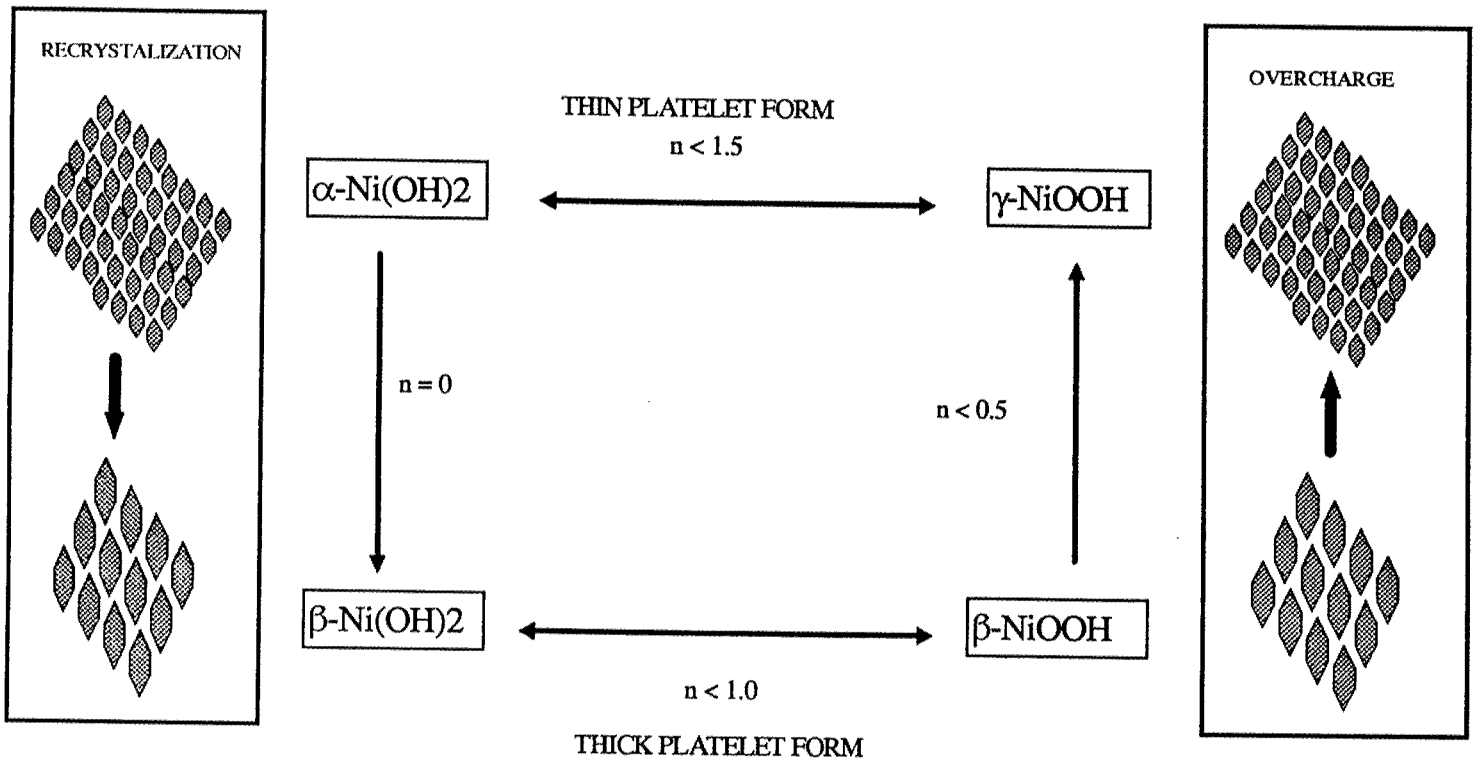

APPLICATION OF FIRST PRINCIPLES MODEL TO SPACECRAFT OPERATIONS

POTENITAL SCALE FOR NICKEL ELECTRODE MODEL

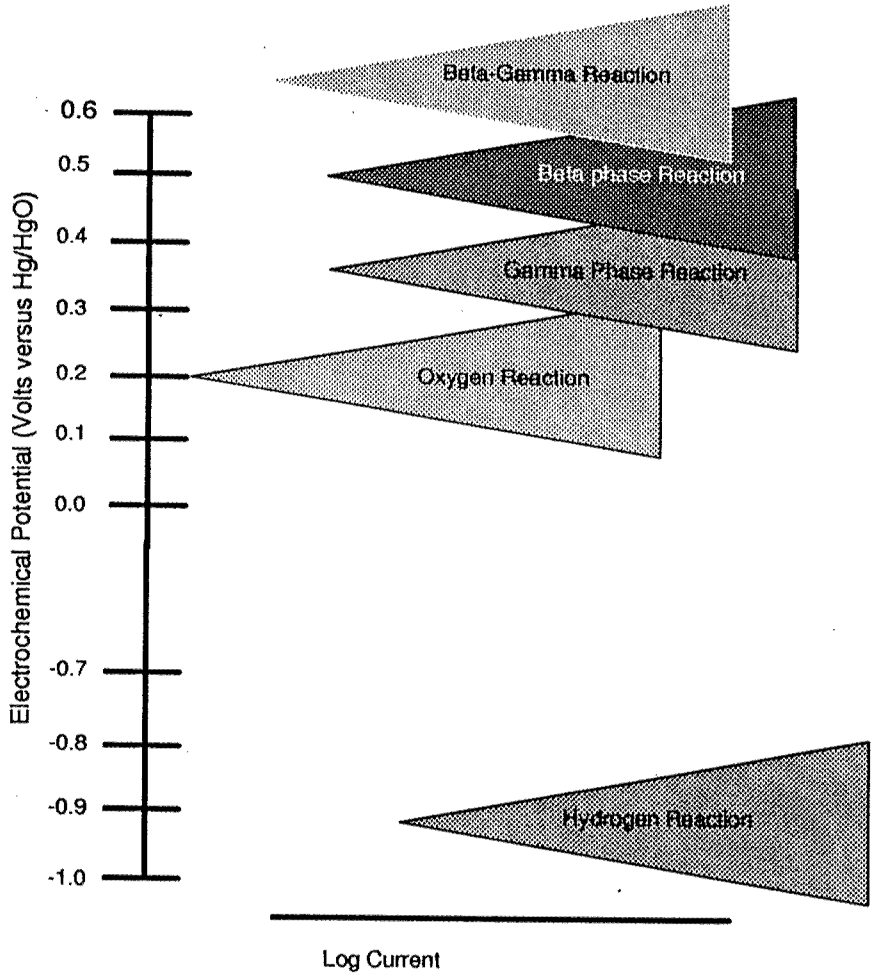

NICKEL ELECTRODE FADING STUDIES

BASED ON INTERPHASE CONVERSION

AND CHANGES IN MORPHOLOGY / CONDUCTION

TOPEX 40% DOD CRANE LIFE TEST DATA USED FOR COMPARISON

ONLY POSITIVE ELECTRODE DEGRADED IN THIS SECTION

SIMULATION OF VOLTAGE FADING OVER LIFE ACHIEVED

SECOND PLATEAU BEHAVIOR INCREASES OVER LIFE

Effect of Gamma Fraction on Discharge Simulation

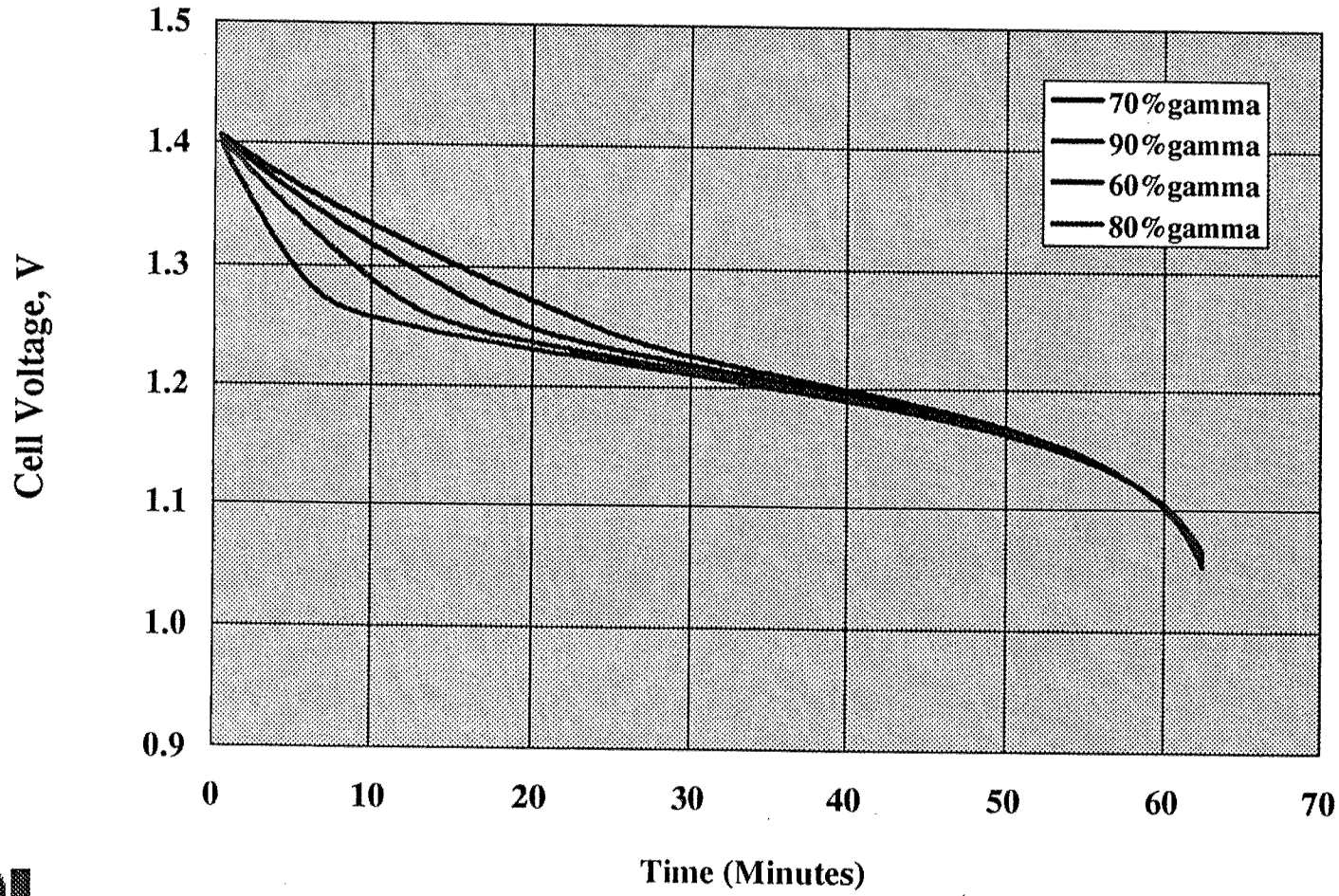

Effect of Conductivity Mixing Parameter (cstp)

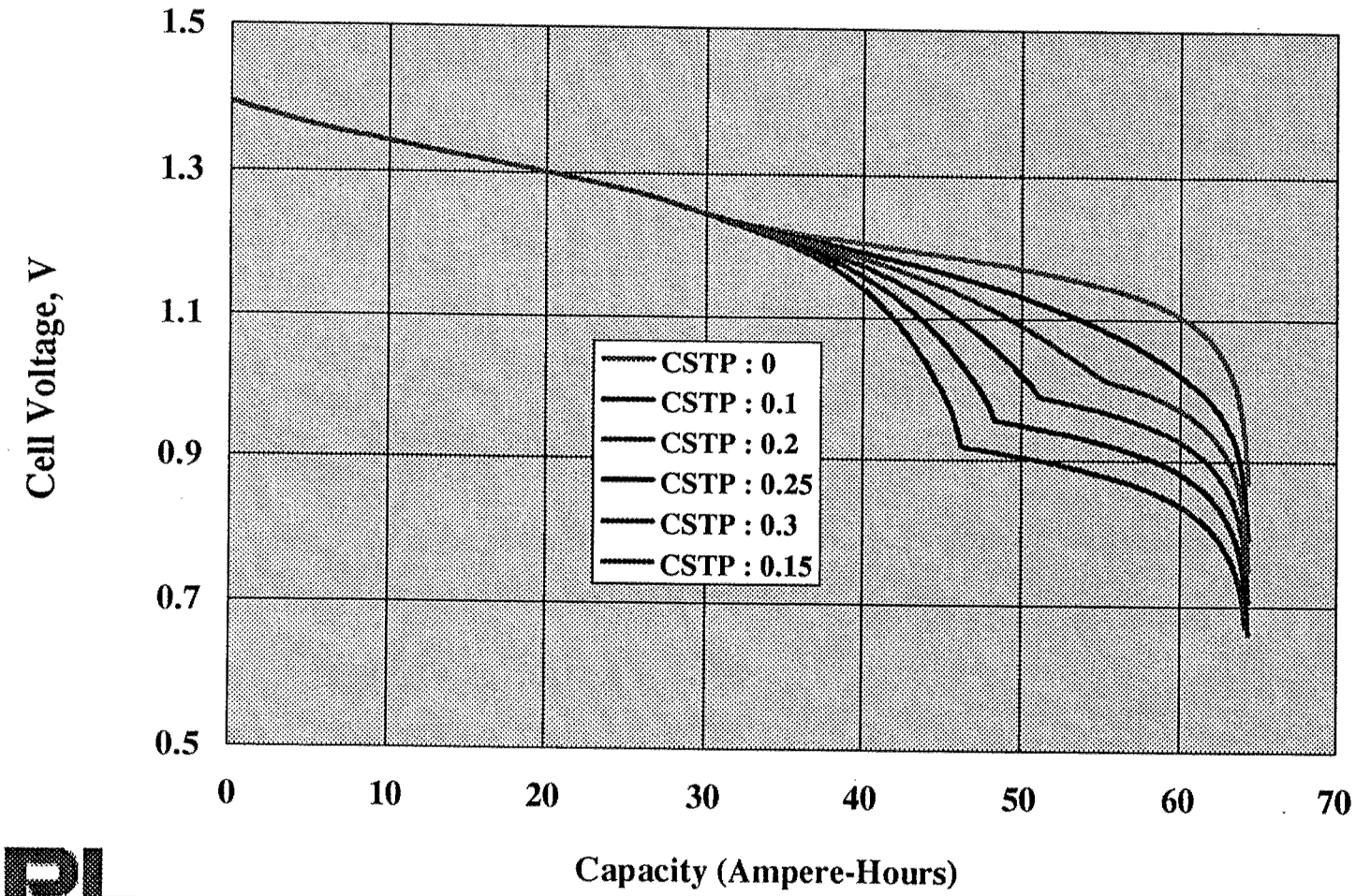

APPLICATION OF FIRST PRINCIPLES MODEL TO SPACECRAFT OPERATIONS

Effect of Gamma Fraction on 40% DOD LEO EON Voltage

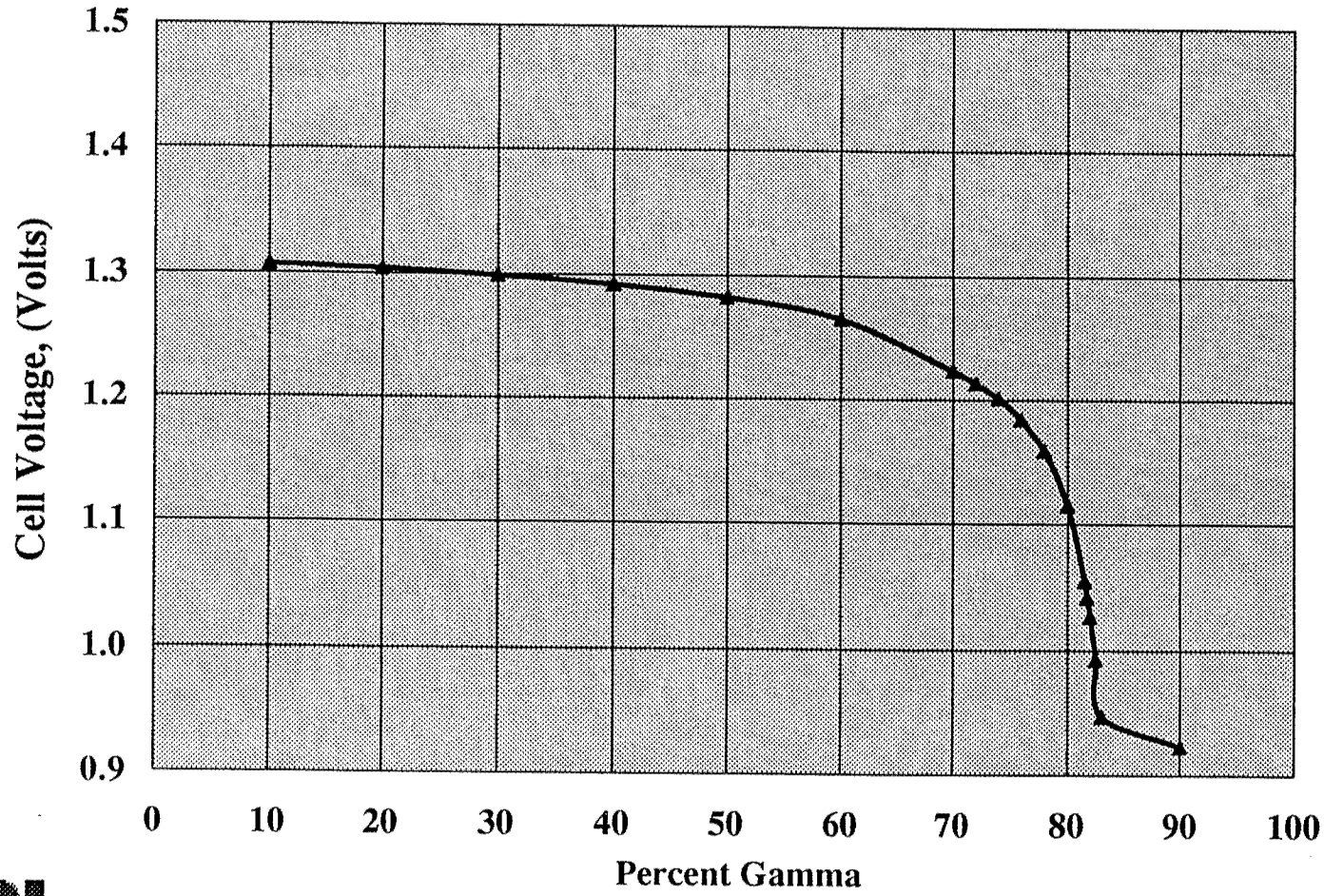

APPLICATION OF FIRST PRINCIPLES MODEL TO SPACECRAFT OPERATIONS

Estimated Gamma Fraction For Life Test

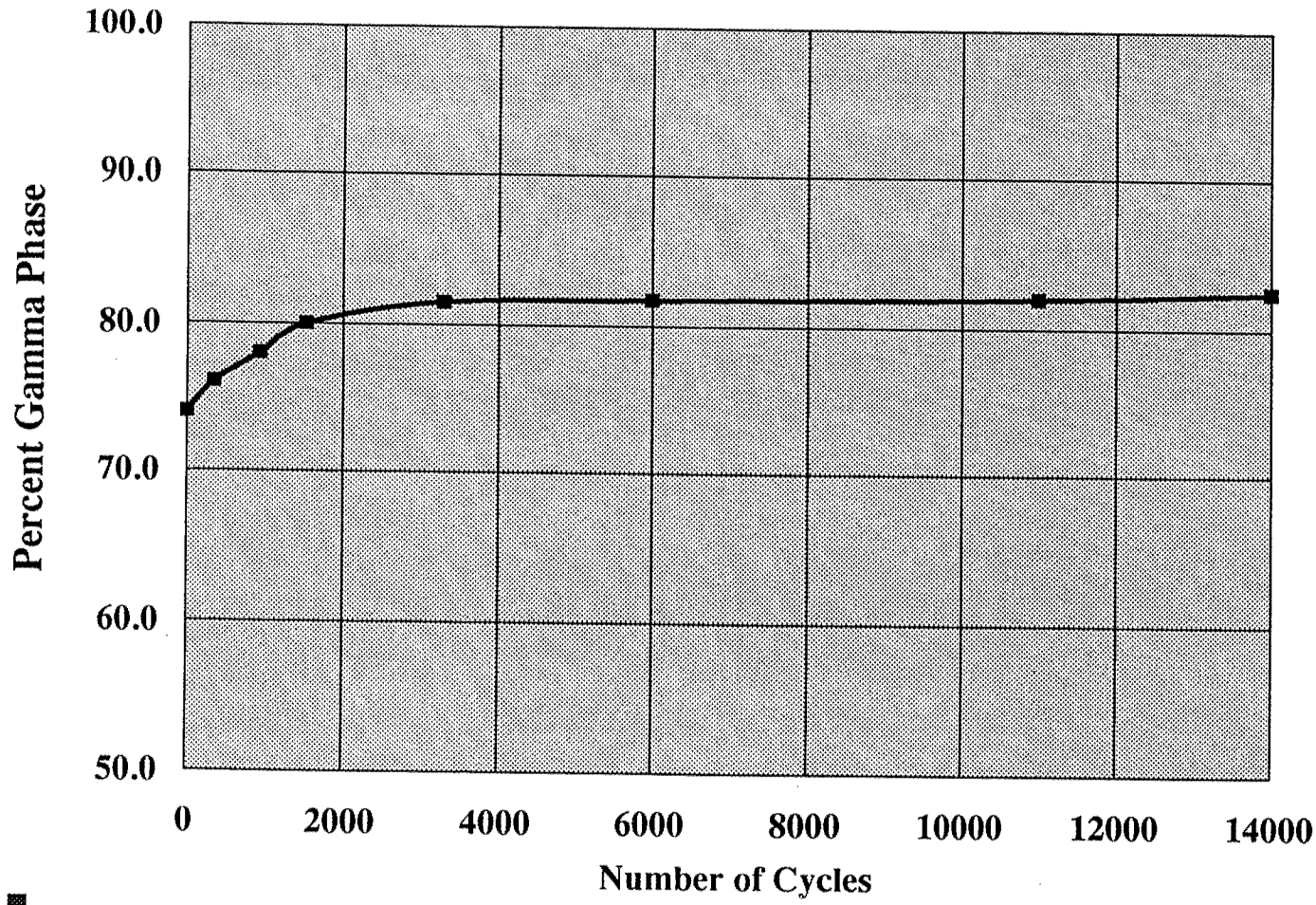

APPLICATION OF FIRST PRINCIPLES MODEL TO SPACECRAFT OPERATIONS

Predicted EON Voltages For Various Percent Gamma Phase

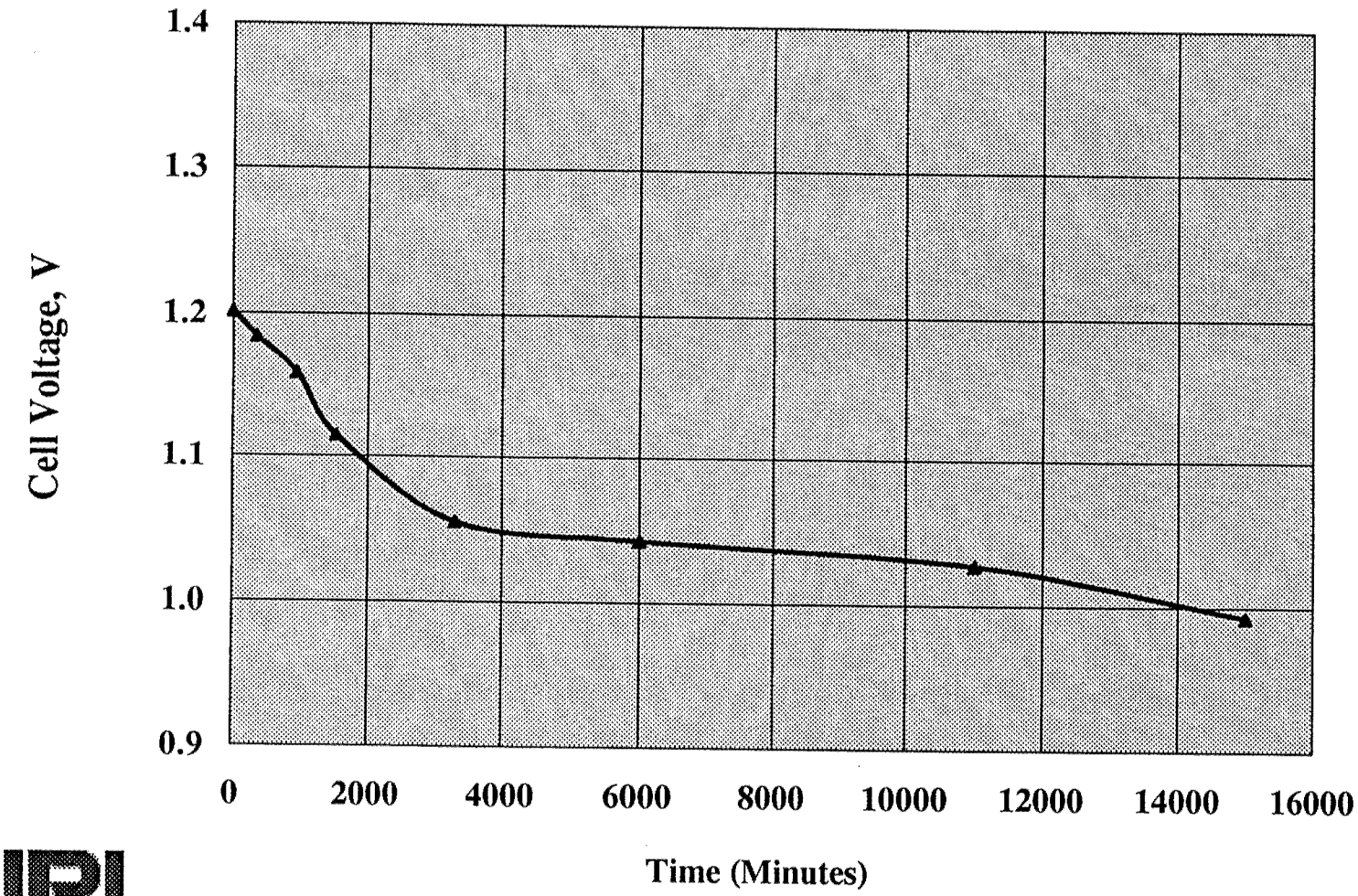

APPLICATION OF FIRST PRINCIPLES MODEL TO SPACECRAFT OPERATIONS

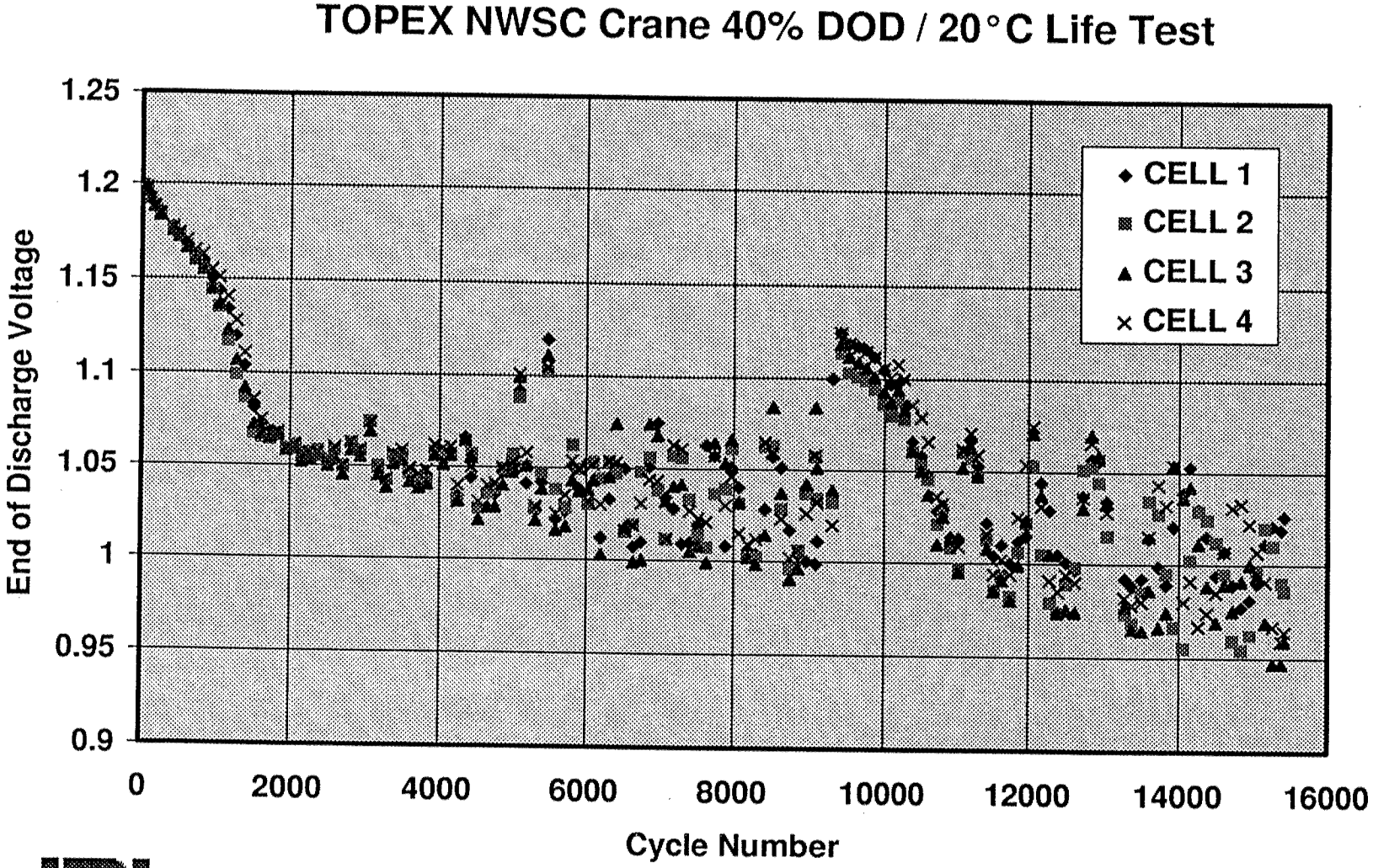

JPL

ELECTROCHEMICAL SYSTEMS GROUP

APPLICATION OF FIRST PRINCIPLES MODEL TO SPACECRAFT OPERATIONS

Predicted Discharge Voltage For Cycled Cell at C/2 Rate

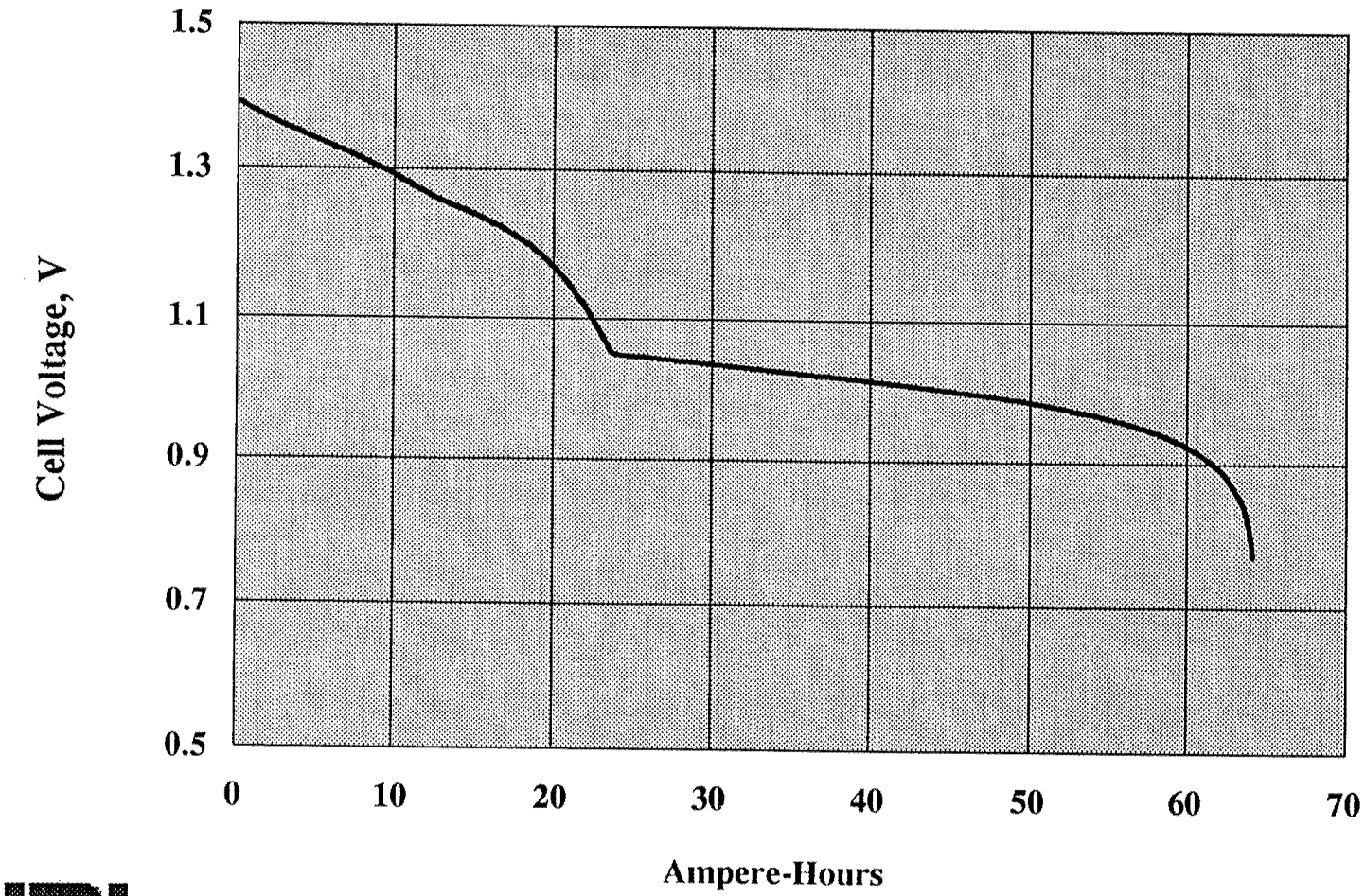

Post Life Test Discharge: Crane Topex Test

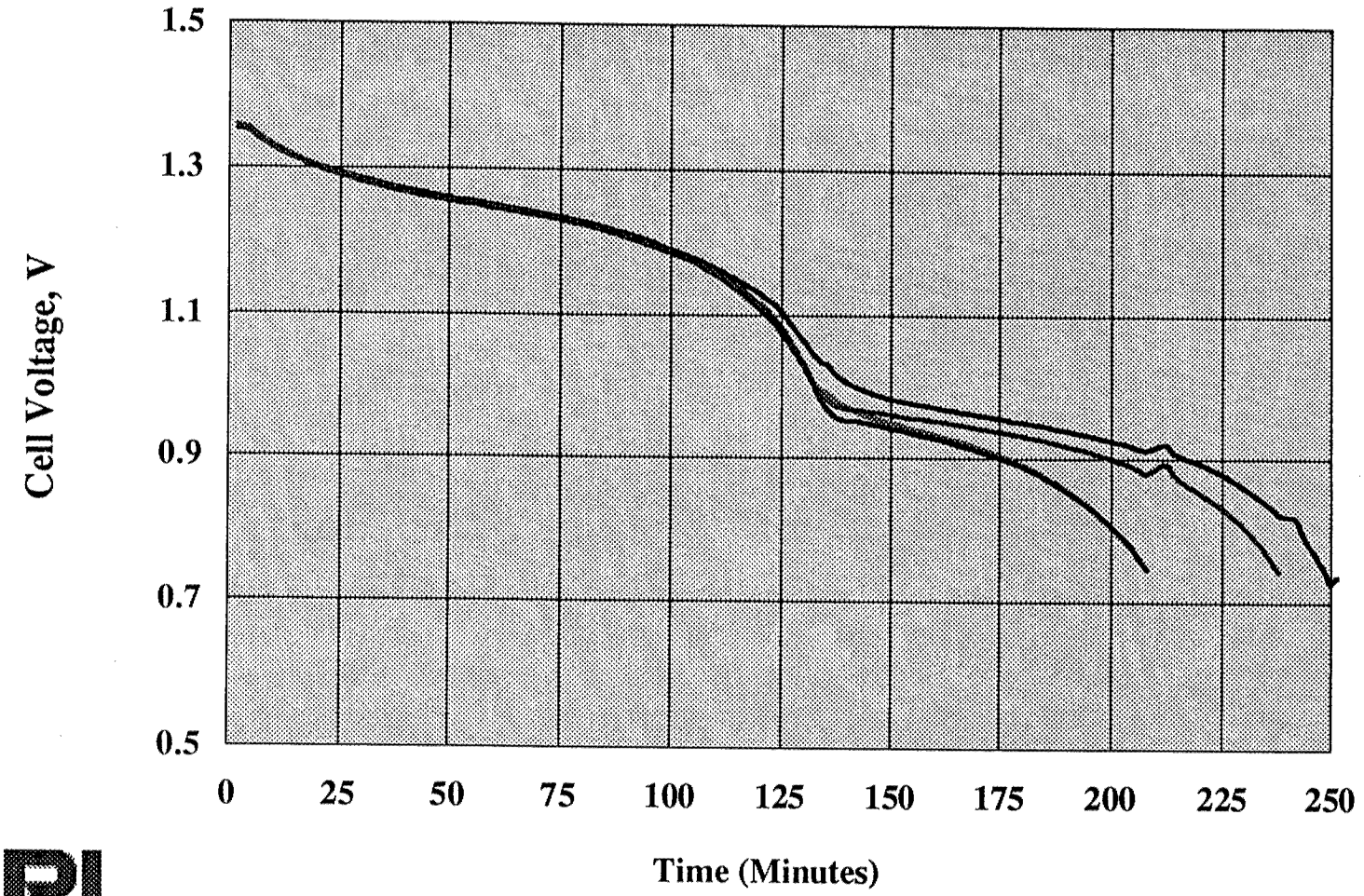

APPLICATION OF FIRST PRINCIPLES MODEL TO SPACECRAFT OPERATIONS

STUDIES OF NEGATIVE LIMITED Ni-Cd CELLS

CAUSES

- INCREASED POSITIVE ELECTRODE CAPACITY
- CADMIUM ELECTRODE CAPACITY FADING
- CHANGES IN THE PRECHARGE LEVEL

EFFECTS

- HIGHER CELL POTENTIALS
- REDUCED CHARGE CURRENTS
- REDUCED CHARGE EFFICIENCY
- REDUCED STATE-OF-CHARGE
- DIVERGENCE OF SOC AND VOLTAGE IN BATTERY PACKS

APPLICATION OF FIRST PRINCIPLES MODEL TO SPACECRAFT OPERATIONS

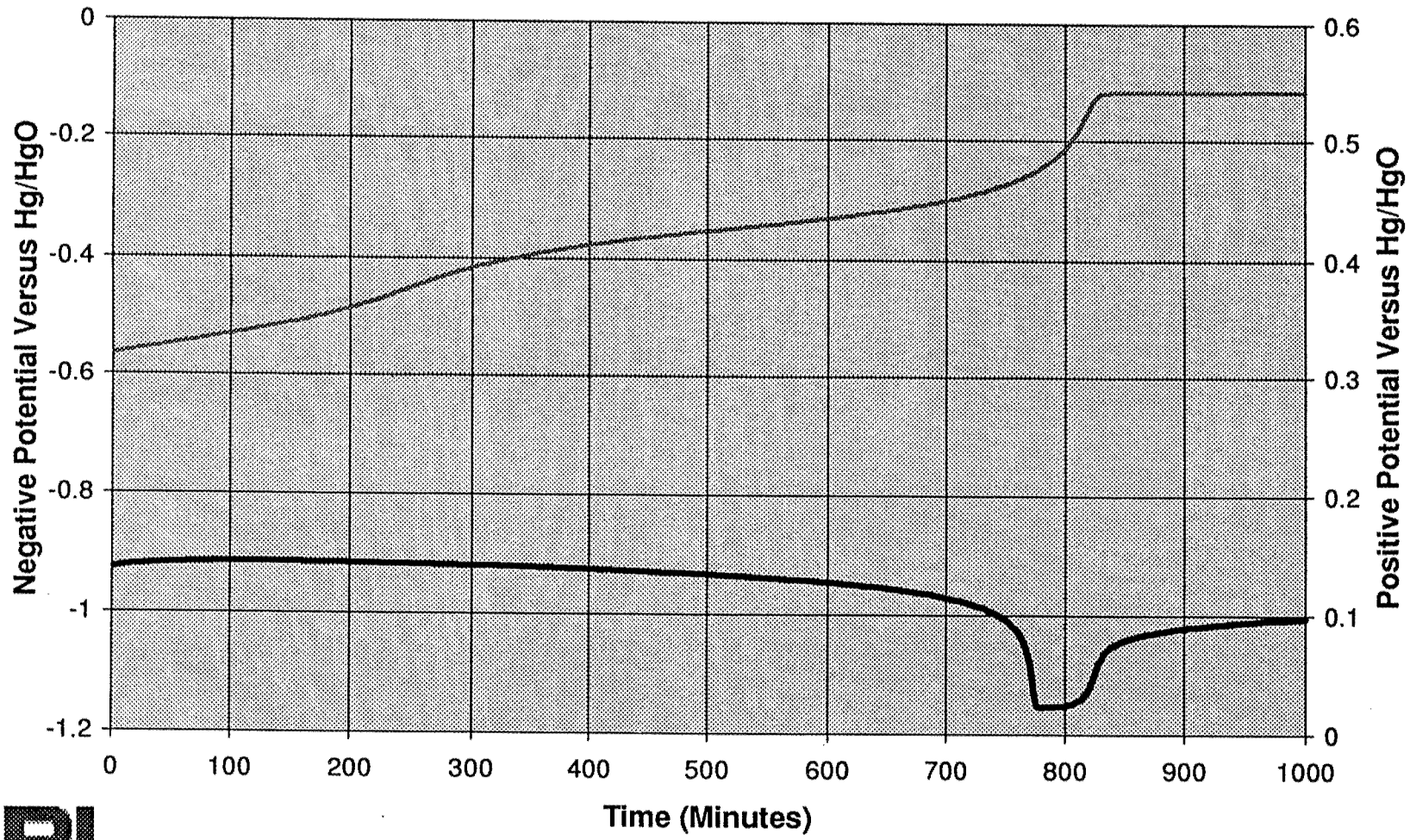

ELECTROCHEMICAL SYSTEMS GROUP

APPLICATION OF FIRST PRINCIPLES MODEL TO SPACECRAFT OPERATIONS

REACTION RATES FOR NEGATIVE LIMITED CELL ON CHARGE

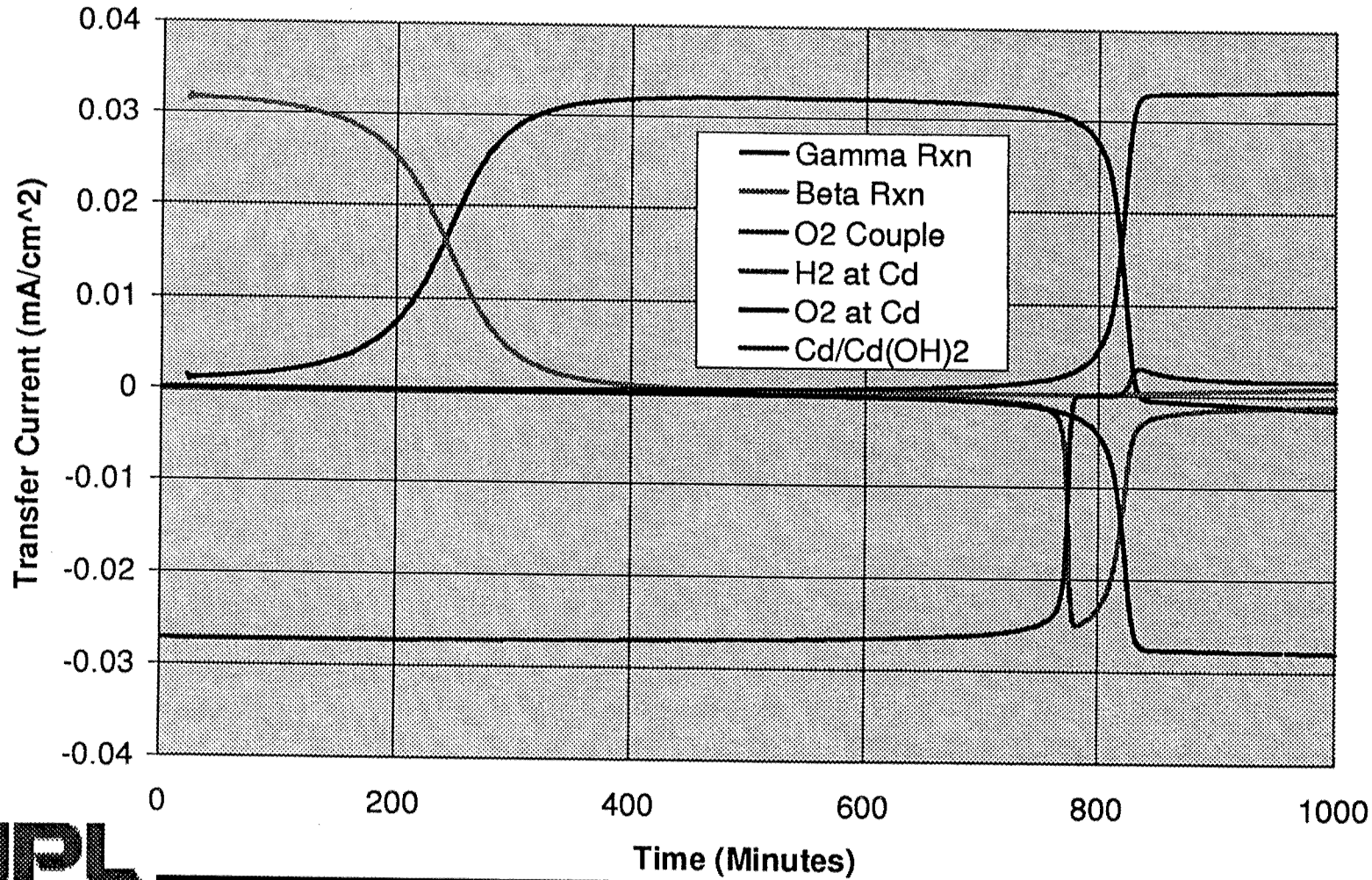

ELECTROCHEMICAL SYSTEMS GROUP

APPLICATION OF FIRST PRINCIPLES MODEL TO SPACECRAFT OPERATIONS

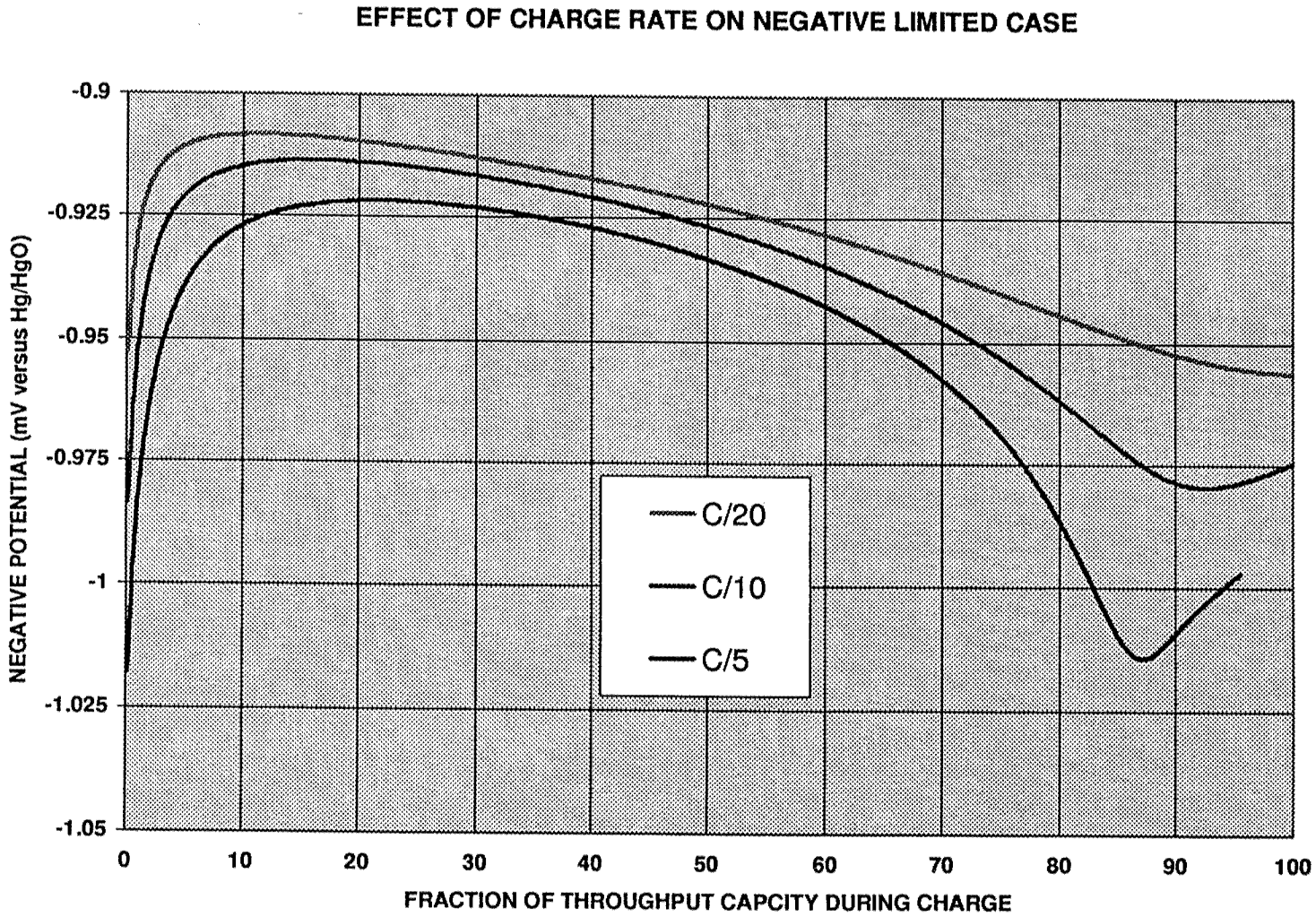

ELECTROCHEMICAL SYSTEMS GROUP

APPLICATION OF FIRST PRINCIPLES MODEL TO SPACECRAFT OPERATIONS

EFFECT OF NEGATIVE LIMITED LEO CYCLING

REGIME SELECTED TO SHOW THE EFFECT OF NEGATIVE LIMITED CELLS

SELECTED REGIME BASED ON RESULTS OF MPS TESTBED / TAGUCHI ANALYSIS

- HIGH CHARGE RATE
- HIGH VT LEVEL
- LOW DOD, 10 MINUTE DISCHARGE DURATION

THESE CONDITION ARE MOST LIKELY TO CAUSE NEGATIVE LIMITED BEHAVIOR

AMOUNT OF PRECHARGE IS VARIED AT THREE LEVELS

SOC's, POTENTIALS, CURRENTS, REACTION RATES WERE PREDICTED

APPLICATION OF FIRST PRINCIPLES MODEL TO SPACECRAFT OPERATIONS

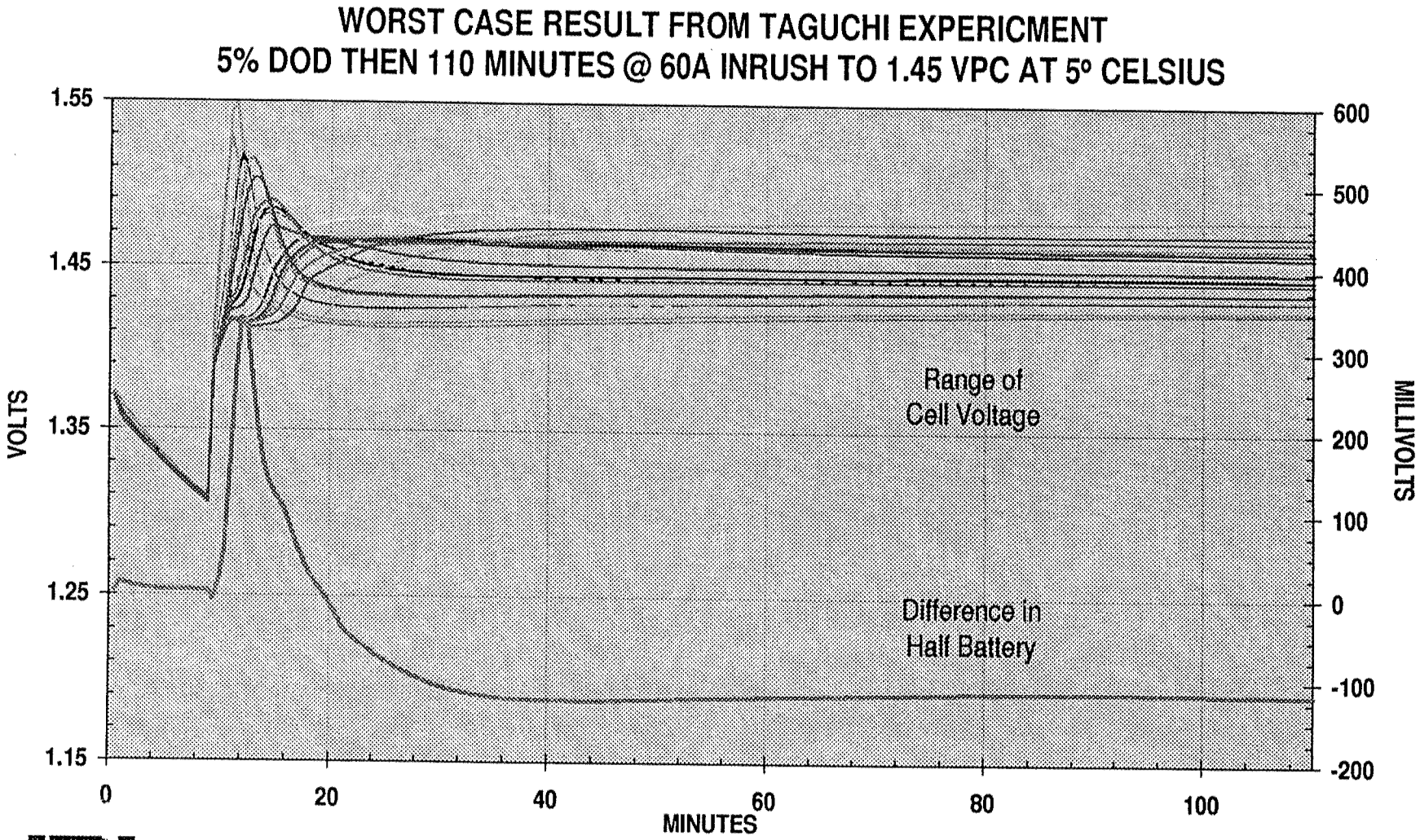

JPL

ELECTROCHEMICAL SYSTEMS GROUP

APPLICATION OF FIRST PRINCIPLES MODEL TO SPACECRAFT OPERATIONS

NEGATIVE ELECTRODE POTENTIALS FOR VARIOUS INTITIAL SOC's

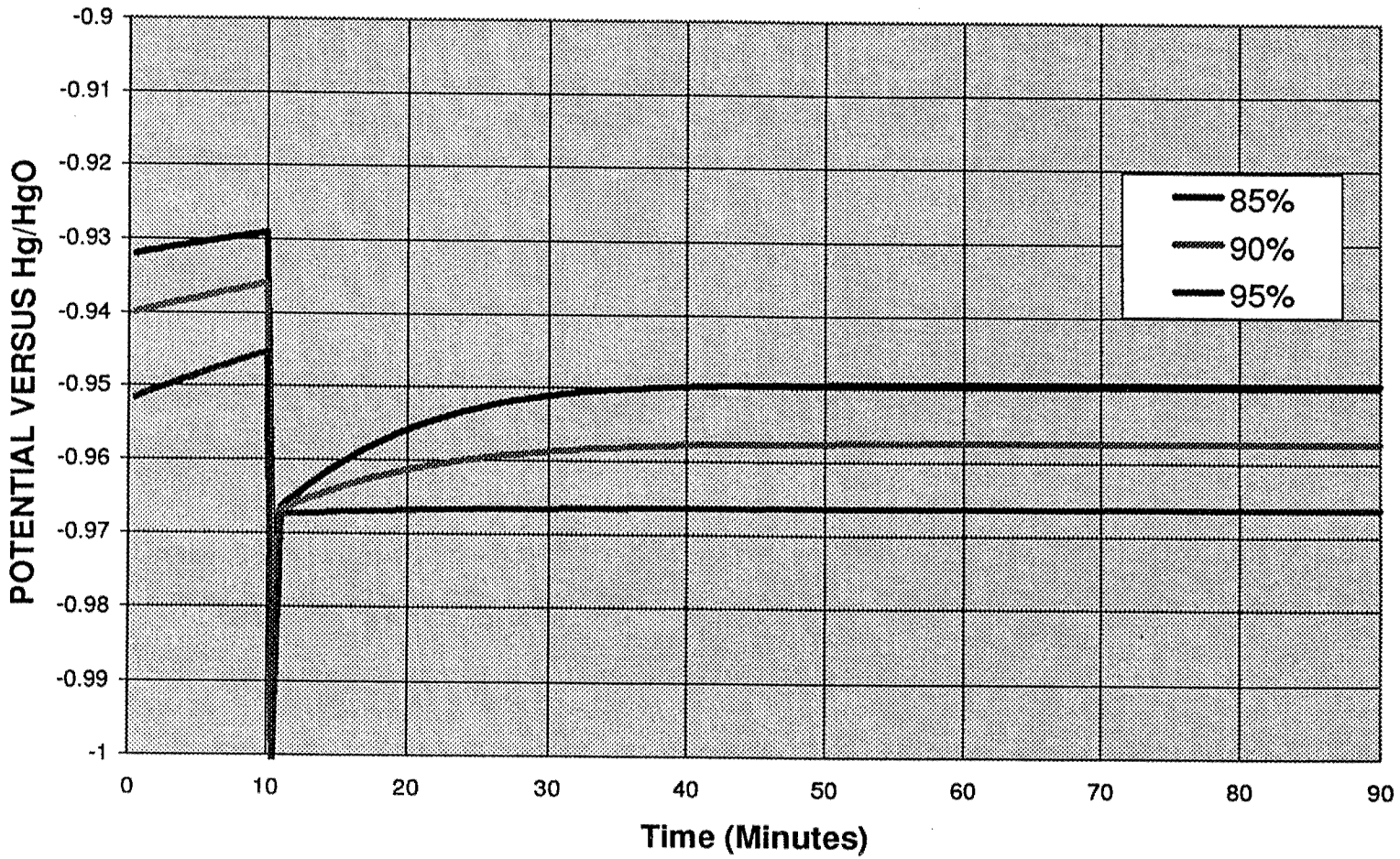

ELECTROCHEMICAL SYSTEMS GROUP

APPLICATION OF FIRST PRINCIPLES MODEL TO SPACECRAFT OPERATIONS

POSITIVE ELECTRODE POTENTIALS FOR VARIOUS INTITIAL Cd SOC's

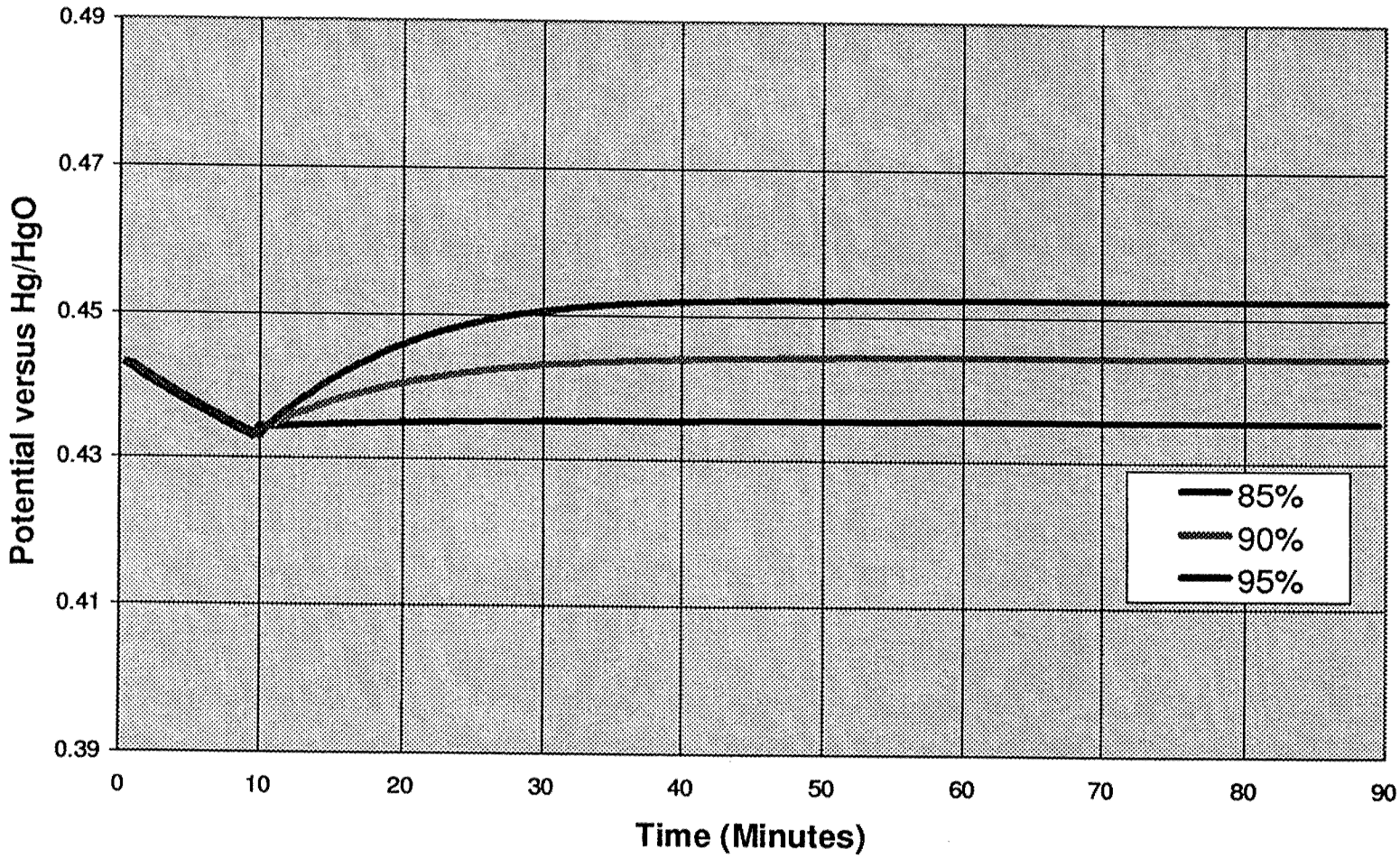

ELECTROCHEMICAL SYSTEMS GROUP

APPLICATION OF FIRST PRINCIPLES MODEL TO SPACECRAFT OPERATIONS

CURRENTS FOR VARIOUS INTITIAL SOC's OF Cd ELECTRODE

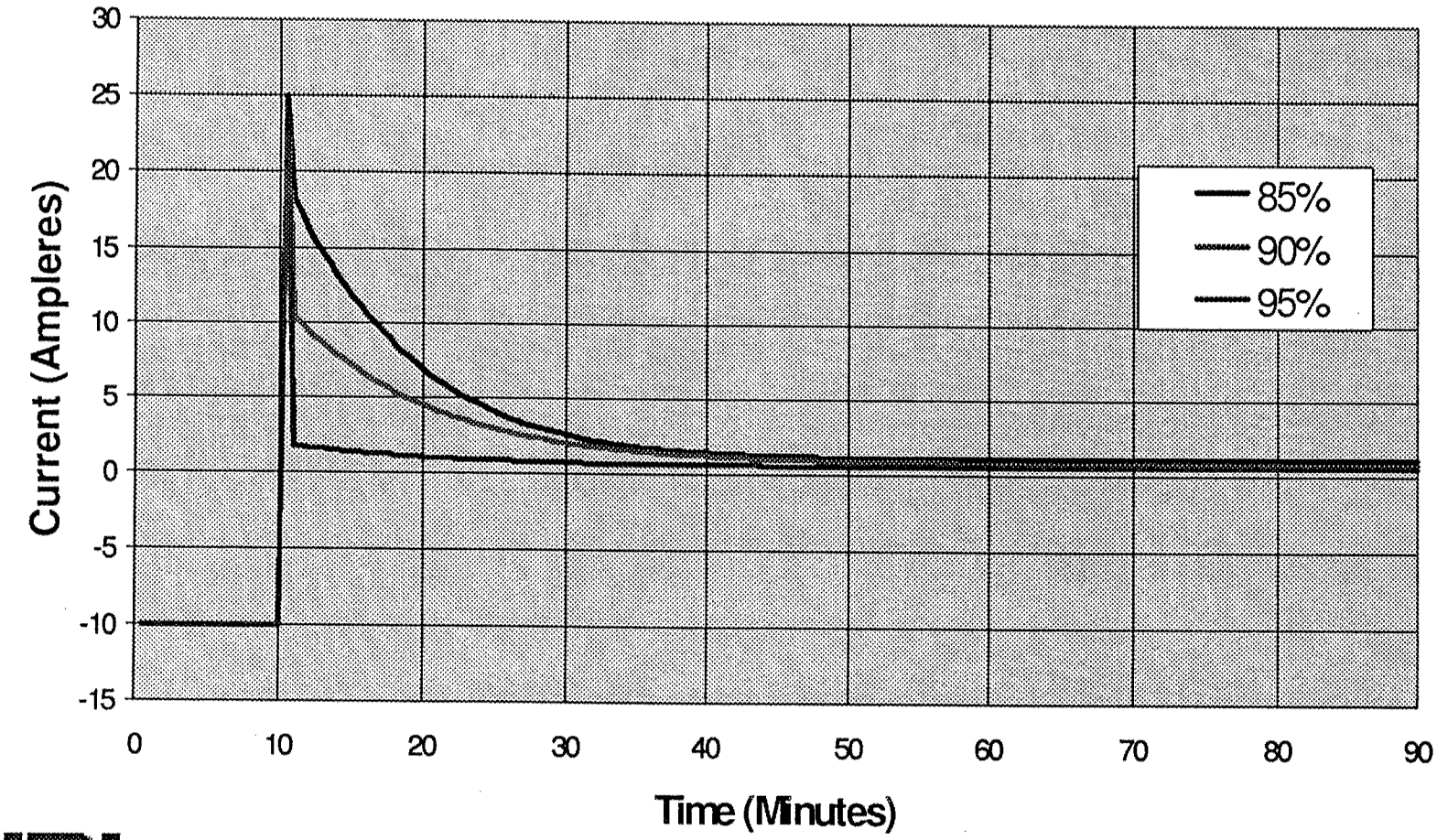

APPLICATION OF FIRST PRINCIPLES MODEL TO SPACECRAFT OPERATIONS

POSITIVE ELECTRODE SOC's FOR VARIOUS INTITIAL Cd SOC's

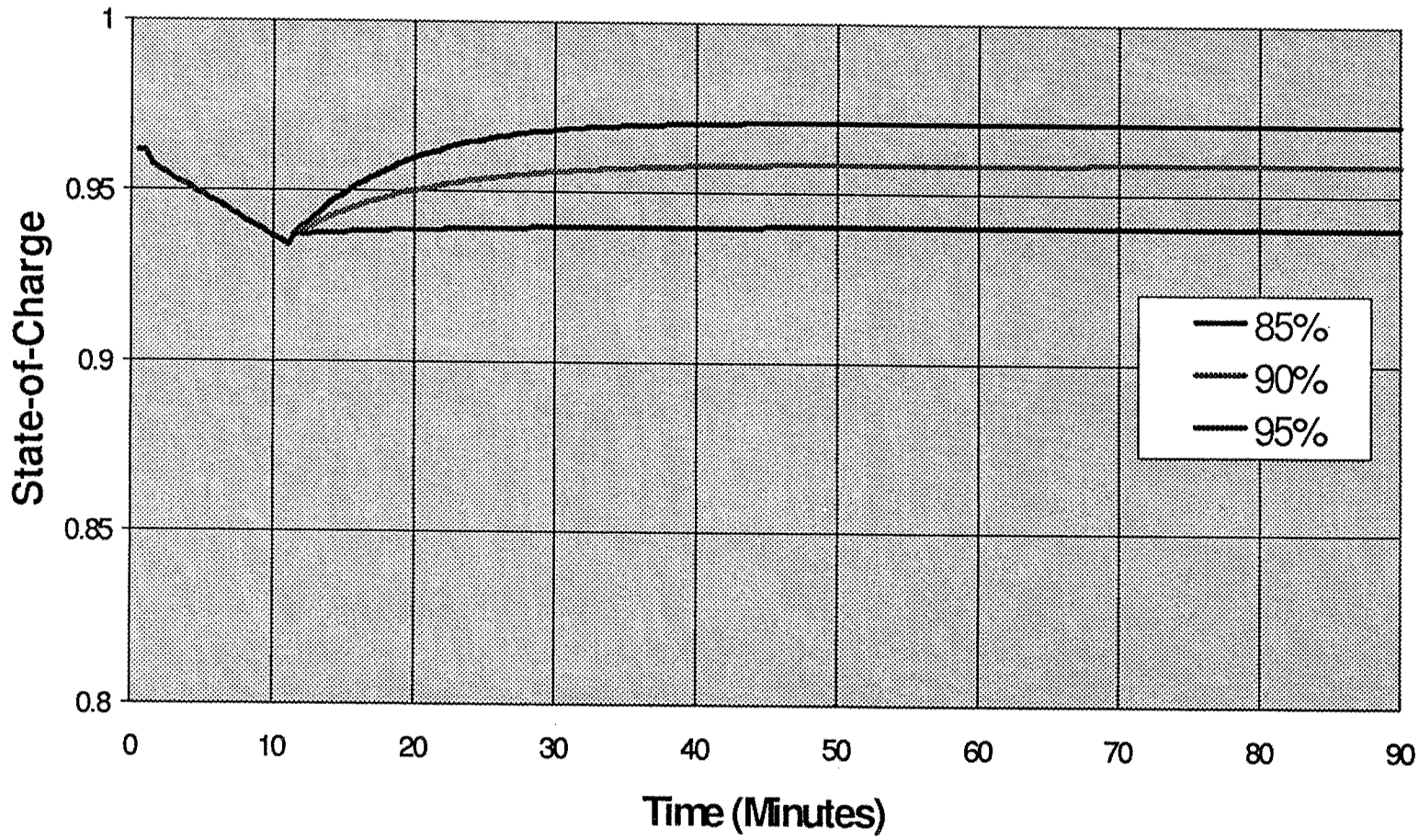

PRESSURE CHANGES IN Ni-H_2 CELLS

H_2 PRESSURE CHANGES EFFECT

- PRESSURE VESSEL SIZING
- PRECHARGE CHANGES

PRESSURE CHANGES DUE TO

- SINTER CORROSION - KNOWN
- PHASE CONVERSION - ADDITIONAL MECHANISM

PRESSURE CHANGES DUE TO PHASE CHANGES

ASSUMING:

1 Liter Void Volume

50 AH Cell Design

1.0 e^-/ Ni Change at BOL

Increased to 1.5 e^-/ Ni at EOL

25 Degrees Celsius

CALCULATIONS:

53.6 AH = 2 Farads

For an increase of 0.5 e^-

1 Equiv. H_2 is produced

Results in 160 psi increase

CONCLUSIONS

FIRST PRINCIPLES BI-PHASIC NICKEL ELECTRODE PRESENTED

MODEL PROVIDES AN EXPLANATION FOR MANY BEHAVIORS

- EON VOLTAGE FADING ON LEO CYCLING
- DEVELOPMENT OF SECOND PLATEAU ON CYCLING
- REDUCTION OF OVERCHARGE PROTECTION IN NiCd CELLS
  - ONSET OF NEGATIVE LIMITED BEHAVIOR
  - CELL DIVERGENCE ON LEO CYCLING
- VARIATION IN HYDROGEN PRECHARGE IN NiH2 CELLS

ACKNOWLEDGMENTS

This work was performed at the Jet Propulsion Laboratory, California Institute of Technology, under contract from NASA. This work was funded by Code AE, the office of the Chief Engineer.

Other Secondary Technologies Session

Page

544

Blank

SODIUM SULFUR BATTERY CELL EXPERIMENT (NaSBE)

Presented to the
1996 NASA Aerospace Battery Workshop
Huntsville, Alabama
December 5, 1996

J. Christopher Garner
U.S. Naval Research Laboratory
Washington, D.C

Naval Research Laboratory
Washington, DC 20375

INTRODUCTION - SODIUM SULFUR

- 1966 FORD MOTOR COMPANY PUBLISH PAPER DESCRIBING NEW TYPE OF SECONDARY BATTERY COMPRISED OF:
  - SOLID, SODIUM ION CONDUCTING ELECTROLYTE
  - LIQUID METAL ELECTRODE
  - REDOX ELECTRODE
  - OPERATING TEMPERATURE BETWEEN 300 AND 400°C
  - SPECIFIC ENERGY OF 150 Wh/Kg
  - NOMINAL VOLTAGE 2.0 V

Naval Research Laboratory
Washington, DC 20375

SODIUM SULFUR BATTERY CELL

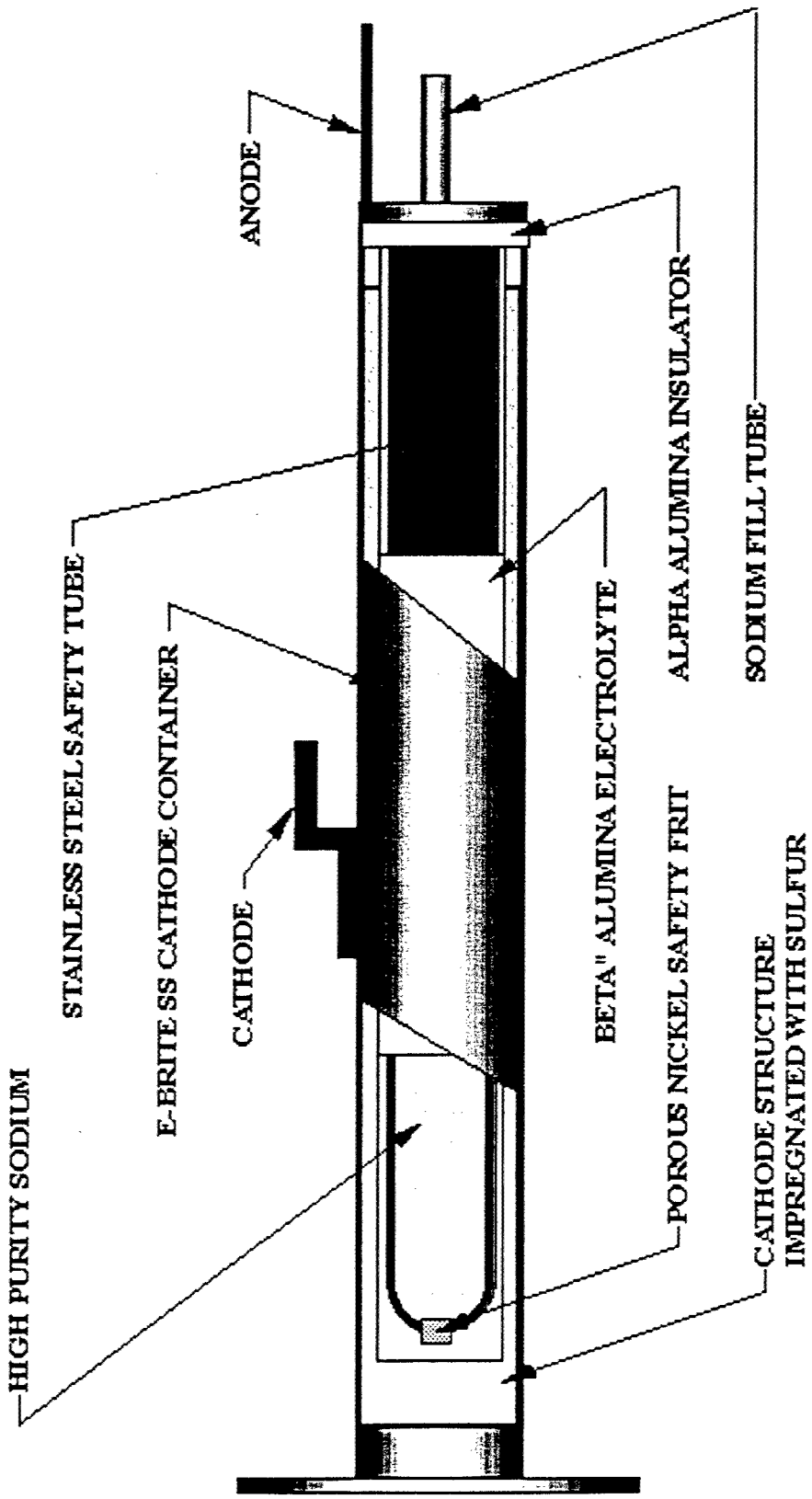

Naval Research Laboratory
Washington, DC 20375

SODIUM SULFUR AEROSPACE HISTORY

- LATE 1970'S USAF BEGINS DEVELOPMENT OF NaS FOR AEROSPACE
  - 1979 AFWAL Tests Ford Aerospace Cells (6,300 Cycles)
  - 1983 AFWAL Funds Ford Aerospace Development of GEO Cells
  - 1986 AFWAL Funds EPI Development of LEO Cells , Hughes HEDRB Effort
  - 1992 NaS Efforts Transferred to USAF PL
- 1993 PL FUNDS EP 40 AH CELLS FOR GROUND TEST AND SAFETY TESTS
  - Ground Test at NWSC, Crane (Simulated Leo,GEO Cycle Tests)
  - Safety Tests at Sandia National Labs
  - Vibration (Hot), Shock, Electrolyte Fracture
- 1994 USAF PL SIGNS MOA WITH NRL FOR FLIGHT EXPERIMENT
  - Design, Build, Test One Brassboard& One Flight Experiment
  - Brassboard to Be Used As Ground Test Bed Delivered to USAF PL

Naval Research Laboratory
Washington, DC 20375

FLIGHT EXPERIMENT PURPOSE

- CHARACTERIZE NaS BATTERY CELL OPERATION IN ZERO-G
  - Perform Post Flight DPA, Compare With Ground Test Cells
- LEARN HOW TO WORK WITH A BATTERY SYSTEM THAT REQUIRES 350°C TEMPERATURES
- NAVIGATE EXPERIMENT THROUGH NASA SAFETY AND INTEGRATION PROCESS

Naval Research Laboratory
Washington, DC 20375

EXPERIMENT DESCRIPTION

- LAUNCH 4 NaS BATTERY CELLS AT AMBIENT TEMP, CHARGED
- PHASE I - HEAT CELLS ON ORBIT TO 350°C
- PHASE II - (2) CAPACITY CYCLES
  - § -20A Discharge to 1.65V, 4A Charge to 2.35V
- PHASE III - (2) SIMULATED GEO CYCLES
  - § -20A Discharge for 1.2 Hr., 2A Charge for 12 Hr., 10.8 Hr. Open Circuit
- PHASE IV - (15) SIMULATED LEO CYCLES
  - § -32A Discharge for 0.5 Hr., 16 a Charge for 1 Hour
- PHASE V - DISCHARGE CELLS TO 0%, 20%, 40%, 60% COOL TO AMBIENT
- FIT ENTIRE EXPERIMENT WITHIN NASA STANDARD GAS CAN
- LAUNCH WITH STS-80 ON WAKE SHIELD FACILITY 03

Naval Research Laboratory
Washington, DC 20375

40 AH SODIUM SULFUR BATTERY CELL

- CAPACITY 40 AMPERE-HOURS
- DIMENSIONS
  - Length 0.240 m (9.44 inches)
  - Diameter 0.035 m (1.39 inches)
- MASS 0.580 KG (1.28 LBS)
- SPECIFIC ENERGY 138 WH/KG
- MANUFACTURE EAGLE PICHER INC., JOPLIN, MO
- ELECTROLYTE B" ALUMINA

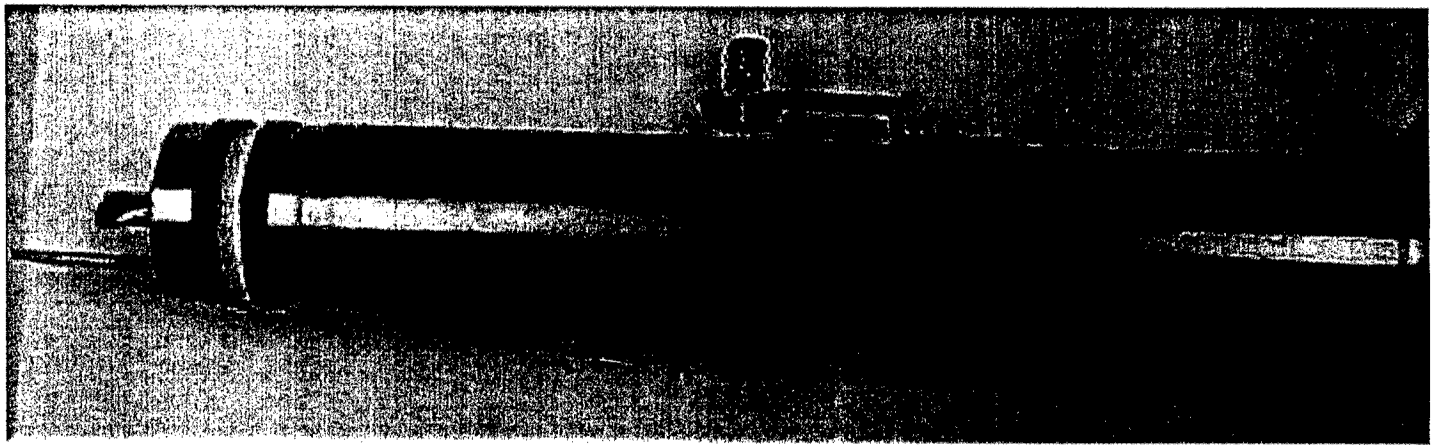

Naval Research Laboratory
Washington, DC 20375

EXPERIMENT BLOCK DIAGRAM

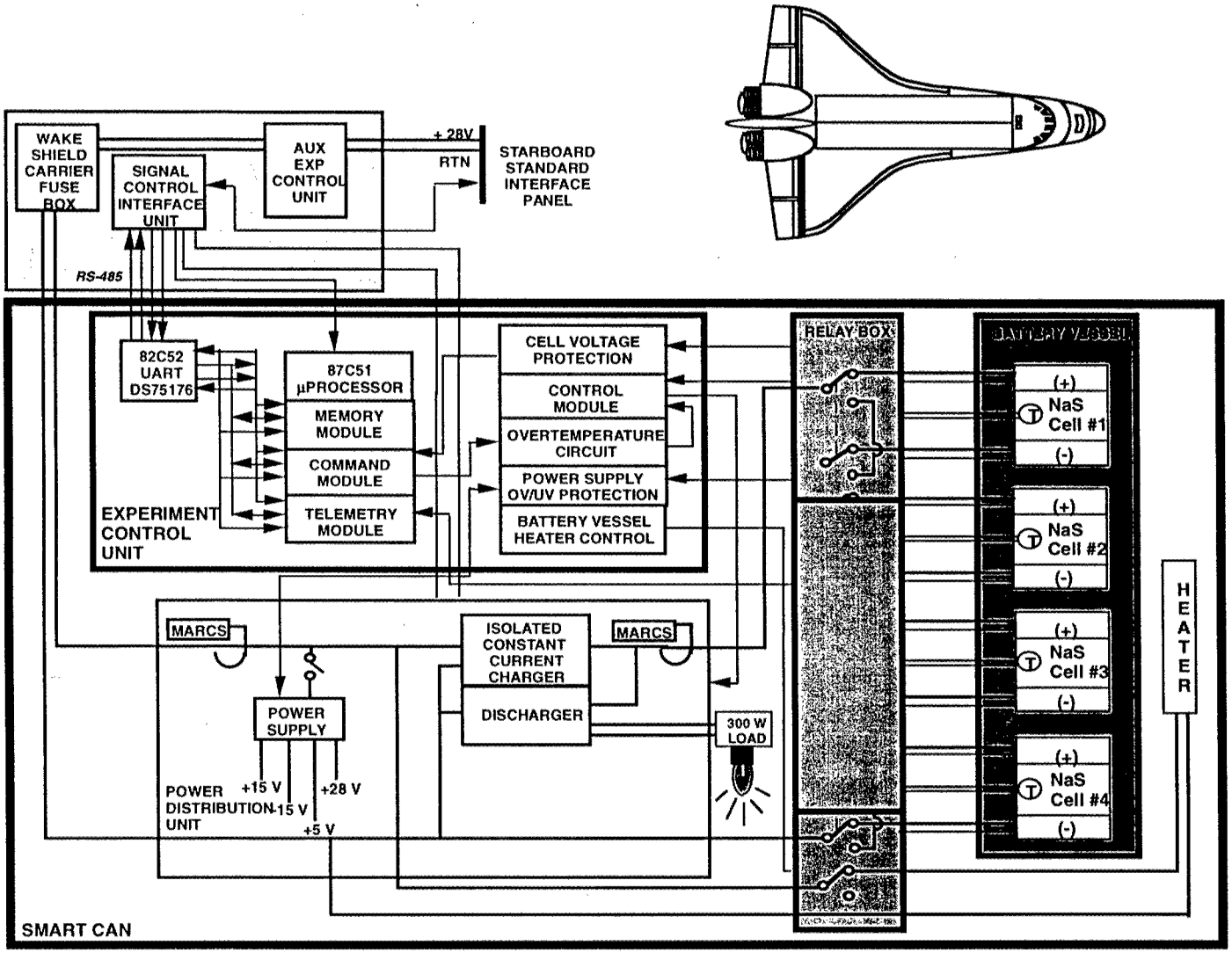

Naval Research Laboratory
Washington, DC 20375

EXPERIMENT POWER ELECTRONICS

- CHARGE BATTERY CELLS AT 2, 4 AND 16 AMP RATES
- DISCHARGE BATTERY CELLS AT -20 AND -32 AMP RATES
  - Discharge 1 Cell to 60% Depth of Discharge
  - Use 3 Halogen Lamps As Discharge Loads
- EXPERIMENT MUST FAIL SAFE
  - Internal Power Supply Failure Shuts Down Entire Experiment
  - NaS Battery Cell Overtemperature Circuit
    - DISABLES BATTERY HEATER
    - DISABLES CHARGER AND DISCHARGER
  - NaS Battery Cell Over/Undervoltage Circuit
    - EACH CELL MONITORED INDIVIDUALLY
      - IF CELL VOLTAGE < 1.65 V OR > 2.5 V CELL IS REMOVED FROM CIRCUIT
  - All Power Lines Are Switched

Naval Research Laboratory
Washington, DC 20375

EXPERIMENT TELEMETRY, COMMAND & CONTROL

- REQUIREMENTS
  - Collects Telemetry From Experiment
    - Individual Cell Voltage, 4 Temperatures/Cell, Experiment Temperatures, Charge/Discharge Currents
  - Send Commands
  - Receive/X-Mit Commands & Telemetry From WSF CBC via RS-485
  - Store One Orbit Of Experiment TLM Data
- IMPLEMENTATION
  - Harris 82C52 UART & Processor For WSF Data Interface
    - Intel 87C51C µController
      - 8051 Heritage
      - 32k EPROM
      - 256 Bytes RAM
      - 10 MHz Clock
      - 2 User Interrupts
  - 48k x 8 Total Memory For Experiment Data & Software
  - 16 Low Level Commands (200µS Pulse Width)
  - 16 High Level Commands (+28V, 40mS)
  - 32 Bi-Level TLM Points
  - 64 Analog TLM (48 Passive, 16 Active)

Naval Research Laboratory
Washington, DC 20375

EXPERIMENT THERMAL DESIGN

- POWER GENERATED BY BATTERY CELLS IS DISSIPATED BY HALOGEN LIGHT BULBS OUTSIDE OF SMART CAN
- HOT VESSEL WRAPPED WITH A 4 PIECE 0.001M THICK MICA HEATER
- NaS CELL TEMPERATURES CONTROLLED WITHIN 350±20°C
  - Monitor NaS Cell and Hot Vessel Temperatures
    - When NaS Cell Temp < 330°C , Thermostat Closes, Heater Power Applied
    - When Hot Vessel Temp < 330°C & NaS Cell Temp < 370°C, Thermostat Closes
    - When NaS Cell or Hot Vessel Temp > 370°C, Thermostat Opens
- USE OF HIGH THERMAL RESISTANCE CERAMIC ISOLATORS TO OBTAIN DT BETWEEN HOT VESSEL & MID-DECK

Naval Research Laboratory
Washington, DC 20375

EXPERIMENT ON-ORBIT DATA TRANSFER

- GroundStation Uses OS Comet*
- RS422 From/To SII & NASA JSC
- RS 485 From/To WSF & NaSBE

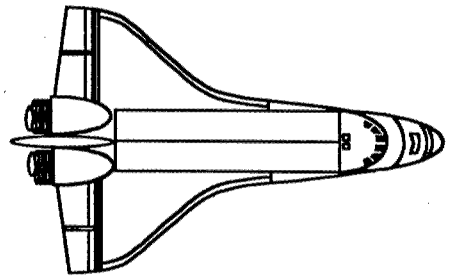

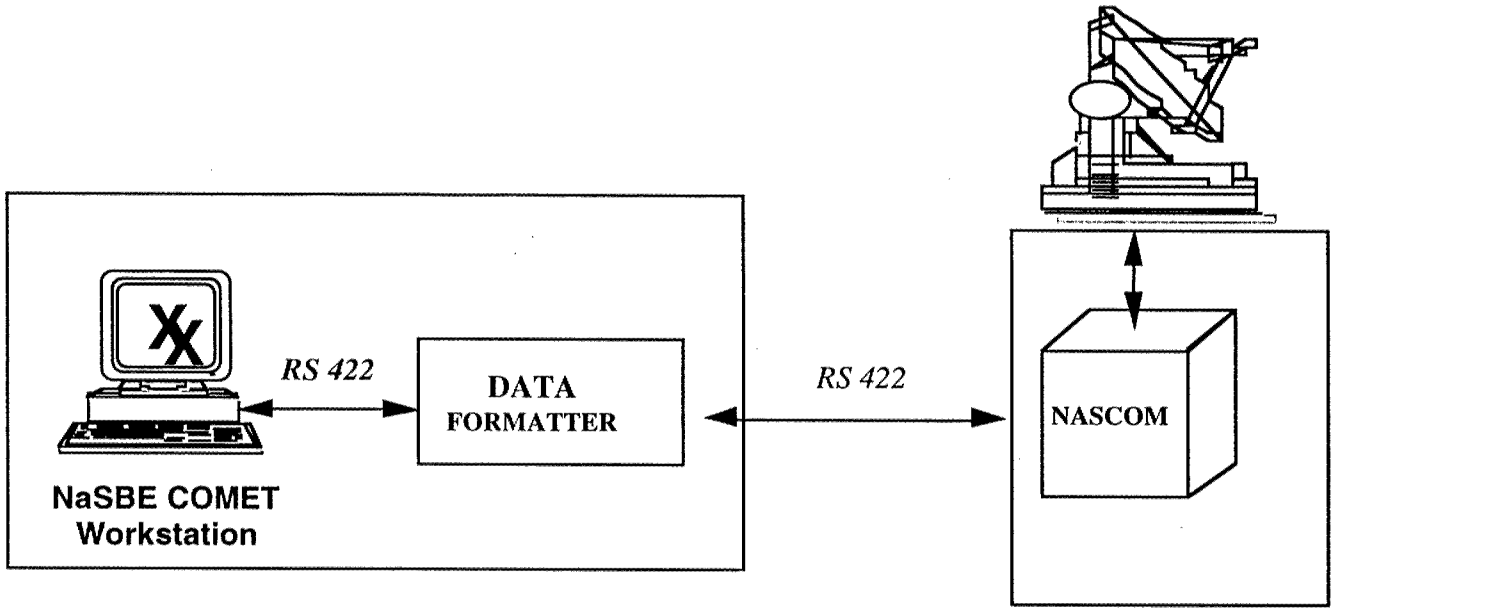

SPACE INDUSTRIES INTERNATIONAL
LEAGUE CITY, TEXAS

NASA JOHNSON SPACE FLIGHT CENTER

Naval Research Laboratory
Washington, DC 20375

THERMAL VACUUM TEST DATA (-20 A DISCHARGE)

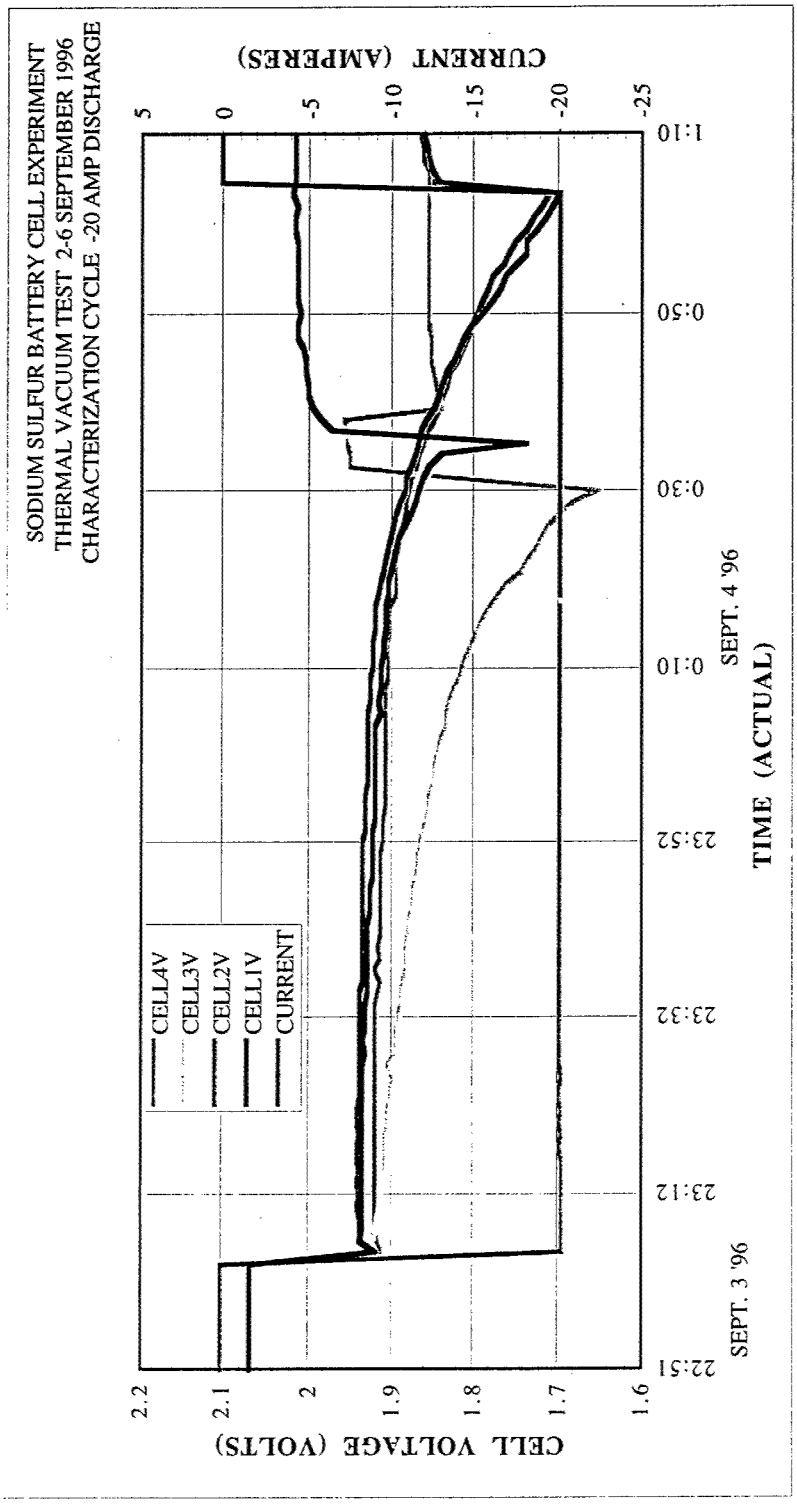

Naval Research Laboratory
Washington, DC 20375

THERMAL VACUUM TEST DATA (4 A CHARGE)

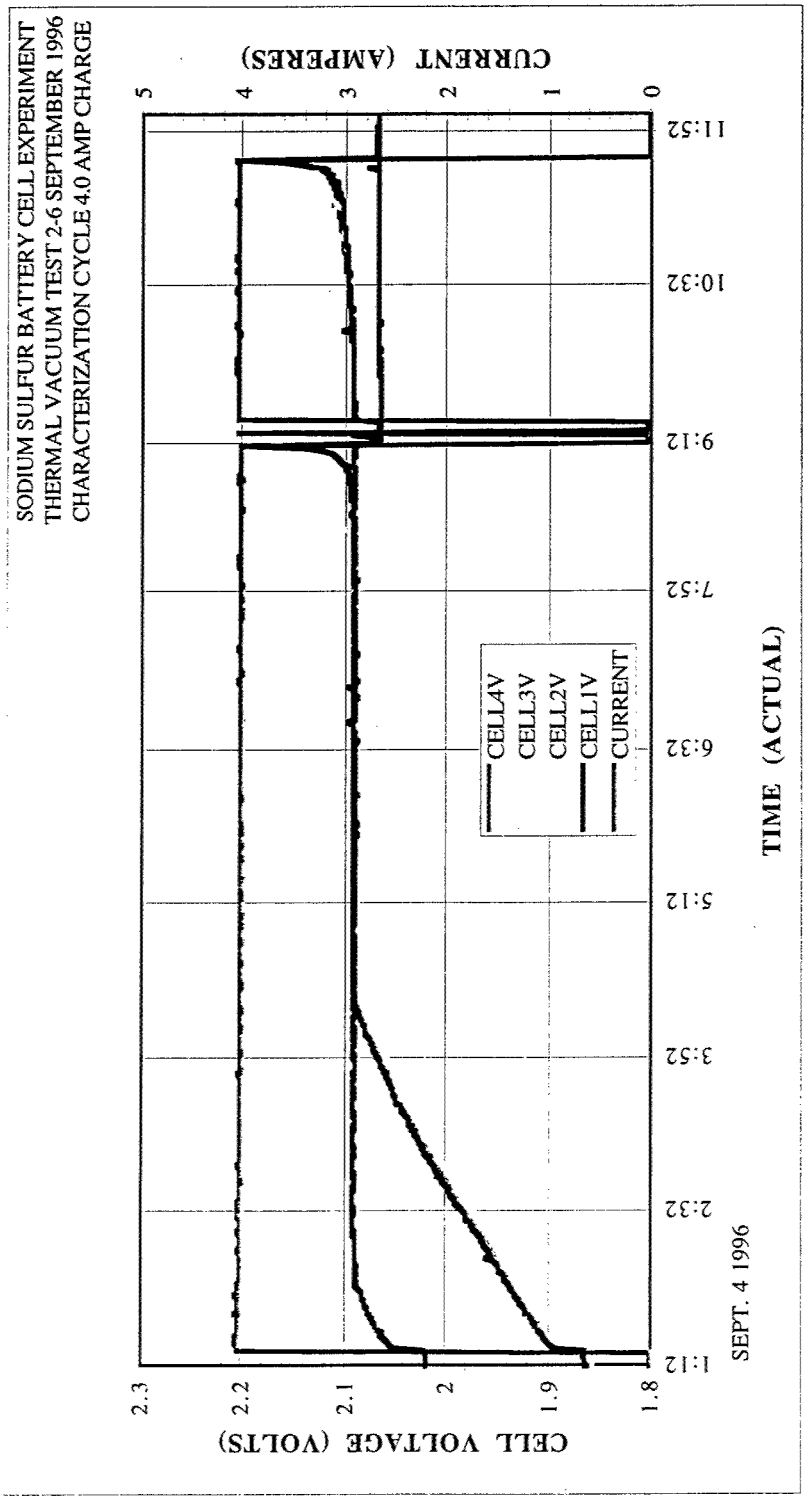

Naval Research Laboratory
Washington, DC 20375

THERMAL VACUUM TEST DATA (LEO 40% DOD)

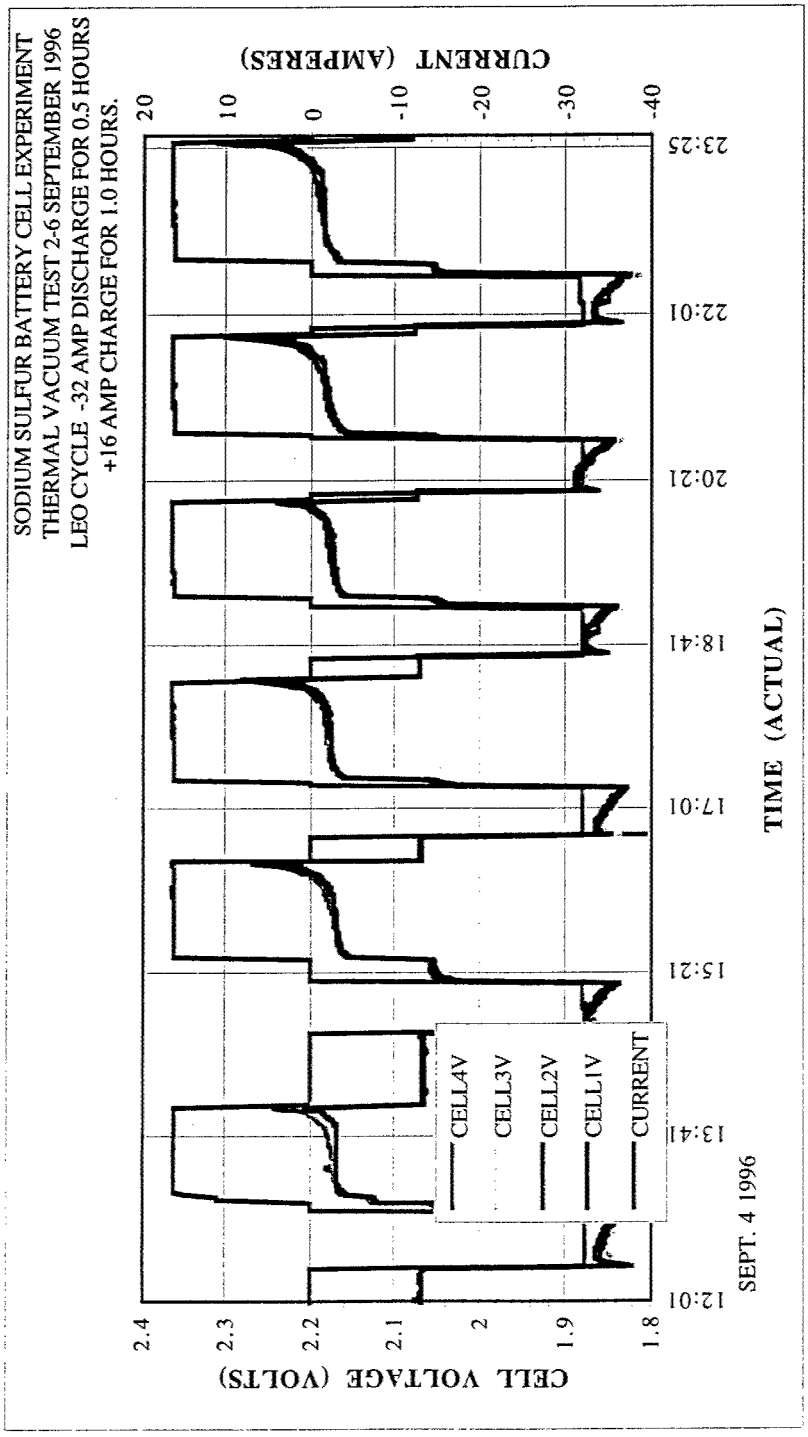

Naval Research Laboratory
Washington, DC 20375

THERMAL VACUUM TEST DATA

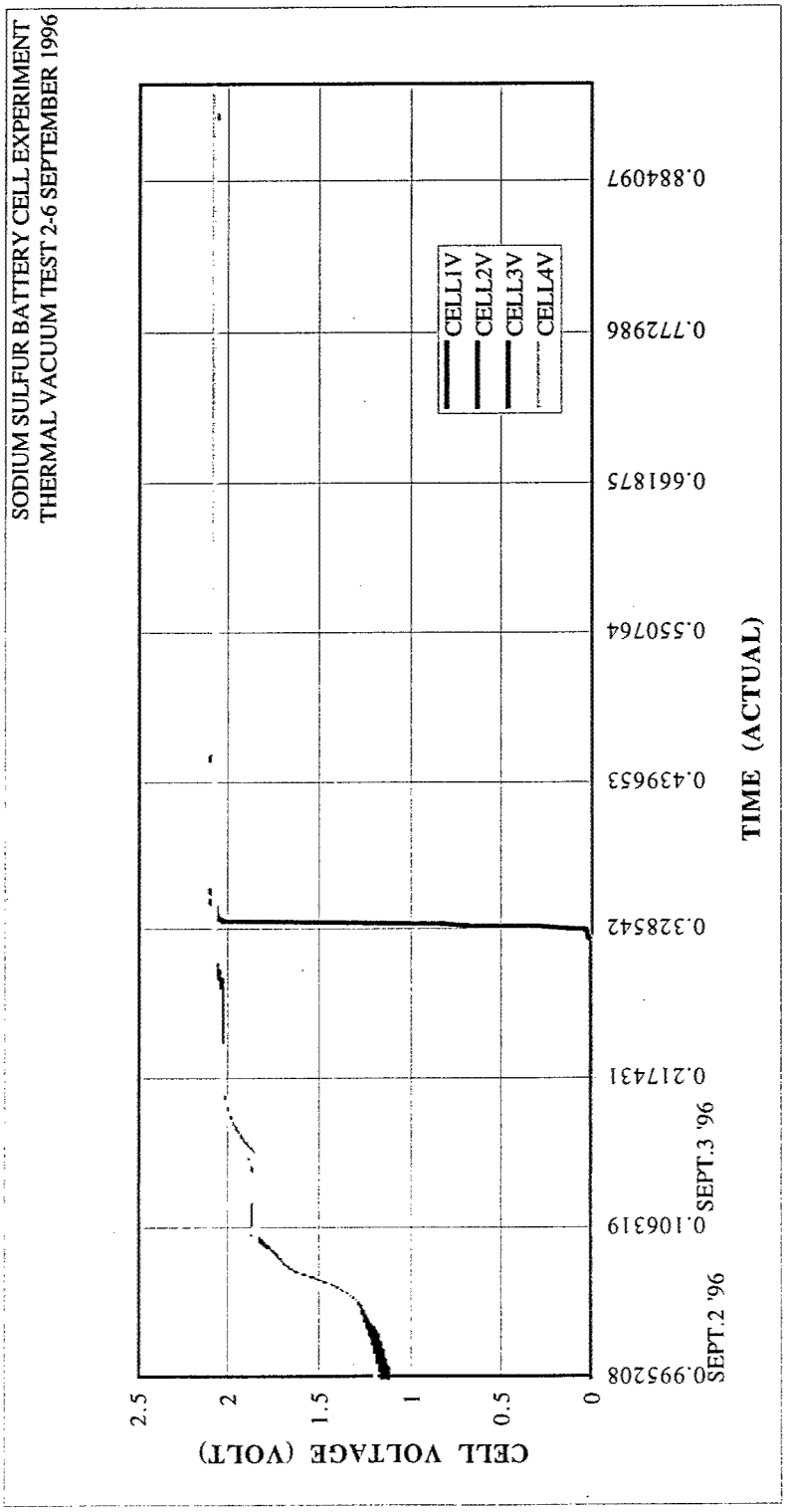

Naval Research Laboratory
Washington, DC 20375

SUMMARY

- USAF PL SPONSOR FOR NaS BATTERY CELL FLIGHT EXPERIMENT
- GROUND TESTS DATA SHOW NaS WITH SPECIFIC ENERGY >100 WH/KG
- EXPERIMENT MODIFICATION IN PROGRESS FOR RIDE AS NASA HITCHHIKER PAYLOAD
- NEGOTIATING FOR LAUNCHES ON STS -89, STS-90, AND STS-91

Naval Research Laboratory
Washington, DC 20375

Page

564

Blank

1996 NASA Aerospace Battery Workshop
Marshall Space Flight Center

LOW-EARTH-ORBIT(LEO) LIFE CYCLE EVALUATION OF NICKEL-ZINC BATTERIES

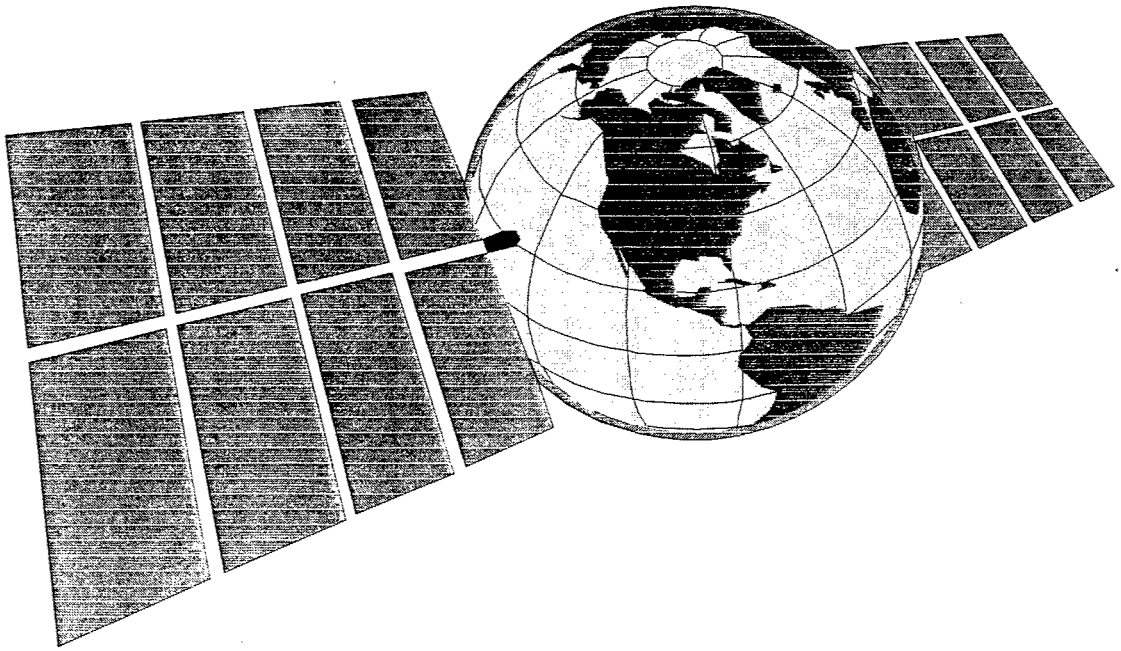

D. COATES, E. FERREIRA,
M. NYCE AND A. CHARKEY
Energy Research Corporation
3 Great Pasture Road
Danbury, CT 06813

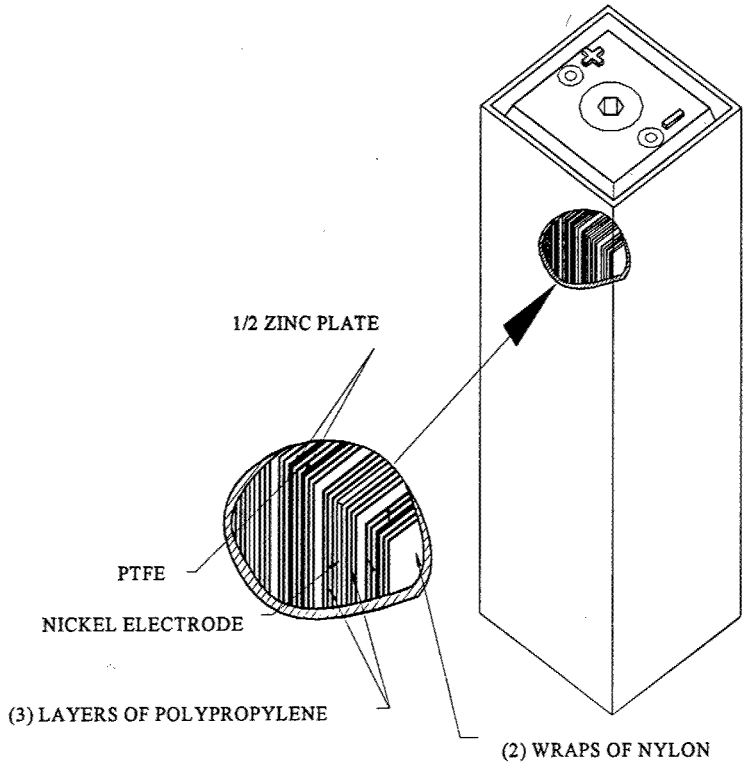

TYPICAL SEALED NICKEL-ZINC CELL DESIGN

- LOW-COST ROLL-BONDED ELECTRODES
- NICKEL/GRAPHITE COMPOSITE ACTIVE MATERIAL
- COBALT SPINEL TREATED GRAPHITE
- LOW METAL CONTENT - HIGH SPECIFIC ENERGY
- REDUCED SOLUBILITY CALCIUM / ZINC ELECTRODE
- MINIMAL SHAPE CHANGE
- POROUS POLYPROPYLENE ZINC MIGRATION BARRIER
- NON-WOVEN NYLON ABSORBER / SEPARATOR
- LOW ELECTROLYTE CONCENTRATION
- 20% POTASSIUM-HYDROXIDE / 1% LITHIUM-HYDROXIDE
- PRISMATIC MOLDED POLYSULFONE CELL CASE
- SOLVENT-WELD COVER TO CASE JOINT
- RESEALABLE PRESSURE RELIEF VALVE (25 psi)

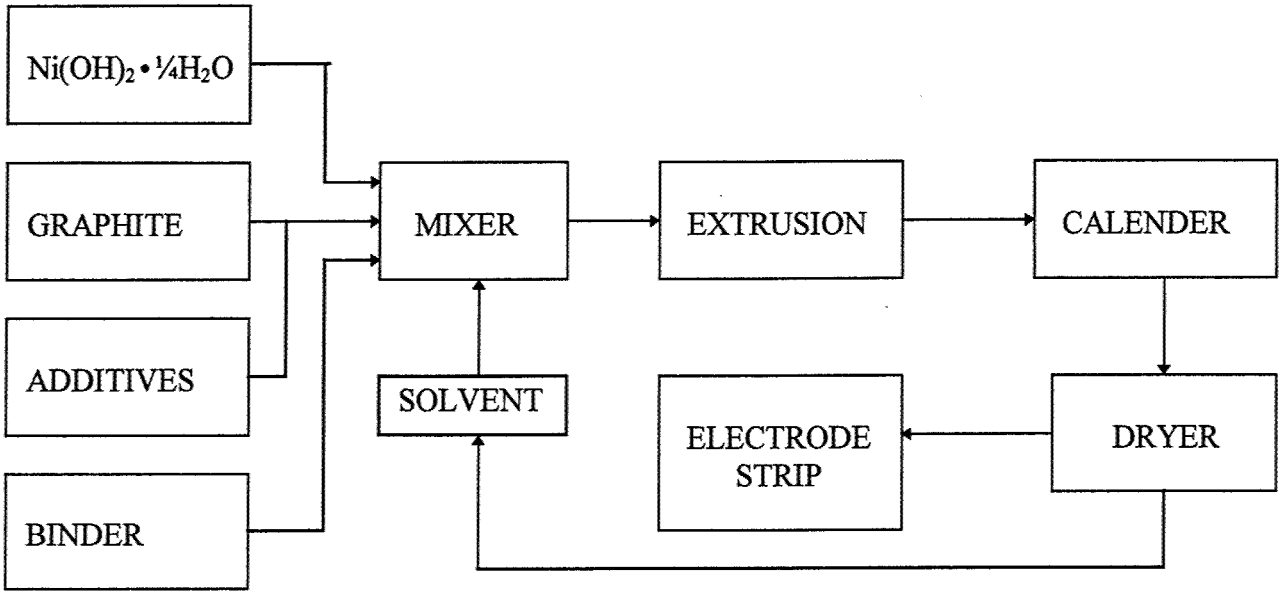

ROLL-BONDED ELECTRODE MANUFACTURING PROCESS

- PATENTED MANUFACTURING PROCESS FOR NICKEL AND ZINC ELECTRODES
- THE NICKEL ELECTRODE IS A GRAPHITE COMPOSITE STRUCTURE
- THE ONLY METAL IN THE NICKEL ELECTRODE IS THE 0.003 INCH NICKEL FOIL CURRENT COLLECTOR
- REDUCED METAL CONTENT REDUCES BOTH COST AND WEIGHT
- THE ZINC ELECTRODE IS A CALCIUM / ZINC FORMULATION
- REDUCED SOLUBILITY ZINC ELECTRODE MINIMIZES SHAPE CHANGE
- LOW COST EXTRUSION BASED MANUFACTURING PROCESS
- PROCESS EASILY SCALEABLE FOR HIGH VOLUME PRODUCTION
- ENVIRONMENTALLY FRIENDLY MANUFACTURING PROCESS
- MINERAL OIL BASED SOLVENT CAN BE RECLAIMED AND RE-USED
- VERY LOW MATERIAL ATTRITION RATE
- ELECTRODE SCRAP MATERIAL CAN BE RE-PROCESSED

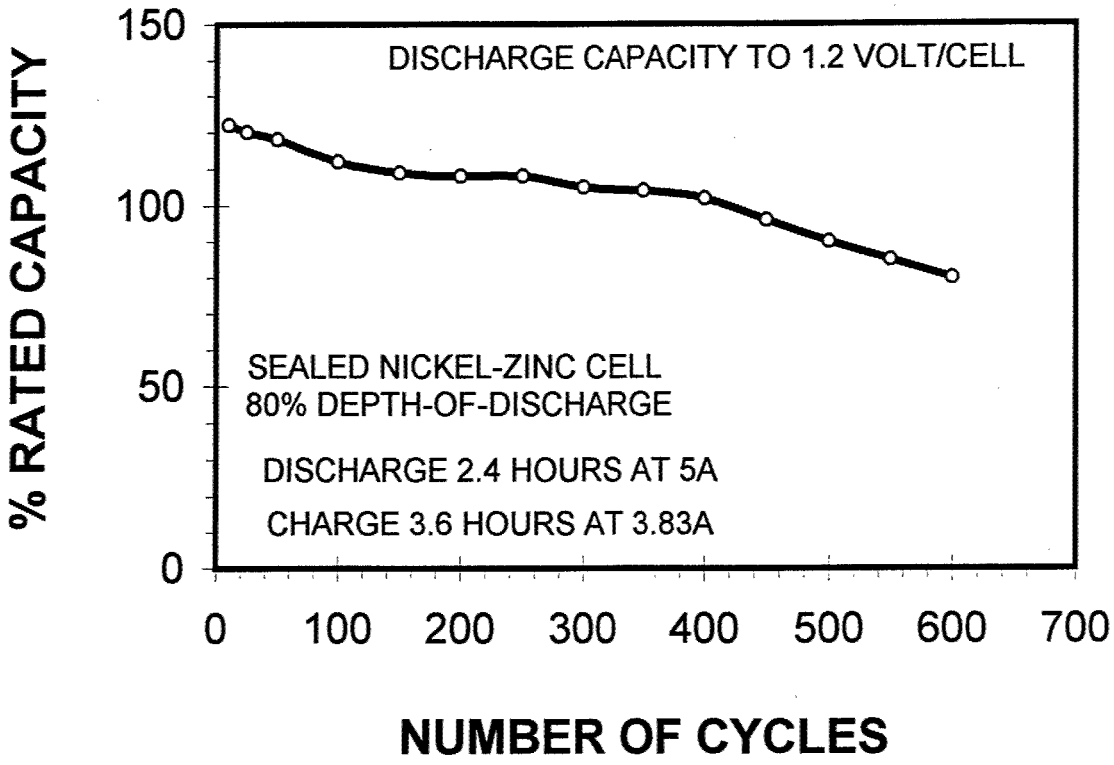

NICKEL-ZINC DISCHARGE CAPACITY VERSUS CYCLE LIFE

- SEALED 15 Ah CELL DESIGN
- ROLL-BONDED COMPOSITE NICKEL AND ZINC ELECTRODES
- PATENTED CALCIUM / ZINC ELECTRODE FORMULATION
- CYCLE REGIME: DISCHARGE @ 5.0 A CHARGE @ 3.8 A
- CAPACITY MEASUREMENT @ 5.0 A TO 1.2 Volts PER CELL
- FULL-DEPTH CAPACITY MEASUREMENT AT 25 CYCLE INTERVALS
- PRIMARY CAPACITY DEGRADATION MECHANISM IS ELECTRODE SWELLING AND CELL STACK DRY-OUT
- ZINC DISSOLUTION AND SHAPE CHANGE ARE MINIMAL

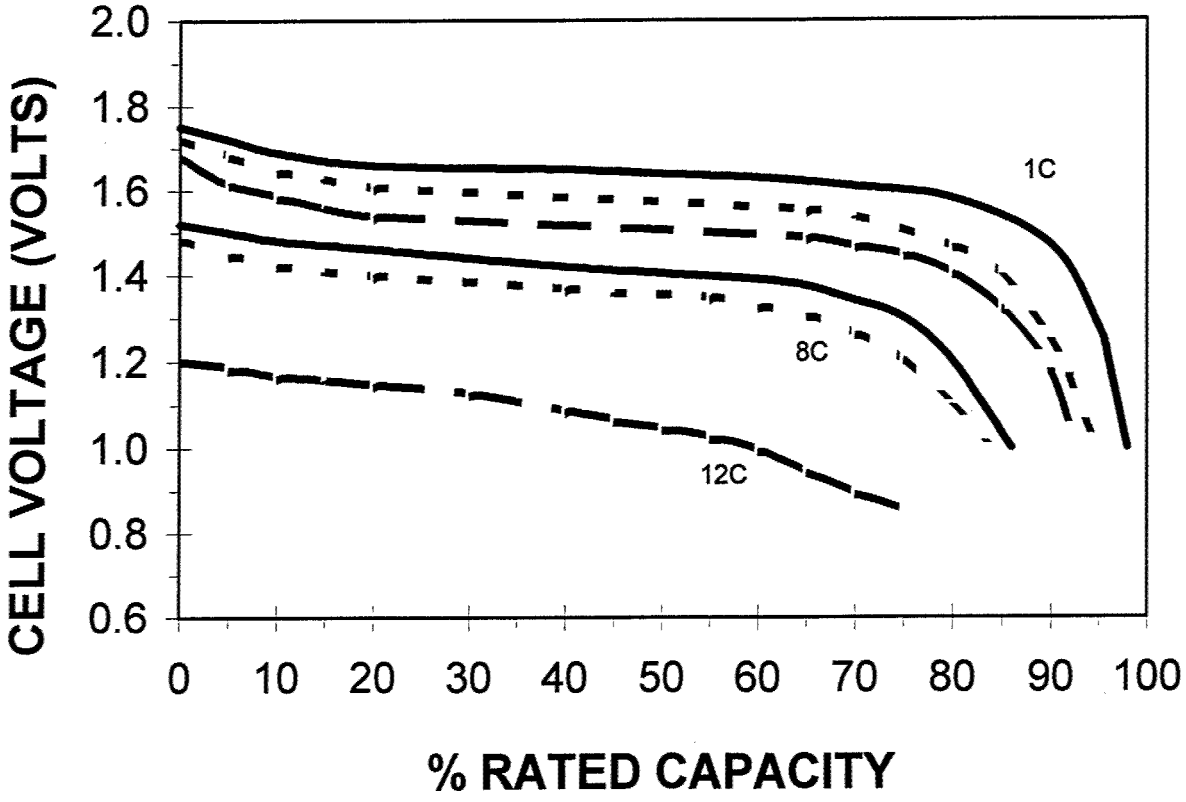

DISCHARGE RATE CAPABILITY OF SEALED NICKEL-ZINC CELL

- SEALED 15 Ah NICKEL-ZINC CELL
- HIGH-RATE DESIGN
- MOLDED POLYSULFONE CELL CASE AND COVER
- PLASTIC BONDED COMPOSITE NICKEL AND ZINC ELECTRODES
- CELL DC INTERNAL IMPEDANCE = 2.5 milliOhms
- DISCHARGE AT 1C, 2C, 4C, 6C, 8C AND 12C (C = 15.0 Amperes)
- ALL DISCHARGES AT ROOM AMBIENT TEMPERATURE
- NO ACTIVE COOLING

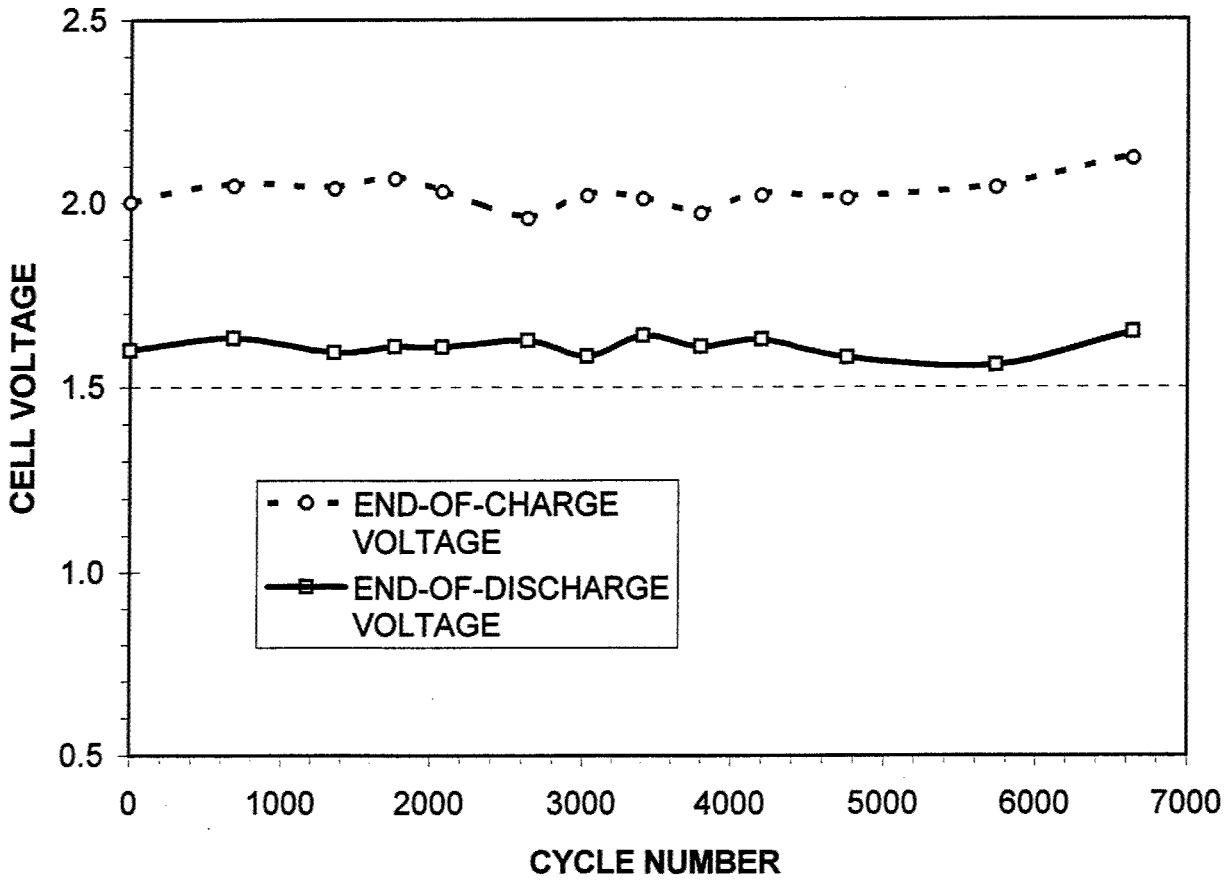

CELL VOLTAGE PERFORMANCE VERSUS CYCLE LIFE

- 14 Ah SEALED NICKEL-ZINC CELL DESIGN
- ROLL-BONDED COMPOSITE NICKEL AND ZINC ELECTRODES
- MOLDED POLYSULFONE CELL CASE AND COVER
- CELL DC INTERNAL IMPEDANCE = 3.0 milliOhms
- CYCLE REGIME: 27.5 MINUTE CHARGE / 17.5 MINUTE DISCHARGE
- CHARGE @ 3.38 A (0.25C RATE) / DISCHARGE @ 5.0 A (0.33C RATE)
- RECHARGE RATIO 1.02 - 1.04
- 10% DEPTH-OF-DISCHARGE BASED ON INITIAL CAPACITY
- CELL OPERATES BETWEEN 80% - 90% SOC BASED ON INITIAL CAPACITY
- CAPACITY MEASURED AT 450 CYCLE INTERVALS
- CELLS REACTIVATED AFTER 6500 CYCLES
- PERFORMANCE IMPROVEMENT AFTER REACTIVATION INDICATES CELL STACK DRY-OUT

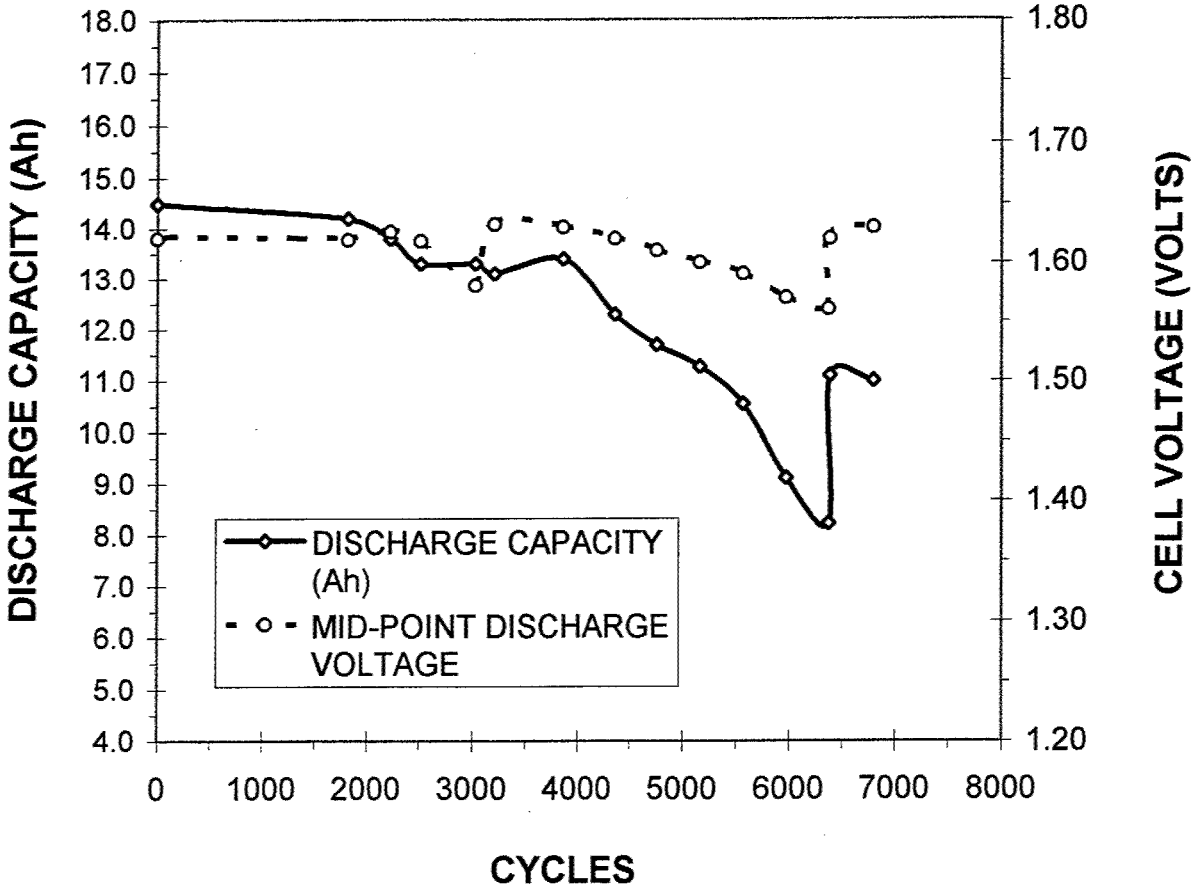

DISCHARGE CAPACITY AND VOLTAGE VERSUS CYCLE LIFE

- TEST ANOMALY OCCURRED AT CYCLE #3130 DUE TO SOFTWARE ERROR
- CELLS WERE BYPASSED ON OPEN-CIRCUIT DURING DISCHARGE PORTION OF CYCLE
- CELLS WERE CHARGED FOR 90 CYCLES WITHOUT DISCHARGE AMOUNTING TO A TOTAL CHARGE INPUT OF 157 Ah (1120% OVERCHARGE)
- CELLS DID NOT VENT DURING THIS EXTENSIVE OVERCHARGE
- PERFORMANCE BEGAN TO DEGRADE RAPIDLY AFTER THIS EVENT
- CELLS WERE REACTIVATED AT CYCLE #6390
- CAPACITY AND VOLTAGE PERFORMANCE IMMEDIATELY RECOVERED
- CELLS CURRENTLY HAVE 75-80% OF ORIGINAL CAPACITY AFTER 7000 CHARGE / DISCHARGE CYCLES

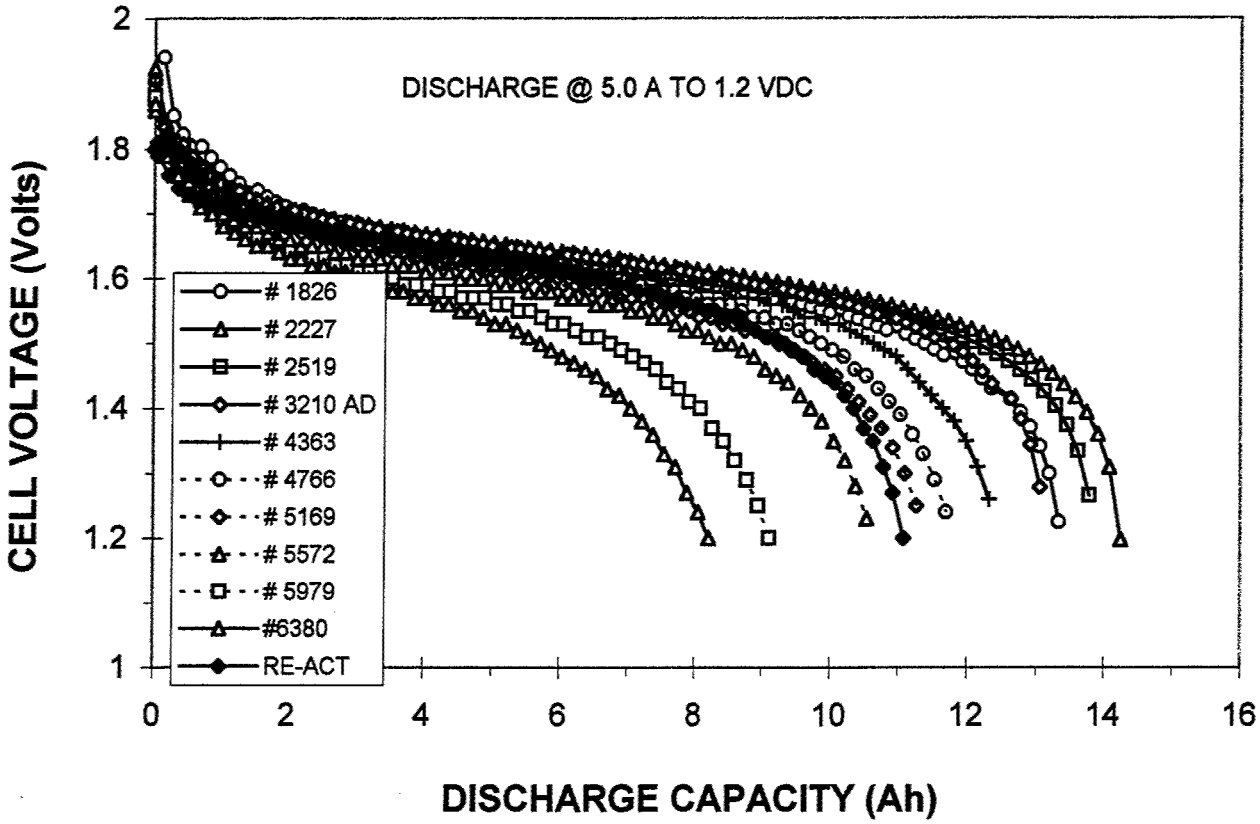

DISCHARGE CAPACITY AS A FUNCTION OF CYCLING

- EACH DISCHARGE IS AT 5.0A TO 1.2V
- PREVIOUS CHARGE FOR EACH CYCLE IS AT 3.8A
- INITIAL CYCLES CHARGE INPUT = 18.0 Ah (28% OVERCHARGE)
- CHARGE INPUT REDUCED TO 15.0 Ah AFTER 2300 CYCLES (8% OVERCHARGE)
- MPDV AT CYCLE #2227 = 1.626V / DECREASED TO 1.560V AT #6380
- INCREASED TO 1.632V AFTER REACTIVATION
- DISCHARGE CAPACITY AT CYCLE #2227 = 13.8 Ah
- DISCHARGE CAPACITY AT CYCLE #6380 = 8.2 Ah (60% OF NOMINAL)
- DISCHARGE CAPACITY INCREASED TO 11.1 Ah (80% OF NOMINAL) AFTER REACTIVATION

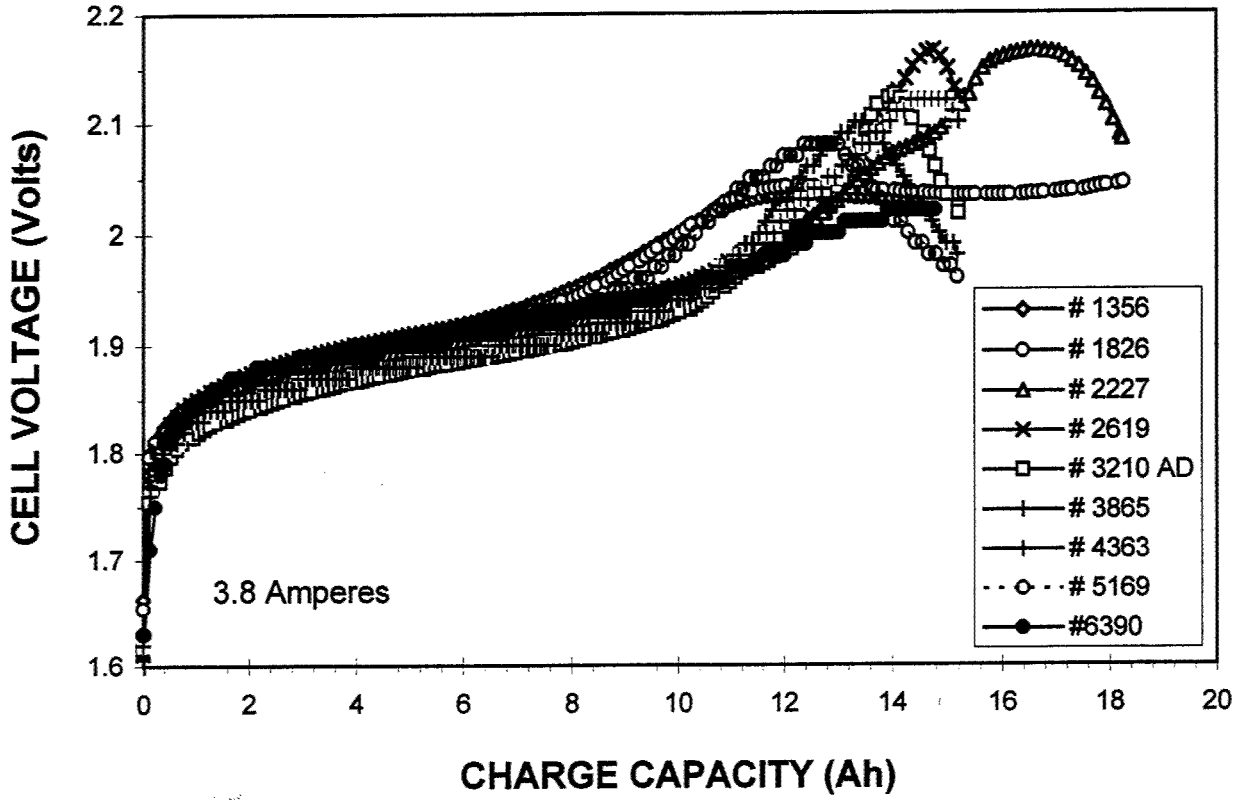

CHARGE VOLTAGE AS A FUNCTION OF CYCLE LIFE

- 3.8A CHARGE PRIOR TO THE FULL-DEPTH CAPACITY MEASUREMENT
- CONSTANT CURRENT / FIXED TIME / AMBIENT TEMPERATURE CHARGE
- OVERCHARGE WAS EXCESSIVE ON INITIAL CYCLES
- TIME WAS REDUCED TO REDUCE TOTAL CHARGE INPUT
- SHAPE OF THE CHARGE CURVE SHOWS A GENERAL TREND TOWARDS THE EARLIER ONSET OF OXYGEN EVOLUTION WITH CYCLING
- THE INFLECTION POINT OCCURS AT 12 Ah FOR CYCLE #2227 (86% SOC BASED ON CELL DISCHARGE CAPACITY)
- THE INFLECTION POINT OCCURS AT 9.5 Ah FOR CYCLE #5169 (116% SOC BASED ON ACTUAL CELL CAPACITY)
- FOR CYCLE #6390 (AFTER REACTIVATION) THE INFLECTION POINT IS AT 12.0 Ah (SAME Ah INPUT AS INITIAL, BUT NOW 109% OF CELL CAPACITY)
- ALSO, CYCLE #6390 SHOWS VERY LITTLE RISE IN VOLTAGE WITH THE ONSET OF OXYGEN EVOLUTION

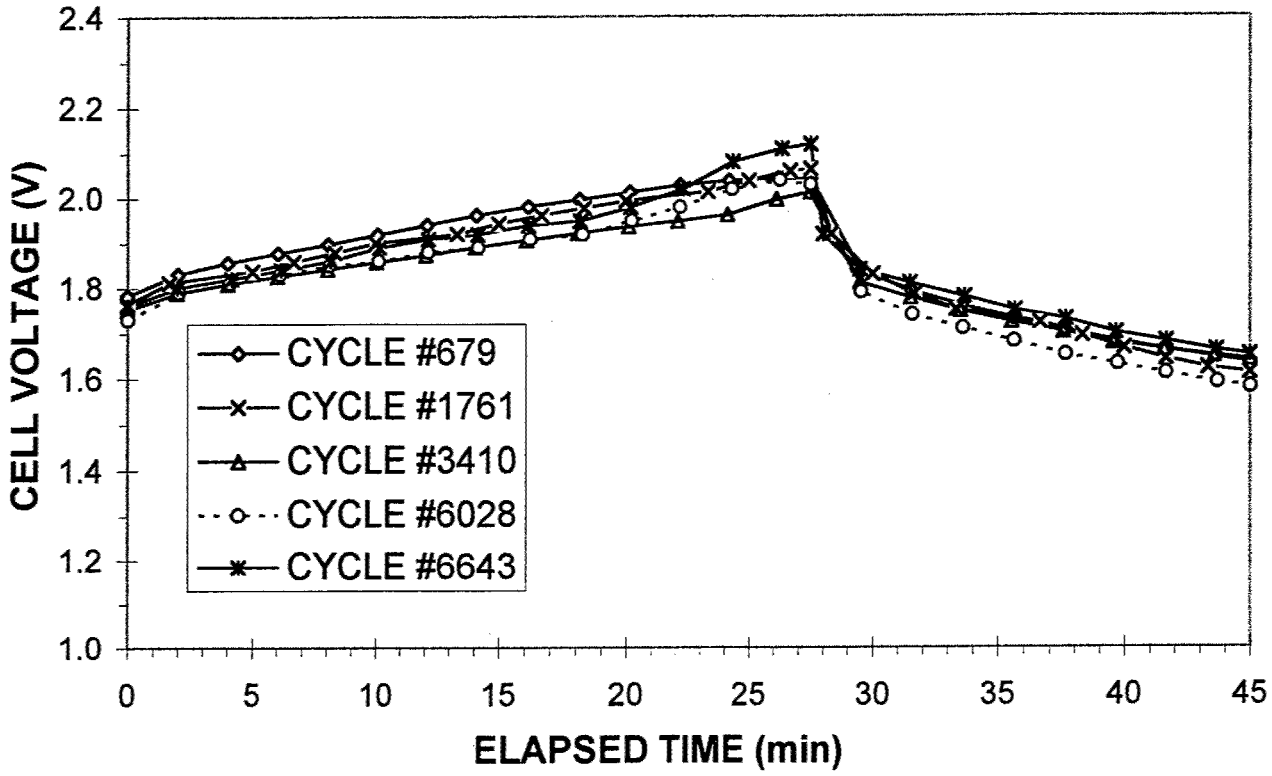

CELL VOLTAGE VERSUS TIME FOR MULTIPLE LEO CYCLES

- CYCLE REGIME: 27.5 MINUTE CHARGE / 17.5 MINUTE DISCHARGE
- CHARGE @ 3.38 A (0.25C RATE) / DISCHARGE @ 5.0 A (0.33C RATE)
- INITIAL RECHARGE RATIO = 1.04 / CURRENT RATIO = 1.02
- 10% DEPTH-OF-DISCHARGE BASED ON INITIAL CAPACITY
- DOD = 15% BASED ON CURRENT CAPACITY AFTER 7000 CYCLES
- CELL OPERATES BETWEEN 80% - 90% SOC BASED ON INITIAL CAPACITY
- CURRENTLY OPERATING BETWEEN 75% - 90% SOC
- MPDV AT #679 = 1.711V / DECREASED TO 1.660V AT CYCLE #6028
- MPDV INCREASED TO 1.724V AFTER REACTIVATION
- EODV AT #679 = 1.633V / DECREASED TO 1.580V AT CYCLE #6028
- EODV INCREASED TO 1.652V AFTER REACTIVATION

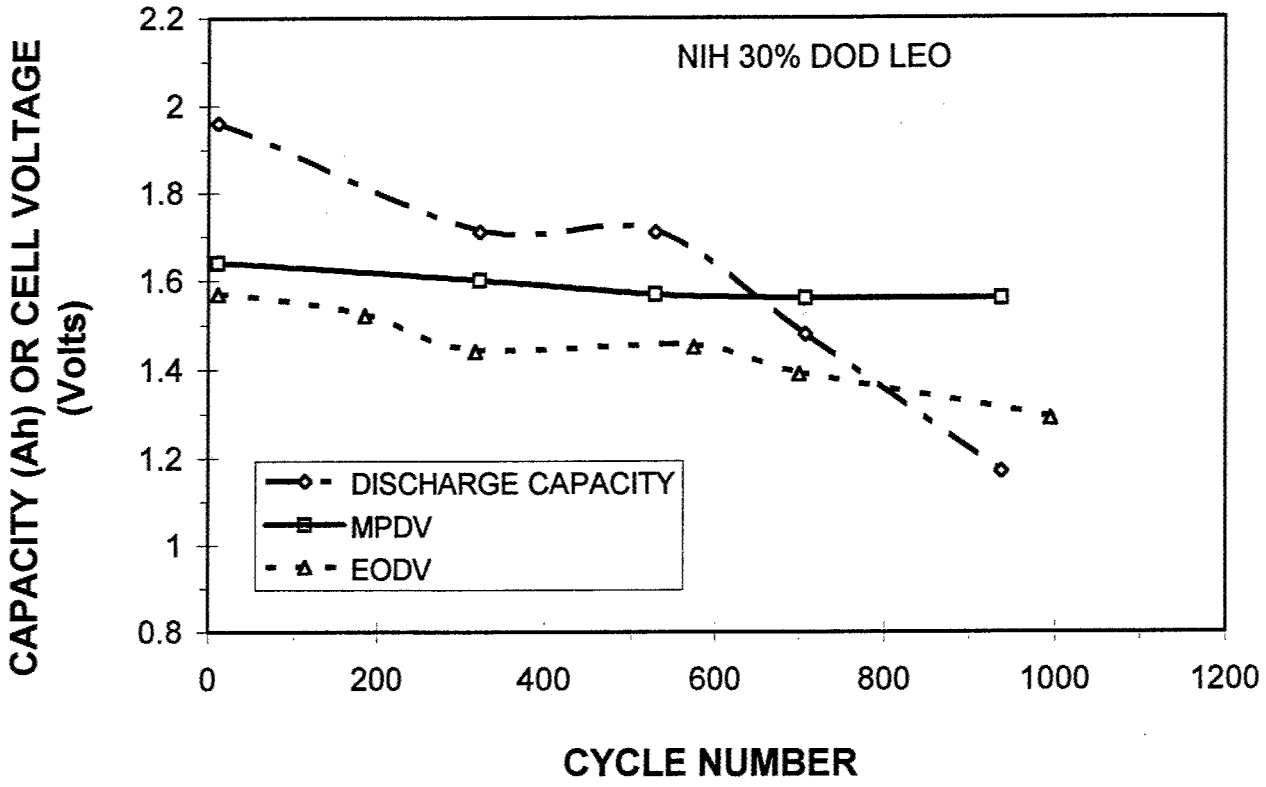

DISCHARGE CAPACITY AND VOLTAGE VERSUS CYCLE NUMBER

- 2 Ah SEALED NICKEL-ZINC CELL
- SPECIFIC ENERGY = 60 Watt-hours per kilogram
- ENERGY DENSITY = 73 Watt-hours per liter
- CELL DC INTERNAL IMPEDANCE = 30 milliOhms
- CYCLE REGIME = 27.5 minute CHARGE @ 1.3 A
  17.5 minute DISCHARGE @ 2.0 A
- 30% DEPTH-OF-DISCHARGE BASED ON INITIAL CAPACITY
- DISCHARGE CAPACITY MEASURED @ 1.0 A TO 1.2 Volts PER CELL
- MPDV = MID-POINT DISCHARGE VOLTAGE DURING ACC LEO CYCLE
- EODV = END-OF-DISCHARGE VOLTAGE AT TIME = 45 minutes DURING THE NORMAL ACCELERATED LEO CYCLE

CONCLUSIONS

- COMPOSITE NICKEL ELECTRODE PROVIDES EXCELLENT PERFORMANCE AT A REDUCED WEIGHT AND LOWER COST
- CALCIUM / ZINC ELECTRODE MINIMIZES SHAPE CHANGE
- UNOPTIMIZED CELL DESIGNS YIELD 60 Wh/kg
- NICKEL-ZINC DELIVERS 600 CYCLES AT 80% DOD
- LONG CYCLE LIFE OBTAINABLE AT LOW DOD
  - > 7000 CYCLES AT 10% DOD
  - > 1000 CYCLES AT 30% DOD
- HIGH RATE CAPABILITY / POWER DENSITY
- LONG-TERM FAILURE MECHANISM IS STACK DRY- OUT
- METAL CASE CELL DESIGN UNDER DEVELOPMENT
- FURTHER TESTING PLANNED AT 50% DOD
- FURTHER WORK PLANNED TO REDUCE ZINC TO NICKEL RATIO
- ANOMALOUS OVERCHARGE (1120%) GREATLY AFFECTED CELL PERFORMANCE BUT DID NOT INDUCE FAILURE AND WAS RECOVERABLE

Burp Charging Nickel Metal Hydride Cells

by

Eric Darcy
NASA-Johnson Space Center
Houston, Texas

and

Richard Pollard
University of Houston
Houston, Texas

Presented by Bob Bragg
to the
1996 NASA Aerospace Battery Workshop
Dec 4, 1996

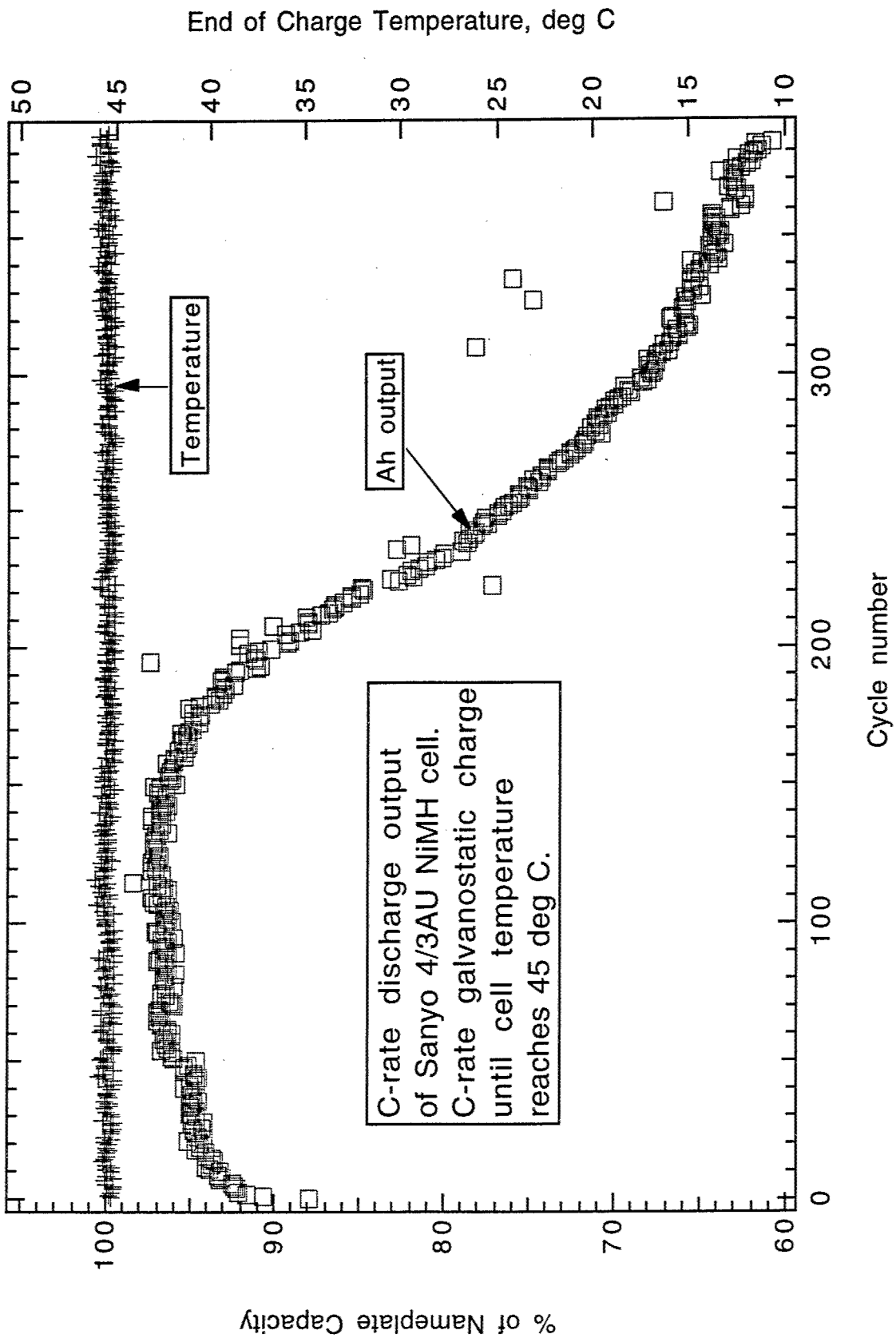
End of Charge Temperature, deg C
50
45
40
35
30
25
20
15
10
Temperature
Ah output
C-rate discharge output
of Sanyo 4/3AU NiMH cell.
C-rate galvanostatic charge
until cell temperature
reaches 45 deg C.
100
90
80
70
60
% of Nameplate Capacity
0
100
200
300
Cycle number

$\partial V/\partial t = -X$ or $\partial T/\partial t = Y$

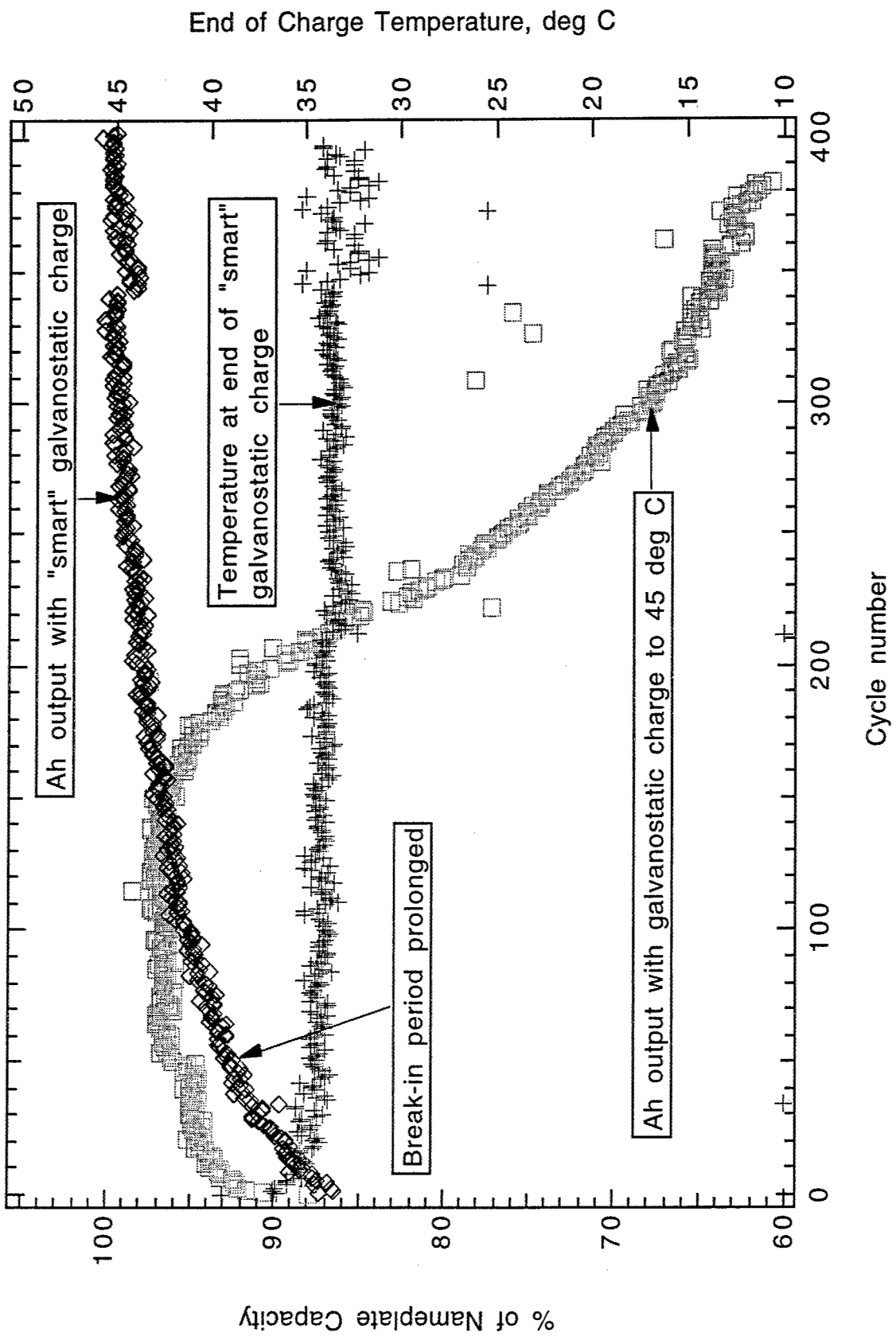

Some methods for improving cell peformance

- Smart termination
  - negative voltage slope, $\partial V/\partial t < 0$
  - rise in temperature, $\partial T/\partial t = Y$
- Charge current waveform changes
  - relaxation, $I = 0$
  - discharge burp, $I < 0$

Areas of improvement remaining

- can break-in period to maximum capacity be accelerated?
- can discharge capacity be increased without compromising cycle life?
- can charge heat be reduced further?

Modifying the current waveform shown effective with NiCd cells

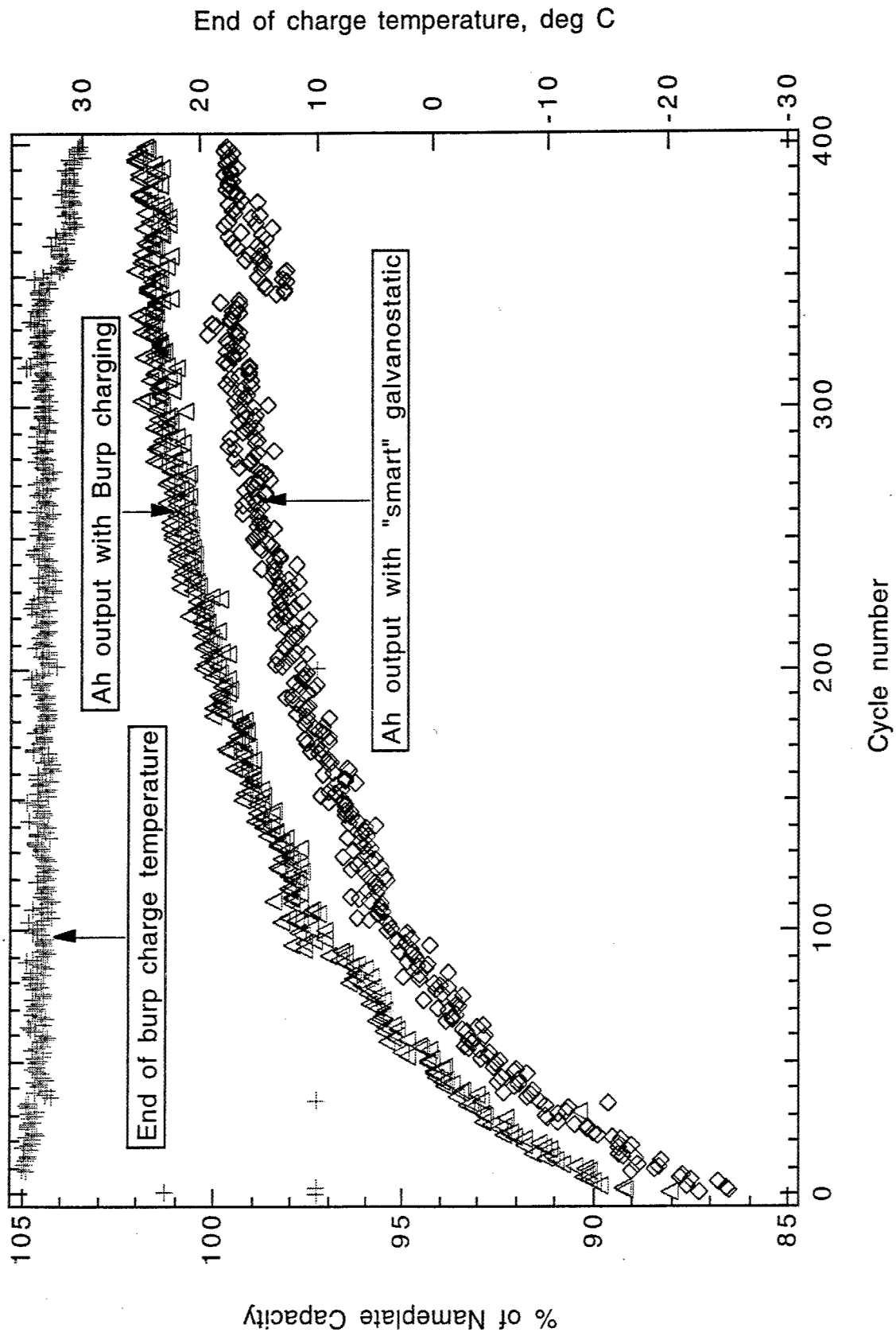
End of charge temperature, deg C
30
20
10
0
-10
-20
-30
Ah output with Burp charging
Ah output with "smart" galvanostatic
End of burp charge temperature
105
100
95
90
85
% of Nameplate Capacity
0
100
200
300
400
Cycle number

What is Burp Charging?

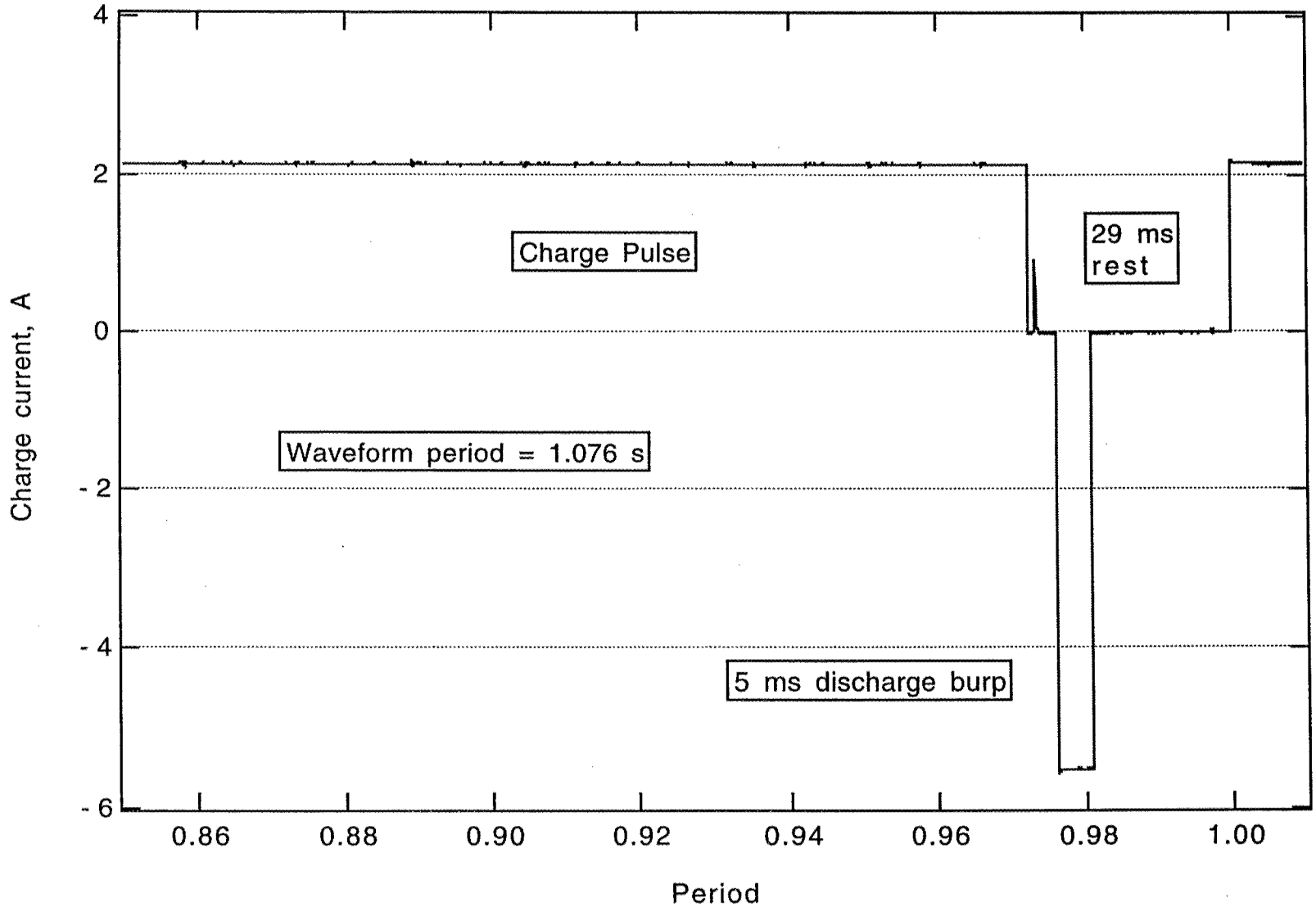

Darcy -12/4/96

Methods to study effects of relaxation and burp discharge

	Charge Waveform	Termination Method		
		$\partial T/\partial t = X$	$\partial V/\partial t = -Y$	$\partial^2 V/\partial t^2 = 0$
Galvanostatic	Constant current	X	X	
Pause	Constant current with short relaxation periods	X	X	X
Burp	Constant current with relaxation periods and discharge burps	X	X	X

Calorimetric Results

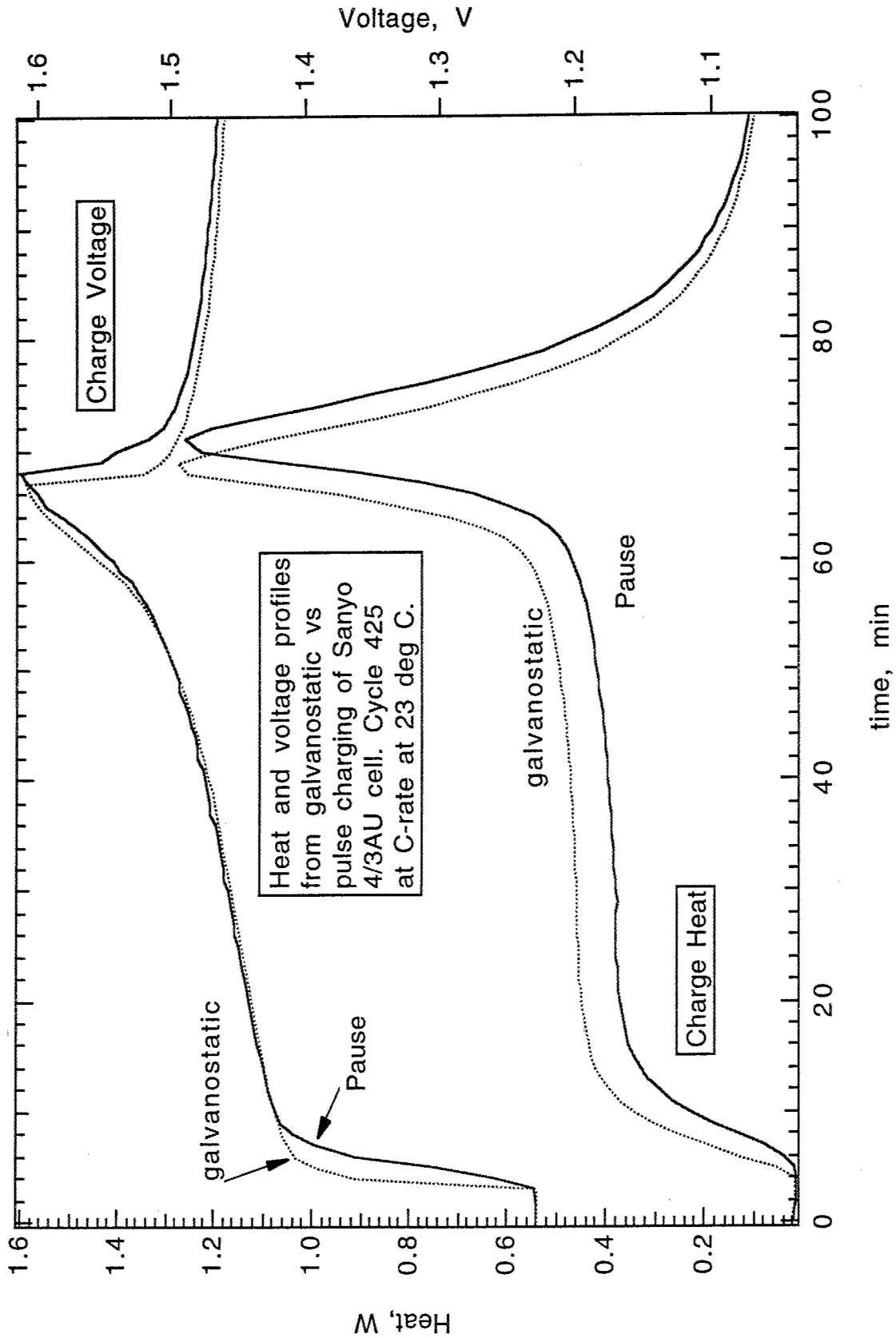

Darcy -12/4/96

Effects of interrupting the galvanostatic charge

- Lowers Ah input rate by 2.7%
- Total Ah input lowered by 4%, while Ah output unchanged
- Overvoltages essentially the same
- Charge heat rate, W, reduced throughout the charge *
- Total charge heat, J, lowered by 8% *
- Rise in cell temperature (T_{final} - T_{init}) not affected *

* evaluated at 425th cycle

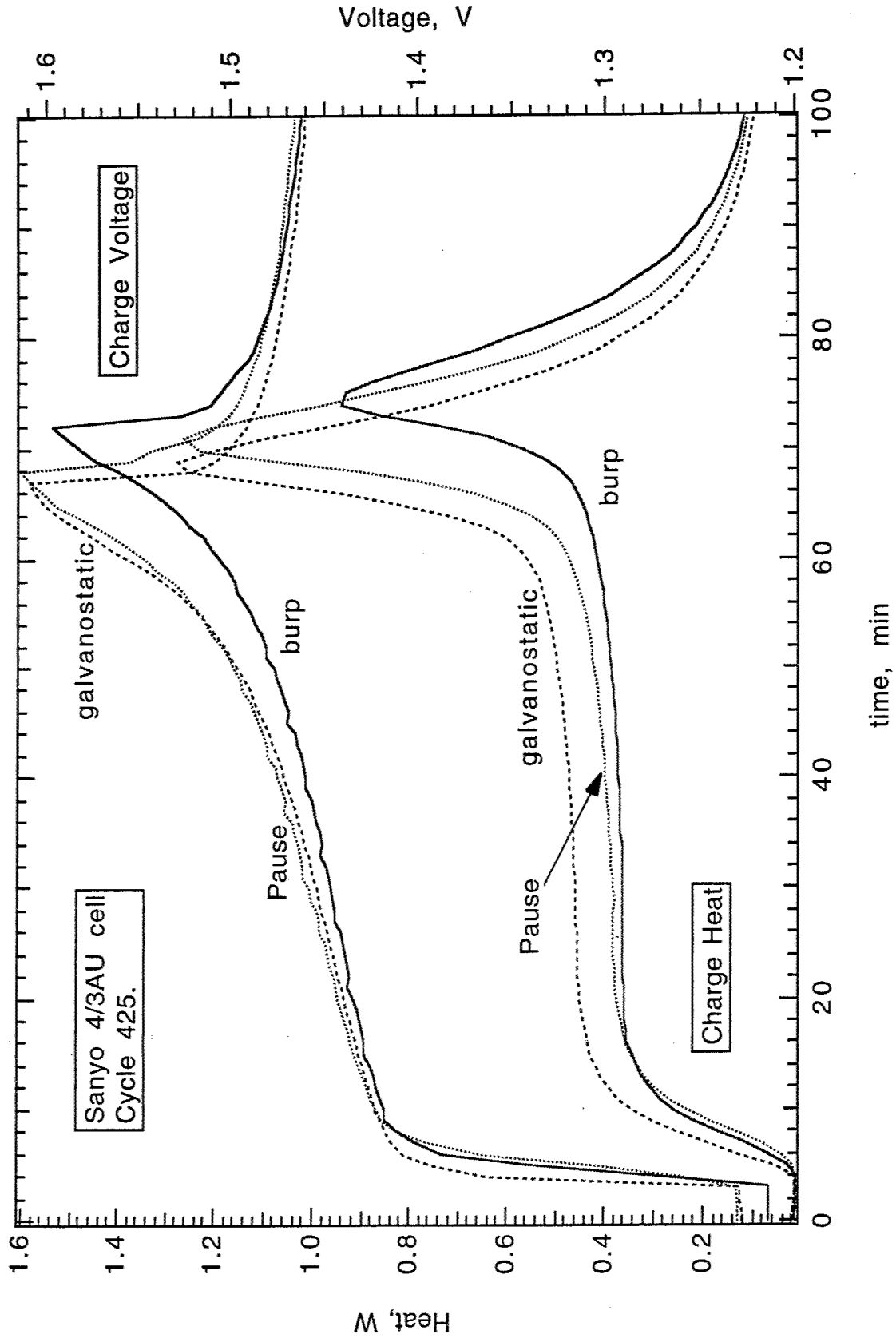
Voltage, V
1.6
1.5
1.4
1.3
1.2
Charge Voltage
galvanostatic
burp
Pause
galvanostatic
burp
Pause
Sanyo 4/3AU cell
Cycle 425.
Charge Heat
Heat, W
1.6
1.4
1.2
1.0
0.8
0.6
0.4
0.2
0
20
40
60
80
100
time, min

Darcy -12/4/96

Results

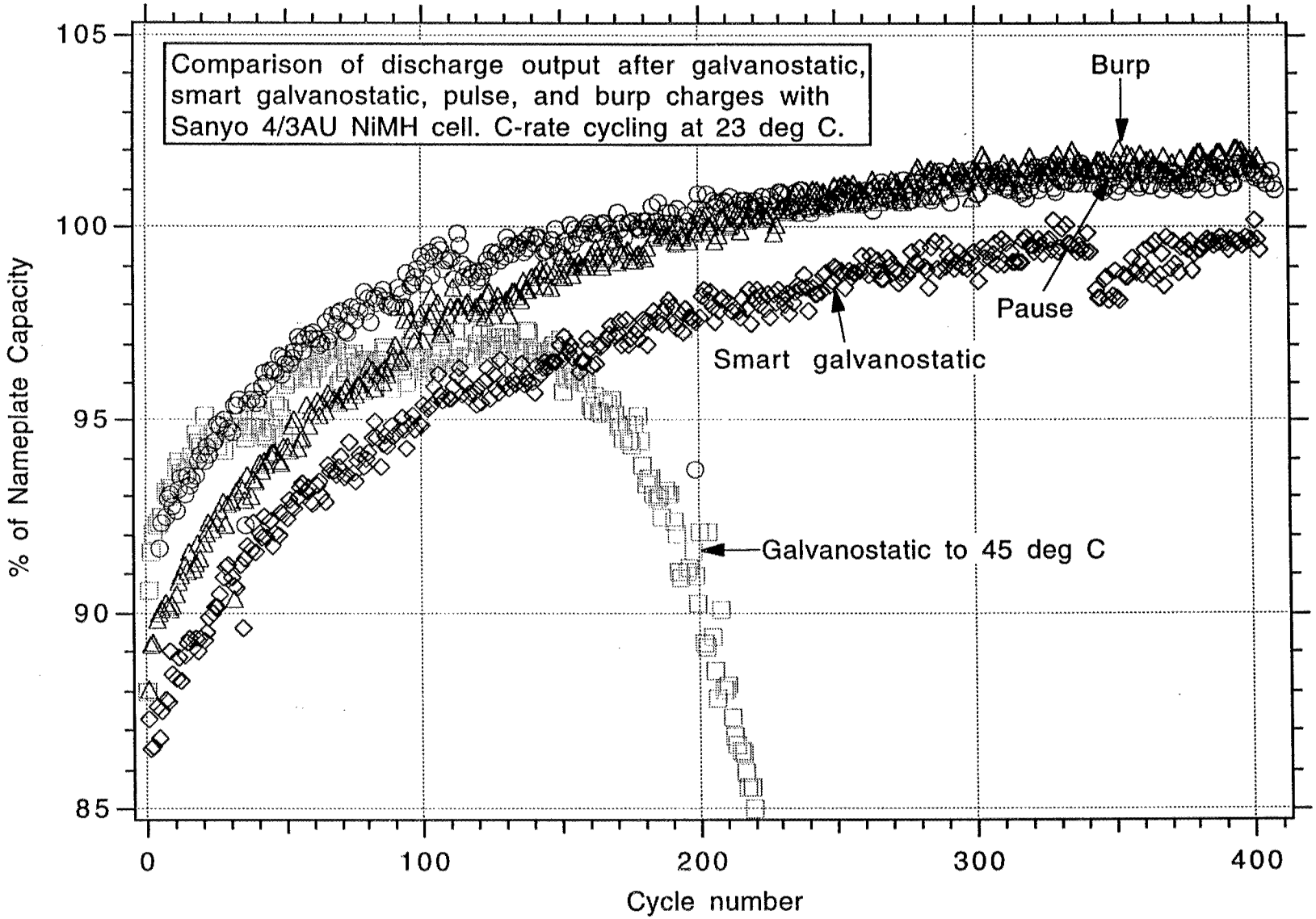

Darcy -12/4/96

Effects of adding 5 ms discharge burps

- Reduces Ah input rate by 1.1%
- Increases total Ah input and output by 5%
- Lowers charge heat rate (e.g., by an additional 6% at midcharge point) *
- Lowers rise in cell temperature by ~1 °C, despite larger Ah input *
- Reduces overvoltage throughout charge
  (e.g., by ~50 mV near end of charge) *

Do differences between burp vs pause charging depend on cycle number?

- break-in period shorter with pause

Is overvoltage reduction developed with cycle number?

* evaluated at 425th cycle

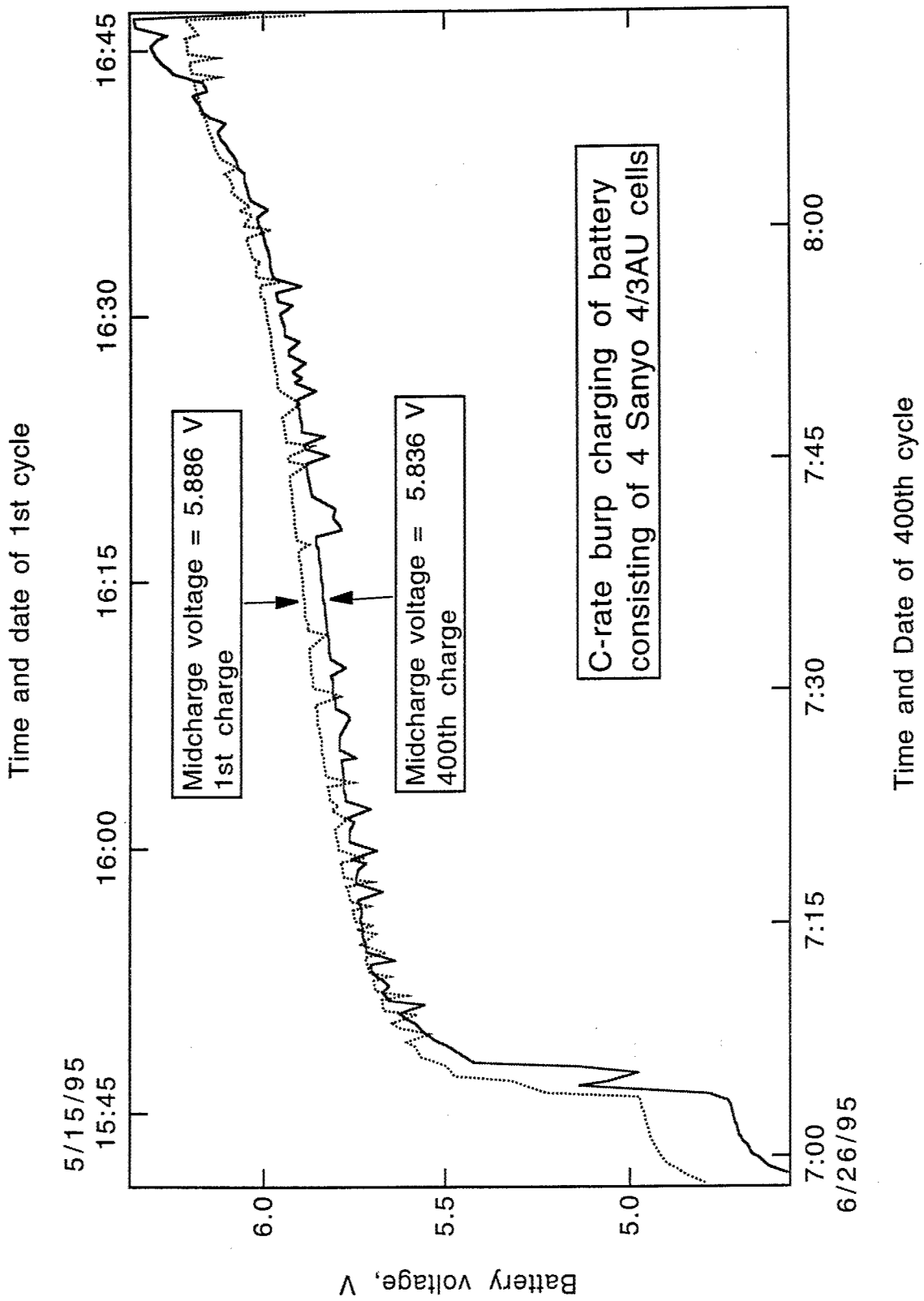
Battery voltage, V
6.0
5.5
5.0
Time and date of 1st cycle
5/15/95
15:45
16:00
16:15
16:30
16:45
Midcharge voltage = 5.886 V
1st charge
Midcharge voltage = 5.836 V
400th charge
C-rate burp charging of battery
consisting of 4 Sanyo 4/3AU cells
Time and Date of 400th cycle
7:00
6/26/95
7:15
7:30
7:45
8:00

Do other NiMH cell designs exhibit similar behavior?

Performance dependent on charge method

- cycle life
- rise in cell temperature
- overvoltage
- break-in period
- etc.

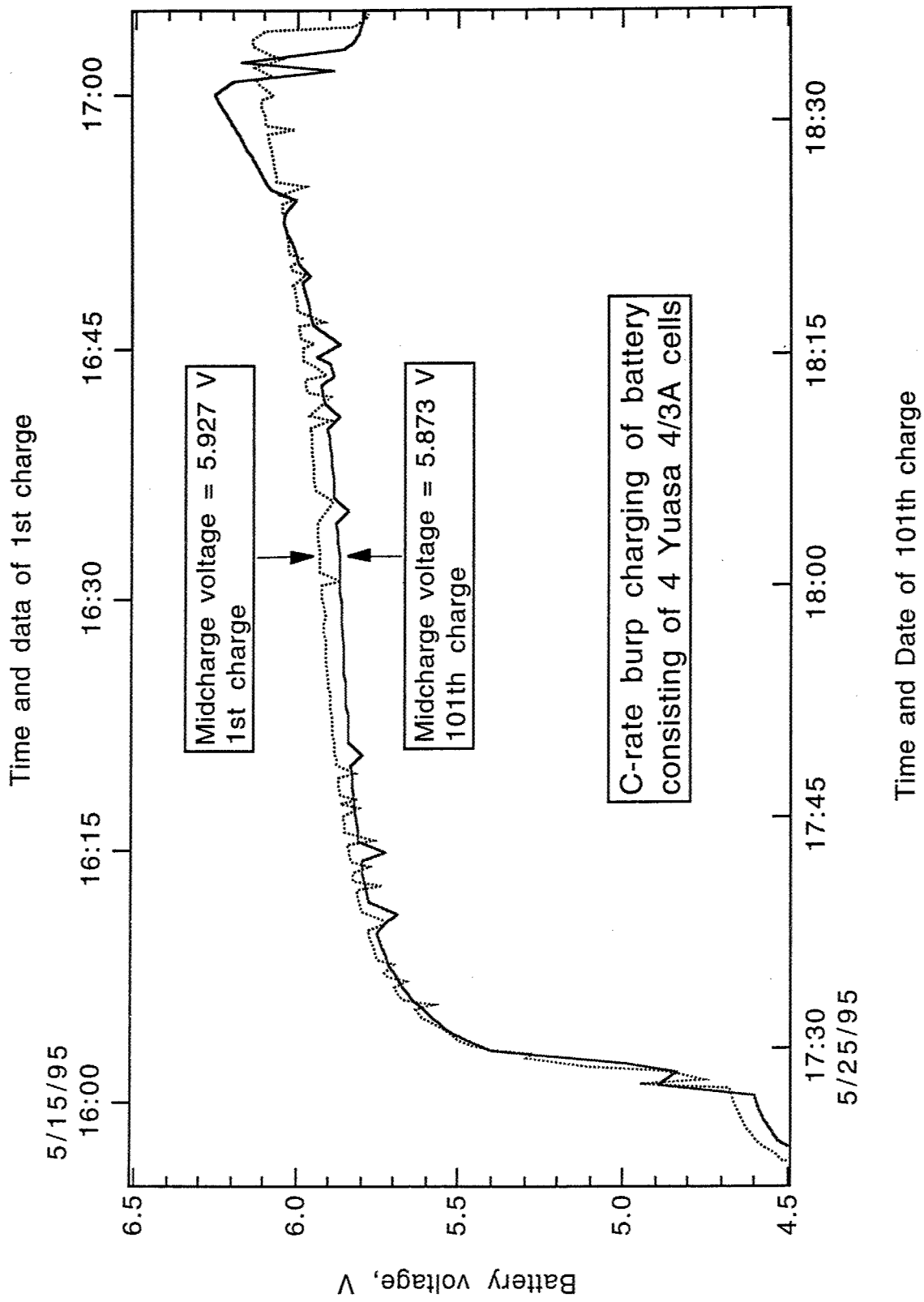
Battery voltage, V
6.5
6.0
5.5
5.0
4.5
Time and data of 1st charge
5/15/95
16:00
16:15
16:30
16:45
17:00
Midcharge voltage = 5.927 V
1st charge
Midcharge voltage = 5.873 V
101th charge
C-rate burp charging of battery
consisting of 4 Yuasa 4/3A cells
17:30
5/25/95
17:45
18:00
18:15
18:30
Time and Date of 101th charge

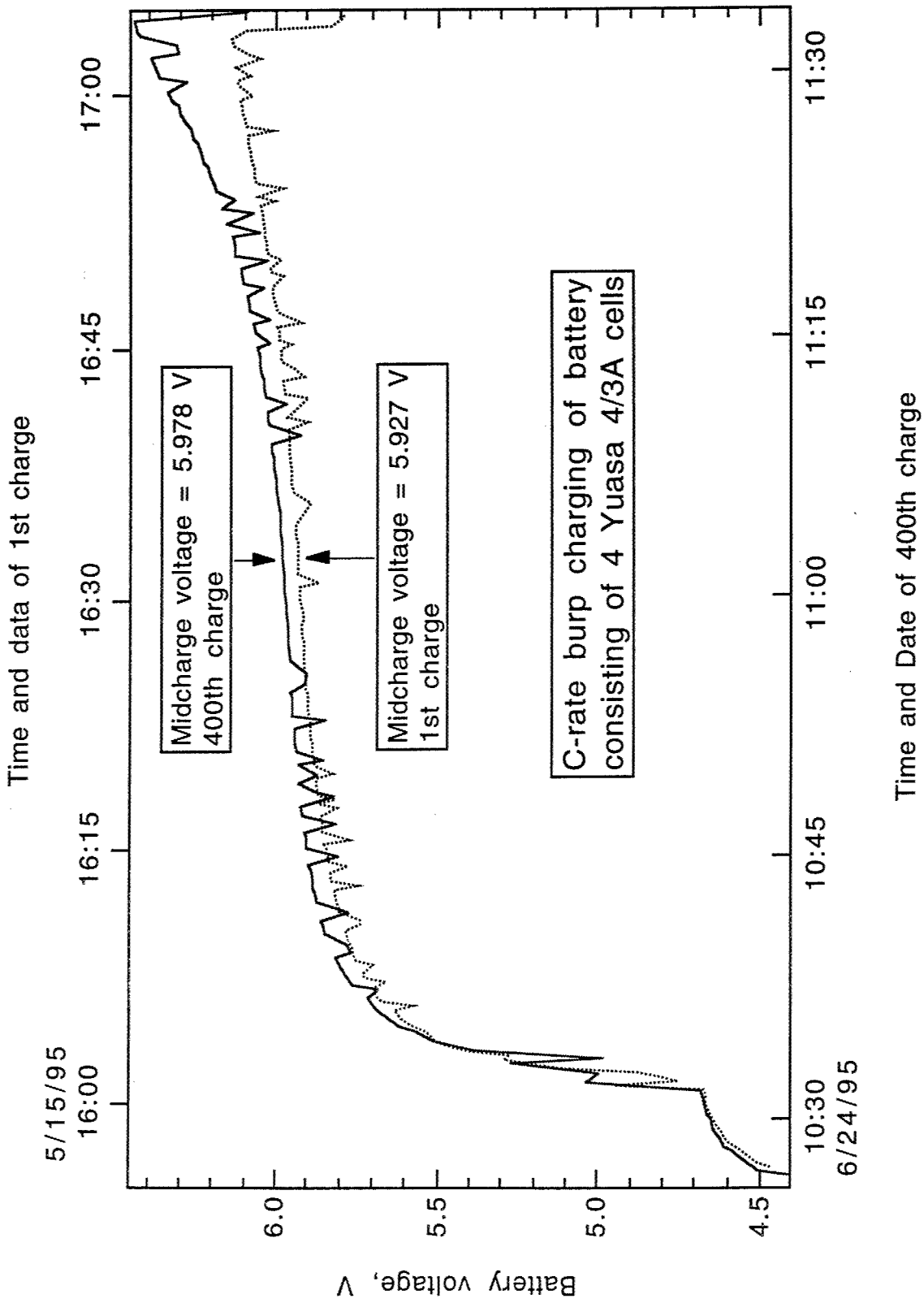
Time and data of 1st charge
5/15/95
16:00
16:15
16:30
16:45
17:00
Midcharge voltage = 5.978 V
400th charge
Midcharge voltage = 5.927 V
1st charge
C-rate burp charging of battery
consisting of 4 Yuasa 4/3A cells
10:30
6/24/95
10:45
11:00
11:15
11:30
Time and Date of 400th charge
6.0
5.5
5.0
4.5
Battery voltage, V

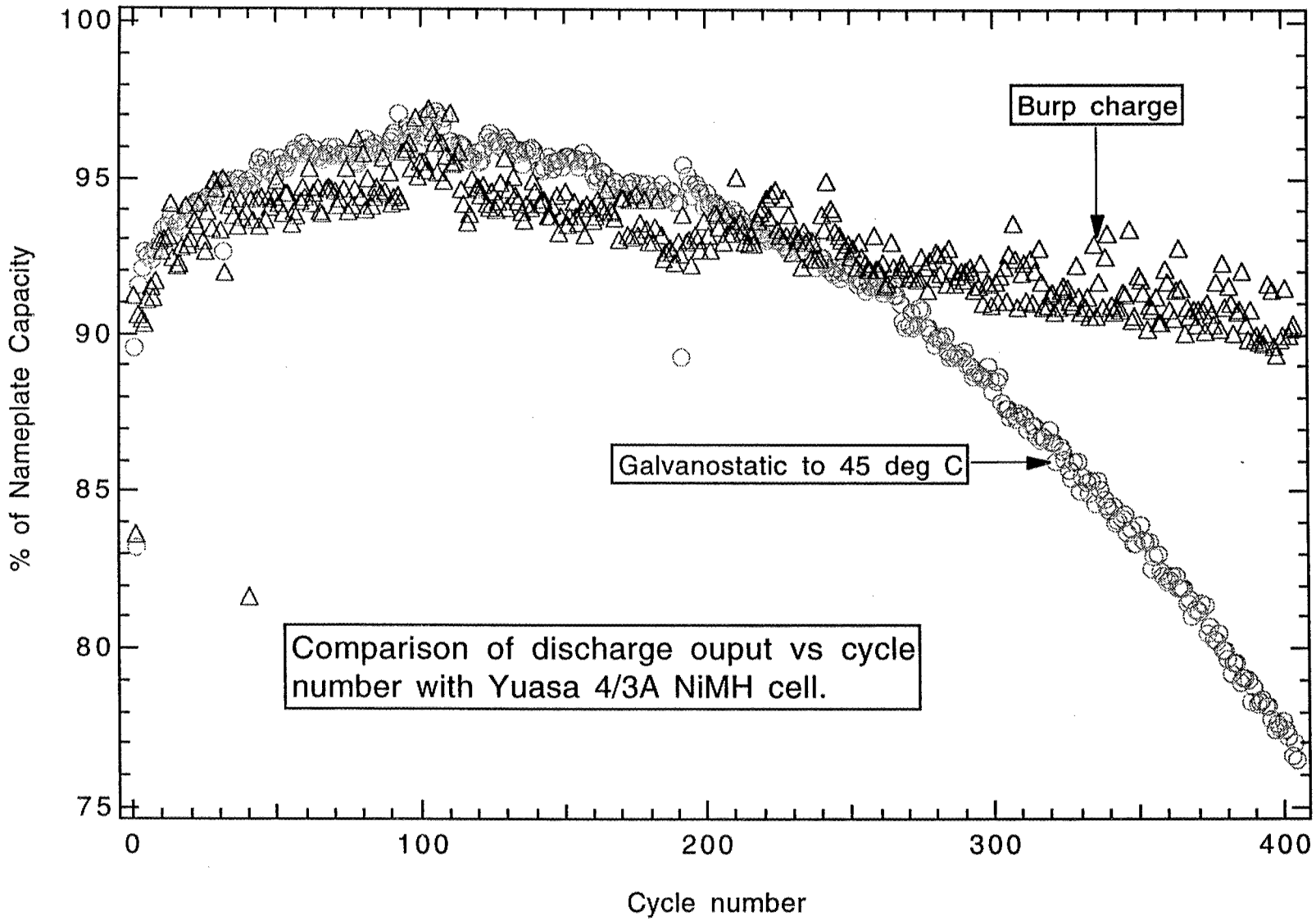
100
95
90
85
80
75
% of Nameplate Capacity
0
100
200
300
400
Cycle number
Burp charge
Galvanostatic to 45 deg C
Comparison of discharge ouput vs cycle number with Yuasa 4/3A NiMH cell.

Darcy -12/4/96

Conclusions

Addition of "smart" termination to simple galvanostatic charge *
- prolongs cycle life
- lengthens break-in period

Addition short relaxation periods to "smart" galvanostatic charge *
- lowers total Ah input without compromising discharge capacity
- shortens break-in period
- no effect on cycle life (to 400 cycles)

Adding very short discharge burps to the relaxation periods *
- increases total Ah input and output by same amount
- lengthens break-in period
- no effect on cycle life (to 400 cycles)

Burp charging improves cycle life with different NiMH cell designs

* Based on studies with 1 cell design

On-going Work

- Continue cycling comparison of galvanostatic, pause, and burp charging

- Compare morphology changes of electrodes
  - particle size distribution
  - porosity

- Compare burp heat effects with other cell designs

- Develop thermal model of NiMH cell based on obtained properties
  - heat capacity
  - thermoneutral potential
  - $\partial E/\partial T$

Why does burping lower overvoltage?

Possible reasons;

- dislodges O_2 from cathode pores, preventing local current density rise
- increases or maintains electrode porosity, aiding ion transport
- results in less O_2 evolution, due to lower charge heat

SEM analysis to date of electrodes after 400 cycles is unsupportive

- particle size differences are small in negative electrode
- porosity differences not yet discernable in positive electrode

In-situ analysis of positive electrode with 7x magnification fibroscope reveals

- bubbling activity increases with SOC during charging
- differences between charge techniques are not discernable

On-going Work

- Compare galvanostatic, pulse, and burp charging with 50x magnification
  - place electrode coil from NiMH cell into a transparent KOH beaker
  - place a reference electrode (Hg/HgO) between the electrodes
  - expose a portion of positive electrode for viewing
  - control waveform with an automated waveform generator
  - mark occurrance of pulses and burps with audio signal
  - record video and audio of bubbling activity on positive during charge

First Application - EMU Helmet Interchangeable Portable (EHIP) Lights

- Battery (P/N SED39130223)
  - 15 Sanyo NiMH cells arranged 3P-5S
  - strings connected in parallel to power 6W lights for 7 hours
  - bottom glide latches allow EVA replaceability from helmet
  - Raychem polyswitches limit current to 1.5 A/cell
  - weighs 1.04 kg

- Charger (P/N QC-1001)
  - charges 4 batteries in <4 hours independently and simultaneously
  - "burp" charge control achieved by 4 ICS-1702 chips
  - uses shuttle 28 $\pm$ 4 Vdc input
  - strings connected in series (18V) during charging
  - thermistors in battery provide temperature input to charger
  - velcro mounted to mid-deck area
  - weighs 1.39 kg

- Charger has passed all certification tests

- New lights, battery, and charger first flight is STS-82 in Feb 97

Low Temperature Synthesis, Chemical and Electrochemical Characterization of $LiNi_xCo_{1-x}O_2$ ($0 < x < 1$) Cathode Materials for Rechargeable Lithium Ion Batteries

K.S. Nanjundaswamy, D. Standlee, C.O. Kelly and, *R. V. Whiteley Jr.
Advanced Electrochemical Systems Group, Technologies Division
Eagle-Picher Industries Inc., P.O. Box 47, Joplin, MO 64802
** Department of Chemistry, Pacific University, 2043 College Way, Forest Grove, OR 97116*
Tel: (417) 623-8000, *Fax* : 417-623-0850, *E-mail*: EPLion@AOL.COM

Abstract

A new method of synthesis for the solid solution cathode materials $LiNi_xCo_{1-x}O_2$ ($0 < x < 1$) involving enhanced reactions at temperatures ≤700°C, between metal oxy-hydroxide precursors MOOH (M = Ni, Co) and Li-salts (Li_2CO_3, LiOH, and $LiNO_3$) has been investigated. The effects of synthesis conditions and sources of Li, on phase purity, microstructure, and theoretical electrochemical capacity (total M^{3+} content) are characterized by powder X-ray diffraction analysis, scanning electron microscopy, chemical analysis and room temperature magnetic susceptibility. An attempt has been made to correlate the electrochemical properties with the synthesis conditions and microstructure.

Introduction

The high voltage (4 V) metal oxide cathode materials $LiMO_2$ (M = Co, Ni) and $Li_{1+x}[Mn_2]O_4$ for lithium rechargeable batteries are very well investigated in literature[1-4]. Several other new high voltage cathode materials based on polyanion framework, spinel and olivine related structures have been reported recently[5-7]. However, only $LiCoO_2$ has so far proven to be successful commercially, as cathode material for Li-Ion batteries that deliver long cycle life. $LiMO_2$ (M = Co, Ni) crystallize in (2D) α-$NaFeO_2$ layered structure[8] at temperatures > 400°C, while the low temperature polymorphs have spinel-like (3D) structures. The ordering of Li and transition metal atoms in the structure depends on thermal history. The electrochemical properties such as voltage, capacity and cyclability are very sensitive to the structural disorder. $LiMn_2O_4$ has a spinel (3D) structure and forms a range of defect spinel compositions that show variable stoichiometry, Mn oxidation state and total oxygen content in the phase diagram[9] $LiMn_2O_4$ - $Li_2Mn_4O_9$ - $Li_4Mn_5O_{12}$, making the processing very difficult[10]. In fact a 50% substitution of Mn atom in $LiMn_2O_4$ by Cr results in α-$NaFeO_2$ type layered structure in a narrow temperature range of synthesis[11]. Although $LiNiO_2$ has marginally higher capacity compared to $LiCoO_2$, the difficulty in processing of $LiNiO_2$ stems form the fact that Ni^{3+} requires higher oxygen partial pressure. In addition, the increased tetrahedral site stability of nickel intermediates favor the occupation of Li-sites by nickel in α-$NaFeO_2$ structure, thereby reducing the capacity and the Li^+-ion mobility in $LiNiO_2$[12]. Also, $LiNiO_2$ suffers from increased safety concerns due to relatively unstable charged state at higher operating temperatures.

The solid solutions $LiNi_xCo_{1-x}O_2$ ($0 < x < 1$) achieve a compromise between the complimentary properties of the end members $LiCoO_2$ and $LiNiO_2$. These soild solutions have strong potential to replace the commercialized $LiCoO_2$ because of their relatively low cost, low volume change[13, 14] during charge/ discharge, as well as higher capacity. The composition with $x = 0.5$, has the advantage of slightly lower, sloping voltage plateau compared to other compositions, which is better from electrolyte stability and overcharge protection[15]. However optimizing the synthesis conditions for such solid solutions by commonly used ceramic techniques, that uses Ni(II)O or Ni(II)-salts as the nickel source is very difficult because of the low reactivity of the Ni(II)O and the unstable Ni^{3+} that requires higher oxygen pressure at elevated tempeartures. A prolonged solid state reaction at high temperatures not only reduces Ni^{3+} to Ni^{2+}, but also leads to substantial Li loss resulting in phase

separations of $LiCoO_2$ and $LiNiO_2$ and impurity phases such as $Li_{1-y}Ni_yO$, Co_3O_4, etc.,. We report here the details of a low temperature method[16] that makes use of very reactive metal oxy-hydroxide precursors MOOH (M= Co, Ni), where in the metal atoms are already in trivalent state. Further, the metal atoms in the precursor are mixed homogeneously at the molecular level, helping to reduce the diffusion barriers for the solid state reaction to occur.

Experimental

The metal oxy-hydroxides precursors MOOH where M is a combination of Co and Ni, were prepared by reacting appropriate amounts of metal nitrates with alkaline NaOCl solution, following the procedure described by Nakagawa et al[17]. The metal oxy-hydroxides were dehydrated in vacuum and further calcined with Li-salts (Li_2CO_3, LiOH, and $LiNO_3$) at elevated temperatures to get the final compositions $LiNi_xCo_{1-x}O_2$ ($0 \le x \le 1$). The reactions occuring at various stages are represented as follows:

$$M(NO_3)_2 \cdot x H_2O \xrightarrow{\text{NaOCl solution}} MOOH \cdot x H_2O \quad [1]$$

$$MOOH \cdot x H_2O \xrightarrow{\text{Vacuum dehydration}} MOOH + x H_2O \quad [2]$$

$$Li_2CO_3 + 2\,MOOH \xrightarrow{\text{Calcination } >500°C} 2\,LiMO_2 + CO_2 + H_2O \quad [3].$$

Solid solution compositions (referred to as "samples A", here afterwards) $LiNi_xCo_{1-x}O_2$ for x = 0.15, 0.40, 0.60, and 0.80 were prepared by direct solid-state reactions in air, starting from stoichiometric amounts of $Ni_xCo_{1-x}OOH$ and Li_2CO_3 at 500, 700, 900 and 1100°C, with annealing durations of 6, 10 and 14 hours. The samples were cooled to room temperature in about 30 minutes.

Compositions (referred to as "samples B", here afterwards) $LiNi_xCo_{1-x}O_2$ for x = 0.3 were prepared from calcination of oxy-hydroxide precursor $Ni_{0.3}Co_{0.7}OOH$, in air at 700°C with three different sources of lithium, Li_2CO_3, LiOH, and $LiNO_3$, employing quenching or slow cooling conditions. Quenching from 700°C to room temperature was done in 5 minutes, while slow cooling to room temperature was done in about 61 hours.

The cobalt and nickel contents were analyzed by atomic absorption spectroscopy and Li content was determined by flame photometry. All samples were characterized for total M^{3+} content ($M^{3+} = Co^{3+} + Ni^{3+}$) by iodometric titration. X-ray powder diffraction (XRD) and SEM were used for structural and microstructural characterization.

Results and Discussion

X-ray phase analysis was used to determine the optimum temperature range for ("samples A") solid solutions $LiNi_xCo_{1-x}O_2$ for x = 0.15, 0.40, 0.60, and 0.80, prepared by direct solid-state reaction in air, from $Ni_xCo_{1-x}OOH$ and Li_2CO_3. A reaction temperature of <500°C in air was too low and for the 'x' values mentioned, XRD showed broad peaks due to unidentified phases and Li_2CO_3. Reactions at temperature 1100°C resulted in range of impurity phases (Co_3O_4, $Li_{1-y}Ni_yO$) and phase separation of blue colored sample indicating Co^{2+} diffusion into the alumina / silicate matrix of the container. Also the chemical analysis showed huge loss of Li (Li contents were as low as 50-60% of the theoretical value, and total transition metal contents were >105% of the theoretical value) at 1100°C. The temperature range between 700-900°C showed much better results in terms of phase purity and chemical analysis. Small amounts (~2-3%)of $Li_{1-y}Ni_yO$ was the only impurity present in the temperature range 700-900°C. The amount of Li present in the samples were close to theoretical values (98-102%) for samples prepared at 700°C, while Li content was reduced to 95-98%, for samples prepared at 900°C.

Figures 1-4 give the variations of unit cell parameters *a*, *c*, *c/a* and $I_{d(003)}/I_{d\,(104)}$ intensity ratios with amount of Ni present in the compositions, respectively for the "samples A". The solid line is drawn in figures 1 and 2, joining the squares that represent the unit cell constants of the end members with the high temperature layered α-$NaFeO_2$ structure[8]. The unit cell parameters show relatively larger deviations from this solid line for all the "samples A", that are prepared at ≥900°C. "Samples A", that are prepared ≤700°C show lesser deviations from the the solid line. These variations from the high temperature polymorph could be attributed to the slight deviation from the nominal compositions, relatively broad [hkl] lines due to short thermal annealing, and possible disorder of Li/ M atoms

in the structures, specially in case of low temperature preparations. It is to be noted that low temperature polymorphs (that have structure more like cubic spinels) of $LiCoO_2$ show a lower *c* and higher *a* values, as compared to the high temperature polymorphs [8,18].

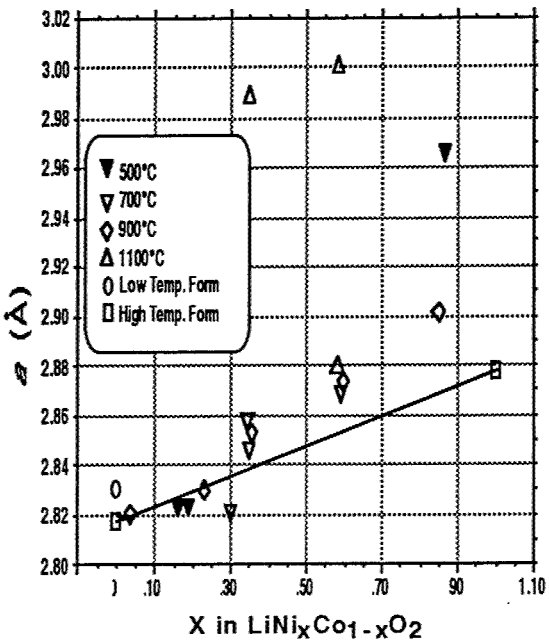

Figure 1. Variation of cell parameter *a* with x for $LiNi_xCo_{1-x}O_2$ compositions.

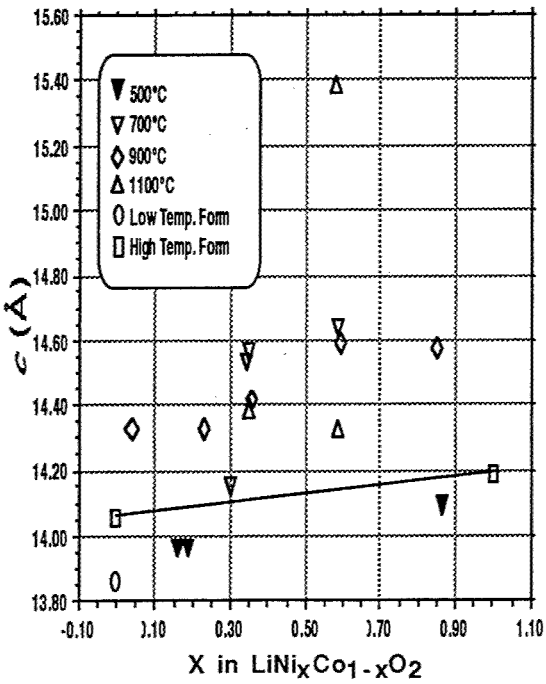

Figure 2. Variation of cell parameter *c* with x for $LiNi_xCo_{1-x}O_2$ compositions.

We have compared the *c /a* ratios in Fig. 3, for all the "samples A" with the literature values reported for high temperature polymorphs[18]. From the plot it is clear that the higher Ni fraction (with $x \geq 0.6$) and higher temperature preparations (1100°C) show larger deviations for the same reasons mentioned above. The *c /a* ratios for these samples do not follow a definite trend since the structure can vary considerably with temperature of preparation. In fact low temperature polymorphs can have Co^{3+} (t_2^6) in low spin state and these are smaller than the Ni^{3+}($t_2^6e^1$)ion. The *c /a* ratio are close to a value of 4.90 for temperatures ≤500°C which is in agreement with the ideal cubic close packed lattice.

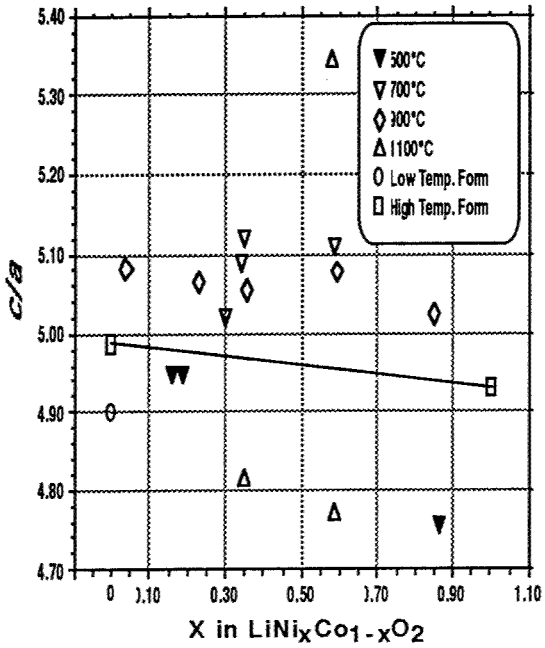

Figure 3. Variation of *c /a* with x for $LiNi_xCo_{1-x}O_2$ compositions.

The intensity ratios of [003] and [104] reflection lines give an indication regarding the structural arrangement of heavy transition metal atom in the structure. This hypothesis is based on the fact that cobalt and nickel are significantly heavier and therefore considerably stronger scatterer of X-rays. Of the "samples A" in Fig. 4, only the ones prepared at 500°C show larger decrease of intensity ratios with Ni fraction, while the intermediate temperature regions show a smaller trend indicating that the structural disorder is more for low temperature preparations.

From the above results, it is clear that the 700°C in air, is the optimum temperature of preparation for the high temperature polymorph of the solid solutions that are richer

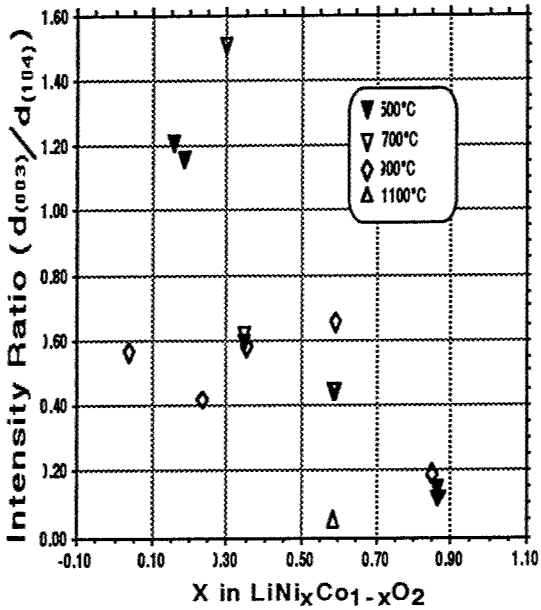

Figure 4. Variation of $I_{d(003)}/I_{d(104)}$ with x and temperature for $LiNi_xCo_{1-x}O_2$.

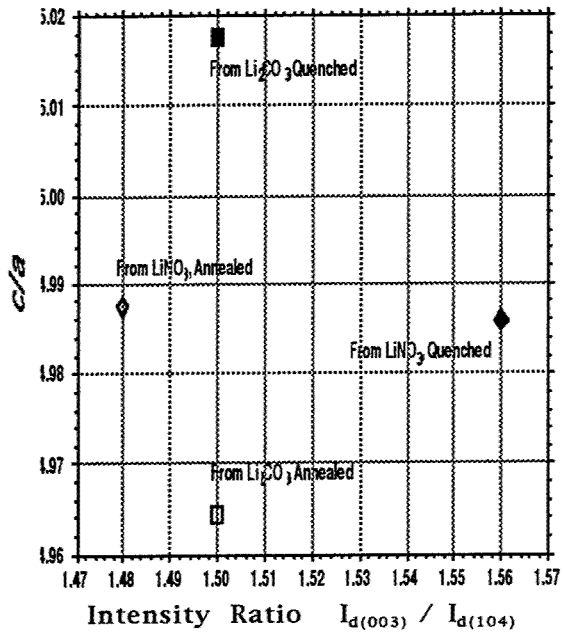

Figure 5. Effect of Li source on *c /a* and $I_{d(003)}/I_{d(104)}$ for $LiNi_{0.3}Co_{0.7}O_2$

in cobalt from precursor method. To determine the effect of Li source on the synthetic conditions, we prepared a set of "samples B" with composition $LiNi_{0.3}Co_{0.7}O_2$ starting from carbonate, nitrate and hydroxide salts of Li. Calcining was done at 700°C for 6 hours, with variations in annealing and quenching conditions.

The "samples B" that are prepared from LiOH showed phase separations to $LiNiO_2$ and $LiCoO_2$, while the ones from nitrate and carbonate sources were single phase. The XRD lines were more sharp for the samples made from $LiNO_3$ with the (006), (102) and (108), (110) lines well separated indicating better crystallization. Figure 5 shows the variations of c / a and the $I_{d(003)}/I_{d(104)}$ for six samples of $LiNi_{0.3}Co_{0.7}O_2$. The *c/a* ratio is close to the one expected for high temperature polymorph for sample prepared from $LiNO_3$ source, while the sample prepared from carbonate source showed slight deviation. Theoretical capacities (total M^{3+} content) estimated from iodometric titration are given in Figure 6, and the samples prepared from $LiNO_3$ source showed higher theoretical capacities. The lower capacities in all these cases are probably due to the small amounts of impurity phases (~2%) present $Li_yNi_{1-y}O$. The room temperature susceptibility values indicate the presence of more Ni^{2+} in samples from carbonate and hydroxide sources of Li, indicating that the partial oxygen pressure to

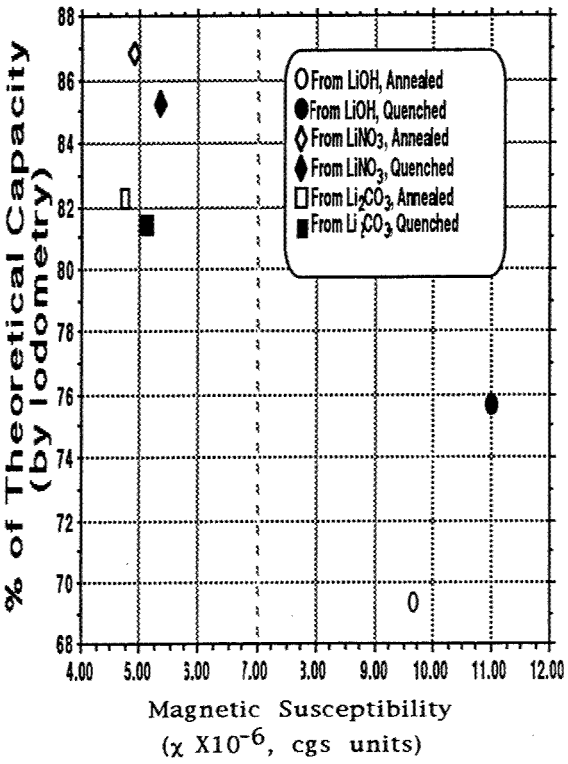

Figure 6. Effect of Li source on theoretical capacity and magneticsuceptibilty for $LiNi_{0.3}Co_{0.7}O_2$

keep all the nickel in Ni^{3+} state is not high enough.

The scanning electron micrographs were taken for "samples B" that are prepared from the carbonate and nitrate salts of lithium. The particle sizes showed a mean distribution around 1 μm.

Soft chemistry methods employ low temperatures and involve decomposition reactions that evolve gases, resulting in fine particles. If, controlled properly they could give uniform particle size distributions for the end product. Fine particles of the cathode materials are important for rate capability, and homogeneous distribution of particle size contributes to better density. On the other hand, larger cathode particles reduce the interface contact with electrolyte solution, resulting in increased cycle life for the battery. There are different approaches to increase the particle sizes such as prolonged annealing, flux induced crystallization and anion substitution. The precursor method reported here could be tuned to get the desired microstructure for the cathode material and such an effort is underway. Also, measurements of cell characteristics for cathode samples $LiNi_{0.3}Co_{0.7}O_2$ made from $LiNO_3$ source is under progress, against carbon.

Conclusions

We have shown that the oxy-hydroxide precursor MOOH that has the transition metals (M= Co, Ni) homogeneously mixed at the molecular level, in M^{+3} state could be effectively used for fine particles synthesis of solid solution $LiNi_xCo_{1-x}O_2$ ($0 \leq x \leq 1$) in air. The method is cheap, fast and better compared to the conventional ceramic route that is constrained by solid state diffusion barrier. Further, a temperature of 700°C, 6-14 hours of annealing time, in ambient oxygen pressure and $LiNO_3$ as lithium source, are better for cobalt-rich compositions, while nickel-rich compositions need a higher partial pressure of oxygen. The method could be conveniently modified to get desirable microstructural changes and suitable anion substitution for fine tuning the elctrochemical properties. We also have shown that iodometric titration and XRD phase analysis could be effectively used to pre-characterize the electrochemical properties.

Acknowledgments

The contributions from Ms. T.M. Nguyen and Ms. Ruth K Long of Pacific University and Dr. Mike Shaw and Mr. Mark Dudley of the Specialty Materials Division of Eagle-Picher, Miami, OK are gratefully acknowledged.

References

1. J.B. Goodenough, M.M. Thackeray, W.I.F. David, and P.G. Bruce, *Rev. Chim. Miner.* 21, 435 (1984).
2. K. Mizushima, P.C. Jones, P.J. Wiseman, and J.B. Goodenough, *Mat. Res. Bull.*, 15, 783 (1980).
3. T. Ohzuku, M. Kitagawa, and T. Hirai, *J. Electrochem. Soc.*, 137, 769 (1990).
4. J.M. Tarascon, F. Coowar, G. Amatucci, F.K. Shokoohi, and D.G. Guyomard, *J. Power Sources*, 59, 103 (1995).
5. K.S. Nanjundaswamy, A.K. Padhi, J.B. Goodenough, S. Okada, H. Ohtsuka, H. Arai, & J. Yamaki, *Solid State Ionics* (1996, in print).
6. A.K. Padhi, K.S. Nanjundaswamy, and J.B. Goodenough, *J. Electrochem. Soc.*, (in print).
7. A.K. Padhi, W.B. Archibald, K.S. Nanjundaswamy, and J.B. Goodenough *J. Solid State Chem.*, (in print).
8. T.W. Hewston and B.L. Chamberland *J. Phys. Chem. Solids*, 48, 97 (1987).
9. R.J. Gummow, A.DeKock, and M.M. Thackeray, *Solid State Ionics*, 69, 59 (1994).
10. C. Masquelier, M. Tabuchi, K. Ado, R. Kanno, Y. Kobayashi, Y. Maki, O. Nakamura, and J.B. Goodenough, *J. Solid State Chem.*, 123, 255 (1996).
11. K.S. Nanjundaswamy, A.K. Padhi, C. Masquelier, S. Okada, and J.B. Goodenough, *37th Power Source Conference*, Cherry Hill, NJ, (June 1996).
12. G.G. Amatucci, J.M. Tarascon, and L.C. Klein, *J. Electrochem. Soc.*, 143, 1114 (1996).
13. C. Delmas, I. Saadoune, and A.Rougier, *J. Power Sources*, 43-44, 595 (1993).
14. M.M. Thackeray, *J. Electrochem. Soc.*, 142, 2558 (1995).
15. T. Ohzuku, "*Lithium Batteries, New Materials, Development and Perspectives*", G. Pistoia (Editor), p 239 (Elsevier Science, 1994).
16. C. O. Kelly and R. V. Whiteley Jr., *37th Power Source Conference*, Cherry Hill, NJ, (June 1996).
17. K. Nakagawa, R. Konaka, and T. Nakata, *J. Org. Chem.*, 27, 1597 (1962).
18. R. J. Gummow, *Ph. D. Thesis*, Dept. of Chem., Univ. of Cape Town, Pretoria, (August 1993).

1996 NASA Aerospace Battery Workshop Attendance List

Mike Allison
Hughes Space and Communication
MS 231/1718
POB 2999
Torrance, CA 90509-2999
Ph: (310) 517-5292 Fax: (310) 517-7676

Menahem Anderman
Acme Electric Corporation
Aerospace Division
528 West 21st Street
Tempe, AZ 85282
Ph: (602) 894-6864 Fax: (602) 921-0470

Bob Axley
McDonnell Douglas Aerospace
M/S AHSV-22D3
689 Discovery Dr.
Huntsville, AL 35806
Ph: (205) 922-7956 Fax: (205) 922-4526

Chris Baker
Acme Electric Corporation
528 W. 21st
Tempe, AZ 85282
Ph: 602 894-6864 Fax:

Mike Bangham
McDonnell Douglas Aerospace
689 Discovery Dr.
Huntsville, AL 35806-2804
E-mail: bangham@humail.mdc.com

L. Krista Barker
Lockheed Martin Technical Operations
Building 100
POB 61687
Sunnyvale, CA 94088-1687
Ph: (408) 752-6510 Fax: (408) 744-2250

Bob Bechtel
Marshall Space Flight Center
EB11
Marshall Space Flight Center, AL 35812
Ph: (205) 544-3294 Fax: (205) 544-5841

Mark Behrman
Acme Electric Corporation
Aerospace Division
528 West 21st Street
Tempe, AZ 85282
Ph: (602) 894-6864 Fax: (602) 921-0470

Charles W. Bennett
Lockheed Martin Astro Space
MS U1219
230 E. Mall Blvd.
King of Prussia, PA 19406
Ph: (610) 354-6155 Fax: (610) 354-3434
E-mail: rf04906@vf.lmms.lmco.com

Samuel Birken
The Aerospace Corporation
MS M4/986
POB 92957
Los Angeles, CA 90009-2957
Ph: (310) 336-6080 Fax: (310) 336-5581
E-mail: samiam@lafn.org

Yannick Borthomieu
SAFT Advanced Batteries
Rue G. Leclanche
BP 1029
86060 Poitiers Cedex
France
Ph: 33-549-55-4014 Fax: 33-549-55-4780

Bobby J. Bragg
Johnson Space Center
MS EP52
NASA Rd. 1
Houston, TX 77058
Ph: (281) 483-9060 Fax: (281) 483-3096
E-mail: bbragg@gp904.jsc.nasa.gov

Rita Brazier
Marshall Space Flight Center
EB11
Marshall Space Flight Center, AL 35812
Ph: (205) 544-3295 Fax: (205) 544-5841

Jeffrey C. Brewer
Marshall Space Flight Center
EB12
Marshall Space Flight Center, AL 35812
Ph: (205) 544-3345 Fax: (205) 544-5841
E-mail: jeff.brewer@msfc.nasa.gov

1996 NASA Aerospace Battery Workshop Attendance List

Harry Brown
Naval Surface Warfare Center - Crane Div.
Code 6095 B2949
Commander
300 Hwy 301
Crane, IN 47522
Ph: (812) 854-6149 Fax: (812) 854-1212
E-mail: brown_harry@crane.navy.mil

Shirley Butler
Marshall Space Flight Center
EB12
Marshall Space Flight Center, AL 35812
Ph: (205) 544-3298 Fax:

William Cabrall
The Boeing Company
MS 8M-02
POB 3999
Seattle, WA 98124
Ph: (303) 365-2556 Fax: (303) 365-2560

Dwight Caldwell
Eagle-Picher Industries, Inc.
Range Line Facility
POB 47
Joplin, MO 64802
Ph: (417) 623-8333 x19 Fax: (417) 623-0233

Joseph A. Carcone
Sanyo Energy (USA) Corporation
2001 Sanyo Avenue
San Diego, CA 92173
Ph: (619) 661-6620 Fax: (619) 661-6743
E-mail: jcarcone@sec.sanyo.com

Dr. Paolo Carosso
Swales Aerospace
5050 Powder Mill Rd.
Beltsville, MD 20705
Ph: (301) 586-1266 Fax: (301) 586-0104
E-mail: pcarosso@pop700.gsfc.nasa.gov

John E. Casey
Lockheed Martin Engineering & Sciences Co.
2400 NASA Rd. 1, C44
Houston, TX 77058-3799
Ph: (281) 483-0446 Fax: (281) 483-3096
E-mail: jcasey@gp904.jsc.nasa.gov

Patricia L. Chilelli
Lockheed Martin Astro Space
MS 501
POB 800
Princeton, NJ 08543-0800
Ph: (609) 490-6507 Fax: (609) 490-4242

Barbara Clark
SAFT R&D Center
107 Beaver Ct.
Cockeysville, MD 21030
Ph: (410) 771-3200 Fax: (410) 771-0234

Dwaine Coates
Energy Research Corporation
3 Great Pasture Road
Danbury, CT 06813
Ph: (203) 825-6187 Fax: (203) 825-6150

Betty Colhoun
Goddard Space Flight Center
Code 440.9
Greenbelt, MD 20771
Ph: (301) 286-7691 Fax: (301) 286-1726

Anne Conley
Hughes Aircraft
Bldg S75 / M/S CHS
16800 E. Centretech Parkway
Aurora, CO 80011
Ph: (303) 341-3327 Fax:

Karen Cunningham
Marshall Space Flight Center
EB12
Marshall Space Flight Center, AL 35812
Ph: (205) 544-5618 Fax:

Bernard P. Dagarin
5511 Huntley Ave.
Garden Grove, CA 92845
Ph: (714) 892-4082 Fax:

1996 NASA Aerospace Battery Workshop Attendance List

Sal Di Stefano
Jet Propulsion Laboratory
MS 277-212
4800 Oak Grove Drive
Pasadena, CA 91109
Ph: (818) 354-6320 Fax: (818) 393-6951

Lt. Charles Donet
USAF
PL/VTVP
Kirtland AFB, NM 87117-5776
Ph: (505) 846-4899 Fax: (505) 846-2885
E-mail: donetc@plk.af.mil

Rajiv Doreswamy
Marshall Space Flight Center
EB12
Marshall Space Flight Center, AL 35812
Ph: (205) 544-3366 Fax:

Geoffrey John Dudley
European Space Agency
POB 299
2200 AG Noordwijk
The Netherlands
Ph: 31 71 565 3834 Fax: 31 71 565 4994
E-mail: gdudley@vmprofs.estec.esa.nl

Andrew F. Dunnet
Fraser-Dunnet Consulting
5112 Bradford Drive
Annandale, VA 22003
Ph: (703) 256-4092 Fax: (703) 256-4094

Ted Edge
Marshall Space Flight Center
EB12
Marshall Space Flight Center, AL 35812
Ph: (205) 544-3381 Fax:

Nicanor A. Flordeliza
GE American Communications Satellites, Inc.
4 Research Way
Princeton, NJ 08540
Ph: (609) 987-4453 Fax: (609) 987-4393

Christopher L. Fox
Eagle-Picher Industries, Inc.
POB 47
Joplin, MO 64802
Ph: (417) 623-8000 X367 Fax: (417) 781-1910

Jennifer Francisco
Eagle-Picher Industries, Inc.
1215 West B Street
Joplin, MO 64801
Ph: (417) 623-8000 Fax: (417) 623-5319

Chris Garner
Naval Research Laboratory
Code 8134
4555 Overlook Ave. SW
Washington, DC 20375
Ph: (202) 767-9075 Fax: (202) 767-4633

Pete George
Marshall Space Flight Center
EB12
Marshall Space Flight Center, AL 35812
Ph: (205) 544-3331 Fax:

Dawn Gregory
Hughes Aircraft
Bldg S75 / M/S CHS
16800 E. Centretech Parkway
Aurora, CO 80011
Ph: 303 342-3327 Fax:

James A. Gucinski
Naval Weapons Support Center - Crane
Code 609 Bldg 2949
Crane, IN 47522-5030
Ph: (812) 854-6150 Fax: (812) 854-1212
E-mail: jag444@smtp.nwscc.sea06.navy.mil

Doug Hafen
Lockheed Martin
B/149 O/E6-01
POB 3504
Sunnyvale, CA 94089-3504
Ph: (408) 743-7220 Fax: (408) 742-7701
E-mail: hafen_doug@mm.ssd.lmsc.lockheed.com

1996 NASA Aerospace Battery Workshop Attendance List

David Hall
Marshall Space Flight Center
EB12
Marshall Space Flight Center, AL 35812
Ph: (205) 544-4215 Fax:

Ian S. Hall
Matra Marconi Space UK Ltd.
Gunnels Wood Road
Stevenage, Hertfordshire
SG1 2AS
England
Ph: 011-44-1438-773347 Fax: 011-44-1438-773200

Steve Hall
Naval Surface Warfare Center - Crane Div.
Code 6095
Crane, IN 47522
Ph: (812) 854-4172 Fax: (812) 854-1212

Alan Harkness
Harkon
Suite 105
444 W. 49th Ave.
Vancouver, BC
Canada V5Y 3V4
Ph: (604) 325-1659 Fax: (604) 325-3180

Dr. Robert J. Hayduk
NASA Headquarters
300 E. St., SW
Washington, DC 20546
Ph: (202) 358-4690 Fax: (202) 358-2697
E-mail: robert.hayduk@hq.nasa.gov

Duane Heier
Boeing Defense & Space
MS 8F-08
POB 3999
Seattle, WA 98124-3039
Ph: (206) 773-3039 Fax: (206) 773-9139

Robert Higgins
Eagle-Picher Industries, Inc.
POB 47
Joplin, MO 64802
Ph: (417) 623-8000 Fax:

Carole A. Hill
The Aerospace Corporation
POB 9045
Albuquerque, NM 87119-9045
Ph: (505) 846-7063 Fax: (505) 846-1445
E-mail: hill@kafb.aero.org

Albert Himy
Navy / JJMA
2341 Jefferson Davis Highway
Suite 715
Arlington, VA 22202
Ph: (703) 418-4257 Fax: (703) 418-4269

Scott Hoover
Orion Satellite Corporation
2440 Research Blvd.
Suite 160
Rockville, MD 20850
Ph: (301) 258-3325 Fax: (301) 258-3319
E-mail: 695-4848@mcimail.com

Sonya Hutchinson
Marshall Space Flight Center
EB12
Marshall Space Flight Center, AL 35812
Ph: (205) 544-3312 Fax:

Nathan Isaacs
MSA
38 Loveton Circle
Sparks, MD 21152
Ph: (410) 628-5440 Fax: (410) 628-0613
E-mail: nedizakmsa@aol.com

Lorna Jackson
Marshall Space Flight Center
EB12
Marshall Space Flight Center, AL 35812
Ph: (205) 544-3318 Fax:

Ralph James
USAF
PL/VTPP
Bldg. 30117, Manzano
3550 Aberdeen Ave SE
Kirtland AFB, NM 87117-5776
Ph: (505) 846-2614 Fax: (505) 846-2885
E-mail: james2@plk.af.mil

1996 NASA Aerospace Battery Workshop Attendance List

Thierry Jamin
CNES / AE / SE / AC
18 Avenue Edouard Belin
31055 Toulouse Cedex
France
Ph: 05 61 27 49 38 Fax: 05 61 28 21 62
E-mail: jamin@ace.esr.cnes.fr

Gwyn Morgan Jenkins
Alabama A&M University
Department of Physics
Normal, AL 35762

Jason E. Jenkins
Johns Hopkins University / APL
MS 23-214
Johns Hopkins Rd.
Laurel, MD 20723-6099
Ph: 410 792-5106 Fax:
E-mail: jason.jenkins@jhuapl.edu

Dr. P. J. Johnson
Matra Marconi Space UK Ltd.
Gunnels Wood Road
Stevenage, Hertfordshire
SG1 2AS
England
Ph: 011-44-1438-773031 Fax: 011-44-1438-773200

David S. Jung
Goddard Space Flight Center
Code 734
Greenbelt, MD 20771
Ph: (301) 286-6104 Fax: (301) 286-1719

Haresh Kamath
Lockheed Martin Missiles & Space
O/E6-01, B/149, Col B3
1111 Lockheed Martin Way
Sunnyvale, CA 94089
Ph: (408) 743-6789 Fax: (408) 743-6745
E-mail: kamath@lmsc.lockheed.com

Bob Kapustka
Marshall Space Flight Center
EB12
Marshall Space Flight Center, AL 35812
Ph: (205) 544-3302 Fax:

Donald R. Kleis
The ENSER Corporation
UAH Johnson Research Center
Huntsville, AL 35899
Ph: (205) 890-6707 x247 Fax: (205) 890-6668
E-mail: slvrstreek@aol.com

Michael D. Koelling
Hughes Aircraft
MS CHSS
16800 E. CentreTech Parkway
Aurora, CO 80011
Ph: (303) 341-3327 Fax: (303) 341-2926
E-mail: mokoe@aol.com

Kiyokazu Koga
National Space Development Agency of Japan
2-1-1 Sengen, Tsukuba-shi,
Ibaraki-ken, 305 Japan
Ph: (81) 298 52 2285 Fax: (81) 298 52 2299
E-mail: koga@rd.tksc.nasda.go.jp

Stanley J. Krol, Jr.
Lockheed Martin Technical Operations Inc.
7474 Greenway Center Drive
Suite 200
Greenbelt, MD 20770
Ph: (301) 901-6101 Fax: (301) 901-6076
E-mail: krol_stanley@mnb2.fss-moses.lo

Ron Lantzy
Lockheed Martin
18605 East Dorado Dr.
Aurora, CO 80015
Ph: (303) 341-3812 Fax:

Erik L. Levine
Space Systems / Loral
3825 Fabian Way
MS G-13
Palo Alto, CA 94303-4604
Ph: (415) 852-5511 Fax: (415) 852-4936

Danny Liu
INTELSAT
INTELSAT VIII Program Office
c/o Lockheed Martin Astro Space
POB 800 / MS 93
Princeton, NJ 08543-0800
Ph: (609) 426-9225 Fax: (609) 426-8968

1996 NASA Aerospace Battery Workshop Attendance List

Eric Lowery
Marshall Space Flight Center
EB12
Marshall Space Flight Center, AL 35812
Ph: (205) 544-0080 Fax:

Chuck Lurie
TRW
MS R4/1082
One Space Park
Redondo Beach, CA 90278
Ph: (310) 813-4888 Fax: (310) 812-4978
E-mail: chuck.lurie@trw.com

Dr. Tyler X. Mahy
U.S. Government
c/o OTS, NHB
Washington, DC 20505
Ph: (703) 874-0739 Fax: (703) 641-9830

Paul A. Malachesky
The Aerospace Corporation
The Hallmark Bldg.
13873 Park Center Rd.
Suite 187
Herndon, VA 22071
Ph: (703) 808-4894 Fax: (703) 808-4955

Michelle Manzo
Lewis Research Center
MS 309-1
21000 Brookpark Rd.
Cleveland, OH 44135
Ph: (216) 433-5261 Fax: (216) 433-6160

Nehemiah Margalit
Tracor Applied Sciences Inc.
1601 Research Blvd.
Rockville, MD 20850
Ph: (301) 838-6223 Fax: (301) 838-6222
E-mail: nmargalit@tracor.com

Jeff Martin
Marshall Space Flight Center
EB12
Marshall Space Flight Center, AL 35812

Dean W. Maurer
McKnight Associates
292 Johnston Dr.
Watchung, NJ 07060
Ph: (908) 753-4457 Fax:

Kurt McCall
Marshall Space Flight Center
EB12
Marshall Space Flight Center, AL 35812
Ph: (205) 961-4501 Fax:

M. J. Milden
2212 So. Beverwil Dr.
Los Angeles, CA 90034-1034
Ph: (310) 836-6694 Fax: (310) 836-0094
E-mail: mmilden@worldnet.att.net

K. S. Nanjundaswamy
Eagle-Picher Industries, Inc.
Technology Division
POB 47
Joplin, MO 64802
Ph: (417) 623-8000 x436 Fax: (417) 623-5556

David O'Dell
Marshall Space Flight Center
EB12
Marshall Space Flight Center, AL 35812
Ph: (205) 544-3416 Fax:

Pat O'Donnell
Lewis Research Center
MS 309-1
21000 Brookpark Rd.
Cleveland, OH 44135
Ph: (216) 433-5248 Fax: (216) 433-6160
E-mail: seodo@lims02.lerc.nasa.gov

Naohito Okobo
Sanyo Electric Company, Ltd.
222-1 Kaminaizen. Sumoto City
Hyogo, Japan
Ph: 81-799-24-4111 Fax:

1996 NASA Aerospace Battery Workshop Attendance List

John L. Palme
ORBCOMM Global
21700 Atlantic Blvd.
Dulles, VA 20166-6801
Ph: (703) 406-5685 Fax: (703) 406-3504
E-mail: jpalme@orbcomm.net

Rick Parmley
Eagle Picher
POB 47
Joplin, MO 64802
Ph: (417) 623-8000 Fax:

Dave Perrone
Jet Propulsion Laboratory
MS 277-212
4800 Oak Grove Dr.
Pasadena, CA 91109
Ph: 818 354-9044 Fax: 818 393-6951
E-mail: david.e.perrone@jpl.nasa.gov

David F. Pickett
Eagle-Picher Industries
Power Systems Department
3820 S. Hancock Expressway
Colorado Springs, CO 80911
Ph: (719) 392-4266 Fax: (719) 392-5103

Dan T. Radzykewycz
U.S. Air Force
Phillips Laboratory
Kirtland AFB, NM 87117-5776
Ph: 505 846-5703 Fax:

Gopal Rao
Goddard Space Flight Center
Code 734
Greenbelt, MD 20771
Ph: (301) 286-6654 Fax: (301) 286-1751

Ron Repplinger
Eagle-Picher Industries, Inc.
POB 47
Joplin, MO 64802
Ph: (417) 623-8000 Fax: (417) 623-5319

Byron Rogers
McDonnell Douglas
101 Victoria Drive
Madison, AL 35758
Ph: (205) 922-4524 Fax:

Darren L. Scoles
Eagle-Picher Industries, Inc.
Technologies Division
Power Systems Department
3820 S. Hancock Expressway
Colorado Springs, CO 80911
Ph: (719) 392-4266 Fax: (719) 392-4381
E-mail: 73024.3615@CompuServe.com

Annie Sennet
SAFT
156 Avenue DeMetz
93230 Romainville
France
Ph: 011 1 33 49 15 36 44 Fax: 011 1 33 48 91 95 53
E-mail: annie.sennet@saft.alcatel-alsthorm.fr

Sat P. Singhal
Computer Sciences Corporation
7404 Executive Place
Seabrook, MD 20706
Ph: 301 464-7400 x7579 Fax: 301 464-3352
E-mail: ssinghal@csc.com

Luther W. Slifer, Jr.
Jackson & Tull, Chartered Engineers
NASA / Goddard Space Flight Center
Code 734.4
J & T Support
Greenbelt, MD 20771
Ph: (301) 286-8433 Fax: (301) 286-1751

Hsiao L. Smith
Goddard Space Flight Center
Code 734
Greenbelt, MD 20771
Ph: (301) 286-4641 Fax:
E-mail: hsiao.smith@gsfc.nasa.gov

Steven Stadnick
Hughes Aircraft Co.
MS D543, Bldg. S24
POB 92919
Los Angeles, CA 90009
Ph: (310) 416-4134 Fax: (310) 416-3922

1996 NASA Aerospace Battery Workshop Attendance List

Dan Standlee
Eagle-Picher Industries, Inc.
1215 West B Street
Joplin, MO 64802
Ph: (417) 623-8000 X301 Fax:

Joe Stockel
Office of Research & Development
LF-7 Rm 6118
Washington, DC 20505
Ph: (703) 613-8833 Fax: (703) 613-8954

Ralph M. Sullivan
Swales & Associates, Inc.
13118 Greenmount Ave.
Beltsville, MD 20705
Ph: (301) 572-1280 Fax: (301) 595-2871

Greg Terry
Kateli Enterprises, Inc.
295 Lakeridge Dr. S.
Lynchburg, TN 37352
Ph: (205) 651-2177 Fax: (615) 759-4728
E-mail: ghterry@hiwaay.net

Vijay V. Thakur
Defence Research Agency
Space Power Systems
Space Department / P234 Building
DERA Farnborough
Hampshire. GU146TD. U.K.
Ph: 011-44-1252 393669 Fax: 011-44-1252 392664

Lawrence Thaller
The Aerospace Corporation
MS M2/275
POB 92957
Los Angeles, CA 90009
Ph: (310) 336-5180 Fax: (310) 336-1636
E-mail: larry_thaller@qmail2.aero.org

Paul Timmerman
Jet Propulsion Laboratory
MS 277-213
4800 Oak Grove Drive
Pasadena, CA 91109
Ph: (818) 354-5388 Fax: (818) 393-6951

Robert F. Tobias
TRW
MS R4/1074
One Space Park
Redondo Beach, CA 90278
Ph: (310) 813-5784 Fax:

Walt Tracinski
Applied Power International
1236 N. Columbus Ave., #41
Glendale, CA 91202-1672
Ph: (818) 243-3127 Fax: (818) 243-3127

Dr. Hari Vaidyanathan
COMSAT Laboratories
22300 Comsat Dr.
Clarksburg, MD 20871
Ph: (301) 428-4507 Fax: (301) 428-3686
E-mail: hari.vaidyanathan@comsat.com

John W. Van Zee
University of South Carolina
Chemical Engineering Dept.
Columbia, SC 29208
Ph: (803) 777-2285 Fax: (803) 777-8265
E-mail: vanzee@engr.engr.sc.edu

Harry Wannemacher
Jackson & Tull
7375 Executive Place
Suite 200
Seabrook, MD 20706
Ph: (301) 805-6090 Fax: (301) 805-6099
E-mail: harry.wan@jnt.com

Margot Wasz
The Aerospace Corporation
MS M2/275
POB 92957
Los Angeles, CA 90009

Steve Westfall
Eagle-Picher Industries, Inc.
POB 47
C & Porter Streets
Joplin, MO 64802-0047
Ph: (417) 623-8000 Fax: (417) 623-5556

1996 NASA Aerospace Battery Workshop Attendance List

Dr. Ralph E. White
University of South Carolina
Dept. of Chemical Engineering
Swearingen Engineering Center
Columbia, SC 29208
Ph: (803) 777-3270 Fax: (803) 777-8265
E-mail: rew@sun.che.sc.edu

Tom Whitt
Marshall Space Flight Center
EB12
Marshall Space Flight Center, AL 35812
Ph: (205) 544-3313 Fax:

Doug Willowby
Marshall Space Flight Center
EB12
Marshall Space Flight Center, AL 35812
Ph: (205) 544-3334 Fax:

Jim Wiser
Marshall Space Flight Center
PD14
Marshall Space Flight Center, AL 35812

Daphne Xu
INTELSAT
3400 International Dr. NW
Box 34
Washington, DC 20008-3098
Ph: (202) 944-7250 Fax: (202) 944-7333
E-mail: daphne.xu@intelsat.int

Albert H. Zimmerman
The Aerospace Corporation
MS M2/275
POB 92957
Los Angeles, CA 90009-2957
Ph: (310) 336-7415 Fax: (310) 336-1636

REPORT DOCUMENTATION PAGE

Form Approved
OMB No. 0704-0188

Public reporting burden for this collecton of information is estimated to average 1 hour per response, including the time for reviewing instructions, searching existing data sources, gathering and maintaining the data needed, and completing and reviewing the collection of information. Send comments regarding this burden estimate or any other aspect of this collection of information, including suggestions for reducing this burden, to Washington Headquarters Services, Directorate for Information Operations and Reports, 1215 Jefferson Davis Highway, Suite 1204, Arlington, Va 22202-4302, and to the Office of Management and Budget, Paperwork Reduction Project (0704-0188), Washington, DC 20503.

1. AGENCY USE ONLY (Leave Blank)	2. REPORT DATE	3. REPORT TYPE AND DATES COVERED
	February 1997	Conference Publication

4. TITLE AND SUBTITLE

The 1996 NASA Aerospace Battery Workshop

5. FUNDING NUMBERS

6. AUTHOR(S)

Jeffrey C. Brewer, Compiler

7. PERFORMING ORGANIZATION NAME(S) AND ADDRESS(ES)

George C. Marshall Space Flight Center
Marshall Space Flight Center, Alabama 35812

8. PERFORMING ORGANIZATON REPORT NUMBERS

M-825

9. SPONSORING/MONITORING AGENCY NAME(S) AND ADDRESS(ES)

National Aeronautics and Space Administration
Washington, DC 20546

10. SPONSORING/MONITORING AGENCY REPORT NUMBER

NASA CP-3347

11. SUPPLEMENTARY NOTES

Proceedings of a workshop sponsored by the NASA Aerospace Flight Battery Systems Program, hosted by the Marshall Space Flight Center, and held at the Huntsville Hilton on December 3-5, 1996

12a. DISTRIBUTION/AVAILABILITY STATEMENT

Unclassified-Unlimited
Subject Category 44

12b. DISTRIBUTION CODE

13. ABSTRACT *(Maximum 200 words)*

This document contains the proceedings of the 29th annual NASA Aerospace Battery Workshop, hosted by the Marshall Space Flight Center on December 3-5, 1996. The workshop was attended by scientists and engineers from various agencies of the U.S. Government, aerospace contractors, and battery manufacturers, as well as international participation in like kind from a number of countries around the world.

The subjects covered included nickel-cadmium, nickel-hydrogen, silver-zinc, nickel-metal hydride, and lithium based technologies, as well as flight and ground test data. Nickel-hydrogen reconditioning was also covered.

14. SUBJECT TERMS

battery, nickel-cadmium, nickel-hydrogen, nickel-metal hydride, lithium, cadmium, battery tests, electrode, pressure vessel, modeling, reconditioning

15. NUMBER OF PAGES

624

16. PRICE CODE

A99

17. SECURITY CLASSIFICATION	18. SECURITY CLASSIFICATION OF THIS PAGE	19. SECURITY CLASSIFICATION OF ABSTRACT	20. LIMITATION OF ABSTRACT
Unclassified	Unclassified	Unclassified	

National Aeronautics and
Space Administration
Code JTT
Washington, DC
20546–0001

Official Business
Penalty for Private Use, $300

Postmaster: If Undeliverable (Section 158 Postal Manual), Do Not Return